15th ECSSC – Vienna, Austria

August 23 to 26, 2015 at the Campus of the University of Vienna

PROGRAM

BOOK OF ABSTRACTS

15th EUROPEAN CONFERENCE
ON SOLID STATE CHEMISTRY

August 23-26, 2015

Vienna, Austria

15th ECSSC – Vienna, Austria
August 23 to 26, 2015 at the Campus of the University of Vienna

15th EUROPEAN CONFERENCE ON SOLID STATE CHEMISTRY
August 23 to 26, 2015
Vienna, Austria

Organized by
Dept. of Inorganic Chemistry (Materials Chemistry), University of Vienna
Austrian Chemical Society (GÖCH)
Division of Solid State and Materials Chemistry (EuCheMS)

COMMITTEES

International Advisory Board

H-J. Deiseroth (University of Siegen, Germany), Chair
E. Antipov (Moscow State University, Russia)
M. Drillon (IPCMS, Université Louis Pasteur, Strasbourg, France)
J. Gonzalez-Calbet (Universidade Complutense, Madrid, Spain)
H. Ipser (University of Vienna, Austria)
M. Jansen (Max Planck Institute for Solid State Research, Stuttgart, Germany)
H. Fjellvåg (University of Oslo, Norway)
S. Lidin (University of Lund, Sweden)
A. Maignan (Université de Caen, France)
J. Hulliger (University of Bern, Switzerland)
M.J. Rosseinsky (University of Liverpool, United Kingdom)
G. Van Tendeloo (University of Antwerp, Belgium)
A.R. West (University of Sheffield, United Kingdom)

Local Organizing Committee

University of Vienna, Department of Inorganic Chemistry / Materials Chemistry

H. Ipser, Chair
H. Flandorfer
K.W. Richter
I. Jandl
J. Polt
M.C. Marker
A. Beutl
P. Kainzbauer
C. Luef
G. Reisinger
P. Wibner

Vienna University of Technology

S. Bühler-Paschen
G. Rupprechter
M. Weil

GÖCH - Austrian Chemical Society

G. Ebner

SPONSORS

GOLD SPONSOR

plansee GROUP

MESSER Gases for Life

VIENNA NOW OR NEVER WWW.VIENNA.INFO

SILVER SPONSOR

MBRAUN

Springer

BRONZE SPONSOR

LACTAN ROTH Chemikalien und Laborgeräte 8020 Graz - Puchstraße 85

VWR We Enable Science

WILEY-VCH

EXHIBITORS

BRUKER

STOE

SINCE 1887

MBRAUN

L+H

TECHNIK

VAKUUM

Generalvertretung für

oerlikon

leybold vacuum

Prager

Elektronik

NETZSCH

Table of Contents

Conference Location

15th ECSSC – Vienna, Austria
August 23 to 26, 2015 at the Campus of the University of Vienna

Conference area
Conference desk

Restaurants for lunch:
“Stiegl Ambulanz”,
“Salettl”,
“Zum Gangl”
Special conditions for conference participant

SOCIAL PROGRAM

Social Program:

- Welcome Reception on Sunday, August 23, 2015
  Starting at 18.00 directly at the conference location
- Reception at the City Hall of Vienna on Tuesday evening, August 25, 2015
  Starting at 19.30, entrance Lichtenfelsgasse 2, 1010 Vienna, from 19.00

Program for Accompanying Persons:

- Welcome Reception on Sunday, August 23, 2015
  Beginning at 18.00 directly at the conference location
- Reception in the City Hall of Vienna on Tuesday evening, August 25, 2015
  Starting at 19.30, entrance Lichtenfelsgasse 2, 1010 Vienna, from 19.00
- Guided Walking Tour through the City of Vienna including coffee and cake in a typical Viennese Kaffeehaus on Monday afternoon, August 24, 2015
- Excursion to the surroundings of Vienna on Tuesday (full day), August 25, 2015
  Excursion destination is the famous monastery "Heiligenkreuz" (Cistercian abbey). Also a visit of the elegant music and shopping city of Baden is scheduled. Once an imperial summer residence.

Reception at the City Hall of Vienna

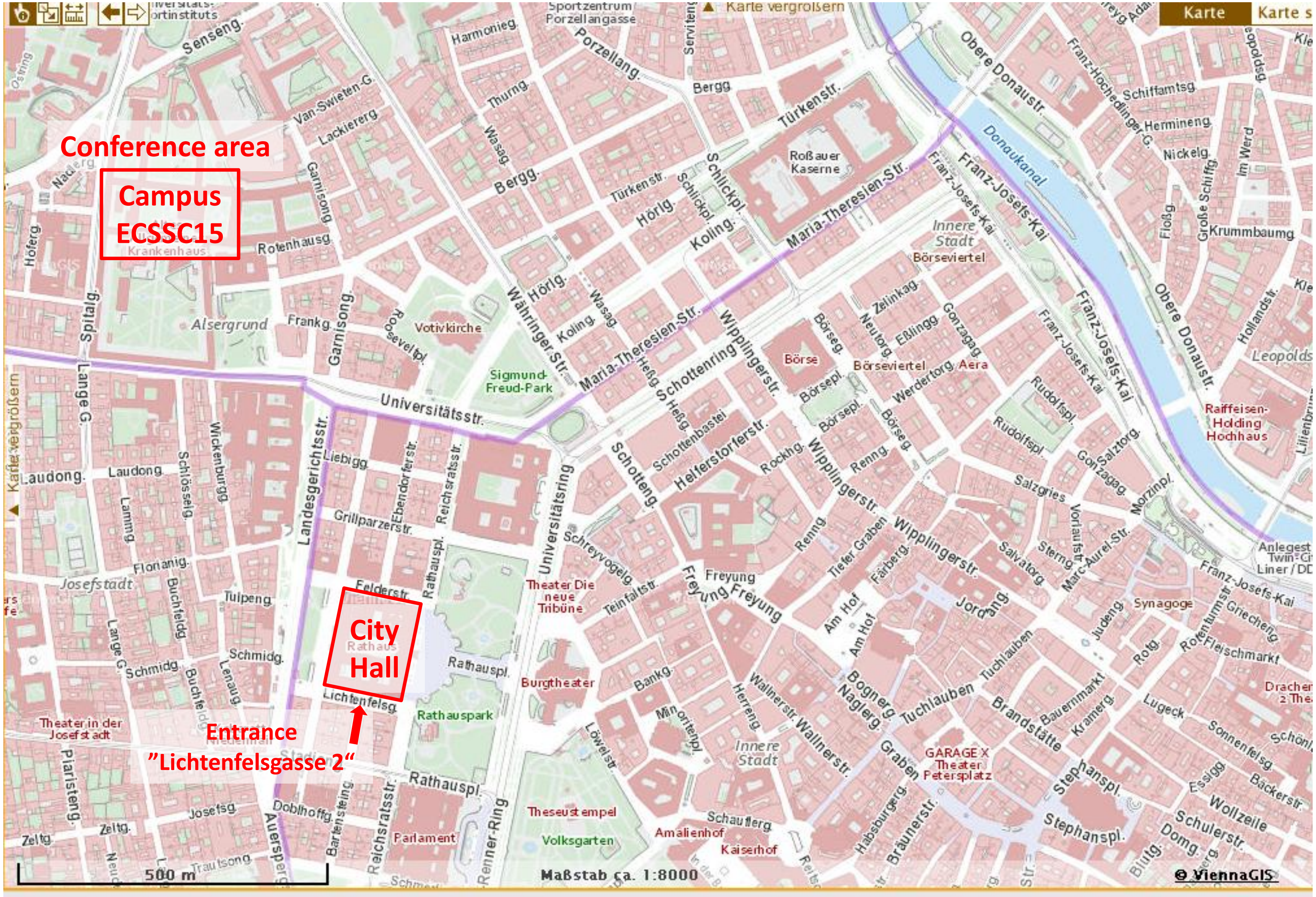

CONFERENCE PROGRAM

Monday 24.08.2015			Tuesday 25.08.2015			Wednesday 26.08.2015		
08.30 – 08.50		Opening						
08.50 – 09.30	**PL1**	Plenary Lecture 1	09.00 – 09.40	**PL4**	Plenary Lecture 4	09.00 – 09.40	**PL7**	Plenary Lecture 7
09.30 – 09.55	**IL1**	Invited Lecture 1	09.40 – 10.05	**IL4**	Invited Lecture 4	09.40 – 10.05	**IL7**	Invited Lecture 7
09.55 – 10.15	**O1**	Short Lecture 1/1	10.05 – 10.25	**O7**	Short Lecture 4/1	10.05 – 10.25	**O13**	Short Lecture 7/1
10.15 – 10.35	**O2**	Short Lecture 1/2	10.25 – 10.45	**O8**	Short Lecture 4/2	10.25 – 10.45	**O14**	Short Lecture 7/2
10.35 – 11.00		Coffee Break 1	10.45 – 11.05		Coffee Break 3	10.45 – 11.05		Coffee Break 5
11.00 – 11.40	**PL2**	Plenary Lecture 2	11.05 – 11.45	**PL5**	Plenary Lecture 5	11.05 – 11.45	**PL8**	Plenary Lecture 8
11.40 – 12.05	**IL2**	Invited Lecture 2	11.45 – 12.10	**IL5**	Invited Lecture 5	11.45 – 12.10	**IL8**	Invited Lecture 8
12.05 – 12.25	**O3**	Short Lecture 2/1	12.10 – 12.30	**O9**	Short Lecture 5/1	12.10 – 12.30	**O15**	Short Lecture 8/1
12.25 – 12.45	**O4**	Short Lecture 2/2	12.30 – 12.50	**O10**	Short Lecture 5/2	12.30 – 12.50	**O16**	Short Lecture 8/2
12.45 – 14.00		Lunch	12.50 – 14.00		Lunch	12.50 – 14.00		Lunch
14.00 – 14.40	**PL3**	Plenary Lecture 3	14.00 – 14.40	**PL6**	Plenary Lecture 6	14.00 – 14.40	**PL9**	Plenary Lecture 9
14.40 – 15.05	**IL3**	Invited Lecture 3	14.40 – 15.05	**IL6**	Invited Lecture 6	14.40 – 15.05	**IL9**	Invited Lecture 9
15.05 – 15.25	**O5**	Short Lecture 3/1	15.05 – 15.25	**O11**	Short Lecture 6/1	15.05 – 15.25	**O17**	Short Lecture 9/1
15.25 – 15.45	**O6**	Short Lecture 3/2	15.25 – 15.45	**O12**	Short Lecture 6/2	15.25 – 15.45	**O18**	Short Lecture 9/2
15.45 – 16.00		Coffee Break 2	15.45 – 16.00		Coffee Break 4	15.45 – 16.00		Closing of Conference
16.00 – 18.00	**P**	Poster session 1	16.00 – 18.00	**P**	Poster session 2			

Monday 24.08.2015					
Time		**Event**	**LECTURER**	**TOPIC**	**TITLE**
08.30 – 08.50		Opening			
CHAIR: Grin Juri					
08.50 – 09.30	**PL1**	Plenary Lecture 1	**Steurer** Walter	**Intermetallics**	Statistics of intermetallics - some remarkable findings
09.30 – 09.55	**IL1**	Invited Lecture 1	**Pay Gómez** Cesar	**Intermetallics**	Icosahedral Quasicrystals and Approximants
09.55 – 10.15	**O1**	Short Lecture 1/1	**Hoch** Constantin	Intermetallics	Polar metal-metal bonding in intermetallic phases from electrocrystallisation near room temperature
10.15 – 10.35	**O2**	Short Lecture 1/2	**Ponou** Simeon	Intermetallics	Conflict management: Lessons from Intermetallic Chemistry
10.35 – 11.00		Coffee Break1			
Time		**Event**	**LECTURER**	**TOPIC**	**TITLE**
CHAIR: Delahaye Emilie					
11.00 – 11.40	**PL2**	Plenary Lecture 2	**Maignan** Antoine	**Functional materials**	Thermoelectric or multiferroic oxides and sulfides: 2D versus 3D magnetic materials
11.40 – 12.05	**IL2**	Invited Lecture 2	**Señarís-Rodríguez** María Antonia	**Functional materials**	Electric order and magnetism in hybrid organic-inorganic compounds with perovskite-like structure
12.05 – 12.25	**O3**	Short Lecture 2/1	**Tsvetkov** Dmitry	Functional materials	Oxygen Nonstoichiometry and Charge Transfer in the Double Perovskite $Sr_2FeMoO_{6-\delta}$
12.25 – 12.45	**O4**	Short Lecture 2/2	**Weller** Mark	Functional materials	Synthesis, structures and optical properties of hybrid lead iodide perovskite phases
12.45 – 14.00		Lunch			
Time		**Event**	**LECTURER**	**TOPIC**	**TITLE**
CHAIR: Bensch Wolfgang					
14.00 – 14.40	**PL3**	Plenary Lecture 3	**Clarke** Simon	**Modern developments in chalcogenide research**	Soft chemical control of iron selenide superconductors and layered oxide chalcogenides
14.40 – 15.05	**IL3**	Invited Lecture 3	**Wágner** Tomáš	**Modern developments in chalcogenide research**	Chalcogenide glass films for nanoscale memories
15.05 – 15.25	**O5**	Short Lecture 3/1	**Valldor** Martin	Modern developments in chalcogenide research	Synthesis and characterization of Ba[CoSO]: magnetic complexity and chalcogen ordering
15.25 – 15.45	**O6**	Short Lecture 3/2	**Berthebaud** David	Functional materials	Looking for new chalcogenides functional Materials in Ba-T-Se systems (T=Cr, Fe)
15.45 – 16.00		Coffee Break2			
16.00 – 18.00	**PMon**	Poster session 1			

Tuesday 25.08.2015					
Time		**Event**	**LECTURER**	**TOPIC**	**TITLE**
CHAIR: Häussermann Ulrich					
09.00 – 09.40	**PL4**	Plenary Lecture 4	**Rosseinsky** Matthew J.	**New methods of synthesis**	Symmetry, calculation and synthesis in the search for coupled property materials
09.40 – 10.05	**IL4**	Invited Lecture 4	**Feldmann** Claus	**New methods of synthesis**	Tailored Synthesis between Water and Liquid Ammonia: Hollow Nanospheres for Medicine and Less-noble Metals for Catalysis
10.05 – 10.25	**O7**	Short Lecture 4/1	**Hector** Andrew L.	New methods of synthesis	Templated growth of small nanowires using supercritical fluid electrodeposition
10.25 – 10.45	**O8**	Short Lecture 4/2	**Moran** Emilio	New methods of synthesis	Microwave-assisted routes for the synthesis of inorganic materials: an overview
10.45 – 11.05		Coffee Break 3			
Time		**Event**	**LECTURER**	**TOPIC**	**TITLE**
CHAIR: Cupid Damian					
11.05 – 11.45	**PL5**	Plenary Lecture 5	**Kresse** Georg	**Solid state theory**	Methods beyond DFT: current status and future developments
11.45 – 12.10	**IL5**	Invited Lecture 5	**Abrikosov** Igor A.	**Solid state theory**	Solid state theory at finite temperature
12.10 – 12.30	**O9**	Short Lecture 5/1	**Bende** David	Solid state theory	Heteropolar Bonds and a Position-Space Representation of the 8-N Rule
12.30 – 12.50	**O10**	Short Lecture 5/2	**Rojo** Teofilo	Ionic and electronic transport in solids	Na ionic conductivity in NaTMO$_2$ layered oxides as cathode Materials for Na-ion Batteries
12.50 – 14.00		Lunch			
Time		**Event**	**LECTURER**	**TOPIC**	**TITLE**
CHAIR: Hulliger Jürg					
14.00 – 14.40	**PL6**	Plenary Lecture 6	**Seshadri** Ram	**Collective magnetic phenomena**	Structural studies of oxide spinel magnets: Magnetocapacitors and frustrated systems
14.40 – 15.05	**IL6**	Invited Lecture 6	**Tsirlin** Alexander	**Collective magnetic phenomena**	Magnetism of Cu minerals: geological insights into quantum effects
15.05 – 15.25	**O11**	Short Lecture 6/1	**Battle** Peter	Collective magnetic phenomena	Relaxor Ferromagnetism in the Perovskite Structure
15.25 – 15.45	**O12**	Short Lecture 6/2	**Delahaye** Emilie	Functional materials	Magnetic and Luminescent hybrid coordination networks based on imidazolium dicarboxylate salts and lanthanides
15.45 – 16.00		Coffee Break4			
16.00 – 18.00	**PTue**	Poster session 2			

Wednesday 26.08.2015

Time		Event	LECTURER	TOPIC	TITLE
			CHAIR: Flandorfer Hans		
09.00 – 09.40	**PL7**	Plenary Lecture 7	**Kolb** Ute	**New methods of characterization**	Automated electron Diffraction Tomography (ADT) - solving crystal structures from nano particles
09.40 – 10.05	**IL7**	Invited Lecture 7	**Evans** John.S.O.	**New methods of characterization**	Put your trust in powder: new diffraction methods for studying functional materials
10.05 – 10.25	**O13**	Short Lecture 7/1	**Bensch** Wolfgang	New methods of characterization	Structural and Electronic Changes During Li Uptake and Removal of Nanosized $CoFe_2O_4$ Revealed by a Detailed in operando X-ray Scattering and X-ray Absorption Spectroscopy Study
10.25 – 10.45	**O14**	Short Lecture 7/2	**Fop** Sacha	Ionic and electronic transport in solids	Complex crystal structure and oxide ion conductivity in the hexagonal perovskite derivative $Ba_3MoNbO_{8.5}$
10.45 – 11.05		Coffee Break5			

Time		Event	LECTURER	TOPIC	TITLE
			CHAIR: Schmetterer Clemens		
11.05 – 11.45	**PL8**	Plenary Lecture 8	**Tarascon** Jean-Marie	**Ionic and electronic transport in solids**	Recent advances on insertion materials for better Li-ion batteries
11.45 – 12.10	**IL8**	Invited Lecture 8	**Hagen** Anke	**Ionic and electronic transport in solids**	Ionic and electronic transport in solid oxide cells – Seen from an applied perspective
12.10 – 12.30	**O15**	Short Lecture 8/1	**Dunst** Andreas	Ionic and electronic transport in solids	Lithium ion dynamics in amorphous Li-Si electrochemically prepared from semiconductor grade, monocrystalline silicon - An NMR Study
12.30 – 12.50	**O16**	Short Lecture 8/2	**Ragoen** Céline	Ionic and electronic transport in solids	Influence of alumina content on Na+/K+ interdiffusion in soda silicate glasses
12.50 – 14.00		Lunch			

Time		Event	LECTURER	TOPIC	TITLE
			CHAIR: Huppertz Hubert		
14.00 – 14.40	**PL9**	Plenary Lecture 9	**Eremets** Mikhail I.	**High pressure synthesis and in situ investigations**	Superconductivity at 195 K and other results of application of megabar pressures
14.40 – 15.05	**IL9**	Invited Lecture 9	**Ovsyannikov** Sergey V.	**High pressure synthesis and in situ investigations**	High-pressure high-temperature synthesis of simple oxides
15.05 – 15.25	**O17**	Short Lecture 9/1	**Hasegawa** Masashi	High pressure synthesis and in situ investigations	Ultra-High Pressure Synthesis and Characterization of Transition Metal Nitrides
15.25 – 15.45	**O18**	Short Lecture 9/2	**Häussermann** Ulrich	Others	Exploring hydrothermal environments at gigapascal pressures for materials synthesis
15.45 – 16.00		Closing of Conference			

Monday 24.08.2015

Poster Session 1 16.00 – 18.00

Intermetallics

Poster No.	PRESENTER		TITLE
PMon001	**Vrestal**	Jan	Ab initio calculated energy of formation of chromium Laves phases in phase equilibrium calculations
PMon002	**Schmetterer**	Clemens	Interactions between Sn-Zn solders and Ni-substrates - the Ni-Sn-Zn system
PMon003	**Schmetterer**	Clemens	Powder Preparation from the nano to the micrometer scale
PMon004	**Yakymovych**	Andriy	Structure transformations during Co/Sn solid/liquid interfacial reactions
PMon005	**Ponou**	Simeon	A Multicomponent Approach to Structurally Complex Zintl Phases for Energy Applications
PMon006	**Pavlu**	Jana	Ab initio and CALPHAD modelling of Laves phases in Mn-based systems
PMon007	**Janka**	Oliver	$Ba_3Pt_4Al_4$ - A Complex Platinide with a Pt/Al Framework Featuring Heterocubane $[Pt_4Al_4]$ Units
PMon008	**Palcut**	Marian	Corrosion behavior of Al-Pd and Al-Co complex metallic alloys
PMon009	**Verchenko**	Valeriy	Evolution of the ground state in the system of binary intermetallics $CrGa_4$ and $MnGa_4$
PMon010	**Nash**	Philip	Experimental investigation of ternary Fe-Sn-Ti phase diagram at 873 K
PMon011	**Kainzbauer**	Peter	Experimental investigations in the binary Mn-Sb and ternary Mn-Sb-Bi System
PMon012	**Prokofiev**	Andrey	Intermetallic rare earth clathrates: synthesis, mechanism of rare earth incorporation and impact of electronic correlations on the thermoelectric properties
PMon013	**Wolf**	Silke	Karlsruhe Institut of Technologie
PMon014	**Jacob**	Aurélie	Liquidus projection of ternary Laves phase containing systems for the development of ferritic steel
PMon015	**Reichmann**	Thomas	Metallurgical preparation, thermodynamic characterisation and cycling measurements of new intermetallic anode materials for Li-ion batteries
PMon016	**Tence**	Sophie	New hydrides $RTXH_{1.5}$ (R = Rare-earth; T = Sc,Ti; X = Si,Ge)

PMon017	**Fürtauer**	Siegfried	New intermetallic anode materials: Experimental investigation of the Cu-Li-Sn system
PMon018	**Matselko**	Oksana	On the room and high temperature modifications of $Pd_3(Ga,Sb)$ ternary phase
PMon019	**Hillebrecht**	Harald	Ordered defect variants of a closest packing in $TaGa_{6-x}Zn_x$ - or packing of $Ta(Ga,Zn)_{12}$ polyhedra like in elemental metals
PMon020	**Hillebrecht**	Harald	Single crystal growth and crystal structures of binary intermetallics Ta_xGa_y
PMon021	**Kuznetsov**	Alexey	Ordering Patterns in Mixed Group 10 Metal Tellurides Based on B8-type Intermetallics
PMon022	**Tambornino**	Frank	Quantifying electron transfer in polar intermetallic phases: structural, NMR and theoretical studies on lithium amalgams
PMon023	**Mahon**	Tadhg	$R_2T_{3-x}Si_x$, a new pseudo-binary phase and prospective magnetocaloric material (R = Ce, Pr, Nd, Gd, Tb, Dy; T = Co, Ni).
PMon024	**Prots**	Yurii	Structural transformation of the $NaZn_{13}$-type derivatives in the La(Ce)-Ni-Ga systems
PMon025	**Wibner**	Patrick	Synthesis of supported intermetallic $Pd_{1-x}Zn_{1+x}$ nanoparticles for catalysis
PMon026	**Pathak**	Manisha	Synthesis, Structure and Properties of Novel Nitridogermanate $Ca_6[Ge_2N_6]$
PMon027	**Feng**	Xianjuan	Synthesis, crystal structure and properties of a new compound Ir_2Cd_{23}
PMon028	**Niehaus**	Oliver	Systematic investigations of Ce-Ru interactions by XPS
PMon029	**Gulo**	Fakhili	Ternary Intermetallic Compound in Ca-Cd-Pt System
PMon030	**Jandl**	Isabella	The NiAs Structure Family: Structure Composition Relations and Thermodynamic Modelling
PMon031	**Kroupa**	Ales	The assessment of the Al-V and Al-Si-V system
PMon032	**Beutl**	Alexander	The systems Li-Sb and Cu-Li-Sb, an experimental approach
PMon033	**Delsante**	Simona	Thermodynamic properties of Mg-Pd alloys
PMon034	**Boller**	Herbert	$V_{18}P_9C_2$ - a Complex Phosphide Carbide
PMon035	**Solokha**	Pavlo	Vacancy ordering phenomena in novel RZn_xGe_2 compounds (R=Tb-Er; 0.15<x<0.25)

Functional materials			
Poster No.	**PRESENTER**		**TITLE**
PMon036	**Vasylechko**	Leonid	Anomalous Thermal Expansion of Mixed Samarium Cobaltites-Ferrites
PMon037	**Jung-König**	Jan	Nanoscaled Gadolinium and Magnesium Carbonate Hollow Spheres
PMon038	**Harm**	Sascha	Phase Relations of Alkali Metal Zinc Phosphates for Application in Lithium-Ion Battery Cathodes
PMon039	**Volkova**	Nadezhda	Phase equilibria, crystal structure and properties of the complex oxides in the Sm-Sr-Fe-Co-O system
PMon040	**Grotz**	Carolin	The two new polyphosphides AgP_{15} and Ag_2GeP_{60} compared to LiP_{15}
PMon041	**Rabu**	Pierre	A versatile tool box for the functionalization of layered materials: ion-exchange, micro-wave assisted reactions and post-functionalization
PMon042	**Safarifard**	Vahid	Amine functionalized metal organic framework for highly efficient reversible adsorption of iodine
PMon043	**Belaroui**	Lala Setti	Adsorption of linuron by an Algerian palygorskite modified with magnetic iron oxides
PMon044	**Bennett**	Matthew	Anion-Deficient Perovskite-type Oxides as New Materials for CO_2 Capture
PMon045	**Piir**	Irena	Bismuth titanate pyrochlore doped with transition metals (Cr, Mn, Cu, Fe, Zn): The thermal stability, structure, properties
PMon046	**Marchuk**	Alexey	$Ba_3P_5N_{10}X:Eu^{2+}$ (X = Cl, Br, I) - Luminescent Nitridophosphates with Zeolite-like Framework Structure
PMon047	**Abdmeziem**	Kaïssa	Characterization and photocatalytic properties of hydrothermally synthesized hydroxyphosphate material
PMon048	**Traiphol**	Nisanart	Colorimetric sensing of various organic acids by using polydiacetylene/zinc oxide nanocomposites: The effects of acid structure
PMon049	**Amara**	Sif-Eddien	Correlation between electrochemical behavior and microstructures of FeNbC ternary alloys
PMon050	**Urusova**	Anastasia	Crystal structure and properties of Y-substituted strontium and barium ferrites
PMon051	**Ivanov**	Ivan	Crystal structure, oxygen nonstoichiometry and electric properties of $PrBaCo_{2-x}FexO_{6-\delta}$

PMon052	**Maier**	Maria	Cubic, ceramic-like solid solutions $Li_{7-x-y}La_3Zr_{2-x-y}NbxTayO_{12}$ with garnet-type structure for all-solid-state Li-ion batteries: synthesis of dense samples and characterisation focussing on Raman spectroscopy
PMon053	**Tsvetkov**	Dmitry	Defect structure and related properties of $YBaCo_2O_{6-\delta}$
PMon054	**Miller**	Stuart	Defect Flourite vs Pyrochlore : the M_2 M'_2 O_7 case
PMon055	**Sereda**	Vladimir	Defect structure and defect-induced properties of $SrTi_{0.5}Fe_{0.5}O_{3-\delta}$
PMon056	**Telegin**	Sergey	Effect of cobalt deficiency on physical properties of the polycrystalline samples $EuBaCo_xO_{6-\delta}$ and the single crystal $EuBaCo_{1.9}O_{6-\delta}$
PMon057	**Dergham**	D.	Elaboration and caractérisation of ZnO-Cu thin films By thermal evaporation
PMon058	**Prodan**	Alina Mihaela	Evaluation of dextran coated iron oxide magnetic nanoparticles toxicity after intratracheal instillation
PMon059	**Slabon**	Adam	Fabrication of Nanoporous Metallic Coatings
PMon060	**Shevelkov**	Andrei	Fe-based layered tellurides $Fe_{3-\delta}GeTe_2$ and $Fe_{3-\delta}As_{1-y}Te_2$: synthesis, neutron diffraction study, Mössbauer spectroscopy and band structure calculations
PMon061	**Cario**	Laurent	Giant Zn deficiency and p-typeness tuned by a nanosize effect in N-doped ZnO nanoparticles
PMon062	**Bos**	Jan-Willem	Glass-like Thermal Conductivity in $SrTiO_3$ Thermoelectrics Induced by A-site Vacancies
PMon063	**Bos**	Jan-Willem	Improved Thermoelectric Performance in Nanostructured half-Heuslers
PMon064	**Bang**	Seong-eun	Hydrothermal synthesis and characterization of novel quaternary yttrium selenites
PMon065	**Huang**	RUI	Improvement of near infrared Long-Persistent Luminescence in Si Substituted $Zn_3Ga_2Ge_2O_{10}$
PMon066	**Lainé**	Fabien	Influence of the cationic substitution on crystal structure and physical properties in the $Fe_{3-x}Mn_xO_2BO_3$ ($0 \leq x \leq 3$) system
PMon067	**Gilyov**	Artyom	$La_{2-x}Sr_xNi_{1-y}FeyO_{4+\delta}$ as cathode materials for SOFC application
PMon068	**Rueff**	Jean-Michel	Low dimensional hybrids with magnetic and luminescence properties
PMon069	**Rueff**	Jean-Michel	Silver based hybrids with potential bactericidal properties
PMon070	**Müller-Buschbaum**	Klaus	Luminescence of Ln-N-MOFs for Sensing and Chromaticity Tuning

PMon071	**Verma**	Naveen	Luminescent characteristics of $CaAl_2O_4:Eu^{3+}$phosphors co-doped with Er^{3+} and Gd^{3+}
PMon072	**Verma**	Naveen	Optical properties of Yb^{3+} doped ZnO/MgO nanocomposites prepared by combustion method
PMon073	**Zagaynov**	Igor	Mesoporous ceria-based catalysts for oxidation reactions
PMon074	**de Laune**	Benjamin	Mixed Transition Metal Phases Relating to Schafarzikite: A Properties Investigation
PMon075	**Sardar**	Kripasindhu	Mixed metal nitride $Ni_{2-x}Co_xMo_3N$ as a heterogeneous catalyst and electro catalyst
PMon076	**Salek**	Guillaume	Mn^{2+} doped $Zn_3(PO_4)_2$ phosphors as thermal sensors
PMon077	**Kolchina**	Liudmila	Modified Ln_2CuO_4 (Ln=La, Pr) as cathode materials for solid oxide fuel cells
PMon078	**Asabina**	Elena	NZP-phosphates, containing metals in oxidation state +2, as new materials with regulated thermal expansion
PMon079	**Alfaifi**	Bandar	Nanostructured Fabrication of $MFeO_3$ (M= La, Y) for Efficient Solar to Chemical Energy Conversion by Photosynthetic Cell
PMon080	**Cherepanov**	Vladimir	New Family of Nanoscale Ordered Quintuple Perovskites $Ln_{2-\varepsilon}Ba_{3+\varepsilon}Fe_5O_{15-\delta}$ (Ln = Sm, Nd)
PMon081	**Isaeva**	Anna	New candidates for topological insulators in the bismuth-halogen systems
PMon082	**Förg**	Andrea	Novel coatings for corrosion and wear protection by thermal spraying
PMon083	**Patureau**	Pascaline	On the incorporation of Jahn-Teller Cu^{2+} ions into multiferroic $MnWO_4$
PMon084	**Matos**	Manuel	Organic light emitting diodes based on conjugated polymers functionalized with calix[4]arenes
PMon085	**Rabia**	Cherifa	Oxidation of cyclohexanone to adipic acid with aqueous hydrogen peroxide on $(NH_4)_xX_yPMo_{12}O_{40}$ with X= Sb, Sn
PMon086	**Tsvetkova**	Nadezhda	Oxygen non-stoichiometry and phase stability of Zn-doped $YBaCo_4O_{7\pm\delta}$ oxide with swedenborgite-type structure
PMon087	**Ciobanu**	Carmen Steluta	Photoluminescence and antimicrobial activity of Ag or Eu doped hydroxyapatite powders
PMon088	**Popa**	Cristina-Liana	Physico-chemical characterizations and cytotoxicity evaluation of novel zinc doped hydroxyapatite embedded in a collagen matrix
PMon089	**Yu**	Jae Su	Preparation and luminescence properties of $SrMoO_4$ optical materials doped with rare-earth ions

PMon090	**Boutamine**	Sultana	Revisite of reactivity of thiosemicarbazide on some divalent ions synthesis of complexes, characterization, DFT calculations, catalase like and biological activities
PMon091	**Uskokovic-Markovic**	Snezana	Raman spectroscopy on the impregnation of tungstophosphoric acid onto mesoporous and microporous supports
PMon092	**Mozharivskyj**	Yurij	Rare-Earth Antimonide and Bismuthide Suboxides: Interplay between the Structure and Transport Properties
PMon093	**Black**	Ashley P.	Red luminescence and ferromagnetism in europium oxynitridosilicates with a β-K_2SO_4 structure
PMon094	**Penkala**	Bartosz	Role of Lattice Oxygen on CO Oxidation Over $Ce_{18}O_2$-Based Catalyst Revealed Under Operando Conditions
PMon095	**Prutsch**	Denise	Self-Organized Amorphous TiO_2 Nanotubes as Na-Ion Battery Anodes
PMon096	**Pralong**	Valerie	Sodium Intercalation into the Iron Hydroxysulfate $NaFe_3(SO_4)_2(OH)_6$: a Topotactic Reversible Reaction from a Crystalline Phase to an Inorganic Polymer-like structure
PMon097	**Hank**	Zakia	Soil Remediation by Using Some Transition Metal Coordination Compounds
PMon098	**Halake**	Shobha	Solvothermal Synthesis and Characterization of Two New Barium-Organic Coordination Compounds
PMon099	**Nazarchuk**	Evgeny	Structural diversity of organically templated uranyl chromates
PMon100	**Zevalkink**	Alexandra	Structurally complex Zintl compounds for high temperature thermoelectric power generation
PMon101	**Nentwig**	Markus	Structure and thermoelectric properties of germanium antimony telluride heterostructures
PMon102	**Bizo**	Liliana	Substitution of couple Sn(IV)/Zn(II) for In(III) in the fluorite-like transparent conductors: $In_{5-2x}Sn_{1+x}SbZn_xO_{12}$
PMon103	**Bae**	Su-whan	Syntheses and Characterization of Two Series of Quaternary Mixed Metal Tellurites with Various Cation Sizes and Te^{4+} Polyhedra
PMon104	**Kim**	Saet Byeol	Synthesis and characterization of a new layered Pb^{2+}-Kemp’s triacid coordination polymer
PMon105	**Farger**	Pierre	Synthesis and characterization of new hybrid coordination compounds based on imidazolium and 3d transition metal salts.
PMon106	**Lee**	Soohyun	Synthesis and detection properties of hydrothermally grown vertically aligned zinc oxide-based nano structures for ultraviolet photodetector applications
PMon107	**Torralvo**	María José	Synthesis and magnetic properties of ferrite nanoparticles
PMon108	**Korolev**	Dmitrii	Synthesis, structure and valence states of 3d-atoms in the matrix of yttrium-gallium garnet

PMon109	**Uitz**	Marlena	The Electrochemical Performance of Rutile Nanorods for Lithium-Ion Batteries
PMon110	**Perz**	Martin	The Influence of Silicon on the Long-term stability of LSCF SOFC-Cathodes
PMon111	**Serras**	Paula	The use of waste biomass as carbon source in the synthesis of sodium vanadium fluorophosphates cathodes for Na-ion batteries
PMon112	**Gaudon**	Manuel	Thermochromic and piezochromic properties of $AMoO_4$ oxides
PMon113	**Amano-Patino**	Midori	Topochemical Reduction of Some Complex Ruthenium Oxides
PMon114	**Cascales**	Concepción	Tunable upconverted visible light and high sensitivity optical thermal sensing of Ln, Yb:$Y_6O_5F_8$ nanotubes
PMon115	**Traiphol**	Rakchart	Versatile route to prepare reversible thermochromic polydiacetylene/ poly(vinylpyrrolidone) nanocomposites: Effects of molecular weight and fabrication process
PMon116	**Röhr**	Martin	$[ZrO]^{2+}[G6P]^{2-}$ Biocompatible Inorganic-Organic Hybrid Nanoparticles for Supported Drug Delivery

Modern developments in chalcogenide research

Poster No.	PRESENTER		TITLE
PMon117	**Lai**	Kwing To	Synthesis and characterization of strong antiferromagnet CaFeSeO
PMon118	**Driss**	Dalel	A new chalcogenide compound $Ba_2F_2Fe_{1.5}Se_3$ with iron selenide layers
PMon119	**Woodruff**	Daniel	Chemical control of superconductivity in layered lithium iron selenide hydroxides
PMon120	**Peschke**	Simon	Flux Synthesis, Modulated Crystal Structures, and Physical Properties of $RE_2O_2MnSe_2$ (RE = La, Ce)
PMon121	**Popcevic**	Petar	High pressure study of intercalated transition metal dichalcogenides $Co_{0.33}NbS_2$ and $Fe_{0.33}TaSe_2$
PMon122	**Ritscher**	Anna	Mechanochemical Synthesis and Neutron Scattering Measurements on Kesterite (Cu_2ZnSnS_4)
PMon123	**Stolze**	Karoline	Mixed-Valent Selenium in the Uncharged Iridium Cluster $[Ir_4Se_{10}Br_{16}]$
PMon124	**Karabyn**	Vasyl	Phase change materials for the $Ge_8Bi_2Te_{11}$ - $Ge_8Sb_2Te_{11}$ system
PMon125	**Yusenko**	Kirill	Polymorphism in Intercalated Iron Selenide Superconductors: Influence of Interlayer Distance and Electron Transfer on the Critical Temperature

PMon126	**Kleeberg**	Fabian	Rare-Earth Metal Cations in a Polar Framework Erected by Thiogallato-closo-Dodecaborate Anions
PMon127	**Blandy**	Jack	Soft chemical control of the crystal structure and properties of $Sr_2MnO_2Cu_{1.5-x}S_2$
PMon128	**Nasonava**	Darya	Structural and properties features of Fe-substituted tetrahedrites
PMon129	**Delacotte**	Charlène	Structures and magneto-electric behaviors of calcium and iron based oxysulfides
PMon130	**Pompe**	Constantin	The crystal structures and polymorphism of Na_2TeQ_3 (Q=S, Se)
New methods of characterization			
Poster No.	**PRESENTER**		**TITLE**
PMon131	**Regoutz**	Anna	Polarisation dependence in hard X-ray photoemission of Sn-doped TiO_2
PMon132	**Regoutz**	Anna	High-pressure photoelectron spectroscopy investigation of the interaction between CO_2 and Cu-based reduction catalysts
PMon133	**Wittich**	Knut	Angular overlap modelling of the vanadyl(IV) chromophore in silver vanadyl(IV) bis(orthophosphate) pyrophosphate in comparison to single crystal EPR measurements
PMon134	**Andre**	Rémi	Assessment of the thermodynamic properties of solids at high temperature with the drop calorimetry technique
PMon135	**Iranmanesh**	Mitra	Combinatorial ceramic synthesis and scanning SQUID microscopy for searching new cuprate superconductors
PMon136	**Slawinski**	Wojciech	Novel crystal structure of MoO_3 nanobelts
PMon137	**Hartmann**	Thomas	Optimising PDF data quality using a laboratory powder diffractometer
PMon138	**Payne**	David	Recent Developments in Laboratory-based High Pressure Photoelectron Spectroscopy
PMon139	**Durach**	Dajana	Unusual Tetrahedra Network Structures of Lanthanum Barium Oxonitridosilicates
PMon140	**Coomer**	Fiona	Using muSR to investigate solid state materials: frustration in double perovskites

Tuesday 25.08.2015

Poster Session 2 16.00 – 18.00

New methods of synthesis

Poster No.	PRESENTER		TITLE
PTue001	**Bouyon**	Tracy	Hybrid Gold/Thiolates Nanoparticles: Control of Surface Properties and Characterizations, Insertion in Porous Materials
PTue002	**Daviero**	Sylvie	New positive nanosheets from the exfoliation of dimensional oxybromide for oriented thin films deposit
PTue003	**de Sousa Filho**	Paulo Cesar	Synthesis and luminescent properties of mixed rare earth phosphate/vanadate hollow particles
PTue004	**Wörsching**	Matthias	Towards new subvalent compounds - the new nitridoborate $Ba_{23}(BN_2)_{11}(B(N/O)_3)_3N_{3-x}$
PTue005	**Renman**	Viktor	Collapsing transition metal oxohalides as negative electrode materials for lithium ion batteries
PTue006	**Rein**	Viktor	Encapsulation of Lipophilic Dyes and Drugs in Hydrophilic $ZrO(HPO_4)$ shells
PTue007	**Penner**	Simon	Enhanced kinetic stability of pure and Y-doped tetragonal ZrO_2
PTue008	**Lee**	Bum Jae	Fracture Toughness of Epoxy Semi-IPN Toughened with In-situ Polymerized Novel Polysulfone via Azide-alkyne Click Reaction
PTue009	**Müller**	Ulrike	Halogenidoaluminate Salts of the Intermetalloid Cluster Cation $[Bi_{12}Ni_2]^{4+}$ - Synthesis in Ionic Liquids, Crystal Structure and Chemical Bonding
PTue010	**Konar**	Sumit	Intercalation Compounds from LiH and Graphite: Relative Stability of Metastable Stages and Thermodynamic Stability of Dilute Stage Id
PTue011	**Schöttle**	Christian	Less-Noble Metal Nanoparticles
PTue012	**Hoehn**	Peter	Lithium and alkaline-earth nitrides of group 13 and 14 metals: millimeter-sized single crystals from lithium melts
PTue013	**Oana**	Carp	Materials synthesis via polysaccharides assisted procedures
PTue014	**Roslova**	Maria	Microwave-assisted Polyol Synthesis of $M_3Bi_2X_2$ (M = Ni, Pd; X =S, Se): Using Solution Chemistry to Access Ternary Metal-Rich Chalcogenides

PTue015	**Raguz**	Branimir	New polymorphs of lithium pyrophosphate
PTue016	**Pet'kov**	Vladimir	Phosphates of rare-earth elements and titanium: synthesis optimization and crystal structure study
PTue017	**Kosaka**	Tomomi	Preparation Pr doped perovskite red phosphors by hydrothermal reaction
PTue018	**Schnabel**	Anke	Silver Chromium(III) Phosphates: Syntheses, Equilibrium Relations, New Crystal Structures and De-intercalation Experiments
PTue019	**Peña**	Alazne	Sodium vanadium fluorophosphates prepared by a new microwave assisted synthesis: electrochemical study of raw and C-coated materials
PTue020	**Roy**	Subrata Chandra	Solid solutions in the quasi-binary system vanadyl(V) phosphate - molybdenyl(V) phosphate
PTue021	**Morsali**	Ali	Sonochemical syntheses of nano lead(II) coordination polymer; precursor for preparation of lead(II) oxide/iodide nano-structures
PTue022	**Schmitz**	Andreas	Synthesis and Crystal Structure of Thallium(I, III) Pyrophosphate
PTue023	**Haumann**	Sebastian	Synthesis and self-assembly of Cobalt and Nickel Nanoparticles
PTue024	**Nedumkandathil**	Reji	Synthesis and structural characterization of $BaTiO_{3-x}H_x$ oxyhydrides
PTue025	**Häbel**	Jan-Peter	Synthesis, Crystal Structures and Topotactic Oxidation of Polynary Silver Transition Metal Phosphates
PTue026	**Nash**	Philip	The Large Scale Synthesis of Aligned Plate Nanostructures
PTue027	**Hertrampf**	Jan	Three Modifications of Barium Tetramidogallate: An Intermediate in Ammonothermal GaN Crystal Growth
PTue028	**Konovalov**	Igor	The synthesis of nanoparticles of metal oxides by supercritical CO_2 anti-solvent precipitation
Solid state theory			
Poster No.	**PRESENTER**		**TITLE**
PTue029	**Kurkcu**	Cihan	An ab initio molecular dynamics study of structural properties of FeF_2 as a function of pressure
PTue030	**Masys**	Sarunas	Elastic Properties of $LaNiO_3$: An Employment of PBE-based Functionals

PTue031	**Kremenetskaya**	Olga	Electron density and ELI-D analysis of the cd → β-Sn phase transition of group IV elements
PTue032	**Deringer**	Volker	Exploring Bonding in Complex Solids with New Theoretical Tools
PTue033	**Azibi**	Mourad	First-principles calculations of the phase stability and surface energy of TiO_2 (100) and (110)
PTue034	**Herzig**	Peter	First-principles study of phase stability, hydrogen ordering, and the metal-insulator transition in hydrogen-rich lutetium hydrides
PTue035	**Touzani**	Rachid	Long looked-for and finally found: Nb_2RuB_2 - theoretical and experimental studies
PTue036	**Kang**	Hong Seok	Mechanical and Electronic Properties of π -Conjugated Organometallic Nanomaterials
PTue037	**Boviatsis**	John	On the correct form of the nonlinear optical susceptibility in strongly-driven semiconductor quantum dots
PTue038	**Tomerini**	Daniele	On the role of computational modelling in the understanding of novel organic electroactive materials for Li-ion batteries
PTue039	**Shipilov**	Alexander	Synthesis, phase formation, structure and thermal expansion behavior of double arsenates of zirconium and alkali earth metals
PTue040	**Azibi**	Mourad	The Vickers microhardness prediction of TiC and TiN: A DFT study
Collective magnetic phenomena			
Poster No.	**PRESENTER**		**TITLE**
PTue041	**Frei**	Maren	Charge and Spin Ordering in Intrinsically Doped Sodium Oxocuprates
PTue042	**Pachmayr**	Ursula	Coexistence of Ferromagnetism and Superconductivity in the iron chalcogenide $[(Li_{0.8}Fe_{0.2})OH]FeSe$
PTue043	**Batuk**	Dmitry	Crystal structure and magnetic phase transitions of $Bi_4Fe_5O_{13}F$, a material with the frustrated magnetic pentagonal Cairo lattice.
PTue044	**Solana-Madruga**	Elena	High pressure synthesis, structures and magnetic properties of Mn_2MSbO_6 oxides
PTue045	**Cussen**	Eddie	Valence Bond Glass Formation and Dynamic Magnetic Ordering in Frustrated Perovskites
PTue046	**Clemens**	Oliver	Ways Out of Frustration?! The Magnetic Structures of the low and high temperature phases of $Mn_3(VO_4)_2$

Ionic and electronic transport in solids

Poster No.	PRESENTER		TITLE
PTue047	**Stanje**	Bernhard	Li-Ion Dynamics of Layer-Structured 2H-Li_xNbS_2 studied by ^{7}Li NMR
PTue048	**Taibl**	Stefanie	Visualization of ion motion in Fe-$SrTiO_3$ thin films by means of impedance spectroscopy under bias
PTue049	**Rettenwander**	Daniel	A Micro-contact Electrochemical Impedance Spectroscopy Study of NASICON Type $Li_{1.5}$ $Al_{0.5}$ $Ti_{1.5}$ $(PO_4)_3$ and $LiTi_2$ $(PO_4)_3$ Single Crystals
PTue050	**Langer**	Julia	Combined ^{6,7}Li NMR study of slow Li diffusion in monoclinic Li_2SnO_3
PTue051	**Fraenkl**	Max	Direct approach for impedance analysis of ion conducting glasses
PTue052	**Kochetova**	Nadezda	Electrical properties of perovskite-type complex oxides $Ba_2Sc_2MO_8$ (M=Ti, Zr)
PTue053	**Chezhina**	Natalia	Electron structure as a foundation for selecting the compositions of doped lanthanum gallate as electron ionic conductors for SOFC
PTue054	**Epp**	Viktor	Extremely High Li^+ Diffusivity in NASICON-type $Li_{1.5}Al_{0.5}Ti_{1.5}(PO_4)_3$
PTue055	**Wohlmuth**	Dominik	Fast Li Ion Transport in the $Li_7P_3S_{11}$ Glass Ceramic as Seen by ^{6,7}Li NMR Relaxometry
PTue056	**Wiedemann**	Dennis	High-Temperature Transformation from 1T- to 3R-Li_xTiS_2 Observed in situ with Neutron Diffraction
PTue057	**Ryabkov**	Y.I.	Ilmenite ceramics for advanced electrical and magnetic materials
PTue058	**Øygarden**	Vegar	Intercalation of water in the $LaSr_3Fe_3O_{10-\delta}$ Ruddlesden-Popper type material
PTue059	**Polt**	Julia	Investigation of the solid-solution Sr_2YNbO_6 - $Sr_3NbO_{5.5}$
PTue060	**Kharitonova**	Elena	$La_2Mo_2O_9$-based compounds with high oxygen conductivity in $La_2Mo_2O_9$ - $Ln_2W_2O_9$ - $Ln_2Mo_2O_9$ (Ln = Pr, Nd, Sm, Gd) ternary systems
PTue061	**Kharitonova**	Elena	Phase formation and conductivity of compounds in Ln_2MoO_6 - Bi_2O_3 (Ln = Pr, Nd) systems
PTue062	**Schrödl**	Nina	$La_2NiO_{4+\delta}$ as anode material for solid oxide electrolyser cells under chromium poisoning conditions

PTue063	**Monchak**	Mykhailo	Li diffusion pathways in LATP-based materials
PTue064	**Brandstätter**	Harald	Li ion dynamics in nanocrystalline and structurally disordered Li_2TiO_3
PTue065	**Walch**	Gregor	Light-induced stoichiometry changes in oxides at high temperatures
PTue066	**Woods**	Michael	Lithium diffusion in mixed conducting polymers
PTue067	**Cussen**	Eddie	Lithium ion Conduction in Disordered Non-Framework Crystalline Borohydrides
PTue068	**Welzl**	Andreas	Local conductivities in Li ion conducting garnet-based ceramics measured by microelectrodes.
PTue069	**Breuer**	Stefan	Mechanochemical synthesis and characterization of the metastable, nanocrystalline F ion conductor $(Ba_xCa_y)La_{(1-x-y)}F_{(3-x-y)}$
PTue070	**Preishuber-Pflügl**	Florian	Mechanochemistry of Fluorine Ion Conductors: Insights into Synthesis and Ion Transport via Impedance Spectroscopy and Solid-State NMR
PTue071	**Blazquez Alcover**	Ignacio	Metal exsolution in $Ba(Fe,M)_2(PO_4)_2$ (M=Li, Co, Ni) : Metal versus alkali cationic mobility
PTue072	**Animitsa**	Irina	NMR study of proton motion in fluorine-doped complex oxides with perovskite and brownmillerite structures
PTue073	**Animitsa**	Irina	The effect of phosphate doping on local structure and ion transport of $Ba_4Ca_2Nb_{2-x}P_xO_{11}$
PTue074	**Pralong**	Valerie	New Rock Salt type Structure from Chemical or Electrochemical insertion Reaction
PTue075	**Greaves**	Colin	New oxygen insertion reactions involving 1-D channels
PTue076	**Evans**	Ivana	Oxide Ion Conductors for Energy Applications: Hops and Twists in the Solid State
PTue077	**Maity**	Avishek	$Pr_2NiO_{4+\delta}$: InSitu electrochemical oxygen intercalation studied by synchrotron diffraction on single crystal
PTue078	**Koroleva**	Mariya	Synthesis, thermal stability and electrical properties of copper- or cobalt-containing bismuth titanates with the pyrochlore type structure
PTue079	**Schmidt**	Walter	Small change-great effect: Steep increase of Li ion dynamics in $Li_4Ti_5O_{12}$ at the early stages of chemical Li insertion (x = 0.1, x = 0.3)
PTue080	**Grebenev**	Vadim	Solid acid proton conductors of CsH_2PO_4 - $CsHSO_4$ - H_2O salt system

PTue081	**Chen**	Min	Space Charge Layer Effect at Nickel/$BaZr_{0.9}Y_{0.1}O_{3-\delta}$ interfaces in Protonic Ceramic Fuel Cells
PTue082	**Hofer**	Johannes	Synthesis and characterization of donor doped barium titanate
PTue083	**Driscoll**	Laura	Synthesis and doping studies of $Na_2M(SO_4)_2.2H_2O$ (where M = Fe, Co and Ni) for potential applications as a cathode material for Na-ion batteries
PTue084	**Krasnov**	Aleksey	Synthesis and properties of $Bi_{2-y}M_xTi_2O_7$-DELTA (M - Sc, In) pyrochlores
PTue085	**Wagner**	Reinhard	Synthesis of garnet-type Li-ion conductor $Li_{7-x}La_3Zr_{2-x}Bi_xO_{12}$
PTue086	**Zhang**	Bo	The mechanism of Ag filament formation in Ag doped AsS_2 thin layer
PTue087	**Kastlunger**	Georg	Theory of charge transport through single redox-active transition metal complexes
			High pressure synthesis and in situ investigations
Poster No.	**PRESENTER**		**TITLE**
PTue088	**Belik**	Alexei	Crystal Chemistry and Physics of Perovskites with Small Cations at the A Site
PTue089	**Pobel**	Roman	Absence of superconductivity in metastable $Ca_{1-x}Pr_xFe_2As_2$ (x = 0-1) synthesized under high pressure conditions
PTue090	**Konatham**	Satish	Hydrothermal syntheses and single crystal X-ray structures of three new vanadium (V) tellurites CaV_2TeO_8, $Sr_4V_4Te_4O_{20}(OH)_4$ and $Cd_2V_2Te_2O_{11}$
PTue091	**Glätzle**	Matthias	High-pressure Synthesis and Single-Crystal Structure of HP-LaOF
PTue092	**Ovsyannikov**	Sergey	High-pressure high-temperature synthesis of bulk $Si_{1-x}B_x$ alloys: two semiconductors form an unusual metal
PTue093	**Castillo**	Rodrigo	High-pressure synthesis of three new Ge-rich compounds in the Ba - Ge system
PTue094	**Yamamoto**	Ayako	High-pressure synthesis, crystal structure and properties of bismuth dicalcogenides, $Bi(Se_{1-x}S_x)_2$ (x = 0, 0.5, 1.0) and its substitutions
PTue095	**Heymann**	Gunter	High-pressure/High-temperature Synthesis and Characterization of the first Palladium and Platinum containing Lithium Transition-Metal Sulfides $Li_2M_3S_4$ (M = Pd, Pt)
PTue096	**Köpf**	Marianne	Investigation on the mineraliser assisted synthesis of black phosphorus via in-situ neutron powder diffraction

PTue097	**Friedrich**	Daniel	Kinetics of the phase transition of $CsGaSe_2$
PTue098	**Kloß**	Simon David	$NdLiP_4N_8$ - The First Rare Earth Nitridophosphate by Metathesis
PTue099	**Bertschler**	Eva-Maria	Surprising Anion Topologies in Lithium Nitridophosphates
PTue100	**Vitzthum**	Daniela	Synthesis and Characterization of the New High-Pressure Gallium Borate $Ga_2B_3O_7(OH)$
PTue101	**Krumeich**	Frank	Thermal behavior of carbon-coated lithium iron phosphate
Others			
Poster No.	**PRESENTER**		**TITLE**
PTue102	**Schildhammer**	Daniel	High-Temperature Synthesis and Characterization of Rare-Earth Molybdenum-Oxynitrides
PTue103	**Schmetterer**	Clemens	Slag to Materials - Possible Applications for Red Mud
PTue104	**Stoiber**	Dominik	Alkaline-earth Metal Dependent Structural Distortion in Inverse Perovskite Nitride Arsenides
PTue105	**Jung**	Joo-hei	Characterization of alumina-graphene composites (AGC) formed by the reaction of carbon monoxide with partially nitrided alumina powder
PTue106	**Sree Rama Murthy**	A	Development of yttria doped thoria solid electrolyte and its performance in liquid sodium systems as oxygen sensors
PTue107	**Sree Rama Murthy**	A	Synthesis, characterization and hydrogen sensing properties of $Cr_{1-x}Fe_xNbO_4$ (x = 0-1)
PTue108	**Mahmoud**	Ahmed	Electrical Conductivity, Gap Width and Sensitivity to CO_2 gas for ITO Powder and Nanoparticle
PTue109	**Weiz**	Alexander	Electrical properties of the bismuth-rich subiodides $Bi_{14}I_4$ and $Bi_{18}I_4$
PTue110	**Scott-Fordsmand**	Janeck James	Environmental Risk Assessment of Nanomaterials
PTue111	**Ovchinnikov**	Alexander	Extended anionic frameworks in the AE-Mn-N systems. Synthesis, structure and physical properties of new nitridomanganates
PTue112	**Lee**	Soo Hyun	Fabrication and properties of polydimethysiloxane films for optical and triboelectric applications

PTue113	**Petschnig**	Lucas	Solution Combustion Synthesis of $CeFeO_3$ under Ambient Atmosphere
PTue114	**Marshall**	Kayleigh	Hydrofluorothermal Synthesis of Novel Transition Metal Fluorophosphate and Fluorosulfate Frameworks
PTue115	**Faria**	Rodolfo	Hydrogenation of ternary intermetallic compounds MTrTt (M = Ca, Sr, Ba; Tt = Al, Ga; Tt = Si, Ge) - A chemical bonding view in position space
PTue116	**Ortner**	Teresa	Hydrothermal Synthesis and Characterization of the Lutetium borate-nitrate $Lu_2B_2O_5(NO_3)_2 \cdot 2\ H_2O$
PTue117	**Malek**	Marcin	Influence of binder type on the SiC-based ceramic slurries properties for casting shell moulds fabrication
PTue118	**Lee**	Kuan-Wei	InAlAs/InGaAs Metamorphic High-Electron-Mobility Transistor With a Sol-Gel Processed TiO_2 as Gate Dielectric
PTue119	**Amara**	Leïla	Interaction between carbides formed in FeTiNbC alloys. Corrosion resistance.
PTue120	**Reisinger**	Gabriel	Isothermal section and new compounds in the system Al-Fe-Ge
PTue121	**Choi**	Yeon-Hee	Luminescence spectra of Ce^{3+}-doped $LaAlO_3$ powders prepared from the La_2O_3-CeF_3-Al_2O_3 reaction system
PTue122	**Cassidy**	Simon	Metal-Ammonia Intercalated Iron Selenide Superconductors Studied In-Situ by Powder X-Ray Diffraction
PTue123	**Rasche**	Bertold	New environment for a two-dimensional topological insulator with hexagonal channels hosting $[BiI_2]$- ions
PTue124	**Mechtaeva**	Elizaveta	Protonation of $A_2Ln_2Ti_3O_{10}$ (A = K, Na, Li; Ln = La, Nd) in aqueous medium
PTue125	**Paidi**	Anil Kumar	Syntheses and structural characterization of new quaternary vanadates of niobium and tantalum AMV_2O_8 (A = K, Rb, Tl, Cs; M = Nb, Ta)
PTue126	**Heppke**	Eva	Sodium Ion Substitution in Barium Zirconate
PTue127	**Taibi**	Kamel	Some compositions $Pb_{1-x}Ba_x(Zr_yTi_{1-y})O_3$ with very small lead content
PTue128	**Jindal**	Jitender	Structural and electrochemical impedance spectroscopic studies of anodic oxide film on zirconium fabricated in different aqueous electrolytes
PTue129	**Benhebal**	Hadj	Synthesis and Characterization of Alkali Metals-doped Tin Oxide Thin Films by Sol-Gel Process
PTue130	**Regus**	Matthias	Synthesis and In-situ X-ray Characterization of New, Metastable Cr-Sb Compounds Using Multilayered Thin Films

PTue131	**Shaqiri**	Halil	Synthesis and characterization of mixed-metal silicophosphates
PTue132	**Najjar**	wahiba	Synthesis, characterization of ZnO and Ag-doped ZnO : Application in photocatalytic degradation of endocrine disrupting under UV irradiation
PTue133	**Rudolph**	Daniel	The First Europium(II) Oxide Hydride Iodide
PTue134	**Hartenbach**	Ingo	The Incorporation of Lithium and Silicon Cations in Yttrium Tungstate
PTue135	**Hillebrecht**	Harald	The new borosulfates $Cs_2B_2S_3O_{13}$ and $Cs_3HB_4S_2O_{14}$ - on the way to the structure of vitreous B_2O_3?
PTue136	**Cupid**	Damian	Thermochemistry of New Anode Materials based on the Li-Si-O System for Li-Ion Batteries
PTue137	**García García**	F. Javier	Oxygen dynamics in $BaFeCl_{0.130(2)}O_{2.50(2)}$
PTue138	**Villesuzanne**	Antoine	Identification of n-type and p-type transparent conducting materials from first-principles

ABSTRACTS

15th ECSSC – Vienna, Austria
August 23 to 26, 2015 at the Campus of the University of Vienna

Oral Presentations

PL1

Statistics of intermetallics - some remarkable findings

Steurer, Walter (Laboratory of Crystallography, Zurich, CHE); Dshemuchadse, Julia (University of Michigan, Ann Arbor, USA)

The talk will focus on the questions why intermetallic compounds are adopting so many different struture types, and what their geometrical ordering principles are. Our statistical analysis is based on the database Pearson's Crystal Data (PCD) [1], and the Mendeleev numbers [2] as parameters, which take some crystal chemistry into account.

In the PCD are listed 20 829 full structures of intermetallic phases, which crystallize in 2166 structure types. 1087 of them are unique, i.e., featuring just one representative compound each. The distribution of unique structure types as a function of symmetry and unit cell size, respectively, is similar to that of the non-unique ones. The top 20 structure types, i.e., 0.9% of all structure types, represent 35.6% of the structures of all intermetallics. Their complexity is low to moderate, ranging between $cI2$-W and $hR57$-$Zn_{17}Th_{12}$. The three most frequent structure types are $cF24$-$MgCu_2$ (3.9%), followed by cF4-Cu (2.8) and cP4-Cu_3Au (2.6%).

The distribution of the stoichiometries of ternary structure types shows interesting features. In the concentration diagram most structure types are rather densely arranged along tie lines such as AB-AC, AC-BC or AB-C ($M(A)<M(B)<M(C)$, with M the Mendeleev number [2]). This is remarkable, since we do not have a substitution of A by B or C in a common structure, but completly different structures along a tie line. This can only be explained by topological considerations.

In contrast to what one may expect from the naive point of view on the chemical bonding present in the metallic elements and the intermetallics, the majority of structure types has a rather low symmetry. What is also amazing is the spread in the number of atoms per unit cell, which ranges from 1 to 23 256. What is still mysterious is that the number of structure types with an even number of atoms per primitive unit cell is much larger than that where this number is odd.

The intermetallic phases we know so far represent just the tip of the iceberg. In case of the 81 elements that we define as metallic, 277 structures (allotropes) and 86 structure types are known. For the 3240 (85 320) possible binary (ternary) intermetallic systems, the numbers are 6441 compounds out of 1401 systems (13 026 out of 5109 systems) and 943 structure types (1391), respectively. This large difference between studied and non-studied systems can be accounted only to a minor amount to toxicity, radioactivity or scarcity of a significant number of elements. Consequently, there is much more left to be explored. Who would have anticipated the existence of quasicrystals before their discovery, for instance?

We hope that our statistical analysis will make a small, but not negligible, contribution to the big picture of intermetallics by structuring the vast amount of intermetallic phases in a proper way.

---

[1] Villars, P. and Cenzual, K., Pearson's Crystal Data: Crystal Structure Database for Inorganic Compounds 2012/13.
[2] Pettifor, D.G., Solid State Commun. 51 (1984) 31.

IL1

Icosahedral Quasicrystals and Approximants

Pay Gomez, Cesar (Uppsala University, Department of Chemistry - Ångström Laboratory, Uppsala, SWE)

Quasicrystals have altered our view on solid matter. In spite of fierce resistance from the scientific community, Dan Shechtman's discovery finally gained recognition resulting in the redefinition of the term "crystal" and a Nobel Prize.[1] Structure determination of quasicrystals still remains one of the most challenging tasks in this field of research. In this talk we will review how the process is carried out to answer the question "where are the atoms?",[2] illustrated by the example of the icosahedral $YbCd_{5.7}$ phase,[3] which today still remains the most complete structure determination of an icosahedral quasicrystal.

---

[1] D. Shechtman, I. Blech, D. Gratias, J. W. Cahn, Phys. Rev. Lett. 1984, 53, 1951-1953.

[2] P. Bak, Phys. Rev. Lett. 1986, 56, 861-864.

[3] H. Takakura, C. Pay Gómez, A. Yamamoto, M. De Boissieu, A. P. Tsai, Nature Materials 2007, 6, 58-63.

O1

Polar metal-metal bonding in intermetallic phases from electrocrystallisation near room temperature

Hoch, Constantin (Ludwig-Maximilians-Universität München, München, GER)

The transition from ionic to metallic bonding is poorly understood, mostly due to a small number of compounds which actually show polarised metal-metal bonding. There are two principal synthetic pathways towards intermetallic phases with considerable but incomplete electron transfer from one constituting element to the other: (1) a metallic and an ionic educt can be reacted in a way suitable to combine both in a „chemical twin“, *e. g.* in alkali metal suboxometallates [1], or (2) reaction of two metallic educts *A* and *B* with an electronegativity difference high enough to result in partial electron transfer from *A* to *B* but not high enough for the formation of Zintl phases. The first pathway leads to phases with metallic and ionic bonding in separated and alternating structural compartments, whereas the second pathway leads to complex structures with pronounced yet incomplete electron transfer and a combination of ionic, metallic and covalent bonding contributions.

In recent years, we have established the synthetic method of isothermal electrolysis to obtain mercury-rich amalgams of the less noble alkali, alkaline earth and rare earth metals [2]. This method consists of an electrolysis process at constant temperature. A drop of liquid mercury serves as reactive cathode. The second component, the less noble metal, is added from solution of a metal salt in an aprotic polar organic solvent by electrolytic deposition. Exploring phase diagrams horizontally by gradually and isothermally changing the composition of the cathode yields many new phases as phase-pure and gram-scale samples. Especially compounds not available from standard inorganic synthesis routes due to high reaction enthalpies combined with low peritectic decomposition temperatures can easily be obtained.

Electrocrystallisation can also be applied on Hg-free systems, as long as there is a possibility of using liquid metals as a cathode. We have extended our work from amalgams towards intermetallic compounds with Ga, In, Sn and others, either using the elemental metals or low melting eutectics. Hg as a solvent for metals not liquid near room temperature can be used as auxiliary in order to form *e. g.* indides at room temperature.

The interplay of ionic and metallic bonding contributions leads to highly complicated structures with long translation periods. Low Ioffe-Regel limit resistances [3] and bad metal behaviour [4] are the consequences. The unusual combination of metallic conductivity with strong electron localisation and correlation together with considerable covalent bonding contributions could open new opportunities for *e. g.* thermoelectric materials or multiferroic properties.

Here we present some new intermetallic crystal structures together with some examples from literature, all synthesised at temperatures between –40 and +80 °C by electrocrystallisation. The structure-property relations of the new compounds illustrate the effect of highly polarised metal-metal bonding.

---

[1] C. Hoch, J. Bender, A. Wohlfarth, A. Simon, *Z. Anorg. Allg. Chem.***635** (2009), 2429; C. Hoch, J. Bender, A. Simon, *Angew. Chem. Int. Ed.***48** (2009), 2415.

[2] C. Hoch, A. Simon, *Z. Anorg. Allg. Chem.***632** (2006), 2288; C. Hoch, A. Simon, *Z. Anorg. Allg. Chem.***634** (2008), 853; C. Hoch, A. Simon, *Angew. Chem. Int. Ed.***51** (2012), 3262; F. Tambornino, C. Hoch, *J. Alloys Compd.***618** (2015), 299; F. Tambornino, C. Hoch, *Z. Anorg. Allg. Chem.***618** (2015), 537.

[3] A. F. Ioffe, A. R. Regel in *Prog. Semicond. Vol. 4* (A. F. Gibson, F. A. Kroger, R. E. Burgess, Eds.), Heywood, London, **1960**, p. 237.

[4] A. F. Hebard, S. B. Arnason, *J. Supercond.***12** (1999), 159; O. Gunnarsson, M. Calandra, J. E. Han, *Rev. Mod. Phys.***75** (2003), 1085.

O2

Conflict management: Lessons from Intermetallic Chemistry

Ponou, Simeon (Department of Chemistry, Lund University, Lund, SWE)

Conflict management is the process of limiting the negative aspects of conflict in a system while increasing its positive aspects. Properly managed conflict can improve system outcomes. This definition is very appealing for solid state chemists, particularly those focusing on structure-properties relationship in intermetallic compounds. Indeed, intermetallic crystal structures are often of daunting complexity, and their rationalization can be very challenging. In addition, many (multi)functional intermetallic materials are characterized by conflicting properties. Typical examples include the thermoelectric materials where the phonon-glass behavior is conflicting with the electron-crystal behavior. Also, conflict between localization and delocalization of bonding electron-pairs has been invoked to explain high Tc in the superconducting MgB_2. Moreover, some superconducting materials are known to be paramagnetic or heavy fermions systems. In more fundamental angles, they are numerous intermetallic structures in which the structure-properties relationship are rationalized only by using counterintuitive approaches. Perhaps, the academically most relevant cases are found in so called electronic intermetallic compounds for which the electron band-structure energy is a large fraction of the total energy, and crystal structure types are related to particular valence electron concentrations (average number of valence electrons per atom): the Hume-Rothery and, the electron precise Zintl-phases. In the latter, typical conflicts are those between closed-shell configuration and metallic properties, or between directed and isotropic interactions as well as between localized and multicentered bonding. The purpose of this talk is to present some striking examples of inherent conflicts in some newly discovered intermetallic structures, and the very original response provide by nature to properly manage the resulting tensions. These range from local symmetry breaking or differential fractional site occupancy to address physico-chemical potential gradient in the homologous series $Ca_{2+n}M_{2+x}Ge_{2-x+n}$ (M = Ag, Mg, Mn), illustrating either the substantive versus affective conflict, or the organizational and interpersonal conflict. Further examples address the conflicts between homo- and heteronuclear bonding in noble metal stuffed Zintl phases and the impact of the relativistic effects, resulting in unusual metal-metal bonding in the ternaries system Ca/Pd-Pt/Ge.

With up to 25% of the manager day being spent on dealing with conflict, education needs to reconsider the importance of this subject. The subject warrants emphasis on enabling students to deal with conflict management and we hope to convince you that more intermetallic chemistry in our chemical education may provide the necessary analytical skill to the students.

PL2

Thermoelectric or multiferroic oxides and sulfides: 2D versus 3D magnetic materials

Maignan, Antoine (Laboratoire CRISMAT, UMR 6508 CNRS, ENSICAEN, UNICAEN, Caen Cedex, FRA); Guilmeau, E. (Laboratoire CRISMAT, UMR 6508 CNRS, ENSICAEN, UNICAEN, Caen Cedex 04, FRA); Hébert, S. (Laboratoire CRISMAT, UMR 6508 CNRS, ENSICAEN, UNICAEN, Caen Cedex 04, FRA); Daou, R. (Laboratoire CRISMAT, UMR 6508 CNRS, ENSICAEN, UNICAEN, Caen Cedex, FRA); Lebedev, O. (Laboratoire CRISMAT, UMR 6508 CNRS, ENSICAEN, UNICAEN, Caen Cedex, FRA); Berthebaud, D. (Laboratoire CRISMAT, UMR 6508 CNRS, ENSICAEN, UNICAEN, Caen Cedex, FRA)

The transition metal oxides (TMO) and sulfides form two large classes of promising candidates for multiferroicity and thermoelectricity. For the former, the quasi-2D magnetism in triangular networks, responsible for both low Néel temperature and complex antiferromagnetic structure, provide key ingredients to generate spin induced ferroelectricity [for a review see reference 1 and references therein]. In that respect, the $CuCrO_2$ delafossite phase [2,3] and the $AgCrS_2$ sulfide [4,5], with a derived structure, are both multiferroics below T_N=25K and T_N=55K, respectively. To approach room temperature spin induced ferroelectricity, more 3D magnetic networks are needed as in $YBaCuFeO_5$ [6], an oxygen deficient ordered perovskite, or in hexaferrites [1]. A major concern for this topic lies in the insulating character of the samples: due to their tendency towards mixed-valency, TMOs can be too leaky. Nevertheless, in that case, the electronic correlations and the magnetic spins are responsible for their unusual T dependence of the Seebeck coefficient (S), which explains why (3D) perovskite metallic ruthenates, such as $SrRuO_3$, are studied for their thermoelectric properties [7].

In contrast to spin induced ferroelectrics, a major limitation for 3D structures of thermoelectrics, in both oxide or sulfide, comes from the easiness of the phonons propagations leading to too large thermal conductivities (k) [at 300K k>10$W.K^{-1}.m^{-1}$ in two itinerant ferromagnets, $SrRuO_3$ and CoS_2 [8], the latter crystallizing in the pyrite structure]. In order to reduce the k values, the layered cobaltites with “misfit” structure [7] and more recently, the compounds derived from TiS_2 [9], have been studied. The CdI_2-type conducting planes of their layered structures have to be optimally doped to first optimize their power factor ($PF=S^2/r$, r=electrical resistivity). In the “misfit” phases, oxides or sulfides, the charge transfer between the separating block to the conducting layer is fixed by the structural mismatch between the different sublattices. This motivated the study of the 1T-TiS_2 dichalcogenide in which intercalation and substitution can be used to optimize PF and, also, the thermoelectric figure of merit, ZT=(PF/k).T, by reducing the lattice part of k in crystals, by a factor of 5 [10].

---

[1] Y. Tokura, S. Seki and N. Nagaosa, Rep. Prog. Phys, 77 (2014) 076501.
[2] S. Seki, Y. Onose and Y. Tokura, Phys. Rev. Lett 101, (2008) 067204.
[3] M. Poienar, F. Damay, C. Martin, V. Hardy, A. Maignan and G. André, Phys. Rev. B 79 (2009) 014412.
[4] K. Singh, A. Maignan, C. Martin and Ch. Simon, Chem. Mater. 21 (2009) 5007.
[5] F. Damay, S. Petit, M. Braedlein, S. Rols, J. Ollivier, C. Martin and A. Maignan, Phys. Rev. B 87 (2013) 134413.
[6] B. Kundys, A. Maignan and Ch. Simon, Appl. Phys. Lett. 94 (2009) 072506.
[7] Review article: S. Hébert, D. Berthebaud, R. Daou, Y. Bréard, D. Pelloquin, E. Guilmeau, F. Gascoin, O. Lebedev and A. Maignan, J. Phys. Cond. Matter (in press).
[8] S. Hébert, E. Guilmeau, D. Berthebaud, O. Lebedev, V. Roddatis and A. Maignan, J. of Appl. Phys. 114 (2013) 103703.
[9] Review article: E. Guilmeau, A. Maignan, C.L. Wan, K. Koumoto, Energy and Environnemental Science (submitted).
[10] R. Daou, H. Takahashi, S. Hébert, M. Beaumale, E. Guilmeau and A. Maignan, J. Appl. Phys. 117 (2015) 165101.

IL2

Electric order and magnetism in organic-inorganic hybrid compounds with perovskite-like structure

Señaris-Rodriguez, Maria Antonia (University of A Coruña, A Coruña, ESP)

Single phase multiferroics, in which magnetic and electric orders coexist and even better couple, have been subjected to extensive research in recent years in view of the scientific interest of these materials and their potential applications in novel devices.

Beyond transition-metal oxides, in which these properties are usually investigated, recent research is also paying increased attention to organic-inorganic hybrid compounds whose crystalline and modular designable nature can provide an interesting new approach to multiferroic behavior.

In this talk I will focus in these latter, in particular in organic-inorganic hybrid perovskites, to discuss with examples the different possibilities found so far to combine electric order and magnetism in these materials and to get a magnetoelectric coupling.

O3

Oxygen Nonstoichiometry and Charge Transfer in the Double Perovskite Sr_2FeMoO_{6-d}

Tsvetkov, Dmitry (Ural Federal University, Ekaterinburg, RUS); Golomolzin, Rodion (Ural Federal University, Ekaterinburg, RUS); Ivanov, Ivan (Ural Federal University, Ekaterinburg, RUS); Zuev, Andrey (Ural Federal University, Ekaterinburg, RUS)

Mixed ionic- and electronic-conducting perovskite-type oxides are the state-of-the-art materials for high-temperature solid-state electrochemical devices such as solid oxide fuel cells (SOFCs), oxygen membranes and sensors. Many of such materials are cobaltite-based oxides.

Recently, double perovskites Sr_2MMoO_{6-d}, where M is a 3d-metal, received great attention as attractive materials for such application. It is generally recognized that defect structure is of key importance for understanding the properties of materials. However, the data on the defect structure and related properties of double perovskites Sr_2MMoO_{6-d} (M=3d-metal) as function of oxygen partial pressure (p_{O2}) and temperature are very restricted to date.

Crystal structure, oxygen nonstoichiometry, total conductivity and Seebek coefficient of the double perovskite Sr_2FeMoO_{6-d} were studied as a function of oxygen partial pressure $-15<\log(pO_2/atm)<0$ and temperature $800 \leq T$, $°C \leq 1050$.

In situ x-ray diffraction measurements of Sr_2FeMoO_{6-d} crystal structure were carried out. Total conductivity and Seebek coefficient of Sr_2FeMoO_{6-d} were measured simultaneously by means of four-probe dc method. Oxygen nonstoichiometry of the double perovskite Sr_2FeMoO_{6-d} was measured using thermogravimetric technique.

Results obtained are discussed on the basis of the defect structure of the double perovskite Sr_2FeMoO_{6-d}

This work was supported by the Russian Foundation for Basic Research (grant No. 15-33-20978).

O4

Synthesis, structures and optical properties of hybrid lead iodide perovskite phases

Weller, Mark (University of Bath, Bath, GBR)

Main group metal iodometallate and bromometallates represent a large class of semiconducting materials that display optical and electronic properties of great interest currently as photovoltaics. Of particular interest are the heavy group 14 iodometalates, since they can adopt perovskitic structures of varying dimensionality and demonstrate large compositional and structural variations that allow the band gap for solar cell applications to be controlled [1,2]. Specifically when the A-site in the perovskite formula, AMI3, is occupied by a small monovalent cation, such as Rb, Cs, methylammonium, or formamidinium, a three-dimensional (3D) framework is obtained [3]. If a larger cation is used two-dimensional (2D) layered, or one-dimensional (1D) chain materials are obtained with formulas AMI3, A2MI4, and A3MI5 which still retain their perovskite (or corner sharing) connectivity [4,5]. The stoichiometry of the final material and the metal-iodide linkages are extremely sensitive to the nature of the cation with both size and the functionality playing a crucial role, particularly for A = alkylylammonium. Structurally these materials show very complex behaviours based on the size of cation, its shape and, for alkyl groups, its orientation in the unit cell. These behaviours as also often temperature dependent with materials demonstrating complex phase behaviours and transitions as the alkylammonium groups reorientate. One further complexity of importance in the synthesis and use of these materials is their ease of hydration and dehydration [6]; a process that involves separating, into [PbI6]2- units, amine, and H2O molecules, and rebuilding the perovskite network. We have recently undertaken a systematic investigation of phases in the lead iodide-amine cation systems forming a variety of new (2-3)- (multiple layer), 2-, 1- and 0- (cluster) dimensional structures. A wide range of amines has been studied extending from small monovalent species such as guanadinium to large fully conjugated aromatic systems. Full structure determination has been undertaken using both single crystal and powder X-ray diffraction. Analysis of these results provides an understanding of the roles of cation size and shape on the dimensionality of the lead-iodide structural element. These results also permit an understanding of the optical absorption spectra of these materials, which are controlled by both the exact lead iodide sub-unit structure (dimensionality and inter PbI6 octahedral bond angles) and, for conjugated amines, the nature of the intercalated organic cation. Detailed structural studies of some of these materials, using neutron powder diffraction, will also be reported as they shed considerable light on the importance of the hydrogen-bonding interactions between amine cations and lead iodide framework. Results on methylammonium lead iodide have been reported previously [7] and results of more recent studies of the 3D formamidium lead iodide and 2D alkylammonium lead iodides will be summarised.

---

[1] Chung, I., Lee, B., He, J., Chang, R. P. H. & Kanatzidis, M. G.. Nature 485, 486–489 (2012). [2] Kojima, A., Teshima, K., Shirai, Y. & Miyasaka. T. J. Am. Chem. Soc. 131, 6050–6051 (2009).

[3] C. C. Stoumpos, C. D. Malliakas, and M. G. Kanatzidis. Inorg. Chem. 2013, 52, 9019−9038; T.Baikie, Y. Fang, J. M. Kadro, M. Schreyer, F. Wei, S. G. Mhaisalkar, M. Graetzel and T.J. White J. Mater. Chem. A, 2013, 1,5628

[4] D. G. Billing and A. Lemmerer, Acta Crystallogr., Sect. B: Struct. Sci., 2007, 63, 735. D. G. Billing and A. Lemmerer, New J. Chem., 2008, 32, 1736; D. G. Billing and A. Lemmerer, CrystEngComm, 2007, 9, 236;

[5] A. Lemmerer and D. G. Billing Dalton Trans., 2012, 41, 1146-1157

[6] B. R. Vincent, K. N. Robertson, T. S. Cameron and K. Osvald, Can. J. Chem., 1987, 65, 1042–1046.

[7] M. T. Weller, O.J. Weber, P. F. Henry A. M. Di Pumpo, T. C. Hansen Chem. Comm., 2015, 51, 4180 – 4183

PL3

Soft chemical control of iron selenide superconductors and layered oxide chalcogenides

Clarke, Simon (University of Oxford, Oxford, GBR)

This talk will discuss the chemical control of the properties of several chalcogenide materials. In one strand of the talk synthetic methods for realising new members of the class of iron based superconductors will be described. One focus will be on compounds containing iron selenide layers with electropositive metals and small molecules, notably ammonia, in the interlamellar space, which have been characterised using neutron diffraction investigations [1,2] and in-situ X-ray powder diffraction investigations carried out during synthesis [2]. A second focus of this strand will be on a series of related hydroxide selenide compounds. Here the ability to control the composition through soft chemical synthesis enables the electronic and structural factors which dictate whether or not layered iron selenides superconduct to be examined and tested [3]. A second strand of the talk will describe soft chemical control of the structures and properties of a series of layered oxide chalcogenides in which the composition of a coinage metal (Cu or Ag) chalcogenide layer is controlled using redox chemistry to control the electronic properties of an intervening transition metal oxide layer.

---

[1] M. Burrard-Lucas et al., Nature Materials 12, 15 (2013).
[2] S. J. Sedlmaier et al., J. Am. Chem. Soc. 136, 630 (2014).
[3] H. Sun et al. Inorg. Chem. 54, 1958 (2015).
[4] J. N. Blandy et al. 2015 Submitted for publication.

IL3

Chalcogenide glass films for nanoscale memories.

Wagner, Tomas (University of Pardubice, Department of inorganic chemistry, Pardubice, CZE); Zhang, Bo (University of Pardubice, Department of inorganic chemistry, Pardubice, CZE); Fraenkl, Max (Department of General and Inorganic Chemistry, Faculty of Chemical Technology, University of Pardubice, Pardubice, CZE); Frumar, Miloslav (Department of General and Inorganic Chemistry, Faculty of Chemical Technology, University of Pardubice, Pardubice, CZE); CHEN, G. (Department. of Physics & Astronomy, Athens, USA); Krbal, Milo¿ (Department of General and Inorganic Chemistry, Faculty of Chemical Technology, and Centre for Materials Science, University of Pardubice, Pardubice, CZE); Valkova, Silvie (Department of General and Inorganic Chemistry, Faculty of Chemical Technology, and Centre for Materials Science, University of Pardubice, Pardubice, CZE)

A range of material systems exist in which nanoscale ionic transport and redox reactions provide the essential for switching as platform for reconfigurable electronic devices and biological like computing. One class relies on mobile cations, which are easily created by electrochemical oxidation of the corresponding electrode metal, transported in the insulating layer, and reduced at the inert counter electrode. These devices are termed electrochemical metallization memories (EMC) or conductive bridge random access memories [1]. The material candidates for electrolytes in such devides have been recently studied. They are amorphous chalcogenides [2, 3] and also oxides (SiO2, WO3, TiO2 and others [1]) containing metal elements (Ag, Cu) or their compounds (Ag2S, CuS) and gaining some portion of ionic conductivity and becoming mixed ionic-electronic conductors [3-8]. The aim of this work is to present our current results on syntesis and resistive switching of chalcogenide based nanowire array cells and planparalel cells.

The authors thanks to project KONTAKT II (CR-USA) LH14059 for financial support.

---

[1] W. Lu, D. S. Jeong, M. Kozicki, R. Waser, MRS Bulletin, 37 (2012) 124.

[2] M. Frumar and T. Wagner, Curr. Opinion Solid St. Mat. Sci. 7 (2003) 117.

[3] M. Frumar, B. Frumarova, T. Wágner, Amorphous and Glassy Semiconducting Chalcogenides. In: Bhattacharya P, Fornari R, and Kamimura H, (eds.), Comprehensive Semiconductor Science and Technology, volume 4, pp. 206–261 (2011)Amsterdam: Elsevier.

[4] Š. Stehlík, J. Kolář, M. Bartoš, Mil.Vlček, M. Frumar, V. Zima, T. Wágner, Sol. State Ionics 181, (2010) 1625.

[5] J. Kolář, T. Wágner, V. Zima, Š. Stehlík, B. Frumarová, L. Beneš, Mil. Vlček, M. Frumar, J. Non-Cryst. Solids, 357 (2011) 2223.

[6] I. Kaban, P. Jóvári, T. Wágner, M. Bartoš, M. Frumar, B. Beuneu, W. Hoyer, N. Mattern, J., Eckert, J. Non-Cryst. Solids, 357 (2011) 3430.

[7] Š. Stehlik, K. Shimakawa, T. Wágner, M. Frumar, J. Phys. D: Appl. Phys. 45 (2012) 205304.

[8] Kolar J., Macak J., Terabe K., Wágner T, Down-scaling of resistive switching to nanoscale using porous anodic alumina membranes, J. Mater. Chem. C 2 (2014) 349-355.

O5

Synthesis and characterization of Ba[CoSO]: magnetic complexity and chalcogen ordering

Valldor, Martin (Max Planck Institute for Chemical Physics of Solids, Dresden, GER); Rößler, Ulrich K. (Leibniz Institute for Solid State and Materials Research, Dresden, GER); Prots, Yurii (Max Planck Institute for Chemical Physics of Solids, Dresden, GER); Kuo, Chang-Yang (Max Planck Institute for Chemical Physics of Solids, Dresden, GER); Chiang, Jen-Che (Institute of Physics, National Chiao Tung University, Hsinchu, TWN); Hu, Zhiwei (Max Planck Institute for Chemical Physics of Solids, Dresden, GER); Pi, Tun-Wen (National Synchrotron Radiation Research Centre, Hsinchu, TWN); Kniep, Rüdiger (Max Planck Institute for Chemical Physics of Solids, Dresden, GER); Tjeng, Liu Hao (Max Planck Institute for Chemical Physics of Solids, Dresden, GER)

We have successfully synthesized the novel compound barium thio-oxocobaltate(II), $Ba[CoS_{2/2}O_{2/2}]$ (*Cmcm*, a = 3.98808(3), b = 12.75518(9), c = 6.10697(4) Å) that is isostructural to Ba[ZnSO]. Soft x-ray absorption spectroscopy confirms that cobalt is in the oxidation state +2 and tetrahedrally coordinated by 2 S and 2 O atoms in an ordered fashion. High temperature magnetic susceptibility data indicate strong low dimensional spin-spin interactions, which are suggested to be closely related to the layer type crystal structure and perhaps the ordered distribution of S and O. Antiferromagnetic long range spin ordering below T_N = 222 K is observed as an anomaly in the specific heat coinciding with a significant lowering of the magnetic susceptibility. Density-functional theory calculations (GGA+U) identify an antiferromagnetic ground-state within the square-like two-dimensional layers of Co with antiferromagnetic correlations for nearest and next-nearest-neighbors along bonds mediated by S or O. However, this magnetic state is subject to frustration by relatively strong interlayer couplings.

O6

Looking for new chalcogenides functional materials in Ba-T-Se systems (T=Cr, Fe)

Berthebaud, David (Laboratoire CRISMAT ENSICAEN UMR CNRS 6508, Caen, FRA); Pelloquin, Denis (Laboratoire CRISMAT ENSICAEN UMR CNRS 6508, Caen Cedex 04, FRA); Lefevre, Robin (Laboratoire CRISMAT ENSICAEN UMR CNRS 6508, Caen Cedex 04, FRA); Perez, Olivier (Laboratoire CRISMAT ENSICAEN UMR CNRS 6508, Caen Cedex 04, FRA); Gascoin, Franck (Laboratoire CRISMAT ENSICAEN UMR CNRS 6508, Caen Cedex 04, FRA); Hebert, Sylvie (Laboratoire CRISMAT ENSICAEN UMR CNRS 6508, Caen Cedex 04, FRA); Maignan, Antoine (Laboratoire CRISMAT ENSICAEN UMR CNRS 6508, Caen Cedex 04, FRA)

Many intermetallic compounds containing chalcogens have already been discovered from a structural point of view but for most of them no physical properties have been reported. Moreover, a literature survey tends to indicate that a large number of unknown phases are expected to be discovered with a systematic approach since many of these systems have not been thoroughly examined. In conclusion, clearly, chalcogenides phases have the potential to bring diverse structures and properties, and their further study is of great importance.

For example, the recent discovery of alkaline metal intercalated FeSe superconductor with Tc~30K [1] has highlighted the properties of materials built of edge-sharing $FeSe_4$ tetrahedra, and motivated us to look for new iron selenide based materials.

In addition, chromium selenides based compounds have shown the potential of this family of compounds for thermoelectric applications. It is for instance the case of the ternary $Ba_xCr_5Se_8$, in which the cations sit within the infinite channels formed by the $[Cr_5Se_8]^-$ anionic sub-network. The complex ordering of the cations lead to an extremely small thermal conductivity of less than 1 W/(mK), that together with a large Seebeck coefficient, produces thermoelectric figure of merit above of 0.1 at 900K. This example validates the fact that, indeed, attractive properties can be unveiled.

In this contribution, the first result of our systematic exploration will show that in certain systems, physical properties are promising and that the richness of these systems probably still hides some interesting materials. In addition to the known phases, new ternary intermediate phases have been isolated. We will present here the crystal structures refinements, based on transmission electron microscopy and X-ray diffraction data, as long with physical properties obtained by means of magnetic and transport properties measurements.

---

[1] F-C. Hsu, J-Y. Luo, K-W. Yeh, T-K. Chen, T-W. Huang, P. M. Wu, Y-C. Lee, Y-L. Huang, Y-Y. Chu, D-. Yan,M-K. Wu, *Proc Natl Acad Sci U S A* . 105(38) (2008) 14262–14264 .

PL4

Symmetry, calculation and synthesis in the search for coupled property materials

Rosseinsky, Matthew J. (Department of Chemistry, University of Liverpool, Liverpool, GBR)

It is attractive to harness the ever-increasing power of computation [1] in the search for new materials, but the scale and nature of the problem make brute force de novo approaches challenging, while “big data” searches for analogues of existing structures in databases, though very useful, cannot identify potentially transformative new structures. Building chemical knowledge into computational tools used together with experiment offers a different approach. I will present an example of crystal chemically-informed computational identification of a new SOFC cathode [2], and an example of a nanostructured SOFC cathode system [3] whose multiple length scale structure exemplifies the challenges in designing materials ab initio. We have recently used this integrated approach to combine permanent magnetism and electrical polarisation in a single phase material above room temperature [4].

---

[1] M. Jansen, I.V. Pentin, J.C.Schoen, Angewandte Chem. Int. Ed. 51, 132, 2012

[2] M. Dyer et al Science 340, 847, 2013

[3] A. Demont et al J. Am. Chem. Soc. 135, 10114, 2013

[4] M. Pitcher et al Science 347, 420, 2015

IL4

Tailored Synthesis between Water and Liquid Ammonia: Hollow Nanospheres for Medicine and Less-noble Metals for Catalysis

Feldmann, Claus (Karlsruhe Institute of Technology (KIT), Karlsruhe, GER)

Hollow nanospheres, less-noble metal nanoparticles and nanoscaled metal nitrides are no doubt highly interesting classes of materials with properties and functions that range from fluorescence and magnetism to drug delivery and catalysis. All these nanomaterials, however, relate to metastable phases that are partially highly sensitive to oxidation and hydrolysis. Thus, specific methods of synthesis are required to realize these nanomaterials with optimal properties. In the recent years, we have developed several new methods of synthesis such as microemulsions for preparing hollow nanospheres [1] or syntheses in liquid ammonia to obtain less-noble metal nanoparticles [2]. The hollow nanospheres include oxides (e.g., AlO(OH), La(OH)3, ZnO, SnO2, TiO2), sulfides (e.g., CuS, Cu1.8S, Cu2S, Ag2S) or metals (e.g., Au, Ag) exhibiting outer diameters of 10-50 nm, a wall thickness of 2-10 nm and an inner cavity of 5 to 30 nm in diameter [1]. Via liquid-ammonia-based synthesis we can obtain less-noble metals (e.g., Bi, Mo, W, Re, Fe, Zn, Ti) as well as metal nitrides (e.g., CoN, GaN, Si3N4) with diameters <10 nm [2]. Based on our synthesis strategies ranging from water to liquid ammonia as the liquid phase, we could address various properties and applications, including sensing, catalysis, drug delivery, optical imaging, and gas sorption [1,2]. The presentation will critically discuss the need of new synthesis strategies including specific advantages and disadvantages.

---

[1] a) H. Goesmann, C. Feldmann, Angew. Chem. Int. Ed. 2010, 49, 1362 (Review). b) H. Gröger, F. Gyger, P. Leidinger, C. Zurmühl, C. Feldmann, Adv. Mater. 2009, 21, 1586. c) P. Leidinger, R. Popescu, D. Gerthsen, C. Feldmann, Small 2010, 6, 1886. d) P. Leidinger, S. Simonato, C. Feldmann, Chem. Commun. 2012, 48, 7046. e) F. Gyger, A. Sackmann, M. Hübner, P. Bockstaller, D. Gerthsen, H. Lichtenberg, J.-D. Grunwaldt, N. Barsan, U. Weimar, C. Feldmann, Part. Part. Syst. Charact. 2014, 31, 591.

[2] a) F. Gyger, P. Bockstaller, D. Gerthsen, C. Feldmann, Angew. Chem. Int. Ed. 2013, 52, 12443. b) F. Gyger, P. Bockstaller, H. Gröger, D. Gerthsen, C. Feldmann, Chem. Commun. 2014, 50, 2939. c) C. Schöttle, P. Bockstaller, D. Gerthsen, C. Feldmann, Chem. Commun. 2014, 50, 4547.

O7

Templated growth of small nanowires using supercritical fluid electrodeposition

Hector, Andrew (University of Southampton, Southampton, GBR)

Supercritical fluids are attractive media for the electrodeposition of metals and semiconductors into complex nanostructures [1], as their essentially zero surface tension allows them to readily penetrate porous and nanoporous structures. They also have low viscosities and hence show enhanced mass transport rates. Depending on the choice of electrolyte and solvent they can also have a wide electrochemical window. These advantages also come with several practical disadvantages including generally low dielectric constants and the necessity to work in sealed systems at elevated temperature and pressure. Hence there is very little published work on electrodeposition from single phase supercritical systems. In order to explore the possibilities of using electrodeposition from supercritical fluids to make sub 20 nm nanostructures and nanostructured devices we have focused on the electrodeposition of a range of p-block elements from supercritical difluoromethane. With many of this elements it has been possible to deposit sub-20 nm nanowires using commercial anodic alumina templates as the hosts. These have been characterized in detail using X-ray diffraction and transmission electron microscopy. To investigate the small size limits of the technique, sub-5 nm templates have been developed from ordered mesoporous silica films [2]. Progress in deposition into these very small pore systems will also be described.

---

[1] P. N. Bartlett, D. A. Cook, A. L. Hector, W. Levason, G. Reid, W. Zhang, M. W. George, J. Ke and D. C. Smith, “Electrodeposition from supercritical fluids”, Phys. Chem. Chem. Phys., 2014, 16, 9202-9219.

[2] C. Robertson, R. Beanland, S. A. Boden, A. L. Hector, R. J. Kashtiban, J. Sloan, D. C. Smith and A. Walcarius, “Ordered mesoporous silica films with pores oriented perpendicular to a titanium nitride substrate”, Phys. Chem. Chem. Phys., 2015, 17, 4763-4770.

O8

Microwave-assisted routes for the synthesis of inorganic materials: an overview

Moran, Emilio (Universidad Complutense Madrid, Madrid, ESP)

The synthesis of complex functional inorganic materials, such as oxides, can be successfully performed by using microwave irradiation as the source of heat. To achieve this, different routes and set-ups can be used: microwave-assisted synthesis may proceed in the solid state or in solution, aqueous or not, and the set ups may be as simple and accessible as a domestic oven or quite sophisticated laboratory equipments. An obvious advantage of this innovative methodology is the considerable reduction in time –minutes rather than hours or days- and, as a consequence of it, energy saving. No less important is the fact that the particle growth is inhibited and the broad variety of different microwave or microwave-assisted synthesis techniques opens up opportunities for the preparation of inorganic nanoparticles and nanostructures. In this work, various microwave synthesis techniques have been employed: solid-state microwaves, single-mode microwaves using a TE_{10p} cavity and microwave-assisted hydrothermal synthesis. The synthesis of relevant examples such as electrode or electrolyte materials for SOFC's, cathodic materials for Li/Na batteries, multiferroics, etc., will be presented and discussed.

PL5

Methods beyond DFT: current status and future developments

Kresse, Georg (University of Vienna, Computational Materials Physics, Vienna , AUT)

The properties of all materials arise largely from the quantum mechanics of their constituent electrons under the influence of the electric field of the nuclei. The solution of the underlying many-electron Schrödinger equation is a non-polynomial hard problem, owing to the complex interplay of kinetic energy, electron-electron repulsion and the Pauli exclusion principle. The dominant computational method for describing such systems has been density functional theory, although the accuracy of this method is not well established for materials under i.e. extreme conditions. Quantum-chemical methods based on an explicit ansatz for the many-electron wavefunctions are potentially more accurate, but they have not been fully explored in the solid state owing to their computational complexity, which ranges from strongly exponential to high-order polynomial in system size. The talk will give a simple to understand introduction to quantum chemistry methods and modern many body perturbation theory and discuss recent advances in the application of these methods to solids. Results for an exact technique, full configuration interaction quantum Monte Carlo to a variety of real solids, are report providing reference many-electron energies. These are used to rigorously benchmark the standard hierarchy of quantum-chemical techniques, up to the ``gold" standard coupled-cluster ansatz [1]. In practice, these methods are however yet too expensive to be applied to questions in materials science. Simpler methods that recover the important ingredients of the many electron solution, such as the random phase approximation to the correlation energy as well as improvements to this method are discussed alongside illustrative examples [2,3,4].

---

[1] George H. Booth, Andreas Grüneis, Georg Kresse, and Ali Alavi, "Towards an exact description of electronic wavefunctions in real solids", Nature 493, 365 (2013).

[2] J. Harl and G. Kresse, "Accurate bulk properties from approximate many-body techniques", Phys. Rev. Lett. 103, 056401 (2009).

[3] L. Schimka, J. Harl, A. Stroppa, A. Gruneis, M. Marsman, F. Mittendorfer, and G. Kresse, "Accurate surface and adsorption energies from many-body perturbation theory", Nature Materials 9, 741 (2010).

[4] M. Kaltak, J. Klimes, and G. Kresse, "A cubic scaling algorithm for the random phase approximation: Self-interstitials and vacancies in Si", Phys. Rev. B 90, 054115 (2014).

IL5

Solid state theory at finite temperature

Abrikosov, Igor A. (Linköping University, Linköping, SWE)

Ab initio electronic structure theory is known as a useful tool for prediction of materials properties, for their understanding, as well as for determination of parameters employed in higher-level modeling. However, majority of simulations still deal with calculations in the framework of density functional theory (DFT) with local or semi-local functionals carried out at zero temperature. In this talk, we present new methodological solutions, which go beyond this approach and explicitly take into account finite temperature effects. Basic ideas behind novel techniques for first-principles theoretical simulations of lattice dynamics, as well as their coupling to systems with magnetic excitations and configurational disorder are introduced. The capabilities of the Temperature Dependent Effective Potential (TDEP) method [1], the Disordered Local Moment Molecular Dynamics (DLM-MD) [2], and the combined technique [3] are demonstrated using transition metal nitrides and their alloys as model systems.

---

[1] O. Hellman, I. A. Abrikosov, and S. I. Simak, Phys. Rev. B **84**, 180301(R) (2011); O. Hellman, P. Steneteg, I. A. Abrikosov, and S. I. Simak, Phys. Rev. B **87**, 104111 (2013); O. Hellman and I. A. Abrikosov, Phys. Rev. B **88**, 144301 (2013).
[2] P. Steneteg, B. Alling, and I. A. Abrikosov, Phys. Rev. B **85**, 144404 (2012).
[3] N. Shulumba, B. Alling, O.Hellman, E. Mozafari, P. Steneteg, M. Odén, and I. A. Abrikosov, Phys. Rev. B 89, 174108 (2014).

O9

Heteropolar Bonds and a Position-Space Representation of the 8-N Rule

Bende, David (Max Planck Institute for Chemical Physics of Solids, Dresden, GER); Wagner, Frank R. (Max Planck Institute for Chemical Physics of Solids, Dresden, GER); Grin, Yuri (Max Planck Institute for Chemical Physics of Solids, Dresden, GER)

The chemical bonding of Zintl phases, main-group MgAgAs-type and zinc-blende-type compounds is analyzed with the aid of quantum chemical position-space indicators.[1] The 8−N rule - basis for the formal description of chemical bonding in Zintl phases - is reformulated in position space and extended for the quantitative and consistent description of heteropolar bonding present in the compounds of the MgAgAs and zinc-blende type. Heteropolar bonds (p) are understood as a superposition of a nonpolar covalent part (b’) and a polar hidden lone-pair part (lp’) according to (p) = (*x*b’,[1-*x*]lp’). The particular ratio of covalent and hidden lone-pair part depends on the atoms’ contributions to the heteropolar bond similar to a classical Lewis formula. A covalent bond is characterized by an equal electronic contribution of the bonding partners, a lone pair is characterized by a component’s complete ownership of the electron population. The intermediate bonding situations represent heteropolar bonding.

The access electron number $N_{\mathrm{acc}}(E)$, the valence electron number $N_{\mathrm{val}}(E)$, and the charge claim $P_E(E)$ recover the 8−N rule in position space and allow the treatment of heteropolar bonding according to the presented model. The equal treatment of compounds with homopolar and heteropolar bonding leads to an interesting analogy of the bonding situations e.g. between NaP and LiAlSi. NaP is a Zintl phase with two nonpolar P-P bonds and two segregated lone pairs per phosphor atom. An equivalent of two nonpolar bonds and two lone pairs is mixed into four heteropolar Al-Si bonds in the MgAgAs-type compound LiAlSi: (p) = (0.5b',0.5lp').

Additionally, the position space variant of the 8–N rule provides a new framework for analysis of non-tetrahedral partial structures with higher coordination numbers and even compounds with non-octet atomic species.

---

[1] D. Bende, F. R. Wagner, Yu. Grin, *Inorg. Chem.* **2015**, *54*, 3970-3978.

O10

Na ionic conductivity in $NaTMO_2$ layered oxides as cathode Materials for Na-ion Batteries

Gonzalo, Elena (CICenergigune, Miñano, ESP); Han, Man H (CICenergigune, Miñano, ESP); Singh, Gurpreet (CICenergigune, Miñano, ESP); Lopez del Amo, Juan M (CICenergigune, Miñano, ESP); Lezama, Luis (Universidad del País Vasco (UPV/EHU), Bilbao, ESP); Rojo, Teofilo (Universidad del País Vasco (UPV/EHU). CICenergigune, Bilbao, ESP)

Sodium ion batteries (SIBs) have been recently chosen as a good alternative to the Li ion batteries (LIBs) for stationary applications. Natural abundancy, geographical distribution, low cost, feasible redox potential and similar intercalation chemistry of sodium to lithium have been the main reasons to reinforce this field of research. The number of publications and research groups working on SIB field has increased exponentially.[1-2] One of the most promising families of cathode materials for Na-ion batteries is $NaTMO_2$ layered oxides (TM =Cr, Mn, Fe, Co, Ni, and mixtures of 2–3 transition metals) because of their excellent electrochemical properties and structural simplicity.[3]

Layered oxides are composed of repeating sheets of TMO_6 layers with Na ions located in between the layers. These structures are classified as O3-, P2-, and P3-phases depending on the surrounding Na environment and the number of unique oxide layer packings.[4] The letter indicates the environment where Na is located (O: octahedral, P: prismatic) and the number indicates the number of interlayers that are surrounded. In the P2-phase, sodium is located in between the MO6 oxide layers resulting in an $AB_{Na1}BA_{Na2}A$…pattern with sodium ions coordinated to oxygen atoms in a trigonal prismatic environment, one edge sharing and one face sharing. In the O3-phase, sodium ions are located between the oxide layers where oxygen stacking is in the $AB_{Na1}CA_{Na2}BC_{Na3}A$... pattern in which each sodium is octahedrally coordinated to oxygen sharing one edge and one face with MO_6 octahedra.

CIC Energigune Na research line has focused its approach on the study of new materials with improved electrochemical performances by following two approaches:
- The first one a direct comparison of the impact of the different structure arrangements of $Na_{2/3}Fe_xMn_{(1-x)}O_2$ phases in their electrochemical performances. P2- and O3- $Na_{2/3}Fe_{2/3}Mn_{1/3}O_2$ have been synthesized as pure phases and electrochemically characterized. [5]
- Dopant substitution with electrochemically inactive species such as Mg in P2- $Na_{2/3}MnO_2$ to suppress the charge ordering in the structure during the electrochemical process in order to improve its electrochemical performance.[6]

Excellent electrochemical capacities (between 150-170 mAh/g) added to a considerable high average voltage (~2.7V), make the mentioned materials very interesting to be further characterized. Mechanism of charge/discharge process or the various structural changes have been studied in detail by analyzing the materials under cell operating conditions with different in-situ techniques.

Spectroscopic techniques (NMR and EPR) combined with electrochemical measurements have allowed us to study the Na ionic conductivity of the mentioned layered oxides. The mobility of Na ions in these phases, which is related to the different local environment of Na ions (prismatic and octahedral sites) and diffusion pathways, will be discussed. [5]

---

[1] Palomares V. et al. *Energy Environ.Sci.***2012**, 5, 5884.
[2] Palomares V. et al. *Energy Environ.Sci.***2013**, 6, 2312.
[3] Han M.H. et al. *Energy Environ.Sci.* **2013**, 6, 2312.
[4] Delmas C. et al. *Physica*, **1980**, 99B, 81.
[5] Gonzalo E. et al. *J. Mater. Chem. A,***2014**, 2, 18523
[6] Billaud J., et al. *Energy Environ. Sci.* **2014**, 7, 1387.

PL6

Structural studies of oxide spinel magnets: Magnetocapacitors and frustrated systems

Kemei, Moureen (University of California Santa Barbara, Santa Barbara, USA); Seshadri, Ram (University of California Santa Barbara, GOLETA, USA)

Insulating, magnetic AB_2O_4 spinel oxides, usually with $B = Cr^{3+}$ in the octahedral site, are fascinating materials that display a number of interesting phenomena. When A is non magnetic Mg^{2+} or Zn^{2+}, these are the canonical geometrically frustrated antiferromagnets with famously depressed magnetic ordering temperatures. In fact, magnetic ordering cannot take place without a structural transition first taking place. For many years now, the complete structures of the phases that form concurrently with magnetic ordering have not been known. These are established with high-resolution synchrotron X-ray diffraction studies carried out as a function of temperature. The structural phase transitions must be regarded in the light of structural changes at magnetic ordering seen also in the Jahn-Teller distorted spinels $NiCr_2O_4$ and $CuCr_2O_4$, where the structural changes clearly do *not* arise as a means of frustration release. The effect of careful addition of magnetic ions on the A-site in the ACr_2O_4 with A = Mg^{2+} and Zn^{2+}allows the different roles of structural changes and magnetic ordering to be understood. Finally, structural transitions accompanying magnetic changes on the spinel compounds $MnMn_2O_4$ and $GeCo_2O_4$ are also presented.

IL6

Magnetism of Cu minerals: geological insights into quantum effects

Tsirlin, Alexander (Experimentalphysik VI, EKM, Universität Augsburg, Augsburg, GER); Lebernegg, Stefan (Max Planck Institute for Chemical Physics of Solids, Dresden, GER); Janson, Oleg (Max Planck Institute for Chemical Physics of Solids, Dresden, GER); Rosner, Helge (Max Planck Institute for Chemical Physics of Solids, Dresden, GER)

Intricate quantum phenomena manifest themselves in real-world materials and, thus, can be observed experimentally. For example, low-temperature behavior of magnetic insulators is conveniently mapped onto quantum spin models. When suitable magnetic ions are chosen and their spatial arrangement is properly adjusted, intriguing effects related to the formation of unconventional magnetic order or absence thereof, magnetic order induced by external field, ballistic heat transport or spin-nematic states emerge. Those have direct connections to fundamental phenomena in quantum physics, such as Bose-Einstein condensation of magnons and unconventional superconductivity.

The manifestation of quantum magnetic properties strongly depends on chemical and structural features of a material, because spatial arrangement of the magnetic ions and the ensuing interaction pathways fully determine the low-temperature behavior. This close combination of chemistry and physics is often extended toward geology , as many of the natural minerals feature magnetic ions and reveal peculiar magnetic behavior at low temperatures.

In this talk, quantum magnetism of several Cu^{2+} minerals will be presented. Malachite $Cu_2(OH)_2CO_3$, a well-known green pigment and even an industrially relevant source of copper, reveals gapped magnetic excitations that bring it close to the unusual regime of quantum criticality [1]. A far less-known copper mineral diaboleite $Pb_2Cu(OH)_4Cl_2$ features unexpected connections to the perovskite crystal structure and demonstrates diluted antiferromagnetism in two dimensions [2]. Finally, dioptase $Cu_6Si_6O_{18} \times 6H_2O$ is a very exotic case of an effectively low-dimensional magnet in three dimensions, where quantum effects are triggered by the small number of magnetic interactions per ion, and the ordered magnetic moment is only half of its full value for Cu^{2+} [3].

We will also discuss methodological issues related to magnetic measurements on natural samples, the selection of samples from the batch, and the control of sample quality.

AAT gratefully acknowledges financial support of the Sofja Kovalevskaya program of Alexander von Humboldt Foundation and of the Mobilitas program of the ESF, grant MTT77.

---

[1] S. Lebernegg *et al. Phys. Rev. B***88**, 224406 (2013).
[2] A. A. Tsirlin *et al. Phys. Rev. B***87**, 064404 (2013).
[3] O. Janson *et al. Phys. Rev. B***82**, 014424 (2010).

O11

Relaxor Ferromagnetism in the Perovskite Structure

Battle, Peter (University of Oxford, Oxford, GBR); Avdeev, Maxim (Bragg Institute, Lucas Heights, AUS); Hadermann, Joke (University of Antwerp, Antwerp, BEL); Sena, Robert (University of Antwerp, Antwerp, BEL); Chin, Chun-Mann (University of Oxford, Oxford, GBR); Tang, Yawei (University of Oxford, Oxford, GBR)

The list of factors that play a role in determining the magnetic behaviour of double perovskites, $AA'BB'O_6$, includes the electron configuration of any diamagnetic 6-coordinate cation, the electron configuration of the magnetic cation and the extent of *(B,B')* cation disorder. These factors together determine the relative strengths of NN and NNN interactions and hence the nature of the magnetic ordering, if any. The interplay between these factors can also be seen in "triple perovskites" with the general formula $A_{3-y}A'_yB_2B'O_9$, for example $La_3Ni_2SbO_9$ which we have recently investigated [1] . The structure of these compounds usually contains two alternating, crystallographically distinct six-coordinate sites that can accommodate the *B* and *B'* cations, but in the case of $La_3Ni_2SbO_9$ these cations occur in a 2:1 ratio, rather than 1:1, so they cannot form a completely ordered array. In fact one of the two sites is fully occupied by Ni^{2+} and the other by 33 % Ni^{2+}, 66 % Sb^{5+}, i.e. the cation distribution is as ordered as it can be given the stoichiometry but some disorder remains. Our ac and dc magnetometry studies both showed the presence of a spontaneous magnetisation below 105 K. A magnetisation of 1.5 μ_B per formula unit was measured at 2 K in a field of 40 kOe. This net magnetisation arises even though the coupling between neighbouring Ni^{2+} cations is antiferromagnetic because the two interacting sublattices are not equally populated by magnetic cations (100 % v 33 %). However, only very weak magnetic scattering was observed in neutron diffraction data collected at 5 K. It was proposed that, as a consequence of the cation disorder, $La_3Ni_2SbO_9$ behaves as a relaxor ferromagnet, analogous to a relaxor ferroelectric [2] , with magnetic domains too small to be detected by neutron diffraction forming below 105 K. The formation of domains was ascribed to the presence of local antimony-rich regions wherein the magnetic coupling between Ni^{2+} cations is disrupted, thus creating a domain wall. We argued that in these regions the variations in composition might lead to changes in the relative influence of NN and NNN interactions and hence to local spin frustration. In this contribution we shall present neutron scattering and electron microscopy data that support this model. We shall also discuss the magnetic properties of other new $A_{3-y}A'_yB_2B'O_9$ compositions, some of which show relaxor behaviour and some of which do not. The possible reasons for the variation in behaviour will be discussed.

---

[1] P.D. Battle, S.I. Evers, E.C. Hunter, M. Westwood, *Inorg. Chem.* 52 (2013) 6648.
[2] A.A. Bokov, Z.G. Ye, *Journal of Materials Science* 41 (2006) 31-52.

O12

Magnetic and Luminescent hybrid coordination networks based on imidazolium dicarboxylate salts and lanthanides.

Farger, Pierre (IPCMS-CNRS-UMR7504, Strasbourg, FRA); Gallart, Mathieu (IPCMS-CNRS-UMR7504, Strasbourg, FRA); Roger, Guillaume (IPCMS-CNRS-UMR7504, Strasbourg, FRA); Delahaye, Emilie (IPCMS-CNRS-UMR7504, Strasbourg, FRA); Rabu, Pierre (IPCMS-CNRS-UMR7504, Strasbourg, FRA)

Metal Organic Frameworks (MOFs) and hybrid coordination frameworks in general have been the subject of considerable research in recent years. This interest comes from the versatility and flexibility of their architecture as well as their potential application in many areas such as gas storage, catalysis, drug delivery…[1-3] More recently, MOFs have been put forward for their multiferroic properties which give them potential application for information storage.[4-7]
MOFs are often obtained by solvothermal reaction between metal salts and neutral ligand bearing coordination functions. In our group, we have focused on the synthesis of MOFs from imidazolium salts or ionic liquids (ILs) bearing carboxylate coordination functions to monitor the structural building process. This strategy has been successfully applied to transition metal salts giving rise to different coordination networks [8] and has been extended to lanthanides since they show a large variety of coordination sphere (unlike transition metal ions showing mainly tetrahedral or octahedral coordination sphere).

We will present in this communication our recent results concerning the synthesis, the crystal structure and characterization of new hybrid coordination networks based on imidazolium dicarboxylate salts or ILs and lanthanides (Ln^{3+} = Nd, Sm, Eu, Gd, Tb, Dy, Ho, Yb). We will focus particularly on the study of their magnetic and luminescent properties. Beyond the interest to explore new families of compounds, the incorporation of imidazolium salts with special functionalities into the coordination networks let glimpse the possibility to obtain new multiferroic materials.

---

[1] G. Férey, *Chem. Soc. Rev.* **2008**, 37, 191.
[2] P. Horcajada, C. Serre, M. Vallet-Regí, M. Sebban, F. Taulelle, G. Férey, *Angew. Chem. Int. Ed.***2006**, 45, 5974.
[3] M. Dinca, J. R. Long, *Angew. Chem. Int. Ed.***2008**, 47, 6766.
[4] G. Rogez, N. Viart, M. Drillon, *Angew. Chem. Int. Ed.***2010**, 49, 1921.
[5] A. K. Cheetam, C. N. Rao, *Science***2007**, 318, 58.
[6] M. Guo, H.-L. Cai, R.-G. Xiong, *Inorg. Chem. Commun.***2010**, 13, 1590.
[7] W.-J. Ji, Q. Zhai, S.-N. Li, Y.-C. Jiang, M.-C. Hu, *Chem. Commun.* **2011**, 47, 3834.
[8] P. Farger, R. Guillot, M. Gallart, F. Leroux, G. Rogez, E. Delahaye, P. Rabu. **Submitted**.

PL7

Automated electron Diffraction Tomography (ADT) – solving crystal structures from nano particles

Kolb, Ute (Johannes Gutenberg Universität, Mainz, GER)

The choice of an appropriate method for structural characterization of a material is strongly dependent on the achievable crystallinity. Single crystal X-ray diffraction, already developed into a standard method for crystal structure solution, is suitable for crystals down to the µm range. X-ray powder diffraction, the method of choice for smaller crystallites, became over the last years more and more popular but is still an expert's task if used for structure solution. Problems arise often from peak overlap due to big unit cells, space groups of low symmetry, some structures remain unsolved due to low data quality, impurity or structural complexity of the material. Electron radiation allows to sample much smaller volumes and to address single nano crystals but structure solution based on intensities from oriented electron diffraction patterns turned out to be extremely problematic mainly due to dynamical scattering effects. In addition the alignment of electron diffraction patterns is time consuming and difficult. Nevertheless, electron diffraction has been frequently used for indexing and assignment of impurity peaks to support the analysis of x-ray powder data affected by the above described problems. A major step towards improved electron diffraction intensities was the development of the precession technique by Vincent and Midgley in 1994 which has been used increasingly since then. These improved electron diffraction intensities can be used to complement powder diffraction data or to support the partitioning of overlapping peaks. In some cases, where an appropriate completeness of the reciprocal space could be achieved, PED data has been used for ab-initio structure analysis standalone through "direct methods" and maximum entropy methods. Automated electron Diffraction Tomography (ADT), an approach for 3D electron diffraction data acquisition and analysis, applies the idea to collect non oriented diffraction patterns in a tilt sequence around an arbitrary crystal axis with fixed tilt steps. In such a way the majority of the accessible reciprocal space can be scanned inside the tilt range of the microscope goniometer. To collect ADT data sets the crystal should be tracked by TEM/STEM) imaging to guarantee the correct diffraction volume. Nano electron diffraction patterns allow a mild illumination. ADT diffraction patterns cannot be analyzed manually. Thus dedicated software was programmed (ADT3D) reconstructing the three-dimensional reciprocal space for cell parameter determination and intensities extraction as well providing the chance to inspect the reciprocal space visually for the detection of crystallographic specialties such as disorder, twinning or polycrystallinity. Cell parameter determination, intensity extraction and detection of crystallographic specialities are straight forward and structure solution can be performed ab-initio by standard X-ray programs. This turned automated electron diffraction tomography into an approach which can be learned and performed in a reasonable time scale. Data sets collected by ADT are of higher quality than those collected by conventional electron diffraction based on oriented patterns. Dynamical effects are strongly reduced so that a standard kinematic approach (intensities proportional to Fhkl2) delivers ab-initio structure solutions. Reflection intensities may be further improved by integration coupling ADT with precession electron diffraction (PED). About 40 structures could be solved using ADT including inorganic, organic or hybrid material; some data sets originating from single nanocrystals down to 50 nm. Remarkably, large cell porous minerals, zeolites and beam-sensitive metal-organic frameworks could be accessed as well. Although structure refinement based on kinematical intensities turned out to be stable, achievable R values of only 20-30% are still high and final refinement should be performed based on X-ray powder data or via dynamically calculated intensities.

IL7

Put your trust in powder: new diffraction methods for studying functional materials

Evans, John (Department of Chemistry, Durham University, Durham, GBR)

Powder diffraction is one of the most powerful structural probes available to the solid state chemist. It invariably plays a critical role in the synthesis of new phases, and in-situ studies are increasingly exploited to understand and control complex synthetic routes to fleetingly stable materials. Ab initio structure solution followed by Rietveld refinement often provides the first structural information on new functional materials before they become available as single crystals. Powder diffraction is also the usual method of choice for probing structure-property relationships under non-ambient or in-operando conditions, or for following the structures of samples undergoing structural phase transitions associated with property changes.

In this invited talk I'll focus on new developments in powder diffraction analysis. I'll discuss how so-called "Symmetry Mode Rietveld Refinement" [1] can be an extremely efficient way of analysing the structures of inorganic materials. I'll use examples from our work on framework oxide and layered transition metal oxychalcogenides to illustrate how the technique allows complex superstructures to be solved and rationalised. If time permits I'll discuss how techniques such as "Parametric Rietveld Refinement" [2] can be used to extract accurate quantitative analysis on evolving systems when conventional independent Rietveld refinements fail.

---

[1] S. Kerman, B.J. Campbell, K.K. Satyavarapu, H. T. Stokes, F. Perselli and J. S. O. Evans, Acta Cryst., 2013, A68, 222–234.

[2] G.W. Stinton, J.S.O. Evans, Journal of Applied Crystallography, 2007, 40, 87–95.

O13

Structural and Electronic Changes During Li Uptake and Removal of Nanosized $CoFe_2O_4$ Revealed by a Detailed in operando X-ray Scattering and X-ray Absorption Spectroscopy Study

Bensch, Wolfgang (Christian-Albrechts-Universität zu Kiel, Kiel, GER)

Much is speculated in literature about the reaction mechanisms occurring during Li uptake/removal of oxidic spinels. An *in operando* XRD and XAS study of the Li insertion and extraction using nanosized $CoFe_2O_4$ as anode material revealed a detailed picture of the different mechanistic reaction steps from the initial Li-uptake until full conversion of the spinel. First a minute amount of Li is inserted into the surface of the nanoparticles being accompanied by a slight expansion of the lattice parameter.

After insertion of two Li per formula unit the spinel structure is converted to a NaCl-like arrangement of the ions. During this reaction step Fe^{3+} is reduced to Fe^{2+} and all cations moved from the tetrahedral sites to the empty octahedral sites. Increasing the Li content the NaCl-like structure is amorphized and simultaneously reduction of Fe^{2+}/Co^{2+} to the metallic state occurs. At the end of discharging nanosized metal particles are embedded in a Li_2O matrix. During the charge process the spinel structure is not recovered. In the first few charge/discharge cycles Fe/Co are reoxidized to Fe^{3+}/Co^{2+} while during further cycling the nanoparticles of metallic Co cannot be reoxidized. This observation suggests that at least the inability of reoxidation of Co is responsible for the capacity loss observed during the investigations. Taking into account results about conversion reactions using MFe_2O_4 (M = Mg, Mn, Fe, Co, Ni, Cu) as anode materials presented in literature, a general reaction pathway for these materials can be formulated.

O14

Complex crystal structure and oxide ion conductivity in the hexagonal perovskite derivative $Ba_3MoNbO_{8.5}$

Fop, Sacha (University of Aberdeen, Aberdeen, GBR); McLaughlin, Abbie C. (The Chemistry Department, Meston Building, University of Aberdeen, Aberdeen, GBR); Skakle, Jan (The Chemistry Department, Meston Building, University of Aberdeen, Aberdeen, GBR)

In the last years, intensive research in finding new electrolytic materials for solid oxide fuel cell (SOFC) applications has led to the discovery of several fast oxide ion conductors [1]. Efforts are being made to lower SOFCs' operating temperature to an intermediate range (400 – 600 °C) [2] to widen their possible field of employment and to reach this goal it is important to discover new structural families of oxide ion conducting materials. As the oxide ion conductivity is strongly dependent on the crystal structure, the perovskite family seems to offer the perfect playground thanks to its capability of adopting numerous structural derivatives. Despite several perovskite materials with significant oxide ion conductivity have already been reported [3, 4], thus far there has been no account of a solid oxide conductor that crystallises with the hexagonal perovskite structure. Hexagonal perovskites form when BO_6 octahedra share faces and different stacking sequences of the cubic (corner-sharing BO_6 octahedra) and hexagonal (face-sharing BO_6 octahedra) AO_3 layers can give rise to different crystal structures.

Here we present the average crystal structure of the hexagonal perovskite derivative $Ba_3MoNbO_{8.5}$, which has previously been described to have intrinsic oxygen vacancies and intertwined regions of Mo/NbO_6 octahedra and Mo/NbO_4 tetrahedra [5]. Rietveld refinement of neutron powder diffraction data shows that $Ba_3NbMoO_{8.5}$ forms in a hybrid structural model formed by the superimposition of two sub-structural units (a 9R hexagonal polytype and palmierite unit), with disorder in the oxygen sub-lattice. Impedance spectroscopy experiments proved that the system is able to support ionic conductivity, as revealed by the presence of a Warburg response in the complex plane plots highlighting a polarisation phenomenon associated with ionic diffusion at the interface between the electrolyte and the electrodes. The ionic nature of the conductivity was confirmed by concentration cell experiments which gave ionic transport number values close to unity in both O_2/Air and 5% H_2 in Ar/Air atmospheres (0.99 and 0.92 at 600 °C respectively). With a bulk conductivity of $1.83 \cdot 10^{-3}$ S/cm at 600 °C, comparable to other prominent oxide ion conductors, $Ba_3MoNbO_{8.5}$ is the first fast oxide ion conductor in the hexagonal perovskites family that could pave the way to the design of a new class of solid oxide fuel cell electrolytes.

---

[1] L. Malavasi, C. A. J. Fisher and M. S. Islam, *Chem. Soc. Rev.* 39, 4370 – 4387 (2010).

[2] E. D. Wachsman and K. T. Lee, *Science* 334, 935 – 9 (2011).

[3] T. Ishihara, H. Matsuda and Y. Takita, *J. Am. Chem. Soc.* 116, 3801 – 3803 (1994).

[4] M. Li, M. Pietrowski, R. A. De Souza, H. Zhang, I. M. Reaney, S. N. Cook, J. A. Kilner and D. C. Sinclair, *Nat. Mater.* 13, 31 – 35 (2013).

[5] E. García-González, M. Parras and J. M. González-Calbet, *Chem. Mater.* 10, 1576 – 1581 (1998).

PL8

Recent advances on insertion materials for better Li-ion batteries.

TARASCON, Jean Marie (Collège de France / Réseau sur le Stockage Electrochimique de l¿Energie (RS2E), Paris , FRA)

Rechargeable lithium ion batteries, because of their high energy density, have conquered most of today's portable electronics and they stand as serious contenders for EV's and grid applications. For the latter to happen, we still need to increase their energy density while making them greener and more sustainable. This is a formidable challenge. Electrode reactions in Li-based technologies are based on the reversible insertion/deinsertion of Li^+ ions into a host material with the concomitant addition/removal of electrons. Such reactions being intrinsically limited to 1 e- per 3d-metal, there is a quest for new materials and new concepts, both of which will be addressed in this presentation.

Firstly, our strategy towards the design of novel high voltage polyanionic compounds [1] involving either Li or Na-based fluorosulfates, sulfates and oxysulfates such as $Li_2CuO(SO_4)_2$ will be described together with i) their electrochemical performance and ii) their ionic conductivities which will be discussed through the Bond Valence Energy Landscape approach.

Turning to new concepts, great hope is presently placed on the Li-rich $Li[Li_xNi_yCo_zMn_{1-x-y-z}]O_2)$ layered electrodes, coined Li-rich NMC, which show staggering capacities of 280 mAh/g as compared to 15 mAh/g for $LiCoO_2$. We will show via the use of structurally related Li2Ru1-ySnyO3 materials [2], combined with the use of complementary techniques (XPS, EPR) [3], that this large capacity results from cumulative cationic and anionic redox processes, hence ending 25 years of belief that insertion reactions solely rely on cationic redox reactions. Therefore, the poor kinetics and large voltage decay of such electrodes upon cycling have plagued their implementation in practical Li-ion cells. Using chemically substituted $Li_2Ru_{1-y}Ti_yO_3$ electrodes we established [4], from *ex-situ* high angle annular dark field scanning transmission electron microscopy imaging (HAADF-STEM), the origin of the voltage decay, which is nested in ionic radii considerations and size bottleneck issues. Lastly, pursuing our chemical substitution work we could design [5] model compounds which enable, for the first time, the visualization, by both microscopy and neutron diffraction, of the perroxo (O-O) dimers involved in the reversible redox process. 11, place Marcelin Berthelot, 75005 Paris CEDEX, FRANCE

The discovery of anionic redox activity among oxides represents a transformational approach for creating advanced electrode materials. However, as is often the case with new discoveries, the fundamental science at work needs to be rationalized and understood. Specifically, what are the mechanisms for ion and electron transport in these Li-driven anionic redox reactions? Mastering these issues, which will require the integration of computational and analytical tools, is a must to harvest all the advantages of this new class of high capacity electrodes and enable their implementation in the next generation of Li-ion cells.

---

[1] G. Rousse, J.M. Tarascon, *Chemistry of Materials*, 26(1), 394, 2014.
[2] M. Sathiya, G. Rousse, K. Ramesha, C.P. Laisa...and J.M. Tarascon J-M, *Nature Materials, 12*, 827, 2013.
[3] M. Sathiya, J.B. Leriche, E. Salager, D. Gourier, J.M. Tarascon, and H. Vezin, *Nature Communications*, February 2015
[4] M. Sathiya, A.M. Abakumov, D. Foix, G. Rousse… and J.M. Tarascon*, Nature Materials* 14, 230–238 (2015)
[5] E. McCalla et al. to be submitted

IL8

Ionic and electronic transport in solid oxide cells – Seen from an applied perspective

Hagen, Anke (Department of Energy Conversion and Storage / Risø Campus, Roskilde, DNK)

Solid oxide fuel and electrolysis cells (SOCs) are considered key technologies in future energy systems dominated by the production of electricity from fluctuating renewable sources.
SOCs are composite devices, where the single components have to fulfil different functions such as catalytic activity for the respective reactions, transport of ions, electrons, and gasses, etc. Ionic and electronic conductivity are important properties for the choice of materials for those components and determine the optimum operating conditions, in particular temperature. The presentation will show that there are – in addition to materials choice - more dimensions to consider in order to achieving high performing and durable SOCs.

One such dimension is structuring. By adjusting optimum particle sizes and distributions, degree of percolation, etc. for a given material, key performance parameters can be affected significantly. The challenge is to identify, understand, and achieve these optimal structural properties, preferably on real SOCs and to validate under real operating conditions.

The presentation will give examples for the interplay between materials (such as ionic and electronic conduction) and structural properties (such as percolation) and how these are assessed on solid oxide cells by advanced electrochemical and microstructural characterization methodology.

O15

Lithium ion dynamics in amorphous Li-Si electrochemically prepared from semiconductor grade, monocrystalline silicon - An NMR Study

Dunst, Andreas (TU Graz, CD Laboratory for Li Ion Batteries, Graz, AUT); Sternad, Michael (TU Graz, CD Laboratory for Li Ion Batteries, Graz, AUT); Epp, Viktor (TU Graz, CD Laboratory for Li Ion Batteries, Graz, AUT); Wilkening, Martin (TU Graz, CD Laboratory for Li Ion Batteries, Graz, AUT)

Silicon is one of the most promising anode materials for lithium-based rechargeable batteries. Provided the volume changes during Li uptake can be brought under control, Li ion diffusivity is expected to crucially determine the performance of such energy storage systems. Therefore, studying diffusion properties in amorphous Li-Si underpins applied research that is being directed towards the development of powerful storage devices. So far, only little information is available on Li self-diffusion in amorphous Si. Here, we used 7Li NMR spectroscopy [1] to precisely quantify microscopic activation energies and Li jump rates in amorphous Li-Si which is primarily formed if monocrystalline Si is lithiated electrochemically. Our results reveal relatively fast Li diffusivity with an average activation energy for long-range ion transport as high as ca. 0.65 eV; jump rates turn out to be in the order of 2.5 × 105 1/s at 246 K, see also ref. [2]. Comparisons with data from laboratory frame NMR relaxometry, which is sensitive to more localized ion hopping, points to complex dynamics that is most likely governed by non-exponential motional correlation functions originating from a large distribution of activation energies. Preliminary 6Li MAS NMR measurements helped characterize local structures in the amorphous sample. We found indications that at temperatures below 373 K, Li12Si7 is formed during our MAS NMR experiments performed at a spinning speed of 30 kHz. The formation of structural motifs of the binary Zintl phase was verified by ex situ X-ray powder diffraction. Noteworthy, a second sample, which is a mixture of amorphous Li-Si and metastable, crystalline Li15Si4 that forms at lower discharge potentials, points to Li diffusivity (0.51 eV) being comparable with that of the amorphous sample. The data obtained might help optimizing Li-based silicon batteries whose performance critically depend on fast Li-ion transport.

Acknowledgement. Financial support by the Federal Ministry of Science, Research and Economy and the National Foundation for Research, Technology and Development is gratefully acknowledged.

---

[1] V. Epp, M. Wilkening, Phys. Rev. B 82 (2010) 020301.

[2] A. Kuhn, P. Sreeraj, R. Pöttgen, H.-D. Wiemhöfer, M. Wilkening, P. Heitjans, J. Am. Chem. Soc. 113 (2011) 11018.

O16

Influence of alumina content on Na^+/K^+ interdiffusion in soda silicate glasses

Ragoen, Céline (Université Libre de Bruxelles, Bruxelles, BEL); Godet, Stéphane (Université Libre de Bruxelles, Bruxelles, BEL); Lambricht, Thomas (AGC Flat Glass Europe, Gosselies, BEL); Scheyvaerts, Florence (AGC Flat Glass Europe, Gosselies, BEL)

The fantastic technological potential and the increasing demand of touch screens is an important driving force for the glass industry to continuously improve and understand the mechanical properties of thin glass sheets. While traditional thermal tempering is well suited for thick (i.e >5mm) sheets, chemical strengthening is the solution to improve both the impact and scratch resistance of thinner sheets. The process consists in exchanging smaller hosts alkali ions such as Na+ by larger ions such as K^+. The exchange is performed in a molten salt at a temperature below the glass transition temperature, leading to the formation of a compression layer at the glass surface that tremendously improves the glass resistance.

Alkali aluminosilicate glasses are most widely used in the glass industry to produced high resistant ionic exchanged glasses. Indeed, they allow achieving both a high surface compressive stress and a large compression layer in reasonable treatment times. There is however a lack of fundamental understanding regarding the exact role of alumina on the interdiffusion processes
In the present work the effect of the alumina content on the Na^+/K^+ interdiffusion in soda silicate glasses was scrutinized together with the associated mechanical properties, such as surface hardness and compressive strength. Moreover, an important characterization effort was carried out in order to correlate the interdiffusion processes to the glass structure.

Consequently, the diffusion profiles were analyzed by Energy dispersive X-Ray spectroscopy in a scanning electron microscope. This enabled the depth of the compression layer to be determined and the interdiffusion coefficients of the different glasses to be calculated.
The mechanical properties of the chemically tempered glasses have been mainly evaluated by nanoindentation. Hardness profiles were measured and were found to compare well with the diffusion profiles. The compressive stress was evaluated by optical methods.

The change in interdiffusion coefficients and mechanical properties with the alumina content is shown to have a structural origin. This was studied by density measurements and DSC analysis. The free volume in the glass is an important parameter that influences the diffusion properties of cations. Moreover, the glass transition temperature affects, inter alia, the relaxation phenomena.

PL9

Superconductivity at 195 K and other results of application of megabar pressures

Eremets, Mikhail (Max-Planck Institut fur Chemie, Chemistry and Physics at High Pressures Group, Mainz, GER)

Megabar pressures dramatically changes interatomic distances in materials eventually leading to phase transformation. Molecular nitrogen, for instance, transforms to a polymer where nitrogen atoms are single bonded. Sodium ? simple metal ? becomes transparent at pressures of ≈200 GPa transforming into ionic- electride-like state. The main focus of the presentation is search for high temperature superconductivity in pressure induced metals. We found that sulfur hydride transforms at P~90 GPa to metal and superconductor with the record critical temperature of superconductivity (T_c) of 195 K at P~150 GPa (arXiv:1412.0460). This superconductivity is likely related to higher hydrides H_nS (n>2) formed due to the dissociation of H_2S. We proved occurrence of superconductivity by the sharp drop of the resistivity at least 50 times lower than the copper resistivity and the decrease of T_c with magnetic field. The isotope shift of T_c in D_2S consists with predictions of the BCS theory and indicates a major role of phonons in the superconductivity. We will discuss these results in connection to metallic hydrogen too.

IL9

High-pressure high-temperature synthesis of simple oxides

Ovsyannikov, Sergey (Bayerisches Geoinstitut, Universität Bayreuth, Bayreuth , GER)

High-pressure high-temperature (HP-HT) synthesis is known to be a powerful tool for preparation of new unique materials and phases of which properties can be very different from those of their ambient pressure analogues. We show that HP-HT synthesis of simple binary oxides can lead to surprising dense polymorphs, e.g., perovskite-type Mn_2O_3 [1] with unique semiconducting properties [2], Th_2S_3-type Ti_2O_3 of shiny golden color [3,4], and others. We also demonstrate that HP-HT synthesis can stabilize simple oxides in unusual stoichiometry and display examples on iron oxides.

---

[1] S. V. Ovsyannikov, A. M. Abakumov, A. A. Tsirlin, W. Schnelle, R. Egoavil, J. Verbeeck, G. Van Tendeloo, K. Glazyrin, M. Hanfland, and L. Dubrovinsky, Angewandte Chemie Intl. Ed. 52, 1494 (2013).

[2] S. V. Ovsyannikov, A. E. Karkin, N. V. Morozova, V. V. Shchennikov, E. Bykova, A. M. Abakumov, A. A. Tsirlin, K. V. Glazyrin, and L. Dubrovinsky, Advanced Materials 26, 8185 (2014).

[3] S. V. Ovsyannikov, X. Wu, A. E. Karkin, V. V. Shchennikov, and G. M. Manthilake, Physical Review B 86, 024106 (2012).

[4] S. V. Ovsyannikov, X. Wu, G. Garbarino, M. Núñez-Regueiro, V. V. Shchennikov, J. A. Khmeleva, A. E. Karkin, N. Dubrovinskaia, and L. Dubrovinsky, Physical Review B 88, 184106 (2013).

O17

Ultra-High Pressure Synthesis and Characterization of Transition Metal Nitrides

Hasegawa, Masashi (Department of Crystalline Materials Science, Nagoya University, Nagoya, JPN); Niwa, Ken (Department of Crystalline Materials Science, Nagoya University, Nagoya, JPN); Terabe, Toshiki (Department of Crystalline Materials Science, Nagoya University, Nagoya, JPN); Suzuki, Kentaro (Department of Crystalline Materials Science, Nagoya University, Nagoya, JPN); Shirako, Yuichi (Department of Crystalline Materials Science, Nagoya University, Nagoya, JPN); Muto, Shunsuke (EcoTopia Science Institute, Nagoya University, Nagoya, JPN); Tatsumi, Kazuyoshi (EcoTopia Science Institute, Nagoya University, Nagoya, JPN); Mizui, Tatsuya (Department of Quantum Engineering, Nagoya University, Nagoya, JPN); Soda, Kazuo (Department of Quantum Engineering, Nagoya University, Nagoya, JPN); Kikegawa, Takumi (Photon Factory, High Energy Accelerator Research Organization, Tsukuba , JPN)

Metal nitrides, especially transition metal nitrides, have been studied from the viewpoints of not only fundamental chemistry and physics but also materials science and engineering because they have attractive chemical and physical properties, such as eminent hardness, distinguished catalytic capability, unique superconductivity, peculiar magnetism and so on. Therefore, they, particularly, nitrogen-rich metal nitrides are paid the most attention to now. High pressure synthesis technique recently provides us a lot of novel ones such as Zr_3N_4, Hf_3N_4 and so on [1]. A diamond anvil cell usually called DAC, is a well-used small ultra-high pressure generation apparatus. It can be easily combined with a laser heating system and the combined system is called LH-DAC. It is a powerful tool to synthesize various kinds of nitrogen-rich metal nitrides because one can utilize a direct nitriding chemical reaction between metal and nitrogen supercritical fluid in a closed sample space in DAC [2-6]. For example, platinum group pernitrides have been successfully synthesized in high pressures and temperatures using this system [7-10]. We have also recently reported the first syntheses of RhN_2 and RuN_2 pernitrides by using the original LH-DAC system [11,12]. Although these are all novel nitrides and lead to grow new fundamental and applied chemistry and physics, there still remain various indistinct points since they are difficult to be characterized because of the extremely tiny size of the synthesized samples. In this study, various kinds of advanced analytical experiments have proceeded systematically in order to investigate the nature of chemical bonding between platinum group metal and nitrogen atoms in these per nitrides. Nitride samples were synthesized by the LH-DAC system and characterized by the synchrotron X-ray diffraction and Raman scattering measurements under both high and ambient pressures. The chemical bonding states between metal and nitrogen atoms of the ambient recovered sample were analyzed by TEM-EELS and synchrotron XPS. It has been found from the high pressure in-situ synchrotron XRD that RhN_2 and RuN_2 show more compressible than the other platinum group pernitrides. This is qualitatively same as the predicted one by theoretical calculation study [13]. Besides, it is also found that Ru d is weakly hybridized with N p. On the other hand, the large shift of binding energy for Ir 4f is observed in the spectrum of IrN2. These systematic experiments and analyses have clarified that their bulk moduli strongly depend on the binding energy between the transition metal and nitrogen atoms.

---

[1] A. Zerr, G. Miehe and R. Riedel, Nature Mater., 2, 185(2003).
[2] M. Hasegawa, T. Kondo and T. Yagi, Proc. 43th Symp. on Synthetic Crystals, 43, 107 (1998).
[3] M. Hasegawa and T. Yagi, J. Crystal Growth, 217, 349 (2000).
[4] M. Hasegawa and T. Yagi, Solid State Commun., 135, 294 (2005).
[5] M. Hasegawa and T. Yagi, J. Alloys Comp., 403, 131 (2005).
[6] K. Niwa, M. Hasegawa and T. Yagi, J. Alloys Comp., 477, 493 (2009).
[7] E. Gregoryanz, C. Sanloup, M. Somayazulu, J. Badro, G. Fiquet, H. K. Mao and R.J. Hemley, Nature Mater. 3, 294 (2004).
[8] J. C. Crowhurst, A. F. Goncharov, B. Sadigh, C. L. Evans, P. G. Morrall, J. L. Ferreira and A. J. Nelson, Science 311, 1275 (2006).
[9] A. F. Young, C. Sanloup, E. Gregoryanz, S. Scandolo, R. J. Hemley and H. K. Mao, Phys. Rev. Lett. 96, 155501 (2006).
[10] J. C. Crowhurst, A. F. Goncharov, B. Sadigh, J. M. Zaug, D. ?berg, Y. Meng and V. B. Prakapenka, J. Mater. Res. 23, 1 (2008).
[11] K. Niwa, D. Dzivenko, K. Suzuki, R. Riedel, I. Troyan, M. Eremets and M. Hasegawa, Inorg. Chem. 53, 697 (2014).
[12] K. Niwa, K. Suzuki, S. Muto, K. Tatsumi, K. Soda, T. Kikegawa and M. Hasegawa, Chemistry-A European Journal 20, 1 (2014). 13. R. Yu, Q. Zhan and L. C. De Jonghe, Angew. Chem. Int. Ed., 46, 1136 (2007).

O18

Exploring hydrothermal environments at gigapascal pressures for materials synthesis

Spektor Kristina (Stockholm University, Stockholm, SWE, Arizona State University, USA);
Leinenweber Kurt (Stockholm University, Stockholm, SWE);
Häussermann, Ulrich (Stockholm University, Stockholm, SWE)

Hydrothermal reactions play an important role in materials synthesis and geochemistry [1]. Extending their pressure range to the gigapascal regime gives opportunities for the synthesis of truly novel materials. Extreme water environments may alter decisively thermodynamic relations (such as solubilities, mixing behaviors, solid – fluid reaction equilibrium constants) and also kinetics for reactions and phase transitions (e.g. through modified (hydroxylated) surfaces). In this case water serves as catalyst, promoting new reactions. However water may as well act as reactant and incorporate e.g. in oxide materials according to H_2O (fluid) + O (oxide) = 2 OH (oxide).

We adapted multi anvil techniques to access aqueous fluids in a pressure range from 2.5 to 10 GPa and at temperatures up to 1000 °C [2]. Initial experiments involved the treatment of amorphous SiO_2 and coesite with water at 10 GPa and at temperatures between 300 °C and 550 °C, which resulted in the formation of ultra-hydrous stishovite. This form of stishovite contains up to several wt.% of water. According to ^1H NMR experiments, there is strong evidence that the primary mechanism for the H_2O uptake is a direct hydrogarnet-like substitution of $4H^+$ for Si^{4+}, with the protons clustered as hydroxyls around a silicon vacancy [3]. Temperature dependent NMR experiments reveal pronounced proton dynamics. The potential of extreme water for materials synthesis is further demonstrated by the hydrothermally catalyzed transition of titania from rutile to TiO_2-II.

---

[1] G. Demazeau, J. Mater. Sci. **43**, 2104 (2008).

[2] E. Stoyanov, U. Häusserman, K. Leinenweber, High Pressure. Res. 30, 175 (2010).

[3] K. Spektor, J. Nylen, E. Stoyanov, A. Navrotsky, R. L. Herwig, K. Leinenweber, G. P. Holland, U. Häussermann Proc. Nat. Acad. Soc. 108, 20918, (2011).

Poster Presentations

PMon001

Ab initio calculated energy of formation of chromium Laves phases in phase equilibrium calculations

Vrestal, Jan (Masaryk University, Brno, CZE); Pavlu, Jana (Masaryk University, Brno, CZE); Sob, Mojmir (Masaryk University, Brno, CZE)

Phase diagrams of many systems exhibit three polytypes of Laves phases (phases with composition A2B): C14, C36 and C15. At high temperatures, the C14 is the equilibrium phase, C15 is stable at low temperatures, and C36 in between. Ab initio calculations give usually similar stability sequence at zero Kelvin temperature with the C15 as the most stable and C14 the least stable structure (again with the C36 structure in between). In the present contribution, the phenomenon described above is analyzed in Cr-Nb, Cr-Ta, Cr-Hf, Cr-Ti, and Cr-Zr systems with the help of temperature dependence of the difference of heat capacities at constant pressure, which is calculated as difference of heat capacity of Laves phase and heat capacities of standard element reference phases. Comparison of published phenomenological assessments [1-3] with experimental data reveals good mutual agreement.

Financial support of Czech Science Foundation by grant No. GA14-155765, and "CEITEC – Central European Institute of Technology" (CZ.1.05/1.1.00/02.0068) from the European Regional Development Fund is gratefully acknowledged.

---

[1] Re-modeling of Laves phases in the Cr-Nb and Cr-Ta systems using first-principles results Pavlu J., Vrest'al J., Sob M.: CALPHAD-COMPUTER COUPLING OF PHASE DIAGRAMS AND THERMOCHEMISTRY, 33 (1) 179-186 (2009)

[2] Stability of Laves phases in the Cr-Zr system Pavlu J., Vrest'al J., Sob M.: CALPHAD-COMPUTER COUPLING OF PHASE DIAGRAMS AND THERMOCHEMISTRY, 33 (2) 382-387 (2009)

[3] Thermodynamic modeling of Laves pohases in th Cr-Hf and Cr-Ti systems: Reassessment using first-principle results. Pavlů J., Vřešťál J., Šob M.: CALPHAD-COMPUTER COUPLING OF PHASE DIAGRAMS AND THERMOCHEMISTRY, 34 (1) 215-221 (2010)

PMon002

Interactions between Sn-Zn solders and Ni-substrates – the Ni-Sn-Zn system

Schmetterer, Clemens (Fraunhofer UMSICHT Institute Branch Sulzbach Rosenberg, Sulzbach-Rosenberg, GER); Rajamohan, Divakar (University of Vienna, Dep. Inorganic Chemistry / Materials Chemistry, Vienna, AUT); Effenberger, Herta Silvia (University of Vienna, Institut für Mineralogie und Kristallographie, Vienna, AUT); Flandorfer, Hans (University of Vienna, Dep. Inorganic Chemistry / Materials Chemistry, Vienna, AUT)

Within the efforts to replace conventional Pb-free solders, Sn-Zn-based alloys have gained attention as possible alternatives. During soldering, the solder chemically reacts with the contact material to form potentially brittle intermetallic phases. As Ni is frequently used as a contact material, knowledge about the Ni-Sn-Zn system is important to describe the behavior of the relevant material combinations. In the present contribution, a largely extended and up-dated Ni-Sn-Zn phase diagram was established based on earlier literature data and a series of new experimental results. The Ni-Sn-Zn system is characterized by the existence of six ternary compounds and large homogeneity ranges of the binary compounds. Close structural relations exist between the ternary compounds and neighboring binary phases. The phase diagram was established based on the available data from experimental results of investigation by SEM/EDX, powder and single-crystal XRD and DTA. Several isothermal structures in the temperature range from 250 to 1100 °C, the reactions scheme, liquidus projection and vertical sections will be shown.

PMon003

Powder Preparation from the nano to the micrometer scale

Schmetterer, Clemens (Fraunhofer UMSICHT Institute Branch Sulzbach Rosenberg, Sulzbach-Rosenberg, GER); Wolf, Gerhard (Fraunhofer UMSICHT, Institute Branch Sulzbach Rosenberg, Sulzbach-Rosenberg, GER); Masset, Patrick (Fraunhofer UMSICHT, Institute Branch Sulzbach Rosenberg, Sulzbach-Rosenberg, GER)

Many modern and innovative production processes use powder materials as feedstock, such as hot isostatic pressing (HIP), powder injection molding (PIM), and additive manufacturing (AM). Each of these processes imposes specific requirements on the powder materials because their properties significantly influence the manufacturing processes and quality of the manufactured components. E.g. in powder bed based AM processes, micro meter sized powders with excellent flow properties are needed in order to achieve a homogeneous powder bed. This means that the individual powder particles must have a spherical shape and must be free from satellites. Nano sized powders open up entirely new possibilities in terms of applications and functionalities, e.g. in coating technology, surface engineering, catalysis and sintering. While it is evident that powders must fulfill the requirements of the process, their properties are governed to a large extent by the production route. Typical techniques for the targeted preparation of powder materials are e.g. mechanical methods, melt atomization techniques or electrochemical methods. In this contribution the characteristics of powders prepared from these methods will be shown (e.g. particle size and distribution) as well as the material and process parameters influencing their properties (e.g. melting behavior). Knowledge of this factors is essential for the targeted design of powder materials. Examples for the various powder preparation techniques, the powder materials and applications of these powders will be given.

PMon004

Structure transformations during Co/Sn solid/liquid interfacial reactions

Yakymovych, Andriy (Institut für Anorganische Chemie (Materialchemie), Wien, AUT); Plevachuk, Yuriy (Dept Metal Physics,National Ivan Franko University, Lviv, UKR); Richter, Klaus W. (Dept Inorg Chem (Mater Chem), University of Vienna, Vienna, AUT)

The interfacial reactions between pure Co and Sn are examined in this study. The wettability of the Co substrate by liquid Sn in the extended temperature range between the melting point of pure Sn and 523 K was investigated. The formation and growth of intermetallic compounds in the reaction zone was evaluated and the wetting angle between liquid Sn and the Co was determined with different methods. After the wettability measurements, the interface cross-sections of the samples were studied by the optical and electron microscopy. The metallographic investigations allowed determining the thickness and composition of the interfacial layers. According to the obtained results, the intermetallic compound $CoSn_3$ is formed in the reaction zone.

PMon005

A Multicomponent Approach to Structurally Complex Zintl Phases for Energy Applications

Lidin, Sven (Lund University, Lund, SWE); Miller, Gordon J. (Department of Chemistry, , AMES, USA); Ponou, Simeon (Department of Chemistry, Lund University, Lund, SWE)

The most common and successful strategy to increase the efficiency of thermoelectric (TE) materials has been to modifying a promising compound by the introduction of point defects through alloying.1 The resulting isostructural solid solutions have much lower lattice thermal conductivity due to the phonon scattering at those point defects. Nevertheless a minimum in the thermal conductivity is reached at some composition which is called the “alloy limit”.2 In a bottom up approach, nano-structuring of the promising TE compounds have led to the best performing materials according to experimental results, due to additional phonon scattering at the grains boundaries.3 Hence, the design of new functional compounds with increasingly complex structure and composition has become one of the major focuses in material sciences. Thus, new high efficient TE materials by design may be accomplished by rational approaches like combining simple building blocks in one single crystal lattice. Due to their narrow band gap and semiconducting properties, Zintl phases are best candidate materials for TE applications.4 In this context, multicomponent compounds with two or more Zintl anions in their crystal structure are intuitively ideal materials to display higher degree of structural complexity and hence, enhanced TE performance. An additional interest of this multicomponent approach is the inherent ability to combine two or more functional building units in the same crystal lattice. Here, each building block offers opportunity to fine-tune specific physical properties of the material.

In this report, we will present some newly obtained compounds illustrating this multicomponent approach, as well as the rational for their synthesis which underscores several challenges including the difficult crystallographic studies of their highly complex structures with huge unit cells, the lattice potential gradient arising from the Madelung energy and packing frustrations.

PMon006

Ab initio and CALPHAD modelling of Laves phases in Mn-based systems

Pavlu, Jana (CEITEC and Faculty of Science, Masaryk University, Brno, AUT); Vrestal, Jan (CEITEC and Faculty of Science, Masaryk University, Brno, CZE); Broz, Pavel (CEITEC and Faculty of Science, Masaryk University, Brno, CZE); Mazalova, Martina (Faculty of Science, Masaryk University, Brno, CZE); Sob, Mojmir (CEITEC and Faculty of Science, Masaryk University, Brno, CZE)

Mn-based systems play an important role in modern materials. Mn and Ta are used in thermoelectric coolers at low temperatures and Mn-Ti system is considered as hydrogen storage material. A good knowledge of phase relations in both Mn-Ta and Mn-Ti systems is therefore crucial for thermodynamic prediction for higher-order systems. From this reason the combined ab initio and CALPHAD modelling of Laves phases was performed including the results of previous studies (Mn-Ta [1-5], Mn-Ti [6-9]).

This work presents new ab initio data which were included in thermodynamic assessments of the above mentioned systems and calculated phase diagrams. The comparison of calculations with recent experimental data [1,10] is presented.

This research was supported by the Czech Science Foundation (Project No. GA 14-15576S), by the Project CEITEC–Central European Institute of Technology (CZ.1.05/1.1.00/02.0068) from the European Regional Development Fund, and by the Ministry of Education, Youth and Sports of the Czech Republic (project MOBILITY 7AMB15AT002). Access to computing and storage facilities owned by parties and projects contributing to the National Grid Infrastructure MetaCentrum, provided under the programme "Projects of Large Infrastructure for Research, Development, and Innovations" (LM2010005), is greatly appreciated.

---

[1] S.V.Meschel, P.Nash, X.-Q. Chen : J. Alloys Compd., 492 (2010) 105

[2] A.K. Niesen, F.R. de Boer, R.Boom, P.F de Chatel, W.C.Mattens, A.R.Miedema: Calphad 7 (1983) 51

[3] C.Colinet, A.Pasturel, P.Hicter: Calphad 9 (1985) 71

[4] P.E.A. Turchi, V. Drchal, J. Kudrnovský, C. Colinet, L. Kaufman, Z.-K. Liu: PRB 71 (2005) 094206

[5] L. Kaufman: Calphad 15 (1991) 243

[6] J.L. Murray (Ed.), The Mn-Ti system, In: Phase diagrams of Binary Titanium Alloys, ASM International, Materials Park, Ohio, 1987, p.159

[7] N. Saunders. System Mn-Ti. In: I. Ansara, T. Dinsdale, M.H. Rand (Eds.), COST 507, Thermochemical Database for Light Metal Alloys. Vol. 2, EUR 18499EN, European Commission, Luxemburg, 1998, p. 241

[8] R. Krendelsberger et al., Experimental Investigation and Thermodynamic Calculation of the Mn -Ti System, unpublished work, University of Vienna, Austria,1997

[9] X.Q. Chen et al., Acta Mater. 51 (2003) 1239

[10] A.U. Khan, Phase relations and crystal structure study in various Ti, Al and Si-based systems, PhD Thesis, University of Vienna, Institute of Physical Chemistry, Austria, November 2011

PMon007

$Ba_3Pt_4Al_4$ - A Complex Platinide with a Pt/Al Framework Featuring Heterocubane [Pt_4Al_4] Units

Stegemann, Frank (Institut für Anorganische und Analytische Chemie, Westfälische Wilhelms-Universität Münster, Münster, GER); Benndorf, Christopher (Institut für Anorganische und Analytische Chemie, Institut für Physikalische Chemie - Westfälische Wilhelms-Universität Münster, Münster, GER); Bartsch, Timo (Institut für Anorganische und Analytische Chemie, Westfälische Wilhelms-Universität Münster, Münster, GER); St. Touzani, Rachid (Institut für Anorganische Chemie, RWTH Aachen, Aachen, GER); Bartsch, Manfred (Physikalisches Institut, Universität Münster, Münster, GER); Zacharias, Helmut (Physikalisches Institut, Universität Münster, Münster, GER); Fokwa, Boniface P. T. (Institut für Anorganische Chemie, RWTH Aachen, Aachen, GER); Eckert, Hellmut (Institut für Physikalische Chemie, Westfälische Wilhelms-Universität Münster, Münster, GER); Janka, Oliver (Westfälische Wilhelms-Universität Münster, Münster, GER)

The number of intermetallic compounds in the systems *AE*-*T*-Al (*AE* = alkaline earth, *T* = platinum group metal) is quite manageable. Besides the equiatomic compounds CaPdAl (CaPdAl type) [1, 2] and CaPtAl (TiNiSi type) [3] the Al-rich compounds $AENi_2Al_9$ (*AE* = Sr, Ba; $BaFe_2Al_9$ type) [4], $CaNiAl_9$ (own structure type) [5], $CaNi_2Al_8$ ($CaFe_2Al_8$ type) [6] and $CaPd_3Al_5$ (own structure type) [7] are known. Furthermore Mg_3T_2Al (*T* = Ni, Pt; Mn_3Ni_2Si type) [8-10], $Be_2Ni_{0.5}Al_{0.5}$ ($MgCu_2$ type) [11] and $Mg_{0.95}Ni_{1.79}Al_{0.26}$ ($MgNi_2$ type) [10] have been reported. $Ba_3Pt_4Al_4$, the first compound in the ternary system Ba-Pt-Al, was prepared from the elements in niobium ampoules and crystallizes in an orthorhombic structure, space group *Cmcm* (*oP*44, a = 1073.07(3), b = 812.30(3), c = 1182.69(3) pm) isopointal to the Zintl phase $A_2Zn_5As_4$ (*A* = K, Rb). The structure features strands of distorted [Pt_4Al_4] heterocubane-like units by condensation over Pt/Al edges. These are arranged in a tetragonal rod packing by condensation over Pt and Al atoms with the barium atoms located inside cavities. Structural relaxation confirmed the electronic stability of the new phase, while band structure calculations indicate metallic behavior. COHP bonding analysis coupled with Bader effective charge analysis suggest a polar intermetallic phase in which strong Al-Pt covalent bonds are present, while a significant electron transfer from Ba to the [AlPt] network is found. This electron transfer has furthermore been confirmed by Pt XPS measurements. For $Ba_3Pt_4Al_4$ the Pt $4f_{5/2}$ and $4f_{7/2}$ energies were found in the range of elemental Pt due to the electron transfer of Ba, while PtAl and $PtAl_2$ show a pronounced shift towards more cationic platinum.

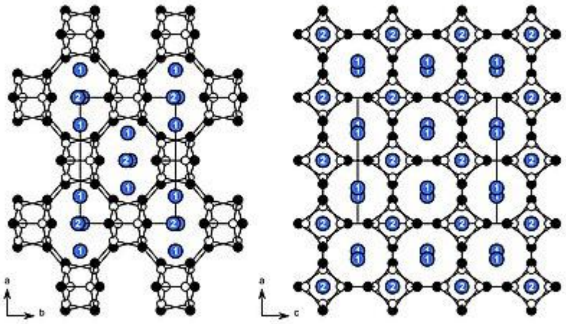

Figure 1. Unit cell of $Ba_3Pt_4Al_4$ along the *a* axis (left) and *c* axis (right), crystallizing with the orthorhombic space group *Cmcm*.

---

[1] G. Cordier, T. Friedrich, R. Henseleit, A. Grauel, U. Tegel, C. Schank, C. Geibel, *J. Alloys Compd.***1993**, *201*, 197-201.
[2] G. Cordier, T. Friedrich, *Z. Kristallogr.***1993**, *205*, 135-136.
[3] P. Kenfack Tsobnang, D. Fotio, S. Ponou, C. Fon Abi, *Acta Crystallogr.* **2011**, *67*, i55.
[4] K. Turban, H. Schäfer, *J. Less-Common Met.***1975**, *40*, 91-96.
[5] M. B. Manyako, O. S. Zarechnyuk, T. I. Yanson, *Kristallografiya***1987**, *32*, 1389-1391.
[6] M. B. Manyako, O. S. Zarechnyuk, T. I. Yanson, *Russ. Metall.***1988**, *3*, 185-187.
[7] G. Cordier, G. Dörsam, T. Friedrich, R. Henseleit, C. Röhr, *J. Alloys Compd.* **1993**, *190*, 201-207.
[8] K. J. Range, F. Rau, U. Klement, *Acta Crystallogr.***1990**, *C46*, 2454-2455.
[9] L. Guanglie, C. Linshen, W. Lianbang, Y. Huantang, *J. Alloys Compd.***2001**, *321*, L1-L4.
[10] C. He, Y. Du, H.-L. Chen, H. Ouyang, *Int. J. Mater. Res.***2008**, *99*, 907-911.
[11] J. A. Carrabine, *J. Nucl. Mater.***1963**, *8*, 278-280.

PMon008

Corrosion behavior of Al-Pd and Al-Co complex metallic alloys

Palcut, Marian (Slovak University of Technology, Trnava, SVK); Duriska, Libor (Slovak University of Technology, Trnava, SVK); Priputen, Pavol (Slovak University of Technology, Trnava, SVK); Janovec, Jozef (Slovak University of Technology, Trnava, SVK)

Al–TM (TM = transition metal element) alloys are an important part of a large family of complex metallic alloys (CMA). These alloys contain also structurally complex intermetallic phases with large unit cells, inclusive of quasicrystals [1]. Quasicrystals are characterized by lack of translational symmetry. A 5-fold and 10-fold symmetry is observed instead [1]. First quasicrystalline Al-TM phases were discovered in mid-1980s by Shechtman et al [1]. Their discovery was later awarded by Nobel Prize in chemistry. Because of their complex crystal structure, the physical properties of CMA differ from traditional metallic materials [1]. Corrosion behavior of most complex Al–TM phases is unknown [1, 2].

In the present work, the phase occurrence and the corrosion behavior of Al-Pd and Al-Co CMA have been investigated. Three Al-Pd alloys (Al-13Pd, Al-23Pd and Al-33Pd, composition given in atomic percent) and six Al-Co alloys (Al–24Co, Al–25Co, Al–26Co, Al–27Co, Al–28Co and Al-29Co) were prepared by arc–melting in Ar from high purity Al, Pd and Co lumps. The microstructure of the alloys was investigated by a field emission gun scanning electron microscope JEOL JSM–7600F coupled with an Oxford Instruments energy dispersive X–ray spectrometer. Furthermore, the phase occurrence was studied by an X–ray Panalytical Empyrean PIXCel 3D diffractometer with Bragg–Brentano geometry, working with a CoKα1,2 radiation beam. Each alloy was heterogeneous as it was found to consist of several microstructure constituents. Structurally complex intermetallic phases in these materials were found. The occurrence of the phases has been interpreted based on both previously published Al–Co and Al-Pd phase diagrams and non–equilibrium processes during casting. The as-cast alloys were subjected to corrosion testing in an aqueous NaCl solution. Open circuit potential of each alloy was measured first, immediately after sample immersion in the electrolyte. The electrochemical polarization was conducted in a standard 3–electrode cell at room temperature (21±2 °C). The reaction was controlled by a PGU 10V–1A–IMP–S potentiostat/galvanostat (Jaissle Electronic Ltd., Germany). The corrosion potential and corrosion current density were determined by the Tafel extrapolation of experimental polarization curves. The effect of the phase occurrence has been evaluated. A large amount of pitting is observed on the alloy surfaces, with some of the phases being preferentially corroded. The local nobility of individual Al–Co and Al-Pd intermetallic compounds is discussed. Conclusions towards the alloy corrosion resistance are provided.

Mr. Dušan Janičkovič (Institute of Physics, Slovak Academy of Sciences) is acknowledged for sample preparation by arc–melting. This work was financially supported by European Regional Development Fund (ERDF) via agreements ITMS:26220120014 and ITMS:26220120048; the Grant Agency VEGA via projects nos. 1/0018/15 and 1/0068/14; the Slovak Research and Development Agency via agreement no. APVV–0076–11 and the Slovak Academy of Sciences via "Centre of Excellence for functional multiphase materials" (FUN–MAT).

---

[1] J. M. Dubois, Chem. Soc. Rev. 41 (2012) 6760–6777.

[2] M. Palcut, P. Priputen, M. Kusý, J. Janovec, Corros. Sci. 75 (2013) 461–466.

PMon009

Evolution of the ground state in the system of binary intermetallics $CrGa_4$ and $MnGa_4$

Verchenko, Valeriy (Lomonosov Moscow State University, Department of Chemistry, Moscow, RUS); Tsirlin, Alexander (National Institute of Chemical Physics and Biophysics, Tallinn, EST); Shevelkov, Andrei (Lomonosov Moscow State University, Department of Chemistry, Moscow, RUS)

The family of intermetallic compounds with the $PtHg_4$ type of crystal structure consists of only 5 members: $CrGa_4$, $MnGa_4$, $ReGa_4$, $NiHg_4$, and $PtHg_4$ [1]. The crystal structure of $PtHg_4$ can be regarded as a defect CsCl motif, where 3/4 of the Cs atoms have been removed such that an arrangement of corner-connected [$PtHg_{8/2}$] cubes is formed, keeping the cubic symmetry. Noticeably, the $PtHg_4$-type intermetallics adopt 18 valence electrons per formula unit in $CrGa_4$, $NiHg_4$, and $PtHg_4$, and 19 valence electrons in $MnGa_4$ and $ReGa_4$, suggesting that these compounds are "electron" intermetallics, i.e. the stability range of the $PtHg_4$ family is determined by the number of valence electrons. The structural stability of "electron" intermetallics is usually referred to the existence of a gap or pseudo-gap at the Fermi level [2]. The gap arises between non-bonding and antibonding states, which are formed by the hybridized *d* and *sp* valence orbitals. Thereby, two fundamental problems appear from the peculiarities of "electron" intermetallic compounds: the detailed analysis of chemical bonding and the investigation of very rare intermetallic semiconductors, for which the band structure has a real band gap at the Fermi level. Both questions could be analyzed in detail for the TGa_4 compounds (T = Cr, Mn, Re). Indeed, due to the simplicity of their crystal structures, extended band structure calculations are possible to perform the analysis of chemical bonding between *d* and *p* metals, T and Ga, which form the compounds. Besides, $CrGa_4$, which has 18 valence electrons per formula unit, is known to possess a pseudo-gap at the Fermi level, indicating bad metallic behavior [1]. Thus, the band structure of $CrGa_4$ and the chemical bonding in this compound are related to those in semiconductor-like intermetallics, and call for a detailed investigation.

In the present study, we analyze band structure and physical properties of TGa_4 intermetallic compounds (T = Cr, Mn). Despite Cr and Mn being neighbors in the 3*d* row of the periodic system, isostructural $CrGa_4$ and $MnGa_4$ do not form a continuous solid solution. Instead, the $CrGa_4$-based limited solid solution $Cr_{1-x}Mn_xGa_4$ is formed with $x_{max} = 0.14(2)$, indicating that there is no continuous transition between the 18 and 19 valence electrons per formula unit for the TGa_4 compounds. To elucidate the origin of this miscibility gap, we studied chemical and physical properties of $Cr_{1-x}Mn_xGa_4$ for $x = 0$-$0.14(2)$, 1, and found that it crystallizes in the parent $PtHg_4$ type of crystal structure and follows the Vegard law. $Cr_{1-x}Mn_xGa_4$ demonstrates bad ($x = 0$-$0.14(2)$) or typical ($x = 1$) metallic behavior and continuous x evolution of $S(T)$ curves, where S is the Seebeck coefficient. Therefore, neither the crystal nor electronic structures can readily account for the discontinuity of the solid solution. However, we have found by the neutron diffraction experiments that at least $MnGa_4$ is antiferromagnetically ordered even above room temperature in a clear contradiction with the Pauli paramagnetic behavior assumed previously [1]. Our results are corroborated by the band structure calculations that reveal the non-magnetic metallic behavior of $Cr_{1-x}Mn_xGa_4$ ($x = 0$-0.15) and the antiferromagnetic metallic ground state of $MnGa_4$.

We gratefully acknowledge the financial support of the Mobilitas program of the ESF, grant MTT77, and Russian Foundation for Basic Research, grant #14-03-31181-mol_a.

---

[1] Haussermann, U.; Viklund, P.; Bostrom, M.; Norrestam, R.; Simak, S.I. *Phys. Rev. B* **2001**, 63, 125118.
[2] Yannello, V.J.; Fredrickson, D.C. *Inorg. Chem.* **2014**, 53, 10627-10631.

PMon010

Experimental investigation of ternary Fe-Sn-Ti phase diagram at 873 K

Nash, Philip (Illinois Institute of Technology, Chicago, USA); Yin, Ming (Illinois Institute of Technology, Chicago, IL, USA)

The 873 K isothermal section of the ternary Fe-Sn-Ti system was investigated over the whole composition range by means of equilibrated alloys analyzed using X-ray powder diffraction, scanning electron microscopy and energy dispersive spectroscopy. Three ternary compounds were found: Fe_2SnTi, $FeSnTi_2$ were confirmed and $Fe_5Sn_9Ti_6$ is reported for the first time. The half-Heusler compound FeSnTi was not found to exist in the temperature range investigated.

PMon011

Experimental investigations in the binary Mn-Sb and ternary Mn-Sb-Bi System

Kainzbauer, Peter (Department of Inorganic Chemistry (Materials Chemistry), University of Vienna, Vienna , AUT); Richter, K.W. (Department of Inorganic Chemistry (Materials Chemistry), University of Vienna, Vienna , AUT); Ipser, Herbert (Department of Inorganic Chemistry (Materials Chemistry), University of Vienna, Vienna , AUT)

Several magnetic phases have been reported and frequently investigated in the two binary systems Mn-Sb and Mn-Bi. For instance, the isostructural NiAs-type phases MnBi and MnSb as well as MnSbBi thin films have been investigated previously due to their superior ferromagnetic and magneto-optical properties. However only few experimental studies have been carried out on the ternary Mn-Sb-Bi phase diagram. In the current study, isothermal sections at 320 °C and 600 °C of the ternary MnSbBi system were investigated.

In addition, the phase diagram of the binary Mn-Sb system which exhibited a number of uncertainties concerning phase boundaries and melting temperatures [1] has been reinvestigated. The investigations were performed by conventional techniques, i.e. powder and single crystal X-ray diffraction, differential thermal analysis and scanning electron microscopy. Based on this new experimental results, an improved version of the binary Mn-Sb phase diagram is proposed.

Moreover, it is planned to preform magnetic measurements with a superconducting quantum interference device magnetometer in cooperation with the MPI of Chemical Physics of Solids in Dresden, Germany.

The experimental work at the University of Vienna was supported by the FWF (Austria Research Foundation) under the Project No. P26023-N19

---

[1] Massalski, T.,B.; Okamoto, H., Subramanian, P.,R.: Binary Alloy phase Diagrams (1992)

PMon012

Intermetallic rare earth clathrates: synthesis, mechanism of rare earth incorporation and impact of electronic correlations on the thermoelectric properties

Prokofiev, Andrey (Institute of Solid State Physics, Vienna University of Technology, Vienna, AUT);
Ikeda, Matthias (Institute of Solid State Physics, Vienna University of Technology, Vienna, AUT);
Sidorenko, Andrey (Institute of Solid State Physics, Vienna University of Technology, Vienna, AUT);
Svagera, Robert (Institute of Solid State Physics, Vienna University of Technology, Vienna, AUT);
Waas, Monika (Institute of Solid State Physics, Vienna University of Technology, Vienna, AUT);
Paschen, Silke (Institute of Solid State Physics, Vienna University of Technology, Vienna, AUT)

Intermetallic type-I clathrates show promise for thermoelectric applications due to their exceedingly low lattice thermal conductivities. They are guest-host systems in which a large electropositive atom, like Ba or alkali metals, fills oversized polyhedral cavities in a covalently bound Si, Ge or Sn framework. It is the interaction of the vibration mode of the guest atom (rattling) with the delocalized vibrations of the framework that results in the anomalously low thermal conductivity. Viewing from another point, in many intermetallic compounds some rare earth (RE) elements lead to strong electronic correlation phenomena including the occurrence of giant thermopower, another important property of an efficient thermoelectric material. Thus, the incorporation of appropriate f-elements into clathrates seems a promising route to drastically increase the thermoelectric efficiency of this material. We report on the successful incorporation of a number of RE elements as guest atoms into the clathrate cages. The synthetic route is briefly described. We discuss the mechanism of RE incorporation based on the trends in the clathrate phase composition along the RE element range. Our investigation reveals that the RE content is mainly governed by two factors, the residual cage space and the electron balance in the sense of the Zintl concept. The thermoelectric and magnetic properties of some RE clathrates are discussed. We observe a 50% enhancement of the thermopower in a cerium-containing clathrate compared with a RE-free reference material [1]. We suggest that a rattling-enhanced hybridization of the conduction electrons with the localize f-electrons underlies this effect.

---

[1] A. Prokofiev, A. Sidorenko, K. Hradil, M. Ikeda, R. Svagera, M.Waas, H.Winkler, K. Neumaier, and S. Paschen. Thermopower enhancement by encapsulating cerium in clathrate cages. Nature Mat. 12 1096-1101 (2013)

PMon13

From Intermetallic Clusters to (bi)metallic Nanoparticles

Wolf, Silke (Karlsruher Institut für Technologie, Institut für Anorganische Chemie, Karlsruhe, GER); Feldmann, Claus (Karlsruhe Institute of Technology (KIT), Karlsruhe, GER)

Ionic liquids have recently been noticed as promising reaction media not only for the synthesis of nanoparticles, zeolithes or metal-organic frameworks but as well for metal clusters.[1,2] Due to their high redox stability, ionic liquids are suitable reaction media for metal carbonyls.[3]

As a part of our studies regarding role and benefit of ionic liquids under reductive conditions,[3] we could obtain several metal carbonyl clusters, such as $[\{Fe(CO)_3\}_4\{SnI\}_6I_4]^{2-}$ (Figure 1, left), $SnI\{Co(CO)_4\}_3$ or $[\{PbMn(CO)_5\}\}_6I_8]^{2-}$ (Figure 1, right) by reacting metal iodides and metal carbonyls in imidazolium based ionic liquids, e.g., [BMIm][NTf_2] (BMIm: 1-butyl-3-methylimidazolium, NTf_2: bistrifuoridomethansulfon-imide). [3-5] Structure and bonding of these compounds are validated by single-crystal structure analysis, FT-IR spectra, and, in two cases, by DFT calculations.

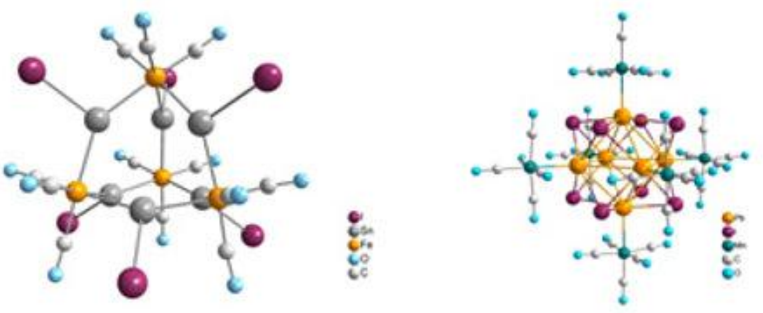

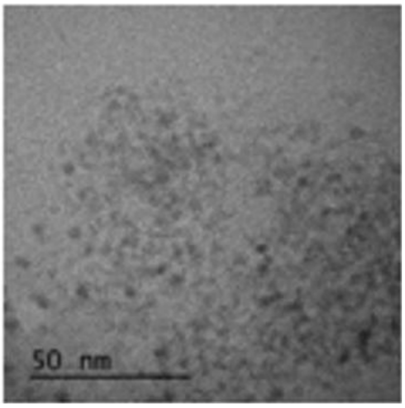

As a continuation, our interest shifted to the thermal decomposition of the above mentioned carbonyl clusters in ionic liquids with regard to the formation of metallic nanoparticles. This approach to form metal nanoparticles comprises several advantages: (1) Only a thermal decomposition of the precursor is necessary to obtain the elemental metal; specific reducing agents are not required. (2) When using these carbonyl compounds, no decomposition products of the precursor remain in the nanoparticle suspension.[6] As a first example, we could obtain nanoparticles, with a diameter of about 5 nm, by thermal decomposition of $[Co\{1,4\text{-}Ph(CN)_2\}_2\{NTf_2\}_2][SnI\{Co(CO)_4\}_3]_2$ in [BMIm][BF_4] as ionic liquid. These nanoparticles were investigated by transmission electron microscopy (Figure 2) and X-ray powder diffraction.

---

[1] D. Freudenmann, S. Wolf, M. Wolff, C. Feldmann, *Angew. Chem. Int. Ed.* **2011**, *50*, 11050 (Review).

[2] E. Ahmed, M. Ruck, *Dalton Trans.***2011**, *40*, 9347 (Review).

[3] S. Wolf, F. Winter, R. Pöttgen, N. Middendorf, W. Klopper, C. Feldmann, C. *Chem. Eur. J.* **2012**, *18*, 13600.

[4] S. Wolf, C. Feldmann, *Dalton Trans.* **2012** , *41*, 8455.

[5] S. Wolf, K. Reiter, F. Weigand, W. Klopper, C. Feldmann, C. *Inorg. Chem.* **2015**, *54*, 3989.

[6] E. Redel, R. Thomann, C. Janiak, *Chem. Commun.***2008**, 1789.

PMon014

Liquidus projection of ternary Laves phase containing systems for the development of ferritic steel

Jacob, Aurélie (Forschungszentrum Juelich, Juelich, GER); Schmetterer, Clemens (Fraunhofer-UMSICHT, Sulzbach-Rosenberg, GER); Grüner, Daniel (Forschungszentrum Juelich, Jülich, GER); Wessel, Egbert (Forschungszentrum Juelich, Jülich, GER); Hallstedt, Bengt (RWTH Aachen, Aachen, GER); Khvan, Alexandra (NUST MISIS, Moscow, RUS); Kondratiev, Alex (NUST MISIS, Moscow, AUT); Singheiser, Lorenz (Forschungszentrum Juelich, Jülich, GER)

Ferritic steels with high Cr-content are potential high temperature materials. Crofer 22H is an example of such a ferritic steel and it is strengthened by Laves phase particles. The formation of Laves phase particles improves the materials properties such as creep strength and corrosion resistance. The Laves phase forms in competition with other phases.

A careful literature survey has shown that certain Laves phase containing ternary systems have not been well established. Nevertheless, the knowledge of these systems is necessary for the further development of ferritic steels, where these systems can be regarded as sub-systems of the overall alloy system.

In the present work, we propose the experimentally determined of the liquidus projection of the ternary Cr-Fe-Nb and Fe-Nb-Si systems. Both systems have their importance in the development of new ferritic alloys.

The liquidus projections were established first from the determination of the primary crystallisation of as-cast samples together with data on the binary invariant reactions. The thermal behaviour of the samples was then studied by DTA measurements. The liquidus projection was finally constructed from the combined results.

PMon015

Metallurgical preparation, thermodynamic characterisation and cycling measurements of new intermetallic anode materials for Li-ion batteries

Reichmann, Thomas (Karlsruhe Institute of Technology, Karlsruhe, GER); Li, Dajian (Karlsruhe Institute of Technology, Karlsruhe, GER); Cupid, Damian (Karlsruhe Institute of Technology, Karlsruhe, GER)

Secondary lithium ion cells are now universally accepted as a viable key components for electrical energy storage in portable, entertainment, computing and telecommunication equipment required by todays information-rich, mobile society. Predominantly, the lack of suitable reversible negative electrode materials hinders the generation of new lithium ion batteries with distinctly higher charge densities and cycling stabilities. Until now, a variety of (semi-)metal anodes have been tested, promising unrivalled capacities as well as safety due to more positive potentials against Li/Li^+ compared to graphite. Sn-based intermetallic anodes are expected to deliver significant capacity increases (960 mAh/g) compared to graphite although they suffer from large volume changes during lithiation/delithiation which lead to electrode degradation and poor cycling stability. A significant improvement of cyclability can be achieved when using intermetallic alloys, *e.g.* Cu-Sn or Sb-Sn as anode materials. As electrochemical performance of a battery strongly depends on intrinsic properties of the electrode materials, a direct link between electrochemistry and solid-state chemistry is beneficial and even required. From that point of view, any attempt to improve the performance of a lithium ion battery must start with the investigation and characterisation of the electrode materials. It is the aim of the current project to combine experimental key data (thermodynamic properties, phase diagram information, crystallographic data) with electrochemically derived data from prototype cells. Consistent thermodynamic descriptions of corresponding material systems will be developed using CALPHAD (Computer Coupling of Phase Diagrams and Thermochemistry) method. The thermodynamic descriptions will then allow the design of new electrode materials with optimally tailored properties based on the ICME (Integrated Computational Materials Engineering) approach. A series of Li-Sn and Cu-Li-Sn alloys were synthesised by metallurgical techniques in our laboratory. The alloys were characterised by powder X-ray diffraction, ICP-OES and electron microscopy. Selected phase-pure alloys were used to determine c_p data by differential scanning calorimetry (DSC). Due to the reactivity of Li, both the synthesis and heat capacity measurements of the respective compounds required the use of tantalum crucibles which were sealed by arc-melting in a glove-box. The measured heat capacities were used to update a thermodynamic description for the Li-Sn system [1] which has been already developed in a previous study. In addition, phase-pure alloys were used as active material for intermetallic electrodes. Powdered Li_xSn alloys were dispersed in N-Methyl-2-pyrrolidone (NMC) together with carbon black to improve conductivity and Polyvinylidene fluoride (PVDF) was added as a binder to facilitate the production of compact electrode materials. Electrochemical cycling tests were performed in a suitable coin cell arrangement against Li/Li^+, varying potential at constant current density (CCVV) .

PMon016

New hydrides $RTXH_{1.5}$ (R = Rare-earth; T = Sc,Ti; X = Si,Ge)

TENCE, SOPHIE (ICMCB-CNRS, PESSAC, FRA); MAHON, TADHG (ICMCB-CNRS, PESSAC, FRA); GAUDIN, ETIENNE (ICMCB-CNRS, PESSAC, FRA); CHEVALIER, BERNARD (ICMCB-CNRS, PESSAC, FRA)

Among the *RTX* (*R* = rare-earth, *T* = transition metal, and *X* = Si, Ge) intermetallics some of them crystallize with the tetragonal CeFeSi-type structure or with the CeScSi-type one which is a derivative of the former one. In both structural types, layers of empty [Ce_4] tetrahedra are observed but the [FeSi] or [ScSi] layers are different. This layer is made of edge-shared [Si_4] tetrahedra filled by Fe in the CeFeSi-type and of [Si_4] square planes with Sc in the center in the CeScSi-type. It is noteworthy that some *RTX* ternaries such as *R*TiGe (R = Gd, Tb) present both structural types corresponding to the low- and the high-temperature forms.

It was shown in the past that, in the case of the CeFeSi-type structure, the [Ce_4] tetrahedra can be filled by hydrogen leading to CeFeSiH-type hydrides. This induces very interesting modulation of the physical properties [1]. More recently, it was also shown that it is possible to stabilize hydrides upon hydrogenation of the CeScSi-type intermetallics such as CeTiGe, CeScSi, NdScSi or TbTiGe. It also yields drastic modulation of the magnetic properties of the pristine compounds by reducing or destroying the magnetic ordering [2, 3]. For the first time the crystallographic positions of hydrogen (or deuterium) atoms have been determined from neutron diffraction data on $NdScSiD_{1.5}$ and $CeTiGeH_{1.5}$. The case of $NdScSiD_{1.5}$ will be presented in details since the deuteration process was precisely studied by in-situ neutron diffraction experiments. The role played by hydrogen in the chemical bonding is analyzed by band structure calculation.

---

[1] B. Chevalier et al., J. Alloys Compd. 2009, 43, 480.
[2] B. Chevalier et al., Chem. Mater 2010, 22, 5013-5021.
[3] E. Gaudin et al., Inorg. Chem. 2011, 50, 11046-11054.

PMon017

New intermetallic anode materials: Experimental investigation of the Cu-Li-Sn system

Fürtauer, Siegfried (Institut für Anorganische Chemie (Materialchemie), Wien, AUT); Flandorfer, Hans (University of Vienna, Vienna, AUT)

Besides carbonaceous and composite materials, intermetallic anodes are promising candidates of new anode materials for lithium ion batteries. Increased gravimetric capacity, sufficient potential towards the cathode and reasonable diffusion at low temperatures are benchmark data for improved anodes. The knowledge of alloy phase diagrams containing lithium is mandatory to understand the nature and mechanisms of charging and discharging intermetallic anodes, like e.g. Cu-Sn alloys. Therefore, the Cu-Li-Sn phase diagram and the constituting binary systems Cu-Sn, Li-Sn and Cu-Li have been investigated extensively by experimental methods. Powder-XRD, SC-XRD studies and thermal analysis were applied to describe the alloy phase diagrams, drop calorimetry was performed to provide supplementary data for the thermodynamic optimization. The outcome of this work is fundamental for further application-oriented studies, e.g. the calculation of the open circuit voltage.

This work has been funded by the FWF under the project I559-N19 within the DFG priority project SPP 1473 "WeNDeLIB".

PMon018

On the room and high temperature modifications of $Pd_3(Ga,Sb)$ ternary phase

Matselko, Oksana (Max-Planck-Institut für Chemische Physik fester Stoffe , Dresden, GER); Matselko, Oksana (Ivan Franko National University of Lviv, Lviv, UKR); Cardoso-Gil, Raul (Max-Planck-Institut für Chemische Physik fester Stoffe , Dresden, GER); Burkhardt, Ulrich (Max-Planck-Institut für Chemische Physik fester Stoffe , Dresden, GER); Grin, Yurii (Max-Planck-Institut für Chemische Physik fester Stoffe , Dresden, GER); Gladyshevskii, Roman (Ivan Franko National University of Lviv, Lviv, UKR)

The ternary Pd-Ga-Sb system is known for $C_{\mathrm{Pd}} \leq 50$ at.% – isothermal section at 500°C and complete reaction scheme (Scheil diagram) were constructed [1]. Up to now, the Pd-rich part was not published, only the formation of one ternary phase $Pd_{25}Ga_{4.5}Sb_{4.5}$ ($Pd_{25}Ge_9$-type structure, *P*-3, *hP*34) was reported [2]. During our investigation of the Pd-rich part of Pd-Ga-Sb system at 500°C we found two tetragonal phases with primitive unit cell and approximate composition $Pd_3Ga_{0.5}Sb_{0.5}$. One of them crystallizes in Pt_3Al structure type (*P*4/*mbm*, *tP*16). There is no binary phase with stoichiometric composition 3:1 in the Pd-Ga system [3], while there exist three modifications for intermatallic compounds Pt_3Al and Pt_3Ga [4] – high temperature cubic (Cu_3Au-type structure, *Pm*-3*m*, *cP*4), intermediate (U_3Si-type structure, *I*4/*mcm*, *tI*16) and low temperature (Pt_3Al – type structure, *P*4/*mbm*, *tP*16). The samples were synthesized from the elements by arc melting, subsequently annealed and quenched. Characterisation was performed by means of powder X-ray diffraction (XRD) analysis, scanning electron microscopy with energy dispersive X-ray spectroscopy (EDXS) and differential thermal analysis (DTA). For the powder XRD analysis samples with $C_{\mathrm{Pd}} \geq 70$ at.% were filed and annealed again at 500°C for 24 hours to remove residual strain. According to results of *in situ* temperature dependent XRD on as cast samples, the tetragonal phase with Pt_3Al-type structure exists till 600°C, whereas the second one is stable till 650°C. At higher temperature some cubic phase forms. After cooling (from 750°C) at room temperature we found only the tetragonal phase with Pt_3Al-type structure. The existence of earlier reported $Pd_{25}Ga_{4.5}Sb_{4.5}$ phase was also confirmed.

---

[1] K. W. Richter, H. Ipser. Ber. Bunsenges. Phys. Chem. 102 (1998) 1245-1251.
[2] M. Ellner, M. El-Boragy. J. Less-Common Met. 161 (1990) 147-158.
[3] H. Okamoto. J. Phase Equilib. 29 (2008) 466-467.
[4] Y. Oya, Y. Mishima, T. Suzuki. Z. Metallkd. 78 (1987) 485-490.

PMon019

Ordered defect variants of a closest packing in $TaGa_{6-x}Zn_x$ – or packing of $Ta(Ga,Zn)_{12}$ polyhedra like in elemental metals

Koffi, Agbelenko (Institut für Anorganische Chemie, Freiburg, GER); Ade, Martin (Institut für Anorganische Chemie, Freiburg, GER); Hillebrecht, Harald (Institut für Anorganische Chemie, Freiburg, GER)

Four different structures were obtained for mixed crystals of the composition $TaGa_{6-x}Zn_x$ with $2.48 \leq x \leq 3.32$. All crystal structures base on the same principle. Hexagonal layers of a composition $Ta(Ga,Zn)_3$ alternate with topologically equivalent layers $[V](Ga,Zn)_3$, where a void [V] substitutes the Ta-atoms. Therefore, all crystal structures can be described as a defect variant of a closest packing AB_3 as an ordered defect variant of a closest packing. The stacking of the two types of layers occurs in a way, that Ta is always surrounded by a metal atom Ga/Zn and not by a void. Therefore, Ta shows a 12-fold coordination, either a cuboctahedron (cubic sequence ABC) or an "anti"cuboctaahedron (hexagonal sequence ABA). In all the four cases, voids and Ta-atoms are completely ordered, while no ordering was observed for Ga/Zn. The Ga/Zn ratio was determined by EDX on cut and polished single crystals.

In cubic $TaGa_{2.68}Zn_{3.32}$ (Fm-3m, Z = 4, a = 779.4(1) pm) all layers are stacked in cubic sequences ...ABC... Accordingly, Ta is coordinated as a cuboctahedron. The coordination number of Ga/Zn is 10, i.e. a cuboctahedron with two missing atoms in trans-position. The arrangement of the $Ta(Ga,Zn)_{12}$ cuboctahedra corresponds to the *fcc* packing of the Cu-type.
In hexagonal $TaGa_{3.52}Zn_{2.48}$ ($P6_3/mmc$, Z = 2, a = 550.2(4), c = 907.07(7) pm) the sequnce of the layers is ...ABAC... with the Ta-atoms in layesr B and C, i.e. in hexagonal sequences. Accordingly, Ta is coordinated as an "anti"cuboctahedron and the $Ta(Ga,Zn)_{12}$ polyhedra are arranged like the *hcp* of the Mg-type.

In the second hexagonal compound $TaGa_{2.75}Zn_{3.25}$ ($P6_3/mmc$, Z = 4, a = 550.35(3), c =1809.6(3) pm) the layer sequence is ...ACBCABCB... with Ta in layers ABAC. Because of this sequence the coordination of Ta alternates from cuboctahedron to "anti"cuboctahedron. This arrangement of polyhedra corresponds to the La-type.

The most complex stacking of layers is realised in rhombohedral $TaGa_{2.96}Zn_{3.04}$ (R-3m, Z = 9, a = 550.35(3), c = 4066.4(3) pm). The Ta-atoms are in hexagonal and in cubic sequences as well with a ratio of 2:1. The pattern of Ta-polyhedra represents the Sm-type.
Obviously, the occurence of the differnt types of $TaGa_{6-x}Zn_x$ is ruled by the valence electron concentration as the ratio between cubic and hexagonal sequences correlates to the Ga/Zn ratio. This is similar to the elemental structures of the rare earth metals and the transition metals.
All single crystals $TaGa_{6-x}Zn_x$ were grown from a melt of the elements with a large excess of Ga/Zn. The formation of the different types is regulated ba the ratio Ga/Zn.

PMon020

Single crystal growth and crystal structures of binary intermetallics Ta_xGa_y

Koffi, Agbelenko (Institut für Anorganische Chemie, Freiburg, GER); Ade, Martin (Institut für Anorganische Chemie, Freiburg, GER); Hillebrecht, Harald (Institut für Anorganische Chemie, Freiburg, GER)

Single crystals of binary intermetallics Ta_xGa_y were obtained from the elements. The variation of composition, temperature and cooling rate resulted in the formation of new compounds and of well-known phases, which were characterised by single crystal investigations for the first time. The composition was additionally checked by EDX.

$Ta_{2-x}Ga_{5+x}$ (x = 0.38) is a new compound. The crystal structure is isotypic to Mn_2Ga_5 ($P4/mbm$, $Z = 2$, $a = 932.1(1)$, $c = 275.72(6)$ pm) and contains rods of pentagonal prisms $TaGa_{10}$ running in direction [001]. The non-stoichiometry results from a mixed Ta/Ga occupation.

Ta_4Ga_5 was mentioned by Schubert et al. [1]. Drys [2] reported a primitive tetragonal unit cell with a = 1180 pm and c = 1690 pm for a compound $TaGa_2$.The crystal structure of Ta_4Ga_5 ($P4_2/mnm$, $Z = 36$, $a = 1179.4(2)$, $c = 1696.7(3)$ pm) represents a new structure type. The complex structure contains 7 independent Ta-positions amd 9 Ga-atoms. The coordination numbers are between 10 and 13 with quite irregular polyhedra. According to the composition near 1:1 and the similar atomic radii, there are Ta-Ta, Ta-Ga and Ga-Ga interactions.

The highest Ga-content was found for the new compounds Ta_8Ga_{41} (R-3, $Z = 3$, $a = 1431.1(2)$, $c = 1534.4(3)$ pm, V_8Ga_{41}-type [3]) and Ta_6Ga_{31} (P-1, $Z = 2$, $a = 969.7(1)$, $b = 968.8(1)$, c = 1488(3) pm, $\alpha = 87.18(1)$, $\beta = 80.18(1)$, $\gamma = 85.18(1)°$, triclinic Mo_6Ga_{31}-type [4]). Both compounds are formed as intergrown crystals. The intergrowth is esplained by the close structural similarity and prevented a reliable refinement of the individual structures. Both crystal structures base on $TaGa_{10}$-polyhedra (combination of icosahedron and cube). These polyhedra are connected to octameric cube-like units. In Ta_8Ga_{41} the "supercubes" are isolated, in Ta_6Ga_{31} they form dimers.

The existence of Ta_5Ga_3 in different modifications was confirmed. Tetragonal Ta_5Ga_3 ($I4/mcm$, $Z = 4$, $a = 1021.99(7)$, $c = 511.21(4)$ pm) was assignet to the W_5Si_3-type. A second tetragonal form ($I4/mcm$, $Z = 4$, $a = 659.86(9)$, $c = 1193.1(2)$ pm) belongs to the Cr_5B_3-type but one of the Ga-sites has an occupaton of 40% ($Ta_5Ga_{2.2}$). Hexagonal Ta_5Ga_3 ($P6_3/mcm$, $Z = 2$, $a = 707.23(4)$, $c = 530.6(3)$ pm, Mn_5Si_3-type) contains small amounts of oxygen, so the composition is $Ta_5Ga_3O_{0.4}$.

---

[1] H. G. Meissner, K. Schubert, *Z. Metallkde.* **1965**, *56*, 475.

[2] M. Drys, J. Less-Common Met. **1978**, 58, 111.

[3] K. Girgis, W. Petter, *Acta Cryst. B*, **1975**, *31*, 113; K. Yvon, *Acta Cryst. B*, **1975**, *31*, 117.

[4] R. Lux, PhD Thesis, University Freiburg, **2004**.

PMon021

Ordering patterns in mixed group 10 metal tellurides based on B8-type intermetallics

Kuznetsov, Alexey (Department of Chemistry, Moscow State University, Moscow, RUS); Zakharova, Elena (Department of Chemistry, Moscow State University, Moscow, RUS); Stroganova, Ekaterina (Department of Chemistry, Moscow State University, Moscow, RUS)

The NiAs/Ni_2In structure type (aka B8 type) represents rather simple structure motif that is adopted by many binary and more complex intermetallic compounds. However, this simplicity is misleading, since superstructures and ordering phenomena for the B8-type compounds can be rather complex [1]. Here we report ordering patterns arising from 'diluting' Group 10 metal – main-group metal binaries with tellurium. We have obtained several compounds featuring different ordering depending on the transition/main-group metal combination, which were investigated using single-crystal and powder X-ray diffraction, electron diffraction and high-resolution electron microscopy, Moessbauer spectroscopy. Electronic structure studies were performed on the DFT/FP-LAPW level.

For nickel, a number of compounds belonging to the $Ni_{3-x}MTe_2$ family [2] was discovered. Their structures are based on the NiAs-type subcell, with the *c* parameter tripled. This superstructure is generated by both main-group elements to form an *hcp* array with an ordered –M–Te–Te– stacking sequence along the *c* axis, with Ni vacancies present both in the heterometallic fragments and between the Te atoms, the latter thus forming a van der Waals gap. Depending on the main group metal type, these compounds exhibit different behavior with respect to the variations of the Ni content. At x=0 the only difference in the structures for different M is in the distribution of Ni between the positions in the heterometallic fragments and van der Waals gap: for M=Ga, Ge this ratio is ca. 70/30, while for In, Sn it is ca. 30/70, for M=Sb it is 50/50. As the 'x' increases, the compounds with M=Ga, Ge lose Ni from the heterometallic layer, and the ordering of the vacancies leads to the new unit cell with $a=b=2xa_{sub}$, while the ones with M=Sn, In, show the ordering of the van der Waals Ni positions resulting in the modulations along the *c* axis.

Palladium-based compounds of this type are formed only for heavier main-group metals (Sn, In, Pb, Bi), and for the most part feature simple NiAs-type structures with no detectable ordering in the As position. The exception being Pd-Sn-Te system, where, along with the NiAs-type compound, ordered structures appear to exist in a limited compositional range. However, the ordering pattern differs drastically from the Ni-based compounds and includes small monoclinic distortion of the parent B8 unit cell.

Electronic structure calculations show dominant contributions from transition metal *d*-orbitals near the Fermi level for all types of compounds. Bonding analysis reveals the network of multi-centered heterometallic bonds.

This work was supported by RFBR (Grants No. 15-03-06459 and 14-03-31802) and Russian Academy of Sciences. The use of MSU supercomputer resources is kindly acknowledged.

---

[1] S. Lidin. *Acta Cryst.***1998**, B54, 97-108

[2] a) H.-J. Deiseroth, K. Aleksandrov et al. *Eur. J. Inorg. Chem*. **2006**, 8, 1561-1567; b) A.A. Isaeva, O.N. Makarevich, A.N. Kuznetsov et al. *Eur. J. Inorg. Chem. 2010*, 1395-1404.

PMon022

Quantifying electron transfer in polar intermetallic phases: structural, NMR and theoretical studies on lithium amalgams

Tambornino, Frank (Ludwig-Maximilians-Universität München, München, GER); Bräuniger, Thomas (Ludwig-Maximilians-Universität München, München, GER); Minke, Christian (Ludwig-Maximilians-Universität München, München, GER); Hoch, Constantin (Ludwig-Maximilians-Universität München, München, GER)

Amalgams of the less noble metals have been studied extensively in the 19th and 20th century. Early studies on the binary system Li-Hg revealed three phases with compositions Li_3Hg, LiHg and $LiHg_3$. All of them have been structurally characterised [1-4], some with single crystal data, others were assigned to known structure types on the basis of their powder diffraction patterns. Here we present single crystal and power diffraction studies on Lithium amalgams, combined with solid-state NMR investigations in order to quantify the electron transfer between them.

The electron affinity of mercury is insufficient for the formation of Zintl-analogous Hg anions. As a consequence, partially negative polarised Hg networks are a recurring structural motif in Hg-rich phases, and the charge is distributed equally over the mercury substructure. Mercury-rich amalgams thus can be taken as model compounds for studies of polar metal-metal bonding. They simultaneously show contributions from ionic, covalent and metallic bonding, leading to complicated structures and „bad metal“ behaviour.

The incomplete electron transfer can be monitored with solid-state NMR utilising the Knight shift [5]. As direct measure of the s-electron density at the atomic core, it is proportional to the electron transfer from Lithium to Mercury. Two NMR-active nuclei (^{7}Li and ^{199}Hg) provides independent probes for NMR.

Our studies show a direct correlation between the mercury content and the signals for both ^{7}Li and ^{199}Hg and hence for the polarisation of the metal-metal bonding. Starting from pure lithium (265 ppm) the Knight shift decreases with increasing mercury content (Li_3Hg: 203.2 ppm, LiHg: 101.7 ppm, $LiHg_3$: 72.9 ppm). The partial positive charge on Lithium increases with increasing Hg content as a consequence of the more efficient charge delocalisation on a larger Hg substructure. This is corroborated by the Knight shift of ^{119}Hg. Metallic Hg shows the highest Knight shift (22480 pm), and with increasing lithium content, the mercury subnet gets subsequently higher charged. With more pronounced ionic bonding contributions the Knight shift decreases ($LiHg_3$: 17172 ppm, LiHg: 4500 ppm, Li_3Hg: 1680 ppm).

Ab-initio calculations on the basis of FP-LAPW (GGA+PBE) methods implemented in the WIEN2k program package [6] support the experimental findings. The calculated total and partial density of states (DOS) show an increasing electron transfer from Li_3Hg to $LiHg_3$. However, all Lithium amalgams show to be metallic, as seen in measurements of the thermal behaviour of the specific electric conductivities.

The combination of structural investigations, solid-state NMR, band structure calculations and conductivity measurements proves to be a robust toolbox for detailed studies on polar metal-metal bonding.

---

[1] W. Kerp, W. Böttger, Z. Anorg. Allg. Chem.**1900**, 25, 1.
[2] G. J. Zukowsky, Z. Anorg. Allg. Chem.**1911**, 71, 403.
[3] E. Zintl, G. Brauer, Z. Phys. Chem.**1933**, 20, 245.
[4] E. Zintl, A. Schneider, Z Elktrochem. Angew. P.**1935**, 41, 771.
[5] W. Knight, Phys. Rev.**1949**, 76, 1259.
[6] P. Blaha, K. Schwarz, G.K.H. Madsen, D. Kvasnicka, J. Luitz, WIEN2k, An Augmented Plane Wave and Local Orbitals Program for Calculating Crystal Properties, Technische Universität Wien, Austria, **2006**.

PMon023

$R_2T_{3\text{-}x}Si_x$, a new pseudo-binary phase and prospective magnetocaloric material (R = Ce, Pr, Nd, Gd, Tb, Dy; T = Co, Ni).

Tence, Sophie (ICMCB-CNRS, Pessac); Gaudin, Etienne (ICMCB-CNRS, Pessac, FRA); Chevalier, Bernard (ICMCB-CNRS, Pessac, FRA); Mahon, Tadhg (ICMCB-CNRS, Pessac, FRA)

In the search for new magnetocaloric materials we investigate ternary intermetallic systems containing magnetic elements such as rare earth and transition metals. During these investigations, we have discovered a new solid solution: $Gd_2Co_{3\text{--}x}Si_x$, with $0.29 < x < 0.5$ [1] which crystalizes in the orthorhombic *Cmce* space group with the La_2Ni_3-type structure. The structure consists of a three-dimensional network of Gd-atoms forming channels running along the a-axis, and puckered two-dimensional layers of Co/Si-atoms with a Kagome-like structure stacked along the c-axis (see Figure). Interestingly, these ferrimagnetic phases have a tuneable Curie Temperature (T_C) between 280 and 338 K depending on the concentration of Co. We have extended the study of this solid solution to other rare earths. In each case, the R_2T_3 pure binaries do not exist ($x = 0$), the phases being stabilised only by a partial substitution of Si for Co. The light rare earths such as Ce, Pr and Nd, have been shown to form the phase with Co and only after an annealing at low temperatures of around 500°C. Their compositions were studied by electron microprobe analysis and their magnetic properties were measured.

The same kinds of systems have been studied with nickel as the transition metal and new phases are only formed with the heavy rare earths Gd, Tb or Dy. We focused on the Gd compounds due to the high magnetic moment of gadolinium. By varying the starting composition we were able to obtain a $Gd_2Ni_{3\text{-}x}Si_x$ solid solution that undergoes a ferromagnetic transition around 96 K which barely changes with the composition (contrary to what was observed with the homologous solid solution with Co). Besides this, these materials have an appreciable magnetocaloric effect of 5 $J.K^{-1}.kg^{-1}$ at the Curie temperature for an applied field of 2 Tesla.

---

[1] Tencé, S.; Caballero Flores, R.; Chable, J; Gorsse, S.; Chevalier, B.; Gaudin, E.; *Stabilization by Si Substitution of the Pseudobinary Compound $Gd_2(Co_{3-x}Si_x)$ with Magnetocaloric Properties around Room Temperature*, Inorganic Chemistry **2014**, 53 (13), pp. 6728-6736.

PMon024

Structural transformation of the $NaZn_{13}$-type derivatives in the La(Ce)-Ni-Ga systems

Prots, Yurii (Max-Planck-Institut für Chemische Physik fester Stoffe, Dresden, GER); Vasylechko, Leonid (Max-Planck-Institut für Chemische Physik fester Stoffe/Lviv Polytechnic National University, Lviv, UKR); Burkhardt, Ulrich (Max-Planck-Institut für Chemische Physik fester Stoffe, Dresden, GER); Fauth, Francois (ALBA Synchrotron, Barcelona, ESP); Kaczorowski, Dariusz (Institute of Low Temperature and Structure Research, Polish Academy of Sciences, Wroclaw, POL); Grin, Yuri (Max-Planck-Institut für Chemische Physik fester Stoffe, Dresden, GER)

The investigation of the $La(Ni_{1-x}Ga_x)_{13}$ and $Ce(Ni_{1-x}Ga_x)_{13}$ systems [1−3] indicated the formation of several $NaZn_{13}$-related phases with (pseudo)cubic ($NaZn_{13}$ aristotype, space group *Fm−3c*), tetragonal ($CeNi_{8.5}Si_{4.5}$ structure type, space group *I*4/*mcm*, $a_t \approx a_c/\sqrt{2}$, $c_t \approx a_c$) and two orthorhombic atomic arrangements ($LaNi_7In_6$ structure type, space group *Ibam*, $a_o \approx a_c/\sqrt{2}$, $b_o \approx a_c/\sqrt{2}$, $c_o \approx a_c$, and own structure type, space group *Fmmm*, $a_o \approx a_c$, $b_o \approx a_c$, $c_o \approx a_c$). In these series, the distortions of the basic $NaZn_{13}$ structure are strongly depend on the composition, which vary between $x = 2.2$ and 7.6 for lanthanum, and between $x = 3.9$ and 7.3 for cerium systems. Thus, a sequence of the morphotropic phase transformations *Fm−3c*↔*I*4/*mcm*(I)↔*Ibam*↔*Fmmm*↔*I*4/*mcm*(II) occurs in both systems. It is evident, that the deformation of the structures also takes place at elevated temperatures as indicated by the multiple twinning of the microstructures. Nevertheless, no signs of the temperature-induced phase transformations are detected by differential thermal analysis up to the melting points of ~1000−1200 °C.

In situ high-temperature high-resolution X-ray synchrotron powder diffraction examinations of the selected $La(Ni_{1-x}Ga_x)_{13}$ and $Ce(Ni_{1-x}Ga_x)_{13}$ samples with *Ibam* and *Fmmm* structures clearly showed complex temperature-induced structural phase transitions. The measurements were performed at BL04-MSPD beamline of ALBA synchrotron facilities (Experiment N 2014071025).

Continuous phase transition *Ibam*↔*I*4/*mcm* occurs in $LaNi_{8.5}Ga_{4.5}$ and $CeNi_{7.25}Ga_{5.75}$ phases at 460 °C and 895 °C, respectively. From the extrapolation of the *c/a* ratio of tetragonal phases the transformation to the high-temperature cubic phase can be predicted for La and Ce samples above 1800 °C and 1500 °C, respectively, which is however much higher than their melting points of 1083 °C ($LaNi_{8.5}Ga_{4.5}$) and 1001 °C ($CeNi_{7.25}Ga_{5.75}$). Complex behavior of the lattice parameters, e.g., negative expansion of the orthorhombic *Ibam* phase along [001], was observed for both phases.

Discontinuous phase transition *Fmmm*↔*Fm*−3*c* has been detected in $LaNi_{6.13}Ga_{6.87}$ and $CeNi_{6.13}Ga_{6.87}$ phases at the temperatures of 750 °C and 700 °C, respectively. Close analysis of the diffraction patterns in the vicinities of the transition temperatures revealed that the transition from the orthorhombic *Fmmm* structure to the parent *Fm*−3*c* cubic arystotype occurs through an intermediate tetragonal phase, existing in a narrow temperature range of 50−80 °C.

---

[1] Yu. Grin, R.E. Gladyshevsky, Gallides, Metallurgia, Moscow, 1989.

[2] L. Vasylechko, Yu. Grin, in: G. Effenberg, O.I. Bodak, T.I. Yanson (Eds.), Red Book. Constitutional Data and Phase Diagrams. Vol. 41, Part 3 MSI GmbH, Germany, 1996, pp. 1545-1547.

[3] L. Vasylechko, Yu. Prots, U. Burkhardt, C. Drathen, D. Kaczorowski, Yu. Grin. New distorted variants of the $NaZn_{13}$ type of structure. 14th European Conference on Solid State Chemistry (ECSSC14). July 7 − 10, 2013, Bordeaux, France. Meeting Abstracts, P. 118.

PMon025

Synthesis of supported intermetallic $Pd_{1-x}Zn_{1+x}$ nanoparticles for catalysis

Wibner, Patrick (Department of Inorganic Chemistry (Materials Chemistry), University of Vienna, Vienna, AUT); Kriegel, René (Institut für Chemie, Technische Universität Chemnitz, Chemnitz, GER); Richter, Klaus W. (Department of Inorganic Chemistry (Materials Chemistry), University of Vienna, Vienna, AUT); Armbrüster, Marc (Institut für Chemie, Technische Universität Chemnitz, Chemnitz, GER)

Many hydrogen storage systems for fuel-cells have been investigated, over the last few years. One possibility is the storage of hydrogen in chemical form as methanol. This type of fuel cell is called *Direct-methanol-fuel-cell* (DMFC) and the release of hydrogen from methanol is named “Methanol-Steam-Reforming” (MSR). Catalysts like $Cu/ZnO/Al_2O_3$ and derivatives were investigated. A promising novel metal catalyst is Pd/ZnO which in situ forms the intermetallic phase PdZn. Since the intermetallic PdZn phase exhibits a broad homogeneity range, it stands to reason that different compositions of the same phase might show different catalytic activity and selectivity.

A phase diagram assessment of the Pd-Zn system was performed and the system modelled via CALPHAD-method, yielding activities, which were used to calculate a temperature gradient for synthesizing a catalyst with controlled composition by gas/solid reaction via a pseudo-isopiestic set-up. The activities obtained by the CALPHAD-method needed to be tested since the activity of a bulk material and nano particles can differ significantly.

$PdZn/Al_2O_3$ catalysts with different compositions and at varying reaction temperatures were produced in order to find the best path for synthesizing a catalyst with high activity and high CO_2-selectivity.

The catalysts were characterised by the means of XRD, ICP-MS, ICP-OES, SEM and TEM. XRD and TEM studies show intermetallic PdZn nanoparticles with a narrow size distribution around 6-7 nm. Neither ICP-OES nor ICP-MS delivered high accuracy results in terms of composition and could only provide the average composition of the PdZn particles, so additional studies are necessary for a good compositional characterization. Activity and CO_2-selectivity of the synthesized catalysts was determined and compared to other model catalysts. A maximum CO_2-selectivity and activity was reached for the catalyst with the highest zinc content.

PMon026

Synthesis, Structure and Properties of Novel Nitridogermanate $Ca_6[Ge_2N_6]$

Pathak, Manisha (Max Planck Institute for Chemical Physics of Solids, Dresden, GER); Ovchinnikov, Alexander (Max Planck Institute for Chemical Physics of Solids, Dresden, GER); Schelle, Walter (Max Planck Institute for Chemical Physics of Solids, Dresden, GER); Bobnar, Matej (Max Planck Institute for Chemical Physics of Solids, Dresden, GER); Hoehn, Peter (Max Planck Institute for Chemical Physics of Solids, Dresden, GER); Grin, Yuri (Max Planck Institute for Chemical Physics of Solids, Dresden, GER)

Characteristic structural features of most of the ternary alkaline earth (*AE*) germanium nitrogen compounds are isolated or condensed nitridogermanates anions $[Ge_xN_y^{z-}]$ surrounded by electropositive *AE* cations; previously known nitridogermanates with Ca include $Ca[GeN_2]$[1], $Ca_2[GeN_2]$[2] $Ca_5[Ge_2N_6]$[2], $Ca_4[GeN_4]$[2], and $Ca_7[GeN_4]N_2$[3], in contrast to anti-perovskite calcium germanide nitride Ca_3GeN[4].

In the present contribution, we report the novel calcium nitridogermanate $Ca_6[Ge_2N_6]$. The new phase crystallizes trigonal (*R*3 (No.148), a = 9.2124(2) Å, c = 9.2675(3) Å, Z = 3). $Ca_6[Ge^{III}{}_2N_6]$ is the first example of a nitridogermanate containing $[Ge_2N_6]^{12-}$ dimers with Ge-Ge bonds. Ge in 3+ oxidation state is tetrahedrally coordinated by Ge and 3 N with Ge-Ge bond length of 2.4188(3) Å and Ge-N distances of 1.903(1) Å, (3x). Previously reported phases $Ca_2[Ge^{II}N_2]$, $Ca_4[Ge^{IV}N_4]$ & $Ca_7[Ge^{IV}N_4]N_2$, $Ca_5[Ge^{IV}N_3]_2$, and $Ca[Ge^{IV}N_2]$, contain nitridogermanates in the form of bent anions of $[GeN_2^{4-}]$, isolated tetrahedra $[GeN_4^{8-}]$, infinite chains of $^1[GeN_2N_{2/2}^{5-}]$, and 3D network of $[GeN_{4/2}^{2-}]$, respectively. The isolated N^{3-} in $Ca_7[Ge^{IV}N_4]N_2$ is coordinated by six Ca^{2+}.

Synthesis of $Ca_6[Ge_2N_6]$ was performed from Ca_3N_2 and Ge in molar ratio of 3 : 1 in sealed tantalum ampoules at 750°C using molten Na as flux and NaN_3 as a source of N_2. After the reaction, excess Na was removed under dynamic vacuum at 300°C. The heavy atom positions of isotypic $Ca_6[Cr_2N_6]H$[5] phase were used as a starting model in Rietveld refinement, however no indications for any occupation of the H-site were observed. Physical properties characterization such as electric resistivity and magnetic susceptibility will be presented as well.

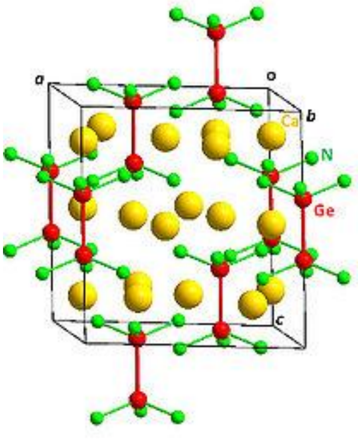

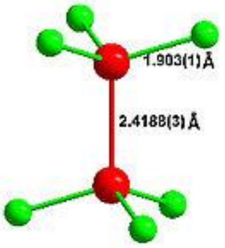

---

[1] Manuaye, M.; Guyader, J.; Laurent, Y.; Lang, J.; Bull. Soc. Fr. Mineral. Cristallogr. 1971, 94, 347-352.
[2] Clarke, S.J.; DiSalvo, F.J.; Inorg. Chem. 2000, 39, 2631-2634.
[3] Junggeburth S.C.; Oeckler O.; Johrendt D.; Schnick W.; Inorg. Chem. 2008, 47, 12018-12023.
[4] Chern, M.Y.; Vennos, D.A.; DiSalvo, F.J.; J. Solid State Chem. 1992, 96, 415-425.
[5] Bailey, M.S.; Obrovac, M.N.; Baillet, E.; Reynolds, T.K.; Zax, D.B.; DiSalvo, F.J.; Inorg. Chem. 2003, 42, 5572-5578.

PMon027

Synthesis, crystal structure and properties of a new compound Ir_2Cd_{23}

Feng, Xianjuan (Max-Planck-Institute for chemical physics of solids, Dresden, GER); Prots, Yurii (Max-Planck-Institute for Chemical physics of solids, Dresden, GER); Bobnar, Matej (Max-Planck-Institute for Chemical Physics of solides, Dresden, GER); Schmidt, Marcus (Max-Planck-Institute for Chemical Physics of Solids, Dresden, GER); Grin, Yuri (Max-Planck-Institute for Chemical Physics of Solids, Dresden, GER)

A new compound Ir2Cd23 was synthesized from elemental components in a sealed tantalum crucible at 1000 °C for 3 hours and subsequent annealing at 600 °C for 4 days. X-ray single-crystal diffraction was performed on the selected crystal which is a twin along [111] direction, simulating reverse-obverse twinning in the rhombohedral setting of the structure. The relationship between two domains can be described by the matrix (2/3 -1/3 2/3; 2/3 2/3 -1/3; -1/3 2/3 2/3) (in cubic setting).

The refinement revealed that, it crystallizes in a new structure type, which is closely related to Rh7Mg44.[1] Compared to Rh7Mg44, Ir atoms occupy two of the three sites of Rh, Cd5 takes the third one(24g). The rest Cd atoms occupy two more positions (24f and 16e) while failing to one of the 48h sites. The relationship between these two structure can be described in the Wyckoff notation as: h5g2fe6 (hh4g2f□e6□) and h4g2f2e7(□h4g2f2e7) for Rh7Mg44 and Ir2Cd23 respectively. The crystal structure of Ir2Cd23 can be described as condensed [Ir1Cd]10, [Ir2Cd]12 polyhedra. The interstitial holes are filled by blocks formed by 6 condensed [Cd5Cd]12 icosahedra. The center of these icosahedra (Cd5 atoms) are located in the apexes of a regular octahedron. Ir-Cd distances vary from 2.72 to 3.00 Å, while Cd-Cd distances from 2.86 to 3.18 Å. No Ir-Ir contact can be expected since the shortest Ir-Ir distance is 4.93 Å. The structural peculiarities of Ir2Cd23 are discussed with those of Ir8Cd41 and V8Ga41.[2-3]

The composition of Ir2Cd23 is confirmed by EDX. According to TG-DTA, it is stable up to 670 °C, followed by decomposition with elimination of Cd. Ir2Cd23 shows a metallic behavior in the electrical resistivity between 2 K and 400 K. Diamagnetic dominants under external magnetic field from 10 mT to 70 T between 2 K and 400 K.

---

[1] L. Westin, L.-E. Edshammar. Acta Chem. Scand. 25, 1480 (1971).
[2] X.-J Feng, Y. Prots, Zeitschrift für Kristallographie. New crystal structures 228, 299 (2013).
[3] K. Yvon. Acta Crystallogr. B30, 853 (1974).

PMon028

Systematic investigations of Ce-Ru interactions by XPS

Niehaus, Oliver (Institut für Anorganische und Analytische Chemie and NRW Graduate School of Chemistry, Universität Münster, Münster, GER); Bartsch, T. (Institut für Anorganische und Analytische Chemie and NRW Graduate School of Chemistry, Universität Münster, Münster, GER); Bartsch, M. (Physikalisches Institut, Universität Münster, Münster, GER); Abdala, P. M. (SNBL at ESRF, European Synchrotron Radiation Facility, Grenoble, FRA); Pöttgen, R. (Institut für Anorganische und Analytische Chemie and NRW Graduate School of Chemistry, Universität Münster, Münster, GER)

In several ternary intermetallic compounds containing cerium and ruthenium, very short Ce–Ru distances are reported.[1,2] These distances are significantly shorter than the sum of the covalent radii of 289 pm, which can only be explained by partially tetravalent cerium.

According to systematic substitution of ruthenium in CeRuSn we were able to prove the dependence of the cerium valence on the transition metal. Therefore, all compounds have been investigated by magnetic measurements and x-ray absorption near edge structure (XANES) spectroscopy. The results of both methods coincide very well.[3,4]

Up to know we were just able to show that different cerium valences have no influence on the third element.[5] In this work we like to use x-ray photoelectron spectroscopy (XPS) as a third method for the determination of the cerium valence by electron spectroscopy for chemical analysis (ESCA). Furthermore we will use ESCA to check any influence of different cerium valences on the binding energies (especially $3d_{5/2}$ and $3d_{3/2}$) of ruthenium. Therefore, a number of different compounds with trivalent and intermediate cerium will be investigated and discussed in comparison to results from magnetic measurements and XANES. In Fig. 1 the x-ray absorption spectra of $CeRu_2Si_2$ and $Ce_2Ru_4Mg_{17}$ are displayed in comparison to CeO_2 and $Ce_2(CO_3)_3$ as tetravalent and trivalent standards, respectively. Fitting of these results leads to a cerium valence 3.06(3) for $CeRu_2Si_2$ and 3.12(3) for $Ce_2Ru_4Mg_{17}$.

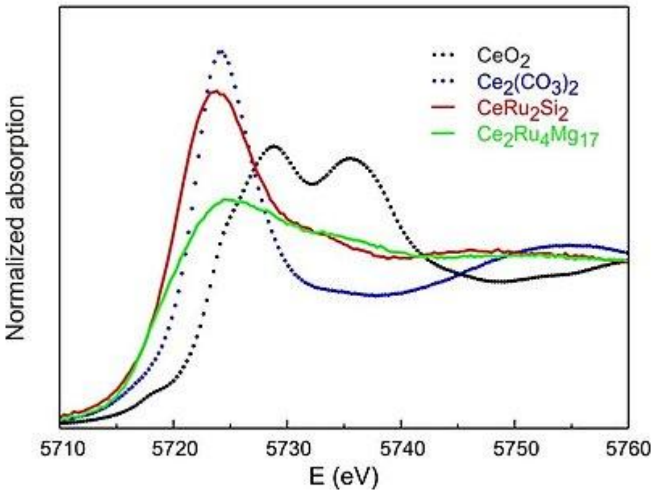

Fig. 1. Normalized L_{III} XANES spectra of $CeRu_2Si_2$ and $Ce_2Ru_4Mg_{17}$ plotted together with$Ce_2(CO_3)_3$ and CeO_2 as reference compounds.

---

[1] F. Hermes, S. F. Matar, R. Pöttgen, *Z. Naturforsch.***2009**, *64b*,901.
[2] T. Mishra, R.-D. Hoffmann, C. Schwickert, R. Pöttgen, *Z. Naturforsch.* **2011**, *66b*, 771.
[3] O. Niehaus, P. M. Abdala, R. St. Touzani, B. P. T. Fokwa, R. Pöttgen, *Solid State Sci.* **2015**, *40*, 36.
[4] O. Niehaus, P. M. Abdala, R. Pöttgen, *Z. Naturforsch.* **2015**, *70b*, 253.
[5] O. Niehaus, P. M. Abdala, J. F. Riecken, F. Winter, B. Chevalier, R. Pöttgen, *Z. Naturforsch*. **2013**, *68b*, 960.

PMon029

Ternary Intermetallic Compound in Ca-Cd-Pt System

Gulo, Fakhili (Sriwijaya University, Palembang, IDN)

Three ternary intermetallic compounds were successfully isolated in the Ca-Cd-Pt system. Cubic $Ca_3Cd_8Pt_4$(*Fm*-3*m*, a = 13.513(1) Å) contains octahedral calcium cluster centered by platinum, Pt@$Ca_6$and tetrahedral star cadmium cluster, Cd_8as main blocks. A simple compound, CaCdPt crystallizes in orthorhombic system (*Pnma*, a = 7.5748 (15) Å, b = 4.4774 (9) Å, and c = 8.6383 (17) Å). Here, calcium atoms are bonded to each other in the form of six-membered rings with chair conformations. The novel structure, $Ca_6Cd_{11}Pt$ crystallizes in orthorhombic system with space group, *Pnma*, a = 18.799(2) Å, b = 5.986(1) Å, c = 15.585(3) Å. It contains novel pentagonal bipyramidal (PBP) Cd_7 clusters. Calcium form pentagonal rings along *ac*-plan which are stuffed between Cd pentagonal bypiramidal clusters.

PMon030

The NiAs structure family: structure-composition relations and thermodynamic modelling

Jandl, Isabella (Institut für Anorganische Chemie (Materialchemie), Wien, AUT); Ipser, Herbert (University of Vienna, Vienna, AUT); Richter, Klaus W. (University of Vienna, Vienna, AUT)

The general NiAs structure includes the related structure types CdI_2, NiAs and Ni_2In. It is composed of transition metals T and main group elements B, out of the 13th to 16th group, forming $T_{1\pm x}B$ structures. Due to its ability to include different amounts of transition metal, large homogeneity ranges can be found, between $T_{0.5}B$ and T_2B. This structure is widespread among transition metal compounds and therefore present in many different alloy systems. Especially in higher order systems, little is known about occurrence and homogeneity ranges of corresponding solid solution phases.

To contribute to this knowledge, a few ternary model systems were investigated experimentally in a current research project. Phase equilibria and structural characteristics were analysed. One of these systems, Ni-Sn-Te, revealed a continuous solid solution between a phase with TB_2-structure ($NiTe_2$) and a phase with T_2B-structure (Ni_3Sn_2 HT), forming an extended single-phase field. To other investigated systems (Ni-Pt-Sn and Ni-Pd-Sn) showed continuous solid solutions of the NiAs phases in the ternary, as well. Moreover, a partial ordering of the transition metals throughout these phase fields was discovered.

As nowadays, alloys are getting more and more complex, consisting of many different components; extrapolations using the Calphad approach are often the method of choice. A detailed knowledge of the underlying crystal chemistry is necessary for consistent models. Based on our investigations, it is necessary to integrate the whole possible homogeneity range of the general NiAs structure into one single model. Hence, a modified sublattice model for NiAs structures is proposed for future Calphad optimisations. Three endmember of this model correspond to the boundary structures of the general NiAs type (CdI_2, NiAs, Ni_2In). In preparation of future Calphad-type modelling, the energies of formation of compounds with these three boundary structures were calculated using ab-initio density functional theory. A small database of energies of formation of (hypothetic) binary Ni-containing NiAs structures with varying main group elements has been developed.

PMon031

The assessment of the Al-V and Al-Si-V system

Kroupa, Ales (Institute of Physics of Materials AS CR, , Brno, CZE); Richter, Klaus W. (Department of Inorganic Chemistry/Materials Chemistry, University of Vienna, Wien, AUT)

The ternary Al-Si-V system was studied experimentally [1,2] and obtained experimental data were used for the theoretical assessment of this system. It was found during the work on the assessment that the latest reassessment of the binary Al-V system [3] is not correct and it is impossible to model the experimental results obtained for the ternary Al-Si-V system. Therefore, the reassessment of the Al-V system was carried out, using experimental data from [4] and using different thermodynamic data for the enthalpies of formation at 298 K than in the case of study [3]. The reassessed binary system was used in the assessment of the ternary system and results are presented in this work.

This work was supported by the Czech Science Foundation in the scope of the project No. 14-15576S.

---

[1] B. Huber, H. S. Effenberger, K. W. Richter, Intermetallics, 18(4)/2010, 606-615.

[2] B. Huber, K. W. Richter, Intermetallics, 19(3)/2011, 369-375

[3] W. Gong, Y. Du, B. Huang, R. Schmid-Fetzer, C. Zhang, H. Xu, Zeit. F. Metallkde., 95(11)/2004, 978-986

[4] K.W. Richter, H. Ipser, Zeit. f. Metallkde., 91(5)/2000, 383-388.

PMon032

The systems Li-Sb and Cu-Li-Sb, an experimental approach

Beutl, Alexander (Institut für Anorganische Chemie (Materialchemie), AUT); Effenberger, Herta Silvia (University of Vienna, Institut für Mineralogie und Kristallographie, Vienna, AUT); Flandorfer, Hans (University of Vienna, Dep. Inorganic Chemistry / Materials Chemistry, Vienna, AUT)

Antimony and its alloys have recently attracted attention in regard of their capability to reversibly uptake Li. With theoretical energy densities far beyond the value for carbon, which is the currently preferred anode material for lithium ion batteries (LIBs), antimony containing systems might play an important role in the development of high performance LIBs in the near future. However the lack of basic thermodynamic information on these materials and their respective phase relations hinders a systematic development of new Li-ion novel anodes.

Our investigations currently focus on a detailed thermodynamic description of the systems Li-Sb and Cu-Li-Sb. XRD, thermal analysis and calorimetry were used to describe the respective phase diagrams. Several new ternary intermetallic compounds were identified and their crystal structures were determined. Isothermal and vertical sections were developed.

This work has been funded by the FWF under the project I559-N19 and by the DFG under the project FL-730/1-2 within the DFG priority project SPP 1473 "WeNDeLIB".

PMon033

Thermodynamic properties of Mg-Pd alloys

Delsante, Simona (Department of Chemistry and Industrial Chemistry, Genoa University, Genova, ITA); Borzone, Gabriella (Department of Chemistry and Industrial Chemistry, Genoa University, Genova, ITA)

A peculiar feature of the Mg-Pd phase diagram is the presence of several “Complex Metal Alloys (CMAs)” which are phases with giant unit cells and inherent structural disorder; their structure can be described with Mackay clusters as fundamental structural unit [1]. The assessment of the Mg-Pd phase diagram was published in 1988 by Nayeb-Hashemi et al. [2] with many uncertainties and subsequently, considering the existence of the CMAs, was revised by Makongo et al. [1]. At present a definitely assessed version of the Mg-Pd phase diagram is not available, and great differences can be found for instance in the formation of the Mg_6Pd phase which is indicated to be a peritectic one by [2] and having a congruent melting by [1]. As for the standard enthalpies of formation ($\Delta_f H°$) there is a great lack in literature for the Mg-Pd phases; nowadays predictive methods are very developed, but it is not trivial to apply common models to giant cells like those of the CMAs. Usually the $\Delta_f H°$ are calculated with ab initio methods and the most used is the Density Functional Theory (DFT), but the problem is that in a multielectronic system the exchange-correlation energy is unknown and so approximation must be used. The great interest on first-principles calculations is also motivated with the possibility to use their results in the CALPHAD method to predict stability and phase boundaries of complex systems. For the Mg-Pd system studied in this work, the $\Delta_f H°$ values have been calculated by [3] and no experimental data can be found in literature. A high temperature drop calorimeter [4, 5] has been employed to directly measure the $\Delta_f H°$ at 300K of the Mg_6Pd phase. The calorimetric results have been validated by X-ray Powder Diffraction (XRD) and Scanning Electron Microscopy (SEM) coupled with Electron Probe Microanalysis (EPMA) analysis. A high sensitive SETARAM 111 Differential Scanning Calorimeter has been employed to determine the formation temperature of the Mg_6Pd phase. An enthalpy of formation value of -28.0±0.5 (kJ/ mol · at) at 300K was obtained for the Mg_6Pd intermetallic phase and the congruent melting behaviour was confirmed at 564°C, in fair good agreement with the value of 571°C proposed by Makongo et al. [1]. A more exothermic formation was measured for the Mg_5Pd_2, to be – 39.5±1.0 (kJ/ mol · at) at 300K. The results will be presented, discussed and compared with literature data.

---

[1] J. Makongo et al., Philosophical Magazine, 86 (3) (2006) 427.
[2] A.A. Nayeb-Hashemi et al., Phase Diagrams of Binary Magnesium alloys, ASM International, Materials Park, OH, (1988) 247.
[3] J.F. Fernandez et al., Intermetallics, 19 (2011) 502.
[4] G. Cacciamani et al., J. Alloys and Compounds 220 (1995) 106.
[5] G. Ghosh et al., Acta Materialia 54 (2006) 4977.

PMon034

$V_{18}P_9C_2$ - a Complex Phosphide Carbide

Boller, Herbert (Institut für anorganische Chemie, Universität Linz, AUT); Effenberger, Herta (Institut für Mineralogie und Kristallographie der Universität Wien, Wien, AUT)

The title compound crystallizes in the orthorhombic space group No.51, *Pmma* with a = 1704.4(3), b = 322.19(7), and c = 1303.0(2) pm, Z=2.The crystal structure is composed of 19 symmetry independent atoms forming a complicatednetwork. These features will be compared with related phases, e.g. V_4P_2C or V_2P. In view of the small amount of carbon in $V_{18}P_9C_2$ this compound can be considered rather as an interstitially stabilised (binary) vanadium phosphide.

PMon035

Vacancy ordering phenomena in novel RZn_xGe_2 compounds (R=Tb-Er; 0.15<x<0.25)

De Negri, Serena (Università degli Studi di Genova, Genova, ITA); Proserpio, Davide (Università di Milano / Samara State University, Milano, ITA); Saccone, Adriana (DCCI, Università di Genova, Genova, ITA); Solokha, Pavlo (DCCI, Università di Genova, Genova, ITA)

Rare-earth (R)-based binary and ternary germanides have been the object of numerous studies, focused on their crystal structure, chemical bonding and physical properties. Within this family, the RM_xGe_2 compounds (M = transition or *p*-block metal) are of particular interest due to their crystallographic peculiarities, *i.e.* the presence of modulated planar Ge layers and partially occupied M sites, coupled with zero thermal expansion behaviour [1-3].

In this work, results on new RZn_xGe_2 (R = heavy rare earth metals) compounds are presented and discussed. These compounds were found for the first time as by-products of syntheses targeted to obtain $R_2Zn_{1-x}Ge_6$ phases, in the framework of our research activity on R-Zn-Ge systems [4].

Ternary samples of nominal composition $R_{32}Zn_5Ge_{63}$ (R = Tb, Dy, Ho, Er) were then synthesized by direct reaction of the constituents, enclosed in an arc sealed Ta crucible, inside a resistance furnace, under a controlled thermal cycle and a continuous rotation. Samples were characterized by scanning electron microscopy coupled with energy dispersive X-ray spectroscopy (SEM-EDXS) and the crystal structures of the new RZn_xGe_2 compounds were studied by single-crystal X-ray diffraction (XRD) analysis.

In the literature, analogue RM_xGe_2 compounds were described mainly as deficiency derivatives of the $CeNiSi_2$ - structure type. Recently, some of them were reinterpreted both as 4-fold superstructures [1] or commensurately modulated structures [2, 3]. These models give a more accurate description of the Ge layers distortion and the M atoms ordered distribution suggested by the presence of weak super reflections in the electron diffraction plots.

The X-ray diffraction patterns of the RZn_xGe_2 studied compounds show similar super reflections, whose intensities and distribution depend on the nature of R. The structural model best fitting our experimental data is a 8-fold superstructure (own structure type, $P2/n$, $mP54$-x–$g^{10}f^4e^3$, for R=Dy a = 5.6705(11) Å, b = 16.144(3) Å, c = 11.319(2) Å, b = 92.12(3)°). For R = Tb, Dy crystals non-merohedral twinning was observed, instead for R = Ho, Er crystals single domains were detected. The relation between the proposed 8-fold superstructure and the $CeNiSi_2$ aristotype is presented by means of symmetry reduction in the Bärnighausen formalism. This representation highlights in a concise manner the ordering of Zn atoms and possible twin formation.

---

[1] M. A. Zhuravleva et al., *Inorg. Chem.* 44 (2005) 2177;
[2] S. C. Peter et al., *J. Am. Chem. Soc.* 133 (2011) 13840;
[3] J. Zhang et al, *Inorg. Chem.* 54 (2015) 722;
[4] P. Solokha et al., *Inorg. Chem.* 54 (2015) 2411.

PMon036

Anomalous Thermal Expansion of Mixed Samarium Cobaltites-Ferrites

Pekinchak, Olga (Lviv Polytechnic National University, Lviv, UKR); Vasylechko, Leonid (Lviv Polytechnic National University, Lviv, UKR); Prots, Yuri (Max-Planck-Institut für Chemische Physik fester Stoffe, Dresden, GER); Chernyshov, Dmitry (Swiss-Norwegian Beam Lines at ESRF, Grenoble, FRA)

The interest in the rare earth (R) cobaltites and ferrites with a perovskite structure is stimulated by their unique fundamental physical properties. In particular, $RCoO_3$ compounds exhibit temperature induced metal-insulator transitions and different types of magnetic ordering, which are strongly dependent on the spin state of Co^{3+} ions. The latter undergo a thermally driven transition from a low-spin (LS) to intermediate-spin (IS) and high-spin (HS) states. Generally $RFeO_3$ ferrites exhibit spin-reorientation transitions at 80-200 K and para- to antiferomagnetic transitions at 620-750 K. Recently, clear sign for the magneto-elastic coupling at the Neel temperature of 675 K has been revealed for $SmFeO_3$ based on *in situ* synchrotron and neutron powder diffraction as well as polarization dependent soft X-ray absorption spectroscopy [1].In order to study a phase and structural behaviour of the mixed cobaltites-ferrites a series of $SmCo_{1-x}Fe_xO_3$ samples with x=0.1-0.9 were prepared by solid state reactions in air at 1573 K. High-temperature X-ray synchrotron powder diffraction has been performed *in situ* at Swiss-Norwegian beam line BM1A of ESRF (Grenoble, France). The measurements were carried out in the temperature range of 298-1100 K at the mulipurpose PILATUS@SNBL diffractometer (WL = 0.69748 A) equipped with hot-air blower. Diffraction patterns were collected at the fixed temperatures with the step of 5-10 K. Analysis of the diffraction data was carried out using the WinCSD program package.

In situ high temperature powder diffraction of the $SmCo_{1-x}Fe_xO_3$ series revealed considerable anomalies in the lattice expansion which are especially pronounced for the cobalt-rich specimens. The anomalies, which are reflected in a sigmoidal dependence of the unit cell parameters and in the considerable increasing of the thermal expansion coefficients, are obviously associated with the changes in the spin state of Co^{3+} ions from LS to IS or HS. Observed deviations in the lattice expansion in the $SmCo_{1-x}Fe_xO_3$ series become less pronounced with the decreasing cobalt content, but they are clearly detectable even in the Fe-richest specimen $SmCo_{0.1}Fe_{0.9}O_3$. Thorough analysis of the selected bond lengths and tilt angles of Co/FeO_6 octahedra, as well as atomic displacement parameters (ADPs) of transition elements and oxygen, revealed further structural anomalies in the $SmCo_{1-x}Fe_xO_3$ series. Significant bond-length stretching inside Co/FeO_6 octahedra in $SmCo_{0.7}Fe_{0.3}O_3$ at 450 K and 720-730 K as well as corresponding extrema at ADPs curves indicate the Jahn-Teller distortion (which may be dynamic). These effects can be associated also with the magnetic and electronic phase transitions occurred in the end members of the system. In particular, "pure" $SmCoO_3$ undergoes magnetic and metal-insulator transitions at 493 K and 693 K, respectively, whereas $SmFeO_3$ shows the spin-reorientation transition at 480 K and para- to antiferomagnetic transition at 670 K. It is evident that the coupling of the electronic and magnetic transitions with the lattice will result in extremely complicated magnetic and electronic phase diagram of the mixed cobaltite-ferrite systems.

The work was supported in parts by the Ukrainian Ministry of Education and Sciences (Project "KMON") and ICDD Grant-in-Aid program. In situ high-temperature synchrotron diffraction measurements were carried out during beamtime allocated to the CRG Experiment No 01-02-1065.

---

[1]. C.-Y. Kuo, Y. Drees, M.T. Fernandez-Diaz, L. Zhao, L. Vasylechko *et al. Phys. Rev. Letters* 113 (2014) 217203 (5pp).

[2] O. Kharko, L. Vasylechko, S. Ubizskii, A. Pashuk, Yu. Prots. *Functional Materials* 21(2) (2014) 226-232.

PMon037

Nanoscaled Gadolinium and Magnesium Carbonate Hollow Spheres

Jung-König, Jan (Institute for Inorganic Chemistry, KIT, Karlsruhe, GER); Feldmann, Prof. Dr. Claus (Institute for Inorganic Chemistry, KIT, Karlsruhe, GER)

Inorganic hollows spheres are highly interesting alternatives to polymer spheres and liposomes as drug delivery systems in medicine.[1] To this regard, we present nanoscaled gadolinium and magnesium carbonate hollow spheres which can be loaded, for instance, with the cytostatic doxorubicin.

Via a modified microemulsion synthesis,[2] we obtained amorphous hollow spheres of gadolinium and magnesium carbonate according to X-ray and electron diffraction data. The w/o microemulsion consists of water (pH 12) saturated with CO_2 and an unpolar phase of dodecane. The unpolar phase of the microemulsion is loaded with an organic gadolinium or magnesium precursor, whereas agents and dyes can be dissolved in the water phase. Under controlled temperature and CO_2-atmosphere hollow spheres can be obtained. STEM and TEM images show that the gadolinium carbonate hollow spheres have a mean diameter of 30 nm and a cavity of 7 nm, whereas the magnesium carbonate hollow spheres are about 42 nm in size and 12 nm of the inner cavity. In vitro studies based on HeLa and HepG2 cells show an enhanced toxicity of doxorubicin filled gadolinium carbonate as compared to free doxorubicin. Nanocapsules of inorganic compounds like gadolinium carbonate and magnesium carbonate show an increased release rate under reduced pH-values, proved by UV/Vis traced dialysis bag release studies.[3] Reduced pH-values are associated to many tumors.[4] It is known from literature that it is possible to minimize side effects of doxorubicin by encapsulation.[5] The doxorubicin filled gadolinium and magnesium carbonate hollow spheres might further decrease toxic effects. In the first step, gadolinium carbonate hollow spheres are administered to trace the amount and body distribution of gadolinium compounds by MRT techniques and benefit of the enhanced release rate of doxorubicin by external magnetic fields. Secondly, the highly biocompatible, chemically related magnesium-based hollow spheres are applied to deliver high amounts of doxorubicin in a personalized therapy to reduce the amount of doxorubicin to a minimum.

---

[1] L. Brannon-Peppas, J. O. Blanchette, *Adv. Drug Delivery Rev.* **2012**, 64, Supplement, 206-212.

[2] P. Leidinger, R. Popescu, D. Gerthsen, C. Feldmann, *Small* **2010**, 6, 1886-1891.

[3] J. Jung-König, R. Popescu, U. S. C. Seidl, D. Gerthsen, C. Feldmann, *in preparation* **2015**.

[4] L. E. Gerweck, K. Seetharaman, *Cancer Res.* **1996**, 56, 1194-1198.

[5] O. Tacar, P. Sriamornsak, C. R. Dass, *J. Pharm. Pharmacol.* **2013**, 65, 157-170.

PMon038

Phase Relations of Alkali Metal Zinc Phosphates for Application in Lithium-Ion Battery Cathodes

Harm, Sascha (Ludwig-Maximilians-Universität München, München, GER); Nimmrich, Kathleen (Ludwig-Maximilians-Universität München, München, GER); Rager, Sabrina (Ludwig-Maximilians-Universität München, München, GER); Hoch, Constantin (Ludwig-Maximilians-Universität München, München, GER)

Transition metal phosphates are promising candidates for application in lithium ion batteries as cathode materials with high cyclic stability [1]. A new candidate material with this respect is $LiZnPO_4{\cdot}H_2O$. It crystallizes in the orthorhombic system (space group $Pna2_1$ with a = 10.575(2), b = 8.0759(9), c = 4.9937(6) Å [2]), isotypic to the zeolite type ABW ($Li[AlSiO_4]{\cdot}H_2O$ [3]). The network is build from vertex-sharing $[ZnO_4]$ and $[PO_4]$ tetrahedral anions and channels parallel to the c axis occupied with Li^+ cations and water molecules. The Li^+ cations are coordinated by water molecules and terminal O atoms from zincate and phosphate anions in tetrahedral $[LiO_3(H_2O)]$ units. Millimeter-sized single crystals for structural investigations can easily be obtained by dissolving lithium and zinc salts in phosphoric acid followed by successively increasing the pH value of the solution by diffusion of NH_3 through a PE membrane separating the aqueous ammonia from the lithium zinc phosphate solution [4].To obtain a redox-active material, Zn^{2+} ions have to be substituted by a divalent transition metal cation like *e. g.* Co^{2+}. For other zinc phosphates as *e. g.* Hopeite, $Zn_3(PO_4)_2{\cdot}4H_2O$, Co^{2+}-substituted single crystals can easily be grown in the same way, just by adding the redox-active bivalent element in the phosphate-containing solution. However, in the case of $LiZnPO_4{\cdot}H_2O$ this substitution process does not yield $LiZn_{1-x}Co_xPO_4{\cdot}H_2O$. Colorless needles are the only result, indicating that no cobalt is incorporated during crystal growth. However, $LiZn_{1-x}Co_xPO_4{\cdot}H_2O$ can be obtained by alkali metal ion exchange starting from $NaZn_{1-x}Co_xPO_4{\cdot}H_2O$. For this purpose, polycrystalline $NaZn_{1-x}Co_xPO_4{\cdot}H_2O$ has to be stirred over night in a saturated aqueous solution of $LiClO_4$. It is notable that $NaZn_{1-x}Co_xPO_4{\cdot}H_2O$ is not isotypic to the lithium compound. It crystallizes in a chiral crystal structure with the enantiomorphic hexagonal spacegroups $P6_122$ or $P6_522$ (a = 10.412(2), c = 15.184(2) Å [5]). This structure is known as zeolite CZP. It transforms to the $LiZn_{1-x}Co_xPO_4{\cdot}H_2O$ with ABW structure during the ion exchange of Na^+ versus Li^+. Cobalt-free $NaZnPO_4{\cdot}H_2O$ in CZP structure would only be obtained under hydrothermal conditions, under ambient conditions a reaction of zinc salt solution with phosphorous acid and NaOH results in the formation of $Na_6(ZnPO_4)_6(H_2O)_8$ with a sodalite-type crystal structure in space group $P4\text{-}3n$ (a = 8.8285(1)). When an exchange of Na^+ versus Li^+ is performed with this cobalt-free material, again the orthorhombic $LiZnPO_4{\cdot}H_2O$ is formed. Here we present an overview of the complex phase formation relations between the different zeolite structures of lithium and sodium zinc phosphates and the respective transformations occuring during exchange of Na^+ versus Li^+ and substitution of Zn^{2+} by Co^{2+}. Phase equilibria and transformations have been investigated by X-ray single crystal, powder diffractometric and thermoanalytical methods. They can be rationalized by consideration the respective lattice energies [6].

---

[1] A. K. Padhi, K. S. Nanjundaswamy, J. B. Goodenough, *J. Electrochem. Soc.* **144** (1997), 1188; C. Kallfaß, C. Hoch, H. Schier, A. Simon, H. Schubert, *Z. Naturforsch.***65B**, (2010), 1427.

[2] W. T. A. Harrison, T. E. Gier, J. M. Nicol, G. D. Stucky, *J. Solid State Chem.***114**, (1995), 249.

[3] E. Fois, A. Gamba, C. Medici, G. Tabacchi, S. Quartieri, E. Mazzucato, R. Arletti, G. Vezzalini, V. Dmitriev, *Micropor. Mesopor. Mat.***115**, (2008), 267.

[4] M. Friedrich, Dissertation, Universität zu Köln, 1992.

[5] W. T. A. Harrison, T. E. Gier, G. D. Stucky, R. W. Broach, R. A. Bedard, *Chem. Mater.***8**, (1996), 145.

[6] R. Hoppe, *Adv. Fluor. Chem.***6** (1970) 387.

PMon039

Phase equilibria, crystal structure and properties of the complex oxides in the Sm-Sr-Fe-Co-O system

Volkova, Nadezhda (Ural Federal University named after the first President of Russia B.N.Yeltsin, Yekaterinburg, RUS); Zubatkina, Lada (Ural Federal University, RUS); Maklakova, Anastasiya (Ural Federal University, Yekaterinburg, RUS); Galaida, Anastasiya (Ural Federal University, Yekaterinburg, RUS); Gavrilova, Ludmila (Ural Federal University, RUS); Cherepanov, Vladimir (Ural Federal University, Yekaterinburg, RUS)

Mixed rare earth and strontium cobaltates or ferrites attract significant attention as promising electrode materials for intermediate-temperature solid oxide fuel cells. The present work is devoted to a study of the phase equilibria in the Sr–Sr–Co–O, Sr–Sr–Fo–O and Sr–Fe–Co–O systems in air at 1100°C and determination of the crystal structure and properties of intermediate phases. The samples were synthesized by solid-state and glycerin nitrate techniques. The changes of oxygen content in the single phase complex oxides were measured by TGA method within the temperature range 25–1100° C . Thermal expansion of the ceramic samples was measured using a dilatometer in air. The total electrical conductivity was studied by the 4-probe DC method within 25–1100° C under atmospheric air. According to the results of XRD analysis three types of solid solutions: $Sr_{1-x}Sm_x(Fe,Co)O_{3-\delta}$, $Sr_{2-y}Sm_y(Fe,Co)O_{4\pm\delta}$, $Sr_{3-z}Sm_zFe_3O_{7-\delta}$ exist in the systems. Formation of the $SmFe_{1-z}Co_zO_{3-\delta}$ solid solutions within the range ($0 \le z \le 1$) has been confirmed. The value of oxygen content in $SmFe_{0.5}Co_{0.5}O_3$ has not noticeably changed within the whole temperature range under investigation. It was found that single-phase Sm-substituted solid solutions $Sr_{1-x}Sm_xMO_{3-\delta}$ (M = Fe, Co) formed within the range $0.00 \le x \le 0.50$. XRD patterns of the single phase samples were refined by Rietveld method within the cubic structure (*Pm3m* sp. gr.) for M = Fe or within the tetragonal structure (*I4/mmm* sp. gr.) for M = Co. On the other hand Sr-substitution for Sm in $Sr_{1-x}Sm_xFeO_{3-\delta}$ is also possible within the range $0.85 \le x \le 1.00$. These solid solutions, like unsubstituted $SmFeO_{3-\delta}$, were indexed in the orthorhombic structure (*Pbnm* space group). An introduction of samarium into the strontium cobaltate and strontium ferrite increases the oxygen content. The bend on the $\Delta L/L = f(T)$ curve for the $Sr_{0.9}Sm_{0.1}CoO_{3-\delta}$ indicates the presence of phase transition at temperature $\sim$ 335° C . The decrease of average values of TEC with the increase of Sm content is probably related to the reduction of the unit cell volume and diminishing of oxygen exchange. The temperature dependencies of the total conductivity of $Sr_{1-x}Sm_xMO_{3-\delta}$ (M = Fe, Co) possess maxima at approximately 300–500ºC in air. Seebeck coefficient for $Sr_{0.9}Sm_{0.1}MO_{3-\delta}$ (M = Fe, Co) and $SmFe_{0.5}Co_{0.5}O_{3-\delta}$ reveals positive values within the entire temperature and oxygen partial pressure ranges that indicate predominant *p*-type conductivity. According to the results of XRD analysis single phase samples $Sr_{2-y}Sm_yMO_{4\pm\delta}$ were formed within the range $0.7 \le y \le 1.1$ for M = Co and $0.7 \le y \le 0.8$ for M = Fe. X-ray diffraction patterns obtained for all single phase samples were indexed in the orthorhombic structure, sp. gr *I4/mmm.* The values of oxygen content in the $Sr_{2-y}Sm_yMeO_{4\pm\delta}$ solid solutions recalculated to the room temperature were nearly equal to 4.0. The miscibility gap was found in the row with the general formula $Sr_{3-z}Sm_zFe_2O_{7\pm\delta}$. The formation of solid solutions was found within the range $0.0 \le z \le 0.3$ and single phase sample was also obtained for z=1.2. The solid solutions based on strontium ferrite ($0.0 \le z \le 0.3$) possess tetragonal structure, *I4/mmm* space group whereas $Sr_{1.8}Sm_{1.2}Fe_2O_{7\pm\delta}$ was described in $P4_2/mmm$ space group. The value of oxygen content in the $Sr_{1.2}Sm_{1.8}Fe_2O_{7\pm\delta}$ was nearly equal to 6.96 at room temperature. The projections of isothermal–isobaric phase diagrams for the Sm – Sr – Co – O, Sm – Sr – Fe – O and Sr–Fe–Co–O systems to the compositional triangle of metallic components were presented.

This work was financially supported by the Russian Foundation for Basic Research (project no. 13-03-00958_a).

PMon040

The two new polyphosphides AgP_{15} and Ag_2GeP_{60} compared to LiP_{15}

Grotz, Carolin (TU München, FG Synthese und Charakt. innov. Mat., Garching, GER); Eckstein, Nadine (Tu München, FG Synthese und Charakt. innov. Mat., Garching, GER); Schäfer, Konrad (TU München, FG Synthese und Charakt. innov. Mat., Garching, GER); Nilges, Tom (TU München, FG Synthese und CHarakt. innov. Mat., Garching, GER)

During our investigations of the Ag/P and Ag/Ge/P systems, new polyphosphides have been synthesized via short way transport reactions, following the mineralizator concept[1]. Two phosphorus-rich compounds AgP_{15} and Ag_2GeP_{60} were discovered and characterized. The phases can be obtained from the corresponding elements adding iodine or GeI_4 as mineralizer, respectively. Both compounds form black, needle-shaped crystals which grow as aggregates at the ampoule wall. AgP_{15} is the first example of a transition metal polyphosphide featuring a $[P_{15}]$ subunit. It represents the third compound in the Ag/P system beside Ag_3P_{11}[2] and AgP_2[3].
The structures of the two polyphosphides were determined by single-crystal X-ray diffraction and were confirmed by powder X-ray diffraction and EDX measurements. Concerning the polyphosphide substructure both compounds show similar structure motifs, known from MP_{15} compounds where M is an alkali metal like Li[4] or K[5] and phosphorus forms a $[P_{15}]$- polyphosphide. According the Baudler nomenclature[6], the strand can be regarded as a $[P_8]$-cage, connected via $[P_2]$ and $[P_3]$ units. A tubular polymeric strand [P8]P2[P3]P2[results. It is carrying one negative charge, which is charge balanced by metal ions.

Recently, we were able to prove, that LiP_{15} and the higher homologues $(K,Rb)P_{15}$ are not isotypic, as stated earlier on.[7] LiP_{15} is characterized by a different orientation of the polyphosphide substructure compared with $(K,Rb)P_{15}$.[5] Going from the alkaline metal ions to the d^{10} ion in AgP_{15}, different coordination modes to the polyphosphide substructure occur. The situation is comparable with Cu_2P_{20}[1] where copper is separating $[P_{20}]$ subunits.

Adding a third component like in Ag_2GeP_{60} the situation is even more complex. While the polyphosphide substructure remains the same the occurrence of silver and germanium leads to a reorientation of the polyphosphide subunits relative to each other.Herein we report on the synthesis, crystal structures and selected physical properties of alkaline and late transition metal polyphosphides.

---

[1] S. Lange, M. Bawohl, R. Weihrich, T. Nilges, *Angew. Chem.***2008**, *120*, 5736-5739; *Angew. Chem. Int. Ed. Engl.***2008**, *47*, 5654 –5657.
[2] M. H. Moeller, W. Jeitschko, *Inorg. Chem.***1981**, *20*, 828-833.
[3] O. Olofsson, *Acta Chem. Scand.* **1965**, *19*, 229-241.
[4] N. Eckstein, L.-A. Jantke, T. F. Faessler, J. Mink, M. Drees, T. Nilges, *Eur. J. Inorg. Chem.***2014**, 5135-5144.
[5] H. G. v. Schnering, H. Schmidt, *Angew. Chem.* **1967**, *79*, 323-323.
[6] M. Baudler, *Angew. Chem.***1982**, *94*, 520 – 539; *Angew. Chem. Int. Ed. Engl.***1982**, *21*, 492 – 512.
[7] W. Wichelhaus, Dissertation, Westfälische Wilhelms-Universität Münster **1973**.

PMon041

A versatile tool box for the functionalization of layered materials: ion-exchange, micro-wave assisted reactions and post-functionalization

Wang, Yanhui (IPCMS UMR7504 CNRS-UNISTRA, STRASBOURG, FRA); Evrard, Quentin (IPCMS UMR7504 CNRS-UNISTRA, STRASBOURG, FRA); Taviot-Guého, Christine (ICCF UMR-CNRS 6296, Université Blaise Pascal, Aubière, FRA); Roger, Melissa (Laboratoire de Chimie Électrochimie Moléculaires et Chimie Analytique, UMR CNRS 6521, Brest, FRA); Jaffrès, Paul-alain (Laboratoire de Chimie Électrochimie Moléculaires et Chimie Analytique, UMR CNRS 6521, Brest, FRA); Delahaye, Emilie (IPCMS UMR7504 CNRS-UNISTRA, STRASBOURG, FRA); RABU, Pierre (CNRS IPCMS UMR7504, STRASBOURG, FRA); Rogez, Guillaume (IPCMS UMR7504 CNRS-UNISTRA, STRASBOURG, FRA)

Since the discovery of the outstanding electronic properties of the graphene derivatives, the research in the field of functional nanomaterials has been increasingly concerned with the conception of new multifunctional nanosheet-based systems, with intensification of research in the field of layered materials.[1]

Among the possible chemical routes, the hybrid organic–inorganic approach is particularly well suited to promote multifunctionality within a single material. In this way, transition metal layered simple hydroxides (LSH), of general formula $MII_2(OH)_3(X).mH_2O$ (M = Co, Cu, Ni and X = nitrate, acetate…), are very well adapted to grafting reactions of various molecules. In this poster, we will present our recent progress in this field [2].

For layered hydroxides, the functionalization essentially proceed by anion-exchange reactions, especially effective in aqueous medium. Even though this strategy has been very successful for obtaining new (multi)functional layered hybrid materials, it also severely limits the type of molecules that can be considered to be grafted in the interlamellar space. To overcome this difficulty, one solution is to synthesize in situ the desired molecules from a pre-grafted functional precursor.[3] Thus, only the first stage (grafting the precursor) requires the use of insertion-grafting conditions by anion exchange. The following reactions may appeal to a much larger panel of conditions, including the use of non-aqueous solvents. Confinement of the reaction space may also have specific effects on the synthesis. This poster will describe some of the LSH specially designed for post-synthetic modification, their synthesis, characterization and reactivity. Finally, going from layered hydroxides to layered oxides, we will present some of our latest results on the micro-wave assisted functionalization of layered materials.[4]

---

[1] a) V. Nicolosi, M. Chhowalla, M. G. Kanatzidis, M. S. Strano, J. N. Coleman, Science 340, (2013); b) R. Ma, T. Sasaki, Adv. Mater. 22, 5082 (2010).

[2] a) H. Shimizu, M. Okubo, A. Nakamoto, M. Enomoto, N. Kojima, Inorg. Chem. 45, 10240 (2006); b) E. Delahaye, S. Eyele-Mezui, M. Diop, C. Leuvrey, D. Foix, D. Gonbeau, P. Rabu, G. Rogez, Eur. J. Inorg. Chem., 2731 (2012); c) S. Eyele-Mezui, E. Delahaye, G. Rogez, P. Rabu, Eur. J. Inorg. Chem. 2012, 5225 (2012); d) R. Bourzami, S. Eyele-Mezui, E. Delahaye, M. Drillon, P. Rabu, N. Parizel, S. Choua, P. Turek, G. Rogez, Inorg. Chem. 53, 1184 (2014); e) G. Rogez, C. Massobrio, P. Rabu, M. Drillon, Chem. Soc. Rev. 40, 1031 (2011).

[3] O. Palamarciuc, E. Delahaye, P. Rabu, G. Rogez, New J. Chem. 38, 2016 (2014).

[4] Y. Wang, E. Delahaye, P. Rabu, G. Rogez, manuscript in preparation.

PMon042

Amine functionalized metal organic framework for highly efficient reversible adsorption of iodine

Safarifard, Vahid (Tarbiat Modares University, Tehran, IRN); Morsali, Ali (Tarbiat Modares University, Tehran, IRN)

The synthesis and characterization of metal-organic frameworks (MOFs) is one of the most rapidly developing areas of chemical science.[1] These materials have enormous potential for many practical structure-related applications such as storage, separation or controlled release of gases, catalysis, drug delivery, as well as adsorptive removal of hazardous materials, which are based on the pore size and shape as well as the host-guest interactions involved.[2] A key to accessing advanced MOF materials suitable for more specialized applications is to introduce different functional groups into these networks.[3] The use of an amine-tagged ligand may enhance the adsorbent-adsorbate interactions through host-guest hydrogen-bonding to enhance iodine adsorption.[4]

A guest-filled phase of two-fold interpenetrated 3D metal–organic framework, (TMU-16-NH_2), was synthesized by the solvothermal reaction of NH_2-BDC (NH_2-BDC = 2-amino-1,4-benzenedicarboxylic acid), 4-bpdh (2,5-bis(4-pyridyl)-3,4-diaza-2,4-hexadiene), and $Zn(NO_3)_2 \cdot 6H_2O$ in DMF at 80 °C for 48 h, and isolated as red color block-shaped crystals. The formula of the compound was determined to be $[Zn_2(NH_2\text{-BDC})_2(4\text{-bpdh})].3DMF$ (TMU-16-NH_2) by single-crystal X-ray diffraction studies, and the phase purity of the bulk material was independently confirmed by powder X-ray diffraction (PXRD). In this way, 1D channels are formed with a width of 13.4 × 17.6 $Å^2$, permitting a double interpenetration that results in four much smaller 1D channels each of 4.6 × 7.1 $Å^2$ in cross-section. In this compound, we successfully loaded the porous crystals with I_2 by suspending them in a solution of I_2 in cyclohexane. The delivery of I_2 from TMU-16-NH_2-I_2 performed in ethanol, a nonaromatic solvent, at room temperature.

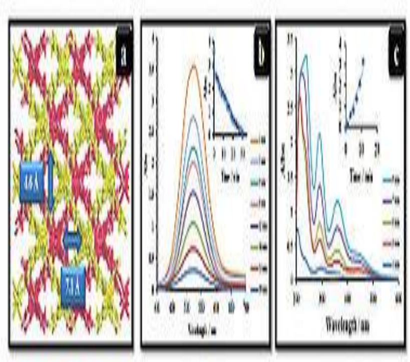

Fig. 1: a) Cylinder model representations of the interpenetrating structure of **TMU-16-NH_2**. b) UV/vis absorption spectra for the I_2 sorption by **TMU-16-NH_2**,c) Temporal evolution of UV/vis absorption spectra for the I_2 delivery from **TMU-16-NH_2**.

---

[1] N. Stock and S. Biswas, Chem Rev, 2012, 112, 933.
[2] H. B. Tanh Jeazet, C. Staudt and C. Janiak, Dalton Trans., 2012, 41, 14003.
[3] S. M. Cohen, Chem Rev, 2012, 112, 970.
[4] M. Felloni, P. Hubberstey, C. Wilson and M. Schroder, CrystEngComm, 2004, 6, 87.

PMon043

Adsorption of linuron by an Algerian palygorskite modified with magnetic iron oxides.

Belaroui, Lala Setti (University of Oran 1, Oran, DZA)

Linuron, 3-[3,4-(dichlorophenyl)-1-methoxy-1-methylurea], one of the most important commercial phenyl urea herbicides, has good contact activity and may kill emergent weed seedlings. In addition, linuron is a weak *in vitro* competitive androgen receptor antagonist, induces a positive response to the Hershberger assay in immature and adult rats, and suppresses androgen dependent gene expression. Half-life in soil ranges from 38 to 67 days, being microbial degradation the primary mechanism for its dissipation. When microbial activity is low, degradation processes slow down and accumulation phenomena can easily lead to toxic levels. Under environmental conditions, phenyl-urea's can persist at the mg L^{-1} level in groundwater for a number of days or weeks depending on temperature and pH.

To reduce the presence of this chemical in water, an adsorption study was started using three types of Algerian clay: purified palygorskite (P-Atta@dz), palygorskite modified with magnetic iron oxides Black1-Atta@dz and palygorskite modified with magnetic iron oxides subjected to hydrothermal treatment Black2-Atta@dz. Palygorskite is a 2:1 phyllosilicate, but, unlike other clay minerals, it has a fibrous morphology resulting from the 180° inversion occurring every four silicon tetrahedra, causing a structure of chains aligned parallel to the "a" axis, each of which has a 2:1 structure. This threedimensional ordering also causes open channels measuring 3.7 x 6.4 Å containing zeolitic and crystallization water. The two mentioned nanoparticles were synthesized by co-precipitation of two iron precursors in alkaline medium on the fibrous material.

The adsorption study was followed by HPLC. Several parameters have been evaluated, such as the mass of the adsorbent, the contact time, the initial concentration of the adsorbate and the effect of temperature. Hence we determined the kinetic order of the reaction and thermodynamic parameters. Modeling of adsorption isotherms was made according to the models of Freundlich, Langmuir. The results show a retention rate of 83%, 55% and 27% for Black1-Atta@dz, Black2-Atta@dz and P-Atta@dz, respectively.

Transformation of available cheap adsorbents is an alternative for improving the retention of pollutants present in water due to anthropogenic activities.

PMon044

Anion-Deficient Perovskite-type Oxides as New Materials for CO_2 Capture

Bennett, Matthew (University of Hull, Hull, GBR); Francesconi, Maria Grazia (University of Hull, Hull, GBR)

In the field of CO_2 capture and storage, two well-researched approaches are the reaction of alkali earth metal oxides, AO (A = Ca, Sr, Ba) with CO_2 to form carbonates ACO_3 and physic/chemisorption of CO_2 molecules in the channels of zeolites [1]. This work investigates a new approach that can be derived from merging the carbonate and the zeolite strategies, the use of oxides of general formula A_2MO_3 with A = Ca, Sr, Ba and M = Cu, Pd. These materials contain alkali metals, which tend to react readily with CO_2 to form stable carbonates and, also show a K_2NiF_4-type structure with anion deficiencies, which can be host sites for $(CO_3)^{2-}$ anions. In fact, in the structure of these materials, the transition metal is coordinated by the oxide anion in square planar fashion and forms chains of corner-linked M-O polyhedral, along which the anion vacancies are ordered.

We intend to exploit these vacant sites for CO_2 storage, aided by the presence of an alkaline earth metal, which will form stable bond with the $(CO_3)^{2-}$ anions. The advantage of this approach is the use of CO_2 as chemical reagent, to modify the anionic lattice in inorganic solids, hence either modify their properties or prepare new materials.

There have been reports of the formation of novel compounds via “filling” of the anion vacancies in A_2MO_3 compounds. In A_2CuO_3 (A = Sr, Ca) the anion stoichiometry was increased via the substitution of 1 oxide with 2 fluoride anions, leading to the formation of $A_2CuO_2F_{2+\delta}$, $(0\leq\delta\leq0.35)$ [2]. A_2PdO_3 was also reported to form the oxide-fluoride $A_2PdO_2F_2$, via substitution of 1 oxide with 2 fluoride anions [3]. Furthermore, Sr_2CuO_3 was reported to form the oxide carbonate $Sr_2CuO_2(CO_3)$ as a result of as a result of O^{2-} being exchanged for a CO^{3-} ion. Sr_2CuO_3 can therefore be considered a very good candidate for CO_2 capture, as it contains widely available low cost elements and it is very easy to prepare.

We have studied the reaction between selected A_2MO_3 compounds and CO_2 gas at various temperature, using a combination of Thermo Gravimetric Analysis and Powder X-Ray Diffraction. We prepared $Sr_2CuO_2(CO_3)$ with low level of $Sr(CO_3)$ impurity in less than one hour. Preliminary results are hinting at the possibility of a family of oxide carbonates with variable $(CO_3)^{2-}$ content, $Sr_2CuO_2(CO_3)_{1\pm x}$. Further work is now concentrating on the preparation of single phase $Sr_2CuO_2(CO_3)$ to measure its properties, on the verification of the existence of the family and on the investigation of more reactions between CO_2 and A_2MO_3 compounds

---

[1] D. M. D’Alessando, B. Smit and J R. Long, *Angew. Chem. Int. Ed.*, 2010, **49**, 6065.

[2] C. Greaves, M. Al-Mamouri, P.R. Slater and P.P. Edwards, *Nature (London)*, 1994, **369**, 382; M.G. Francesconi, P.R. Slater, J.P. Hodges, C. Greaves, P. P. Edwards, M. Al Mamouri and M. Slaski, *J. Solid State. Chem.*, 1998, **135**, 17.

[3] T. Baikie, E. L. Dixon, J. F. Rooms, N. A. Young and M. G. Francesconi, *Chem Commun.*, 2003, 1580; T. Baikie, N. A. Young, M. G. Francesconi, *Prog. Solid St. Chem.*, 2007, **35**, 265.

PMon045

Bismuth titanate pyrochlore doped with transition metals (Cr, Mn, Cu, Fe, Zn): The thermal stability, structure, properties

Piir, Irena (Institute of Chemistry, Komi Scientific Center , UBRAS, Syktyvkar, RUS); Koroleva, Maria (Institute of Chemistry, Komi Scientific Center , UBRAS, Syktyvkar, RUS); Sekushin, Nikolay (Institute of Chemistry, Komi Scientific Center , UBRAS, Syktyvkar, RUS); Korolev, Dmitry (St. Petersburg State University, St. Petersburg, RUS); Piskaikina, Maria (Ukhta State Technical University, Ukhta, RUS)

A new group of pyrochlores based on doped bismuth niobate has been studied intensively in the last decade. It was found that high-temperature interaction of equimolar amounts of zinc, magnesium, or 3-d metals oxides with bismuth and niobium oxides leads to the formation of the stable compounds with pyrochlore-type structure [1]. Analogously, a doping of $Bi_2Ti_2O_7$ with smaller ionic radii metals allows to obtain a bismuth titanates with a pyrochlore structure, stable in a wide temperature range up to melting point. Conditions of metal-containing bismuth titanates synthesis and fields of homogeneity in systems $Bi_{2(1.6)}MTi_2O_{7-\delta}$, ($M$ = Cr, Mn, Fe, Cu) were determined. Preferential distribution of the metal atoms in the A- sites of the pyrochlore structure was established based on the results of synthesis, X-ray diffraction, pycnometric density measurements. In the case of copper- and manganese-containing bismuth titanate, compounds with a sufficiently high amount of doped metal can be prepared, that is unambiguously associated with the replacement with copper or manganese atoms of a significant proportion (~ 30 %) of titanium atoms occupying the B sites. It was shown that magnetic behavior of bismuth titanate pyrochlore containing atoms of paramagnetic metal depends on the distribution of these metals atoms in the crystallographic positions. It was found that appreciable exchange interactions (anti-ferromagnetic type) occur as a result of the distribution of paramagnetic atoms in the B (titanium)-sites. The magnetic behavior of compounds with a low amount of paramagnetic atoms (M = Cr, Fe) substituted A (bismuth)-sites is determined by the behavior of M (III) as single atoms in the high-spin state. The electrical properties of the doped bismuth titanate pyrochlores were studied using impedance spectroscopy method. It was shown that these compounds exhibit mixed conductivity due to electronic and ionic type charge carriers. The electronic or ionic type conductivity depends on the nature and amount of the doping atoms. Revealed that a significant number of compounds with doping 3d metal atoms that are replace of titanium atoms (copper- and manganese-containing bismuth titanate pyrochlores) have the dominating of electronic conductivity.

This work is supported by the RFBR (project № 15-03-09173 A, project № 13-03-00132 A).

---

[1] Vanderah T.A., Levin I., Lufaso M.W. An Unexpected Crystal-Chemical Principle for the Pyrochlore Structure // Eur. J. Inorg. Chem. 2005. V. 14. P. 2895–2901.

PMon046

$Ba_3P_5N_{10}X$:Eu^{2+} (X = Cl, Br, I) - Luminescent Nitridophosphates with Zeolite-like Framework Structure

Schnick, Wolfgang (University of Munich (LMU), Department of Chemistry, Munich, GER);
Marchuk, Alexey (Ludwig-Maximilians-Universität, München, GER)

Illumination sources based on phosphor converted light emitting diodes (pc-LEDs) technology increasingly gain importance. Due to their energy efficiency, pc-LEDs have been successfully established in the market and are about to replace inefficient common light sources. Consequently, further investigation of luminescent materials is an important research target.

Here we report on the synthesis, structural characterization and luminescence properties of novel nitridophosphates, namely $Ba_3P_5N_{10}X$ with X = Cl, Br and I.[1] These isotypic compounds have been synthesized by the reaction of stoichiometric amounts of $Ba(N_3)_2$, BaX_2 (X = Cl, Br, I) and P_3N_5. 2 mol-% EuX_2 (X = Cl, Br, I) were used as doping agent. The synthesis was carried out in a Walker-type multi-anvil assembly at 1000 °C and pressures between 1 and 5 GPa.

The crystal structures (*Pnma* (no. 62), $Z = 8$, **$Ba_3P_5N_{10}Cl$**: $a = 12.566(1)$, $b = 13.224(1)$, $c = 13.803(1)$ Å; **$Ba_3P_5N_{10}Br$**: $a = 12.566(1)$, $b = 13.224(1)$, $c = 13.803(1)$ Å; **$Ba_3P_5N_{10}I$**: $a = 12.566(1)$, $b = 13.224(1)$, $c = 13.803(1)$ Å) were solved and refined on the basis of single-crystal X-ray diffraction data and confirmed by Rietveld refinement and FTIR spectroscopy. The crystal structure is built up of all-side vertex-sharing PN_4 tetrahedra leading to a zeolite-like framework with three-dimensional *achter*-ring [2] channels. These contain alternately Ba and halide atoms Cl, Br and I, respectively. The framework topology is analogous to that of the JOZ zeolite.[3] The PN_4 tetrahedra form condensed *dreier*, *vierer* and *achter* rings. This condensation results in turn in two slightly distorted composite building units made up of $3^4 4^2 8^6$-cages.

Upon excitation by near-UV light, orange ($Ba_3P_5N_{10}Cl$:Eu^{2+}), natural-white ($Ba_3P_5N_{10}Br$:Eu^{2+}) and cyan ($Ba_3P_5N_{10}I$:Eu^{2+}) luminescence can be observed. All three compounds exhibit several bands in the emission spectrum, which can be explained by Eu^{2+} occupying different Ba lattice sites.

With $Ba_3P_5N_{10}X$:Eu^{2+} (X = Cl, Br, I), we have demonstrated that nitridic zeolites are generally suited as host lattices for high performance luminescent materials.

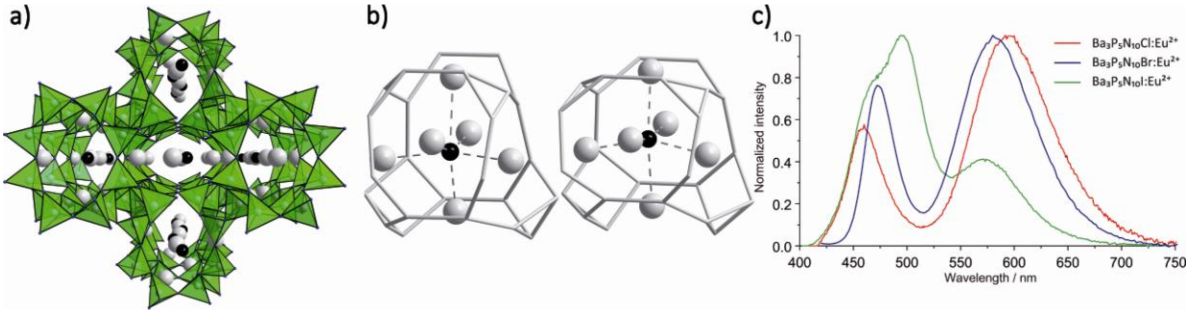

Figure 1: a) Crystal structure of $Ba_3P_5N_{10}X$ (X = Cl, Br, I), viewed along [100]. Atom colors: Ba = gray, X = black, N = blue, PN_4 tetrahedra = green. b) Topological representation of the two different $3^4 4^2 8^6$ cages with cage content. c) Emission spectra of $Ba_3P_5N_{10}X$: red (X = Cl), blue (X = Br) and green (X = I).

---

[1] A. Marchuk, W. Schnick**,** *Angew. Chem.* **2015**, *127*, 2413*; Angew. Chem. Int. Ed.* **2015**, *54*, 2383.
[2] F. Liebau, *Structural Chemistry of Silicates*, Springer, Berlin, **1985**.
[3] J. A. Armstrong, M. T. Weller, *J. Am. Chem. Soc.* **2010**, *132*, 15679.

PMon047

Characterization and photocatalytic properties of hydrothermally synthesized hydroxyphosphate material

Roumila, Yasmina (USTHB University, Faculty of Chemistry, Algiers, DZA); Bagtache, Radia (USTHB University, Faculty of Chemistry, Algiers, DZA); Meziani, Djaafar (USTHB University, Faculty of Chemistry, Algiers, DZA); Abdmeziem, Kaïssa (USTHB University, Faculty of Chemistry, Algiers, DZA)

Syntheses of metal phosphates materials have attracted widespread attention because of their various applications in many fields. In this kind of view, our work is devoted to the synthesis of transition metal phosphates, prepared under hydrothermal conditions. It should be pointed out that the structure and properties of such materials are very dependent upon the synthesis method and many other experimental factors. In the present work, as a contribution, we report on the hydrothermal synthesis of a copper hydroxyphosphate material.The influence of the starting molar composition of the reaction mixture and that of other chemical parameters, such as adding of organic structure directing agents, crystallization temperature and time, pH…. have been investigated. The material has been characterized using several physicochemical techniques including: X-Ray diffraction, chemical and thermal analyses, scanning electron microscopy, UV-Vis diffuse reflectance measurements and Fourier transform infrared spectroscopy. Moreover, some photo- electrochemical properties of the synthesized material were investigated. The thermal variation of the conductivity follows an exponential type law, characteristic of a semi-conductor behaviour. The photocatalytic properties were assessed through the degradation of organic molecules. We present herein the results obtained with azo-dye pollutants. The photocatalytic activity was investigated under visible and UV light, with varying some experimental factors, such as: dye solution concentration and pH, photocatalyst dose, irradiation time and effect of the addition of hydrogen peroxide.

The results of the study highlighted a good performance of the synthesized material, in such application. It would be a promising candidate for various other ones, in the field of photocatalysis.

PMon048

Colorimetric sensing of various organic acids by using polydiacetylene/zinc oxide nanocomposites: The effects of acid structure

Chanakul, Amornsak (Chulalongkorn University, Bangkok, THA); Traiphol, Rakchart (Naresuan University, Phitsanulok, THA); Traiphol, Nisanart (Chulalongkorn University, Bangkok, THA)

In this study, we demonstrate the utilization of polydiacetylene(PDA)/zinc oxide(ZnO) nanocomposites as colorimetric sensors for various types of organic acids. Series of 14 organic acids with systematic variation of molecular structure and dissociation constant (K_a) are investigated. The PDA/ZnO nanocomposites are prepared by using three types of monomers with different alkyl chain length, 5,7-hexadecadiynoic acid, 10,12-tricosadiynoic acid and 10,12-pentacosadiynoic acid. Our results show that all PDA/ZnO nanocomposites clearly exhibit color transition upon the addition of organic acids with concentration range of about 0.01 to 100 mM. The change of PDA structure provides the ability to manipulate the color transition at desired concentration of each acid. Color transition behaviors of the nanocomposites are also found to depend significantly on the dissociation ability and structure of the acids. For system of linear carboxylic acids, the higher of K_a value leads to the higher sensitivity of PDA/ZnO nanocomposites. When the K_a values are comparable, the architecture of organic acids becomes a dominant factor. The increase of chain length promotes the color transition of PDA/ZnO nanocomposites while the presence of some brancheswithin the acid structure causes an opposite result. This study also investigates the colorimetric response of the nanocomposites to some organic acids commonly used in food industry such as sorbic acid, oxalic acid, malic acid, citric acid, salicylic acid, acetylsalicylic acid.

PMon049

Correlation between electrochemical behavior and microstructures of FeNbC ternary alloys.

AMARA, Sif-Eddien (University of Sciences and Technology Houari Boumediene, Algiers, DZA); HADDAD, Farida (Laboratory of Electrochemistry-Corrosion, Metallurgy and Inorganic Chemistry, Bab Ezzouar, DZA); BENCHETTARA, Abdelkader (Laboratory of Electrochemistry-Corrosion, Metallurgy and Inorganic Chemistry, Algiers, DZA)

The refractory nature and high resistance to chemical corrosion make metals such as niobium attractive for several applications. Niobium is used as an alloying element to strengthen high-strength low-alloy steels. It is used to provide creep strength in superalloys operating in the hot section of aircraft gas turbine engines and in stainless steel automobile exhaust systems. In the present study, the electrochemical behaviour of four based iron FeNbC ternary alloys was related to the observed microstructures. The alloys were arc melted from pure metals and graphite, under argon atmosphere. The solidification sequences of FeNbC alloys were established using different techniques (differential thermal analysis, optical microscopy, scanning electron microscopy with energy dispersive X-ray analysis, and quantitative electron probe microanalysis). Thus, the primary crystallization phases, d(Fe) and NbC_{1-x} are identified. In addition, two invariant ternary reactions are proposed: an invariant eutectic ternary reaction: $L \rightarrow d(Fe) + Fe_2Nb + NbC_{1-x}$ and a quasi-peritectic reaction: $L + d(Fe) \rightarrow g(Fe) + NbC_{1-x}$. The potentiodynamic technique was applied to study the electrochemical behaviour of the FeNbC ternary alloys in non deaerated solution. This latter contained; 10-3 M $NaHCO_3$ and 10-3 M Na_2SO_4. It was found that the evolution of corrosion current density was to be related to the niobium content and the presence of carbides as well as their distribution in the microstructure. It shown that, the evolution of corrosion current densities depends on the composition in niobium except for the alloy containing at the same time primary and eutectic NbC_{1-x} carbides (fig. 1). Indeed, for some alloys, the corrosion current densities decrease with the increase of niobium content. However, the alloy with 90.62 at % Fe and 2.00 at % Nb has the highest corrosion current density. This would be assigned to the quantity of pearlite formed, in addition to the formation of Widmanstätten cementite.

PMon050

Crystal structure and properties of Y-substituted strontium and barium ferrites

Urusova, Anastasia (Federal State Autonomous Educational Institution of Higher Professional Education «Ural Federal University named after the first President of Russia , Ekaterinburg, RUS); Rudik, Viktoria (Federal State Autonomous Educational Institution of Higher Professional Education «Ural Federal University named after the first President of Russia , Ekaterinburg, RUS); Bryuzgina, Anna (Federal State Autonomous Educational Institution of Higher Professional Education «Ural Federal University named after the first President of Russia , Ekaterinburg, RUS); Aksenova, Tatiana (Federal State Autonomous Educational Institution of Higher Professional Education «Ural Federal University named after the first President of Russia , Ekaterinburg, RUS); Cherepanov, Vladimir (Federal State Autonomous Educational Institution of Higher Professional Education «Ural Federal University named after the first President of Russia , Ekaterinburg, RUS)

The crystal structure and physicochemical properties of B-site substituted complex oxides $MeFe_{1-y}Y_yO_{3-d}$ (Me=Sr, Ba) were studied in present work. Powder samples were synthesized by means of glycerol-nitrate method. Final annealing was performed at 1373 K in air with subsequent slow cooling or quenching to room temperature.The crystal structure of both oxides was strongly depended on oxygen content. Whereas slowly cooled $SrFeO_{3-\delta}$ possesses tetragonal structure (sp.gr. I4/mmm), strontium ferrite quenched from 1373 K revealed a cubic structure (sp. gr. Pm3m). High-temperature XRD analyses of barium ferrite in air was proved an existence of single orthorhombic $BaFeO_{3-\delta}$ (sp.gr. $P2_12_12$) below 673 K, a single phase cubic structure (sp. gr. Pm3m) at temperature above 1273 K, and a mixture of both orthorhombic and cubic phases within the temperature range 673–1273 K.

Yttrium can be implemented to the crystal structure of both strontium and barium ferrites but in a different way. In a case of strontium ferrite Y-substitution occurs in both A- and B-site of perovskite $ABO_{3-\delta}$ structure. Single phase solid solutions $Sr_{1-x}Y_xFeO_{3-\delta}$ ($0.05 \le x \le 0.20$) and $SrY_{0.1}Fe_{0.9}O_{3-\delta}$ with cubic structure and $Sr_{1-x}Y_xFeO_{3-\delta}$ ($0.85 \le x \le 1$) with orthorhombic structure were found in the Sr-Fe-Y-O system by the XRD of slowly cooled samples. The refined unit cell parameters and unit cell volume of $Sr_{1-x}Y_xFeO_{3-\delta}$ were decreased with the increase of yttrium content due to larger ionic radius of Sr^{2+}compared to that of Y^{3+}. The oxygen content in $Sr_{1-x}Y_xFeO_{3-\delta}$ ($0.05 \le x \le 0.20$) was measured by TGA within the temperature range 298–1273 K in air. The absolute values of oxygen content were determined using iodometric titration. The oxygen content in $Sr_{1-x}Y_xFeO_{3-\delta}$ was decreased with the increase of yttrium concentration.

Because of larger difference between the ionic radii of yttrium and barium only yttrium for iron substitution took place in barium ferrite . The formation of cubic $BaFe_{1-y}Y_yO_{3-d}$ solid solutions stable in air at all studied temperatures and single phase complex oxide $YBa_3Fe_2O_{8-d}$ were detected . The ED patterns of $YBa_3Fe_2O_{8-d}$ and corresponding HRTEM image confirm the orthorhombic structure (sp. gr. Pnma) that is in agreement with the XRD results. According to the high temperature XRD study performed within the temperature range 298–1273 K in air $BaFe_{0.9}Y_{0.1}O_{3-d}$ is stable at all temperatures and possesses cubic structure (sp. gr. Pm3m) . The change of oxygen content in the samples was measured by means of thermogravimetric technique within the temperature range 300 – 1373 K in air. The absolute value of oxygen content in the samples was determined using both iodometric titration of the slowly cooled sample and reduction by hydrogen inside the TGA cell.

The thermal expansion measurements show the absence of phase transition in all complex oxides within the studied temperature range. Temperature dependency of conductivity for the single phase Y-substituted oxides was measured and discussed.

PMon051

Crystal structure, oxygen nonstoichiometry and electric properties of $PrBaCo_{2-x}FexO_{6-\delta}$

<u>Ivanov, Ivan (Ural Federal University, Yekaterinburg, RUS)</u>; Tsvetkov, Dmitry (Ural Federal University, Yekaterinburg, RUS); Malyshkin, Dmitry (Ural Federal University, Yekaterinburg, RUS); Zuev, Andrey (Ural Federal University, Yekaterinburg, RUS)

The layered rare-earth cobaltites $LnBaCo_2O_{6-\delta}$ have attracted great attention in last decades due to their fascinated properties such as high mixed ionic-electronic conductivity and electrochemical activity, which make them suitable for application as cathodes in high- and intermediate temperature solid oxide fuel cells.

Powder samples of $PrBaCo_{2-x}Fe_xO_{6-\delta}$ (PBCF) were synthesized using glycerol-nitrate technique. X-ray diffraction analysis of PBCF samples obtained accordingly showed no indication for presence of a second phase. Crystal structure of $PrBaCo_{2-x}Fe_xO_{6-\delta}$ (x=0–1) was investigated by “in situ” x-ray diffraction in the temperature range 25-1000 °C and in the oxygen partial pressure range 10^{-5} – 0.21 atm. Oxygen nonstoichiometry of the $PrBaCo_{2-x}Fe_xO_{6-\delta}$ (x=0–1) double perovskites was measured as a function of oxygen partial pressure and temperature 700≤T, °C≤1000 using thermogravimetric technique and coulometric titration. Fe-doping was shown to increase oxygen content at a given temperature in the double perovskites $PrBaCo_{2-x}Fe_xO_{6-\delta}$. All $PrBaCo_{2-x}Fe_xO_{6-d}$ (x=0-1) samples studied were found to have P4/mmm crystal structure in air at all temperatures investigated. PBC was found to undergo the P4/mmm→Pmmm structure transition under reducing conditions at temperatures from 500 °C at $pO_2 = 10^{-3}$ atm down to 350 °C at $pO_2 = 10^{-4}$ atm.Therefore, results obtained indicate in favor of both temperature and oxygen content influence on the P4/mmm – Pmmm phase transition in double perovskites. Total conductivity and Seebeck coefficient of PBCF samples were measured simultaneously as functions of T and pO_2 using the standard 4-probe DC technique. Total conductivity was found to increase with pO_2 growth whereas positivethermo-EMF simultaneously decreases. Such behavior indicates in favor of electron holes as predominant charge carriers in PBCF. Total conductivity and thermo-EMF of PBCF were shown to decrease and increase, respectively, with Fe content growth.

This work was supported by the President of the Russian Federation (grants No. MK-6206.2014.3 and No. SP-3215.2015.1).

PMon052

Cubic, ceramic-like solid solutions $Li_{7-x-y}La_3Zr_{2-x-y}NbxTayO_{12}$ with garnet-type structure for all-solid-state Li-ion batteries: synthesis of dense samples and characterisation focussing on Raman spectroscopy

Maier, Maria (University of Salzburg, Salzburg, AUT); Musso, Maurizio (University of Salzburg, Salzburg, AUT); Amthauer, Georg (University of Salzburg, Salzburg, AUT); Rettenwander, Daniel (University of Salzburg, Salzburg, AUT)

Delocalized stationary and mobile energy storage systems are key technologies for the present and for the immediate future. Fast solid-state Li-ion electrolytes – complying with safety requirements, high ionic conductivity, and further desirable properties – have therefore been extensively studied in recent years. *Cubic*, garnet-like structured ceramics $Li_{7-x-y}La_3Zr_{2-x-y}Nb_xTa_yO_{12}$ ($0 \leq x, y \leq 2$) (LLZNTO) are promising solid-state electrolytes, not least because of their good chemical stability against various electrode materials, especially Li metal. The cubic structure is a necessary – although not a sufficient – condition for high ionic conductivity in these oxides. Not all LLZNTOs show a cubic structure (at ambient conditions): (i) the endmember $Li_7La_3Zr_2O_{12}$ has a tetragonal structure $I4_1/acd$; (ii) the endmembers $Li_5La_3Nb_2O_{12}$ and $Li_5La_3Ta_2O_{12}$ exhibit a cubic structure $Ia\text{-}3d$; (iii) the transition from tetragonal to cubic phase occurs in $Li_{7-x-y}La_3Zr_{2-x-y}Nb_xTa_yO_{12}$ around $(x+y) = 0.25$, according to X-ray diffraction.
Practical applications in all-solid-state batteries demand electrolytes with (i) ionic conductivities σ between 10^{-4} and 10^{-3} Scm^{-1}, roughly speaking, and (ii) dense materials. Ad (i): as far as we know up to now, only low-doped solid solutions $Li_{7-x-y}La_3Zr_{2-x-y}Nb_xTa_yO_{12}$ – i.e. compounds with $(x+y)$ slightly higher than the phase transition concentration – show an adequately high ionic conductivity. Beside a large number of charge carriers a highly disordered Li-ion distribution over the Li-sites 24*d*, 48*g*, and 96*h* in the garnet structure (molten/liquid-like Li-sublattice) is inevitable in order to achieve a high ionic conduction. A defect structure may promote the Li-ion mobility, too. Ad (ii): dense-sintered, ceramic-like LLZNTOs are supposed to enhance the total ionic conductivity by reducing the grain-boundary resistance. Moreover, they exhibit the mechanical stability required for solid-state electrolytes.

For the characterisation of crystalline solids, in terms of phases and crystal chemistry, powder X-ray diffraction is the method of choice. In addition, Raman spectroscopy is a well-known, non-invasive, and very powerful technique to study materials of all kinds. Nevertheless, Raman scattering is often an underestimated method for acquiring useful information on the structure of solids. A comparison of the two techniques verifies that Raman spectroscopy provides a much more sensitive measure of the impact of the structural differences in the solid solutions LLZNTO, compared to XRD. This study presents synthesis routes for the preparation of dense ceramic-like LLZNTOs. The samples are characterised by various techniques, whereupon the merits of Raman spectroscopy are pointed out. LLZNTOs are investigated by Raman scattering in order to determine (i) phases, (ii) phase transition concentrations, (iii) structural inhomogeneities, (iv) chemical inhomogeneities, (v) doping/substitu-tion concentrations, and (vi) static and/or dynamic disorder [1,2,3]. To achieve these aims, conventional Raman spectra as well as Raman maps have been recorded, followed by peak-analyses concerning intensities, broadening, and Raman shifting. No attempt is made to identify the origins of peaks in detail.

---

[1] Larraz G. et al. (2013), *J. Mater. Chem. A*, **1**, 11419.
[2] Tietz F. et al. (2013), *Solid State Ionics*, **230**, 77.
[3] Thompson T. et al. (2014), *J. Mater. Chem. A*, **2**, 13431.

PMon053

Defect structure and related properties of $YBaCo_2O_{6-\delta}$

Tsvetkov, Dmitry (Ural Federal University, Ekaterinburg, RUS); Sednev, Anton (Ural Federal University, Ekaterinburg, RUS); Malyshkin, Dmitry (Ural Federal University, Ekaterinburg, RUS); Ivanov, Ivan (Ural Federal University, Ekaterinburg, RUS); Zuev, Andrey (Ural Federal University, Ekaterinburg, RUS)

Double perovskite $YBaCo_2O_{6-\delta}$ have received great attention as a potential cathode material for SOFCs due to high mixed ionic–electronic conductivity, fast oxygen transport and small thermal expansion coefficient close to that of YSZ. However, the defect structure of the $YBaCo_2O_{6-\delta}$ has not been studied so far as well as its oxygen nonstoichiometry, total conductivity and Seebeck coefficient.

Powder sample of $YBaCo_2O_{6-\delta}$ was prepared using glycerol–nitrate technique. Metallic Co, preliminary annealed Y_2O_3 and $BaCO_3$ were used as starting materials. All the materials used had purity 99.99%. The final calcination was carried out at 1100 ^{o}C for 48 h. Phase composition of the as synthesized powder sample was controlled by X-ray diffraction.

Oxygen nonstoichiometry of the double perovskite $YBaCo_2O_{6-\delta}$ was measured as a function of oxygen partial pressure (pO_2) and temperature (T) using two independent techniques: thermogravimetry and solid state coulometric titration. Oxygen content in $YBaCo_2O_{6-\delta}$ as a function of T and *pO2* was found to vary in a relatively narrow range as compared to similar double perovskites like, for example, $GdBaCo_2O_{6-\delta}$.

Total conductivity and Seebeck coefficient of $YBaCo_2O_{6-\delta}$ were measured as a function of T and *pO2* by four probe dc-method. A significant drop in the total conductivity of $YBaCo_2O_{6-\delta}$ was found below the certain value of *pO2* at given T suggesting the thermodynamic stability limit of this double perovskite with respect to pO_2 decrease. It was shown that both total conductivity and Seebeck coefficient of $YBaCo_2O_{6-\delta}$ are almost independent of pO_2 within the range of its thermodynamic stability due to weak pO_2 dependence of the oxygen content. Positive value of Seebeck coefficient as well as decrease of the conductivity of $YBaCo_2O_{6-\delta}$ suggests electron holes as dominating charge carriers. The experimental results obtained were discussed on the basis of the proposed defect structure model of $YBaCo_2O_{6-\delta}$.

PMon054

Defect Flourite vs Pyrochlore : the M_2 M'_2 O_7 case

Miller, Stuart (University of the Witwatersrand, Braamfontein, ZAF); Billing, Dave (University of the Witwatersrand, Braamfontein, ZAF)

In recent times we have prepared a considerable number of mixed metal oxides with the a M_2 M'_2 O_7 stoichiometry. Our interest principally being to investigate the thermoresponsive behaviour of these materials via VT-PXRD methods and to assess their potential as energy materials in Solid Oxide Fuel Cells.

Crystallographically, the defect fluorite structure with space group Fm3m (No 225) and pyrochlore structures with space group Fd3m (No 227) are isometric. In the defect fluorite (DF) phase, the M and M’ cations are completely disordered and oxygen atoms are evenly distributed into all the tetrahedral sites formed by cations. Each oxygen position having a 7/8 occupancy, and hence the description as a ‘defect fluorite’ phase. The pyrochlore (P) phase is a superstructure of the DF phase with the a-axis doubled.

Upon heating the DF phase converts to the P phase and although there are a number of reports in the literature reporting on this phase transition, the detailed phase behaviour of most of these materials remain relatively unexplored. Further heating in our experience has occasionally resulted into the decomposition of the mixed metal oxide into simpler, primary oxides.

We have focused our studies on materials prepared via the sol-gel method. Typically materials are prepared as the DF phase and then subsequently converted to the P phase by heating. The materials produced have been extensively characterised via VT-PXRD, COXA, Rietveld, Raman, TGA and EIS.

Selected results of the study are to be presented. Including thermal expansion coefficients of materials studied and a COXA study of the phase transition.

PMon055

Defect structure and defect-induced properties of $SrTi_{0.5}Fe_{0.5}O_{3-\delta}$

Sereda, Vladimir (Ural Federal University, Yekaterinburg, RUS); Ivanov, Ivan (Ural Federal University, Yekaterinburg, RUS); Tsvetkov, Dmitry (Ural Federal University, Yekaterinburg, RUS); Zuev, Andrey (Ural Federal University, Yekaterinburg, RUS)

Various perovskite-type oxides with general formula ABO_3 are commonly regarded as promising materials for different high-temperature electrochemical devices. The possibility of doping enables precise tailoring of the physical properties of these materials, vastly expanding their applicability ranges. Thus, doped with Fe strontium titanates $SrTi_{0.5}Fe_{0.5}O_{3-\delta}$ combine the high stability of $SrTiO_3$ with the elevated mixed ionic-electronic conductivity of $SrFeO_3$. That is why they have received great attention over the past few decades as materials for solid oxide fuel cell (SOFC) cathodes, oxygen separation membranes and oxygen sensors. So far, the important properties of $SrTi_{0.5}Fe_{0.5}O_{3-\delta}$ such as oxygen nonstoichiometry, chemical expansion, total conductivity and Seebeck coefficient were studied in the relatively narrow range of temperature and oxygen partial pressure (pO_2). Therefore, the main purposes of the work were (i) to study these properties in wide range of pO_2 and temperature and (ii) to find the relationship between them and the defect structure of $SrTi_{0.5}Fe_{0.5}O_{3-\delta}$.

Powder samples of $SrTi_{0.5}Fe_{0.5}O_{3-\delta}$ were synthesized using the standard ceramic and spray-pyrolysis techniques. XRD analysis of the samples obtained accordingly showed no indication for the presence of a second phase. Oxygen nonstoichiometry of $SrTi_{0.5}Fe_{0.5}O_{3-\delta}$ was measured using the coulometric titration method in the ranges of temperature and $\log(pO_2, atm)$ $750 \leq T \leq 1050$°C and $-18 \leq \log(pO_2) \leq -0.7$, respectively. Total conductivity and Seebeck coefficient of $SrTi_{0.5}Fe_{0.5}O_{3-\delta}$ as functions of T and pO_2 were measured simultaneously using the standard 4-probe DC technique. Chemical expansion was measured using two different methods: dilatometric method using original setup, and the high-temperature XRD. The experimental results obtained were discussed on the basis of the defect structure model proposed for $SrTi_{0.5}Fe_{0.5}O_{3-\delta}$.

This work was supported by Russian Fund for Basic Research, grant No 15-03-07446.

PMon056

Effect of cobalt deficiency on physical properties of the polycrystalline samples EuBaCo$_x$O$_{6-\delta}$ and the single crystal EuBaCo$_{1.9}$O$_{6-\delta}$

Telegin, Sergey (IMP UB RAS, Ekaterinburg,, RUS); Naumov, Sergey (IMP UB RAS, Ekaterinburg, RUS); Reznitskih, Olga (IHTE UB RAS, Ekaterinburg, RUS); Solin, Nikolai (IMP UB RAS, Ekaterinburg, RUS)

Previously double layered perovskites LnBaCo$_2$O$_{6-\delta}$ (where Ln – rare earth element) have been widely studied because of their fascinating magnetic, electric and magnetotransport properties [1]. They have a rich phase diagram since the electronic states of Co and surrounding oxygen can be changed with δ [2]. These oxides also exhibit high oxygen surface exchange and diffusivity rates which combined with their electrical conductivity makes them suitable for intermediate temperature electrochemical devices, such as oxygen separation membranes and solid oxide fuel cells [3]. A structure of these compounds is very flexible and sensitive to tiny variations of the oxygen and cation content [2]. This paper deals with a systematic study of the structure and properties of the EuBaCo$_x$O$_{6-\delta}$. All of the samples EuBaCo$_x$O$_{6-\delta}$ (where x = 1.92 – 2.04 by step 0.02) were prepared under the same conditions by the Pechini technique using Eu$_2$O$_3$, BaCO$_3$ and Co as starting materials. The samples then were annealed at 900-1150 °C temperatures with the step 50 °C and grounded after every step. Finally, the powders were pressed into bars, heated for 24 h in air at 1200 °C, and slowly cooled to room temperature. The single crystal EuBaCo$_{1.9}$O$_{6-\delta}$ was grown by the zone melting method. The purity of the compounds was determined by X-ray diffraction. The powder X-ray patterns were recorded by using the DRON-2.0 diffractometer with Cr*Kα* radiation. The crystal structures of the samples were analyzed using the PowderCell2.3 program. The unit cell volumes are given in the Table 1. Table 1. The volume of the unit cell, the energy phase transition (*Pmmm – P4/mmm*) and the Curie temperature of polycrystalline samples EuBaCo$_x$O$_{6-\delta}$ for x = 1.92 – 2.04 and single crystal EuBaCo$_{1.9}$O$_{6-\delta}$ (H || *ab*)

EuBaCo$_x$O$_{6-\delta}$	1.9 (single crystal)	1.92	1.94	1.96	1.98	2.00	2.02	2.04
V, A^3	231.6	229.8	229.8	229.8	229.7	229.7	229.8	229.7
E, J/g	3.3	3.1	3.1	3.3	3.3	3.2	3.3	3.5
T$_C$, K	264.2	266.5	265.2	263.8	261.8	261.1	263.5	265.0

The composition was examined by the energy dispersive X-ray spectroscopy using an Inspect F (FEI) electron microscope equipped with an EDX analyzer. Differential scanning calorimetry measurements were carried out with thermal analyzer Netzsch STA 409 F1 Jupiter in air flow in the temperature range 50 – 1000 °C and heating/cooling rate 5 °C/min. DSC measurements show the complex behavior of the thermal effect near the temperature of the phase transition from orthorhombic (*Pmmm*) to tetragonal (*P4/mmm*) space symmetry. Samples with nonstoichiometric content of cobalt present two heat effects comparing with the EuBaCo$_2$O$_{6-\delta}$ (only one heat effect). Single crystal shows the similar behavior. Phase transition energy decreases with decreasing the cobalt content (see Table 1). Magnetic susceptibility was measured by a differential method in the zero magnetic field at an alternating current (1 kHz). In cobalt nonstoichiometric samples we observed the formation of an additional maximum on the curve and the Curie temperature shift (see the Table 1). In this respect magnetic and DSC measurements do not contradict to each other. We can assume the formation of clusters of several unit cells around cobalt and oxygen vacancies. In these clusters the energy of cobalt-oxygen bonds is changed. The results were obtained within the state assignment of FASO of Russia (theme "Spin», No 01201463330), the RFBR grant (project № 14-02-00432) and the program of UB RAS (project № 15-9-2-4).

---

[1] A.A. Taskin, A.N. Lavrov, Y. Ando. Phys. Rev. B **71**, 134414 (2005)
[2] C. Frontera, J.L. Garcia-Munoz, A. Llobet, M.A.G. Aranda. Phys. Rev. B **65**, 180405 (2002).
[3] A.J. Jacobson. Chem. Mater. **22**, 660 (2010)

PMon057

Elaboration and caracterisation of ZnO-Cu thin films By thermal evaporation

Dergham, D. (Centre OF Development OF Advanced Technologies, Baba Hassen, Algiers, DZA);
Hassani, S. (Centre OF Development OF Advanced Technologies, Baba Hassen, Algiers, DZA);
Lekoui, F. (Centre OF Development OF Advanced Technologies, Baba Hassen, Algiers, DZA);
Ouchaabane (Centre OF Development OF Advanced Technologies, Baba Hassen, Algiers, DZA)

ZnO, and ZnO-Cu thin films were synthesis by vacuum thermal evaporation technique, the samples were annealed at 300°C, 500°C, for one hour, the as deposited samples were characterized by X-ray diffraction (XRD), scanning electron microscopy (SEM), UV-VIS Spectroscopy and nanoindentation were used to study the optical and Nano hardness properties, of the films, respectively. The transmittance of ZnO-Cu thin films in the visible region was ≥90%, the grain size of the thin films was estimated from the Scherer's formula [1] by measuring the Full Width at Half Maximum peak Intensity (FWHM). Annealing at 300 ° C has no effect on the optical properties as annealing at 500 ° C improves the transparency of the films, on the other hand, the resistivity of the films increases for 300 ° C then decreases

Keys words: ZnO-Cu, vacuum thermal evaporation

---

[1] Y. Xu, L. Li , X. Cai and P.K. Chu: Surf.Coat.Technol., 2007, 201, 6824

PMon058

Evaluation of dextran coated iron oxide magnetic nanoparticles toxicity after intratracheal instillation

Prodan, Alina Mihaela (1. Emergency Hospital Floreasca, 2. University Politehnica of Bucharest, Faculty of Applied Chemistry and Materials Science, Bucharest, , ROU); Ciobanu, Carmen Steluta (National Institute for Materials Physics,, Magurele, ROU); Beuran, Mircea (Emergency Hospital Floreasca, Carol Davila University of Medicine and Pharmacy, Bucharest, , ROU); Turculet, Claudiu (Emergency Hospital Floreasca, , Bucharest, , ROU); Pavelescu, Cezar (Emergency Hospital Floreasca, , Bucharest, , ROU); Teleanu, Gabriel (Emergency Hospital Floreasca, , Bucharest, , ROU); Chapon, Patrick (Horiba Jobin Yvon S.A, Longjumeau , FRA)

The synthesis of dextran coated iron oxide magnetic nanoparticles (DIO-NPs) with spherical shape exhibiting uniform size distribution is reported in this study.The XRD analysis of DIO-NPs by Rietveld refinement of X-ray diffraction patterns clearly identified a single phase of maghemite and the spinel cubic structure with Fd3m space group has been confirmed. The resulting Bragg R-factor (RB) and chi squared ($\chi 2$) were 0.574 and 1.05 respectively. The average size, deduced from the XRD data refinement, has a value of 7.08 nm for DIO-NPs, consistent with the mean sizes deduced from TEM observations. Therefore, the X-ray diffraction patterns and HR-TEM give feature characteristics of the maghemite structure. The adsorption of dextran on the surface of iron oxide was evidenced by Attenuated Total Reflectance Fourier transform Infrared (ATR-FTIR) spectroscopy.

The biocompatibility of DIO-NPs was assessed by cell viability and cytoskeleton analysis. Histopathology analysis was performed after 24 hours, 7 and 30 days respectively from the intratracheal instillation of a solution containing 0.5, 2.5 or 5 mg/kg DIO-NPs. The pathological micrographs of lungs derived from rats collected after the intratracheal instillation with a solution containing 0.5 mg/kg and 2.5 mg/kg DIO-NPs show that the lungs have preserved the architecture of the control specimen with no significant differences. However, even at concentrations of 5 mg/kg the effect of DIO-NPS on the lungs was markedly reduced at 30 days post-treatment.

This work was financially supported by the PN-II-131/2014 funded by the Ministry of Education-UEFISCDI. Also this work was funded by the Sectoral Operational Programme Human Resources Development 2007-2013 of the Ministry of European Funds through the Financial Agreement POSDRU/159/1.5/S/134398.

PMon059

Fabrication of Nanoporous Metallic Coatings

Slabon, Adam (RWTH Aachen, Institut für Anorganische Chemie, Aachen, GER)

Porous metals have received recently increased attention as catalysts, filters, lightweight and composite materials and current collectors in electrochemical energy storage systems. [1] Today, the metal current collector on the anode side is a 10 µm thick copper sheet, representing a heavy component in a lithium-ion cell. Its mass is comparable to the anode active material and accounts for around 10% of the total weight of the cell. [2] There remain still two challenging tasks in the synthesis of porous metals: 1) a precise control of the morphology and 2) pore sizes in the submicron range.

A precise control over the morphology and porosity of metallic thin films is demonstrated on the nanoscale. Porous nickel nanostructures in the form of hollow spheres and tubes were synthesized by electrochemical co-deposition of nickel and copper and subsequent electrochemical etching. [3]

---

[1] Y. Hongbin , L. A. Remer, C. Mian , B. Huisheng , T. Qian, Y. Tianle , Z. Yan, Science 2012 , 337 , 563-566

[2] L. B. Hu, H. Wu, F. La Mantia , Y. A. Yang, Y. Cui, ACS Nano 2010 , 4 , 5843-5848.

[3] A. Slabon, F. Krumeich, F. Wächter, R. Nesper, ChemElectroChem 2014 , 1 , 536-538.

PMon060

Fe-based layered tellurides $Fe_{3-\delta}GeTe_2$ and $Fe_{3-\delta}As_{1-y}Te_2$: synthesis, neutron diffraction study, Mössbauer spectroscopy and band structure calculations

Verchenko, Valeriy (Lomonosov Moscow State University, Moscow, RUS); Tsirlin, Alexander (National Institute of Chemical Physics and Biophysics, Tallinn, AUT); Sobolev, Alexey (Lomonosov Moscow State University, Moscow, RUS); Presniakov, Igor (Lomonosov Moscow State University, Moscow, RUS); Shevelkov, Andrei (Lomonosov Moscow State University, Moscow, RUS)

Ni-based layered tellurides form a class of compounds, which possess some peculiarities in the crystal structure and physical properties. Different isostructural representatives with the general formula $Ni_{3\pm\delta}E_{1-y}Te_{2+y}$ (E – *p* element of groups 13-15) are known, such as $Ni_{3-\delta}GaTe_2$ [1], Ni_3GeTe_2 [2], $Ni_{3\pm\delta}In_{1-y}Te_{2+y}$ [3], and Ni_2SbTe_2 [4]. All of them have crystal structures, which could be regarded as a derivative of the NiAs motif. In this derivative, $[Ni_3E]$ heterometallic slabs are confined by Te atoms in layers, which alternate along the *c* direction of a hexagonal unit cell. Thereby, the crystal structure leads to the following feature: it consists of alternating layers each containing metallic blocks of *d* and *p* elements. Both the *d-p* bonding and layered character of the crystal structure may lead to peculiarities in physical properties, which call for a detailed study. However, Ni-based layered tellurides were found simply to be metals and Pauli paramagnets [1, 2, 4]. Among all of these isostructural compounds only one Fe-based representative is known, Fe_3GeTe_2, which differs significantly from the Ni-based layered tellurides. [2]. Fe_3GeTe_2 is also metallic, but shows much more pronounced magnetism. The compound is reportedly ferromagnetic below $T_C \sim 230$ K, however a closer look at the magnetization data reveals non-typical behavior: the magnetization continues increasing in higher magnetic fields, and even at 7 T the saturation of magnetic moment is not reached yet [2]. This observation makes other magnetic structures feasible including ferrimagnetic and canted antiferromagnetic types of order for Fe_3GeTe_2. Neutron diffraction could be directly used to probe all of these configurations. In this study we report on the synthesis, homogeneity range, crystal and electronic structure and physical properties of two Fe-based representatives of layered tellurides, $Fe_{3-\delta}As_{1-y}Te_2$ and $Fe_{3-\delta}GeTe_2$, of which the former is reported for the first time. Both compounds exhibit metallic behavior accompanied with the low-temperature magnetism. As $Fe_{3-\delta}GeTe_2$ shows ferromagnetic transition below 230 K, the phase transition in $Fe_{3-\delta}As_{1-y}Te_2$ at $T \sim 125$ K is less pronounced, and we focused on the properties of $Fe_{3-\delta}GeTe_2$. We employed the neutron diffraction technique and ^{57}Fe Mössbauer spectroscopy to investigate $Fe_{3-\delta}GeTe_2$ magnetism in detail. Our study reveals few peculiarities of the compound in comparison with the previous work [2]: we found $Fe_{3-\delta}GeTe_2$ to possess a homogeneity range $0 < \delta < 0.3$ and to order ferromagnetically below $T_C \sim 225$ K with the local moments of 2.07(2) μ_B and 1.66(2) μ_B at zero temperature on the Fe1 and Fe2 sites, respectively. The obtained magnetic moments are in agreement with the results of band structure calculations, which predict itinerant ferromagnetism for Fe_3GeTe_2. Interestingly, the combination of itinerant ferromagnetic behavior with the layered character of crystal structure give rise to a strong magnetocrystalline anisotropy, which energy was carefully extracted within the full relativistic band structure calculations. To entirely describe functional properties of $Fe_{3-\delta}GeTe_2$, we also report thermoelectric and magnetocaloric effects of the compound.

We gratefully acknowledge the financial support of the Russian Science Foundation, grant #14-13-00089, and the Mobilitas program of the ESF, grant MTT77.

---

[1] Isaeva, A.A.; Makarevich, O.N.; Kuznetsov, A.N.; Doert, T.; Abakumov, A.M. *Eur. J. Inorg. Chem.* **2010**, 1395-1404.

[2] Deiseroth, H.J.; Aleksandrov, K.; Reiner, C.; Kienle, L.; Kremer, R.K. *Eur. J. Inorg. Chem.* **2006**, 1561-1567.

[3] Larsson, A.K.; Noren, L.; Withers, R.L.; Rundlöf, H.*J.Solid State Chem.* **2007**, 180, 2723-2733.

[4] Reynolds, T.K.; Kelley, R.F.; DiSalvo, F.J. *J. Alloys Compd.* **2004**, 366, 136-144.

PMon061

Giant Zn deficiency and p-typeness tuned by a nanosize effect in N-doped ZnO nanoparticles

Cario, Laurent (Institut des Matériaux Jean Rouxel, CNRS Université de Nantes, Nantes, FRA); Renaud, Adèle (Institut des Matériaux Jean Rouxel, CNRS Université de Nantes, Nantes, FRA); Chavillon, Benoit (Institut des Matériaux Jean Rouxel, CNRS Université de Nantes, Nantes, AUT); Rocquefelte, Xavier (Institut des Matériaux Jean Rouxel, CNRS Université de Nantes, Nantes, AUT); Faulques, Eric (Institut des Matériaux Jean Rouxel, CNRS Université de Nantes, Nantes, FRA); Deniard, Phillipe (Institut des Matériaux Jean Rouxel, CNRS Université de Nantes, Nantes, FRA); Cheviré, François (UMR CNRS 6226 "Sciences Chimiques de Rennes", Rennes , FRA); Tessier, Franck (UMR CNRS 6226 "Sciences Chimiques de Rennes", Rennes, FRA); Jobic, Stephane (Institut des Matériaux Jean Rouxel, CNRS Université de Nantes, Nantes, FRA)

Owing to its high technological importance for optoelectronics, zinc oxide received much attention. In particular, the role of defects on its physical properties has been extensively studied as well as their thermodynamical stability. In particular, a large concentration of Zn vacancies in ZnO bulk materials is so far considered highly unstable. Here we report that the thermal decomposition of zinc peroxide produces wurtzite-type ZnO nanoparticles with an extraordinary large amount of zinc vacancies (>15%). These Zn vacancies segregate at the surface of the nanoparticles, as confirmed by ab initio calculations, to form a pseudo core-shell structure made of a dense ZnO sphere coated by a Zn free oxo-hydroxide mono layer [1]. Such Zn-deficient $Zn_{1-x}O$ nanoparticles exhibit an unprecedented photoluminescence signature suggesting that the core-shell-like edifice drastically influences the electronic structure of ZnO. This argument is supported by the synthesis of nanoparticles by ammonolysis at low temperature (e.g. 250 °C) of zinc peroxide which leads to p-type zinc oxide material with the wurtzite structure [2]. The nature of the charge carriers was identified without ambiguity by photoelectrochemistry, complex impedance spectroscopy and transient spectroscopy. P-typeness in ZnO would result from an extraordinary huge amount of Zn vacancies (up to 20%) coupled with the insertion of nitrogen within nanoscale spherical particles. Remarkably, the p-type conductivity remains stable for periods longer than two years in ambient conditions. This discovery could open the door to the achievement of n-ZnO/p-ZnO:N colorless homo-junctions.

---

[1] A. Renauld et al. under revision, *Scientific Report* (2015).
[2] B. Chavillon et al., *J. Am. Chem. Soc.*, 2012, 134, 464

PMon062

Glass-like Thermal Conductivity in $SrTiO_3$ Thermoelectrics Induced by A-site Vacancies

Popuri, Srinivas (Heriot-Watt University, Edinburgh, GBR); Suard, Emma (Institut Laue Langevin, Grenoble, FRA); Decourt, Rodolphe (University of Bordeaux, Bordeaux, FRA); Pollet, Michael (University of Bordeaux, Bordeaux, FRA); Bos, Jan-Willem (Heriot-Watt University, Edinburgh, GBR)

A central challenge in the development of efficient thermoelectric materials is to unite “phonon-glass” and “electron crystal” properties. Reduced $SrTiO_3$ has a large Seebeck coefficient (S) and low electrical resistivity (ρ), leading to promising thermoelectric power factors (S^2/ρ [1]. Despite enormous effort through atomic substitutions and nanostructuring, the thermal conductivity (κ) of $SrTiO_3$ has remained characteristic of a crystalline solid ($\kappa \sim 1/T$). We have used a less-explored approach: the introduction of vacancies on the perovskite A-site through the replacement of Sr^{2+} by La^{3+}. This results in a glass-like state with an almost temperature independent $\kappa = 2.5$ W m^{-1} K^{-1}, close to the predicted minimum for $SrTiO_3$ [2]. We will discuss these results and the potential of A-site deficient $SrTiO_3$ for thermoelectric applications in this poster contribution.

---

[1] T. Okuda, K. Nakanishi, S. Miyasaka and Y. Tokura, Phys. Rev. B 63, 113104 (2001).

[2] Srinivasa. R. Popuri, A. J. M. Scott, R. A. Downie, M. A. Hall, E. Suard, R. Decourt, M. Pollet and J.-W. G. Bos, RSC Advances 4, 33720 (2014).

PMon063

Improved Thermoelectric Performance in Nanostructured half-Heuslers

Downie, Ruth (Heriot-Watt University, Edinburgh, GBR); MacLaren, Donald (University of Glasgow, Glasgow, GBR); Smith, Ronald (ISIS Facility, Didcot, GBR); Bos, Jan-Willem (Heriot-Watt University, Edinburgh, GBR)

It is widely recognized that a sustainable energy future will rely on a range of generation and energy saving technologies. Thermoelectric generators harvest waste heat from any heat generating process but have so far not found widespread use. This is largely due to the relatively poor efficiency of the semiconductors used in these modules. The thermoelectric performance of a material is determined by its figure of merit, $zT = S^2\sigma T/\kappa$, which contains the Seebeck coefficient (S), the electrical conductivity (σ), the sum of lattice and electronic thermal conductivities ($\kappa = \kappa_{lat} + \kappa_{el}$), and the absolute temperature. The underlying problem in attaining high zT values is that all variables except κ_{lat} are linked through the electronic structure of the material.

Half-Heuslers have long been recognised as promising thermoelectric materials with large $S^2\sigma$ values but limited by their relatively large κ_{lat}. One possible approach to enhance zT is through nanostructuring as this offers additional possibilities to reduce κ_{lat} [1].

The first route explored involved the preparation of XNiSn half-Heuslers where X is a mixture of Ti, Zr and Hf. Rietveld analysis of X-ray and neutron powder diffraction data, combined with electron microscopy, reveals the presence of multiple half-Heusler compositions that differ in the ratio of the X-metals [2]. This multiphase behaviour extends over large length scales and has been linked to reductions in κ_{lat}.

The second approach involved control over the segregation into half-Heusler and Heusler phases that occurs for Ni-rich compositions. For arc-melted $TiNi_{1+y}Sn$ (y = 0-0.06) samples low κ_{lat} and zT = 0.7 were observed [3]. Employing other excess metals led to the observation of efficient electron doping for Cu, demonstrating that the electronic properties can also be modified [4].

In all cases, we have used Rietveld analysis of neutron powder diffraction data to give insight into the distributions of metals over the available sites within the structure. This careful structural analysis, enabling links to properties to be made, is the central tenet of our work, and will be a major theme of the presentation.

---

[1] J.W.G. Bos and R.A. Downie. Journal of Physics Condensed Matter 26, 433201 (2014)

[2] R.A. Downie, D.A. Maclaren and J.W.G. Bos. Journal of Materials Chemistry A 2, 6107 (2014)

[3] R.A. Downie, D.A. Maclaren, R.I. Smith and J.W.G. Bos Chemical Communications 49, 4184 (2013)

[4] R.A. Downie, R.I. Smith, D.A. Maclaren and J.W.G. Bos. Chemistry of Materials 27, 2449 (2015)

PMon064

Hydrothermal synthesis and characterization of novel quaternary yttrium selenites

Bang, Seong-eun (Chung-Ang University, Seoul, KOR); Ok, Kang Min (Chung-Ang Univeristy, Seoul, KOR)

Materials containing noncentrosymmetric (NCS) crystal structures exhibit several useful properties such as second-harmonic generation (SHG), piezoelectricity, pyroelectiricity, and ferroelectircity. Thus, huge efforts have been made to search superior performing NCS materials. One successful synthetic approach toward NCS materials is combining second-order Jahn-Teller (SOJT) distortive cations, i.e., d^0 transition metals and stereoactive lone pair cations.[1] However, many locally asymmetric polyhedra of cations caused by SOJT distortions tend to crystallize in macroscopic centrosymmetric (CS) space groups, when they are aligned in an antiparallel manner. We have systematically studied how the alkali metal cations with different sizes influence the overall framework geometries and centricities in a series of stoichiometrically similar yttrium selenites.

A series of alkali metal yttrium selenites, $AY(SeO_3)_2$ (A = K, Rb, and Cs) have been synthesized using A_2CO_3, $Y(NO_3)\cdot 6H_2O$, and SeO_2 under hydrothermal conditions. Although all four reported materials reveal 3D framework geometries, they have different channel structures. $NaY(SeO_3)_2$ with the smallest cation crystallizes in the polar NCS space group, $P2_1cn$ (No. 33). However, those with larger alkali metal cations, $KY(SeO_3)_2$ and $RbY(SeO_3)_2$, show centrosymmetric space group, Pnma (No. 62) and they are isostructural to each other. $CsY(SeO_3)_2$ containing the largest cation crystallizes in the centrosymmetric cubic space group, *Pa-3* (No. 205). The cation size and the subsequent coordination numbers significantly influence the framework geometries as well as the centricities.[2] Powder nonlinear optical (NLO) properties measurements on the NCS selenite, $NaY(SeO_3)_2$ show that the material has a SHG efficiency of 10 α-SiO_2. Thorough characterizations such as Infrared spectroscopy, UV-Vis spectroscopy, thermal analysis, and dipole moment calculation are also discussed.

---

[1] Halasyamani, P. S., Poeppelmeier, K. R., *Chem. Mater.*, **1998**, *10*, 2753-2769.
[2] Bang, S. E., Lee, D. W., and Ok, K. M., *Inorg. Chem.*, **2014**, *53*, 4756-4762.

PMon065

Improvement of near infrared Long-Persistent Luminescence in Si Substituted $Zn_3Ga_2Ge_2O_{10}$

Zhang, Yi (Department of Physics and Electronic Engineering, Hanshan Normal University, Chaozhou, Guangdong, Chaozhou, AUT); HUANG, RUI (Department of Physics and Electronic Engineering, Hanshan Normal University, Chaozhou, Guangdong, Chaozhou, CHN); Lin, Huihong (Department of Physics and Electronic Engineering, Hanshan Normal University, Chaozhou, Guangdong, Chaozhou, CHN)

Long persistent phosphors (LPPs) are known as their characters of persistent luminescence which can emit for hours after the stoppage of irritation. LPPs have already displayed their potential in night-vision assistants, security signs and medical diagnostics. Until now, most of long persistent phosphors such as $SrAl_2O_4:Eu^{2+}$, Dy^{3+} (green, >30 h),[3] $Sr_2MgSi_2O_7:Eu^{2+}$, Dy^{3+} (blue, >10 h)[4] and $CaS:Eu^{2+}$, Tm^{3+} (red, >1 h)[5] have been applied to commercialization of primary color emitters. However, it's hard to satisfy the need of LLPs with near infrared (NIR) emitting. Recently, Pan et al. reported a new NIR Cr^{3+}-doped zinc gallogermanates ($Zn_3Ga_3Ge_2O_{10}:Cr^{3+}$) phosphor with a super long persistence time of more than 360h excited by sunlight.[5] The bright and super long persistent NIR luminescence make it potential candidates for many applications. In this work, the improved NIR long-persistent $Zn_3Ga_3Ge_2O_{10}:Cr^{3+}$phosphors with the substitution of silicon were synthesized using a classic solid state method. The NIR long-persistent luminescence properties were investigated systematically using photoluminescence spectra, persistent d ecay curves , persistent luminescence spectra, thermoluminescence curves, and trap filling spectra. Experimental results reveal that the substitution of silicon can effectively improve the NIR long-persistent luminescence intensity as well as decay time for $Zn_3Ga_3Ge_{2-x}Si_xO_{10}:Cr^{3+}$ phosphor. The improved performance of $Zn_3Ga_3Ge_{2-x}Si_xO_{10}:Cr^{3+}$ phosphors is explained in terms of the substitution mechanism that creates distorted octahedral sites surrounded by octahedral Si positive defects which acts as new efficient traps.

---

[1] T. Matsuzawa, Y. Aoki, N. Takeuchi and Y. Murayama, J. Electrochem. Soc., 1996, 143, 2670.
[2] Y. Lin, Z. Tang, Z. Zhang, X. Wang and J. Zhang, J. Mater. Sci. Lett., 2001, 20, 1505.
[3] D.Jia, W. Jia, R. Evans, W.M. Dennis, H. Liu, J. Zhu and W.M. Yen, J. Appl. Phys. 2000, 88, 3402.
[4] Z. Pan, Y. Y. Lu and F. Liu, Nat. Mater. , 2012, 11, 58.

PMon066

Influence of the cationic substitution on crystal structure and physical properties in the $Fe_{3-x}Mn_xO_2BO_3$ ($0 \leq x \leq 3$) system.

Lainé, Fabien (CRISMAT, UMR CNRS Ensicaen Unicaen, Caen, FRA); Martin, Christine (CRISMAT, UMR CNRS Ensicaen Unicaen, Caen, FRA); Horvath, Barbara (CRISMAT, UMR CNRS Ensicaen Unicaen, Caen, FRA); Malo, Sylvie (CRISMAT, UMR CNRS Ensicaen Unicaen, Caen, FRA); Poienar, Maria (National Institute for Research and Development in Electrochemistry and Condensed Matter, Timisoara, ROU); Rouquette, Jerome (Institut Charles Gerhardt, UMR CNRS, Université Montpellier II, Montpellier, FRA); Damay, Francoise (Laboratoire Leon Brillouin, UMR12, CEA-CNRS, Gif-sur-Yvette, FRA); Beran, Premysl (Nuclear Physics Institute, Rez, CZE); Maignan, Antoine (CRISMAT, UMR CNRS Ensicaen Unicaen, Caen, FRA); Guesdon, Anne (CRISMAT, UMR CNRS Ensicaen Unicaen, Caen, FRA)

Charge ordering in transition metals oxides induces interesting physical properties as shown with Colossal MagnetoResistance in manganites [1] or multiferroism in $LuFe_2O_4$ [2]. Among iron oxides, the ludwigite $Fe^{2+}{}_2Fe^{3+}O_2BO_3$ has sparked particular interest with its exciting electronic and magnetic properties [3, 4]. This oxyborate crystallizes at RT in an orthorhombic cell (SG: Pbam with a = 9.45 Å, b = 12.30 Å and c = 3.07 Å) in which iron cations are distributed over four independent crystallographic sites. Its structure is built from FeO_6 edge-sharing octahedra forming zigzag walls connected through apices and BO_3 triangles [4]. A structural transition occurs at T_{CO} = 283 K, involving a doubling of the c-parameter (SG: Pbnm) due to alternate displacements of iron ions along the rung of one of the two "three leg ladders". Moreover, at decreasing temperature, two magnetic transitions are observed at 112 K and 75 K, each one corresponding to the magnetic ordering of one ladder. Many studies have been performed on $Fe^{2+}{}_2Fe^{3+}O_2BO_3$ and on substituted compounds $Fe_{3-x}M_xO_2BO_3$ where M = Ni, Co, Cu, Mg with different x values [5-8] to understand this complex physical behavior. But, curiously, there are no reported studies for mixed Fe-Mn ludwigite. In this context, we have decided to examine the influence of the cationic substitution in the $Fe_{3-x}Mn_xO_2BO_3$ solid solution for x ranging from 0 to 3. All the samples were synthesized by solid state reaction in evacuated quartz ampoule to control the oxygen content. In order to link the crystal chemistry and physical properties of $Fe_{3-x}Mn_xO_2BO_3$ compounds, X-Ray and electron diffraction studies were performed systematically at room temperature, as well as magnetic and transport properties measurements in the 2 to 400K temperature range. The evolution of the cell parameters vs x shows that the Vegard's law is not followed and the magnetic susceptibility measurements evidence a decrease of the magnetic transition temperatures as x increases. A particular attention was given to the composition $MnFe_2O_2BO_3$ (x=1) with a neutron diffraction study vs. T. The distribution of the manganese and iron cations over the four crystallographic sites has been determined: two sites are fully occupied by iron whereas the two others are mixed, each of these couples corresponding to one "three leg ladder". The refinement of the magnetic structure is still in progress, but the preliminary results show an ordering of only one of these ladders, the fully occupied iron one.

---

[1] Ramirez ; *J. Phys.: Condens. Matter*, **1997**, 9, 8171-8199.

[2] Ikeda et al ; *Nature*, **2005**, 436, 1136-1138.

[3] Bordet et al ; *Phys. Rev. B*, **2009**, 79, 144408.

[4] Larrea et al ; *Hyperfine Interactions*, **2005**, 161, 237-24.

[5] Perkins and Attfield ; *J. Chem. Soc, Chem. Commun*, **1991**, 229-231.

[6] Freitas et al ; *Phys. Rev. B*, **2008**, 77, 184422.

[7] Continentino et al ; *Eur. Phys. J. B*, **1999**, 9, 613-618.

[8] Mitov et al ; *Journal of Alloys and Compounds*, **1999**, 289, 55-65.

PMon067

$La_{2-x}Sr_xNi_{1-y}FeyO_{4+\delta}$ as cathode materials for SOFC application

Gilyov, Artyom (Ural Federal University, Yekaterinburg, RUS); Kiselyov, Evgeny (Ural Federal University, Yekaterinburg, RUS); Cherepanov, Vladimir (Ural Federal University, Yekaterinburg, RUS)

At the moment the K_2NiF_4-type $La_2NiO_{4+\delta}$ is considered as possible a candidate for SOFC application. Its advantages include high ionic conductivity (via interstitial oxygen and vacancies), moderate thermal expansion and high electrocatalytic activity. The properties of $La_2NiO_{4+\delta}$ are well investigated. Nevertheless, some of them such as electron conductivity and chemical stability do not meet the requirements for successful application in SOFC. One of the standard ways to improve the properties of materials is heterovalent doping of A-site and/or B-site. Simultaneous doping of A-site and B-site in $La_2NiO_{4+\delta}$ with strontium and iron has not been fully studied yet. The purposes of this work are to assess the effect of strontium and iron doping on properties of $La_2NiO_{4+\delta}$ and to find the most suitable material in the La-Sr-Ni-Fe-O system for SOFC application.The present work is focused on such properties of the $La_{2-x}Sr_xNi_{1-y}Fe_yO_{4-\delta}$ (x=0.5, 0.6, 0.8; y=0.1-0.5) as electric conductivity, oxygen permeation, oxygen non-stoichiometry and their dependence on temperature and oxygen partial pressure. Thermal expansion and chemical stability to the commonly used electrolytes (YSZ, LSGM etc.) were also examined. The four probe method was used for conductivity measurements. Conductivity values vary significantly with dopants concentration. It was observed that addition of strontium leads to an increase of conductivity whereas iron doping shows opposite effect. Such changes could be attributed to the charge compensating processes and also to the electronic state of iron. The maximum of conductivity (271 S/cm in air at 1123K) corresponds to the $La_{1.2}Sr_{0.8}Ni_{0.9}Fe_{0.1}O_{4\pm\delta}$ composition. Temperature dependencies of oxygen content were obtained by thermogravimetric measurements. The dependencies show that oxygen content gradually decreases with addition of strontium. This also slows the rate of oxygen exchange with atmosphere due to smaller concentrations of highly mobile interstitial oxygen. Addition of iron, in opposite, increases the oxygen content. The highest value of oxygen excess (δ=0.11) was found for $La_{1.5}Sr_{0.5}Ni_{0.6}Fe_{0.4}O_{4+\delta}$ composition.Oxygen permeation studies show that doping with strontium and iron, in general, decrease oxygen transport in the $La_{2-x}Sr_xNi_{1-y}Fe_yO_{4\pm\delta}$. Calculated values of ionic conductivity do not exceed 1% of total conductivity. Activation energies of oxygen permeability vary in range 150-200kJ/mol which is higher than that for undoped La2NiO4 [1]. It should be noted that oxygen flux through the dense $La_{2-x}Sr_xNi_{1-y}Fe_yO_{4-\delta}$ membrane along with ionic conductivity slightly increases at high iron concentrations (y>0.3). Thermal expansion of the $La_{2-x}Sr_xNi_{1-y}Fe_yO_{4-\delta}$ was examined by high temperature XRD analysis and dilatometry in temperature range 25-1100°C in air. No phase transitions were observed in all temperature range studied. The lowest value of thermal expansion coefficient (TEC) obtained for $La_{1.5}Sr_{0.5}Ni_{0.9}Fe_{0.1}O_{4-\delta}$ is $12{,}74\times10^{-6}$ K^{-1}. Further doping with strontium and iron significantly increases TEC and for $La_{1.2}Sr_{0.8}Ni_{0.6}Fe_{0.4}O_{4-\delta}$ its value is equal to $16{,}53\times10^{-6}$ K^{-1}.Chemical stability to electrolytes was examined in air at sintering temperature 1250°C. XRD analysis shows that solid solutions $La_{2-x}Sr_xNi_{1-y}Fe_yO_{4-\delta}$ chemically interact with YSZ and LSGM electrolytes, but are stable to samarium doped CeO_2. For fuel cell tests the $La_{1.5}Sr_{0.5}Ni_{0.6}Fe_{0.4}O_{4-\delta}$ was chosen as a cathode material. Planar-type fuel cell included LSGM (0.7 mm-thick pellet) as an electrolyte and $Sr_2MoNi_{0.75}Mg_{0.25}O_6$ as an anode material. $Ce_{0.8}Sm_{0.2}O_{1.8}$ was used as a buffer layer between the cathode and the electrolyte. The maximum power density of 390 mW/cm^2 was obtained at 850°C.

---

[1] V.V. Kharton et al. Journal of Solid State Chemistry 181 (2008) 1425– 1433.

PMon068

Low dimensional hybrids with magnetic and luminescence properties

Rueff, Jean-Michel (Laboratoire CRISMAT / CNRS UMR 6508, Caen, FRA); Hugot, Nathalie (Laboratoire CRISMAT / CNRS UMR 6508, Caen, FRA); Bloyet, Clarisse (Laboratoire CRISMAT / CNRS UMR 6508, Caen, FRA); Pautrat, Alain (Laboratoire CRISMAT / CNRS UMR 6508, Caen, FRA); Perez, Olivier (Laboratoire CRISMAT / CNRS UMR 6508, Caen, FRA); Raveau, Bernard (Laboratoire CRISMAT / CNRS UMR 6508, Caen, FRA); Caignaert, Vincent (Laboratoire CRISMAT / CNRS UMR 6508, Caen, FRA); Cardin, Julien (Laboratoire CIMAP / CEA CNRS UMR6252 ENSICAEN UCBN, Caen, FRA); Lohier, Jean-François (Laboratoire LCMT / CNRS UMR 6507, Caen, FRA); Rogez, Guillaume (IPCMS / CNRS UMR 7504 , Strasbourg, FRA); Roger, Melissa (CEMCA UBO / CNRS UMR 6521, Brest, FRA); Jaffres, Paul-Alain (CEMCA UBO / CNRS UMR 6521, Brest, FRA)

During this last decade our work has concerned the synthesis of novel hybrid materials for potential applications in the field of magnetism, luminescence and gas or drug storage by using original rigid poly-functional organic precursors. These materials, also called Metal Organic Frameworks (MOF's) or coordination polymers, are obtained by hydrothermal synthesis from an inorganic salt and an organic building block bearing at least one phosphonic acid and one carboxylic acid grafted on a rigid scaffold (e.g. a benzene ring or a heterocycle) that act as organic 'pillar' in the structure.

To understand and to control the dimensionality of these materials (1D, 2D or 3D network) several parameters were considered: structure of the organic precursors (rigidity, position, number and type of functional groups), nature of the inorganic precursor and influence of the experimental conditions (solvent, concentration, pH, temperature).

By this strategy we have underlined the crucial importance of the pH of the reaction media on the control of the dimensionality of magnetic materials when 3- or 4-phosphonobenzoic acid where used with 3d paramagnetic cationic salts (Co^{2+}, Mn^{2+}, Cu^{2+}). Indeed, at low pH only the phosphonic acid is bonded to the inorganic network while at higher pH both functional groups are linked to the inorganic network producing, a columnar, homochiral helical (1D), lamellar (2D), or 3D architectures.

In this work we present the first result concerning three new hybrid materials obtained from new fluorene phosphonic acids derivatives and 3d cationic salts (Co^{2+}, Zn^{2+}, Cu^{2+}).
These three materials exhibit luminescence properties due to the organic subnetwork, and two of them show low dimensionality magnetism.

The synthesis, single crystal structure, thermal stability and the results of magnetic and luminescence characterization will be presented.

PMon069

Silver based hybrids with potential bactericidal properties

Rueff, Jean-Michel (Laboratoire CRISMAT / CNRS UMR 6508, Caen, FRA); Perez, Olivier (Laboratoire CRISMAT / CNRS UMR 6508, Caen, FRA); Raveau, Bernard (Laboratoire CRISMAT / CNRS UMR 6508, Caen, FRA); Caignaert, Vincent (Laboratoire CRISMAT / CNRS UMR 6508, Caen, FRA); Hix, Gary (School of Science and Technology, Nottingham, GBR); Berchel, Mathieu (CEMCA UBO / CNRS UMR 6521, Brest, FRA); Quentel, François (CEMCA UBO / CNRS UMR 6521, Brest, FRA); Jaffres, Paul-Alain (CEMCA UBO / CNRS UMR 6521, Brest, FRA)

Hybrid organic-inorganic materials are wildly studied for their potential applications in the field of magnetism, luminescence, gas or drug storage/release and energy production.
On our side, we have decided to investigate the use of silver hybrid materials for their potential bactericidal properties. In a recent work in this field we have shown that silver-based hybrid materials were able to release silver ions in aqueous solution thus exhibiting a bactericidal effect against six bacterial strains and, especially, against Gram-negative strains. The materials presented here are obtained from a silver salt and from: a) rigid polyfunctional organic building blocks possessing at least one phosphonic acid and one carboxylic acid grafted on a benzene ring (3- or 4-phosphonobenzoic acid) b) n-alkylphosphonates.

To reach the targeted applications, one of the fundamental questions deals with the structure of the hybrid materials. In order to understand and control the dimensionality of the final materials (1D, 2D or 3D network) several parameters have been considered in this work: geometry of the organic precursors (bent or linear), type of reactive functions, influence of the experimental conditions (solvent, concentration, pH, temperature).

Accordingly, this strategy has permitted to underline the crucial importance of the pH of the reaction media on the control of the dimensionality. Indeed, at low pH only the phosphonic acid is bonded to the inorganic network while at higher pH both functional groups are linked to the inorganic. Several materials were obtained and their structure solved by X-ray diffraction on single crystals. The synthesis, structure, thermal stability and the quantification of silver release in aqueous solution will be presented.

The influence of the rigidity, polarity and the number and type of reactive functions of the organic ligand involved in the synthesis will be also discussed.

PMon070

Luminescence of Ln-N-MOFs for Sensing and Chromaticity Tuning

Müller-Buschbaum, Klaus (Universität Würzburg, Würzburg, GER)

Interesting photophysical properties like luminescence contribute to the multifunctionality of metal-organic frameworks (MOFs). This especially includes lanthanide based N-functionalized MOFs, as they can show effective luminescence by organic chromophore based and metal based luminescence processes. Additional energy transfer mechanisms between linker ligands and metal centers can be highly beneficial. N-donor ligands prove useful as antenna for such processes and thereby show an opposite behaviour to OH groups. Lanthanide metal ions can contribute typical 4f-emission as well as less typical 5d-state participation. Concepts of solid-state chemistry such as co-doping of host lattices with metal ions can be utilized to incorporate a defined and low amount of luminescence centers in the MOF, which can be achieved by replacement of the connectivity centers or by utilization of the pore system. Proper choice of luminescence centers can be used to set the chromaticity point and thus the colour of the MOF. Deliberate choice and mixing of metal dopants enable such tuning of the chromaticity up to the emission of white light . Low dopant degrees prevent cross relaxation and reduce quenching by concentration, which increases the overall efficiency. The combination of porosity and luminescence gives a multifunctionality that renders sensing and detection of chemical species accessible based on a dependence of the interaction of guests/MOF on the luminescence. Thereby, an easily observable detection signal becomes available either by intensity change (luminescence turn-on/turn-off sensing), or by a change in the chromaticity. The range of detectable species includes gases, liquids and metal ions. Thus, luminescent MOFs are a hot topic for future sensing applications.

---

[1] a) M. D. Allendorf. C. A. Bauer, R. K. Bhakta, R. J. T. Houk, *Chem. Soc. Rev*. **2009**, *38*, 1330; b) Y. Cui, Y. Yue, G. Qian, B. Chen, *Chem. Rev.* **2012**, *112*, 1126; c) K. Müller-Buschbaum, F. Beuerle, C. Feldmann, Micropous Mesoporous Mater. **2015** , DOI: 10.1016/j.micromeso. 2015.03.036; d) D. Liu, K. Lu, C. Poon and W. Lin, *Inorg. Chem*. **2014**, *53*, 1916.

[2] a) P. Falcaro, S. Furukawa, *Angew. Chem.***2012**, *51*, 8431; b) D. F. Sava, L. E. S. Rohwer, M. A. Rodriguez, T. M. Nenoff, *J. Am. Chem. Soc.***2012**, *134*, 3983.

[3] J.-C. Rybak, M. Hailmann, P. R. Matthes, A. Zurawski, J. Nitsch, A. Steffen, J. G. Heck, C. Feldmann, S. Götzendörfer, J. Meinhardt, G. Sextl, H. Kohlmann, S. J. Sedlmaier, W. Schnick, K. Müller-Buschbaum, *J. Am. Chem. Soc.* **2013**, *135*, 6896.

PMon071

Luminescent characteristics of $CaAl_2O_4$:Eu^{3+}phosphors co-doped with Er^{3+} and Gd^{3+}

Verma, Naveen (M D University, Rohtak, India, Rohtak, IND); Mari, Bernabe (Universitat Politècnica de València, Camí de Vera s/n, 46022 València, Spain, Valencia, ESP); Singh, Krishan Chander (Department of Chemistry, M D University, Rohtak, IND); Mollar, Miguel (Universitat Politècnica de València, Camí de Vera s/n, 46022 València, Spain, Valencia, ESP); Jindal, Jitender (Department of Chemistry, M D University, Rohtak, Rohtak, IND)

$CaAl_2O_4$: Eu^{3+} (1mol %) co-doped with varying concentration of Er^{3+} (1, 2, and 5 mol %) and Gd^{3+} (1, 2, 5 and 10mol %) were prepared by combustion synthesis method at 600 °C. All the compositions were investigated for their structural and photoluminescence properties. Samples were prepared in open atmosphere and show the presence of both Eu^{3+} and Eu^{2+} states and, the ratio of these states changes on annealing at 1000°C. The prepared materials at 600ºC show high intense peak around 440 nm corresponding to $Eu^{2+}$and less intense peaks in the red region which are attributed to the presence of Eu^{3+}. In the annealed compounds at 1000ºC the intensity of 440 nm peak decreases and the intensity of peaks in the red region increases significantly due to Eu^{3+}. The $^5D_0 \rightarrow {}^7F_3$ transition at 657 nm appears as the highest intensity peak. The second rare- earth ion (Er^{3+}or Gd^{3+}) acts as sensitizer and enhances the photoluminescence intensity. The XRD spectra reveal the monoclinic phase of $CaAl_2O_4$ and Eu^{3+}, Er^{3+} and Gd^{3+} doped samples do not change the crystalline structure of calcium aluminate .

The study observed the effect of Er^{3+} or Gd^{3+} co-doping on structural and luminescence properties of $CaAl_2O_4$: Eu^{3+} (1mol %) compound. We vary the concentration of co-dopant to tune the color. The annealing effect also studied on the existence of prominent valence state of europium (Eu^{2+} /Eu^{3+}) in $CaAl_2O_4$: Eu. The reported materials can be used as spectral convertor to enhance the light absorption in the solar cells so that solar cell efficiency may be increased.

PMon072

Optical properties of Yb^{3+} doped ZnO/MgO nanocompositesprepared by combustion method

Verma, Naveen (M D University, Rohtak, India, Rohtak, IND); Mari, Bernabe (Universitat Politècnica de València, Camí de Vera s/n, 46022 València, Spain, Valencia, AUT); Singh, Krishan Chander (Department of Chemistry, M D University, Rohtak, IND); Jindal, Jitender (Department of Chemistry, M D University, Rohtak, IND)

Yb^{3+} doped ZnO/MgOnanocomposite were prepared by combustion synthesis method. The samples were further heated to 1000^{o} C to improve their crystallinity and photoluminescent efficiency. The concentrations of Yb^{3+} and Mg^{2+} were varied between 1 to2% and 5 to 70%respectively in prepared samples. The nano-powders were characterized by Scanning Electron Microscopy and XRay Diffraction for morphology and structural determination. XRD studies have revealed the wurtzite structure for $Mg_xZn_{1-x}O$ for Mg concentrations below 30%. Higher concentrations of Mg results in Yb^{3+} doped ZnO/MgOnanocompositecontainingthree phases; the wurzite hexagonal phase typical of ZnO, the cubic phase of MgO and a small amount of cubic Yb_2O_3 phase. As expected, the amount of cubic phase innano-powders increased with the increase of Mg concentration in ZnO.The crystallite sizeof ZnO/MgO composites decreased from 55nm to 30nm with increase of Mg content.SEM images of Yb^{3+} doped ZnO/MgOnanocomposite with higher Mg content (>50%) showed clearly distinct hexagonal and cubical shaped nano-particles.Photoluminescentemission showed a broad band in the range (435 nm to 700 nm).Pure ZnOnano-phosphor showedan emission peak around 545nm, which isblue shifted with Mg content. The photoluminescenceintensity increased with increase of Mg content in ZnO and it became maximum with 30% Mg concentration.Time resolved decay curves of photoluminescence indicated decay time in micro second time scale.

PMon073

Mesoporous ceria-based catalysts for oxidation reactions

Zagaynov, Igor (A.A. Baikov Institute of Metallurgy and Materials Science, Moscow, RUS); Liberman, Elena (D. Mendeleev University of Chemical Technology of Russia, Moscow, RUS); Buryak, Aleksey (A.N. Frumkin Institute of Physical Chemistry and Electrochemistry, Moscow, RUS)

Nanoscale ceria is very attractive for TWC, SOFC, etc. Doped CeO_2-materials are considered as more promising solid solutions for use in these goals. The introduction of smaller isovalent non-reducible cations like Zr^{4+} and Ti^{4+} into the ceria lattice enhances OSC by creating intrinsic oxygen vacancies thereby increasing the oxygen mobility by facilitating the Ce^{3+}/Ce^{4+} redox process. Whereas doping of aliovalent non-reducible cations (Gd^{3+}) into the ceria lattice enhances oxygen storage capacity (OSC) mainly through the extrinsic oxygen vacancies. It is clear that the quality of the synthesized powder changes with the preparation method. However, the simplest method for production of nanoscale ceria, especially for catalytic applications, is necessary to be used for obtaining a large quantity of intermediates. Among them, the most suitable and simplest method is co-precipitation with ultrasonic treatment (sonochemical method). Ultrasound irradiation can induce the formation of particles with a much smaller size and higher surface area than those reported by other methods and this technique has good reproducibility.

$Gd_xZryTizCe_{1-x-y-z}O_2$ solid solutions with a crystallite size of 5-10 nm have been prepared by sonochemical method from inorganic salts [1]. Ceria-based materials have a mesoporous structure with the diameter of 2-10 nm. The activity of the solid solution in the oxidation of carbon monoxide is determined by the flow method within a temperature range of 20-500°C at atmospheric pressure for the following gas mixture composition, vol. %: CO – 4.2; O_2 – 9.6; N_2 – balance or CO – 1.8; CH_4 – 1.6; O_2 – 9.6; N_2 – balance. It was shown that the temperature of full conversion of CO was 250-270°C for $CO\text{-}O_2\text{-}N_2$ mixture and 380-420°C for $CO\text{-}CH_4\text{-}O_2\text{-}N_2$ mixture without methane oxidation. The method of matrix assisted laser desorption/ionization time of flight (MALDI-TOF) mass spectrometry was used to establish the composition of surface and thus the catalytic sites (active sites of oxidation) [2].

This work was supported by RFBR grants.

---

[1] Mater Lett 139 (2015) 237; Ceram Int doi 10.1016/j.ceramint.2015.03.081.
[2] J Sol-Gel Sci Technol 74 (2015) 103.

PMon074

Mixed Transition Metal Phases Relating to Schafarzikite: A Properties Investigation

de Laune, Benjamin (The University of Birmingham, Birmingham, GBR); Whitaker, Mariana (The University of Birmingham, Birmingham, GBR); Greaves, Colin (The University of Birmingham, Birmingham, GBR)

The mineral schafarzikite ($FeSb_2O_4$, $P4_2/mbc$ $a = 8.61574(9)$ Å, $c = 5.92069(8)$ Å) [1] is analogous to the rutile structure with infinite chains of edge sharing octahedra; the octahedral A site is occupied by the transition metal (Fe^{2+}). However, a significant difference exists. The chains are separated and arranged by Sb^{3+} (B site) cations resulting in a channel running parallel to the chains of octahedra along the [001] direction. The versatility of the system has been demonstrated through the number of substitutions which can be made on the A site by first row transition metals (A = Mn, Fe, Co, Ni, Zn) [2]. To enhance the properties of the system, attempts have been made to manipulate the oxidation sate of the A site cation through substitution of Sb^{3+} by a divalent cation e.g. Pb^{2+} with varying degrees of success [1,3,4].

The magnetic structures of these systems are typically dominated by two types of magnetic order, termed A and C modes. These represent, ferromagnetic ordering within a plane and antiferromagnetic order within a chain (A mode), and ferromagnetic ordering within a chain and antiferromagnetic ordering within a plane (C mode). A complex interplay between intra-chain direct exchange, 90º super exchange, and inter-chain exchange give rise to the overall magnetic ordering of the phase. Most systems are antiferromagnetic overall with one exception; ferromagnetism has recently been discovered in a related phase, $CuAs_2O_4$ [2].

Here we present a series of mixed Co/Fe phases relating to the schafarzikite system. The results from high resolution neutron powder diffraction, magnetic susceptibility, and conductivity measurements are reported. As will be shown, a transition from A ($FeSb_2O_4$) to C ($CoSb_2O_4$)type magnetic ordering has been observed for the first time upon altering the Co-Fe ratio.

---

[1] Whitaker M. J., Bayliss R. D., Berry F. J., Greaves C., *J. Mater. Chem.*, 2011, **21**, 14523.

[2] Caslin K., Kremer R. K., Razavi F. S., Schulz A., Munoz A., Pertlik F., Liu J., Whangbo M.-H., Law J. M., *Phys. Rev. B,* 2014, **89**, 014412-1.3.

[3] de Laune B. P., Greaves C., *J. Solid State Chem.,* 2012, **187**, 225-30.

[4] Abakumov A. M., Rozova M. G., Antipov E. V., Hadermann J., Van Tendeloo G., Lobanov M. V., Greenblatt M., Croft M., Tsiper E. V., Llobet A., Lokshin K. A., Zhao Y., *Chem. Mat.,* 2005, **17**, 1123.

PMon075

Mixed metal nitride $Ni_{2-x}Co_xMo_3N$ as a heterogeneous catalyst and electro catalyst

Sardar, Kripasindhu (University of Southampton, Southampton, GBR); Hector, Andrew L (Chemistry, University of Southampton, Southampton, GBR); Levason, William (Chemistry, University of Southampton, Southampton, GBR); Hargreaves, Justin S. J. (School of Chemistry, University of Glasgow, Glasgow, GBR); McFarlane, Andrew R. (School of Chemistry, University of Glasgow, Glasgow, GBR); Hriljac, Joseph (School of Chemistry, University of Birmingham, Birmingham, GBR)

Mixed metal nitrides are emerging as excellent catalyst for reactions such as electro- chemical redox processes and ammonia synthesis reaction. The catalytic activity of these materials is often found to be comparable with precious metal containing materials. [1] However, the origin of such remarkable activity is least understood and also found to vary in similar samples prepared using varying synthetic routes. [2] We have developed a citrate-gel route for the synthesis of high quality $Ni_{2-x}Co_xMo_3N$ (x = 0.0-0.6). The materials have been characterised with Rietveld refinement, pair distribution function and X-ray absorption spectroscopy (XAS) analysis methods with the use of synchrotron X-ray radiation. The end member Ni_2Mo_3N crystalises in filled β-manganese structure. It has been demonstrated that the use of mild sol-gel process enables one to incorporate Co into Ni_2Mo_3N maintaining β-manganese type structure when synthesised at much lower temperature than used in conventional solid state methods.[3] These materials show hydrogen evolution activity in the range of 4-6 mA/cm^2 (at -0.4V SHE under electrochemical conditions) at room temperature and 150-300 µmol/hr/gm activity towards synthesis of ammonia from N_2 and H_2 at 400°C.

---

[1] J. S. J. Hargreaves, Coord. Chem. Rev. 2013, 257, 2015-2031.

[2] N. Bion, F. Can,J. Cook, J.S.J. Hargreaves, A.L. Hector, W. Levason, A.R.McFarlanec, M. Richard, K. Sardar, Applied catalysis A 2015 (in press)

[3] T.J. Prior and P.D. Battle, J. Solid State Chem. 2003, 172, 138-147.

PMon076

Mn^{2+} doped $Zn_3(PO_4)_2$ phosphors as thermal sensors

Salek, Guillaume (ICMCB, Bordeaux, FRA)

Over the past few decades, research on phosphors based thermometry systems are becoming increasingly important in different fields: engineering [1] ,nanosciences etc….. The temperature dependence characteristics of the thermographic phosphors can be evaluated by a spectral and/or a temporal modification of the phosphorescence emission. Within the different thermometric phosphors, $Zn_3(PO_4)_2$ doped by phosphor activator can be used as an irreversible thermographic sensor. T hree allotropic monoclinic forms with notations: α, β, γ exist for the anydrous form. $Zn_3(PO_4)_2$ doped by Mn^{2+} exhibit an emission-changing characteristics with temperature due to irreversible surrounding of the Mn^{2+}. The main emission of this phosphor dopant corresponds to a $^4T_1$ $^6A_1$ transition, which is strongly dependent on the ligand field and the coordination number. The relationship between the annealing temperature and the phosphorescence due to a modification of the crystal field of Mn2+ ions in the matrix was established combining X-ray diffraction and luminescence spectroscopy. Interpretation of chromaticity coordination will present the potentiality of the use as a thermographic phosphor by a spectral modification behavior.

---

[1] Aldén, M.; Omrane, A.; Richter, M.; Särner, G. Prog. Energy Combust. Sci. 2011, 37, 422–461.

PMon077

Modified Ln_2CuO_4 (Ln=La, Pr) as cathode materials for solid oxide fuel cells

Kolchina, Liudmila (Moscow State University, Moscow, RUS)

In recent decade, the concerns of the solid oxide fuel cells (SOFCs) development are commonly associated with implementation of new cathode materials, which stipulates the fact that the main efforts were directed on an investigation of several types of transition metal oxides with perovskite-related structure. Ones of the perspective oxides for the SOFCs application as a cathode material are cuprates of rare earth elements. Therefore, cuprates of the Ln_2CuO_4 composition, where Ln = La or Pr, related to different structure types (T and T', respectively) were chosen as initial compounds for their further modification.

The presented work is focused on a systematic investigation of different approaches for a modification of the material composition, notably the study how both iso- and heterovalent cation substitution influences the structural and electrochemical properties of rare earth cuprates that are important for their application as cathode materials for intermediate temperature SOFCs. In order to improve conductivity and the electrocatalytic activity of Ln_2CuO_4 in oxygen reduction reaction, the heterovalent substitution of Ce, Pr and/or Sr for Ln were performed in order to obtain the compositions of $La_{1.8-x}Pr_xSr_{0.2}CuO_4$ (x=0.2, 0.4); $La_{2-x}Pr_xCuO_4$ ($0 \leq x \leq 0.4$); $Pr_{2-x}Sr_xCuO_4$ ($0 \leq x \leq 1$), and $Pr_{2-x}Ce_xCuO_4$ ($0 \leq x \leq 0.2$). Phase composition, microstructure and electrochemical properties of the modified cuprates were investigated by X-ray powder diffraction, scanning electron microscopy, four-probe DC conductivity measurements and AC impedance spectroscopy, respectively. The oxygen reduction reaction on the cuprate electrodes deposited on GDC electrolyte was studied in an electrode/electrolyte/electrode symmetrical cell by AC impedance spectroscopy at SOFC operating temperatures (500-800ºC).

The main points of the presented research include a comprehensive study of conducting properties of the materials as well as an investigation of their compatibility with $Ce_{0.9}Gd_{0.1}O_{1.95}$ (GDC) solid electrolyte. The obtained results allow determining the most promising materials for their electrochemical characterization as the SOFC cathode material as well as factors stipulating the best electrochemical cathode performance. Comprehensive analysis of polarization resistances as a function of both temperature and oxygen partial pressure allowed to establish rate-determining steps of oxygen reduction reaction at an electrode/electrolyte interface for different types of electrode materials.

This work was supported by Skolkovo Institute of Science and Technology (Center of electrochemical energy), Russian Foundation for Basic Research (grant no. 15-38-20247) and MSU-development Program up to 2020.

PMon078

NZP-phosphates, containing metals in oxidation state +2, as new materials with regulated thermal expansion

Asabina, Elena (Lobachevsky State University of Nizhni Novgorod, Department of Chemistry, Nizhni Novgorod, RUS); Pet'kov, Vladimir (Lobachevsky State University of Nizhni Novgorod, Nizhni Novgorod, RUS); Schelokov, Igor (Lobachevsky State University of Nizhni Novgorod, Nizhni Novgorod, RUS); Shatunov, Vasiliy (Lobachevsky State University of Nizhni Novgorod, Nizhni Novgorod, RUS); Mayorov, Pavel (Lobachevsky State University of Nizhni Novgorod, Nizhni Novgorod, RUS)

The phosphates of the $NaZr_2(PO_4)_3$ (NZP/NASICON) structural type are known as compounds with low thermal expansion and wide possibilities of ionic substitutions in the structural sites. The NZP family may be described by general crystal-chemical formula $(M1)_{0 \rightarrow 1}(M2)_{0 \rightarrow 3}\{[L_2(PO_4)_3]^{p-}\}_{3\infty}$, where $\{[L_2(PO_4)_3]^{p-}\}_{3\infty}$ represents framework from corner-shared LO_6-octahedra and PO_4-tetrahedra, M1 and M2 are cavities sites. The behaviour of NZP structure in response to heat treatment depends on the nature, the ratio of sizes and the number of cations that occupy crystallographic sites, the number of vacant sites and the unit cell symmetry. The aim of the present work is to describe the synthesis, the phase formation and thermal expansion of the phosphates $M_{0.5(1+x)}Fe_xTi_{2-x}(PO_4)_3$ (M – Mg, Ca, Sr, Ba; $0 \leq x \leq 1$) and $M_{0.5+x}M'_xZr_{2-x}(PO_4)_3$ (M – Ca, Sr, Cd, Ba, Pb; M' – Mg, Mn, Co; $0 \leq x \leq 2.0$). Basing on thermal expansion behavior of the complex phosphates of titanium (zirconium) and metals in oxidation state 2+, we have undertook systematic search for materials with low average thermal expansion and near-zero thermal expansion anisotropy. The compounds were synthesized by sol-gel method. The reaction mixtures were dried at 90°C and then heat-treated in air at 600–1200°C with alternating grinding. The obtained samples were polycrystalline powders. Their chemical composition and homogeneity were checked with the aid of a CamScan MV-2300 microprobe (Link INCA ENERGY detector). Their phase purity was established by powder X-ray diffraction at Shimadzu XRD-6000 diffractometer. The crystal structures of the triple phosphates representatives were refined by the Rietveld method. High temperature studies were carried out in the range 25–800 ° C using Shimadzu HA-1001 heating attachment). The functional composition of the samples was confirmed by IR spectroscopy on a Shimadzu FTIR 8400S spectrometer. The results showed that the NZP structure solid solutions are formed in the studied systems. The Fe^{3+} is close to Ti^{4+} by charge and ionic radii, so the phosphates $M_{1+x}Fe_xTi_{2-x}(PO_4)_3$ crystallized in the NZP type within large compositional range $0 \leq x \leq 1.0$. There is more charge and chemical nature difference between Ti4+ and cations in oxidation state +2. So the homogeneity concentration limits in the systems $M_{0.5+x}M'_xZr_{2-x}(PO_4)_3$ in were lower than in the previous case. The structural data illustrate the preferable distribution of 2-valent cations in crystallographic framework and cavities sites in these compounds. The largest solid solution limits ($0 \leq x \leq 1.0$) were observed in Ca-containing rows (M' – Mg, Co, Mn). This fact may be explained by the optimal Ca^{2+} radii for the NZP structure cavities and its ability to ionic bonds formation. The obtained data on solid solutions limits expand the whole picture of isomorphic ability of the NZP-frameworks. We used it in crystal chemical design of materials with controllable thermal expansion coefficients. The studied compounds belong to materials with low and middle thermal expansion behavior. The thermal expansion anisotropy decreases from 11.8 to 3.7 $°C^{-1}$ in the triple phosphates $MFeTi(PO_4)_3$ ($x = 1$) and from 17.1 to 0.7 $MMg_{0.5}Zr_{1.5}(PO_4)_3$ ($x = 0.5$) series, when little to large M^{2+} cation substitution takes place. The thermal expansion anisotropy regulation was performed on the example of $Ca_{0.5(1+x)}Fe_xTi_{2-x}(PO_4)_3$ solid solution. The predicted compound composition with the lowest anisotropy was $x = 0.30 \pm 0.10$. So the studied phosphates represent considerable practical interest for modelling new thermal-shock resistant materials.

The reported study was supported by RFBR, project 15-03-00716 a.

PMon079

Nanostructured Fabrication of $MFeO_3$ (M= La, Y) for Efficient Solar to Chemical Energy Conversion by Photosynthetic Cell

TAHIR, ASIF (UNIVERSITY OF EXETER, PENRYN, GBR); ULLAH, HABIB (UNIVERSITY OF EXETER, PENRYN, GBR); ALFAIFI, BANDAR (University of Exeter, Penryn, GBR)

The rapid depletion of fossil fuel reserves and increasing energy demands makes it imperative to ascertain a renewable and sustainable energy vector. It is widely believed that hydrogen is the fuel of the future. Splitting water in a photosynthetic cell is an environmentally-sustainable and low-cost route to produce hydrogen by splitting water molecules into its constituents, using sunlight. The photoelectrolysis employing appropriate semiconducting electrodes in a photosynthetic cell has received considerable attention as an efficient way of harnessing sunlight, since the pioneering work of Fujishima and Honda in 1972 [1]. The bottle-neck in realizing the concept of photosynthetic cell practically has been the difficulty in identifying stable low-cost semiconductors that meet the thermodynamic and kinetic criteria for photoelectrolysis of water [2]. Suitable materials for photosynthetic cell should be capable of absorbing maximum photons from sunlight and function as effective catalyst for water splitting. Therefore, the semiconductor electrode must have low electron affinity, good photocorrosion stability and bandgap of 1.8 -2.2 eV for maximum solar to chemical energy conversion [2]. Harvesting maximum solar light, while overcoming the electron hole recombination is a key challenge in solar water splitting for H_2 generation. There has been a considerable interest in recent years in low cost scalable fabrication, characterisation and testing of metal ferrites as a new class of potential semiconductor materials for water photoelectrolysis. This recent interest is ignited by a number of factors; (i) ferrites are a class of oxides hence capable of withstanding rigorous water redox reactions (ii) many metal ferrites have moderate band gaps, hence absorb visible light (iii) ferrites are available as anodes as well as cathodes (iv) they are easy to fabricate. Hence, metal ferrites have been considered as potential candidate materials that fulfil most of the stringent requirements (i.e. optical, energetic, chemical, electrochemical, photoelectrochemical, economic, and environmental requirements) demanded in water photoelectrolysis process. The present work is a continuation of our latest efforts to design a suitable material for solar water splitting by photosynthetic cell [3]. We have recently studied $MFeO_3$ (M = La, Y) as a candidate photocatalytic materials for water photoelectrolysis. Photoelectrochemical properties of those electrodes show that they are suitable for the photoelectrolysis. The present work describes our latest efforts on the fabrication and characterisation of $MFeO_3$ as potential semiconductor photoelectrodes for water electrolysis in photosynthetic cells.

---

[1] A. Fujishima, K. Honda, Nature, 1972, 238, 37.

[2] Grätzel, M.; Photoelectrochemical cells, Nature, 2001, 414, 338.

[3] Tahir, A.A. et al., J. Am. Chem. Soc., 2012, 134, 1228.; Chem. Commun., 2012, 48, 2027.; Faraday Discuss., 2012, 155, 309.;Chem. Mater, 2009, 21, 3763.; J. Phys. Chem. C 2009, 113, 4768.; Mater. Lett. 2009, 63, 523, J. Electroanal. Chem. 2010, 646, 124.; J. Am. Ceram. Soc., 2011, 94, 3540.; Inter. J. Hydrogen Energy 2013, 38, 4315-4323.; J. Photochem. Photobiol. A: Chem. 2010, 216, 119.

PMon080

New Family of Nanoscale Ordered Quintuple Perovskites $Ln_{2-\varepsilon}Ba_{3+\varepsilon}Fe_5O_{15-\delta}$ (Ln = Sm, Nd)

Cherepanov, Vladimir (Ural Federal University, Yekaterinburg, RUS); Raveau, Bernard (Laboratoire CRISMAT, ENSICAEN, Caen, FRA); Volkova, Nadezhda (Ural Federal University, Yekaterinburg, RUS); Lebedev, Oleg (Laboratoire CRISMAT, ENSICAEN, Caen, AUT); Caignaert, Vincent (Laboratoire CRISMAT, ENSICAEN, Caen, FRA); Kundu, Asish (Laboratoire CRISMAT, ENSICAEN, Caen, FRA); Mychinko, Mikhail (Ural Federal University, Yekaterinburg, RUS); Deryabina, Ksenia (Ural Federal University, Yekaterinburg, RUS); Turner, Stuart (University of Antwerp, Antwerp, BEL); Gauquelin, Nicolas (University of Antwerp, Antwerp, BEL)

The investigations of Ln-Ba-*M*-O systems, where *Ln* is a lanthanide and *M* is a 3d-transition metal, (such as Cu, Co, Mn and Fe) have shown an existence of several ordered layered perovskite related phases with attractive transport and magnetic properties. High flexibility of oxygen sublattice, and as a consequence wide homogeneity ranges favours an appearance of oxygen vacancy ordering in the anion sublattice, whereas the large size difference between A-site cations (Ln^{3+}/Ba^{2+}) causes their separation for different layers. Two classes of layered perovskites, called double and triple perovskites were described previously. The double perovskites $LnBaM_2O_{5+\delta}$ corresponds the alternation of the BaO and LnO layers which exhibit a 1:1 ordering were detected for *M* = Co, Fe, Mn. The triple perovskites, which are characterized by a 1:2 ordering of the Ln/Ba layers are mainly represented by the high Tc superconductors $LnBa_2Cu_3O_7$ and their oxygen deficient derivatives and by the magnetic ferrites $LnBa_2Fe_3O_{8+\delta}$. Phase equilibria study in the Ln – Ba – Fe – O system allow to detect a new phase with general composition $Ln_{0.4-y}Ba_{0.6+y}FeO_{3-\delta}$ that according to XRD analysis reveals a cubic structure. Howevera detailed transmission electron microscopy (TEM) study shows that the structure is perfectly ordered at the nanoscale. The electron diffraction (ED) patterns of this phase show that "$a_p \times a_p \times 5a_p$" tetragonal cell was identified. The HRTEM images show that these tetragonal nanodomains are chemically twinned along the three cube directions of the perovskite basic structure and therefore powder XRD patterns display a cubic structure. Taking into account 5-fold perovskite structure actual formula of such tetragonal cell should be written as $Ln_{2-\varepsilon}Ba_{3+\varepsilon}Fe_5O_{15-\delta}$. It consists of 5 LnO/BaO layers stacked alternately with 5 FeO_2 layers along *c*. It should be noted that in Sm-containing system only $Sm_{2-\varepsilon}Ba_{3+\varepsilon}Fe_5O_{15-\delta}$ (ε~0.125) was obtained as a single phase, while for Ln = NdXRD confirmed that a pure perovskite can be synthesized for a larger compositional range, $0 \leq \varepsilon \leq 0.50$. The detailed TEM study of these neodymium based perovskites shows that $Nd_{1.5}Ba_{3.5}Fe_5O_{15-\delta}$and $Nd_2Ba_3Fe_5O_{15-\delta}$ are completely different. $Nd_{1.5}Ba_{3.5}Fe_5O_{15-\delta}$ does not exhibit any ordering of the Nd^{3+} and Ba^{2+}cations and can be described as a simple perovskite with the formula $Nd_{0.3}Ba_{0.7}FeO_{3-y}$, involving a statistical distribution of neodymium and barium on the cationic sites. In contrast $Nd_2Ba_3Fe_5O_{15-\delta}$ exhibits tetragonal "$a_p \times a_p \times 5a_p$" nanodomains coherently intergrown within the cubic perovskite matrix. The contrast segregation on high angle annular dark field scanning TEM (HAADF-STEM) images makes possible to establish a periodic stacking sequence of the A cationic layers in $Sm_{2-\varepsilon}Ba_{3+\varepsilon}Fe_5O_{15-\delta}$ along the *c* axis: "Sm-Ba-Sm/Ba-Sm/Ba-Ba-Sm". This chemical ordering is confirmed by elementalelectron energy-loss spectroscopy (EELS) mapping, which proves that the Sm layers, spaced by $5a_p$ along the *c* axis, and the surrounding Ba layers are practically pure, whereas the median mixed Sm/ Ba layers are found to contain approximately equal amounts of each element. The values of oxygen content at room temperature determined by iodometric titration yields following formulas: $Sm_{1.875}Ba_{3.125}Fe_5O_{14.25}$, $Nd_2Ba_3Fe_5O_{14.54}$ and $Nd_{1.5}Ba_{3.5}Fe_5O_{14.45}$ ($Nd_{0.3}Ba_{0.7}FeO_{2.89}$). The changes of oxygen content were measured by TGA. Transport and magnetic properties of these oxides have been investigated and are discussed.

PMon081

New candidates for topological insulators in the bismuth-halogen systems

Isaeva, Anna (Dresden University of Technology, Dresden, GER); Groh, Matthias F. (Technische Universität Dresden, Dresden, GER); Autès, Gabriel (École Polytechnique Fédérale de Lausanne , Lausanne, CHE); Yazyev, Oleg (École Polytechnique Fédérale de Lausanne, Lausanne, CHE); Moreschini, Luca (Lawrence Berkeley National Laboratory, Berkeley, California, USA)

The notion “topological insulators” (TIs) encompasses compounds/materials that host a new quantum state of matter under normal conditions [1]. Thanks to the special features of their electronic structure, TIs are insulating in bulk and accommodate spin-resolved currents on their surface that may provide dissipationless transport and are immune to backscattering. Due to these exciting properties TIs are envisioned as information transmitters in quantum computing. This rapidly expanding field of research has a high demand on new TI candidates. Since topological properties go hand in hand with strong spin-orbit coupling effects, compounds of heavy main-group elements are closely studied suspects. Following the discovery of the first 3D weak TI $Bi_{14}Rh_3I_9$ [2], our work aims at the search and characterization of new TIs among bismuth-rich halogenides.In [3] we have outlined bismuth subhalides, which are built by stacks of halogen-terminated one-dimensional bismuth stripes, as possible TI candidates. Very recently this idea has found theoretical [4] and experimental [5] support in the case of bismuth monohalides Bi_4X_4 (X = I, Br).Under an assumption that these compounds can foster an entire family of TIs, we explore the mixed bismuth subhalides $Bi_4I_{4-n}Br_n$ ($0 \leq n \leq 1$). According to [6] mixed bismuth iodido-bromides crystallize in two stacking variants, which differ from the Bi_4I_4 or Bi_4Br_4 structures, and exhibit statistical distribution of halogen atoms over their sites for $0 \leq n \leq 1$. Our synthesis has yielded single crystals of a new stacking variant, $Bi_4I_{1.8}Br_{2.2}$, that crystallizes in the $C2/m$ (No. 12) space group with a = 13.239(1) Å, b = 4.3978(3) Å, c = 10.519(1) Å, β = 110.945(1)°, Z = 8, R_1 = 0.025, wR_2 = 0.057. The distinctive feature of $Bi_4I_{1.8}Br_{2.2}$ is mostly ordered site-occupancy for halogen atoms, despite a certain degree of mixing (up to 25% of I in the Br site and 15% of Br in the I site). As a result, bismuth–halogen distances are clearly distinguishable and are equal to 3.12 Å for Bi–I and 2.99 Å for Bi–Br. The shortest intra-layer bismuth–halogen contacts are 4.19 Å for Bi–I and 3.65 Å for Bi–Br. Bismuth-bismuth distances within the stripes lie in the range of 3.03–3.05 Å. Our DFT-based band-structure calculations and computed topological invariants [7] predict weak 3D topological properties for $Bi_4I_{1.8}Br_{2.2}$ and assign it to the same topological class as $Bi_{14}Rh_3I_9$ [2].

This work is supported by the DFG SPP 1666 “Topological Insulators”, Swiss NSF and the ERC “TopoMat”.

---

[1] M. Z. Hasan, C. L. Kane, *Rev. Mod. Phys.* **82** (2010), 3045.

[2] B. Rasche et al., *Nature Mater.* **12** (2013), 422; B. Rasche et al., *Chem. Mater.* **25** (2013), 2359; C. Pauly et al., *Nature Phys.* **11** (2015), 338.

[3] A. Isaeva, B. Rasche, M. Ruck, *Phys. Stat. Solidi RRL* **7** (2013), 39.

[4] J.-J. Zhou, W. Feng, Ch.-Ch. Liu, S. Guan, Y. Yao, *Nano Lett.* **14** (2014), 4767.

[5] O. Yazyev, G. Autès, A. Isaeva, L. Moreschini, J.C. Johannsen et al., *Bull. Amer. Phys. Soc. APS March Meeting*, **60** (2015). http://meetings.aps.org/link/BAPS.2015.MAR.B10.10.

[6] E. V. Dikarev, B. A. Popovkin, A. V. Shevelkov, *Russ. Chem. Bull.* **50** (2001), 2304.

[7] L. Fu, C. L. Kane, *Phys. Rev. B* **76** (2007), 045302.

PMon082

Novel coatings for corrosion and wear protection by thermal spraying

Förg, Andrea (Fraunhofer UMSICHT, Institute Branch Sulzbach Rosenberg, Sulzbach-Rosenberg, GER); Wöllmer, Silke (Fraunhofer UMSICHT, Institute Branch Sulzbach Rosenberg, Sulzbach-Rosenberg, GER); Schmetterer, Clemens (Fraunhofer UMSICHT Institute Branch Sulzbach Rosenberg, Sulzbach-Rosenberg, GER); Masset, Patrick (Fraunhofer UMSICHT, Institute Branch Sulzbach Rosenberg, Sulzbach-Rosenberg, GER)

Coatings are commonly applied whenever a component is exposed to corrosion, wear, chemical attack or a combination thereof. Applications cover practically all aspects of daily life, i.e. from anti stick coatings in cook ware to sophisticated multi-layer or functionally graded coatings for turbine blades. Recent developments focus on functional coatings, e.g. for anti-bacterial, self-cleaning or anti-icing applications. Coating technologies range from vapour deposition via electrochemical plating to spray coatings. The choice of materials and technologies largely depends on the final applications. Post processing steps such as annealing can also be required. By enlarging the lifetime of components coatings can significantly contribute to raise efficiency and lower operating costs. The thermal spray process is a relatively cheap and environmentally friendly technique that can be applied for a wide range of coating materials not only on steel or alloys, but also on substrates that are sensitive to heat such as wood or paper. In the present contribution, thermally sprayed coatings for wear and corrosion protection will be presented. Current issues include (a) the substitution of hard chromium and cadmium coatings on steel parts in the aviation sector by materials that are not potentially harmful to the environment and human health, and (b) the modification of combined coating layers comprising a resistant bond coat and chemically inert ceramic top coat for use in highly aggressive environments where they act as a protective system against high temperature corrosion (e.g. in super heaters in biomass and waste incineration plants). Furthermore, the degradation of thermal spray coatings can be minimized by functionalizing their surface to prevent the deposition of ashes and slags that can initiate corrosion.

PMon083

On the incorporation of Jahn-Teller Cu^{2+} ions into multiferroic $MnWO_4$

Patureau, Pascaline (Institut des matériaux Jean Rouxel (IMN), Nantes, FRA); Deniard, Philippe (Institut des matériaux Jean Rouxel (IMN), Nantes, FRA); Josse, Michaël (Institut de la chimie de la matière condensée de Bordeaux (ICMCB), Pessac, FRA); Dessapt, Rémi (Institut des matériaux Jean Rouxel (IMN), Nantes, FRA); Mevellec, Jean-Yves (Institut des matériaux Jean Rouxel (IMN), Nantes, FRA); Porcher, Florence (Laboratoire Léon Brillouin (LLB), gif sur Yvette, FRA); Maglione, Mario (Institut de la chimie de la matière condensée de Bordeaux (ICMCB), Pessac, FRA); Payen, Christophe (Institut des matériaux Jean Rouxel (IMN), Nantes, FRA)

$MnWO_4$ is regarded as a typical example of a type II multiferroic material with helical spin ordering.[1] The wolframite crystal structure of $MnWO_4$ consists of zigzag chains, running parallel to the c-direction, of either edge-sharing MnO_6 octahedra or edge-sharing WO_6 octahedra. The distorted MnO_6 and WO_6 octahedra contain Jahn-Teller inactive Mn^{2+} (d^5, $S = 5/2$) and nonmagnetic W^{6+} ions, respectively. Competing intrachain and interchain magnetic exchange interactions among Mn^{2+} spins result in spin frustration. As a consequence, three different magnetically ordered states are observed between $T_N = 13.5$ K and $T_2 = 12.3$ K, T_2 and $T_1 = 8$ K, and for $T < T_1$. Between T_2 and T_1, the helical shaped spin alignment makes the crystal structure non-centrosymmetric and MnWO4 becomes ferroelectric.[2] Several recent studies showed that chemical substitution of metallic cations for Mn or W is a useful tool to understand and tune the magnetic and multiferroic properties of $MnWO_4$.[3–5]

Here, we chose to partially substitute Mn^{2+} by Jahn-Teller (JT) active Cu^{2+} ($S = 1/2$) ions because JT distortions are capable of enabling new intriguing relationships between structural and electronic properties.

Polycrystalline samples of $Mn_{1-x}Cu_xWO_4$ solid solution have been synthesized by solid state reaction and a sol-gel method and characterized by different techniques for $x \leq 0.25$. We will discuss the crystal structure of these new materials as seen by X-Ray and neutron diffraction and Raman spectroscopy. We will also study the influence of Cu/Mn substitution on the magnetic and dielectric properties.

---

[1] D. Khomskii, Physics 2009, 2, 1–8.

[2] K. Taniguchi, N. Abe, T. Takenobu, Y. Iwasa, T. Arima, Physical review letters 2006, 97, 097203.

[3] L. Meddar, M. Josse, P. Deniard, C. La, G. André, F. Damay, V. Petricek, S. Jobic, M.-H. Whangbo, M. Maglione, C. Payen, Chemistry of Materials 2009, 21, 5203–5214.

[4] M. Josse, L. Meddar, P. Deniard, S. Jobic, C. Payen, R. Decourt, M. Maglione, Ferroelectrics 2012, 428, 94–100.

[5] K.-C. Liang, R. P. Chaudhury, B. Lorenz, Y. Q. Wang, Y. Y. Sun, C. W. Chu, Integrated Ferroelectrics 2011, 131, 47–55.

PMon084

Organic light emitting diodes based on conjugated polymers functionalized with calix[4]arenes

Matos, Manuel (ISEL/IPL, IT-Lisboa, Lisboa); Morgado, Jorge (IST/IT, Lisboa); Costa, Alexandra (ISEL/IPL - ADEQ, Lisboa); Pinto, Hugo (ISEL/IPL - ADEQ, Lisboa); José, Prata (ISEL/IPL - ADEQ, Lisboa)

Organic light emitting diodes (OLEDs) show several advantages over other materials in display devices. Used as an illumination light source and backlight in LCD displays, new materials and colors are hot research topics. We produced a new OLEDs family based in calix[4]arene poly(*p*-phenylene ethynylene).

This new materials show several advantages in display assemblies as compared to their inorganic counterparts. The solution processability, the possibility of making large and flexible areas of illuminating surfaces, the low fabrication costs and the production of devices capable of emitting most of the light colors is some of the outstanding features normally associated with these materials.

The OLEDs were fabricated using our previous described techniques [3] by the successive deposition of the layers ITO/PEDOT:PSS/CALIX-PPE/metal (aluminum and calcium). The characteristics of the produced OLEDs are shown in figure. These OLED’s produce various light colors including a very interesting white emission with a good efficiency and show a typical light-onset voltage of 6V, reaching a maximum of luminance at 20 V.

The interesting properties observed in these OLEDs pave the way for the development of a diversity of other calixarene-based PPE polymer-OLEDs, which can be structurally tailored to match various light color emissions. The different light color emission can be achieved either by structurally changing the core chromophores or, much more easily, using the capability of different ion complexation by the calixarene scaffolds.

---

[1] - A.I. Costa, L.F.V. Ferreira, J.V. Prata, *J. Polym. Sci. Part A: Polym. Chem.* , 2008, 46, 6477.
[2] - A.I. Costa, H.D. Pinto, L.F.V. Ferreira, J.V. Prata, *Sensors and Actuators B* , 2012, 161, 702.
[3] - G. Bernardo, A. Charas, L. Alcácer, J. Morgado, *J. Appl. Phys*., 2008, 103, 084510.

PMon085

Oxidation of cyclohexanone to adipic acid with aqueous hydrogen peroxide on $(NH_4)_xX_yPMo_{12}O_{40}$ with X= Sb, Sn

RABIA, CHERIFA (Laboratoire de Chimie du Gaz Naturel, Faculté de Chimie, USTHB, ALGIERS, DZA)

The use of solid catalysts in the production environmentally clean processes, that can reduce or eliminate the use of hazardous substances, is the aim of the “green chemistry” application. The HNO_3 substitution, source of pollutant gas as nitrous oxide, by Keggin type polyoxometalates (POMs), non-toxic, non-pollutant and non-corrosive catalysts and the use of hydrogen peroxide (H_2O_2) in the adipic acid synthesis, make the object of this study. Adipic acid (AA) is the basic compound for the polyamide fibers and resins production especially nylon (6.6-polyamide).
A series of Keggin-type POMs of formula $(NH_4)_xX_yPMo_{12}O_{40}$ with X= Sb, Sn, (noted $XPMo_{12}$) have been prepared, characterized by (FT-IR), 31P NMR and UV-Visible spectroscopies and used as catalysts for the liquid phase oxidation of cyclohexanone to adipic acid in presence of hydrogen peroxide at 90°C.

The obtained charaterization results showed that the substituted salts have the Keggin structure and the cubic structure of pure ammonium salt, NH_4PMo_{12}. The presence of the charge transfer between the tin (or antimony) counter-cation and molybdenum (VI) in the Keggin unit was shown by UV–Visible analysis. Thus, the introduction of tin and antimony can lead to partially reduced phosphomolybdates.

The catalytic results showed that the chemical composition, amount of catalyst (0.031 g - 0.250 g) and that of cyclohexanone (15 and 30mmol) and reaction time (10-25 h) have an effect on the AA yields. $SnPMo_{12}$ exhibited the highest performance with an AA yield of ca.80% when the mol number of cyclohexanone is of 30mmol, catalyst mass of 0.125 g and reaction time of 20 h.
The clean synthesis of adipic acid can be obtained from liquid-phase oxidation of cyclohexanone in the presence of hydrogen peroxide and Keggin -type POMs as catalyst.

PMon086

Oxygen non-stoichiometry and phase stability of Zn-doped $YBaCo_4O_{7\pm\delta}$ oxide with swedenborgite-type structure

Tsvetkova, Nadezhda (Ural Federal University, Ekaterinburg, RUS); Zuev, Andrey (Ural Federal University, Ekaterinburg, RUS); Tsvetkov, Dmitriy (Ural Federal University, Ekaterinburg, RUS); Ivanov, Ivan (Ural Federal University, Ekaterinburg, RUS)

The $YBaCo_4O_{7\pm\delta}$ oxide with swedenborgite-type structure is considered as a promising material for oxygen-storage application, solid oxide fuel cells and oxygen separation membranes. The unique feature of this oxide is the high capability for reversible oxygen absorption/desorption at temperature as low as 200 – 400 °C. However, the practical application of $YBaCo_4O_{7\pm\delta}$ oxide is limited to the low-temperature range because of its phase decomposition upon heating above 600 °C in an oxygen-containing atmosphere. The improvement of phase stability at high temperature is possible due to considerable flexibility of $YBaCo_4O_{7\pm\delta}$ structure to different chemical substitutions. Therefore, the main aim of the current work was to study thermodynamic stability, oxygen nonstoichiometry and electrical properties of $YBaCo_{4-x}Zn_xO_{7\pm\delta}$ (x = 1, 3) oxides.

The $YBaCo_{4-x}Zn_xO_{7\pm\delta}$ (x = 1, 3) powders were prepared by solid state reaction in the temperature range 1000 – 1200 °C. After the final heat treatment at 1200 °C for 24 h the samples were quenched to room temperature. The products obtained were characterized by X-Ray diffraction (XRD) using DRON-6 diffractometer.

Oxygen non-stoichiometry, δ, of $YBaCo_{4-x}Zn_xO_{7\pm\delta}$ (x = 1, 3) as a function of temperature (25–1000 °C) in air was investigated by means of thermogravimetric analysis using Rubotherm DynTherm LP-ST thermobalance. Oxygen nonstoichiometry as a function of oxygen partial pressure was measured using coulometric titration method. The experiment was carried out in the range of temperatures 800–1050 °C and oxygen partial pressures 10^{-5}–0.21 atm. Absolute value of δ of $YBaCo_{4-x}Zn_xO_{7\pm\delta}$ (x = 1, 3) samples was determined by means of carbonization of the oxides in CO_2 flux in the thermobalance, as well as by red-ox titration of the quenched samples.

Electrical conductivity and thermo-EMF of $YBaCo_{4-x}Zn_xO_{7\pm\delta}$ (x = 1, 3) oxides were measured with a 4-probe direct current method in the temperature range 30–1000 °C and the range of oxygen partial pressures 10^{-5}–0.21 atm.

As a result, partial substitution of Zn for Co was found to enhance the phase stability of $YBaCo_4O_{7\pm\delta}$ oxide under oxidizing conditions. For example, $YBaCoZn_3O_{7\pm\delta}$ sample is thermally stable in the whole temperature range investigated. At the same time introduction of Zn in the $YBaCo_4O_{7\pm\delta}$ oxide leads to sharp degradation of its low-temperature absorption capability and decreases the total conductivity.

This work supported by the Russian Foundation for Basic Research grant No. 13-03-01031.

PMon087

Photoluminescence and antimicrobial activity of Ag or Eu doped hydroxyapatite powders

Ciobanu, Carmen Steluta (1.NIMP; 2. University Politehnica *of Bucharest, Faculty of Applied Chemistry and Materials Science, Departme, Magurele, Bucharest, ROU); Popa, Cristina Liana (National Institute for Materials Physics,, Magurele, ROU); Prodan, Alina Mihaela (Emergency Hospital Floreasca, , Bucharest, , ROU); Turculet, Claudiu (Emergency Hospital Floreasca, , Bucharest, , ROU); Iconaru, Simona Liliana (National Institute for Materials Physics,, Magurele, ROU); Surugiu, Alina (4Hospital of obstetrics and gynecology,5SC medical center POLIMED srl, Buftea,Ilfov, ROU); Le Coustumer, P. (Institut des Sciences Analytiques et de Physico-Chimie pour l¿Environnement et les Matériaux (IPREM),, Pau, FRA); Predoi, Daniela (National Institute for Materials Physics,, Magurele, ROU)*

In this research study the synthesis of Ag or Eu doped hydroxyapatite in simulated body fluid (SBF) nanoparticles and the optical and biological studies are presented. We have developed two photoluminescent samples based on Ag/Eu:HAp SBF with biological properties. The PL studies on Ag/Eu:HAp SBF nanoparticles revealed that the concentrations of Ag or Eu have an important role on the photoluminescent properties. On the other hand, the antimicrobial activity is also strongly influenced by the Ag or Eu concentration in the samples. The efficiency of microbial activity of the Ag:HAp SBF samples is more obvious than in the case of Eu:HAp SBF samples. However, the bacterial adhesions tests showed that the Ag/Eu:HAp SBF nanoparticles reduce the adhesion of S. aureus and E. coli bacterial strains. All in all, the results suggest that Ag/Eu:HAp SBF nanoparticles could be used as promising materials for biomedical applications.

This work was supported by projects PN II 259/2014. Also this work was funded by the Sectoral Operational Programme Human Resources Development 2007-2013 of the Ministry of European Funds through the Financial Agreement POSDRU/159/1.5/S/134398.

PMon088

Physico-chemical characterizations and cytotoxicity evaluation of novel zinc doped hydroxyapatite embedded in a collagen matrix

Popa, Cristina-Liana (National Institute of Materials Physics, Magurele, ROU); Ciobanu, Carmen Steluta (National Institute for Materials Physics,, Magurele, ROU); Albu, Madalina (Collagen Department, National Research & Development Institute for Textiles and Leather (INCDTP), Bucharest, ROU); Motelica-Heino, Mikael (Institute for Earth Sciences, UMR 7327, Orleans, FRA); Predoi, Daniela (National Institute of Materials Physics, Magurele, ROU); Surugiu, Alina (Hospital of obstetrics and gynecology / SC medical center POLIMED srl , Bucharest, ROU)

The aim of this study was to obtain at low temperature a functional nanocomposite with characteristics similar to the natural bone by using an inexpensive method. The physico-chemical properties of collagen coated zinc doped hydroxyapatite nanopowders (Zn:HAp-Coll) were investigatetd by X-Ray diffraction (XRD), Scanning Electron Microscopy (SEM) and Fourier transform infrared spectroscopy (FTIR). The XRD analysis confirmed that the structure of the obtained nanopowders is characteristic to hexagonal $Ca_{10}(PO_4)_6(OH)_2$ - (P_{63m} space group). Moreover, the cytotoxicity of the Zn:HAp-Coll samples was studied using HeLa cell lines. The cell cycle distribution was examined by flow cytometry analysis after treatment. Our first in vitro studies show that the obtained composites have excellent biocompatibility and support further characterization by *in vivo* approaches.

This work was supported by projects IFA-CEA C4-05/2014. Also this work was supported by the strategic grant POSDRU/159/1.5/S/137750, "Project Doctoral and Postdoctoral programs support for increased competitiveness in Exact Sciences research" cofinanced by the European Social Found within the Sectorial Operational Program Human Resources Development 2007 – 2013.

PMon089

Preparation and luminescence properties of $SrMoO_4$ optical materials doped with rare-earth ions

Du, Peng (Kyung Hee University, Yongin, KOR); Yu, Jae Su (Kyung Hee University, Yongin, KOR)

In recent years, trivalent rare-earth ions doped materials have attracted considerable attention as luminescent materials since the applications in white light-emitting diodes, photovoltaic devices, bioimaging, and optical temperature sensors are very promising. Although erbium (Er^{3+}) ions exhibit their convenient energy level structure and good infrared-induced visible light properties, the absorption in the near-infrared region is low. For example, thus, ytterbium (Yb^{3+}) ions with high and broad absorption in the near-infrared region are required as a sensitizer. Generally, fluorides and glasses have been used in temperature sensor applications. However, they have some limitations on their further applications in temperature sensors due to the relatively poor physical, chemical, and thermal stabilities. Thus, the search for new host material to replace the glasses and fluorides is needed. Meanwhile, a non-invasive optical temperature sensor offers many advantages, based on the infrared-to-visible emission, i.e., upconversion. In this presentation, the $SrMoO_4$ luminescent materials were prepared with doping of various rare-earth ions by a high-temperature solid-state reaction method and their infrared-to-visible emission properties were studied for optical temperature sensor applications. The temperature sensing behavior of the samples was evaluated for low- and high-temperature thermometry. To analyze the optical temperature sensing property in these samples, the fluorescence intensity ratio technique was employed. From room-temperature luminescent spectra, the samples exhibited strong upconversion properties. These results suggest that the rare-earth ions-codoped $SrMoO_4$ phosphors have potential applications in the temperature thermometry.

PMon090

Revisite of reactivity of thiosemicarbazide on some divalent ions synthesis of complexes, characterization, DFT calculations, catalase like and biologica activities

Boutamine, Sultana (USTHB Faculty of chemistry, Bab Ezzouar Alger, DZA)

In this work, we revisited the reactivity of thiosemicarbazide (TSC) (HL^1) on Co(II) and Cu(II) ions by incorporating in the synthesis' medium, a second nitrogenized ligand, namely urea (U)(H_2L^2). The interest of the introduction of a second ligand to the reactional medium is to support the formation of mixed or polymetallic complexes which the physico-chemical properties are completely different from the basic complexes. Also, no study relating to urea-thiosemicarbazide binary system was reported.

Some new metal complexes of Co(II) and Cu(I) have been prepared and characterized by elemental chemical analysis, molar conductance, spectral (IR , ^{1}H NMR) and TGA studies. The IR spectral data suggest the involvement of sulfur and terminal amino-nitrogen in coordination to central metal ion.

On the basis of spectral studies, Oh N_3O_3 environment high spin environment has been assigned for the $Co^{(II)}(L^1)(SCN)(H_2O)_3$ compound and dimeric form for Cu(I) complexe of general formula $Cu^{(I)}{}_2(HL^1)_2(SCN)_2(H_2O)_2$.

The complexes have been tested in catalase-like activity in order to assess their catalytic properties. The results seem encouraging. The antibacterial and antifungal activity of the ligand and its metal complexes is evaluated.

PMon091

Raman spectroscopy on the impregnation of tungstophosphoric acid onto mesoporous and microporous supports

Bajuk-Bogdanovic, Danica (Faculty of Physical Chemistry, Belgrade); Holclajtner-Antunovic, Ivanka (Faculty of Physical Chemistry, University of Belgrade, Belgrade, AUT); Uskokovic-Markovic, Snezana (Faculty of Pharmacy, University of Belgrade, Belgrade)

Heteropoly acids (HPAs) are a class of solid acids constituting units of polyoxometalate (POM). HPAs exhibiting the Keggin structure are the most stable ones and, among others, have found industrial application as acid catalysts. One of the main drawbacks of the HPAs as heterogeneous catalysts is their very low surface area, typically below 10 $m^2\ g^{-1}$. One strategy to overcome this disadvantage is to impregnation HPAs onto high surface area solids such as SiO2, TiO2, ZrO2 or zeolites. Depending mainly on the pH of the solution and concentration of HPA several molecular species originated from HPA persist in equilibrium in HPA solutions. Accordingly, the nature of HPA supported on carriers depends on several parameters, such as the concentration of the impregnating solutions, the nature of used solvent, the pH of solution and some others. Raman spectroscopy is a useful technique for HPAs characterization and their spectra were already explained in details by many authors. This paper screens molecular speciation of tungstophosphoric acid (WPA) in the solutions during impregnation of various supports by Raman spectroscopy. The chosen supports were microporous (BEA and NaY zeolite) and mesoporous (SBA-15, Si-MCM-41 and TiO2-hombikat). In this study, WPA was supported from aqueous solutions in different concentrations and different initial pH values. The Keggin anion is present only in a very acidic solution, while the increasing of pH leads to the decomposition of Keggin anion to various components. However, it cannot be excluded the possible influence of interaction between Keggin anion and the support which was followed by the Raman spectra. For this reason, spectra of suspensions of WPA solution and support were compared with the spectra of pure solutions of the WPA, adjusted to the same pH value by adding NaOH. After comparing these spectra, it can be concluded that the changes in the spectra of WPA/TiO2, WPA/BEA zeolite and WPA/NaY zeolite were caused by the interaction of the anion and the carrier. On the other hand, results of Raman spectroscopy indicated that the primary Keggin structure remained intact after immobilization WPA onto SBA-15 and Si-MCM-41 network.

---

[1] I. Holclajtner-Antunovic, D. Bajuk-Bogdanovic, A. Popa, S. Uskokovic-Markovic, Spectroscopic identification of molecular species of 12-tungstophosphoric acid in methanol/water solutions Inorganica Chimica Acta, 2012, 383, 26–32.

[2]. I. Holclajtner-Antunovic, D. Bajuk-Bogdanovic, M . Todorovic, U. Mioc, J. Zakrzewska, S. Uskokovic-Markovic, Spectroscopic study of stability and molecular species of 12-tungstophosphoric acid in aqueous solution, Canadian Journal of Chemistry, 2008, 86, 996-1004.

PMon092

Rare-Earth Antimonide and Bismuthide Suboxides: Interplay between the Structure and Transport Properties

Mozharivskyj, Yurij (Department of Chemistry and Chemical Biology, McMaster University, Hamilton, Ontario, CAN)

The rare-earth antimonide and bismuthides suboxides with general formulas $RE_n(Sb,Bi)_mO_n$ and $(RE,Ca)_nSb_mO_n$ were investigated as potential thermoelectric materials. These materials can be viewed to consist of the Sb/Bi and *RE*-O building blocks with different transport properties. The substructure approach allows tuning the thermoelectric properties of these materials by modifying the structural features of only one block, without adjusting the number of charge carriers. In the case of the *anti*-$ThCr_2Si_2$ type $RE_2(Sb,Bi)O_2$ phases, substitution of smaller *RE* atoms into the *RE*O slabs or larger Bi atoms into the Sb layer yields different charge carrier activation mechanisms. As a result, the electrical conductivity and Seebeck coefficient are improved simultaneously, while the number of charge carriers in the series remains constant. The charge transport properties can be explained within the framework of the Anderson/Mott-type localization.

PMon093

Red luminescence and ferromagnetism in europium oxynitridosilicates with a β -K_2SO_4 structure

Black, Ashley P. (ICMAB-CSIC, Bellaterra, ESP); Denault, Kristin A. (Department of Materials and Materials Research Laboratory, santa barbara, USA); Oró-Sole, Judith (ICMAB-CSIC, Bellaterra, ESP); Goñi, Alejandro R. (ICMAB-CSIC, Bellaterra, ESP); Fuertes, Amparo (ICMAB-CSIC, Bellaterra, ESP)

The introduction of nitrogen in oxidic compounds involves changes in the electronic structure affecting the physical properties. The lower electronegativity and higher polarizability of nitrogen increases the covalent character of bonds with cations decreasing the interelectronic repulsion. The larger electrical charge of nitride increases the crystal field splitting and the bond polarization. [1] Anion order may influence the physical properties and is driven by the different charge of oxide and nitride and by covalency. [2] In recent years important oxynitride materials have been reported showing dielectric properties, colossal magnetorresistance, [3] photocatalytic activity under visible light [4] and orange-red luminescence.[5] Nitride-based silicates of alkaline earth and rare earth metals have been intensively investigated as hosts for Eu^{2+} or Ce^{3+} doped phosphor light-emitting diode (LED) components with long wavelengths and broad emission bands. Among oxy(nitridosilicates) only few examples of orthosilicates with isolated silicon tetrahedra have been reported. For Li_8SiN_4, an example of nitridosilicate with isolated $[SiN_4]$ tetrahedra, no precise structural data has been reported. Few oxynitrido apatites are known, being poorly nitrided and containing some nitrogen either in the channel anion sites or in the silicate groups. $Gd_3(SiON_3)O$ has been reported as example of orthosilicate-type (oxy)nitridosilicate containing $[SiON_3]^{7-}$ ions [5] and Marchand et al. reported the rare earth oxynitridosilicates $LnEuSiO_3N$ (Ln= La, Nd, Sm) with β-K_2SO_4 structure containing $[SiO_3N]^{5-}$ groups. [6] Alkaline-earth oxysilicates with β-K_2SO_4 structure (α' phases) activated with Eu^{2+} are important, highly efficient luminescent materials. The crystal structure is orthorhombic with space group Pmnb and shows two crystallographically independent sites for cations with coordination numbers (CN) 10 and 9. α'-Sr_2SiO_4:Eu and α'-Ba_2SiO_4:Eu exhibit emission wavelengths of approximately 500 nm under blue-UV light excitation.[7] Here we report the concomitant substitution in Sr_2SiO_4 and Ba_2SiO_4 of one alkaline earth cation by La^{3+} and one oxide by nitride in the $[SiX_4]$ group, producing new orthosilicate-type oxynitridosilicates with formula $LaMSiO_3N$ (M=Sr, Ba) that contain $[SiO_3N]^{5-}$ anions. These show selective occupation (80 %) of the two cation sites in the β-K_2SO_4 structure by La^{3+} in the CN=9 site and Sr^{2+} and Ba^{2+} in the CN=10 site, and partial nitrogen order in two of the three available anion sites. These features make possible the design of new phosphors by doping with either Ce^{3+} or Eu^{2+} that preferentially occupy these two sites respectively, showing longer emission wavelengths than the alkaline earth oxysilicates as a consequence of the oxide/nitride substitution and the larger crystal field splitting induced by the introduction of La^{3+}. The analogous europium compound $LaEuSiO_3N$ is, in addition of a red phosphor material, a soft ferromagnet with Curie temperature of 3 K.[8]

---

[1] A.Fuertes, Dalton Trans. 2010, 39, 5942.

(2] M. Yang, J. Oró-Solé, J.A. Rodgers, A.B. Jorge, A. Fuertes and J.P. Attfield, Nature Chem., 2011, 3, 47.

(3] M. Yang, J.Oró-Solé, A. Kusmartseva, A. Fuertes and J.P. Attfield, J. Am. Chem. Soc., 2010, 132, 4822.

(4] A.B. Jorge, Y. Sakatani, C. Boissière, C. Laberty-Roberts, G. Sauthier, J. Fraxedas, C. Sanchez and A. Fuertes, J. Mater. Chem. 2012, 22, 3220.

[5] M. Zeuner, S. Pagano and W. Schnick, Angew. Chem. Int. Ed., 2011, 50, 7754.

[6] R. Marchand, C.R. Acad. Sci. Paris, 1976, 283, 281.

[7] S.H.M. Poort, W. Janssen, G. Blasse, J. All. Comp. 1997, 260, 93.

[8] A.P. Black, K.A. Denault, J. Oró-Solé, A.R. Goñi and A. Fuertes, Chem. Comm., 2015, 51, 2166.

PMon094

Role of Lattice Oxygen on CO Oxidation Over $Ce_{18}O_2$-Based Catalyst Revealed Under Operando Conditions

Penkala, Bartosz (Universite de Montpellier/Saint-Goabin CREE, Montpellier, FRA); Kaper, Helena (Saint-Gobain CREE, Cavaillon, FRA); Paulus, Werner (Universite de Montpellier, Montpellier, FRA)

Since humankind became a lot less dependent on evolution to progress, our invention of technology has been one of our defining features [1]. Technological development achieved so high level that in order to continue constant improvement of products, industries are commonly using the most sophisticated tools of modern science-large scale facilities, including synchrotron and neutron sources.

Investigation of $CaFeO_{2.5}$ with characteristic Brownmillerite structure by inelastic neutron scattering combined with ab inito molecular dynamical calculation proved existence of low energy lattice modes, which trigger and amplify oxygen mobility in solids [2]. Structural instabilities in Brownmillerite-type materials, which promote migration of oxygen ions, where at the origin for designing novel $CaFeO_{2.5}$ catalysts with structural disorder controlled by the preparation technique. Using polycarbonates as surfactants, nano-$CaFeO_{2.5}$ could be prepared with a controlled amount of extended defects i.e. anti phase boundaries. This is equivalent to the loss of the 3D ordering of (FeO_4) tetrahedral chains, causing a reduction of oxygen mobility activation energy [3]. The catalytic oxidation of CO is enhanced for samples with a total loss of the 3D ordering of (FeO_4) tetrahedral chains.

Projecting the influence of lattice dynamics for oxygen mobility activated at already ambient temperature, we investigated modified $CeO_{2-\delta}$, to correlate the low temperature catalytic activity of ceria based compounds commercialized by Saint-Gobain, with diffraction (X-ray and neutron) and spectroscopic methods as a function of temperature. Combining TGA, Raman spectroscopic experiments and Isotope Labeling Pulse Temperature Programed Oxidation Reaction (ILPTPOR),coupled with mass spectrometric analysis on ^{18}O doped ceria, we explored here the oxygen uptake/release kinetics under operando conditions together with the catalytic activity related either to surface and/or quantitative lattice oxygen mobility and exchange. Specific changes in the lattice dynamics induced by $^{18/16}O$ isotope exchange were analyzed by Raman spectroscopy, allowing to study selectively the temperature dependent onset of lattice oxygen mobility and exchange behavior. Compared to the traditional CO conversion under continuous gas flow conditions, here employed ILPTPOR technique importantly allows together with the ^{18}O labelling, to simultaneously analyse important parameters to explore the mechanism of the catalytic reaction.

---

[1] A. Rutherford, Guardian, 08.10.2010.

[2] W.Paulus, H. Schober, S. Eibl, M. Johnson, T. Berthier, O. Hernandez, M.

[3] Ceretti, M. Plazanet, K. Conder, C. Lamberti, J. Am. Chem. Soc., 130, (47), 16080-85, (2008).

[4] S. Inoue, M. Kawai, N. Ichikawa, H. Kageyama, W. Paulus, Y. Shimakawa, Nature Chemistry, 2, 213-217, (2010).

PMon095

Self-Organized Amorphous TiO_2 Nanotubes as Na-Ion Battery Anodes

Prutsch, Denise (Graz University of Technology, Graz, AUT); Wilkening, Martin (Graz University of Technology, Graz, AUT); Hanzu, Ilie (Graz University of Technology, Graz, AUT)

There is a growing interest in the emerging sodium-ion technology for grid energy storage due to the lower costs projected and the much higher abundance of sodium compared to lithium [1]. Despite several studies on suitable positive electrodes, there is a relatively limited choice of suitable compounds operating at low Na^+ insertion potentials and, thus, being able to serve as negative electrode active materials in sodium-ion batteries [2].

Here, self-organized amorphous titania nanotubular arrays of various lengths and diameters were investigated as possible anode materials. Highly oriented TiO_2 nanotubes were prepared from Ti foil via anodic oxidation using a fluoride containing viscous electrolyte based on ethylene glycol [3]. The length and diameter of the tubes obtained can be adjusted by the anodization conditions chosen. The morphology of the nanoarchitectured samples prepared was thoroughly followed up by scanning electron microscopy. To examine the electrochemical performance of our samples, they were tested in Na half-cells using two different electrolyte formulations. Worth mentioning, the charge-discharge experiments were performed on TiO_2 anodes without any additives such as conductive agents and binders. Galvanostatic cycling experiments were carried out at constant current rates of 50 mA/g and 25 mA/g at potentials ranging from 0.8 to 2.0 V and 0.1 to 2.0 V, respectively. In addition, cyclovoltammetry was used for an in-depth electrochemical characterization of sodium insertion into the self-assembled amorphous nanotubes. These measurements form the basis for further studies on the dynamics of Na ions in Na_xTiO_2 nanotubes via ^{23}Na solid-state NMR spectroscopy.

Most importantly, the TiO_2-based electrodes prepared exhibit high reversibilities and good rate capabilities. Depending on the dimensions of the tubes specific capacity values of up to 70 mAh/g can be reached. Furthermore, a stable cycling performance can be shown for 300 cycles without significant capacity fade; this clearly confirms the outstanding durability at such current rates. Our results, combined with the intrinsic advantages of TiO_2 such as high abundance, non-toxicity, low costs as well as the simple fabrication technique used, point out the capability of TiO_2 nanotubes to work as powerful anode materials in Na-ion batteries.

---

[1] Pan, H.; Hu, Y.-S.; Chem, L.; *Energy Environ. Sci.***2013**, 6, 2338.
[2] Palomares, V.; Casas-Cabanas, M.; Castillo-Martinez, E.; Han, M. H.; Rojo, T.;
*Energy Environ. Sci.***2013**, 6, 2312-2337.
[3] Roy, P.; Berger, S.; Schmuki, P.; *Angew. Chem. Int. Ed. Engl.***2011**, 50, 2904-2939.

PMon096

Sodium Intercalation into the Iron Hydroxysulfate $NaFe_3(SO_4)_2(OH)_6$: a Topotactic Reversible Reaction from a Crystalline Phase to an Inorganic Polymer-like structure

Gnanavel, Muthayian (CNRS, Caen, FRA); Lebedev, Oleg (CNRS, Caen, FRA); Bazin, Philippe (CNRS, Caen, FRA); Raveau, Bernard (CNRS, Caen, FRA); Pralong, Valerie (CNRS, Caen, FRA)

Polyanionic frameworks have been the object of numerous studies for the realisation of electrode materials rechargeable Li/Na-Ions batteries [1-2]. This is exemplified by the iron compounds, which have been investigated, due to the reasonably high voltage of the Fe^{2+}/Fe^{3+} redox couple. Among these systems, rather few iron sulfates were studied since the discovery of lithium insertion in the NASICON type $Fe_2(SO_4)_3$ framework [3]. Importantly, the introduction of hydroxyl groups into the sulfate matrix has opened the route to materials with promising electrode performances, as shown for the hydroxysulphate $LiFeSO_4OH$ [4, 5]. In the search of new matrix for sodium insertion, we explore the hydroxysulfates phases. In the system Na-Fe-SO_4-OH, only four phases are reported: the Natrojarosite $NaFe_3(SO_4)_2(OH)_6$, the Jarosite $Na_{0.84}Fe_{2.86}(SO_4)_2(OH)_6$ and two hydrated phases the Sideronatrite $Na_2FeOH(SO_4)_2.3H_2O$ and the Metasideronatrite $Na_2FeOH(SO_4)_2.H_2O$; these phases are minerals but could be prepared by precipitation or under hydrothermal conditions. In the present study, we report for the first time the formation of the reduced phase $Na_3Fe_3(SO_4)_2(OH)_6$. Interestingly, we will show that the latter phase, prepared by electrochemical sodium insertion, is completely amorphous but crystallizes back to the Natrojarosite structure upon re-oxidation through a reversible solid solution process [6]. This material could then be proposed as positive electrode material for Na ion batteries with a reversible capacity of 120 mAh/g at 2.72V vs Na^+/Na. Moreover, this unique topotactic reaction between an amorphous and a well crystallized phase is interpreted on the basis of the formation of an inorganic polymer and will be discuss in the presentation.

---

[1] B.L. Ellis, L.F. Nazar, Chem. Mater., 2010, 22, 691

[2] G. Rousse, J.M. Tarascon, Chem. Mater., 26, 1, 406, 2014

[3] A.K. Padhi, K.S. Nanjundaswamy, J.B. Goodenough, J. Electrochem. Soc, 1997, 144, 1188.; J.B. Goodenough, K.S. Park, J .Am. Chem. Soc, 2013, 135(4), 1167

[4] M. A. Reddy, V. Pralong, V. Caignaert, U. V. Varadaraju, B. Raveau, Electrochem. Commun, 2009, 11, 1807

[5] M. Reynaud, M. Ati, B. C. Melot, M. T. Sougrati, G. Rousse, J.-N. Chotard, J.-M. Tarascon, Electrochem. Com, 2012, 21, 77 ; M. Reynaud, G. Rousse, A. M. Abakumov, M. T. Sougrati, G. Van Tendeloo, J.N. Chotard, J.M. Tarascon, J. Mater. Chem. A., 2014, 2, 2671

[6] M. Gnanavel, V. Pralong, O. I. Lebedev, V. Caignaert, P. Bazin, B. Raveau, Chem. Mater, 2014, 26, 4521-45 ; M. Gnanavel, O. I. Lebedev, V. Caignaert, P. Bazin, B. Raveau and V. Pralong, Solid State Ionics. , submitted, 2015

PMon097

Soil Remediation by Using Some Transition Metal Coordination Compounds

Hank, Zakia (USTHB Faculty of chemistry, Bab Ezzouar Alger, DZA)

Particular chemicals like pesticides which use, in agriculture, became inescapable are engendering an environmental pollution and more particularly that of the waters as well of surfaces as ground-water sheets. It is urgent, for preservation of public health, to reduce at most our exposure to these substances and to operate everything to reduce and control these pollutants.

So, the presence of pesticides in drinkable waters is severely regulated and the producing companies of water, to conform to the established standards, are obliged to include in their networks of water treatment, processes to eliminate them. The adsorption on the synthetized metal organic complexes may be a technique to disinfect waters polluted by pesticides and other chemicals. In this context, some coordination compouds of manganese were tested in the adsorption of mitrobuzin present in contaminated water. The retained organic molecules are natural products (glucose and caffeine).

PMon098

Solvothermal Synthesis and Characterization of Two New Barium-Organic Coordination Compounds

Halake, Shobha (Chung-Ang University, Seoul, KOR); Ok, Kang Min (Chung-Ang University, Seoul, KOR)

Two novel barium-organic frameworks have been solvothermally synthesized by using $Ba(NO_3)_2$ and aromatic organic linkers such as 4, 4'-sulfonyldibenzoic acid (H_2SBA) and 1, 2, 4, 5-benzenetetracarboxylic acid (H_4BTEC). Pure phases of single crystals have been successfully isolated from the solvothermal reactions. The crystal structures of the resulting materials have been determined by X-ray diffraction. The pinkish plate crystals of Ba-SBA compound crystallize in the monoclinic space group, $P2_1/n$ (no. 14) and exhibit a three-dimensional framework that is composed of zigzag 1D chains formed by edge-shared BaO_8 polyhedra and SBA linkers. The colorless rod crystals of Ba-BTEC materials crystallize in the monoclinic space group, $C2/c$ (no. 15) and reveal another three-dimensional framework structre consisting of 1D chains constructed by the corner-shared BaO_9 and BaO_{10} polyhedra, and BTEC linkers. Interestingly, while the Ba-SBA material exhibits porous channels, the Ba-BTEC compound is non-porous. The PXRD and IR spectra confirm the reversible coordination of the respective solvent molecules, DMF and H_2O. With the porous Ba-SBA framework, gas adsorption properties towards nitrogen, hydrogen and carbon dioxide have been investigated and the differential gas adsorption characteristics will be presented.

PMon099

Structural diversity of organically templated uranyl chromates

Nazarchuk, Evgeny (Saint-Petersburg State University, Saint-Petersburg, RUS)

Investigations of uranyl chromates are of great importance due to the environmental issues and fundamental crystal chemical aspects. Hexavalent chromium is one of the significant constituents of spent nuclear fuel (SNF). $K_2Cr^{6+}{}_2O_7$ is widely used as an oxidant in the REDOX process to manipulate the valence states of Pu and U. It is also used as an effective corrosion inhibitor for magnesium alloys used in some SNF rod arrays.

Uranyl chromates are less studied comparing to all other uranyl compounds with tetrahedral oxyanions. There is well-known tendency of Cr^{6+} to reduce to Cr^{3+} in relatively high-temperature hydrothermal solutions. We have used Cr(VI) trioxide as a starting material for the syntheses in aqueous solutions with various organic molecules at room temperature. Variety of novel zero-, one-, two- and three-dimensional uranyl chromates, dichromates[1], trichromates[2] and chromate-dichromates[1] were obtained. 24 novel uranyl chromates templated by different organic molecules were obtained. All of these structures are based on structural architectures consisting of weakly bonded inorganic uranyl-chromate and organic substructures. Generally, structural richness of uranyl chromates arises from the following features of $[CrO_4]^{2-}$ anions: ability of CrO_4 tetrahedra to polymerizeinto di-, tri-, and tetrachromate units; flexibility of U-O-Cr linkages. Some of obtained compounds demonstrate very complex topologies [3] and nanoscale curved architectures [4].

This work was supported by the Russian Foundation for Basic Research (grant # 14-05-31252) and St. Petersburg State University through the internal grant 3.38.238.2015. Technical support by the SPbSU X-Ray Diffraction Resource Center is gratefully acknowledged.

---

[1]. Siidra, O.I., Nazarchuk, E.V.; Suknotova, A.N.; Kayukov, R.A.; Krivovichev, S.V. Inorganic Chemistry, 2013, 52, 4729–4735

[2]. Siidra, O.I., Nazarchuk, E.V., Sysoeva, E.V., Kayukov, R.A., Depmeier, W. European Journal of Inorganic Chemistry, 2014, 2014, 5495-5498.

[3]. Siidra, O.I., Nazarchuk, E.V., Petrunin, A.A., Kayukov, R.A., Krivovichev, S.V. Inorganic Chemistry, 2012, 51, 9162-9164.

[4]. Siidra, O.I., Nazarchuk, E.V., Krivovichev S.V. European Journal of Inorganic Chemistry, 2012, 2012, 194-197.

PMon100

Structurally complex Zintl compounds for high temperature thermoelectric power generation

Zevalkink, Alexandra (Max Planck Institute of Chemical physics of solids, Dresden, GER); Aydemir, Umut (Caltech, pasadena, USA); Chanakian, Sevan (Caltech, pasadena, USA); Ormeci, Alim (Max Planck Institute of Chemical physics of solids, Dresden, GER); Snyder, Jeffrey (Caltech, pasadena, USA)

Zintl phases, characterized by covalently-bonded substructures separated by electropositive cations, exhibit many of the characteristics desired for thermoelectric applications. Recently, we demonstrated promising thermoelectric performance (*zT* values between 0.4 and 0.9) in a class of Zintl antimonides that share a common structural motif: anionic moieties resembling infinite chains of linked tetrahedra. These compounds ($A_5M_2Sb_6$ and A_3MSb_3, where *A* = Ca or Sr and *M* = Al, Ga and In) crystallize as four distinct, but closely related chain-forming structure types. Most of these phases behave as semiconductors, and exhibit exceptionally low lattice thermal conductivity due to their structural complexity. Here, we show that chemical substitutions on the *A* and *M* sites can be used to control the electronic and thermal transport properties and optimize the thermoelectric figure of merit. Doping with alio-valent elements allows for rational control of the carrier concentration, while isoelectronic substitutions can be used to fine-tune the intrinsic properties. A combination of density functional calculations and classical transport models was used to investigate the relationship between the observed transport properties and the structural chemistry of these compounds.

PMon101

Structure and thermoelectric properties of germanium antimony telluride heterostructures

Nentwig, Markus (IMKM Leipzig, Leipzig, GER); Fahrnbauer, Felix (IMKM Leipzig, Leipzig, GER); Schwarzmüller, Stefan (IMKM Leipzig, Leipzig, GER); Wagner, Gerald (IMKM Leipzig, Leipzig, GER); Oeckler, Oliver (IMKM Leipzig, Leipzig, GER); Maier, Stefan (LMU München, München, GER)

Doping and heterostructuring often lead to a higher efficiency of thermoelectric materials.[1] Compounds (GeTe)nSb2Te3 (GST materials) are good thermoelectric materials with figures of merit ZT of up to 1.5 at 450 °C for n = 12.[2] Complex phase transitions upon quenching lead to a pronounced parquet-like nanostructure with low thermal conductivity. Various substitutions as well as elaborate thermal treatment were found to further optimize the thermoelectric performance.[2,3] The replacement of one Ge2+ by two monovalent cations such as Ag+ formally yields the well-known TAGS materials (GeTe)x(AgSbTe2)2.[4] Substitution by Cu+, on the other hand, results in samples with the nominal compositions Cu2-xGe11+x/2Sb2Te15 ($0 \leq x < 2$). According to powder diffraction patterns, heterogeneous ($x < 1$) or homogeneous phases ($x \geq 1$) are formed depending on the Cu content. High Cu concentrations afford the precipitation of the minority phase Cu2Te. SEM-EDX maps of Cu2Ge11Sb2Te15 show Cu2-xTe precipitates ($0 \leq x < 1$) ranging from 50 to 200 µm in size in the matrix. ZT values approach 2 at 480 °C for $x \approx 1.3$. Heterostructures with the nominal composition [CoSb2(GeTe)0.5]x(GeTe)10.5Sb2Te3 ($0.2 \leq x < 2$) exhibit nano- to microscale skutterudite-type precipitates in a matrix of pseudocubic or trigonal GST. The matrix itself exhibits pronounced nanostructures that probably enhance phonon scattering.[5] In addition, Sb in the precipitates can be partially replaced by GeTe; this can significantly modify the electronic structure of skutterudite-type compounds. As a result, ZT values of ~1 at 320 °C were reached for low skutterudite-type fractions ($x = 0.2$), which is a significant improvement compared to the corresponding pure (GeTe)10.5Sb2Te3. Crystal structure analyses of the constituents of this complex system were performed using a combination of electron microscopy and microfocused synchrotron radiation. They reveal twinning of the crystalline matrix as well as the substitution on the skutterudite anion position. No residual electron densities were found in the voids of the skutterudite structure. Thermal treatment strongly influences the phase composition as well as the micro- and nanostructure of the heterostructures and, as a result, the thermoelectric performance. A further improvement of the thermoelectric properties over the whole temperature range was achieved for several quenched GST materials with varying precipitate contents.

---

[1] J. R. Sootsman, D. Y. Chung, M. G. Kanatzidis, Angew. Chem. Int. Ed. 2009, 48, 8616.

[2] T. Rosenthal, P. Urban, K. Nimmrich, L. Schenk, J. de Boor, J. Stiewe, O. Oeckler, Chem. Mater. 2014, 26, 2567.

[3] H. S. Lee, B.-S. Kim, C.-W. Cho, M.-W. Oh, B.-K. Min, S.-D. Park, H.-W. Lee, Acta Mater. 2015, 91, 83.

[4] S. H. Yang, T. J. Zhu, T. Sun, J. He, S. N. Zhang, X. B. Zhao, Nanotechnology 2008, 19, 245707.

[5] T. Rosenthal, M. N. Schneider, C. Stiewe, M. Döblinger, O. Oeckler, Chem. Mater. 2011, 23, 4349.

PMon102

Substitution of couple Sn(IV)/Zn(II) for In(III) in the fluorite-like transparent conductors: $In_{5-2x}Sn_{1+x}SbZn_xO_{12}$

Bizo, Liliana (Babes-Bolyai University, Faculty of Chemistry and Chemical Engineering, Department of Chemical Engineering, Cluj-Napoca, ROU)

Transparent conducting oxides (TCOs) are important materials used in a wide variety of applications such as transparent contacts for solar cells, liquid crystal displays, flat panel displays, high resolution screens of portable computers, thin film photovoltaics and electrochromic windows [1]. Besides the most famous ITO (In_2O_3:Sn), which crystallizes with the bixbyite structure, another oxide was identified for the composition $In_4Sn_3O_{12}$, with properties close to ITO. The synthesis of solid solution $In_{4+x}Sn_{3-2x}Sb_xO_{12}$, previously reported, has shown that introduction of antimony revealed a great abillity to form M_7O_{12} ordered oxygen-deficient fluorite structure [2]. Moreover the electrical properties of In_5SnSbO_{12} composition were improved by increasing the electronic conductivity up to one order of magnitute if compare to $In4Sn_3O_{12}$. Taking into account all of these three new compositions (x = 0.1, x = 0.2 and x = 0.3) belonging to $In_{5-2x}Sn_{1+x}SbZn_xO_{12}$ system, have been successfully synthesized by substitution of pair Sn(IV)-Zn(II) for In(III). The compositions were studied from point of view of structural, optical and electrical properties. Structure calculations have been performed by Rietveld analysis of the X-ray powder diffraction (XRPD) data. For $In_{4.4}Sn_{1.3}SbZn_{0.3}O_{12}$ composition a small amount of unreacted SnO_2 was identified. By increasing temperature from 1300 °C to 1350 °C a decrease of secondary phase amount, from 5.76 wt % to 3.17 wt %, was evidenced. The electrical conductivity of the latter was enhanced by approximately one order of magnitude with respect to $In_4Sn_3O_{12}$.

---

[1] D. S. Ginley, H. Hosono, and D. C. Paine: Handbook of Transparent Conductors, Springer, Berlin, 2010, DOI: 10.1007/978-1-4419-1637-2.

[2] J. Choisnet, L. Bizo, R. Retoux, S. Hebert, B. Raveau, J. Solid State Chem. 177 (10), 3748-3751, 2004, DOI:10.1016/j.jssc.2004.07.039

PMon103

Syntheses and Characterization of Two Series of Quaternary Mixed Metal Tellurites with Various Cation Sizes and Te^{4+} Polyhedra

Bae, Su-whan (Chung-Ang University, Seoul, KOR); Ok, Kang Min (Chung-Ang University, Seoul, KOR)

Syntheses and Characterization of Two Series of Quaternary Mixed Metal Tellurites with Various Cation Sizes and Te^{4+} Polyhedra Two novel series of quaternary mixed metal tellurites, specifically, four new alkali metal indium tellurites (A = Na, K, Rb, Cs) and three new transition metal vanadium tellurites (M = Al, Ga, Fe) have been synthesized through both hydrothermal and standard solid-state reactions. The structures of the reported compounds have been determined by X-ray single crystal diffraction analyses. The alkali metal indium tellurites exhibit various coordination modes of Te^{4+} cations. The TeO_3 and TeO_4 polyhedra surround central alkali metal cations with different ionic radii. The variable structural environments of Te^{4+} cations influence the materials' framework structures. The materials containing Na^+ and K^+ crystallize in the space groups, *Pbca* and *Pnma*, respectively. The isostructural rubidium and cesium indium tellurites, however, crystallize in the space group, *P-1*. We found out that, in sodium compound, relatively compact Na^+ ion requires 8-MR coordination environments. On the other hand, potassium compound has 12-MR coordination environment, which is attributable to the larger K^+ cation. In rubidium and cesium compound, even larger Rb^+ and Cs^+ cations repel lone pairs of Te^{4+} from their 12-MRs. Intriguingly, sodium and potassium indium tellurites reveal only TeO_3 in their backbones, whereas rubidium and cesium materials have both TeO_3 and TeO_4 in their frameworks. Three novel transition metal vanadium tellurites show dissimilar structural behaviors from those of alkali metal indium tellurites, due to the comparable ionic radii of their transition metal cations. The cationic size differences in the vanadium tellurites do not give significant contributions to the change of their crystal structures. SXRD analyses show that they are isostructural and crystallize in the same space group, $P2_1/n$. All three compounds have two dimensional layered structures with MO_6, VO_4, TeO_3, and TeO_4 polyhedra. Interestingly, though Al^{3+}, Ga^{3+}, and Fe^{3+} have different valence electronic configurations, the compounds have the same structural arrangements. In other words, the contribution of second-order Jahn-Teller distortion (SOJT) in the reported materials is negligible to the crystal structures of these compounds.

---

[1] D. W. Lee, S.-J. Oh, P. S. Halasyamani, K. M. Ok, *Inorg. Chem.***2011**, 50, 4473-4480.
[2] S.-w. Bae, C.-Y. Kim, D. W. Lee, K. M. Ok, *Inorg. Chem.***2014**, 53, 11328-11334.

PMon104

Synthesis and characterization of a new layered Pb^{2+}-Kemp's triacid coordination polymer

Kim, Saet Byeol (Chung-Ang University, Seoul, KOR); Kim, Kang Min (Chung-Ang University, Seoul, KOR)

A new Pb^{2+}-Kemp's triacid coordination polymer has been synthesized by a solvothermal reaction using $Pb(NO_3)_2$, Kemp's triacid (*cis,cis*-1,3,5-Trimethylcyclohexane-1,3,5-tricarboxylic acid), and N,N-dimethylformamide (DMF) as reagents. Colorless hexagonal plate crystals have been grown in a phase pure form. The crystal structure of the newly synthesized material has been determined by single crystal X-ray diffraction. The reported material with an extended structure is crystallizing in a trigonal space group, *R*-3 (No. 148). The compound reveals a layered structure, in which Pb^{2+} is coordinated by seven oxide ligands. The unsymmetrical coordination environment of Pb^{2+} cation is due to the stereoactive lone pair on it. When the coordinated DMF molecules are excluded, a void space is observed from the material. Thermogravimetric analysis suggests that the framework of the reported material is thermally stable up to 390 °C. The loss of coordinated solvent molecules from the material is fully reversible. A complete re-coordination of DMF to Pb^{2+} cations in the activated sample has been monitored by powder X-ray diffraction. The selectivity of the cations during the crystallization has been also studied. A competing crystallization reaction with two toxic cations, Pb^{2+} and Cd^{2+}, reveals that the Kemp's triacid has a higher selectivity toward Cd^{2+} over Pb^{2+}.

---

[1] S. Das, H. Kim, K. Kim. *J. Am. Chem. Soc.***2009**, *131*, 3814.
[2] N. Stock, S. Biswas. *Chem. Rev.***2012**, *112*, 933.
[3] N. H. Lee, D. W. Lee, H. Yeo, K. Kwak, H. S. Chun, K. M. Ok. *CrystEngComm.***2014**, *16,* 5619.

PMon105

Synthesis and characterization of new hybrid coordination compounds based on imidazolium and 3d transition metal salts.

Farger, Pierre (CNRS IPCMS UMR7504, STRASBOURG, FRA); Roger, Guillaume (IPCMS-CNRS-UMR7504, Strasbourg, FRA); Delahaye, Emilie (IPCMS-CNRS-UMR7504, Strasbourg, FRA); Rabu, Pierre (IPCMS-CNRS-UMR7504, Strasbourg, FRA)

Metal Organic Frameworks (MOFs) are hybrid compounds built from inorganic part (3d metal, lanthanides…) linked together by organic part (ligands). The synthesis of such components has known a growing interest for the last decades due to the versatility of their synthesis and their potential applications (for gas storage/separation, catalysis, drug delivery…).[1-3]

MOFs are usually obtained by solvothermal synthesis and more recently using ionothermal synthesis which means that solvent is replaced by ionic liquid (IL).[4, 5] This approach has already proved to be efficient to obtain new hybrid materials. Yet, in the examples of the literature the role of the IL is not well-defined since it can play the role of solvent, charge balancer and/or structuring agent. In our group, we have decided to synthesize hybrid materials from ILs bearing specific coordination functions, developing a solvo-ionothermal synthesis, in order to control the role of the ILs as ligand.

The synthesis and complete characterization of new hybrid frameworks based on imidazolium and first row transition metal ions will be presented. We will specially emphasize the effect of the solvent and the kind of metal salt on the formation of new hybrid compounds and their physical properties.[6]

---

1. G., Ferey, *Chem. Soc. Rev.***2008**, 37, 191.
2. P. Horcajada, C. Serre, M. Vallet-Regí, M. Sebban, F. Taulelle, G. Férey, *Angew. Chem. Int. Ed.***2006**, 45, 5974.
3. J.L.C, Rowsell, O.M. Yaghi, *Microp. Mesopor. Mat.***2004**, 73, 3.
4. P. J. Calderone, P. M. Forster, L. A. Borkowski, S. J. Teat, M. Feygenson, M. C. Aronson, J. B. Parise, *Inorg. Chem.***2011**, 50, 2159.
5. W.-J. Ji, Q. Zhai, S.-N. Li, Y.-C. Jiang, M.-C. Hu, *Chem. Commun.***2011**, 47, 3834.
6. P. Farger, R. Guillot, M. Gallart, F. Leroux, G. Rogez, E. Delahaye, P. Rabu. **Submitted**.

PMon106

Synthesis and detection properties of hydrothermally grown vertically aligned zinc oxide-based nanostructures for ultraviolet photodetector applications

Lee, Soohyun (Kyung Hee University, Yongin-si, KOR)

Zinc oxide (ZnO) nanostructures based ultraviolet (UV) photodetectors (PDs) have attracted great interest in various applications such as flame sensors, spatial optical communications, and calibrations due to wide direct bandgap (3.37 eV), large surface area, and strong chemical stability. In most research, ZnO based UV PDs in the form of metal-semiconductor-metal (MSM) structures have been investigated due to the difficulty in the fabrication of p-type ZnO films with high quality for ZnO p-n homojunction PDs. Since the photoresponse characteristics of ZnO arrays are strongly dependent on their crystallinity, vacuum deposition systems are employed to improve the crystal quality. However, these techniques also exhibit several drawbacks because of the expensive and sophisticated equipment, high growth temperature, or long process time required. On the other hands, a hydrothermal growth method provides a simple and cost-effective process at low temperature. In this presentation, we fabricated the UV PDs based on the hydrothermally grown vertically-aligned ZnO nanostructures. Under different molar concentrations, their photoresponse characteristics were studied. The crystallinity and morphology of ZnO nanostructures were investigated by using a field emission scanning electron microscope and an X-ray diffractometer. The photocurrents of ZnO nanostrucures based UV PDs were measured by utilizing a semiconductor characterization system under an illumination of a 365 nm UV light-emitting source.

PMon107

Synthesis and magnetic properties of ferrite nanoparticles

Torralvo, María José (Universidad Complutense de Madrid, Facultad de Químicas, Madrid, ESP); Virumbrales, Maider (Universidad Complutense de Madrid, Facultad de Químicas, Madrid, ESP); Blanco, Verónica (Universidad Complutense de Madrid, Facultad de Químicas, Madrid, ESP); Delgado, Álvaro (Universidad Complutense de Madrid, Facultad de Químicas, Madrid, ESP); Sáez-Puche, Regino (Universidad Complutense de Madrid, Facultad de Químicas,Madrid, ESP)

Magnetic materials with nanometric particle size have been widely investigated due to their applications in different areas such as data storage, ferrofluid technology, catalysts and medical applications, including magnetically guided drug delivery, contrast agents in magnetic resonance imaging (MRI) or hyperthermia. In these sense, nanosized ferrites are ones the most investigated materials due to their physico-chemical properties that make them potential candidates to be used in the different applications mentioned above. These type of magnetic materials have investigated in our research group during the last decade, where different synthetic routes have been used to prepare ferrite nanoparticles with MFe_2O_4 (M=Fe, Co, Ni y Zn) composition and particle sizes ranging from 2-70 nm. Hydro/solvothermal method [1] has allowed to prepare nanoparticles with sizes between 4-15 nm but these nanoparticles tend to agglomerate and this fact modifies the magnetic properties and it makes difficult to use these materials in many applications. Therefore it is crucial to develop strategies to avoid or minimize the nanoparticle agglomeration. In this connection, ferrite nanoparticles have been synthetized inside different silica matrices such as sepiolite, faujasite and MCM-41 or SBA-15 type materials [2-4]. In these samples the silica porous structure limits the particle size and affects the interparticle interaction and the magnetic behavior. Ferrite nanoparticles have been also synthetized by a precursor thermal decomposition method using high-boiling point solvents. Monodisperse nanoparticles have been obtained and the effect of the organic surrounding layer on the magnetic properties has been analyzed [5]. On the other hand, magnetic nanoparticles functionalized with different groups can be used in biomedical applications and for environmental problems. In this context, magnetite nanoparticles have been functionalized with carboxylic, amine and thiol group and the effect of the surface functional groups on the properties of nanoparticles has been studied. The structural characterization of the samples was carried out by X-ray and neutron diffraction and the morphological studies have been done by transmission electron microscopy. In some samples, Mössbauer spectroscopy, XAS and XANES measurements have been used to evaluate the inversion degree. Magnetic properties have been studied from magnetic susceptibility and magnetization measurements at different temperatures and magnetic fields. The magnetic properties of the studied nanoparticles mainly depends on the chemical composition, but the different preparation methods, particle size and interactions between the particles or with inorganic or organic surrounding matrix are very important factors that must be also considered.

---

[1] V. Blanco-Gutiérrez, M.J. Torralvo-Fernández, R. Sáez-Puche, J. Mater. Chem, (2010) 22 (7) 2992-3003

[2] V. Blanco-Gutiérrez, E. Urones-Garrote, M. J. Torralvo-Fernández, and R. Sáez-Puche, Chem. Mater., (2010) 22 (22) 6130–6137

[3] V. Blanco-Gutiérrez, M. Virumbrales, R. Sáez-Puche and M. J. Torralvo-Fernández, J. Phys. Chem. C, (2013) 117 (40) 20927-20935

[4] M. Virumbrales, A. Delgado, R. Sáez and M. J. Torralvo, 18th International Symposium on the Reactivity of Solids (Saint Petersburg, June 2014)

[5] M. Virumbrales, A. Delgado, R. Sáez and M. J. Torralvo, 14th European Conference on Solid State Chemistry (Bourdeaux, July 2013)

PMon108

Synthesis, structure and valence states of 3d-atoms in the matrix of yttrium-gallium garnet

Korolev, Dmitrii (St. Petersburg State University, St. Petersburg, RUS)

The matrix of yttrium-gallium garnet (YGG) doped with various elements is of substantial interest in the context of its application as materials for laser technologies and for electron-ionic conductors. The properties of such systems must be determined by the distribution of 3*d*-elements over various sites of garnet structure – octahedral and tetrahedral, which has an essential impact on the interatomic interactions in the structure. Those latter will undoubtedly influence the optical properties and conductivity of garnets.

In this work $Y_3M_xGa_{5-x}O_{12}$ solid solutions (M = Cr, Mn, Ni, Cu; $x = 0.01$-0.30) were synthesized by ceramic and sol-gel methods. All of them appeared to belong to cubic syngony (S.G. *Ia*-3). The unit cell parameters were refined by Rietveld method and the dependences of unit cell parameter on the concentration of the doping element were examined. By the data of magnetic susceptibility measurements the distribution of doping elements over nonequivalent sites of the structure was determined. Chromium(III) atoms were found to occupy only octahedral sites in the YGG structure and to be isolated no interacting magnetic atoms. Nickel, manganese, and copper occupy both octahedral and tetrahedral sites in the structure in various ratios. Based on the model of diluted solution the fractions of paramagnetic clusters and single atoms (nickel, manganese, copper) were calculated for the structure of yttrium-gallium garnet. The fundamentals of the influence of the nature and concentration of doping elements on electron structure of garnets and their possible impact on physical and chemical properties of promising materials based on yttrium-gallium garnets are discussed.

PMon109

The Electrochemical Performance of Rutile Nanorods for Lithium-Ion Batteries

Uitz, Marlena (Graz University of Technology, Graz, AUT); Bottke, Patrick (Graz University of Technology, Graz, AUT); Schmidt, Walter (Graz University of Technology, Graz, AUT); Wark, Michael (University of Oldenburg, Oldenburg , GER); Hanzu, Ilie (Graz University of Technology, Graz, AUT); Wilkening, Martin (Graz University of Technology, Graz, AUT)

The development and thorough characterization of new active materials for lithium-ion batteries (LIBs) with enhanced performance and lifetime has reached an unprecedented level. For instance, nanocrystalline transition metal oxides have been intensively studied to act as promising anode materials showing good cyclability and excellent rate performance [1].

Compared to their coarse grained counterparts the increased electrochemical properties are due to the large specific surface area and pore volume. This is beneficial for long-range transport because it reduces both the diffusion lengths of electrons and lithium ions. Here, we studied the possibilities of rutile TiO_2 nanorods to act as anode materials in LIBs. Besides the small volume expansion during Li insertion, the 1D nanostructure of the nanorods investigated might be beneficial for their overall performance [2].

After structural characterization of the TiO_2 nanorods by X-ray powder diffraction (XRD) and high-resolution (HR) transmission electron microscopy (TEM), Li half-cells were assembled under Ar gas atmosphere by taking advantage of the Swagelok-technique. Depending on the charge/discharge rate applied (0.1 C … 20 C), capacities of up to 250 mAh/g (0.1 C) can be obtained. Starting with an initial value of 200 mAh/g (1 C), the capacity reaches approximately 160 mAh/g at a rate of 1 C; for comparison, ca. 120 mAh/g at a rate of 20 C is reached after 1000 cycles.

Besides galvanostatic cycling, cyclovoltammetry was used to study the Li insertion behaviour of the active material. The measurements will build the basis for a systematic analysis of Li ion dynamics in the Li_xTiO_2 nanorods via ^{7}Li solid-state NMR spectroscopy [3]. Such measurements will help to understand how Li ion dynamics change as a function of Li content.

---

[1] A. S. Aricò, P. G. Bruce, B. Scrosati, J.-M. Tarascon, W. van Schalkwijk, Nat. Mater. 4 (2005) 366.
[2] H. Qiao, Q. Luo, Q. Wei, Y. Cai, F. Huang, Ionics 18 (2012) 667.
[3] J. Heine, M. Wilkening, P. Heitjans, Diff. Fundam. 12 (2010) 95.

PMon110

The Influence of Silicon on the Long-term stability of LSCF SOFC-Cathodes

Perz, Martin (Montanuniversitaet Leoben, Chair of Physical Chemistry, Leoben, AUT); Bucher, Edith (Montanuniversitaet Leoben, Chair of Physical Chemistry, Leoben, AUT); Gspan, Christian (Institute for Electron Microscopy and Nanoanalysis (FELMI), Graz University of Technology & Graz Center for Electron Microscopy (ZFE), Graz, AUT); Hofer, Ferdinand (Institute for Electron Microscopy and Nanoanalysis (FELMI), Graz University of Technology & Graz Center for Electron Microscopy (ZFE), Graz, AUT); Sitte, Werner (Montanuniversitaet Leoben, Chair of Physical Chemistry, Leoben, AUT)

Silicon Poisoning has to be taken into account as a degradation mechanism of cathodes in Solid Oxide Fuel Cells (SOFCs) due to the existence of Si in various components of SOFC stacks, e.g. in glass seals. In this study the influence of Si on the long-term stability of $La_{0.6}Sr_{0.4}Co_{0.2}Fe_{0.8}O_{3-\delta}$ (LSCF) cathodes was investigated. A symmetrical cell containing two screen-printed LSCF layers on a GDC substrate was characterized by electrochemical impedance spectroscopy at 700°C for overall 2000 hour. During the first 1000 hours an intrinsic degradation of the cathode performance was observed, causing an increase of the area specific polarisation resistance (ASR) from 0.3 Ωcm^2 to 1.4 Ωcm^2. Subsequently, silicon was brought into the system by sputtering a 10 nm thick silicon layer on both cathodes. This poisoning lead to a strong further increase of the ASR up to 8 Ωcm^2 during additional 1000 hours at 700°C. Analyses of the degraded cathodes by scanning electron microscopy (SEM) and transmission electron microscopy (TEM) showed, that the degradation is caused by reactions of the Cathode Material with Si in a surface-near region down to approx. 50 nm, where the perovsike phase of LSCF is decomposed into La-Sr-silicate and Co-Fe-oxide. The appearance of these phases drastically reduces the kinetics of the oxygen reduction reaction. The present results indicate that even small amounts of silicon can have a negative influence on the in the oxygen exchange activity of LSCF.

PMon111

The use of waste biomass as carbon source in the synthesis of sodium vanadium fluorophosphates cathodes for Na-ion batteries

Serras, Paula (University of Basque Country, Leioa, ESP); Palomares, Veronica (Inorganic Chemistry Department University of Basque Country, Bilbao, ESP); Blas, Maitane (Inorganic Chemistry Department University of Basque Country, Bilbao, ESP); Lopez-Urionabarrenechea, Alexander (Chemical and Environmental Engineering Department, faculty of Engineering, University of the Basque Country, Bilbao, ESP); Lezama, Luis (University of the Basque Country UPV/EHU, Bilbao, ESP); Rojo, Teófilo (CIC Energigune, Miñano, ESP)

Sodium vanadium fluorophosphates have recently shown very good electrochemical performance *vs.* Na/Na^+ providing high working voltages (3.6 and 4 V *vs.* Na/Na^+) and good specific capacity values.The vanadyl (IV) $Na_3V_2O_2(PO_4)_2F$ compound which belongs to the $Na_3V_2O_{2x}(PO_4)_2F_{3-2x}$ family of compounds can be successfully synthesized by a novel single-step hydrothermal method. However the absence of *in-situ* carbon in the final product makes necessary to employ an *ex-situ* carbon coating impregnation method, usually using sucrose. This carbon has demonstrated to increase the electronic conductivity and Na^+ diffusion ability, enhancing the electrochemical performance of the sodium-vanadium fluorophosphate material. The derived composites exhibit good rate capability for charging rates up to 5C and excellent cycling stability.

On the other hand, Hydrothermal Carbonization (HTC) process is a widely used method for the synthesis of functional carbonaceous materials from biomass [6], so it can be an alternative way to get a carbonaceous coating during the hydrothermal synthesis of the fluorophosphate. The biomass usually used for this process includes crude plant materials like agricultural residues, wood and herbaceous energy crops, and carbohydrates like sugars, starch, or cellulose. Moreover, organic electroactive materials derived from biomass are promising candidates for the next generation of rechargeable batteries, due to the low cost, sustainablity and environmental benefits. However their application for electrodic materials in batteries is still a field under development.

In this work, three different carbon sources have been employed in the hydrothermal synthesis in order to obtain a carbon containing vanadyl (IV) $Na_3V_2O_2(PO_4)_2F$ phase in a unique step by HTC. The employed carbon sources consisted on sucrose, vine shoots and eucalyptus wood, these latter two as waste biomass carbon sources. Obtained samples have been characterized by X-ray diffraction, elemental analysis, transmission electron microscopy and Raman spectroscopy. The vanadium oxidation state of the compounds has been estimated by analyzing electron paramagnetic resonance spectra.Electrochemical evaluation of the sodium vanadium fluorophosphates has been made on laminate cathodes in Swagelok cell *vs.* a metallic sodium anode. Differences in obtained specific capacities, rate capability and cycle life will be analyzed and related to the compositional, crystallographic and morphological changes induced by the use of different carbon sources and the use of different synthesis temperatures. When vine shoots are employed as carbon source, preliminary results show that the increasing of the synthesis temperature from 170 to 200ºC increases the particle size of the sodium vanadium fluorophospate material up to 10 µm. However, it must be remarked that the differences in the background of the X-ray diffraction patterns of samples at 170 and 200ºC. indicate the obtaining of a more crystalline carbon when a higher temperature is employed.

PMon112

Thermochromic and piezochromic properties of $AMoO_4$ oxides

Gaudon, Manuel (ICMCB - University of Bordeaux, 33608, FRA); Demourgues, Alain (ICMCB, 33608, FRA)

Without presuming of the reversible or irreversible character of the phenomenon, X-chromic materials may be defined as compounds whose color changes with an external stimulus. Namely, thermochromism and piezochromism refer to the ability of a material to change color with the temperature or the external pressure.

Our contribution will focus on the $CuMoO_4$ [1-5] and $CoMoO_4$ [6,7] X-chromic materials. These molybdates exhibit an abrupt color modification due to a severe structural rearrangement associated to a first order transition which can be produced by pressure, temperature or surface protonation [8]. Indeed, for both oxide families, the high temperature / low pressure modifications exhibit [*MoO4*] tetrahedra while the low temperature / high pressure modifications exhibit [*MoO6*] octahedra.

Two ways can be used in order to tune the thermochromic transition temperature and or the piezochromic transition pressure: (i) the doping of the $(Cu/Co)MoO_4$ oxide with various transition metals (Mg, Ni, Zn…) [1,4, 5,7], (ii) the control of the oxide morphology, especially its crystallite size [6]. It can be also added, that for the piezochromism phenomenon, the application mode of the pressure (isostatic, uniaxial) significantly affects the pressure answer of these materials [5,6]. The results of the chemical/morphological impacts on the transition parameters will be discussed basing on the fundamentals of first-order phase transition thanks to X-Ray/Neutron diffraction, optical characterizations, calorimetric measurements and microscopic observations... Thermosalient effects observed on the material series, opening a new window for likely actuator applications, will be also discussed.

Finally, it will be shown that nowadays, such materials receive attention due to their potential applications as convivial temperature/pressure indicators, especially in the areas of safety/security improvements, gadgets, packaging, motorization, autoclaves…while the oxide powder is incorporated into a paint/varnish, for the shock detection on fragile substrates.

---

[1] M. Gaudon et al. Advanced Materials, 19, 3517-3519, 2007.
[2] M. Gaudon et al. Inorganic Chemistry, 48, 2136-2139, 2009.
[3]. A.-E. Thiry et al. Chemistry of Materials, 20, 2075-2077, 2008.
[4] M. Gaudon et al. Inorganic Chemistry, 46, 10200-10207, 2007.
[5] M. Gaudon et al. Inorganic Chemistry, 47, 2404-2410, 2008.
[6] L. Righetti et al. ACS Appl. Mater. Interfaces, 3, 1319-1324, 2011
[7] L. Robertson et al. Inorganic Chemistry, 50, 2878-2884, 2011.
[8] M. Gaudon et al. Chemistry of Materials, 22, 5905-5911, 2010

PMon113

Topochemical Reduction of Some Complex Ruthenium Oxides

Amano-Patino, Midori (University of Oxford, Oxford, GBR); Bower, Ryan (University of Oxford, Oxford, GBR); Hayward, Michael (University of Oxford, Oxford, GBR)

Complex transition metal oxides are of widespread interest due to the wide variety of electronic and magnetic behavior they exhibit. Low-temperature topochemical (structure conserving) reactions offer pathways to the preparation of novel metastable transition metal oxide phases with unusual combinations of oxidation states and coordination geometries.

Recently, the first oxide phase containing Ru^{2+} centres was prepared via topochemical anion deintercalation using CaH_2 (400ºC), of the mixed-metal perovskite phase $Sr(Ru_{0.5}Fe_{0.5})O_3$ to form $Sr(Ru_{0.5}Fe_{0.5})O_2$.(1) Magnetic measurements and DFT calculations indicate that the ruthenium centres adopt an intermediate spin state of $S = 1$.

Building on this work, the cation ordered double perovskite phases $LaSrNiRuO_6$ and $LaSrCoRuO_6$ have also been reduced to form novel anion deficient materials which exhibit rather unusual magnetically ordered states. The structural and magnetic characterization will be presented.

---

[1] Denis Romero, F.; Burr, S. J.; McGrady, J. E.; Gianolio, D.; Cibin, G.; Hayward, M. A. *J Am Chem Soc***2013**, *135*, 1838.

PMon114

Tunable upconverted visible light and high sensitivity optical thermal sensing of Ln, Yb:$Y_6O_5F_8$ nanotubes

Cascales, Concepción (Inst. Ciencia de Materiales de Madrid, CSIC, Madrid, ESP); Zaldo, Carlos (Inst. Ciencia de Materiales de Madrid, CSIC, Madrid, ESP)

Micron-sized bundles of highly crystalline individual nanotubes of *Pbcm* Vernier-type Yb^{3+}-sensitized Ln^{3+} (Er, Pr)-doped $Y_6O_5F_8$ oxyfluorides have been prepared through efficient low-temperature hydrothermal syntheses. Under near infrared (NIR) 978 nm diode laser excitation, the color of the upconverted light in codoped Pr, Er, Yb:$Y_6O_5F_8$ nanotubes can be selected by the control of the Pr^{3+} concentration, and by the excitation regime and power density. Samples with low Pr^{3+} concentration emit predominantly green light, and the selection between bluish-green light and white light has been demonstrated with large Pr^{3+} concentration (2 mol%), under pulsed or continuous wave excitation, respectively. Involved Er^{3+} and Pr^{3+} electronic transitions and mechanisms to populate their corresponding emitting levels have been analyzed for a large number of 2 mol% Yb^{3+}-sensitized, 0.05 mol% Er^{3+}-doped oxyfluoride samples within the Pr^{3+} concentration span 0.2 - 2 mol% [1].

Furthermore, the ratiometric analysis of the thermal evolution of intensities of NIR excited green upconverted emissions from thermally coupled $^2H_{11/2}$ and $^4S_{3/2}$ multiplets of Er, Yb:$Y_6O_5F_8$ indicates thermal sensing potential with better sensitivity S (0.0041 K^{-1}) than hexagonal Er, Yb:beta-$NaYF_4$ (0.0032 K^{-1}) in the temperature range of physiological interest.

Work supported by the Spanish Ministry of Economy and Competitiveness and by the European Regional Development Fund through MAT2011-29255-C02-01 and MAT2014-56607-R projects.

---

[1] C. Zaldo, C. Cascales, Phys. Chem. Chem. Phys., 2014, 16, 23274-23285.

PMon115

Versatile route to prepare reversible thermochromic polydiacetylene/ poly(vinylpyrrolidone) nanocomposites: Effects of molecular weight and fabrication process

Kamphan, Anothai (Naresuan University, Muang, THA); Traiphol, Rakchart (Naresuan University, Muang, THA)

In this study, we introduces a versatile method to prepare polydiacetylene(PDA)-based materials with reversible thermochromism. Poly(vinylpyrrolidone)s(PVP) are incoporated into the system, enhancing inter- and intrachain interactions within the PDA assemblies via hydrogen bonding. Small angle x-ray scattering reveals that the PVP chains insert into the layer structure of PDA assemblies. The PDA/PVP nanocomposites are fabricated by using three diacetylene(DA) monomers, 10,12-pentacosadiynoic acid(PCDA), 10,12-tricosadiynoic acid(TCDA) and 5,7-hexadecadiynoic acid(HDDA). The pure PDA assemblies prepared from these DA monomers exhibit irreversible blue-to-red color transition upon increasing temperature. The enhanced interactions within the PDA/PVP nanocomposites result in reversible thermochromism, which takes place in a two-step fashion, blue-to-purple and purple-to-red. The color reversibility of these PDA/PVP nanocomposites in thin films persist upto 200 oC. The color-transition temperature can be controlled by varying the PDA structure. The effect of PVP molecular weight(MW) on the formation of the nanocomposites is studied by using three MWs, 10,000, 55,000 and 360,000 g/mol. We have found that the the variation of PVP MW significantly affects the color reversibility and morphology of the nanocomposites. The use of PVP with MW of 10,000 and 55,000 g/mol as additives provides the nanocomposites with fully reversible thermochromism. While the color-transition temperature of the two systems are comparable, the color stability of nanocomposite increases with the MW of PVP. When the MW of PVP is increased to 360,000 g/mol, the nanocomposite exhibites partial color reversibility. We also observe that morphology of the PDA/PVP nanocomposites varies significantly with the MW of PVP and preparation method. This simple approach provides the improvement of stability and color reversibility of PDA-based materials, which is very important for their utilization in sensing applications.

PMon116

$[ZrO]^{2+}[G6P]^{2-}$ Biocompatible Inorganic-Organic Hybrid Nanoparticles for Supported Drug Delivery

Roehr, Martin (Karlsruhe Institute of Technology (KIT), Karlsruhe, GER); Feldmann, Claus (Karlsruhe Institute of Technology (KIT), Karlsruhe, GER)

In the last few years there has been an increased interest in biocompatible hybrid nanomaterials.[1] In this context, a new class of inorganic-organic hybrid nanoparticles was synthesized, that is obtainable by a water-based synthesis and can be readily dispersed in water. The hybrids consist of an inorganic cation ($[ZrO]^{2+}$) and an organic phosphate like flavin mononucleotide $[FMN]^{2-}$ or betamethasone phosphate $[BMP]^{2-}$. This results in fluorescent biomarkers like [ZrO][FMN][2] or DDSs (Drug Delivery System) like [ZrO][BMP].[3,4] The concept is based on the low solubility of zirkonyl phosphate, so that nanoscale particles are formed by precipitation. The advantage of this concept is the low toxicity of zirconium.[5]
In relation to [ZrO][FMN] and [ZrO][BMP], [ZrO][G6P] particles were synthesized in aqueous solution ($[G6P]^{2-}$: D-glucose-6-phosphate). DLS analysis resulted in an average diameter of 160 nm. The assumed chemical composition was confirmed by EDX, TG, XRD and elementary analysis.
[ZrO][G6P] was combined with phenolphthalein bisphosphate $[PPP]^{2-}$ and risedronate $[RDT]^{2-}$. In this case the compounds $[ZrO][G6P]_{0.6}[PPP]_{0.4}$ and $[ZrO][G6P]_{0.3}[RDT]_{0.7}$ were obtained. While [PPP] is used for the detection of the pH value, [RDT] is used for treatment or prevention of osteoporosis.

The nanoparticles have a diameter of about 20-100 nm and are much smaller than human cells (10-100 µm). For this reason they can pass easily through the cell membrane and therefore, they are interesting for medical application. Consequently, nanoparticles can be highly interesting as drug carrier and delivery systems.[6] While [ZrO][FMN] and [ZrO][BMP] show passive drug targeting, [ZrO][G6P] could be a new carrier system for active drug targeting, since D-glucose is an energy source of human cells.[7] Moreover, a faster uptake into human cells should be possible. In this context further compounds may be introduced in order to achieve therapeutic or diagnostic effects.

---

[1] E. Katz, I. Willner, *Angew. Chem. Int. Ed.***2004**, *43*, 6042-6108.

[2] M. Roming, H. Lünsdorf, K. E. J. Dittmar, C. Feldmann, *Angew. Chem. Int. Ed.***2010**, *49*, 632.

[3] J. G. Heck, J. Napp, S. Simonato, M. Lange, J. Möllmer, R. Staudt, F. Alves, C. Feldmann, *J. Am. Chem. Soc., in revision*.

[4] J. G. Heck, M. Poß, H. Reichardt, J. Napp, F. Alves, W. Stühmer, C. Feldmann, patent application **2014**, DE 10 2014 004 512.9.

[5] S. Ghosh, A. Sharma, G. Talukder, *Biol. Trace Elem. Res.***1992**, *35*, 247-271.

[6] Q. A. Pankhurst, J. Connolly, S. K. Jones, J. Dobson, *J. Phys. D: Appl. Phys.***2003**, *36*, R167-R181.

[7] S. Walker-Samuel, R. Ramasawmy, F. Torrealdea, M. Rega, V. Rajkumar, S. P. Johnson, S. Richardson, M. Goncalves, H. G. Parkes, E. Arstad et al., *Nat. Med.***2013**, *19*, 1067-1072.

PMon117

Synthesis and characterization of strong antiferromagnet CaFeSeO

Lai, Kwing To (Max Planck Institute for Chemical Physics of Solids, Dresden, GER); Chang, Pi-Shan (Max Planck Institute for Chemical Physics of Solids, Dresden, GER); Huh, Sungjoon (University of British Colombia, Vancouver, CAN); Burkhardt, Ulrich (Max Planck Institute for Chemical Physics of Solids, Dresden, GER); Rosner, Helge (Max Planck Institute for Chemical Physics of Solids, Dresden, GER); Hu, Zhiwei (Max Planck Institute for Chemical Physics of Solids, Dresden, GER); Kuo, Chang-Yang (Max Planck Institute for Chemical Physics of Solids, Dresden, GER); Pi, Tun-Wen (National Synchrotron Radiation Research Centre, Hsinchu, TWN); Tjeng, Liu Hao (Max Planck Institute for Chemical Physics of Solids, Dresden, GER); Valldor, Martin (Max Planck Institute for Chemical Physics of Solids, Dresden, GER)

We have successfully synthesized the new compound CaFeSeO with high purity. Revealed by x-ray diffraction, this compound belongs to a non-centrosymmetric orthorhombic lattice, with Fe-Se-O quasi-2D tetrahedral layers separated by Ca ions. Inside the tetrahedra, Fe ion is coordinated by two Se and two O ions, while two different Fe-O bond lengths are unexpectedly found. We have also characterized its physical properties through resistivity, heat capacity, magnetic measurements, and x-ray absorption spectroscopy. It is observed that this system is an electrically insulating canted antiferromagnet with T_N = 160 K. However, an anomalous behavior is observed in the field dependence of magnetization, in which the magnetization slowly decreases with decreasing field instead of the sharp decrease near zero fields, indicating that this system is more complex than a conventional canted antiferromagnet.

PMon118

A new chalcogenide compound $Ba_2F_2Fe_{1.5}Se_3$ with iron selenide layers

Driss, Dalel (Institut de Matériaux de Nantes, Nantes, FRA); Janod, E. (Institut des Matériaux Jean Rouxel (IMN), CNRS Université de Nantes, Nantes cedex 3, FRA); Corraze, B. (nstitut des Matériaux Jean Rouxel (IMN), CNRS Université de Nantes, Nantes cedex 3, FRA); Cario, Robert (Institut des Matériaux Jean Rouxel (IMN), CNRS Université de Nantes, Nantes cedex 3, FRA)

Recently, chalcogenide compounds FeSe [1] and $KxFe_2Se_2$ [2] with a layered structure containing anti fluorine sheets Fe_2Se_2 were found to be superconductors with critical temperatures as high as 30K. This critical temperature was even raised above 100K in a single FeSe layer [3]. These discoveries of new iron superconductors have renewed interest in the study of the electronic properties for this class of iron layered materials containing FeSe layers. This work reports on a layered compound $Ba_2F_2Fe_{1.5}Se_3$ containing a new type of iron selenide layer. $Ba_2F_2Fe_{1.5}Se_3$ was synthesized with a high temperature ceramic method. The X-ray refinement on single crystal revealed a layered structure isotopic of the sulfide compound $Ba_2F_2Fe_{1.5}S_3$ [4]. The structure results from an alternative stacking of fluorite type blocks Ba_2F_2 and $Fe_{1.5}Se_3$ layered blocks (see Figure 1). In this $Fe_{1.5}Se_3$ layer, the iron has a mixed valence Fe^{2+} /Fe^{3+}, which is associated with the occupation of different atomic sites, octahedral and tetrahedral, respectively. Owing to its peculiar structure containing this new iron selenide layer the study of the electronic properties of $Ba_2F_2Fe_{1.5}Se_3$ is particularly appealing. In that respect, the magnetic and transport properties of this new compound were investigated and will be reported.

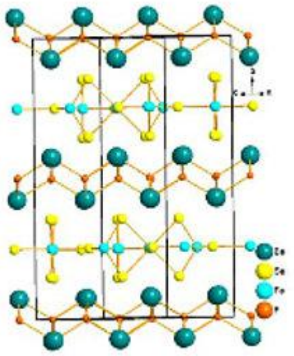

Figure 1: Structure of the $Ba_2F_2Fe_{1.5}Se_3$ compound.

---

[1] F.C. Hsu, J.Y. Luo, K.W. Yeh, T.K. Chen, T.W. Huang, P. M. Wu, Y.C. Lee, Y.L. Huang, Y.Y. Chu, D.C. Yan et M.K. Wu, PNAS, vol. 105 no. 38, 14262-14264, 2008.

[2] Guo, J.; Jin, S.; Wang, G.; Wang, S.; Zhu, K.; Zhou, T.; He, M.; Chen, X. Physical Review B, 2010, 82, 180520.

[3] Jian-Feng Ge, Zhi-Long Liu, Canhua Liu, Chun-Lei Gao, Dong Qian, Qi-Kun Xue, Ying Liu, Jin-Feng Jia, Nature materials, vol. 14, 2015.

[4] L. Cario, H. Kabbour, Inorganic chemistry, 2008, 47, 1648-1652.

PMon119

Chemical control of superconductivity in layered lithium iron selenide hydroxides

Woodruff, Daniel (University of Oxford, Oxford, GBR); Sun, Hualei (Inorganic Chemistry Laboratory, University of Oxford / Beijing Synchrotron Radiation Facility, Institute of High Energy Physics, Chinese Academy of Sc, Oxford , GBR); Cassidy, Simon J. (Inorganic Chemistry Laboratory, University of Oxford / Diamond Light Source Ltd., Harwell Science and Innovation Campus, GBR); Allcroft, Genevieve M. (Inorganic Chemistry Laboratory, University of Oxford / Beijing Synchrotron Radiation Facility, Institute of High Energy Physics, Chinese Academy of Sc, Oxford, GBR); Sedlmaier, Stefan J. (Inorganic Chemistry Laboratory, University of Oxford / Diamond Light Source Ltd., Harwell Science and Innovation Campus, Oxford, GBR); Thompson, Amber L. (Inorganic Chemistry Laboratory, University of Oxford, Oxford, GBR); Bingham, Paul A. (Materials and Engineering Research Institute, Sheffield Hallam University, Sheffield, GBR); Forder, Susan D. (Materials and Engineering Research Institute, Sheffield Hallam University, Sheffield, GBR); Cartenet, Simon (Materials and Engineering Research Institute, Sheffield Hallam University, Sheffield, GBR); Mary, Nicolas (Materials and Engineering Research Institute, Sheffield Hallam University, Sheffield, GBR); Ramos, Silvia (School of Physical Sciences, Ingram Building, University of Kent, Kent, GBR); Foronda, Francesca R. (epartment of Physics, University of Oxford, Clarendon Laboratory, Oxford, GBR); Williams, Benjamin H. (Department of Physics, University of Oxford, Clarendon Laboratory, Oxford, GBR); Li, Xiaodong (Beijing Synchrotron Radiation Facility, Institute of High Energy Physics, Chinese Academy of Science, Beijing, CHN); Blundell, Stephen J. (Department of Physics, University of Oxford, Clarendon Laboratory, Oxford, GBR); Clarke, Simon J. (norganic Chemistry Laboratory, University of Oxford, Oxford, GBR)

Hydrothermal synthesis of layered lithium iron selenide hydroxides $\mathrm{Li}_{1-x}\mathrm{Fe}_x\mathrm{(OH)Fe}^{1-y}\mathrm{Se}$ ($x \sim 0.2$; $0.02 < y < 0.15$) with a wide range of iron site vacancy concentrations in the iron selenide layers is reported. The iron vacancy concentration is revealed to be the only significant compositional variable and as the key parameter controlling the crystal structure and the electronic properties of the reported material. A combination of Single crystal X-ray diffraction, X-ray powder diffraction, neutron powder diffraction and X-ray absorption spectroscopy measurements are used to demonstrate that superconductivity at temperatures as high as 40 K is observed in the hydrothermally synthesised samples when the iron vacancy concentration is low ($y < 0.05$) and when the iron oxidation state is reduced slightly below +2. Samples with higher vacancy concentrations and correspondingly higher iron oxidation states are not superconducting. We demonstrate that reductive post-synthetic lithiation (or sodiation) of the samples turns on superconductivity with critical temperatures exceeding 40 K by displacing iron atoms from the $\mathrm{Li}_{1-x}\mathrm{Fe}_x\mathrm{(OH)}$ reservoir layer to fill vacancies in the selenide layer (see Figure). This work underlines and quantifies the importance of structure and electron count in controlling superconductivity in iron selenide superconductors. The effects of doping the iron selenide layer with other first row transition metals and the subsequent affect this has on the magnetic behaviour of the resultant materials is also investigated.

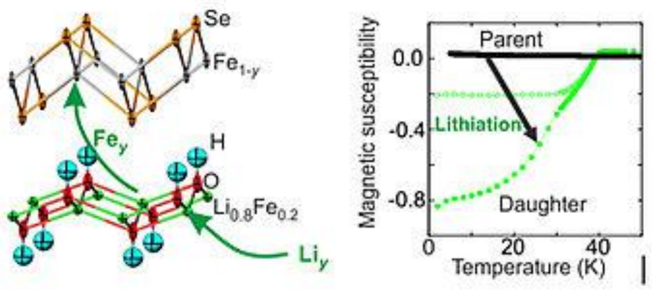

PMon120

Flux Synthesis, Modulated Crystal Structures, and Physical Properties of $RE_2O_2MnSe_2$ (RE = La, Ce)

Peschke, Simon (LMU München, Munich, GER); Nitsche, Fabian (Bruker-AXS GmbH, Karlsruhe, GER)

The discovery of high-T_c superconductivity in iron pnictides and iron selenides with critical temperatures up to 56 K has revived the search for new superconducting materials. Among the different structure types of iron arsenides, compounds with the tetragonal ZrCuSiAs-type structure such as *RE*FeAsO (*RE* = rare-earth metal) exhibit the highest critical temperatures.

During our current investigations into ZrCuSiAs-related compounds with magnetic transition metals, the quaternary transition metal oxyselenides $RE_2O_2MnSe_2$ (*RE* = La, Ce) have been prepared in high purity in a NaI/KI-flux synthesis. X-ray single crystal and powder diffraction experiments revealed a ZrCuSiAs-related, modulated crystal structure with an interesting new vacancy ordering motif at the manganese site which is probably caused by the lattice mismatch between the $[RE_2O_2]^{2+}$ and the $[MnSe_2]^{2-}$ layers. The resulting modulations of both compounds can be approximated by $10a \times 10b \times 2c$ and $51a \times 51b \times 2c$ supercells in $La_2O_2MnSe_2$ and $Ce_2O_2MnSe_2$, respectively. The arrangement of Mn^{2+} cations within the $[MnSe_2]^{2-}$ layers consists of both, edge and corner-sharing $MnSe_{4/2}$-tetrahedra in different ratios which results in a mixture of checkerboard- and stripe-like pattern. The structures can therefore be considered as intermediate structures between $Ce_2O_2FeSe_2$ and $La_2O_2CdSe_2$. Both compounds are insulators with band gaps of 2.13 and 2.01 eV for $La_2O_2MnSe_2$ and $Ce_2O_2MnSe_2$, respectively. Magnetic measurements indicate antiferromagnetic ordering of the Mn^2+ moments with Néel points well above room temperature.[1]

---

[1] S. Peschke, F. Nitsche, D. Johrendt, *Z. Anorg. Allg. Chem*. **2015**, *641*, 529.

PMon121

High pressure study of intercalated transition metal dichalcogenides $Co_{0.33}NbS_2$ and $Fe_{0.33}TaSe_2$

Popcevic, Petar (Institute of Solid State Physics, TU Wien, Wien, AUT); Smontara, Ana (Institute of Physics, Zagreb, HRV); Jacimovic, Jacim (École polytechnique fédérale de Lausanne, Lausanne, CHE); Surija, Vinko (Institute of Physics, Zagreb, HRV); Zivkovic, Ivica (Institute of Physics, Zagreb, HRV); Batistic, Ivo (Department of Physics, Faculty of Science, Zagreb, HRV); Tutis, Eduard (Institute of Physics, Zagreb, HRV); Forró, László (École polytechnique fédérale de Lausanne, Lausanne, CHE); Bari¿ic, Neven (Institute of Solid State Physics, Vienna University of Technology, Wien, AUT)

During the last several decades layered transition metal dichalcogenides are attracting scientific attention due to their lower dimensionality which enhances electronic correlations. Consequently, different orderings that include various density waves as well as superconductivity are found in those systems. There are more than forty different layered transition metal dichalcogenides thus serving as playground for investigation of those correlation effects.

PMon122

Mechanochemical Synthesis and Neutron Scattering Measurements on Kesterite (Cu_2ZnSnS_4)

Ritscher, Anna (Helmholtz Zentrum Berlin, Technische Universität Berlin, Berlin, GER); Lerch, Martin (Technische Universität Berlin, Berlin, AUT); Dolotko, Oleksandr (Heinz Maier-Leibnitz Zentrum, FRM II, Garching b. München, GER)

With respect to absorber materials in solar cells, Cu_2ZnSnS_4 has been a focus of interest in recent years. Up to now, the synthesis of phase-pure kesterite powder is a challenging problem. CZTS crystallizes in the kesterite type (space group $I-4$). This space group is useful describing a complete or partial ordering of Cu and Zn. In addition, kesterite-type phases exhibiting a statistical distribution of Cu/Zn are also known. Such a structure can be described in space group $I-42m$.

The motivation of the here-presented research is the development of a new chemical route for the synthesis of a single-phase material and the structural and compositional characterization of the CZTS powder. A low-temperature formation process was created where the elements should be already mixed at room temperature at an atomic level. This can be realized by a mechanochemical treatment of the binary sulfides in a planetary ball mill. Second, the poorly crystalline product is annealed in H_2S-atmosphere to get a well crystalline and ordered product.Analysis of the synthesized powder has been performed by X-ray diffraction, Neutron scattering, WDS analysis and XANES. There is no indication for the presence of secondary phases.

For a deeper understanding of the correlation between structural parameters and physical properties the knowledge of the cation distribution is required. With standard X-ray techniques it is not possible to determine the Cu/Zn distribution. For a reliable structural characterization neutron diffraction measurements at the SPODI (FRM II, Garching) were performed.
The obtained diffraction patterns show a kesterite-type phase with full Sn/(Cu/Zn) order. The results of first Rietveld refinements using the neutron data predict that Cu fully occupies the 2a (0,0,0) position. Zn and the remaining Cu do not show a complete order or a statistical distribution on the 2c (0,½,¼) and 2d (0,½,¾) positions but rather reveal a partial disorder of the cations.

PMon123

Mixed-Valent Selenium in the Uncharged Iridium Cluster $[\mathrm{Ir}_4\mathrm{Se}_{10}\mathrm{Br}_{16}]$

Stolze, Karoline (TU Dresden, Dresden, GER); Rasche, Bertold (TU Dresden, Dresden, GER); Ruck, Michael (TU Dresden, Dresden, GER)

The reaction of iridium with an excess of selenium and selenium bromide at 200 °C for two weeks yields shiny vermillion, slate-like crystals of the new compound $\mathrm{Ir}_4\mathrm{Se}_{10}\mathrm{Br}_{16}$. Single-crystal X-ray diffraction revealed an orthorhombic unit cell, space group *Pccn*, with lattice parameters a = 1515.0(1) pm, b = 1534.4(1) pm and c = 1514.5(1) pm at 296(1) K. The crystal structure consists of uncharged tetranuclear iridium clusters $[\mathrm{Ir}_4\mathrm{Se}_{10}\mathrm{Br}_{16}]$ with C_2 symmetry. The structured formula $[(\mathrm{Ir}^{3+})_4(\mu_4\text{-}\eta^2\text{-}\mathrm{Se}_2^{2-})_2(\mu\text{-}\eta^{\mathrm{Se}}\text{-}[\mathrm{SeBr}]^-)_2(\eta^{\mathrm{Se}}\text{-}\mathrm{SeBr}_2)_4(\mu\text{-}\mathrm{Br}^-)_2(\mathrm{Br}^-)_4]$ describes the cluster in greater detail. Similar to the $[\mathrm{Ir}_8\mathrm{Se}_{28}\mathrm{Br}_{14}]$ and $[\mathrm{Ir}_8\mathrm{Se}_{40}\mathrm{Br}_{10}]$ clusters [1, 2], each iridium(III) atom is coordinated octahedrally by four selenium and two bromine atoms. The four coordination polyhedra share edges and form a ring. If the coordinating atoms were regarded as electron-pair donors, the transition metal atom would achieve the electron count of 18. Selenium adopts three different oxidation states: –I in the fourfold-connecting diselenide dumbbell, ± 0 in the bridging $[\mathrm{SeBr}]^-$ entity, and +II in the terminal SeBr_2 ligand. A $\mu\text{-}\eta^{\mathrm{Se}}\text{-}[\mathrm{SeBr}]^-$ anion bridging two transition metal atoms is known from $\mathrm{Ru}_2\mathrm{Se}_6\mathrm{Br}_{12}$ [3].

Because selenium and bromine atoms are indistinguishable in the X-ray diffraction experiment, the total energies for a cluster with $\mu\text{-}\mathrm{Br}^-$, i.e. $[\mathrm{Ir}_4\mathrm{Se}_{10}\mathrm{Br}_{16}]$, and a hypothetical cluster with $\mu\text{-}\mathrm{Se}^{2-}$, i.e. $[\mathrm{Ir}_4\mathrm{Se}_{12}\mathrm{Br}_{14}]$ were calculated. The total energies per electron for the two clusters differ by approximately 2.8 eV in favour of the bromide-bridged variant. In addition, a semi-quantitative EDX analysis of a crystal points towards the composition of the bromide-richer cluster (at.-%; measured/calculated): Ir 14.3(1)/13.3, Se 29.1(4)/33.3, Br 56.7(4)/53.3. Very similar structural motifs, including μ-bridging chloride ions and $[\mathrm{SeCl}]^-$ units, were found in the recently solved structure of $\mathrm{Ir}_6\mathrm{Se}_8\mathrm{Cl}_{30}$ [4].

---

[1] K. Stolze, A. Günther, H. C. Hoffmann, M. Ruck, *Z. Anorg. Allg. Chem.***2014**, *640*, 719–723.

[2] K. Stolze, M. Ruck, *Z. Anorg. Allg. Chem.* **2014**, *640*, 1559–1563.

[3] S. A. Baranets, P. Y. Demchenko, *Ukr. Khim. Zh. (Russ. Ed.)* **2013**, *79*, 7–9.

[4] K. Stolze, M. Ruck, unpublished results.

PMon124

Phase change materials for the $Ge_8Bi_2Te_{11}$ - $Ge_8Sb_2Te_{11}$ system

Karabyn, Vasyl (Department of General and Inorganic Chemistry, Faculty of Chemical Technology, University of Pardubice, Pardubice, CZE); Prikryl, Jan (Department of General and Inorganic Chemistry, Faculty of Chemical Technology, University of Pardubice, Pardubice, CZE); Strizik, Lukas (Department of General and Inorganic Chemistry, Faculty of Chemical Technology, University of Pardubice, Pardubice, CZE); Benes, Ludvik (Joint Laboratory of Solid State Chemistry of Inst. of Macromolecular Chem. of the AS CR, v.v i., Prague and University of Pardubice, Pardubice, CZE); Svoboda, Roman (Department of Physical Chemistry, Faculty of Chemical Technology, University of Pardubice, Pardubice, CZE); Frumarova, Bozena (Joint Laboratory of Solid State Chemistry of Inst. of Macromolecular Chem. of the AS CR, v.v i., Prague and University of Pardubice, Pardubice, CZE); Frumar, Miloslav (Department of General and Inorganic Chemistry, Faculty of Chemical Technology, University of Pardubice, Pardubice, CZE)

Materials based on ternary tellurides have been intensively studied for optical and electrical non-volatile memories such as DVD, Blu-ray and PRAM. In our study we focus on the Ge8Sb2Te11 - Ge8Bi2Te11 system. Thin films with thickness d ≈ 200 nm were prepared by Flash Thermal Evaporation (FE) and by Pulsed Laser Deposition (PLD) techniques. The electrical sheet resistance Rs of as-deposited thin films was measured by four probe method according to van der Pauw [1]. It was found that the Ge8Bi2Te11 thin films have Rs ≈ 108 Ω/sqr., Ge8SbBiTe11 thin films have Rs ≈ 108 Ω/sqr. and Ge8Sb2Te11 thin films have Rs ≈ 109 Ω/sqr. at room temperature. The electrical sheet resistance of all as-deposited thin films slightly decreases with increasing temperature according to Arrhenius relation [2]. The activation energies of electrical conductivity Eaσ were found to be Eaσ = 0.38 eV (Ge8Bi2Te11), Eaσ = 0.42 eV (Ge8SbBiTe11) and Eaσ = 0.4 eV (Ge8Sb2Te11) for thin films deposited by FE and Eaσ = 0.3 eV (Ge8Bi2Te11), Eaσ = 0.35 eV (Ge8SbBiTe11) and Eaσ = 0.33 eV (Ge8Sb2Te11) for thin films deposited by PLD. When the temperature further grows, there was observed abrupt decrease of Rs by 2–4 orders of magnitude at higher temperature to a final value of Rs ≈ 102 Ω/sqr. The crystallization temperature Tc as well as activation energy of crystallization Eac was obtained by Kissinger method [3]. Structure of all as-deposited films as determined by X-ray diffraction was amorphous, all films crystallized into cubic rock salt like structure with space group Fm−3m and with lattice parameter a ≈ 6 Å. In the case of bulk samples was observed hexagonal phase P−3m1 for Ge8Bi2Te11. The refractive index of as-deposited PLD films was higher than that one of FE films. This feature can be attributed to higher density of PLD films in comparison with the FE films. The refractive index of as-deposited Ge8Bi2Te11 thin films (n ≈ 4.6 for FE, n ≈ 4.9 for PLD at λ = 1 500 nm) was higher in comparison with Ge8SbBiTe11 thin films (n ≈ 4.1 for FE , n ≈ 4.4 for PLD at λ = 1 500 nm) and Ge8Sb2Te11 thin films (n ≈4.2 for FE , n ≈4.3 for PLD at λ = 1 500 nm). The reason can be seen in higher polarizability of Bi comparing to Sb under assumption of validity of the Clausius-Mossotti realation [4-5].

---

[1] L.J. van der Pauw, Philips Tech. Rev. 20 (1958) 220.
[2] Mott N. F., Davis E. A.,Electronic Processes in Non-Crystalline Materials, Oxford Clarendon Press; London, 1971
[3] H. E. Kissinger, Anal. Chem. 29 (1957) 1702.
[4] R. Clausius, Die Mechanische Wärmlehre. Vol. II. 1879, Brunswick: Vieweg-Verlag.
[5]O. Mossotti, Mem. e Fisica di Modena 24 (1850) 49

PMon125

Polymorphism in Intercalated Iron Selenide Superconductors: Influence of Interlayer Distance and Electron Transfer on the Critical Temperature

Yusenko, Kirill (Swansea University, Swansea SA2 8PP, GBR); Margadonna, Serena (Swansea University, Swansea, GBR)

Since superconductivity with critical temperature up to 50 K was found in iron-pnictide systems, evident progress in understanding the phenomenon has been achieved [1]. Tetragonal β-FeSe with layered structure and transition temperature T_c = 8 K has been found as one of the most promising model system for a deeper understanding of the unconventional pairing mechanism in iron-based superconductors. It has been shown that its superconducting transition is extremely sensitive to applied pressure, reaching the value of 39 K at 7 GPa [2]. Recently, an intercalation of alkali/alkali-earth metals (mainly, Li, Na, K, Cs, Rb, Ca, Ba, Sr, Eu, and Yb) between the layers at low temperature using liquid ammonia as reaction medium, has been employed for the synthesis of phases with critical temperatures between 30 and 46 K (*e.g.* [3]). Due to particular significance of the β-FeSe reaction in liquid ammonia solutions for the preparation of single-phase vacancy-free intercalates, studies of composition/properties relations and dependence on the preparatory conditions is of timely importance. Herein, we report our recent investigation of Na and Ba intercalates prepared using different synthetic methodologies [4-5]. Furthermore, both reactions were investigated using *in situ* time resolved powder X-ray diffraction and magnetic susceptibility measurements.In the case of Na intercalated β-FeSe, the use of an autoclave for the synthesis leads to the formation of a superconducting phase with d = 8.7 Å and T_c = 40 K. However, performing the same reaction on a Schlenk line, results in inhomogeneous samples with T_c = 30 K but very small superconducting fractions. Synchrotron PXRD measurements performed on these systems provided strong evidence of the formation of phases adopting a vacancy ordered superstructure which has never been obtained before with low-temperature solution-based methods. β-FeSe phases intercalated with alkali-earth metals have been barely investigated. Nevertheless, detailed studies of the reaction between Ba solution in liquid ammonia and β-FeSe gives important information about general trends in liquid-NH_3—M—β-FeSe systems. Briefly, Ba solution at 200 K quickly (τ½ ~ 2-3 min) reacts with β-FeSe forming a hyper-expanded $Ba_{0.29(1)}(NH_3)_{0.35(5)}Fe_2Se_2$ intermediate with d = 13.125(1) Å which on heating slowly transforms (τ½ ~ 70 min) into $Ba_{0.24(1)}(NH_3)_{1.92(3)}Fe_2Se_2$ with T_c = 39 K (d = 11.527(1) Å). Further heating of the reaction mixture above 250 K results in the stabilization of a new phase, $Ba_{0.37(1)}(NH_3)_{1.04(2)}Fe_2Se_2$, with lower ammonia content and smaller interlayer distance. This is stable under ammonia pressure and can be characterized by T_c = 36 K. Evacuation reveals the ammonia release and a formation of stable ammonia-free phase $Ba_{0.28(5)}Fe_2Se_2$ with T_c = 34 K.Phase relations in Na and Ba intercalates and the presence of unstable intermediates clearly show the importance of considering the size and chemical nature of the metal employed during the ammonothermal synthesis of superconducting β-FeSe intercalates. Exact metal content and doping level appear to be playing an important role in determining the value of the T_c, which can then be further tuned by modulation of the interlayer spacing.

---

[1] Malavasi, Margadonna (2012): *Chem. Soc. Rev.* 41, 3897;
[2] Margadonna et al. (2009): *Phys. Rev. B* 80, 064506;
[3] Burrard-Lucas et al. (2013): *Nature Mater.* 12, 15;
[4] Yusenko, Margadonna et al. (2015): *ChemCommun* 51, 7112;
[5] Yusenko, Margadonna et al. (2015): *Inorg. Chem, submitted.*

PMon126

Rare-Earth Metal Cations in a Polar Framework Erected by Thiogallato-closo-Dodecaborate Anions

Kleeberg, Fabian (Universität Stuttgart, Stuttgart, GER); Stromsky, Ronja (Universität Stuttgart, Stuttgart, GER); Zimmermann, Lucas (Universität Stuttgart, Stuttgart, GER); Schleid, Thomas (Universität Stuttgart, Stuttgart, GER)

Thioborates consisting of dodecathio-*closo*-dodecaborate units $[B_{12}S_{12}]^{14-}$ are still not set in focus by researchers due to their difficile preparation techniques. Unique examples are $A_8[B_{12}(BS_3)_6]$ (A = Rb and Cs) described by *Krebs et al.* in 2003 [1] and $(K_3I)Sm[B_{12}(GaS_4)_3]$ from *Guo et al.* in 2009 [2]. However, we now present the synthesis and structural characterization of three additional rare-earth metal(III) dodecathio-*closo*-dodecaborates with scandium, yttrium and lanthanum [3], all crystallizing isotypically to the samarium archetype $(K_3I)Sm[B_{12}(GaS_4)_3]$ [2].

The hexagonal crystal structure of $(K_3I)RE[B_{12}(GaS_4)_3]$ (RE = Sc, Y and La) with the space group $P6_322$ contains B_{12} icosahedra (d(B–B) = 172 – 186 pm), which are completely saturated with six tetrahedral $[GaS_4]^{5-}$ units, attached via one edge each. The corresponding *trans*-oriented edge of each tetrahedron is connected to another B_{12} cluster, thus erecting a three-dimensional $[B_{12}(S_2GaS_2)_{6/2}]^{5-}$ framework, wherein the B–S and Ga–S bond lengths fall into the ranges of about 187 pm for d(B–S) and 224 – 234 pm for d(Ga–S). These distances are similar to those found in other compounds containing dodecathio-*closo*-dodecaborate units, such as $A_8[B_{12}(BS_3)_6]$ (A = Rb and Cs) (d(B–S) = 176 – 186 pm [1]), or Ga^{3+} in tetrahedral S^{2-} surrounding, just like Ga_2S_3 (d(Ga–S) = 219 – 237 pm [4]). The de facto $[B_{12}S_{12}]^{14-}$ anions are furthermore interconnected to chains along the crystallographic c-axis via the rare-earth metal trications $(RE)^{3+}$, which reside in sixfold coordination of sulfur atoms arranged as trigonal antiprisms. A further building block of the structure consists of hexagonal channels oriented parallel to [001], which are filled up with one-dimensional columns of *trans*-face sharing $[IK_6]^{5+}$ octahedra (d(I–K) = 361 pm, for comparison: d(I–K) = 353 pm in rocksalt-type KI [5]). All three compounds show almost the same unit cell parameters a and b with $a \approx 1280$ pm, but a varying c-axis ($c \approx 908$ pm for RE = Sc, $c \approx 925$ pm for RE = Y, $c \approx 956$ pm for RE = La) to fulfill the coordinative demands of the differently sized rare-earth metal trications (d(Sc–S) = 267 pm, d(Y–S) = 278 pm, d(La–S) = 293 pm) within their sulfur octahedra.

---

[1] J. Kuchinke, A. Hammerschmidt, B. Krebs, *Solid State Sci.***2003**, *5*, 189 – 196.

[2] S.-P. Guo, G.-C. Guo, M.-S. Wang, J.-P. Zou, H.-Y. Zeng, L.-Z. Cai, J.-S. Huang, *Chem. Commun.* **2009**, *2009*, 4366–4368.

[3] R. Stromsky, F. M. Kleeberg, L. W. Zimmermann, Th. Schleid, *Z. Kristallogr.***2014**, *34*, 147.

[4] J. Goodyear, G. A. Steigmann, *Acta Crystallogr.* **1963**, *16*, 946–949.

[5] L. Vegard, *Z. Phys.***1921**, *5*, 17–26.

PMon127

Soft chemical control of the crystal structure and properties of $Sr_2MnO_2Cu_{1.5-x}S_2$

Blandy, Jack (University of Oxford, Oxford, GBR); Abakumov, Artem (University of Antwerp, Antwerp, BEL); Christensen, Kirsten (University of Oxford, Oxford, GBR); Hadermann, Joke (University of Antwerp, Antwerp, BEL); Adamson, Paul (University of Oxford, Oxford, GBR); Free, David (University of Oxford, Oxford, GBR); Cohen, Harry (University of Oxford, Oxford, GBR); Thompson, Amber (University of Oxford, Oxford, GBR); Clarke, Simon (University of Oxford, Oxford, GBR)

$Sr_2MnO_2Cu_{1.5-x}S_2$[1] is a constituent compound of the wider class $A_2MO_2X_2Ch_2$ (A = Sr, Ba; M = 1st row transition metal, X = Cu, Ag; Ch = S, Se). The compounds in this class are composed of layers of [$SrMnO_2$] and [$Cu_{1.5-x}S_2$] Previous work on this compound has included investigation of its potential as a Li^+ ion host in batteries[2] and examination of the solid solution $Sr_2MnO_2Cu_{1.5}S_{2-y}Se_y$.[3] This work explores the topotactic oxidation of the manganese ions to synthesise metastable compositions with larger copper deficiencies.[4]

$Sr_2MnO_2Cu_{1.5}S_2$ was prepared via traditional high temperature solid state synthesis, before being stirred in solutions of I_2/MeCN of varying concentrations at 0°C for 2 – 4 days. The high mobility of copper in this compound meant that a range of copper occupancies could be obtained between 1.5 and 1.33 with a phase gap in the region 1.39 – 1.35.

Reduction in copper content led to changes in the copper vacancy ordering pattern from that described by Adamson et al.[3], which only appears at temperatures below an ordering temperature of *c.* 250 K, to an incommensurately modulated ordering pattern, which is present in room temperature samples. This incommensurate ordering pattern was solved using a (3 + 1)D model approach, with modulation vector $q = 0.2418\ \mathbf{a_0}^*$ and space group Xmmm(α00)00s. It was found that, as well as occupational modulation of the Cu atoms, there was also significant positional modulation of the oxide layers, which moved closer to the [$Cu_{2-x}S_2$] layers to ensure that the S atoms did not become underbonded in low Cu regions (see fig. 1).

The presentation will also describe the effect of tuning the composition and structure on the physical properties.

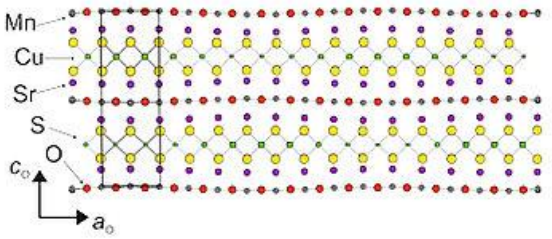

Fig. 1 A representation of the modulated structure obtained from analysis of the single crystal diffraction data. The occupational modulation of the Cu sites is depicted using the size of the green circles

---

[1] W. J. Zhu and P. H. Hor, *Journal of Solid State Chemistry*, 1997, **130**, 319-321.

[2] S. Indris, J. Cabana, O. J. Rutt, S. J. Clarke and C. P. Grey, *Journal of the American Chemical Society*, 2006, **128**, 13354-13355.

[3] P. Adamson, J. Hadermann, C. F. Smura, O. J. Rutt, G. Hyett, D. G. Free and S. J. Clarke, *Chemistry of Materials*, 2012, **24**, 2802-2816.

[4] J. N. Blandy, A. M. Abakumov, K. E. Christensen, J. Hadermann, P. Adamson, S. J. Cassidy, S. Ramos, D. G. Free, H. Cohen, D. N. Woodruff, A. L. Thompson and S. J. Clarke, *APL Materials*, 2015, **3**, 041520.

PMon128

Structural and properties features of Fe-substituted tetrahedrites

Nasonava, Darya (Lomonosov Moscow State University, Department of Chemistry, Moscow, RUS);
Shevelkov, Andrei (Lomonosov Moscow State University, Department of Chemistry, Moscow, RUS)

Currently tetrahedrite ($Cu_{12}Sb_4S_{13}$, I-43m space group) and its substituted analogs (mainly $Cu_{12-x}T_xSb_4S_{13}$, where T = Fe, Ni, Mn, Co, Zn) are among the most attracting attention potential thermoelectric materials. The main reason of tetrahedrites high thermoelectric efficiency is the favorable combination of crystal and electronic structures, which strongly depend on the nature of the substituting element T and its concentration. Thus the key of the thermoelectric properties control is the rigorous structure details study in each particular case.

Our research is devoted to Fe-substituted tetrahedrites ($Cu_{12-x}Fe_xSb_4S_{13}$), which were synthesized and partly investigated by previous researchers [1,2], but still remain interesting objects for complete understanding the correlations between the crystal and electronic structures and magnetic and thermoelectric properties and thus controlling the latter via composition alteration. The aim of our work lies in detailed investigation of the electronic and crystal structures features of Fe-substituted tetrahedrites.

Accurate structural analysis, Mossbauer spectroscopy, magnetic susceptibility, and heat capacity measurements were used for the Fe-substituted tetrahedrites investigation. As the result, the atomic distribution features being in good agreement with literature data [2] were shown. The coexistence region of Fe^{2+} and Fe^{3+} was found, moreover the magnetic susceptibility and Mossbauer spectroscopy data are suggesting the presence of iron in mixed valence state, which can be described by an equation: $Cu^{2+} + Fe^{2+} \leftrightarrow Cu^{+} + Fe^{3+}$. Heat capacity data show no rattling modes of copper atoms, thus pseudo-localized vibrations cannot be the reason for the low thermal conductivity experimentally observed.

The work was supported by Russian Science Foundation, grant no. 14-13-00089

---

[1] J. Heo, G. Laurita, S. Muir, M.A. Subramanian, D.A. Keszler. *Chemistry of Materials 26 (2014) 2047-2051*
[2] J.W. Andreasen, E. Makovicky, B. Lebech, S. K. Møller. *Phys Chem Minerals 35 (2008) 447–454*

PMon129

Structures and magneto-electric behaviors of calcium and iron based oxysulfides

Delacotte, Charlène (CRISMAT, Caen, FRA); Pérez, O. (CRISMAT Laboratory, Caen, FRA); Pautrat, A. (CRISMAT Laboratory, Caen Cedex 04, FRA); Hébert, S. (CRISMAT Laboratory, Caen, FRA); Pelloquin, D. (CRISMAT Laboratory, Caen, FRA); Maignan, A. (CRISMAT Laboratory, Caen, FRA)

Transition metal oxides exhibit such a wide range of physical and chemical properties that they find applications in numerous sectors. In parallel to the search for new phases, a large attention has been devoted to the metal/ion substitutions to improve the properties of oxides or to induce new ones. Especially, a peculiar attention has been given to the control of these properties taking advantage of the anion framework. Some recent and promising results have been reported in the area of mixed anion chemistry as for instance some superconductivity or optical properties in oxychalcogenides or oxypnictides [1-2]. Considering the existence of several layered Ae-M-O-Ch phases (Ae= alkaline earth, M=Mn, Fe, Co, Cu, Zn and Ch=S, Se), the introduction of sulfur can be also considered in the Ca-Fe-O system. Only one compound, CaOFeS, is referred and although its synthesis had been reported for more than twenty years [3], neither refined structural model nor magnetic features have been reported.

We have revisited the Ca-Fe-O-S system and in a recent study [4], an efficient synthesis route is proposed to obtain single crystals and ceramic powder of the CaOFeS phase. Its structure has been established at room temperature by combining data from transmission electron microscopy (TEM) observations together with X-ray single crystal and neutron powder diffraction data. These structural analyses lead to a stoichiometric hexagonal non centrosymmetric polar model built from alternating layers made of $FeOS_3$ tetrahedra sharing S apices and stacked with Ca^{2+} planes. CaOFeS compound exhibits a semi-conducting behavior and a sufficient resistivity under 100K. Thermal dependence of dielectric permittivity has so been measured at low temperatures and evidenced a dielectric transition at 36K. In addition, a new compound $CaO_xFe_{1.25}S$ has been also isolated jointly as bulk and single crystal materials. Its first structural and magnetic properties will be also presented.

---

[1] S.J. Clarke, P. Adamson, S.J.C. Herkelrath, O.J. Rutt, D.R. Parker, M.J. Pitcher and C.F. Smura, Inorg. Chem., 2008, 47 (19), pp 8473–8486

[2] D. Johrendt, H. Hosono, R.D. Hoffmann, R. Pöttgen, Z. Kristallogr. 226 (2011) 435-446

[3] A. Jha, U. O Igiehon and P. Grieveson, Scand. J. Metall., Vol. 20, (1991)

[4] C. Delacotte, O. Pérez, A. Pautrat, D. Berthebaud, S. Hébert, E. Suard, D. Pelloquin and A. Maignan, Inorg. Chem. (Submitted)

PMon130

The crystal structures and polymorphism of Na_2TeQ_3 (Q=S, Se)

Pompe, Constantin (Universität Regensburg, Regensburg, GER); Weihrich, Richard (Universität Regensburg, Regensburg, GER); Pfitzner, Arno (Universität Regensburg, Regensburg, GER)

Alkali metals M=Li, Na, K, and Cs form chalcogenido tellurates with the composition M_2TeQ_3. The trigonal TeQ_3 units therein are arranged in layers. Whereas the Cs cation in Cs_2TeS_3 is eight- and sevenfold coordinated by sulfur [1], the smaller cations M=Li, Na, K are octahedrally surrounded by the chalcogenido anions. Each potassium compound K_2TeQ_3 establishes its own structure type.[2-4] Preitschaft reported a third structure type for the lithium and sodium compounds.[5, 6] The structural differences between K_2TeQ_3 and the lighter homologues are due to a varying orientation of the TeQ_3 units. We investigated the sodium compounds in more detail since in the case of Na_2TeSe_3 these results seemed to contradict former work of Zagler and Eisenmann, who found another crystal structure for it.[4] Systematic variation of the reaction conditions revealed the high-temperature modification Na_2TeSe_3-mC48, which was obtained by heating a stoichiometric mixture of the elements up to 1170 K and subsequent quenching to room temperature. The cell parameters of Na_2TeSe_3-mC48 are a=21.6801(9) Å, b=5.9730(2) Å, c=11.9736(7) Å, β=121.166(6)°, and V=1326.8(2) $Å^3$ (Z=8) in space group C2/c. The low-temperature modification Na_2TeSe_3-mP24 was yielded by annealing a stoichiometric mixture at 670 K for 10 days. The cell parameters of Na_2TeSe_3-mP24 are a=5.990(3) Å, b=12.658(4) Å, c=8.784(3) Å, β=93.51(3)°, and V=664.8(5) $Å^3$ (Z=4) in space group $P2_1/c$. DFT-calculations predict a difference in total energies of both modifications of ΔE=0.18 kJ/mol. Na_2TeS_3, is isotypic with Na_2TeSe_3-mP24. The cell parameters were refined to a=5.776(1) Å, b=12.202(3) Å, c=8.405(3) Å, β=92.03(2)°, and V=592.0(4) $Å^3$ (Z=4). The difference in total energies between Na_2TeS_3-mP24 and hypothetical Na_2TeS_3-mC48 were calculated to ΔE=1.8 kJ/mol. This high difference in total energy matches the experimental observation, that the modification mC48 was not yet accessible. The calculated electronic band gaps for Na_2TeSe_3-mP24 (1.18 eV) and Na_2TeSe_3-mC48 (1.20 eV) are almost identical. Both modifications of Na_2TeSe_3 are reddish, whereas Na_2TeS_3 has a yellow shade, which was also verified by DFT-calculations (1.71 eV). Raman spectra show the vibration modes ν(Te-Q) between 367 and 331 cm^{-1} (TeS_3^{2-} in Na_2TeS_3 and Li_2TeS_3), and between 238 and 217 cm^{-1} for the two modifications of Na_2TeSe_3.

---

[1]J.-M. Babo, K. K. Wolff, T. Schleid, Z. Anorg. Allg. Chem. **2013**, *639*, 2875.
[2]B. Eisenmann, H. Katzer, H. Schäffer, A. Weiss, Z. Naturforsch. **1969**, *B24*, 456.
[3]C. Rumpf, C. Näther, W. Bensch, Acta Cryst. **1999**, *C55*, 1046.
[4]R. Zagler, B. Eisenmann, Z. Kristallogr. **1988**, *183*, 193.
[5]C. Preitschaft, A. Pfitzner, Z. Anorg. Allg. Chem. **2005**, *631*, 1227.
[6]C. Preitschaft, PhD-Thesis, Universität Regensburg **2004**.

PMon131

Polarisation dependence in hard X-ray photoemission of Sn-doped TiO_2

Regoutz, Anna (Imperial College London, Department of Materials, London, GBR); Panaccione, Giancarlo (Consiglio Nazionale delle Ricerche, Istituto Officina dei Materiali, Lab TASC, Trieste, ITA); Borgatti, Francesco (Consiglio Nazionale delle Ricerche, Istituto per lo Studio dei Materiali Nanostrutturati, Bologna, ITA); Tsuei, Ku-Ding (National Synchrotron Radiation Research Centre, Hsinchu, TWN); Agrestini, Stefano (Max Planck Institute for Chemical Physics of Solids, Dresden, GER); Utsumi, Yuki (Max Planck Institute for Chemical Physics of Solids, Dresden, GER); Liao, Yen Fa (National Synchrotron Radiation Research Centre, Hsinchu, TWN); Palgrave, Robert (University College London, Department of Chemistry, London, GBR); Watson, Graeme W. (University Dublin, Dublin); Poll, Christopher (Imperial College London, Department of Materials, London, GBR); Payne, David (Imperial College London, Department of Materials, London, GBR); Egdell, Russell G. (Department of Chemistry, University of Oxford, Oxford, GBR)

Polarisation dependence in hard X-ray photoemission of Sn-doped TiO_2 Recently, the Egdell group has demonstrated that Sn-doped rutile has superior photocatalytic activity to N-doped anatase [1]. An increase in the bandgap would be expected when doping of the wider gap SnO2 into the lower gap TiO_2. However, pronounced bandgap bowing has been observed at low Sn concentrations, with the bandgap reaching a minimum value at x=0.02 [2]. Previous investigations of Sn-doped TiO_2 anatase thin films with X-ray photoemission spectroscopy (XPS) show a weak peak at the bottom of the main O 2p valence band. This peak increases in intensity with increasing Sn doping level. A peak at this position could stem from hybridisation between Sn 5s and O 2p states. However, hydroxides on the sample surface can also lead to a peak at this binding energy. It was possible to identify the contributions of Sn 5s and Ti 4s states to the valence band electronic structure of Sn-doped anatase by polarisation dependent hard XPS. The metal s state intensity is strongly enhanced relative to that of O 2p states at high photon energies due to matrix element effects when photoelectrons are detected along the direction of the electric vector of the incident radiation, but the contribution of s states becomes negligible when photoelectrons are detected in a direction orthogonal to the polarisation vector. The experimental spectra in both polarisations are in good agreement with cross section and asymmetry parameter weighted partial densities of states derived from density functional theory calculations.

---

[1] F. E. Oropeza et al., Phys.Chem.Chem.Phys. 13, 7882 (2011).

[2] M. H. Harunsani et al., Chem.Mater. 22, 1551 (2010).

PMon132

High-pressure photoelectron spectroscopy investigation of the interaction between CO_2 and Cu-based reduction catalysts

Regoutz, Anna (Imperial College London, Department of Materials, London, GBR); Villar Garcia, Ignacio J. (Imperial College London, Department of Materials, London, GBR); Williams, Charlotte (Imperial College London, Department of Materials, London, GBR); Egdell, Russell G. (Department of Chemistry, University of Oxford, Oxford, GBR); Payne, David (Imperial College London, Department of Materials, London, GBR)

High-pressure photoelectron spectroscopy investigation of the interaction between CO_2 and Cu-based reduction catalysts Fossil fuels have become increasingly scrutinised due to their environmental impact, extraction risks, and the depletion of resources. An alternative to fossil fuels is presented by the usage of CO_2 as source for the production of carbon based fuels, including methanol. The development of an efficient CO_2 reduction catalyst necessary for fuel production faces many research challenges, in particular the development of a catalyst able to direct reactions through stable intermediates, e.g. CO. Nanoscale copper is an ideal candidate; however, high overpotentials have to be used to overcome the competition with H_2O reduction to H_2. Recently, so-called “oxide-derived” copper has been shown to overcome this problem, working at moderate overpotentials of around -0.2 V vs. RHE. This system is complicated by the fact that most oxide-derived copper samples still show a considerable amount of copper oxide (Cu_2O) present at the surface. Therefore, it is not clear if the increase in catalytic activity originates solely in the change in surface morphology of the copper or also in the presence of the oxide. As this system promises to be an excellent catalyst for the reduction of CO_2 a detailed understanding of the basis of its catalytic activity is essential and absolutely necessary for any further development. Photoelectron spectroscopy (PES) is used widely in the solid state sciences but due to its nature as a UHV technique, a study of the solid-gas interface, which is intrinsic to the CO_2 reduction catalysis, is not possible. High-pressure photoelectron spectroscopy (HiPPES) is a recent advanced method which allows the measurement of solid samples at elevated pressures of between 1 and 30 mbar (in comparison to 10-9 mbar in conventional XPS). Using this method a study of the surface chemistry of the solid state catalysts as a function of sample preparation, the presence of oxide, temperature, and the influence of co-adsorbates (O_2/H_2O) becomes possible. This work presents results on the interaction of CO_2 with the surface of oxide-derived Cu foil and nanoparticles used in actual catalysis processes. In addition, the results of CO_2 interaction with Cu single crystals as well as Cu_2O thin films are presented to pinpoint differences between metallic and oxidic surfaces. The measurements are conducted both at room temperature as well as at elevated temperatures to investigate possible temperature dependence. Cu 2p and 3p core levels, as well as the Cu LMM Auger lines are used to investigate the state of the copper surfaces. The C 1s and O 1s core levels are used to track free CO_2 gas passing over the sample surface as well as CO_2 adsorption. Furthermore, valence band spectra of the as-presented samples and samples under the presence of CO_2 are compared and contributions of CO_2 identified. Ultimately, the presented results provide a starting point for the detailed understanding of these catalysts and lead to the identification of possible ways to further improve and develop their catalytic characteristics.

PMon133

Angular overlap modelling of the vanadyl(IV) chromophore in silver vanadyl(IV) bis(orthophosphate) pyrophosphate in comparison to single crystal EPR measurements

Wittich, Knut (Bonn University, Bonn, GER); Glaum, Robert (Bonn University, Bonn, GER); Abdullin, Dinar (Bonn University, Bonn, GER); NejatyJahromy, Yaser (Bonn University, Bonn, GER); Schiemann, Olav (Bonn University, Bonn, GER)

$Ag_6(V^{IV}O)_2(PO_4)_2(P_2O_7)$ was obtained by reaction of Ag_3PO_4 and $(VO)_2P_2O_7$ (sealed ampoule, 550 °C, 3d). Its crystal structure [1] exhibits only one independent $[(V^{IV}{=}O)O_5]$ chromophore, therefore this compound appeared well suited for an in-depth investigation of the electronic structure of the $(V{=}O)^{2+}$ group in a phosphate environment. Polarized electronic absorption spectroscopy shows two bands: $\nu_{1a} = 9450\ \text{cm}^{-1}$, $\nu_{1b} = 9950\ \text{cm}^{-1}$, $\nu_2 = 14750\ \text{cm}^{-1}$). EPR provided an orthorhombic crystal g-tensor with $g_1 = 1.9445$, $g_2 = 1.9521$, $g_3 = 1.9695$.
In our contribution we report on angular overlap modelling (AOM) [2-5] of the $[(V^{IV}{=}O)O_5]$ chromophore in $Ag_6(V^{IV}O)_2(PO_4)_2(P_2O_7)$ using the computer program CAMMAG [6-8]. Within the calculation the relations $e_\sigma(V^{IV}\text{-O}) \sim d(V^{IV}\text{-O})^{-5.0}$ [2] and $e_{\pi,x} = e_{\pi,y} = 1/4\cdot e_\sigma$ were used to reduce the number of fit parameters. Using the latter assumption for all π-interactions, the AOM results in too small values for the first excitation observed in the electronic absorption spectrum. Therefore the π-contribution of oxygen in the vanadyl-group was set to $e_{\pi,x} = e_{\pi,y} = 0.47\cdot e_\sigma$. In that way the electronic structure of $Ag_6(V^{IV}O)_2(PO_4)_2(P_2O_7)$ can be described with a small number of independent parameters ($e_{\sigma,max}(V^{IV}\text{-O}) = 24050\ \text{cm}^{-1}$ at $d(V^{IV}\text{-O}) = 1.61$ Å, $\lambda(V^{4+}) = 195\ \text{cm}^{-1}$, $k_x = k_y = 0.79$, $k_z = 0.77$). Within this model the molecular g-tensor of the chromophore was calculated with its components $g_z = 1.9160$, $g_x = 1.9673$ and $g_y = 1.9726$ with the *z*-axis of the reference coordinate system along the $(V^{IV}{=}O)$ bond.The molecular g-tensor is not oriented along the axes of the unit cell of $Ag_6(V^{IV}O)_2(PO_4)_2(P_2O_7)$. Therefore the molecular g-tensor is not identical to the crystal g-tensor obtained by EPR measurements. During the single crystal EPR measurements (Q-band) the crystal was rotated about its *c*- and *b*-axes whereby the values $g_1 = 1.9445$, $g_2 = 1.9521$ and $g_3 = 1.9695$ of the crystal g-tensor could be determined. Taking into account the orientation of the molecular g-tensor related to the axes of the unit cell and assuming co-linearity of the crystal g-tensor to these axes the molecular g-tensor (from AOM) can be transformed to a crystal g-tensor. With equations (1-3) and α_i, β_i, and γ_i referring to the angles between the molecular g-tensor axes i (x, y and z) and the crystallographic axes the values of the crystal g-tensor are calculated as

$g_a = 1.9339 \approx g_1$, $g_b = 1.9517 \approx g_2$, and $g_c = 1.9707 \approx g_3$.

$$g_a^2 = \cos^2(\alpha_x)\cdot g_x^2 + \cos^2(\alpha_y)\cdot g_y^2 + \cos^2(\alpha_z)\cdot g_z^2 \qquad (1)$$
$$g_b^2 = \cos^2(\beta_x)\cdot g_x^2 + \cos^2(\beta_y)\cdot g_y^2 + \cos^2(\beta_z)\cdot g_z^2 \qquad (2)$$
$$g_c^2 = \cos^2(\gamma_x)\cdot g_x^2 + \cos^2(\gamma_y)\cdot g_y^2 + \cos^2(\gamma_z)\cdot g_z^2 \qquad (3)$$

The values of the crystal g-tensor obtained from single crystal EPR experiments ($g_{1\text{-}3}$) are close to those derived within the AOM framework ($g_{a\text{-}c}$).

---

[1] R. Glaum, C. Welker-Nieuwoudt, C.-K. Dobner, M. Eichelbaum, F. Gruchow, C. Heine, A. Karpov, R. Kniep, F. Rosowski, R. Schlögl, S. A. Schunk, S. Titlbach, A. Trunschke, *Chem. Ing. Tech.***2012**, *84*, 1766-1779.

[2] B. N. Figgis, M. A. Hitchman, *Ligand field Theory and its Applications*, Wiley-VCH, New York **2000**.

[3] C. K. Jørgensen, R. Pappalardo, H.-H. Schmidtke, *J. Chem. Phys.***1963**, *39*, 1422.

[4] D. E. Richardson, *J. Chem. Ed.***1993**, *70*, 372.

[5] E. Larsen, G. N. LaMar, *J. Chem. Ed.***1974**, *51*, 633.

[6] D. A. Cruse, J. E. Davies, J. H. Harding, M. Gerloch, D. J. Mackey, R. F. McMeeking, *"CAMMAG" a FORTRAN Computing Package*, Univ. of Cambridge **1991**.

[7] M. Gerloch, *Magnetism and Ligand Field Theory*, Cambridge Univ. Press. **1983**. [8] M. Riley, *CAMMAG for PC*, version 4.0; Univ. of Queensland, St. Lucia, Australia, **1997**.

PMon134

Assessment of the thermodynamic properties of solids at high temperature with the drop calorimetry technique

Andre, Rémi (SETARAM Instrumentation, CALUIRE, FRA)

Drop calorimetry is not the most well-known calorimetric method. However a lot of the high-temperature heat capacity and enthalpy of formation data found in the literature come from the use of this technique. Moreover, since the 1960's, the number of published papers mentioning the use of the drop calorimetry technique has been increasing [1-4]. Different types of drop calorimeters have been designed, especially because it has historically been a home built technique. But in most of the systems, tens or hundreds of milligrams scale samples, initially held at a set temperature (most of the time room temperature) above the calorimeter are pushed into the calorimetric well at the bottom of which a calorimetric vessel sits. The sample falls into this vessel because of its own weight. The vessel, which is held isothermally at the test temperature, is surrounded by a calorimetric detector. The experimental assessment of accurate and reliable thermodynamic properties of solids at high temperatures (above 500°C) is a challenge. Throughout the past decades, SETARAM Instrumentation has been designing and improving drop calorimeters for such purposes. They now reach extreme accuracy and reliability with the latest versions of the Alexys calorimeter. Two kinds of commercially available drop calorimeters were employed for the presented exemples: - MultiHTC is an isothermal or temperature scanning calorimeter with operating temperatures up to 1600°C. It can be equipped with a standard heat flow DSC detector, but also with a quasi-Calvet drop sensor. - Alexys is a true, high-sensitivity Calvet calorimeter optimized for high temperature drop calorimetry isothermal operations at temperatures up to 1000 °C. In both detectors, the arrangement of thermocouple welding (thermopile) on the surface of the experimental chamber at varying heights provides good integration of the heat exchanges. The calibration of the drop calorimetric detectors is achieved by using 30-40mg samples of standard materials with known specific heat capacity such as sapphire (α-Al2O3) or platinum. The employed standard material in the presented tests is NIST standard material 720, synthetic sapphire.

---

[1] S.V. Ushakov and A. Navrotsky, J. Am. Ceram. Soc., 1–20 (2012).

[2] O. Benes, P. Gotcu-Freis, F. Schwörer, R.J.M. Konings, Th. Fanghänel, J. Chem. Thermodynamics 43 (2011).

[3] R. Kandan, R. Babu, K. Nagarajan, J Therm Anal Calorim 99 (2010).

[4] S. Dash, Z. Singh, Journal of Nuclear Materials 404 (2010).

PMon135

Combinatorial ceramic synthesis and scanning SQUID microscopy for searching new cuprate superconductors

Iranmanesh, Mitra (Bern University, Bern, CHE); Stir, Manuela (Bern University, Bern, CHE); Kirtley, John R (Stanford University, California, USA); Hulliger, Jürg (Bern University, Bern, CHE)

A single sample synthesis concept based on multi-element ceramic samples can produce a variety of local products [1]. Applied to cuprate superconductors (SC) statistical modeling predicts the occurrence of about 50 ppm of possible compounds [2]. such a sample need local probe analytical [3] or separation techniques [2] to identify compounds of interest.

Here, we report on results obtained from random mixtures of Ca, Sr, Ba, La, Zr, Pb, and Cu oxides reacted at different conditions. The bulk state is showing superconductivity up to about 125 K. By magnetic separation many SC grains in the size range of 50 to 200 were collected for further analysis. Scanning SQUID microscopy applied to a single grain has detected local µm sized areas of SC up to 115 K. Further techniques such as magneto-optic measurements and transmission electron microscopy will be applied. Following data from literature [4], SC for these compositions are obtained only at high pressure. Here, we have either found a new synthetic approach for known compounds or even a new type of cuprate, reaching a high Tc without containing Bi, Tl, Hg.

---

[1] J. Hulliger, M. A. Awan, Chem. Eur. J. 2004, 10, 4694 – 4702.

[2] J. B. Willems, D. Perez, G. Couderc, B. Trusch, L. Dessauges, G. Labat, J. Hulliger, Solid State Sci. 2009, 11, 162 –169.

[3] M. Iranmanesh. M. Stir, J. R. Kirtley, J. Hulliger, Chem. Eur. J, 2014, 20, 15816 –15823.

[4] Ch. P. Poole, Jr., Handbook of Superconductivity, Academic Press, San Diego, 2000.

PMon136

Novel crystal structure of MoO_3 nanobelts

Slawinski, Wojciech (University of Oslo, Oslo, NOR); Fjellvåg, Øystein (University of Oslo, Oslo, NOR); Ruud, Amund (University of Oslo, Oslo, NOR); Fjellvåg, Helmer (University of Oslo, Oslo, NOR)

One of the most applied power sources today are rechargeable lithium-ion batteries. This is due to its high energy density, high voltage, no memory effect and long cycle life [1]. The most commonly used anode material is graphite. There is now lot of efforts done to discover new materials to improve batteries properties. One interesting candidate is molybdenum trioxide MoO_3, either as anode or cathode material [2]. Its anodic capacity of 1100 mAh/g is well above 372 mAh/g for graphite [3]. However, our focus is rather on MoO_3 as cathode material. Importantly, it has been reported that changing the MoO_3 crystallite size into the nano scale regime significantly improves its electrochemical properties [4-5]. It is therefore essential to gain insight into the crystal structure of material with different particle morphologies at the nanoscale in order to better understand the mechanism behind enhanced electrochemical properties.

We present an extensive study on the disordered structure of MoO_3 nanobelts. Bulk and nanobelt samples of MoO_3 were investigated by synchrotron radiation powder diffraction, supplemented by TEM. The observed diffraction patterns for nanobelt and bulk sample reveal significant differences which cannot be explained just by diffraction line broadening due to limited crystallite size. The MoO_3 structure can be described as consisting of two layers (A and B) stacked alternatingly (AB-AB…). In the nanobelts these layers are no longer stacked perfectly (probability of stacking fault determined to 0.48), while the bulk MoO_3 is perfectly ordered in an ABAB... sequence. It is proposed that the stacking faults may influence electrochemical properties of the nanobelts compared to the bulk material. This is reasonable since the stacking faults occur in interlayers being likely candidates for Li-ion intercalation.

---

[1] Scrosati, B. Nature 1995 , 373 , 557-558.

[2] Wang, X.; Nesper, R.; Villevieille, C.; novak, P. Adv. Energy Mater. 2013, 3, 5, 606-614

[3] Chernova, N.; Roppolo, M.; Dillon, A.; Whittingham, M. Journal of Materials Chemistry 2009 , 19 , 2526-2552.

[4] Brezesinski, T.; Wang, J.; Tolbert, S.; Dunn, B. Nature Materials 2010, 9, 146-151.

[5] Hashem, A.; Askar, M.; Winter, M.; Albering, J.; Besenhard, J. Ionics 2007, 13, 3-8.

PMon137

Optimising PDF data quality using a laboratory powder diffractometer

Hartmann, Thomas (STOE & Cie GmbH, Darmstadt, GER)

In the recent past, the calculation of the pair distribution function (PDF) became more and more common as a new method to obtain structural information from complex materials beyond the Bragg equation and crystallographic PXRD analysis [1].

The atomic PDF $G(r)$ gives the number of atoms in a spherical shell of a normalised thickness at a distance r from an atom, it is the sine Fourier transform of the total scattering structure function $S(Q)$

$G(r)=2/\pi \int Q\, [S(Q) - 1] \sin Q(r) \mathrm{d}Q$

where Q is the magnitude of the scattering vector and $S(Q)$ the corrected and normalised powder diffraction pattern of the material. $S(Q)$ has to be measured to as high Q-values as possible to achieve the best resolution in real-space. With

$| Q | = 4\, \pi \sin\theta \cdot \lambda^{-1}$

it is evident that synchrotron radiation with shortest wavelengths will be preferred to attain the best PDF data. Nevertheless, standard laboratory powder diffractometers can yield sufficient data quality in a reasonable measuring time when Mo K a $_1$ - (0.7093Å) or Ag K a $_1$ -radiation (0.5594Å) has been used.

An impressive comparison of $G(r)$ calculated with PDFgetX3 [2] from data of naphthalene taken at room temperature with a STOE STADI P powder diffractometer in Transmission mode, equipped with a Ag-tube, a Ge(111)-monochromator for pure Ag K a $_1$ -radiation as well as the Dectris MYTHEN 1K detector with 1 mm chip thickness and from synchrotron data, beam line X17A, NSLS Brookhaven with a wavelength of 0.1839 Å resulted into amazingly similar peak widths for both experiments.

Therefore the same powder diffractometer has been chosen to investigate the influence of the wavelength, sample volume, temperature and detector technique to optimise the data quality for laboratory PDF data acquisition.

---

[1] Dinnebier, R. E. and Billinge, S. J. L., *“Powder Diffraction: Theory and Practice”*, **2008**, The Royal Society of Chemistry, Cambridge, UK.
[2] Juhas, P., Davis, T., Farrow, C.L. and Billinge, S .J. L., *J. Appl. Cryst.* **2013**, *46*, 560-566.

PMon138

Recent Developments in Laboratory-based High Pressure Photoelectron Spectroscopy

Payne, David (Imperial College London, London, GBR)

Photoelectron spectroscopy (PES) is one of the most direct probes of electronic structure available to the experimental scientist, as well as an invaluable tool for elucidating bulk and surface chemical composition. It is commonplace to use PES for the characterization of samples held in high or ultra-high vacuum (HV, UHV), yet what is gained in understanding the fundamental surface physics of a material, is lost when this knowledge needs to be transferred to the material operating in real-world conditions. This so-called “pressure-gap” has been the focus of intense technological development over the last 40 years, culminating in the latest generation of HiPPES instruments.

This presentation will introduce a state-of-the-art laboratory-based high-pressure photoelectron spectroscopy (HiPPES) system housed in the Department of Materials, Imperial College London. The system is equipped with a monochromatic X-ray and UPS sources and R4000 HiPP-2 analyser This dual capability instrument can operate at pressures from UHV (10-10 mbar) up to 30 mbar using a variety of gases (a ir, N_2, O_2, H_2, H_2O, CO_2, etc) and over a wide temperature range (100-1110 K) using a two-piece titanium reaction-cell fitted with the cone and aperture necessary for HiPPES measurements. The high-pressure retractable reaction-cell is designed to provide flexibility between near-ambient pressure and UHV conditions.

The system enables key in-situ and in-operando XPS analysis of the surfaces of materials in a wide range of technologically relevant areas including energy, catalysis, electronic materials, biomaterials and environmental science applications. Some areas of recent research will be highlighted including technological advances with equipment [1-3], as well as some very recent results on functional oxide materials.

---

[1] A versatile photoelectron spectrometer for pressures up to 30 mbar. S.K. Eriksson, D.J. Payne et al., Rev. Sci. Instrum. 85 075119 (2014).

[2] Increased photoelectron transmission in High-pressure photoelectron spectrometers using “swift acceleration” M.O.M. Edwards, D.J. Payne et al., Nuclear Instruments and Methods in Physics Research Section A, 785, 191 (2015).

[3] A Study of the Pressure Profiles near the First Pumping Aperture in a High Pressure Photoelectron Spectrometer J.M. Kahk, D.J. Payne et al., submitted (2015).

PMon139

Unusual Tetrahedra Network Structures of Lanthanum Barium Oxonitridosilicates

Fahrnbauer, Felix (Faculty of Chemistry and Mineralogy, Institute for Mineralogy, Crystallography and Materials Science, Leipzig University, Leipzig, GER); Neudert, Lukas (Department of Chemistry, University of Munich (LMU), Munich, GER); Oeckler, Oliver (Faculty of Chemistry and Mineralogy, Institute for Mineralogy, Crystallography and Materials Science, Leipzig University, Leipzig, GER); Schnick, Wolfgang (University of Munich (LMU), Department of Chemistry, Munich, GER); Durach, Dajana (University Munich (LMU), Munich, GER)

Nitridosilicates are highly interesting materials as they show a great structural variability correlated with promising materials properties such as luminescence of Eu^{2+}/Ce^{3+}-doped samples.[1] As their syntheses often lead to heterogeneous and microcrystalline samples, investigations with microfocused synchrotron radiation, often in combination with electron diffraction and microscopy and EDX spectroscopy are necessary for a precise structure determination.[2] Here, we report about $La_6Ba_3Si_{17}N_{29}O_2Cl$ and $La_3BaSi_5N_9O_2:Ce^{3+}$, two oxonitridosilicates with intriguing framework topologies, which were investigated with a sub-micron synchrotron beam (ID11, ESRF, Grenoble). $La_3BaSi_5N_9O_2:Ce^{3+}$ consists of an interrupted three-dimensional tetrahedra network, which is characterized by dreier, sechser and zehner rings of vertex–sharing SiN_4 and SiN_2O_2 tetrahedra.[3-4] The SiN_4 tetrahedra form sechser rings. These rings are connected via common edges to zehner rings. The latter are interconnected by dreier rings, which are composed of two SiN4 and one SiN_2O_2 tetrahedra (Fig. 1a,b) [Pmn21 (no. 31), a = 9.5505(8), b = 19.0778(16), c = 12.1134(9) Å and Z = 8]. High-resolution TEM and Z-contrast scanning TEM confirm the structure. Next to its intriguing structure, $La_3BaSi_5N_9O_2:Ce^{3+}$ shows intense yellow luminescence (λmax = 578 nm; fwhm~4700 cm^{-1}).

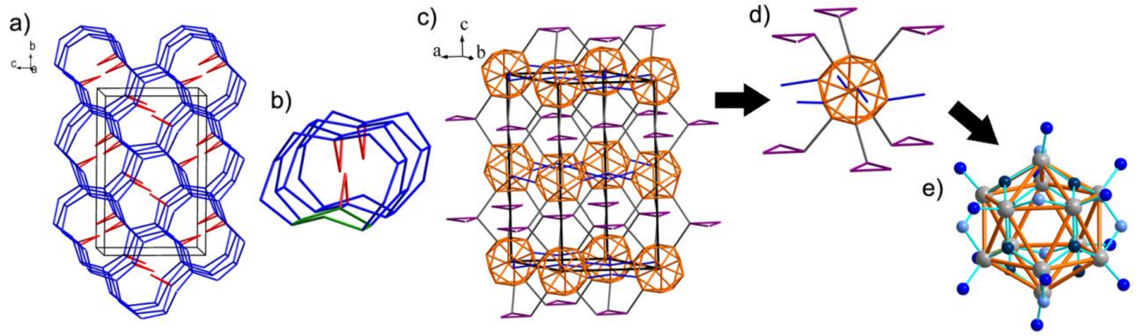

Fig. 1: (a) Topological representation of $La_3BaSi_5N_9O_2$ (zehner rings: blue; dreier rings: red). (b) representation of zehner rings (blue), which are condensed with sechser (green) and dreier (red) rings. Each connecting line represents a Si–N–Si bond. (c) Topological representation of $La_6Ba_3Si_{17}N_{29}O_2Cl$; (d) icosahedra (orange) connected via six dreier rings (violet) and six Si atoms (blue) e) interconnection of the Si atoms of one icosahedron (Si gray; N[3] dark blue ; N[2] blue/light blue). Each Si-N[2]-Si bond corresponds to an edge of the icosahedron

$La_6Ba_3Si_{17}N_{29}O_2C_l$ is characterized by an interrupted three-dimensional tetrahedra network containing vertex-sharing SiN_4 and SiN_3O tetrahedra. The SiN_4 tetrahedra form dreier rings. Twenty of them condense in a way that the Si atoms form icosahedra. These building units are interconnected via six corners by six dreier rings and via the remaining six corners with the Si atom of the SiN_3O-tetrahedra (Fig. 2) [P63/m (no. 176), a = 9.8117(14), c = 19.286(6) Å, Z = 2].

---

[1] M. Zeuner, S. Pagano,W. Schnick. Angew. Chem., Int. Ed. 2011, 50, 7754. [2] F. Fahrnbauer, T. Rosenthal, T. Schmutzler, G. Wagner, G. Vaughan, J. Wright, O. Oeckler, 2015, DOI: 10.1002/anie.201503657 [3] F. Liebau, Structural Chemistry of Silicates; Springer, Berlin, 1985. [4] The term dreier (sechser, zehner)ring was coined by Liebau and is derived from the German word “drei” (”sechs”, “zehn”). A dreier (sechser, zehner) ring comprised three (six, ten) tetrahedra centers.

PMon140

Using muSR to investigate solid state materials: frustration in double perovskites

Coomer, Fiona (ISIS Neutron & Muon Source, Didcot, GBR); Cussen, Edmund (University of Strathclyde, Glasgow, GBR)

Muon spectroscopy, using spin polarised muons, has many applications in the field of solid state chemistry. The magnetic moment of the muon means that implanted muons can act as a local magnetometer, probing the behaviour of magnetic systems, as well as that of superconductors and of charge transport in materials. Positively charged muons can also act as a light analogue of the proton, giving rise to applications such as investigating the behaviour of hydrogen in materials and light particle diffusion.

An overview of the µSR technique and the capabilities of the ISIS pulsed muon source will be presented, focusing in particular on areas that will be of interest to the solid state chemistry community. Examples will be given of cases where µSR has been used, along with other complimentary techniques, to elucidate unusual behaviour in some geometrically frustrated magnetic systems including the valence bond glass $Ba_2LuMoO_{6,1}$ and unusual magnetic ordering in $Ba_2MnMoO_{6.2}$

---

[1] F. C. Coomer and E. J. Cussen, J. Physics: Condens. Matter 2013, 25, 082202.
[2] F. C. Coomer, E. J. Cussen, A. D. Hillier and S. Ramos. In preparation.

PTue001

Hybrid Gold/Thiolates Nanoparticles: Control of Surface Properties and Characterizations, Insertion in Porous Materials

Bouyon, Tracy (Aix Marseille Université CNRS MADIREL UMR 7246, MARSEILLE cedex 20, FRA); Prabhakaran, Rathinasabapathi (Bharathiar University, Coimbatore, IND); Denoyel, Renaud (Aix Marseille Université CNRS MADIREL UMR 7246, MARSEILLE cedex 20, FRA); Dallemer, Frederic (Aix Marseille Université CNRS MADIREL UMR 7246, MARSEILLE cedex 20, FRA)

Based on our skill related to synthesis, characterizations and applications of metal complexes, (1) we extend it up to the nanometric scale, in order to benefit from controlled surface properties.

Syntheses of nanoparticles are developed according to the bottom-up approach. The reduction of gold salts, in the presence of ligands, leads to the formation and stabilization of gold nanoparticles embedded in organic ligands. We optimized synthesis protocols, developed efficient purification and separation processes, for the preparation of nanoparticles combining:

- Metallic core atoms, with a large proportion of surface atoms, are offering high sensitivity to the environmental molecules. We are developing gold nanoparticles, as they are exhibiting stable metallic properties, relative to humidity and oxygen.
- An organic functional shell, based on different functionalized thiolates, controlling the surface properties (the way the nanoparticles interact with their environment). According to this control, the hybrid nanoparticles can be solubilized in different solvents (organic or aqueous), and dried from them. The first benefit is acceding to a large array of quantitative molecular characterization methods, including NMR and UV-visible spectroscopy.

In combination with material science analysis, based on MADIREL’s expertise (mainly thermogravimetry, absorption studies and electronic microscopy), we are able to us to study the metallic/organic interface. So, we can get an accurate picture of the nanoparticle surface. This is critical to control their behavior and acceed to the fine tuning of their properties, for demanding applications.
We took advantage of this approach to control the homogeneous impregnation of the nanoparticles into the matrix of mesoporous SBA-15 silica. So, we developed either dispersed nanoparticles or inserted ones, for their use in liquid state or solid state.

Hybrid metallic nanoparticles are versatile materials, leading to unique properties. (2) Development of this work is allowing us to target two specific areas, where the strict control of the purity of the object and their surface properties is crucial.
In one hand, we are targeting homogeneous and heterogeneous oxidation catalysis, based on previous industrial involvement. This is a major tool for synthesis and for various applications, with the still living challenge to get both high productivity and high selectivity.
On the other hand, we are looking forward therapeutic uses. The control of the surface properties should address biocompatibility issues and the tuning of the interactions with drugs, in order to protect and to vectorise them.

---

[1] New palladium(II) complexes of 3-methoxysalicylaldehyde-4(N)-substituted thiosemicarbazones: Synthesis, spectroscopy, X-ray crystallography and DNA/protein binding study, Kalaivani P., Umadevi C., Prabhakaran R., Dallemer F., Mohan P. S., Natarajan K.,
Polyhedron, 2014, 80, 97

[2] Gold Nanoparticles: Assembly, Supramolecular Chemistry, Quantum-Size-Related Properties, and Applications toward Biology, Catalysis, and Nanotechnology, Astruc D., Daniel M.C., Chem. Rev., 2004, 104, 293

PTue002

New positive nanosheets from the exfoliation of dimensional oxybromide for oriented thin films deposit

Daviero, Sylvie (Unité de Catalyse et Chimie du Solide, Villeneuve d'Ascq, FRA); Blázquez Alcover, Ignaicio (UCCS UniteŽ de Catalyse et Chimie du Solide, Villeneuve d'Ascq, FRA); Huvé, Marielle (UCCS UniteŽ de Catalyse et Chimie du Solide, Villeneuve d'Ascq, FRA); Roussel, Pascal (UCCS UniteŽ de Catalyse et Chimie du Solide, Villeneuve d'Ascq, FRA); Mentre, Olivier (UCCS UniteŽ de Catalyse et Chimie du Solide, Villeneuve d'Ascq, FRA)

Nowadays, there is a growing interest for “designing” new solids through “chimie douce” processes, which involve low-temperature modifications of solids where elementary structural units are re-organized into metastable phases.[1] In this context, the proposition of novel elementary blocks to be assembled is sought, especially in form of highly reactive exfoliated 2D-inorganic nanosheets. Various layered phases like smectite clays, metal chalcogenides, oxides or hydroxides etc… have been delaminated into their elementary layers in aqueous or organic solvent via soft chemical procedures.[2] However, most exfoliations lead to negatively charged nanosheets, which can be recombined with positive-charged counter-ions (inorganic or organic polycations…). Available positive blocks remain limited because only few structural types are compatible. They mostly belong to LDHs phases or rare-earth hydroxides, where various anions can intercalate (hydroxides, carbonates, organics anions…).

To develop new positive 2D-building blocks, we have focused on the mixed $Co^{3+/4+}$ oxo-bromides, 14H-$Ba_7Co_6BrO_{17}$ and 18R-$Ba_6Co_5BrO_{14}$ developed in our laboratory.[3] They are built of ferromagnetic hexagonal-perovskite blocks, separated by $[Ba_2O_2Br]^-$ spacers, where presence of disorder and CO_3^{2-} defects strongly suggests an easy anion-exchange. In the present communication, we show the efficient exfoliation of these compounds in butanol, leading to nanoflakes and Zetametry measurements confirm that particles in colloidal suspension are positively charged. Full structural characterizations were performed by TEM, EDS, Raman and IR spectroscopies and AFM, completed by X-ray absorption spectroscopy (XANES and DANES) and synchrotron X-ray diffraction (in-plane and out of plane) performed at SOLEIL (Saint Aubin, France). Combination of all these techniques shows crystalline flat particles ~50nm large. XAS and DANES spectra, confirm the preservation of the local cobalt environment after the exfoliation process as well as the $Co^{3+/4+}$ mixed oxidation degree. In addition, synchrotron X-ray diffraction, has allowed direct characterization of the sheets after deposition on silicon substrate, ie. a strong preferential orientation along the 00l direction, confirmed by a small mosaicity (3.4°). Furthermore, diffractograms recorded in-plane are close to the original phase, confirming the preservation of the elementary blocks structure. Thus, we can conclude that exfoliation process occurs keeping the global structure of the elementary blocs, creating new positive elementary units with potential intrinsic ferromagnetic properties, which can be used for thin film deposition.

---

[1] Clearfield A. Chem. Rev. (1988) 88 (1):125-148; Ranmohotti K . et al. Advanced Materials (2011) 23 (4):442-460; Schaak R.E. et al. Chem. Mater. (2000), 12, 2513-25; Hayward M. Semicond. Sci. Technol (2014) 29, 064010

[2] Smith R. J.et al. Adv. Mater. 2011, 23, 3944–3948; Sasaki, T., J. Ceram. Soc. Jpn. 2007, 115, 9-16. ; Ma R. Z. et al. Recent Patents on Nanotechnology, vol. 6, pp. 159-168, Nov 2012

[3] Kauffmann M. et al., Acta Cryst. B63, 589-596 (2007); Mentré O. et al. Solid State Sci (2008) 10 (4):471-475

PTue003

Synthesis and luminescent properties of mixed rare earth phosphate/vanadate hollow particles

de Sousa Filho, Paulo Cesar (University of São Paulo, Ribeirão Preto, BRA); Gacoin, Thierry (Ecole Polytechnique, Palaiseau, FRA); Boilot, Jean-Pierre (Ecole Polytechnique, Palaiseau, FRA); Serra, Osvaldo (University of São Paulo, Ribeirão Preto, BRA)

Rare earth (RE) phosphates and vanadates comprise two of the most important classes of inorganic luminescent materials, and their advantageous emission properties are widely explored from a long time [1]. Despite displaying similar crystal structures, RE phosphates and vanadates present remarkably distinct spectroscopic properties due to the particular microenvironments provided to RE ions, as well as to different absorption/energy transfer mechanisms and band structures.[1] This, in turn, enables the design of $REPO_4$-$REVO_4$ heteromicro- and nano- structures with several compositions, which can combine the advantageous properties of the two phases in order to provide luminescent materials with improved activity. In this sense, the $REPO_4$-$REVO_4$ structures can be tuned with focus on different applications, such as phosphors for solid state lighting (illumination/visualisation), biological labeling, and (photo)catalysis, for instance. For this, properties such as crystallinity, density/porosity, and particle sizes, shapes and defects must be adequately controlled by means of the synthetic methodologies, which makes liquid phase approaches notably important to this end. Moreover, for the particular aim of biolabeling systems, RE-based hollow structures are proved to be highly attractive, since they can provide an enhanced contact between the active sites and the biological medium, thus resulting in more efficient agents for cell or tissue bioimaging. In addition, the cavities of this class of structures can be applied to drug storage and delivery, which enables these compounds to act as sophisticate platforms for theranostics[2].

In this sense, this work describes the preparation of hollow $REPO_4$-$REVO_4$ particles for potential applications in biolabeling systems. For this, a two-step sacrificial template methodology is applied, starting from colloidal RE hydroxycarbonate microspheres [3]. The solid $RECO_3OH.xH_2O$ particles are hydrothermally treated in the presence of the phosphate and, subsequently, vanadate precursors, which leads to the decomposition of the hydroxycarbonate phase and to the formation of highly crystalline $REPO_4$-$REVO_4$ domains. As the diffusion of RE3+ ions from the particle core to the solid-liquid interface is faster than the diffusion of PO_4^{3-}/VO_4^{3-} groups from the solution towards the particle core, the crystallization is favoured to occur towards the exterior of the precursor structures, thus resulting in the hollow particles. Due to the application of separated growth steps, the final particles consist in a phosphate-rich inner shell and in a vanadate-rich outer shell. The obtained solids were characterized with regard to their structure, morphology and surface properties, which point to the efficient obtainment of tetragonal phosphates/vanadates. The phase separation between the phosphate and vanadate phases is further confirmed by the acquired luminescent properties, in which the distinct spectroscopic behaviour of Eu^{3+} in the YVO_4 and YPO_4 hosts can be observed. Therefore, the obtained hollow particles can be applied for the development of luminescent biosensors, particularly for the intracellular detection of oxidizing agents through the emissions of Eu^{3+} in the phosphate and vanadate phases.

PCdSF and OAS thank the Brazilian agencies CAPES, CNPq, and FAPESP for the financial support.

---

[1] J.C. Batista, P.C. de Sousa Filho, O.A. Serra; *Dalton Trans.*, **2012**, *41*, 6310.

[2] X. Kang, C. Li, Z. Cheng, P. Ma, Z. Hou, J. Lin; *WIREs Nanomed. Nanobiotech.* **2014**, *6*, 80.

[3] Y. Jia, T.-Y. Sun, J.-H. Wang, H. Huang, P. Li, X.-F. Yu, P.K. Chu; *CrystEngComm* **2014**, *16*, 6141.

PTue004

Towards new subvalent compounds - the new nitridoborate $Ba_{23}(BN_2)_{11}(B(N/O)_3)_3N_{3-x}$

Wörsching, Matthias (Ludwig-Maximilians-Universität München, München, GER); Datz, Stefan (Ludwig-Maximilians-Universität München, München, GER); Hoch, Constantin (Ludwig-Maximilians-Universität München, München, GER)

Since the discovery of the alkali metal suboxides by Simon in the 1970s the coexistence of ionic and metallic bonding in cluster compounds has been subject to much research. [1] In the 1990s earth alkaline metal subnitrides extended the number of subvalent compounds. [2]

Recent studies of ternary suboxometallates Cs_9MO_4 (M = Al, Ga, In, Fe, Sc) [3] and $Cs_{10}MO_5$ (M = Al, Ga, Fe) with oxometallate anions instead of uniatomar oxide or nitride anions embedded in the metallic matrix lead to new cluster entities and a greater variety for the anionic substructure. The comparison of suboxides and subnitrides with the new suboxometallates suggested the synthesis of alkaline earth metal subnitridometallates to extent the plethora of subvalent compounds.

In analogy to the synthesis of suboxometallates from Cs_2O, Cs and M_2O_3, a synthetic route based on the reaction of Ba_2N, Ba and the respective metal nitrides was chosen. Significantly higher reaction temperatures were needed for the subnitridometallates than for suboxometallates in order to achieve sufficient reactivity of the reagents, affording for *h*-BN as crucible material.

The reaction mixture showed considerable reactivity towards *h*-BN at temperatures as high as 1000 °C, leading to several ternary and quaternary B and N-containing compounds. When not precleaned properly, larger amounts of oxygen in the crucible led to the formation of $Ba_4(BN_2)_2O$. [4] In the presence of minor traces of oxygen the reaction yielded a mixture of $Ba_3(BN_2)_2$ [5] and the new compound $Ba_{23}(BN_2)_{11}(B(N/O)_3)_3N_{3-x}$ forming black, brittle crystals with metallic luster. It crystallizes in the trigonal space group P-31c with a = 11.4087(16) and c = 23.045(5) Å. Structure solution and refinement with anisotropical treatment of all atomic displacement parameters yielded the residual coefficients $R1$ = 0.0367 and $wR2$ = 0.0895. The crystal showed rotational twinning.

The structure features linear $[BN_2]^{3-}$, trigonal planar $[B(O/N)_3]^{y-}$ and isolated N^{3-} anions. The N^{3-} anions are coordinated octahedrally by six Ba atoms. The N atoms in $[BN_2]^{3-}$ are coordinated in the form of a strongly distorted octahedron of six Ba atoms, whereas the disordered N/O atoms in the $[B(O/N)_3]^{y-}$ units are coordinated by a strongly distorted octahedron of five equidistant Ba atoms and one B atom.

Existence of the anionic entities was verified by single crystal Raman spectroscopy and is in accordance with literature data.[5, 6]

---

[1] A. Simon, H. J. Deiseroth, *Rev. Chim. Miner.* 1976, **13**, 98-112.

[2] P. E. Rauch, A. Simon, *Angew. Chem.* 1992, **104**, 1505-1506; *Angew. Chem. Int. Ed.* 1992, **31**, 1519-1521; P. E. Rauch, A. Simon, *Angew. Chem.* 1994, **106**, 713-715; *Angew. Chem. Int. Ed.* 1994, **33**, 689-691; G. J. Snyder, A. Simon, *J. Am. Chem. Soc.* 1995, **117**, 1996-1999.

[3] C. Hoch, J. Bender, A. Simon, *Angew. Chem.* 2009, **121**, 2451-2453; *Angew. Chem. Int. Ed.* 2009, **48**, 2415-2417; C. Hoch, J. Bender, A. Wohlfahrt, A. Simon, *Z. Anorg. Allg. Chem.* 2009, **635**, 1777-1782.

[4] J. Curda, U. Herterich, K. Peters, M. Somer, H. G. von Schnering, *Z. Kristallogr.* 1994, **209**, 181.

[5] O. Reckeweg, F. J. DiSalvo, M. Somer, *J. Alloys Compd.* 2003, **361**, 102-107.

[6] G. Padmaja, P. Kistaiah, *J. Phys. Chem.* 2009, **A113**, 2397-2404.

PTue005

Collapsing transition metal oxohalides as negative electrode materials for lithium ion batteries

Renman, Viktor (Dept. of Chemistry - Ångström Laboratory, Uppsala University, Uppsala, SWE); Hu, Shichao (Dept. of Materials and Environmental Chemistry, Stockholm University, Stockholm, SWE); Zimmermann, Iwan (Dept. of Materials and Environmental Chemistry, Stockholm University, Stockholm, SWE); Pay-Gómez, Cesar (Dept. of Chemistry - Ångström Laboratory, Uppsala University, Uppsala, SWE); Johnsson, Mats (Dept. of Materials and Environmental Chemistry, Stockholm University, Stockholm, SWE); Edström, Kristina (Dept. of Chemistry - Ångström Laboratory, Uppsala University, Uppsala, SWE)

The main types of negative electrode materials for Li-ion cells are based either intercalation, alloying or conversion reactions - with the conventional material of choice being the intercalation material graphite, which can accommodate one lithium for every six carbon atoms . Some alloying materials include silicon, tin and antimony. Alloying-type reactions generally occur at low potentials vs. Li/Li^+ and show relatively good reaction kinetics. The main concern regarding alloying reactions, however, is the expansion/contraction exerted by repeated insertion of Li^+ , which leads to poor cyclability over time. Storage of Li in the family of conversion materials is based on the reversible conversion of metal oxides into metallic nanoclusters and lithium oxide. This generally occurs at higher potentials and with larger voltage polarization between the charge and discharge processes. We have performed an electrochemical and structural investigation on two transition metal oxohalides of varying dimensionality - Ni3Sb4O6F6 [1] which has a framework structure and the layered $Mn_2Sb_3O_6Cl$ [2].

These materials allow for the combination of the two previously described reaction mechanisms within the same cell, giving rise to interesting electrochemical behaviours. The relatively open structures are believed to facilitate insertion of Li. Both compounds are shown to react reversibly with Li, with good cyclability, in complex systems where competing reactions occur sequentially and/or simultaneously. Operando XRD studies reveal both materials undergo amorphization during the early stages of lithiation, leading to finely dispersed nanoclusters of Sb and the TM, which then undergoes conversion reactions as well as alloying reactions with continued cycling. In addition to the electrochemical interpretation, XANES was used to more closely monitor the reaction mechanism during the first discharge-charge cycle.

---

[1] Hu, S., et al., Acentric Pseudo-Kagome Structures: The Solid Solution (Co1–xNix)3Sb4O6F6. Chemistry of Materials, 2014. 26(12): p. 3631-3636.

[2] Zimmermann, I. and M. Johnsson, A Synthetic Route toward Layered Materials: Introducing Stereochemically Active Lone-Pairs into Transition Metal Oxohalides. Crystal Growth & Design, 2014. 14(10): p. 5252-5259.

PTue006

Encapsulation of Lipophilic Dyes and Drugs in Hydrophilic ZrO(HPO_4) shells

Rein, Viktor (Karlsruhe Institute of Technology (KIT), Karlsruhe, GER); Feldmann, Claus (Karlsruhe Institute of Technology (KIT), Karlsruhe, GER)

The use of lipophilic compounds (dyes, drugs) in medical diagnostics and therapy is generally limited due to poor water solubility and, therefore, low bioavailability. In order to enable oral or parenteral administration, these compounds require appropriate carrier systems composed of a lipophilic core and a hydrophilic shell. Although many examples such as *o/w*-micelles, solid-lipid nanoparticles or liposomal formulations have been described in the literature, until now only a few resulted in commercial products [1].

A promising approach is the encapsulation of lipophilic compounds in inorganic nanoparticles exhibiting hydrophilic surfaces and, therefore, good dispersibility in aqueous media. Thereby, zirconyl phosphate emerged as a capable inorganic material for carrier systems in medical applications, as it shows high biocompatibility [2].

Microemulsions are defined as optically isotropic and thermodynamically stable systems of water, oil and surfactant. As the diameter of micelles in microemulsions is in the 5 – 50 nm range, they represent suitable templates for nanoparticle synthesis [3]. In addition, *o/w*-microemulsions offer the opportunity to dissolve considerable amounts of lipophilic compounds inside of the micelles.
In this contribution, we report on the template-assisted encapsulation of lipophilic compounds via a novel *o/w*-microemulsion based approach. For this purpose, an *o/w*-microemulsion composed of water, sodium monododecylphosphate as surfactant, *n*-butanol as cosurfactant and toluene as oil-phase was established. The encapsulation was performed by coating the micelles with a ZrO(HPO_4) shell, thus enclosing the dissolved lipophilic compound inside of the formed nanoparticles.

Due to sensitivity of fluorescence spectroscopy, first of all, the concept was tested with the organic fluorescent dye Lumogen® Red. The obtained nanoparticles are spherical in shape and have an average diameter of 50 nm. Aqueous suspensions show intense red fluorescence as well as considerably increased photostability [4]. Finally, the strategy can be extended to the encapsulation of lipophilic drugs in order to improve their availability for medical therapy.

---

[1] A. Fahr, X. Liu, *Expert Opin. Drug Deliv.***2007**, *4*, 403.
[2] M. Roming, H. Lünsdorf, K. E. J. Dittmar, C. Feldmann, *Angew. Chem.* **2010**, *122*, 642.
[3] D. H. M. Buchold, C. Feldmann, *Adv. Funct. Mater.***2008**, *18*, 1002.
[4] V. Rein, C. Feldmann, **2015**, *in preparation*.

PTue007

Enhanced kinetic stability of pure and Y-doped tetragonal ZrO_2

Penner, Simon (Institute of Physical Chemistry, University of Innsbruck, Innsbruck, AUT); Kogler, Michaela (Institute of Physical Chemistry, University of Innsbruck, Innsbruck, AUT); Köck, Eva-Maria (Institute of Physical Chemistry, University of Innsbruck, Innsbruck, AUT); Vanicek, Stefan (Institute of Inorganic and Theoretical Chemistry, University of Innsbruck, Innsbruck, AUT); Schmidmair, Daniela (Institute of Mineralogy and Petrography, University of Innsbruck, Innsbruck, AUT); Götsch, Thomas (Institute of Physical Chemistry, University of Innsbruck, Innsbruck, AUT); Stöger-Pollach, Michael (University Service Center for Transmission Electron Microscopy (USTEM), Vienna, AUT); Klötzer, Bernhard (Institute of Physical Chemistry, University of Innsbruck, Innsbruck, AUT)

The kinetic stability of pure and yttrium-doped tetragonal zirconia (ZrO_2) polymorphs prepared via a pathway involving decomposition of pure zirconium and zirconium+yttrium isopropoxide is reported. Following this preparation routine, high-surface area, pure and structurally stable polymorphic modifications of pure and Y-doped tetragonal zirconia are obtained in a fast and reproducible way. Combined analytical high-resolution *in-situ* transmission electron microscopy, high-temperature X-ray diffraction, chemical and thermogravimetric analysis reveals that the thermal stability of the pure tetragonal ZrO_2 structure is very much dominated by kinetic effects. Tetragonal ZrO_2 crystallizes at 400°C from an amorphous ZrO_2 precursor state and persists the further substantial transformation into the thermodynamically more stable monoclinic modification at higher temperatures at fast heating rates. Lower heating rates favor the formation of an increasing amount of monoclinic phase in the product mixture, especially in the temperature region around 600°C and during/after re-cooling. If the heat treatment is restricted to 400°C even under moist conditions, the tetragonal phase is permanently stable, regardless of the heating or cooling rate and, as such, can be used as pure catalyst support without the addition of cationic or anionic stabilizers. In contrast, the corresponding Y-doped tetragonal ZrO_2 phase retains its structure independent of the heating or cooling rate or reaction environment. Pure tetragonal ZrO_2 can now be obtained in a structurally stable form, allowing its structural, chemical or catalytic characterization without in-parallel triggering of unwanted phase transformations, at least if the annealing or reaction temperature is restricted to $T \leq 400°C$.

PTue008

Fracture Toughness of Epoxy Semi-IPN Toughened with In-situ Polymerized Novel Polysulfone via Azide-alkyne Click Reaction.

Lee, Bum Jae (Chungnam National University, Daejeon, KOR); Sat Byeol, Park (Chungnam National University, Daejeon, KOR); Wu Bin, Ying (Chungnam National University, Daejeon, KOR); Ji Uk, Jang (Chungnam National University, Daejeon, KOR); Jin Yong, Seol (Chungnam National University, Daejeon, KOR); Jong Kyu, Park (Agency for Defense Development, Daejeon, KOR)

In order to maintain the thermal resistance and toughness of a cured toughened epoxy resin together with the reduced viscosity of resin composition in the high performance thermoplastic-toughened epoxy resins, the novel synthetic methodology in which the thermoplastic polymer, novel polysulfone, was formed simultaneously via azide-alkyne click reaction during the epoxy cure process, was investigated. The epoxy resin based on triglycidyl p-aminophenol(TGAP) and 4,4'-diaminodiphenylsulfone(DDS) was mixed with the diazide monomer (1,4-bis(azidomethyl)benzene, BAB) and diacetylene monomer (4,4-sulfonylbis(propynyloxy)benzene, SPB), and the novel polysulfone-type thermoplastic engineering polymer as toughening agent was formed the thermoplastic polymer by in-situ azide-alkyne click polymerization reaction during the cure process of the epoxy resin. The click reaction and epoxy-amine cure reaction was revealed to proceed independently. When even 20wt% polyethersulfone (PES) was replaced by the same percentage of BAB and SPB monomers, the viscosity of resin composition(61cP at 135℃) decreased drastically by about 1/4800 compared with that of the preformed PES-toughened system(2.97×105cP at 135℃). The fracture tougheness (K1c) of semi-IPN’s of crosslinked epoxy and linear novel polysulfone was improved to 1.9MN · m3/2 which was about 2.11 times higher than that of the unmodified epoxy resin(0.9MN · m3/2) at the level of 5wt% in-situ toughening agent. The Tg of in-situ poly(p-BAB/SPB) toughened epoxy resin was similar to the unmodified TGAP-DDS resin(Tg~200℃). The improvement in heat and fracture toughness of in-situ poly(p-BAB/SPB) toughened epoxy resin is attributed to the characteristic uniform dispersity of finer spherical domain(50~200nm) revealed by SEM observation, compared with the counterpart with the preformed polyethersulfone-toughened epoxy resin.

PTue009

Halogenidoaluminate Salts of the Intermetalloid Cluster Cation $[Bi_{12}Ni_2]^{4+}$- Synthesis in Ionic Liquids, Crystal Structure and Chemical Bonding

Müller, Ulrike (Technische Universität Dresden, Dresden, GER); Isaeva, Anna (Technische Universität Dresden, Dresden, GER); Ruck, Michael (Technische Universität Dresden, Dresden, GER)

Endohedral clusters can possess interesting properties, for example superconductivity in $M@C_{60}$ (M = La^+, K^+, Cs^+) [1]. In the past decade also polyhedral clusters of the heavier main group elements embedding transition metal elements were discovered [2]. Such intermetalloid cluster compounds are typically synthesized via solid state reactions or in solution with organic solvents. In our group, the crystallization of the tetrabromidoaluminate salts of the filled polycations $[Rh@Bi_9]^{4+}$ and $[Pd@Bi_{10}]^{4+}$ was reported by dissolution of solid state precursors in ionic liquids (ILs) [3].

ILs are salts that are liquid below 100 °C. In comparison to other reaction media, ILs show several advantages, for instance negligible vapor pressure, low melting point, high polarity and a wide liquid range. Their versatility for inorganic material syntheses is currently under investigation [4].

Crystals of the halogenidoaluminate salts of the binary intermetalloid cluster cation $[Bi_{12}Ni_2]^{4+}$ were obtained by reacting bismuth and the respective nickel dihalide in the Lewis-acidic IL $BMImX{\cdot}5AlX_3$ (X = Cl, Br) at 180 °C. $[Bi_{12}Ni_2]^{4+}$ is isoelectronic to the ternary intermetalloid cluster anion $[Pb_7Bi_5Ni_2]^{3-}$ [5]. In $[Bi_{12}Ni_2]^{4+}$ the Ni atoms are embedded in two base-sharing square antiprisms of Bi atoms. In a first description the $[Bi_{12}Ni_2]^{4+}$ cluster can be regarded as a triple-decker complex of Ni^{2+} ions and two terminal Bi_4^{2-} squares and four equatorial Bi^+ ions. The 18 electron rule for the transition metal in oxidation state +II (8 valence electrons) is fulfilled with the Hückel aromatic Bi_4^{2-} rings being 6e− donors and the four Bi atoms donating one electron to each of the Ni atoms. DFT-based calculations, however, propose Ni^{2+} cations surrounded by almost uncharged Bi atoms.

---

[1] a) J. R. Heath, S. C. O'Brien, Q. Zhang, Y. Lin, R. F. Curl, H. W. Kroto, F. K. Tittel, R. E. Smalley, *J. Am. Chem. Soc.***1985**, *107*, 7779−7780; b) F. D. Weiss, J. L. Elkind, S. C. O'Brien, R. F. Curl, R. E. Smalley, *J. Am. Chem. Soc.***1988**, *110*, 4464−4465; c) J. H. Schön, C. Kloc, B. Batlogg, *Nature***2000**, 408, 549−552.

[2] a) M. Ruck, V. Dubenskyy, T. Söhnel, *Angew. Chem.***2003**, *115*, 3086−3090; *Angew. Chem. Int. Ed.***2003**, *42*, 2978−2982; b) M. Ruck, *Angew. Chem.***1997**, *109*, 2059−2062; *Angew. Chem. Int. Ed.***1997**, *36*, 1971−1973; c) B. Wahl, M. Erbe, A. Gerisch, L. Kloo, M. Ruck, *Z. Anorg. Allg. Chem.***2009**, *635*, 743−752; d) F. Lips, S. Dehnen, *Angew. Chem.***2009**, *121*, 6557−6560; *Angew. Chem. Int. Ed.***2009**, *48*, 6435−6438; e) V. Hlukhyy, H. He, L.-A. Jantke, T. F. Fässler, *Chem. Eur. J.***2012**, *18*, 12000−12007.

[3] M. F. Groh, M. Ruck, *Z. Anorg. Allg. Chem.***2014**, 640, 2391.

[4] a) P. Wasserscheid, T. Welton, *Ionic Liquids in Synthesis* Wiley-VCH, Weinheim, **2007**; b) E. Ahmed, J. Breternitz, M. F. Groh, M. Ruck, *CrystEngComm***2012**, *14*, 4874−4885; c) A. M. Guloy, R. Ramlau, Z. Tang, W. Schnelle, M. Baitinger, Y. Grin, *Nature***2006**, *443*, 320−323; d) D. Freudenmann, C. Feldmann, *Dalton Trans.***2011**, *40*, 452−456.

[5] R. Ababei, J. Heide, M. Holynska, G. Thiele, B. Weinert, X. Xie, F. Weigend, S. Dehnen, *Chem. Commun.***2012**, *48*, 11295−11297.

PTue010

Intercalation Compounds from LiH and Graphite: Relative Stability of Metastable Stages and Thermodynamic Stability of Dilute Stage Id

Konar, Sumit (Stockholm University, Stockholm, SWE); Häussermann, Ulrich (Stockholm University, Stockholm, SWE); Svensson, Gunnar (Stockholm University, Stockholm, SWE)

Lithium graphite intercalation compounds (Li-GICs) were revisited by heating homogeneous mixtures of lithium hydride (LiH) and graphite.[1] Stages I (LiC_6, Aα), IIa ($Li_{0.5}C_6$, AαA), IIb ($Li_{\sim0.33}C_6$, AαABβB), III ($Li_{\sim0.22}C_6$, AαAB), IV ($Li_{\sim0.167}C_6$), and dilute stage lithium Id have been analyzed by powder X-ray diffraction (PXRD) and Raman spectroscopy. Rietveld refinement of PXRD patterns allowed unambiguous structure characterization of the various Li-GICs as well as the determination of weight fractions of phases in the multicomponent product. The essence of our findings is as follows: (1) Formations of metastable Li-GICs and thermodynamically stable lithium carbide (Li_2C_2) are competitive and dependent on time, temperature and stoichiometry. (2) Kinetically driven intercalation is favored over carbide formation at temperatures below 500 °C. (3) Increasing temperature in the interval of 400- 500 °C and increasing LiH activity promotes the rate and degree of intercalation. The highest intercalated stage achieved at 400, 450, and 500 °C is IIb, IIa, and I, respectively. (4) Lower staged (highly intercalated) Li-GICs are metastable with respect to deintercalation into higher staged (less intercalated) Li-GICs with the exception of stage IIa, which can be preserved for several days in the presence of LiH. This distinguished behavior of IIa toward thermally induced deintercalation is attributed to a kinetic barrier for altering AA- into AB-type layer stacking. (5) At temperatures above 500 °C, stage I was observed and it was followed by Li_2C_2 carbide formation. Most likely, the thermodynamically stable carbide is a product of the decomposition of stage I. (6) Dilute stage lithium Id coexists with Li_2C_2 at temperatures up to 800 °C and that the Li content of Id (solubility of Li in graphite) increases between 550 and 800 °C. Consequently, Id with a temperature-dependent homogeneity range should be added as a stable phase in the Li-C phase diagram. A sketch of a revised Li-C phase diagram is provided.

---

[1]S. Konar, U. Häusserman, G. Svensson, Intercalation Compounds from LiH and Graphite: Relative Stability of Metastable Stages and Thermodynamic Stability of Dilute Stage Id, Chem. Mater. 27 (2015) 2566-2575. doi:10.1021/acs.chemmater.5b00235.

PTue011

Less-Noble Metal Nanoparticles

Schöttle, Christian (Karlsruhe Institute of Technology (KIT), Karlsruhe, GER); Feldmann, Claus (Karlsruhe Institute of Technology (KIT), Karlsruhe, GER)

A general synthesis of reactive, less-noble metal nanoparticles is performed via reduction of simple metal chlorides in ethers. This includes Mo^0, W^0, Fe^0, Ru^0, Re^0 and Zn^0 nanoparticles, which are obtained with diameters ≤ 10 nm and a narrow size-distribution. All nanoparticles are available either as powder samples or long-term stable suspensions.[1]

Metal nanoparticles, in general, show interesting and unusual properties due to their small size, large surface-to-volume ratio and quantum-confinement effects.[2] The relatively high number of surface atoms leads to a high reactivity of metal nanoparticles that, on the one hand, can be advantageous for the application in catalysis or chemical synthesis. Especially for less-noble metal nanomaterials, the high reactivity, on the other hand, is a challenge. Synthesis and handling becomes the more difficult, due to oxidation, hydrolysis and agglomeration, the smaller the particles are and the less noble the metal is.[3,4] Therefore, access to high-quality nanoparticles of less-noble metals is still limited.

We addressed the challenge based on liquid-phase syntheses by using strong reducing agents.[5] In addition to our work on less-noble metal nanoparticles, the high reactivity of the nanoparticles is used in direct follow-up reactions. Metal sulfide, arsenide, carbide, nitride or alloy nanoparticles are prepared of similar size (≤ 10 nm) as the pristine metal nanoparticles. To meet the requirements of the synthesis, all reactions are carried out under strict inert-gas conditions, using purified, water- and oxygen-free solvents and chemicals.

---

[1] C. Schöttle, P. Bockstaller, R. Popescu, D. Gerthsen, C. Feldmann, *submitted*.
[2] C. Schöttle, P. Bockstaller, D. Gerthsen, C. Feldmann, *Chem. Commun.* **2014**, *50*, 4547–4550.
[3] F. Gyger, P. Bockstaller, D. Gerthsen, C. Feldmann, *Angew. Chem.* **2013**, *125*, 12671–12675.
[4] H. Goesmann, C. Feldmann, *Angew. Chem.* **2010**, *122*, 1402–1437.
[5] N. G. Connelly, W. E. Geiger, *Chem. Rev.* **1996**, *96*, 877–910.

PTue012

Lithium and alkaline-earth nitrides of group 13 and 14 metals: millimeter-sized single crystals from lithium melts

Hoehn, Peter (MPI-CPfS, Dresden, GER); Borrmann, Horst (MPI-CPfS, 01187, GER); Burkhardt, Ulrich (MPI-CPfS, Dresden, GER); Ovchinnikov, Alexander (MPI-CPfS, Dresden, GER); Schnelle, Walter (MPI-CPfS, Dresden, GER); Zechel, Kerstin (MPI-CPfS, Dresden, GER)

Metalide-nitrides [1] and nitridometalates [2] of main-group metals *M* represent interesting classes of solid state phases, which contain nitrogen as isolated N^{3-} anions or complex anions $[M_xN_y{}^{z-}]$ of different dimensionality with coordination numbers of *M* by N typically between two and four, respectively. Whereas the bonding within these complex anions and frameworks is essentially covalent, nitridometalates are stabilized by predominantly ionic bonding through counterions like alkali (*A*) or alkaline-earth (*AE*) cations. In contrast, bonding in metalide-nitrides is dominated by metallic and ionic interactions. Structural data for the majority of phases reported up to now had been derived from X-ray single crystal data, whereas single phase powder samples had to be employed for investigation of physical properties, since no suitably large single crystals were available.

Here we report on crystal growth experiments in lithium melts [3], which resulted in single crystalline specimens of up to 5 mm in length and 50 mm^3 in volume. Generally, due to the mode of preparation, the thermodynamically most stable phases are precipitated from the reaction mixtures of Li, Li_3N, AE_2N, and *M*, which leads to significantly different results concerning composition of products with respect to reaction temperatures and the alkaline-earth and main-group elements involved.

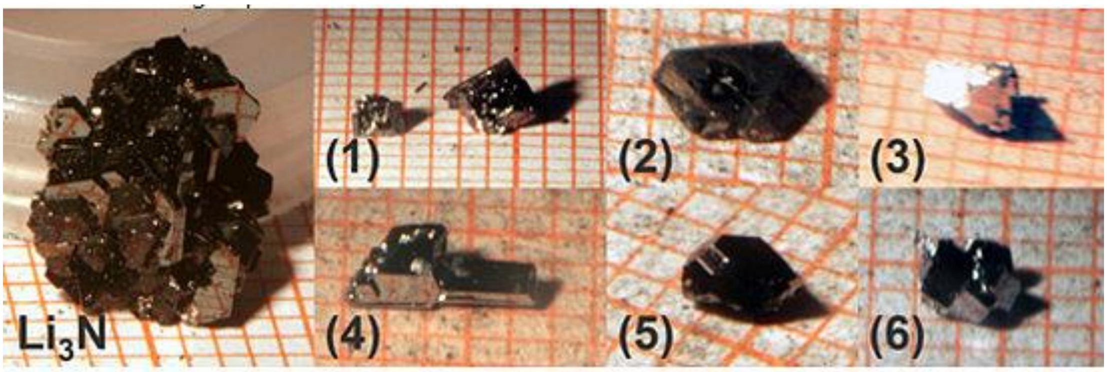

Millimeter-sized single crystals of a plethora of new phases (e.g. $Li_2Sr_6[Ga_4]N_2$ (**3**); $Li_{22}Ba_{12}[Ga_4]_4GaN_9$; $Li_{16}Sr_6M_6N$ (*M* = Ge, Sn (**6**), Pb); $Sr_3MN_{0.67}$ (*M* = Sn (**1**), Pb (**2**)); $Ba_3MN_{0.5}$ (*M* = Sn (**4**), Pb (**5**))) were obtained and their physical properties investigated as a function of crystal orientation.

---

[1] P. Höhn, G. Auffermann, R. Ramlau, H. Rosner, W. Schnelle, R. Kniep; *Angew. Chem. Int. Ed.***2006**, *45*, 6681-6685.
[2] G. Cordier, P. Höhn, R. Kniep, A. Rabenau; *Z. Anorg. Allg. Chem.* **1990**, *591*, 58-66.
[3] A. Jesche et al., *Nat. Commun.* 5:3333 doi: 10.1038/ncomms4333 (**2014**).

PTue013

Materials synthesis via polysaccharides assisted procedures

Stan, Alina (Institute of Physical Chemistry "Ilie Murgulescu", Bucharest, ROU); Munteanu, Cornel (Institute of Physical Chemistry "Ilie Murgulescu", Bucharest, ROU); Raut, Iulia (National Research and Development Institute for Chemistry and Petrochemistry - ICECHIM , Bucharest, ROU); Barjega, Ruxandra (National Institute for Lasers, Plasma and Radiation Physics, Magurele, ROU); Oana, Carp (Institute of Physical Chemistry "Ilie Murgulescu", Bucharest, ROU)

In the last decade, the increase receptiveness towards the environment, forced a reinventing of the nanotechnology in a green context. One of the Green Chemistry principles is the use of renewable raw materials and feedstocks whenever technically and economically practical, rather than depleting non-renewable materials. Certainly, the biomass is the most renewable feedstock in terms of volume produced. Unfortunately, far too little of the produced amounts of polysaccharides are currently used, the most decays and recycles along natural pathways. In these circumstances, finding efficient applications that add supplementary value should represents one the multidisciplinary research topic of this beginning of the millennium. Despite their indisputable green attributes (renewability, highly availability and nontoxic nature) associated with outstanding versatile functionalities, the implication of polysaccharides in the synthesis of different materials (metals, oxides, composites) is an insufficiently explored research issue of materials science. Herein we present several polysaccharides mediated protocols for oxides and oxide/polisaccharide and oxide/sulfides composites synthesis, procedure tailored in our case to zinc oxide. The selection of this oxide is not accidental, being known its extraordinary combination of properties (semiconducting, piezoelectric, pyroelectric, optical, antibacterial and (photo)catalytical ones) that generate a wide range-applications.

PTue014

Microwave-assisted Polyol Synthesis of $M_3Bi_2X_2$ (M = Ni, Pd; X =S, Se): Using Solution Chemistry to Access Ternary Metal-Rich Chalcogenides

Roslova, Maria (Department of Chemistry and Food Chemistry, Technische Universität Dresden, Dresden, GER); Heise, Martin (Department of Chemistry and Food Chemistry, Technische Universität Dresden, Dresden, GER); Ruck, Michael (Department of Chemistry and Food Chemistry, Technische Universität Dresden, Dresden, GER)

Traditionally, intermetallics and their chalcogenides are synthesized using high-temperature melting or powder sintering techniques, which generally provide thermodynamically stable structures and offer little control over morphology. Solution methods remain largely unexplored but in fact low-temperature solution strategies, which were recently shown to yield known binary intermetallic phases [1-3], may be attractive for synthesizing compounds with more complex structures and compositions. Here we report on a general strategy for synthesis of ordered antiperovskites with parkerite or shandite structure in the form of submicron particles that have not been previously reported. Our method doesn’t involve a classical solid state route and is based on microwave-assisted reduction of metal salts in ethylene glycol. For the ternary sulfides synthesis the corresponding metal salts and thiosemicarbazide (TSC) as a sulfur source were refluxed at 300 W for approximately 20 min. The described synthetic approach prevents binary sulfides formation due to a complexation reaction between M^{2+} as well as Bi^{3+} ions and TSC. Se powder or SeO_2 dissolved in the mixture of ethylenediamine and ethylene glycol proved to be a suitable selenium feedstock for the selenides preparation. The choice of reaction parameters allows control of particle size distribution.

---

[1] M. Heise, J.-H. Chang, R. Schönemann, T. Herrmannsdörfer, J. Wosnitza, M. Ruck, *Chem. Mater.* **2014**, *26*, 5640–5646.

[2] D. Köhler, M. Heise, A. I. Baranov, Y. Luo, D. Geiger, M. Ruck, M. Armbrüster, *Chem. Mater.* **2012,** *24*, 1639–1644.

[3] S. Jana, J. W. Chang, R. M. Rioux, *Nano Lett.* **2013,** *13,* 3618–3625.

PTue015

New polymorphs of lithium pyrophosphate

Raguz, Branimir (Bonn University, Bonn, GER); Glaum, Robert (Bonn University, Bonn, GER)

Up to now, two different polymorphs (monoclinic [1] and triclinic [2]) of lithium pyrophosphate have been described in literature. The triclinic form is typically obtained in high temperature solid state syntheses.

Here we report on two new polymorphs of $Li_4P_2O_7$ (trigonal and monoclinic). Those two, previously unknown phases were obtained by heating triclinic $Li_4P_2O_7$ for five minutes at 1000°C, well above its melting temperature of $T = 881.2$°C (determined by DTA), and quenching of the melt to ambient temperature. The quenched solid always consists of the two new forms. The ratio of these phases is variable. Careful annealing of the mixtures transforms them into the well-known triclinic form as single phase. Interestingly, the trigonal phase is converted at $T = 400$°C already, while for the monoclinic phase higher temperatures of $T = 470$°C are required [3].

The trigonal crystal structure was solved and refined from X-ray single crystal data ($Li_4P_2O_7$, $P3_212$, $Z = 3$, $a = 5.1699(2)$ Å, $c = 18.9722\ (8)$ Å, R1 = 0.018, wR2 = 0.051, Goof = 1.14). This crystal structure can be derived from a cubic close-packed array of oxide ions. There are two different types of oxide layers. The first type (layer A and C) contains the terminal oxide ions of the pyrophosphate groups and is fully occupied. In contrast, every third oxide layer (B, B', B") containing the bridging oxide ions of the pyrophosphate groups is occupied by only one third of the possible number of oxide ions. This leads to the stacking sequence A, $B_{1/3}$, C, A', $B'_{1/3}$, C', A", $B''_{1/3}$, C", A, … . The phosphorus atoms occupy the tetrahedral vacancies between layers A and B as well as B and C. The lithium ions are located in two thirds of the tetrahedral voids between layers C and A' (C'A", C"A), respectively.

By subtracting the reflections of the trigonal polymorph from the XRPD pattern of the phase mixture and indexing the remaining reflections with the computer program DICVOL [4], the unit cell for the unknown phase was obtained ($a = 7.899(3)$ Å, $b = 5.157(2)$ Å, $c = 7.549(3)$ Å, $\beta = 115.26(3)$°, FOM = 27.4 for 16 reflections). With this unit cell a structure model for the new monoclinic phase was derived by real space methods using the computer program ENDEAVOUR [5, 6]. The XRPD pattern simulated for the model complies reasonably well with the observed pattern.

Eventually, it was possible to substitute some lithium by copper(I) in the trigonal pyrophosphate according to $(Li_{1-x}Cu^{I}_{x})_4(P_2O_7)$. Cu, $Cu_2P_2O_7$ and $Li_4P_2O_7$ were used as starting materials in stoichiometric amounts. The reaction was performed in a sealed silica tube at 900°C for 10 days. To exclude reaction between the starting materials and the silica, the mixture was enveloped in copper foil. Up to 10% lithium could be substituted by copper(I), leading to the composition $(Li_{0.9}Cu^{I}_{0.1})_4(P_2O_7)$. Its crystal structure was also solved and refined from X-ray single crystal data ($(Li_{0.9}Cu^{I}_{0.1})_4(P_2O_7)$), $P3_212$, $Z = 3$, $a = 5.1978(3)$ Å, $c = 19.125(1)$ Å, R1 = 0.04, wR2 = 0.12, Goof = 1.09). In contrast to the tetrahedral coordination of the Li^+ ions in trigonal $Li_4P_2O_7$, the Cu^+ ions are shifted to the basal plane of the corresponding tetrahedral void, leading to a coordination by three oxide ions in the A and C layers. Interestingly, as indicated by the Guinier photographs, formation of the trigonal pyrophosphate phase seems to be favored by the incorporation of copper(I).

---

[1] O. V. Yakubovich, O. K. Mel'nikov, *Crystallogr. Rep.***1994**, *39*, 737.

[2] A. Daidouh, M. L. Veiga, C. Pico, M. Martinez-Ripoll, *Acta Cryst.***1997**, *C53*, 167. [3] B. Raguž, *part of planned Ph.D. thesis*, Bonn University.

[4] A. Boultif, D. Louër, *J. Appl. Cryst.***2004**, *37*, 724.

[5] Crystal Impact GbR, Endeavour 1.7, Bonn, Germany, **2009**. [6] H. Putz, J .C. Schön, M. Jansen, *J. Appl. Cryst.***1999**, *32*, 864.

PTue016

Phosphates of rare-earth elements and titanium: synthesis optimization and crystal structure study

Asabina, Elena (Lobachevsky State University of Nizhni Novgorod, Nizhni Novgorod, RUS); Shvarev, Ruslan (Lobachevsky State University of Nizhni Novgorod, Nizhni Novgorod, RUS); Pet'kov, Vladimir (Lobachevsky State University of Nizhni Novgorod, Nizhni Novgorod, RUS)

Phosphates with kosnarite structure ($KZr_2(PO_4)_3$, isostructural $NaZr_2(PO_4)_3$, NZP, and $Na_{1+x}Zr_2Si_xP_{3-x}O_{12}$, NASICON) exhibit high stability against high temperature, and aggressive media, efficient luminescent properties, high ionic conductivity. In the NZP structure, LO_6 octahedra (L is cation) and PO_4 tetrahedra share corners to form an $\{[L_2(PO_4)_3]^{p-}\}_{3\infty}$ framework. The extraframework sites with coordination numbers 6 and 8 may be occupied by cations in the oxidation states from +1 to +4 or remain vacant. The NZP phosphates of rare-earth elements and zirconium $R_{1/3}Zr_2(PO_4)_3$ are well-known and structurally studied, the literature data on their titanium analogues $R_{1/3}Ti_2(PO_4)_3$ may be found only for R = La [1]. This fact is explained by lower stability of $R_{1/3}Ti_2(PO_4)_3$ compared with other NZP compounds because of small titanium ionic radius, that determines structural cavity sizes for large R-cations. The purpose of the investigation is to study the possibilities of $R_{1/3}Ti_2(PO_4)_3$ (R = Y, La–Lu) compound synthesis, optimization of methodic for their obtaining and crystal structure peculiarities.

Among known synthesis methods of NZP phosphates, sol-gel or crystallization method from a solution of salts allows obtaining compounds at comparatively low temperatures, atmospheric pressure and doesn't require special equipment. Sol-gel and Pechini methods, the ceramic synthesis (including use of sintering aids) were tested for $R_{1/3}Ti_2(PO_4)_3$ obtaining. The starting reagents for synthesis were R^{3+} nitrate, $TiOCl_2$ and $NH_4H_2PO_4$ (or H_3PO_4) aqueous solutions. To choose the thermal treatment regime, the reaction mixtures were dried at 80°C, heated at 400°C and studied by differential thermal analysis (a Labsys TG-DTA/DSC device) between 25–900°C. The phase composition of the samples was studied by X-ray diffraction at a Shimadzu XRD-6000 diffractometer. The exothermic effects have been observed on the DTA curves at 730–790°C. Under the X-ray results, the samples, thermally treated at 750–1000°C, were phase mixtures of NZP-compound, TiP_2O_7 and R^{3+}-phosphates. Decomposition temperatures decreased from >1000°C for $La_{1/3}Ti_2(PO_4)_3$ to 750°C for $Lu_{1/3}Ti_2(PO_4)_3$.

The Pechini method, with using of ethylenglycol and citric acid, decreased the synthesis temperature due to high homogeneity of the starting reaction mixture. This method allowed us to increase the mass fraction of the target NZP product in the samples from 50 to 100%. For ceramic preparation, the samples were pressed from the reaction mixtures after treatment at 400°C; idem, but with the aid of 2% ZnO or with 3% V_2O_5. The results have shown that the most effective sintering aid is ZnO. Analogues to [2], the proposed sintering mechanism is based on Zn^{2+} substitution on the Ti^{4+} site in the phosphate structure, that should be compensated by the formation of oxygen vacancies in order to maintain charge neutrality. The thermal treatment of ceramics (with ZnO aid) at 750–800°C leaded to obtaining of single-phase NZP phosphates.

The dependence of unit cell parameters on R^{3+} ionic radii had anomaly on the Gd^{3+} compound, connected with its half-occupied 4f-electronic level. The $Pr_{1/3}Ti_2(PO_4)_3$ and $Gd_{1/3}Ti_2(PO_4)_3$ phosphates, obtained by the Pechini method, were structurally studied by the Rietveld method from the powder X-ray data. This compounds crystallized in the the R-3 space group with two types of octahedrally coordinated cavities, one of them is 2/3 occupied by R^{3+} ions.

The reported study was supported by RFBR, project 15-03-00716 a .

---

[1] Lightfoot P., Woodcock D. ICDD, No. 490611.

[2] Sukhanov M.V., Pet'kov V.I., Firsov D.V. // Inorganic Materials. 2011. V. 47. P. 753–757.

PTue017

Preparation Pr doped perovskite red phosphors by hydrothermal reaction

Kosaka, Tomomi (Tokyo Gakugei University, Koganei, Tokyo, JPN); Tanaka, Yuji (Tokyo Gakugei University, Koganei, Tokyo, JPN)

Pr^{3+} doped $CaTiO_3$ red phosphor has been commonly prepared by solid phase synthesis. The reason comes from that titanium reagents for liquid phase synthesis are susceptible to hydrolysis. Recently, water-soluble titanium complexes consisting of hydroxycarboxylic acid ligands were developed by professor Kakihana and his group. They also reported that pH condition of the complex solution has affected polymorphism of TiO_2 obtained by the hydrothermal reaction. They concluded that the structural similarity between the dissolved titanium complex molecules and the nuclei of TiO_2 phase is important for selective preparation. These interesting information imply that the structure of titanium complex has also effect to electric structure of titanium compound obtained from this complex. In this paper, we prepared Pr^{3+} doped $CaTiO_3$ powder from an aqueous solution consisted of water-soluble Titanium complex, $CaCl_2$, and $Pr(NO_3)_3{\cdot}6H_2O$ by hydrothermal method at 423K for 24h and investigated effects of ligands to the red emissions. The powders obtained by hydrothermal reaction were calcined at 923~1073K for 1h in air after drying at 358K for 18h. Glycolic, citric, and lactic acids were used for ligand of water-soluble titanium complex. The compositional ratios of titanium/glycolic, citric, and lactic acid in these complexes are reported 2/3, 1/1, and 1/3, respectively. On the case of glycolic and citric acid ligands, white precipitate was produced when calcium ion was added to titanium complex solution, whereas no precipitate was observed with lactic acid ligand. Because the stability of titanium complex has influenced to these phenomena, we controlled glycolic and citric acid concentrations for conducting the hydrothermal reaction under same condition. X-ray diffraction and Photoluminescence spectroscopy were employed to investigate crystal structure and fluorescence intensity of samples. With lactic acid ligand, XRD revealed that rutile phase was dominant structure indicating large amount of calcium ion weren’t precipitated. It was found that 30% of calcium ion still remain in supernatant solution by EDTA titration. Therefore we considered ways to increase calcium concentration in the precipitate produced after hydrothermal reaction. Then, it was clarified that increasing pH value of sample solution from 6 to 10 using NH3 solution lead to a formation of perovskite structure in the precipitate indicating calcium and titanium coprecipitation was occurred. Perovskite structure was also observed in the precipitate produced from glycolate solution at pH=9 and citrate solution at pH=6. Though, XRD analysis revealed that synthesis of perovskite single phase was difficult under our experimental condition, the red emission peak at 612nm was increased upon sintering above 923K in all samples consisting of perovskite structure. We also prepared reference sample through solid-state reaction of TiO_2, $CaCO_3$, and $Pr(NO_3)_3{\cdot}6H_2O$. However, the intensity of red emission was weak even if it sintered at 1023K. These findings indicated that our method enable us to develop electric structure for red emission by sintering at relatively low temperature due to homogeneously-dispersed metal ions in the precipitate.

PTue018

Silver Chromium(III) Phosphates: Syntheses, Equilibrium Relations, New Crystal Structures and De-intercalation Experiments

Schnabel, Anke (Universität Bonn, Bonn, GER); Glaum, Robert (Universität Bonn, Bonn, GER)

Up to now in the ternary system $AgO_{0.5}$ / $CrO_{1.5}$ / $PO_{2.5}$ only one chrystallographically well characterized phosphate, $AgCr_2(P_2O_7)(PO_4)$ [1], was known. Another one is mentioned in literature with cell parameters only, $AgCrP_2O_7$ [2, 3]. In the group of NASICON type phosphates $AgCrTa(PO_4)_3$ [4] has already been reported.

Syntheses of the silver chromium(III) phosphates as well as the studies on equilibrium relations were carried out by calcining precursors obtained by precipitation from aqueous solutions and subsequent calcining at various temperatures. Three new phosphates were synthesized: $Ag_3Cr(PO_4)_2$, $Ag_3 Cr_3(PO_4)_4$ and $Ag_9Cr_3(P_2O_7)_3(PO_4)_2$. Silver chromium phosphates $AgCrM(PO_4)_3$ (M = Ta [4], Nb) with NASICON type structure were also prepared by precipitation from aqueous solution followed by annealing in air. Crystallization of $Ag_3Cr_3(PO_4)_4$ was achieved by isothermal heating in sealed silica tubes (1000 °C, 14 days, I_2 as mineralizer).

Single-crystal structure analysis of $Ag_3Cr_3(PO_4)_4$ ($P2_1/a$, $Z = 2$, $a = 10.4444(6)$ Å, $b = 6.3257(3)$ Å, $c = 11.0065(7)$ Å, $\beta = 115.742(3)$ °, 154 param., 2416 ind. refl., $R1 = 0.096$, $wR_2 = 0.21$, Goof = 1.32) revealed a layer structure with two crystallographically independent chromium sites and a strong disorder of the silver ions. The structure consists of layers $[Cr_3(PO_4)_4]^{3-}$ which alternate with layers of silver ions.
Cell parameters of $Ag_3Cr(PO_4)_2$ ($C2/m$, $a = 8.4991(13)$ Å, $b = 5.2900(7)$ Å, $c = 7.3438(11)$ Å, $\beta = 95.014(12)$ °) and $Ag_9Cr_3(P_2O_7)_3(PO_4)_2$ (P-3c1, $a = 9.8697(6)$ Å, $c = 15.0460(14)$ Å) were determined from XRPD data in analogy to the isotypic phosphates $Ag_3In(PO_4)_2$ [5] and $Li_9Cr_3(P_2O_7)_3(PO_4)_2$ [6], respectively. Both structures are composed of layers where $[CrO_6]$ octahedra are connected to $[PO_4]$ tetrahedra via vertices while the silver ions are located in between the layers.

De-intercalation experiments were carried out with an excess of NO_2BF_4 in acetonitrile under argon atmosphere at room temperature. Other oxidants used were iodine and bromine. Topotactic de-intercalation was achieved for $AgCrTa(PO_4)_3$ according to eq. (1). The silver content was determined by indexing of the XRPD pattern, the change in intensities could only be described by a reduction of the silver occupancy. EDX measurements confirm these results, a reduced silver content is observed (Ag 10 %, Cr 22 %, Ta 24 %, P 44 %) compared to the starting material (Ag 20 %, Cr 22 %, Ta 19 %, P 39 %).

$$AgCrTa(PO_4)_3 + 0.3\ Br_2 \rightarrow Ag_{0.4}CrTa(PO_4)_3 + 0.6\ AgBr \quad (1)$$

For the other phosphates no topotactic de-intercalation was observed but a breakdown of the original structure, probably due to the formation of dangling bonds from phosphate groups during the de-intercalation process. The corresponding powder reflectance spectra before and after the de-intercalation experiments show transitions typical for Cr^{3+} in an octahedral environment (15000 cm^{-1}, 21000 cm^{-1}) which leads to the assumption that no oxidation of chromium occurs during the de-intercalation of these phosphates.

---

[1] B. Ayed, C. R. Chimie **2012**, 15, 603.
[2] M. Gabelica-Robert, Proceedings of the Second European Conference on Solid State Chemistry, Elsevier, Amsterdam, **1983**, 475.
[3] J. Bennazha, F. Erragh, A. Boukhari, E. M. Holt, J. Chem. Cryst. **2000**, 30, 705.
[4] K. Koteswara Rao, G. Rambabu, M. Raghavender, G. Prasad, G. S. Kumar, M. Vithal, Solid State Ionics **2005**, 176, 2701.
[5] M. A. Strelkov, M. G. Zhizhin, L. N. Komissarova, J. Solid State Chem. **2006**, 179, 3664-3671.
[6] F. Capitelli, N. Dridi, E. H. Arbib, V. Valentini, G. Mattei, Z. Kristallogr. **2007**, 222, 521-526.

PTue019

Sodium vanadium fluorophosphates prepared by a new microwave assisted synthesis: electrochemical study of raw and C-coated materials

Peña, Alazne (University of the Basque Country UPV/EHU, Bilbao, ESP); Palomares, Verónica (University of the Basque Country UPV/EHU, Bilbao, ESP); Serras, Paula (BCMaterials, Derio, ESP); Blas, Maitane (University of the Basque Country UPV/EHU, Bilbao, ESP); Gil de Muro, Izaskun (University of the Basque Country UPV/EHU, Bilbao, ESP); Lezama, Luis (University of the Basque Country UPV/EHU, Bilbao, ESP); Rojo, Teófilo (CIC Energigune, Miñano, ESP)

Sodium vanadium fluorophosphates belonging to $Na_3V_2O_{2x}(PO_4)_2F_{3-2x}$ family have demonstrated to play a relevant role in the field of Na-ion batteries due to their high operating voltages (3.6 and 4 V vs. Na/Na^+) and good specific capacities (up to 90 mAh/g at 2C) , giving rise to high energy density [1-6].
In this work, sodium vanadium fluorophosphates have been prepared by microwave assisted synthesis. The preparative method consists on an aqueous suspension of the reactants exposed to controlled temperature and pressure. Microwave assisted process reduces the reaction time and the energy used to synthesize this material compared to other synthesis methods such as ceramic, sol-gel method or hydrothermal synthesis. Some samples were C-coated by impregnation with sucrose and annealing step after the microwave preparation.

Obtained samples have been characterized by X-ray diffraction, transmission electron microscopy, elemental analysis and electron paramagnetic resonance. The x value in $Na_3V_2O_{2x}(PO_4)_2F_{3-2x}$ family has been estimated analyzing electron paramagnetic resonance spectra (EPR).

It has been proved that microwave process produces pure fluorophosphate samples by X-ray diffraction. The transmission micrographies of these materials show nanorods and prismatic crystals ranging from 5 to 180 nm width. EPR spectra indicate that the vanadium oxidation state is very close to +4.

Coated and raw sodium vanadium fluorophosphates have been electrochemically tested on laminate cathodes in Swagelok cell versus Na/Na^+. Differences in obtained specific capacities, rate capability and cycle life will be analyzed and related to the use of a C-coating.

---

[1] V. Palomares, M. Casas-Cabanas, E. Castillo-Martinez, M.H. Han, T. Rojo, Energy & Environmental Science, 2013, 6, 2312-2337.
[2] P. Serras, V. Palomares, A. Goñi, I. Gil de Muro, P. Kubiak, L. Lezama, T. Rojo, Journal of Materials Chemistry, 2012, 22, 22301-22308.
[3] Y.U. Park, D.H. Seo, B. Kim, K.P Kon, H. Kim, S. Lee, R.A. Shakoor, K. Miyasaka, J.M. Tarascon, K. Kang, Scientific Reports, 2012, 2, 704/1-704/7.
[4] P. Serras, V. Palomares, P. Kubiak, L. Lezama, T. Rojo, Electrochemistry Communications, 2013, 34, 344-347.
[5] P. Serras, V. Palomares, A. Goñi, P. Kubiak, T. Rojo, Journal of Power Sources, 2013, 241, 56-60.
[6] Y.U. Park, D.H. Seo, B. Kim, J. Kim, S. Lee, B. Kim, K. Kang, Advanced Functional Materials, 2014, 24, 4603-4614.

PTue020

Solid solutions in the quasi-binary system vanadyl(V) phosphate - molybdenyl(V) phosphate

Roy, Subrata Chandra (Bonn University, Bonn, GER); Glaum, Robert (Bonn University, Bonn, GER); Kollek, Sarah (Bonn University, Bonn, GER)

Semiconducting behaviour and average oxidation state of vanadium (4.1 to 4.2) in $(VO)_2P_2O_7$ are considered as descriptors for a good catalyst in selective oxidation of n-butane [1]. Here we report on experiments aiming at the setting of an intermediate oxidation state for vanadium via substitution of V^{5+} in $VOPO_4$ by V^{4+}/Mo^{6+} in the quasi-binary system $VOPO_4$ - $MoOPO_4$.

The thermodynamically stable solid solution $V_{1-x}Mo_xOPO_4$; $0.0 \leq x \leq 0.30$ (β-$VOPO_4$ type structure [2]) is obtained via solution combustion synthesis (SCS) [3] followed by heating the reaction intermediates in air. The maximum temperature required to obtain the thermodynamically stable phase decreases with increasing concentration of molybdenum. The pure vanadyl phosphate $V_{1-x}Mo_xOPO_4$ (x = 0) was obtained at 725 °C while the upper phase boundary (x = 0.30) forms already at 600 °C as microcrystalline powder. At higher temperatures the solid solutions of the corresponding composition start to melt. Several other metastable polymorphs of molybdenum-doped $VOPO_4$ (with α_I-, α_{II}-, β-, ω-, ω(ht)-, ε-VOPO4 structure type) were also observed during the heating procedure after ignition. In contrast, only one intermediate with the α_I-type structure was obtained during the synthesis of tungsten doped $VOPO_4$ ($V_{1-x}W_xOPO_4$; $0.0 \leq x \leq 0.26$, α_{II}- and β-$VOPO_4$ type structures) [4]. Upon exposure to lab atmosphere all metastable polymorphs $V_{1-x}Mo_xOPO_4$ are converted into the corresponding di-hydrates with $VOPO_4{\cdot}2H_2O$ [5] type structure. The metastable solid solution $V_{1-x}Mo_xOPO_4$; $0.0 \leq x \leq 0.20$) with γ-$VOPO_4$ type structure [6] was obtained as penultimate phase before transformation into the stable β-phase. The simulated XRPD pattern of the γ-type solid solution reveal that molybdenum replaces vanadium on the octahedral site.
Substitution of V^{5+} by V^{4+}/Mo^{6+} leads to an increase of the *b*- and *c*-axis as a result of increasing $d(V\text{-}O_{eq})$ distances which are aligned along these axes. The *a*-axis, along the chain of alternating short/long distances $d(O_{ax}{=}V\text{-}O_{ax})$ decreases as observed for the solid solution $(V^{IV}_xV^{V}_{1-2x}W^{VI}x)OPO_4$ [4]. The solid solution $V_{1-x}Mo_xOPO_4$; $0.0 \leq x \leq 0.30$ should correspondly be formulated as $(V^{IV}_xV^{V}_{1-2x}Mo^{VI}x)OPO_4$. The olive green color of the members of this solid solution reveals the existence of V^{4+} within the structure which is identified by the weak and broad IVCT($V^{4+} \rightarrow V^{5+}$) absorption band at 14300 cm-1. In addition the UV/VIS spectra show the broad LMCT[O^{2-}(s,p)→V^{5+}(dxy)] at 23500 (shoulder at 25500) cm^{-1}. The single isotropic chemical shift of ^{31}P-MAS-NMR spectra of the β-type solid solution reveals its phase purity. Moreover, the unexpected presence of V^{4+}/Mo^{6+} besides V^{5+} is evidenced by EPR, magnetic and conductivity measurements.

Experiments aiming at $V_{1-x}Mo_xOPO_4$ with x = 0.95 via SCS followed by heating in air (475 °C for 6 days) led to formation of a single phase yellowish powder of vanadium doped α-$(Mo^{VI}O_2)_2P_2O_7$ [7]. Further characterization of this phase will be presented on the poster.

---

[1] M. Eichelbaum, M. Hävecker, C. Heine, A. Karpov, C.-K. Dobner, F. Rosowski, A. Trunschke, R. Schlögl, *Angew. Chem.***2012**, *124*, 6350.

[2] R. Gopal, C. Calvo, *J. Solid State Chem.* **1972**, *5*, 432.

[3] M. S. Hedge, G. Madras, K. C. Patil, *Acc. Chem. Res.***2009**, *42*, 704.

[4] S. C. Roy, R. Glaum, D. Abdullin, O. Schiemann, N. Q. Bac, K.-H. Lii, *Z. Anorg. Allg. Chem.***2014**, *640*, 1876.

[5] H. R. Tietze, *Aus. J. Chem.* **1981**, 34, 2035.

[6] R. L. Harlow, Z. G. Li, N. Herron, H. S. Horowitz, E. M. McCarron, J. W. Richardson. Jr., B. H. Toby, ICSD 2014/02, no. 415213, **2005**.

[7] S. E. Lister, A. Soleilhavoup, R. L. Withers, P. Hodgkinson, J. S. O. Evans, Inorg. Chem. **2010**, *49*, 2290.

PTue021

Sonochemical syntheses of nano lead(II) coordination polymer; precursor for preparation of lead(II) oxide/iodide nano-structures

Morsali, Ali (Tarbiat Modares University, Tehran, IRN); Safarifard, Vahid (Tarbiat Modares University, Tehran, IRN)

During the last two decades, the rational design and syntheses of novel metal coordination polymers have made considerable progress in the field of crystal engineering [1]. The size and shape of solid materials influence on the chemical and physical properties. Hence making coordination polymers in any form in nano-scale is certainly a major step forward toward the technological applications of these new materials [2].A nano-sized Pb(II) coordination polymer, { $[Pb(L)(\mu_2\text{-}I)]_n$ (**1**) , L^- = 1H-1,2,4-triazole-3-carboxylate } was synthesized by sonochemical irradiation (Fig. 1). Calcination of the compound **1** at 630 ºC in air for 4 h yields PbO nanoparticles whereas PbI_2 nanoparticles were prepared by thermal decomposition of compound **1** in oleic acid as a surfactant at 200 °C.

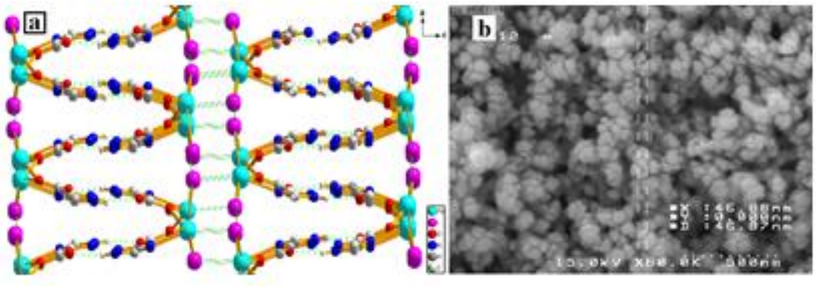

Fig . 1 (a) A fragment of the 3D framework in compound **1** and (b) FE-SEM photograph of compound **1** nanoparticles prepared by ultrasonic generator

---

[1] Leong, W.L. and Vittal, J.J. *Chem. Rev.*, **111**, (2010) 688-764.
[2] Lu, W., Chui, S.S.-Y., Ng, K.-M. and Che, C.-M., *Angew. Chem. Int. Ed.***47**, (2008) 4568-4572.

PTue022

Synthesis and Crystal Structure of Thallium(I, III) Pyrophosphate

Schmitz, Andreas (Bonn University, Bonn, GER); Glaum, Robert (Bonn University, Bonn, GER)

The structure of the mixed-valent indium(I,III) pyrophosphate, $In^{I}In^{III}P_2O_7$ was the first example for an In^+ cation in plein oxygen coordination [1]. Recent experiments led to the new thallium(I,III) pyrophosphate, $Tl^{I}Tl^{III}P_2O_7$, which is isostructural to $In_2P_2O_7$.

A colorless powder of thallium(I,III) pyrophosphate has been obtained from a nitric solution of Tl_2O_3 and $(NH_4)_2HPO_4$ which was evaporated to dryness at 150°C. The residue was finely ground and calcined at 500°C for 24h. At this conditions, a thermal reduction from intermediately formed $Tl^{III}PO_4$ to $Tl^{I}Tl^{III}P_2O_7$ was observed. Single crystals of this pyrophosphate were obtained via chemical vapor transport (CVT) in a temperature gradient (575 → 475 °C; 12 days), using HCl as transport agent.

The crystal structure of $Tl^{I}Tl^{III}P_2O_7$ (P-1 , $Z = 4$, $a = 7.5610(1)$ Å, $b = 10.4143(2)$ Å, $c = 8.4719(1)$ Å, $\alpha = 88.308(1)°$, $\beta = 104.759(1)°$, $\gamma = 89.660(1)°$, R1 = 0.056, wR2 = 0.136, 5641 independent reflections, 200 parameters) was refined from single crystal data.

The structure of $Tl^{I}Tl^{III}P_2O_7$ shows strong similarities to that of the already known indium(I,III) pyrophosphate. Both pyrophosphates show identical connectivity of slightly distorted $[M^{III}O_6]$ octahedra along with $[P_2O_7]^{4-}$ anions. The structure contains channels extending along the crystallographic *c*-axis. These are occupied by Tl^+ cations forming irregular $[TlO_{10}]$ and $[TlO_{11}]$ coordination polyhedra. These polyhedra exhibit free space in the coordination sphere where no oxygen ligands are found. However, there is no reliable indication for the lone-pairs of both Tl^+ or In^+ affecting the structure in this way. Compounds isotypic to $In_2P_2O_7$, e.g. $CsCrP_2O_7$ [2], show similar coordination of Cs^+ cations. In addition, observed distances $d(Tl^{I}\text{-}O)$ and $d(In^{I}\text{-}O)$ are exceptionally long ($d_{min}(Tl^{I}\text{-}O) = 2.72$ Å, $d_{min}(In^{I}\text{-}O) = 2.82$ Å) supporting the assumption of mainly s character for the lone-pair at the monovalent cations.
While $In_2P_2O_7$ forms a monoclinic structure, the unit cell of $Tl_2P_2O_7$ is distorted, leading to triclinic symmetry. Thus the number of independent atoms is doubled and the number of reflections in the XRPD increased. The infrared spectrum of $Tl_2P_2O_7$ will be reported, an assignment of selected vibrational modes for Tl-O and P-O provided. The 31P-MAS-NMR spectrum of $Tl_2P_2O_7$ shows an isotropic chemical shift of $\delta_{iso} = 21.1$ ppm. Other Pyrophosphates show comparable values (β-$Mg_2P_2O_7$: $\delta_{iso} = 19.2$ ppm [3]).

---

[1] H. Thauern, R. Glaum, *Z. Anorg. Allg. Chem.***2003**, *629*, 479.
[2] S. A. Linde, Y. E. Gorbunova, *Neorg. Mater.***1982**, *18*, 464.
[3] F. Fayon, D. Massiot, K. Suzuya, D. L. Price, *J. Non-Crystalline Solids***2001**, *283*, 88.

PTue023

Synthesis and self-assembly of Cobalt and Nickel Nanoparticles

Haumann, Sebastian (Universität Regensburg, Regensburg, GER); Weihrich, Richard (Universität Regensburg, Regensburg, GER)

Cobalt and Nickel nanoparticles were synthesized with different reducing agents in a polyol medium and observation of magnetic self-assembly between nearly spherical nanoparticles [1].

In the last years metal nanoparticles attracted interest particularly due to their magnetic properties and use in different applications like data storage, DNA sequencing, drug delivery, biomedical sensors, microelectronics, radiation therapy and catalysis [2-3]. Therein, the synthesis of Cobalt and Nickel nanoparticles seems very promising from pioneering work [4]. But besides these promising utilizations in everyday life, there are still problems in the production of well-shaped nanoparticles with a certain size and a narrow size distribution. That is why the development of the synthetic routes has to improve constantly with a look at the physical and chemical properties of the nanoparticles.

To understand and improve the processes in the synthesis of Cobalt and Nickel nanoparticles and the resulting properties, nanometer-scale particles were produced in a typical polyol process. Therefore various solvents, different reducing agents and reaction conditions were investigated with respect to the size shape, and self-organization of the particles. The size and shape of the nanoparticles were determined with the Scherrer-equation out of the powder patterns and scanning electron microscope (SEM) measurements.

---

[1] S. Haumann, Master's Theses ,Universität Regensburg (2014).
[2] J. Park, E. Kang, S.U. Son, H.M. Park, M.K. Lee, J. Kim, K.W. Kim, H.-J. Noh, J.-H. Park, C.J. Bae, J.-G. Park, T. Hyeon, Adv. Mater. 17 (2005) 429.
[3] O. Santini, A.R. de Moraes, D.H. Mosca, P.E.N. de Souza, A.J.A. de Oliveira, R.Marangoni, F.Wypych, J. Colloid Interface Sci. 289 (2005) 63.
[4] C. B. Murray, S. Sun, H. Doyle, T. A. Betley, Mat. Res. Bull. 985(2001**).**

PTue024

Synthesis and structural characterization of $BaTiO_{3-x}H_x$ oxyhydrides

<u>Nedumkandathil, Reji (Stockholms universitet, Stockholm, SWE)</u>; Häussermann, Ulrich (Stockholms universitet, Stockholm, SWE)

Recently it has been shown that the reaction of CaH_2 with the archetypical perovskite $BaTiO_3$ affords $BaTiO_{3-x}H_x$ with large amounts (x up to 0.6) of hydrogen incorporated [1]. The cubic perovskite oxy-hydride $BaTiO_{3-x}H_x$ is remarkable in several respects. It represents a defect/vacancy-free solid solution of O^{2-} and H^- ions which commonly form the octahedral environment around Ti that is now in a mixed IV/III oxidation state. $BaTiO_{3-x}H_x$ is electrically conducting and stable in air and water. Further, it is stable at elevated temperature up to approximately 400 ^oC above which hydrogen is released. Here we show the results of a systematic study of the hydride reduction of $BaTiO_3$ leading to perovskite oxyhydrides $BaTiO_{3-x}H_x$. A broad range of reducing agents including LiH, NaH, MgH_2, CaH_2, $LiAlH_4$ and $NaBH_4$ was employed and temperature and dwelling conditions for hydride reduction examined. Samples were characterized by powder X-ray diffraction, thermal gravimetric analysis and scanning electron microscopy. We find that the concentration of H that can be incorporated in $BaTiO_{3-x}H_x$ strongly depends on the kind of reducing agent. The maximum amount is about x = 0.7 which exceeds the originally reported value. Inelastic neutron scattering experiments show that bands corresponding to Ti-H vibrations attain wavenumbers around 1000 cm^{-1}. We further show that H in $BaTiO_{3-x}H_x$ can be conveniently and completely exchanged by D when annealing $BaTiO_{3-x}H_x$ at 500 ^oC in pressurized deuterium (30 bar). This opens for neutron total scattering studies where the local structure of $BaTiO_{3-x}D_x$ (i.e. differences in Ti-O and Ti-H distances) can be elucidated by pair distribution analysis.

References [1] Y. Kobayashi et al., Nat. Mater. 11 (2012) 507.

PTue025

Synthesis, Crystal Structures and Topotactic Oxidation of Polynary Silver Transition Metal Phosphates

Häbel, Jan-Peter (Bonn University, Bonn, GER); Glaum, Robert (Bonn University, Bonn, GER)

Up to now, only ill-defined phases of anhydrous phosphates with transition metals in unusually high oxidation states are known. These are formed during topotactic delithiation of cathode materials like Li*M*PO_4 (*M*: Mn [1], Co [2], Ni [3]) in lithium ion batteries. This projects aim are synthesis and characterization of silver transition metal phosphates and their topotactic de-intercalation. By this means, metastable phosphates with transition metals in unusually high oxidation states in an environment of "innocent" ligands should be accessible.

Syntheses of the silver transition metal phosphates were carried out by calcining precursors, which were obtained by precipitation from aqueous solutions ($AgNO_3$, $(NH_4)_2HPO_4/H_3PO_4$, $Ni(OH)_2$ and $Fe(NO_3)_3\cdot 9H_2O$, respectively, as starting materials). Four new phosphates were synthesized: $Ag_4Ni_7(PO_4)_6$, $Ag_4Ni_2(P_2O_7)_2$, $Ag_4Ni_3(PO_4)_2(P_2O_7)$ and $Ag_3Fe(PO_4)_2$. Single crystals of $Ag_4Ni_7(PO_4)_6$ and $Ag_4Ni_2(P_2O_7)_2$ were obtained by treating the corresponding sodium compounds in a flux of $AgNO_3$. Both structures form a 3-dimensional network of $[NiO_6]$ octahedra and $[PO_4]$ tetrahedra. The silver atoms are located within these networks.

Single crystal structure analysis of $Ag_4Ni_2(P_2O_7)_2$ (P-1, Z = 2, a = 6.3786(13) Å, b = 9.4100(19) Å, c = 10.8700(22) Å, α = 64.837(30)°, β = 80.362(30)°, γ = 73.051(30)°, 3070 ind. refl., R1 = 0.076, wR2 = 0.22, Goof = 0.710) revealed 12 independent sites for the silver atoms with s.o.f. between 0.06 and 0.55.
Single crystal structure analysis of $Ag_4Ni_7(PO_4)_6$ (C 2/m, Z = 2, a = 10.6025(9) Å, b = 14.0082(11) Å, c = 6.4705(5) Å, β = 104.502(3) °, 1481 ind. refl., R1 = 0.069, wR2 = 0.185, Goof = 1.101) revealed 13 independent sites for the silver atoms with s.o.f. between 0.05 and 0.26.

The cell parameters of the new phosphates $Ag_4Ni_3(PO_4)_2(P_2O_7)$ and $Ag_3Fe(PO_4)_2$ were determined based on the powder diffraction pattern of the isotypic phosphates sodium transition metal phosphates [4, 5].
Oxidative de-intercalation experiments were carried out in evacuated sealed silica tubes with iodine at 215 °C and 300 °C, respectively. De-intercalation with bromine as oxidizing agent were realised in acetonitrile at room temperature. The XRPD patterns of the products reveal the formation of silverbromide (silveriodide).

---

[1] C. Delacourt, P. Poizot, M. Morcrette, J.-M. Tarascon, C. Masquelier, *Chem. Mater.***2004**, *16*, 93-99.
[2] H. Ehrenberg, N. N. Bramnik, A. Senyshin, H. Fuess, *Solid State Sci.***2009**, *11*, 18-23.
[3] M. Minakshi, P. Singh, D. Appadoo, D. E. Martin, *Electrochim. Acta***2011**, 56, 4356-4360.
[4] F. Sanz, C. Parada, J.M. Rojo, C. Ruiz Valero, *Chem. Mater. 2001*, 13, 1334-1340.
[5] V. A. Morozov, B. I. Lazoryak, A. P. Malakho, K. V. Pokholok, S. N. Polyakov, T. P. Terekhina, *J. Solid State Chem.***2001**, *160*, 377-387.

PTue026

The Large Scale Synthesis of Aligned Plate Nanostructures

Nash, Philip (Illinois Institute of Technology, Chicago, USA); Zhou, Yang (Illinois Institute of Technology, Chicago, IL, USA)

A novel process for the large-scale synthesis of nanostructures is proposed and demonstrated using alloys in the Ni-Co-Al system. The synthesis technique involves developing nanoscale two-phase microstructures through discontinuous precipitation followed by selective etching to selectively remove one of the phases. The technique has been demonstrated using the discontinuous precipitation of a γ' phase $(Ni, Co)_3Al$, followed by selective dissolution of the γ matrix phase. Through control of the composition and aging parameters it is possible to produce plates of different thickness and different spacings. The method is easily scaled up and may be generally applied to any alloy system undergoing a complete discontinuous precipitation transformation. This synthesis technique opens up a vast new area of potential applications through selection of the plate composition and additional functionalization.

PTue027

Three Modifications of Barium Tetramidogallate: An Intermediate in Ammonothermal GaN Crystal Growth

Hertrampf, Jan (Institute of Inorganic Chemistry, Stuttgart, GER); Alt, N. S. A. (Institute of Process Machinery and Systems Engineering, Erlangen, GER); Schlücker, E. (Institute of Process Machinery and Systems Engineering, Erlangen, GER); Niewa, R. (Institute of Inorganic Chemistry, Stuttgart, GER)

Single crystals of group III nitrides are of great importance for semiconductor industries. Gallium nitride is characterized by its wide bandgap (3.2 ~ 3.4 eV), high chemical and thermal durability. Those features are required for a number of applications such as blue laser diodes, transistors or high power amplifiers [1,2].

Ammonothermal synthesis (critical point of ammonia: p = 11.3 MPa, T = 403.5 K) is suitable for growth of high-quality GaN wafers of several inch. Within this technique, mineralizers are responsible for reasonable solubility of GaN in ammonia, thus, for material transport (ammono-basic: alkali metals, their amides or azides, ammono-acidic: gallium halides or ammonium halides) [3-5]. The chemical nature of dissolved species in general is still in question, but several potential intermediates, for ammono-basic as well as for ammono-acidic regime, have been recently characterized [6,7]. Under ammono-basic conditions the possible intermediates $NaGa(NH_2)_4$ [8,9], $Na_2[Ga(NH_2)_4]NH_2$ [6] and $Li[Ga(NH_2)_4]$ in two modifications [6] were obtained and characterized with $NaNH_2$ and $LiNH_2$ as mineralizers, respectively.

To the best of our knowledge no studies report GaN crystal growth using alkaline-earth metal amides as mineralizers so far. We performed GaN transport under ammono-basic conditions (T = 523 K, p = 900 to 1600 bar) using barium amide as mineralizer and observed formation of $Ba[Ga(NH_2)_4]_2$ as possible intermediate. Further we present the characterization of three modifications of $Ba[Ga(NH_2)_4]_2$ (space groups P-4, $P2/c$ and $P21/n$) obtained under slightly different conditions. IR and Raman measurements show a doublet for the symmetric and asymmetric amid vibration, each caused by two chemically different amide groups present in the crystal structures. Thermal analysis reveals a step-wise decomposition with the loss of 4 molecules ammonia per formula unit to finally yield $BaGa_2$.

---

[1] O. Ambacher, *J. Phys. D. Appl. Phys.* **1998**, *31*, 2653.

[2] M. R. Krames, O. B. Shchekin, R. Müller-Mach, G. O. Müller, L. Zhou, G. Harbers, M. G. Craford, *J. Disp. Technol.* **2007**, *3*, 160.

[3] R. Dwilinski, R. Doradzinski, J. Garczynski, L. Sierzputowski, R. Kucharski, M. Zajac, M. Rudzinski, R. Kudrawiec, J. Serafinczuk, W. J. Strupinski, *J. Cryst. Growth* **2010**, *312*, 2499.

[4] H. W. Xiang, *J. Phys. Chem. Ref. Data* **2004**, *33*, 1005.

[5] D. Ketchum, J. Kolis, *J. Cryst. Growth* **2001**, *222*, 431.

[6] S. Zhang, N. S. U. Alt, E. Schlücker, R. Niewa, *J. Cryst. Growth* **2014**, *403*, 22.

[7] S. Zhang, F. Hintze, W. Schnick, R. Niewa, *Eur. J. Inorg. Chem*. **2013**, *31*, 5374.

[8] P. P. Molinier, R. Brec, J. Rouel, P. Herpin, *Acta Cryst*. **1973**, *B29*, 925.

[9] H. Jacobs, B. Nöcker, *Z. anorg. allg. Chem*. **1993**, *619*, 381.

PTue028

The synthesis of nanoparticles of metal oxides by supercritical CO_2 anti-solvent precipitation

Fomichev, Valery (Lomonosov Moscow state university of fine chemical technologies, Moscow, RUS);
Konovalov, Igor (Lomonosov Moscow state university of fine chemical technologies, Moscow, RUS);
Drobot, Dmitry (Lomonosov Moscow state university of fine chemical technologies, Moscow, RUS);
Smirnova, Ksenia (Lomonosov Moscow state university of fine chemical technologies, Moscow, RUS)

Nanoscale metal oxides are of tremendous current interest to scientists and engineers because of the potential of their emerging applications spanning catalysts, ceramics, sensors, fuel cells, etc. Today there are a variety of synthetic techniques of metal oxide nanomaterials, including sol−gel, micelle, hydrothermal, solvothermal, sonochemical, microwave, electrodeposition, physical vapor deposition, and chemical vapor deposition methods.The crystal sizes and crystal structures of the oxides strongly depend on the synthesis parameters including temperature, solvent, additives, acidity, and aging during the solution-based preparation processes.

In our work we synthesized such nanomaterials as TiO_2, ZrO_2, Nb_2O_5, Ta_2O_5 by supercritical CO_2 anti-solvent precipitation. As precursors we applied solutions of metal alkoxides in corresponding alcohol (for example, tantalum methoxide in methanol, titanium isopropoxide in isopropanol) .The study revealed that the size of oxide particles strongly depend on synthesis parameters namely on temperature, pressure, concentration and stream velocity of CO_2. Experiments were carried out under the following conditions: pressure range 8,5-30 kPa , temperature range 40-80 ^oC, molar concentration 1/85-1/200.

So, one can vary the size of the obtained product by changing conditions of the process. The influence of temperature, pressure and concentration of precursor on the average particle size was studied. Thus, when the pressure increases the average particle size decreases. When the temperature increases the average size decreases. With decreasing concentration of the precursor in an alcoholic solution particle size decreases.

It expected to oxides formed by hydrolysis of initial alkoxides. Water is present in small amounts of CO_2 (up to 0.02%), which is sufficient for reaction behavior. Chromatographic methods of analysis found to contain ethers in the exhaust gas after the reactor.

The results of X-ray and TEM(HR) analyzes have demonstrated that the obtained oxides are amorphous. The measuring of the particle size by electron microscopy and by the method of dynamic light scattering has shown that the product is monodisperse with a narrow size distribution and that size is in the nanoscale range. The particle size of the oxides is obtained in the range of 10 to 100 nm with a narrow particle distribution (±2 nm). SSA has shown that the oxides have a high porosity and a large specific surface area (for example, SSA TiO_2 200m^2/g).

In the modern electronic technology has been a sharp increase in the role of the dielectric and semiconductor materials based on these oxides. Using of these materials meet modern requirements such as operational reliability electronics items and development of industrial production of small capacitors, occupying a prominent place in electronic equipment. Amorphous oxides are promising precursors for producing various types of ceramics with high performance.

PTue029

An ab initio molecular dynamics study of structural properties of FeF_2 as a function of pressure

Kurkcu, Cihan (Ahi Evran University, Kirsehir, TUR); Merdan, Ziya (Gazi University, Ankara, TUR); OZTURK, Hulya (Ahi Evran University, Kirsehir, TUR); Kurkcu, Cemile (Ahi Evran University, Kirsehir, TUR)

We have studied the structural properties of the antiferromagnetic FeF_2 in tetragonal structure with $P4_2/mnm$ symmetry using density functional theory (DFT) under rapid hydrostatic pressure up to 300 GPa. The AF_2-type compounds crystallize in rutile-type structure at ambient conditions. The FeF_2 compound undergoes a phase transformation from the tetragonal structure to orthorhombic structure with Pnnm symmetry at 136 GPa. This phase change is also studied by total energy and enthalpy calculations.

Because of the novel phase transitions and geophysical importance, the difluoride compounds have been studied under the influence of temperature and pressure [1-9]. The FeF_2 compound crystallizes in a tetragonal rutile-type structure ($P4_2/mnm$, Z=2) at ambient conditions. Ming and Manghnani [6] obtained that rutile-structure FeF_2 transform into the $CaCl_2$ structure at 4.5 GPa.

In this study the tetragonal rutile-type structure of FeF_2 was firstly equilibrated at zero pressure and pressure was gradually increased up to 300 GPa with an increment of 4 GPa. The structure of FeF_2 transforms from rutile-type structure with space group $P4_2/mnm$ to $CaCl_2$-type structure with space group Pnnm at 136 GPa

The structural properties of the tetragonal FeF_2 compound are investigated in the local density approximation of density functional theory with the functional of Ceperley and Adler (CA) [10] using the ab-initio program SIESTA [11]. The self-consistent “norm-conserving” pseudopotentials are generated using the Troullier–Martins scheme [12]. For the Brillouin zone (BZ) integration, we use the Monkhorst–Pack (MP) [13] mesh 6x6x8 for rutile-type structure and 8x10x12 for $CaCl_2$-type structure. The simulation cells consist of 96 atoms with periodic boundary conditions. Pressure was applied via the method of conjugate-gradient to the system and increased with an increment of 4 GPa for FeF_2. In order to analyze each minimization step we use the KPLOT program and RGS algorithm [14-15] that give elaborated knowledge about cell parameters, atomic positions and space group of an analyzed structure.

---

[1] A.E. Austin, J. Phys. Chem. Solids **30**, 1282 (1969).
[2] J.D. Jorgensen, T.G. Worlton and J.C. Jamieson, Phys. Rev. B **17**, 2212 (1978).
[3] H. Wang, X. Liu, Y. Li, Y. Liu and Y. Ma, Solid State Commun. **151**, 1475 (2011).
[4] A.Y. Wu, Phys. Lett. A **60**, 260 (1977).
[5] J.C. Jamieson and A.Y. Wu, J. Appl. Phys. **48**, 4573 (1977).
[6] L.C. Ming, M.H. Manghnani, T. Matsui and J.C. Jamieson, Phys. Earth Planet. Inter. **23**, 276 (1980).
[7] L. Nagel and M. O’Keeffe, Mater. Res. Bull. **6**, 1317 (1971).
[8] P. Duffek, K. Schwarz and P. Blaha, Phys. Rev. B **48**, 12 672 (1993).
[9] I.de P.R. Moreira, R. Dovesi, C. Roetti, V.R. Saunders and R. Orlando, Phys. Rev. B **62**, 7816 (2000).
[10] D.M. Ceperley and B.J. Adler, Phys. Rev. Lett. **45**, 566 (1980).
[11] P. Ordejon, E. Artacho and J.M. Soler, Phys. Rev. B **53**, (R10) 441 (1996).
[12] N. Troullier and J.L. Martins, Phys. Rev. B **43**, 1993 (1991).
[13] H.J. Monkhorst and J.D. Pack, Phys. Rev. B **13**, 5188 (1976).
[14] R. Hundt, J.C Schön, A. Hannemann and M. Jansen, J. Appl. Crys. **32**,413(1999).
[15] A. Hannemann, R. Hundt, J.C. Schön and M. Jansen, J. Appl. Cryst. **31**, 922 (1998).

PTue030

Elastic Properties of $LaNiO_3$: An Employment of PBE-based Functionals

Masys, Sarunas (Vilnius University, Vilnius, LTU); Jonauskas, Valdas (Vilnius University, Vilnius, LTU)

Among the remarkable family of perovskite oxides, lanthanum nickelate $LaNiO_3$ is a rare example characterized by paramagnetic metallic behaviour down to the lowest temperatures and being structurally compatible with many active functional layers. This compound has attracted significant theoretical and experimental research efforts due to its tremendous potential to be used in developing solid oxide fuel cells, high-temperature superconductors, colossal magnetoresistance materials, and ferroelectric thin-film devices.

It is interesting to note that although one can find a variety of theoretical studies based on conventional density functional theory (DFT) and beyond-DFT techniques in which the electronic structure of $LaNiO_3$ is extensively investigated and compared to the experimental data, in the literature scarcely any first-principles calculations on the elastic properties of $LaNiO_3$ have been reported to date. The situation is not much better with the experiment, especially regarding the single-crystal measurements. Having in mind that the list of potential applications of $LaNiO_3$ continues to grow, it becomes obvious that the deep knowledge of elastic features could be useful for both technological and fundamental reasons.

In this work, we present theoretical calculations of single-crystal elastic constants and polycrystalline moduli of rhombohedral (space group No. 167) $LaNiO_3$ employing a well known family of PBE-based functionals: PBE [1], PBEsol [2], and PBE0 [3]. Our calculations carried out using CRYSTAL14 code [4] indicate that elastic properties of $LaNiO_3$ evaluated within different DFT approaches substantially vary. The obtained results are presented in Table 1.

Table 1. Single-crystal elastic constants C_{ij} together with bulk B, shear G, and Young's E moduli (in GPa) calculated for rhombohedral $LaNiO_3$ using different DFT approaches.

	C_{11}	C_{12}	C_{13}	C_{15}	C_{33}	C_{44}	C_{66}	B	G	E
PBE	220.9	141.5	144.2	Mär.26	306.9	77.9	39.7	176.6	57.5	155.5
PBEsol	264.6	161.6	150.1	17.Jun	341.1	98.8	51.5	198.4	71.9	192.6
PBE0	279.3	164.4	138.8	51.9	367.2	31.2	57.5	200.4	14.Jun	42.8

Thus, in order to distinguish the most reliable values of calculated elastic features, one should be aware of the subtle differences in the structure and performance of PBE-based functionals.

---

[1] J. P. Perdew, K. Burke, and M. Ernzerhof, Phys. Rev. Lett. **77**, 3865 (1996).
[2] J. P. Perdew, A. Ruzsinszky, G. I. Csonka, O. A. Vydrov, G. E. Scuseria, L. A. Constantin, X. Zhou, and K. Burke, Phys. Rev. Lett. **100**, 136406 (2008).
[3] C. Adamo and V. Barone, J. Chem. Phys. **110**, 6158 (1999).
[4] R. Dovesi, R. Orlando, A. Erba, C. M. Zicovich-Wilson, B. Civalleri, S. Casassa, L. Maschio, M. Ferrabone, M. De La Pierre, P. D'Arco, Y. Noel, M. Causa, M. Rérat, and B. Kirtman, Int. J. Quantum Chem. **114**, 1287 (2014).

PTue031

Electron density and ELI-D analysis of the cd → β-Sn phase transition of group IV elements

Kremenetskaya, Olga (MPI for Chemical Physics of Solids, Dresden, GER); Kohout, Miroslav (MPI for Chemical Physics of Solids, Dresden, GER); Grin, Juri (MPI for Chemical Physics of Solids, Dresden, GER)

The group IV elements Si, Ge and Sn exhibit a pressure-induced phase transition from the cubic diamond (*cd*) to the *β-Sn* phase, while for C this phase transition was not observed. Can this fact be understood from the point of view of the quantum chemical topological analysis?

Both *cd* and *β-Sn* structures can be described by the body centered tetragonal lattice, where c/a=√2 for the *cd* and c/a≈0.5 for the *β-Sn* phase. The *cd→β-Sn* phase transition is simulated by a continuous decrease of the c/a ratio. An enthalpy barrier calculation reveals the structure with c/a≈0.8 as the transition one for Si, Ge and Sn. For carbon the enthalpy increases monotonically along the transition pathway. This difference in the energetic behavior can be attributed to the exchange-correlation term of the DFT energy (E_{xc}), while the classical terms (Coulomb interaction and kinetic energy) behave similarly for all the elements.

The topological analysis of the electron density (ED) is widely used to describe the bonding situation. During the phase transition a topological catastrophe occurs at c/a≈0.8, where new bond critical points (BCP) between the atoms in the [001] direction are formed for all the elements. This is commonly attributed to a new bonds formation, however, apparently in this case it is due to the change of the unit cell symmetry and is only slightly influenced by the electron density reorganization.

During the phase transition the primary bond distances increase and the new ones in the [001] direction decrease. To estimate the change in the covalent interaction between atoms the sum of ED values in the middle of the primary (ρ_1) and new (ρ_2) bonds for an atom was calculated ($4\cdot\rho_1+2\cdot\rho_2$). The negative value of this function mirrors the behavior of the E_{xc} term along the transition pathway. It behaves for carbon differently than for the other elements. It has to be noted that for Ge and Sn a clear correlation is observed only for valence density (excluding the contribution of d electrons).

ρ_1 and ρ_2 separately have similar respective behavior for all the elements (ρ_1 decreases and ρ_2 increases during the phase transition). This allows to describe an absence of the energy minimum for the *β-Sn* carbon as a result of two factors, fast weakening of the covalent interaction for the primary bonds and slow strengthening for the new ones.

Similar conclusion can be made from the topological analysis of the electron localizability indicator (ELI-D), which shows chemically significant regions of space (core shells, lone pairs, bonds). For normal interatomic distances the atoms have one shared valence ELI-D maximum, but for long distances it splits into two maxima. For Si, Ge and Sn during the phase transition the new ELI-D maxima along [001] direction are formed before the four primary ones split, and for the experimental *β-Sn* structures with c/a≈0.5 six ELI-D attractors around each atom are observed. For carbon the primary bond maxima split before the formation of new ones and the structure with six ELI-D maxima around each atom cannot be formed. This again brings us to the conclusion that the *cd→β-Sn* phase transition is a result of an interplay of the primary bond weakening accompanied by the strengthening of the new bonds.

PTue032

Exploring Bonding in Complex Solids with New Theoretical Tools

Deringer, Volker (RWTH Aachen University, Aachen, GER); Maintz, Stefan (RWTH Aachen University, Aachen, GER); Tchougréeff, Andrei (RWTH Aachen University, Aachen, GER); Dronskowski, Richard (RWTH Aachen University, Aachen, GER)

The notion of bonding between atoms is at the heart of chemistry, not only in the molecular realm but likewise in the solid state. To interpret the electronic structures of crystalline solids in a chemical language, a number of orbital-based bonding indicators are widely used, such as the crystal orbital overlap and Hamilton population (COOP and COHP). Traditionally, these tools rely on atom-centred basis functions—hence, by definition, they cannot be directly combined with numerically efficient plane-wave basis sets, which are ingredients for many of today's density-functional theory (DFT) workhorses. Recently, we have shown that one *can* re-extract bonding indicators such as the COHP from plane-wave computations [1], and subsequently developed an analytical framework (and the computer program LOBSTER) for this purpose [2]. Here, two applications will be presented which have been enabled by precisely such projection techniques: first, we analyse chemical bonding at competing quartz-type GeO_2 surfaces, lending numerical support to Pauling's iconic third rule [3]; second, we explore the bonding nature of local structural fragments in amorphous GeTe, a prototype phase-change material which is used for data storage [4].

---

[1] V. L. Deringer, A. L. Tchougréeff, R. Dronskowski, *J. Phys. Chem. A* **2011**, *115*, 5461; see also references therein.
[2] S. Maintz, V. L. Deringer, A. L. Tchougréeff, R. Dronskowski, *J. Comput. Chem.* **2013**, *34*, 2557.
[3] V. L. Deringer, R. Dronskowski, *Chem. Sci.* **2014**, *5*, 894.
[4] V. L. Deringer, W. Zhang, M. Lumeij, S. Maintz, M. Wuttig, R. Mazzarello, R. Dronskowski, *Angew. Chem. Int. Ed.* **2014**, *53*, 10817.

PTue033

First-principles calculations of the phase stability and surface energy of TiO_2 (100) and (110)

Azibi, Mourad (Centre for development of advanced technologies (CDTA), Algiers, DZA); Saoula, Nadia (Centre for development of advanced technologies (CDTA) , Algiers, DZA)

First-principles calculations of the crystal structures, bulk moduli, and relative stabilities of TiO_2 rutile and anatase were successfully calculated and simulated by a plane wave pseudopotential. The minimum total energy of the structure is achieved by relaxing automatically the internal coordinates using the Broyden-Fletcher-Goldfarb-Shanno (BFGS) algorithm. The calculated unit cell data agree to within 2% of the corresponding experimental determination and calculated bulk moduli are within 10% of the most reliable experimental results. Rutile TiO_2 (100) and (110) slabs are constructed before the calculation by cleaving a bulk TiO_2 after geometry optimization. A vacuum region with the thickness of 15 Å is included in the supercell to prevent the interaction between the slab and its periodic images. The calculated results of structural relaxation and surface energy for TiO_2 (110) and (100) slab indicate that A 12 and 10 layers slab, respectively, were found to be a good surface model. The surface energy of TiO_2 (100) and (110) are calculated to be 1.1 and 0.9 J/m^2, respectively.

PTue034

First-principles study of phase stability, hydrogen ordering, and the metal-insulator transition in hydrogen-rich lutetium hydrides

Kerscher, Tobias (University Medical Center Göttingen, Göttingen , GER); Müller, Stefan (Hamburg University of Technology, Hamburg, GER); Karsai, Ferenc (Institut für Materialchemie, Wien, AUT); Wolf, Walter (Materials Design s.a.r.l., Montrouge, FRA); Herzig, Peter (Institut für Physikalische Chemie, Wien, AUT)

This contribution focusses on the ab-initio investigation of the lutetium–hydrogen system for LuH_{2+x}, $0 \leq x \leq 1$. Lutetium hydrides, together with the hydrides of La, Sc, and Y, can be considered as prototype materials for the other rare-earth hydrides with their additional complications due to incompletely filled f states. In a slightly simplified picture one can distinguish between two classes of hydride-forming metals, the lighter lanthanoid metals (La, Ce, and Pr) on the one hand, which have larger atomic radii, and the heavier (and smaller) lanthanoids (from Tb to Lu) together with Sc and Y on the other hand. In the above-mentioned concentration range ($0 \leq x \leq 1$) the structures of all the former hydrides can be derived from an fcc arrangement of the metal atoms, while for the latter hydrides the structure is derived from an fcc lattice of the metal atoms for the dihydrides and an hcp lattice for the trihydrides.

Investigations performed previously dealt with the influence of hydrogen-vacancy ordering on the stability and the optical properties of La di- and trihydrides [1, 2]. We report here on an investigation of the corresponding Lu hydrides, but will also consider the situation in some of the hydrides of Sc, Y, and La for comparative purposes. The main strategy has been to perform a large set of DFT calculations with VASP and to use the resulting energies as input for a cluster expansion (CE) [3]. In order to examine the vibrational stability of those structures which have minimum formation energies for the respective compositions, phonon calculations have been performed. The results of which will also be used for obtaining the contribution of lattice vibrations to the thermodynamic functions.

From the calculated formation energies one can see higher stability of the hcp-like structure for higher hydrogen concentrations ($x \geq 0.75$) and for the fcc-like structure at lower concentrations. For the stoichiometric Lu (Y) trihydride the former structure is more stable by ca. 0.2 eV (0.15 eV) per Lu (Y) atom. While for the corresponding La-H system the removal of H atoms from a tetrahedral site is energy expensive, this is not normally the case for the Lu-H system. For example, creating two tetrahedral H vacancies in hcp-$Lu_{12}H_{36}$ leads to a structure which is lower in energy compared to the other possible cases.

For the Lu-H system band gaps have been found for the fcc-like structures down to $x \approx 0.7$, for the hcp-like structures only for the stoichiometric or almost stoichiometric trihydrides.

The presented computational results have been obtained using the Vienna Scientific Cluster (VSC).

---

[1] T. C. Kerscher, G. Schöllhammer, P. Herzig, W. Wolf, R. Podloucky, and S. Müller:
First-principles study of hydrogen ordering in lanthanum hydride and its effect on the metal-insulator transition, Phys. Rev. B 86, 014107/1–8 (2012).
[2] G. Schöllhammer, F. Karsai, and P. Herzig:
Fluorite-Type Rare-Earth Hydrides Studied from First Principles. In “Properties of Fluorite Structure Materials”, Editors: P. Vajda and J. M. Costantini, Nova Science Publishers (N.Y., USA), ISBN: 978-1-62417-458-2 (2013).
[3] D. Lerch, O. Wieckhorst, G. L. W. Hart, R. W. Forcade, and S. Müller:
UNCLE: a code for constructing cluster expansions for arbitrary lattices with minimal user-input. Modelling Simul. Mater. Sci. Eng. 17, 055003 (2009).

PTue035

Long looked-for and finally found: Nb_2RuB_2 - theoretical and experimental studies

Touzani, Rachid (Institute of Inorganic Chemistry RWTH Aachen, Aachen, GER); Mbarki, Mohammed (RWTH Aachen University, Aachen, GER); Fokwa, Boniface P. T. (Institut für Anorganische Chemie, RWTH Aachen, Aachen, GER)

We recently discovered a new twofold superstructure of U_3Si_2-type (Nb_2OsB_2, space group P4/mnc, no.128) [1] and also investigated the Nb_2MB_2 phases (M = Fe, Ru, Os) theoretically (DFT calculations) [2]. The synthesis of Nb_2RuB_2 was not successful in the past. At first Nb_2RuB_2 was predicted to crystallize with the Nb_2OsB_2 structure type [2]. Calculations with the Universal Structure Predictor Evolutionary Xtallography (USPEX) program, however, revealed Nb_2RuB_2 to crystallize with the $AlMn_2B_2$-type structure with a lower total energy than the Nb_2OsB_2-type structure. Further calculations with the PHONOPY program showed that Nb_2RuB_2 with the $AlMn_2B_2$-type structure is thermodynamically unstable, while the Nb_2OsB_2-type structure for this compound is stable (see Fig.1). Eventually, we successfully synthesized Nb_2RuB_2 and according to X-ray diffraction it crystallizes with the Nb_2OsB_2-type structure. Further experimental investigations confirmed the presence of distorted Nb-layers and Ru_2-dumbbells in the crystal structure as already predicted in Ref. 2. According to chemical bonding analysis, the homoatomic B–-B interactions present in this structure are optimized and very strong, but relatively strong heteroatomic M–-B, B–-Nb and Ru–-Nb bonds are also found: These interactions, which together build a three-dimensional network, are mainly responsible for the structural stability of this ternary boride, just like in the homologous Nb_2OsB_2. The density-of-states at the Fermi level predicts metallic behavior, as expected from a metal-rich boride.

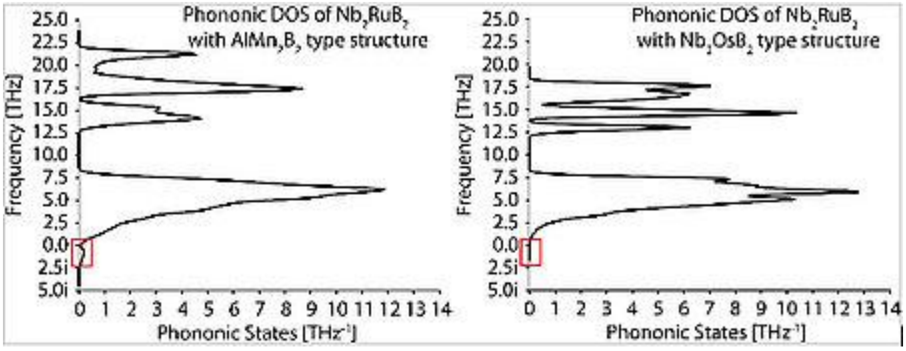

Fig.1 The phononic DOS of Nb_2RuB_2 with $AlMn_2B_2$-type structure (left) shows occupied imaginary frequencies and therefore is thermodynamically unstable, while the phononic DOS of Nb_2RuB_2 with Nb_2OsB_2-type structure (right) does not show any occupied imaginary frequencies.

---

[1] M. Mbarki, R. St. Touzani, B. P. T. Fokwa, *J. Solid State Chem*, **2013**, *203*, 304.
[2] R. St. Touzani, B. P. T. Fokwa, *J. Solid State Chem*, **2014**, *211*, 227.

PTue036

Mechanical and Electronic Properties of π -Conjugated Organometallic Nanomaterials

Kang, Hong Seok (Jeonju University, Chonju, Chonbuk, KOR)

Using first-principles calculations, we have investigated elastic and electronic properties of single sheets of two-dimensional (2D) π-Conjugated M-Bis(dithiolene) Nanosheet (M-C4S4) (M= Ni, Pd), between which the NiC4S4 sheet was recently synthesized. Under isotropic strain, our calculation of the in-plane stiffness parameter C and Poisson ratio ν indicates that the 2D M-C4S4 are even softer than grapyne-4, which is the most porous among all graphyne analogs considered. In addition, different configurations are found to correspond to local energy minima for the bilayer of NiC4S4, when one of the layer is slided with respect to the other one by an application of shear stress. Overall, the sliding brings about a continuous tuning of the band gap of the NiC4S4 bilayer from a semiconductor to a metal, rendering it potentially useful in nanoelectromechanical devices. Furthermore, we have shown that double-stranded zinc(II) porphyrin ladder polymer (Zn-LADDER) arrays recently synthesized exhibits a giant Stark effect upon application of transverse electric field, which is as strong as that in boron nitride nanotubes.

PTue037

On the correct form of the nonlinear optical susceptibility in strongly-driven semiconductor quantum dots

Paspalakis, Emmanuel (University of Patras, Patras); Boviatsis, John (Technological and Educational Institute of Western Greece, Patras); Baskoutas, Sotirios (University of Patras, Patras)

In recent years, significant attention has been given to nonlinear optical phenomena, such as nonlinear optical absorption and dispersion, derived from a driven quantum transition of semiconductor nanostructures, such as semiconductor quantum wells, quantum disks and mainly quantum dots. An important issue that is widely studied is the effect of probe electromagnetic field intensity on the total (nonlinear) absorption coefficient and on the total (nonlinear) index of refraction. Some of the phenomena that are commonly found for large electromagnetic field intensities are the creation of a strong dip in the absorption spectrum near or at resonance (the so-called bleaching effect), negative absorption near or at resonance that leads to optical gain and the change of the slope of the total index of refraction near or at resonance from negative to positive that changes the behavior of the system from fast to slow light.

Unfortunately, these phenomena do not exist and are artifacts of a common abuse of the theoretical methodology for the study of the total absorption coefficient and the total index of refraction. The main error is that the total absorption coefficient and the total index of refraction was initially derived from density matrix equations using perturbation theory and includes first-order (linear) as well as third-order (nonlinear) terms. This method gives correct results for small electromagnetic field intensities and it leads to saturation of absorption and dispersion in this regime. However, for larger intensities it gives the misleading results mentioned above due to either failure of the order of perturbation theory considered in the derivation of the total absorption coefficient and the total index of refraction or even failure of perturbation theory at all in the treatment of the problem.

In this work, we revisit the problem of the total absorption coefficient and the total index of refraction in a symmetric semiconductor quantum dot structure (we choose the example of a core-shell quantum dot) under a strong probe field excitation. We use the two-level model, solve the relevant density matrix equations under the rotating wave approximation and under steady state conditions, and obtain the correct form of the nonlinear optical susceptibility that is then used for the derivation of the formulae of the total absorption coefficient and the total index of refraction under the interaction with a strong probe field. Actually, the commonly used perturbation theory formulae can be obtained by our formulae using a series expansion and keeping terms up to second order in electric field amplitude. We also derive the electronic structure of the quantum dot system by solving numerically the time-independent Schrödinger equation, under the effective mass approximation, using the potential morphing method and obtain the energy difference and the electric dipole matrix element for the relevant transitions of the quantum dot system. Then, for the specific quantum dot system we compare the results of the total absorption coefficient and the total index of refraction for the two methodologies (the perturbation result and our result) for different electromagnetic field intensities.

This research has been co-financed by the European Union (European Social Fund - ESF) and Greek national funds through the Operational Program "Education and Lifelong Learning" of the National Strategic Reference Framework (NSRF) - Research Funding Program: Archimedes III.

PTue038

On the role of computational modelling in the understanding of novel organic electroactive materials for Li-ion batteries

Tomerini, Daniele (Laboratoire de Réactivité et Chimie des Solides, Amiens, FRA); Dupradeau, François-Yves (Laboratoire de Glycochimie, des Antimicrobiens et des Agroressources, Amiens, FRA); Frayret, Christine (Laboratoire de Réactivité et Chimie des Solides, Amiens, FRA)

In the search for cost-effective and less ecological footprint Lithium-ion batteries, redox-active organic compounds could offer great promise to contribute to the future sustainable supply of the energy. In this “nascent” research area, computational modeling can play a crucial role. Beyond the possible design of new promising redox active compounds through molecular quantum theory approaches [1], simulation applied to the periodical structures may offer the possibility to gain insight in the electrochemical process of the actual material at the atomic scale. More specifically, despite current extensive efforts in experimental research, this field is sometimes facing some deficiencies in the knowledge of either the lithiated or delithiated phase structure or even both of them. Indeed, large difficulties are still encountered when dealing with in-situ XRD studies during electrochemical experiments, in such a way that few crystals of alkali salts of semiquinone anion radicals are reported to date for instance. From some case studies, we were able to highlight the success of DFT approach in helping a lot experimentalists for the knowledge of the lithiated phase of tetramethoxy-para-benzoquinone (which was unknown experimentally and for which the computationally identified structure agrees with the experimental voltage) [2]. Moreover, X-Ray Diffraction (XRD) analysis may be insufficient in precisely locating Hydrogen positions, which are however fundamental for the understanding of intermolecular interactions. When neutron diffraction data are unavailable, a great benefit can thus be afforded by combining experiments with theoretical calculations. In such context, we proved that providing an adjustment of the semi-empirical treatment for the dispersion component (added to the DFT one), dispersion-corrected DFT computations are really reliable to account for geometrical features of organic crystals (including lattice parameters, bond lengths, stacking inter-plane distance, …) [2-5]. Starting from heavy atoms positioning issued from XRD data, improvement in Hydrogen location was provided on the Li2DHDMQ□4H2O compound along with the differentiation of bonding between 100K and ambient forms from topological analysis of the electron density through the Atoms in Molecules theory [5]. However, one of the great challenges remains the identification of most probable oxidized or reduced crystalline forms in some complicated cases especially when structural solvent molecules can be present in the lattice. Moreover, there is no guarantee to be able to reach the global minimum structure by simply calling to the manual insertion/depletion of lithium ions. Beyond periodical DFT computations, we then initiated a Crystal Structure Prediction approach (combining for instance force fields molecular calculations / simulated annealing treatments and dispersion-corrected DFT modelling) with some promising success on a few examples. Within this context and through the selection of the most striking examples, we will present the lessons and challenges of solid state modelling for organic electrodes in Lithium-ion batteries.

---

[1] D. Tomerini et al., PCCP, 2015, 17, 8604.
[2] G. Bonnard et al., RSC Adv., 2013, 3, 19081.
[3] C. Frayret, et al.,PCCP, 2012, 14, 11398.
[4] A.-L. Barrès et al. Chem. Eur. J., 2012, 18, 8800.
[5] G. Bonnard et al., CrystEngComm, 2013, 15, 2809.

PTue039

Synthesis, phase formation, structure and thermal expansion behavior of double arsenates of zirconium and alkali earth metals

Shipilov, Alexander (Lobachevsky State University of Nizhni Novgorod, Nizhni Novgorod, RUS); Pet'kov, Vladimir (Lobachevsky State University of Nizhni Novgorod, Nizhni Novgorod, RUS); Sukhanov, Maksim (Lobachevsky State University of Nizhni Novgorod, Nizhni Novgorod, RUS); Borovikova, Elena (Lomonosov Moscow State University, Moscow, RUS)

Compounds with kosnarite structure ($KZr_2(PO_4)_3$, isostructural $NaZr_2(PO_4)_3$, NZP, and $Na_{1+x}Zr_2Si_xP_{3-x}O_{12}$, NASICON) are researched intense due to wide cation isomorphism in all crystallographic positions and opportunity of using these compounds as solid electrolytes, low thermal expansion ceramics, matrix for immobilization of radioactive waste, etc. The goal of this research is a synthesis, studying of phase formation, refinement of the crystal structure and studying of thermal expansion of arsenates in the $M_{0.5}Zr_2(AsO_4)_3$ series (M = Mg, Ca, Sr, Ba).

Individual compounds were synthesized with sol-gel method. Gels were dried at 90 ° C and after were heated at 600−850 ° C until ending of the synthesis. Products were explored with X-ray diffraction, IR-spectroscopy and X-ray microanalysis methods. Research was performed with using equipment of Shimadzu firm.

Compounds $M_{0.5}Zr_2(AsO_4)_3$ form at ~800° C . $Mg_{0.5}Zr_2(AsO_4)_3$ is crystallized in $Sc_2(WO_4)_3$ structural type and stable until 850° C . Arsenates $M_{0.5}Zr_2(AsO_4)_3$ with M = Ca, Sr, Ba are crystallized in NZP structural type and stable until 1000° C . There is linear dependence between unit cell parameters and alkaline earth cation radius. When the radius of M-cation increases, parameter *c* increases and *a* reduces. This feature of NZP structure connected with following reason: increasing size of M-cation leads to increasing of extra-frameworkcavity inside the column between two surfaces of nearby octahedra ZrO_6, which situated along *c*-axis, and as a consequence to increasing of *c* parameter. At the same time there is a correlated rotation of ZrO_6-octahedra and AsO_4-tetrahedra which bind parallel columns. This rotation leads to reducing of distance between columns and *a* parameter.

There are nine bands in IR-spectrum of $Mg_{0.5}Zr_2(AsO_4)_3$ in the region of AsO_4^{3-} stretching vibrations (1024–780 cm^{-1}). The same spectra character has zirconium phosphates with Co , Ni, Cu and Mn (sp. gr. $P2_1/n$). According to this and X-ray diffraction data we classified $Mg_{0.5}Zr_2(AsO_4)_3$ to the same space group. The asymmetric stretching vibrations ν_3 of the AsO_4^{3-} ion in IR-spectra of this compound were shown by bands at 1024–831 cm^{-1}, the symmetric stretching vibrations ν_1 − by bands at 808, 798, 782 cm^{-1}, the bending vibrations ν_4 − by big amount of bands at 516−418 cm^{-1}. IR-spectra of zirconium arsenates which include bigger alkaline earth cations (Ca, Sr, Ba) than Mg, were classified to R–3 space group. The five bands in the range 1020–850 cm^{-1} are assigned to the symmetric stretching As−O vibrations of the AsO_4^{3-} ion; the band at ~820 cm^{-1} corresponds to the symmetric stretching vibrations (a factor group analysis of the vibrations of the AsO_4^{3-} ion predicts that there are six stretching IR-active vibrations). The bands in 500–400 cm^{-1} correspond to the bending vibrations (ν_4) of the ion.

$M_{0.5}Zr_2(AsO_4)_3$ (M = Ca, Ba) structures were refined by the Rietveld method. The basic element of the crystal structure of the arsenates is a three-dimensional framework. Topologicalunit of framework is formed with “lanterns”, built with 3 AsO_4 -tetrahedra and 2 ZrO_6-octahedra, connected by vertices. “Lanterns” form infinite columns, which are parallel to the axis of –3 order. Ba and Ca cations are half placed extra-frameworkpositions.

Temperature dependences of the unit cell parameters of $M_{0.5}Zr_2(AsO_4)_3$ (M = Ca, Sr, Ba) were studied by high-temperature X-ray diffraction, and thermal expansion coefficients of the compounds were determined. α_{av} were $5.5\cdot10^{-6}$, $5.0\cdot10^{-6}$, $4.5\cdot10^{-6}$ ° C^{-1} respectively (middle expansion substances).

The reported study was supported by RFBR, project No. 15-03-00716.

PTue040

The Vickers microhardness prediction of TiC and TiN: A DFT study

Azibi, Mourad (Centre for development of advanced technologies (CDTA), Algiers, DZA); Saoula, Nadia (Centre for development of advanced technologies (CDTA), Algiers, DZA)

The Vickers microhardness of NaCl-type TiC and TiN is calculated using elastic properties obtained by first principle pseudopotential method within generalized gradient approximation (GGA) proposed by Perdew–Burke–Ernzerhof (PBE) combined with theoretical model developed by Chen which established a correlation between hardness and elasticity.

Calculated lattice parameters, elastic constants and theoretical Vickers hardness are in excellent agreement with available experimental and theoretical results.

The method developed by Chen,to obtain the Vickers microhardness, could be applied to a systematic study of a wide variety of crystalline materials.

PTue041

Charge and Spin Ordering in Intrinsically Doped Sodium Oxocuprates

Frei, Maren (Max-Planck-Institute for Chemical Physics of Solids, Dresden, GER); Ali, N.Z. (Max-Plank-Institut for Chemical Physics of Solids, Dresden, GER); Sirker, J. (Max-Plank-Institut for Chemical Physics of Solids, Dresden, GER); Nuss, J. (Max-Plank-Institut for Chemical Physics of Solids, Dresden, GER); Horsch, P. (Max-Plank-Institut for Chemical Physics of Solids, Dresden, GER); Jansen, M. (Max-Plank-Institut for Chemical Physics of Solids, Dresden, GER)

Using alkali azides and the respective nitrates as starting materials for alkali oxometallates offers the option of precisely fixing the oxygen content and therefore the valence state of the transition metals in respective multinary oxides. This so called “azide/nitrate route” [1] has allowed us to gain access to a family of intrinsically doped Mott insulators, the charge ordered sodium oxocuprates (II/III) of general composition $Na_{1+x}CuO_2$, with the end members $NaCuO_2$ and the still elusive Na_2CuO_2. The first candidates of edge-sharing chain cuprates $Na_3Cu_2O_4$ (x = 1/2) and $Na_8Cu_5O_{10}$ (x = 3/5) are the first unambiguous manifestations of one-dimensional Wigner lattices, where long-range Coulomb interactions determine the charge ordering pattern [2]. The magnetic properties of the latest member of this family $Na_5Cu_3O_6$, with less stable hole doping 1/3, reveal a new scenario of charge-ordered cuprates [3]. Here, in addition to classical charge ordering, the antiferromagnetic coupling is weakened by virtual excitations across the Wigner gap: the third-nearest-neighbor coupling dominates the magnetic interaction. A numerical calculation for an effective long-range Heisenberg model with parameters from detailed analysis of the magnetic exchange constants as a function of the Wigner gap fits the susceptibility data fairly well. Newly realized spin patterns will be discussed.

---

[1] M. Jansen, *Z. anorg. allg. Chem.***2012**, 638, 1910.

[2] P. Horsch, M. Sofin, M. Mayr, M. Jansen, *Phys. Rev. Lett.***2005**, 94, 076403.

[3] N. Z. Ali, J. Sirker, J. Nuss, P. Horsch, M. Jansen, *Phys. Rev. B***2011**, 84, 035113.

PTue042

Coexistence of Ferromagnetism and Superconductivity in the iron chalcogenide $[(Li_{0.8}Fe_{0.2})OH]FeSe$

Pachmayr, Ursula (Ludwig-Maximilians-Universität München, München, GER); Johrendt, Dirk (Ludwig-Maximilians-Universität München, München, GER); Nitsche, Fabian (Ludwig-Maximilians-Universität München, München, GER); Luetkens, Hubertus (Paul Scherrer Institut PSI, Villigen, CHE); Brückner, Felix (Technische Universität Dresden, Dresden, GER); Kamusella, Sirko (Technische Universität Dresden, Dresden, GER); Sarkar, Rajib (Technische Universität Dresden, Dresden, GER); Klauss, Hans-Henning (Technische Universität Dresden, Dresden, GER)

Superconductivity is generally considered incompatible with ferromagnetism. The latter generates magnetic flux, while superconductivity expels magnetic flux from the interior of a solid. In $[(Li_{0.8}Fe_{0.2})OH]FeSe$ we recently observed the astonishing coexistence of these ordering phenomena.[1] The crystal structure exhibits alternately stacked lithium-iron-hydroxide layers and iron selenide layers. The latter provide superconductivity up to 43 K, whereas the magnetic ordering emerges from iron ions in the hydroxide layer at 10 K. Even though the internal dipole field of the ferromagnet acts on the superconductor, superconductivity is not suppressed but a spontaneous vortex phase is formed. Magnetization measurements, ^{57}Fe-Mössbauer spectra, ^{7}Li-NMR spectra and µSR experiments confirm these findings.

---

[1] U. Pachmayr, F. Nitsche, H. Luetkens, S. Kamusella, F. Brückner, R. Sarkar, H.-H. Klauss and D. Johrendt, *Angew. Chem. Int. Ed.*, **2015**, *54*, 293-297.

PTue043

Crystal structure and magnetic phase transitions of $Bi_4Fe_5O_{13}F$, a material with the frustrated magnetic pentagonal Cairo lattice.

Batuk, Dmitry (EMAT, University of Antwerp, Antwerp, BEL); Abakumov, Artem M. (Electron microscopy for material science (EMAT), University of Antwerp / Department of Chemistry, Moscow State University, Moscow, RUS); Tsirlin, Alexander A. (National Institute of Chemical Physics and Biophysics, Tallin, EST); Hadermann, Joke (Electron microscopy for material science (EMAT), University of Antwerp, Antwerp, BEL)

Frustrated magnetic systems demonstrate a plethora of unusual magnetic ground states, which makes them an attractive research subject form both theoretical and experimental perspectives. Most of the geometrically frustrated systems are based on spin lattices that comprise closed triangular loops. Five-bond loops are rare and can be found in the so-called Cairo lattice. Since regular pentagonal units do not form a tiling on the plane, the Cairo lattice, unlike the triangular lattice, contains non-equivalent bonds. Recent theoretical works put forward a number of unconventional ground states, including spin nematics, and other interesting properties of the Cairo spin lattice. These predictions remain highly challenging for experimental verification. The pentagonal arrangement of magnetic ions in the crystals is very rare, which is partly related to the fact that periodic crystals cannot have five-fold symmetry. Presently, the only known magnetic prototype material with the Cairo lattice is $Bi_2Fe_4O_9$ having a mullite-type crystal structure.

In this contribution, we present a new mullite-based structure of $Bi_4Fe_5O_{13}F$ featuring the pentagonal Cairo lattice. The crystal structure of this material was determined using a combination of neutron powder diffraction, synchrotron X-ray powder diffraction, and transmission electron microscopy. $Bi_4Fe_5O_{13}F$ crystallizes in the tetragonal $P4_2/mbc$ space group with the lattice parameters at room temperature $a = 8.2995(1)$ Å and $c = 18.0573(3)$ Å. The crystal structure is preserved in a wide temperature range 1.5 – 700 K. Similar to the mullite structure, it is built of infinite rutile-like chains of edge-sharing FeO_6 octahedra, which are interconnected with Fe_2O_7 bow-tie fragments of double FeO_4 tetrahedra. These bow-tie fragments together with the double octahedral fragments from the chains form quasi-two-dimensional Cairo lattice. Unlike the mullite structure, where the pentagonal layers are found at every second octahedra in the chains, they appear at every third octahedra in $Bi_4Fe_5O_{13}F$. The structural cavities between the pentagonal layers are filled with anion-centered Bi_4F tetrahedra.

The magnetic structure of the material was characterized using neutron powder diffraction data, thermodynamic measurements and density-functional band-structure calculations. Below $T_N = 178$ K, the long-range magnetic order sets in. The topology of the structure gives rise to the frustrated exchange couplings and induces a sequence of magnetic phase transitions at $T_1 = 62$ K, $T_2 =71$ K. Below T_1, $Bi_4Fe_5O_{13}F$ forms a fully ordered non-collinear antiferromagnetic structure, whereas the two magnetic states between T_1 and T_N feature lower ordered moments and different spin arrangements. The magnetic phase transitions are associated with changes in the orientation and the magnitude of the ordered magnetic moments. While the magnetic ground state below T_1 follows expectations for the Cairo spin lattice, the behavior at finite temperatures and the sequence of magnetic transitions are highly unusual and so far unanticipated by theory.

The work was partially supported by the Russian Science Foundation (grant 14-13-00680)

PTue044

High pressure synthesis, structures and magnetic properties of Mn_2MSbO_6 oxides

Sáez-Puche, Regino (Universidad Complutense de Madrid, Madrid, ESP; Solana-Madruga, Elena (Universidad Complutense de Madrid, Madrid, ESP); Dos Santos-García, Antonio J. (Universidad Politécnica de Madrid, Madrid, ESP); Ritter, Clemens (Institut Laue-Langevin, Grenoble, FRA); Arévalo-López, Ángel M. (Centre for Science at Extreme Conditions and School of Chemistry, University of Edinburgh, Edinburgh, GBR); Attfield, J. Paul (Centre for Science at Extreme Conditions and School of Chemistry, University of Edinburgh, Edinburgh, GBR)

ABO_3 ternary oxides, where A and B cations can be distributed either randomly or ordered into the crystallographic sites, have been widely studied due to their potential applications arising from their diverse electric and magnetic behaviors [1]. Among the ordered oxides, the most commonly studied compounds belong to the perovskite family. These are the so called double perovskites, of general formula $A_2BB'O_6$, where B and B’ cations arrange in a rock-salt ordered fashion within the octahedral network and A cations occupy the cuboctahedral voids. However, when A and B cations segregate into alternate layers perpendicular to the c-axis, an ilmenite-type structure can also be found. Our recent studies have shown that cation distribution ranges from one polymorph to another depending on size and/or charge ratios, oxidation state stability and kinetics effects. In this work we present a detailed study on the synthesis and magnetic properties of Mn_2MSbO_6 (M=Sc, Cr, Fe) compounds. High pressure and temperature synthesis is needed for the occurrence of these polymorphs. The use of moderate pressures (~3-4 GPa) leads to the formation of the ilmenite structure but stabilizing the small Mn^{2+} cation in the A site of the denser perovskite structure is only possible at high pressures (~8-12 GPa) [2]. Mn_2MSbO_6 (M= Sc, Cr) perovskites present antiferromagnetic (AFM) ground states at low temperatures, where their magnetic structures are ruled by the $\kappa = [0\ 0\ 0]$ and $\kappa = [½\ 0\ ½]$ propagation vectors respectively [3]. Otherwise, the Mn_2FeSbO_6 perovskite [4] shows a more complex magnetic behavior due to the presence of ferromagnetic inhomogeneities within an AFM matrix. The incommensurate magnetic structure at low temperatures is described by $\kappa = [0\ 0.426\ 0]$, where both Mn and Fe moments run parallel to the b-axis of an elliptical helix. It is well know that helical spin structures can break inversion symmetry and generate multiferroicity, but in this case our electrical polarization measurements on a dense pellet did not show any ferroelectric behavior. Mn_2MSbO_6 (M= Fe and Cr) ilmenite polymorphs show a complex magnetic behavior. Magnetic susceptibility, magnetization and powder neutron diffraction data confirm the AFM helical ordering of Cr^{+3} and Mn^{+2} spins in an incommensurate magnetic structure with $\kappa = [0\ 0\ 0.46]$ below 60 K, and a temperature dependence of κ up to [0 0 0.54] at about 10 K. On the other hand, Mn_2FeSbO_6 ilmenite presents an antiparallel alignment of the $2Mn^{+2}$ and the Fe^{+3} spins below 260 K with a magnetic propagation vector $\kappa_1 = [0\ 0\ 0]$. This ferrimagnetic structure represents, however, not the magnetic ground state of the system: it undergoes, then, a second magnetic transition at ∼ 50 K where the high temperature magnetic phase leaves place to an incommensurate magnetic structure described by $\kappa_2 = [0\ 0\ 0.07]$, as deduced from the appearance of new satellite peaks around (003) reflection. A specially worthwhile example is the Mn_2ScSbO_6 compound when synthesized at moderate pressures. Order-disorder effects occur within the ilmenite structure (S.G. R-3), thereby allowing Sc and Sb ordering by lowering the symmetry (R3). The charge/size relationship induces an unusual cation ordering, giving rise to its crystallization with the Ni_3TeO_6-type structure [5]. Since Sc and Sb are displaced from each other becoming no longer coplanar, this structure breaks the inversion symmetry, allowing a spontaneous polarization of the material.

---

[1] Greenblatt et al. *Angew. Chem. Int. Ed.* 2013, **52**.

[2]M. A. Alario-Franco et al., *J. Am. Chem. Soc.*, 2011, **133**, 8552.

[3] R. Sáez-Puche et al. *Dalton Trans.*, 2015, Advance Article. **DOI**: 10.1039/C4DT03849E.

[4] R. Sáez-Puche et al. *J.Phys.:Condens.Matter.*, 2013, **25**, 206004.

[5] C. J. Fennie, *Phys. Rev. Lett.* 2008, **100**, 167203.

PTue045

Valence Bond Glass Formation and Dynamic Magnetic Ordering in Frustrated Perovskites

Coomer, Fiona (Isis Neutron and Muon Source, Didcot, GBR); Cussen, Eddie (University of Strathclyde , Glasgow, GBR)

Antiferromagnetic coupling between magnetic centres classically leads to the formation of an antiferromagnetically ordered ground state. In many cases the interactions conflict leading to frustration that inhibits the formation of a long-range magnetically ordered state. If the magnetic centres are distributed on a face-centred cubic (*fcc*) lattice then coupling between points of an equilateral triangle leads to perfect frustration. The perovskite structure can accommodate a range of cations in the six-coordinate octahedral site. We have used cation-ordering to generate *fcc* lattices containing the paramagnetic ions Mo^{5+} and Mn^{2+} on half of these sites in Ba_2LuMoO_6 and Ba_2MnMoO_6 respectively.

Ba_2LuMoO_6 contains diamagnetic Lu^{3+} and almost complete chemical ordering between this and Mo^{5+} leads to an *fcc* lattice of Mo^{5+}, $S={}^1/_2$ cations. Neutron diffraction and magnetic measurements show that there is no long-range ordering of these spins despite strong antiferromagnetic coupling and that the cubic structure is maintained to 2 K. However, in common with the isostructural compound Ba_2YMoO_6, [1, 2] this compound shows a loss of magnetic moment and a weakening of the magnetic exchange interaction indicative of the formation of a valence bond glass.[3]

Ba_2MnMoO_6 contains an *fcc* lattice of Mn^{2+}, $S={}^5/_2$ cations that are paramagnetic at room temperature with antiferromagnetic coupling, $\theta = -78(1)$ K, between moments of 4.5 μ_B per Mn^{2+}. Neutron diffraction data collected at 2 K show an antiferromagnetically ordered phase with *ca.* $4\mu_B$ per Mn^{2+} forming a degenerate, non-collinear magnetic structure. The magnetic Bragg peaks are lost by 10.8(1) K. Remarkably, the bulk magnetisation gives no indication of this complete spin cancellation, but shows only a weak transition around 3.5 K whilst muon spin relaxation shows a magnetic transition at 8 K. The dependence of the apparent ordering temperature on the timescale of the measurement technique suggests that the long-range antiferromagnetism evident in the neutron diffraction measurements represents a spin arrangement that is dynamic over the longer timescales sampled by the other techniques.

---

[1] M. A. de Vries, A. C. McLaughlin and J. W. G. Bos *Physical Review Letters* 2010, 104, 177202.

[2] T. Aharen, J. E. Greedan, C. A. Bridges, A. A. Aczel, J. Rodriguez, G. MacDougall, G. M. Luke, T. Imai, V. K. Michaelis, S. Kroeker, H. D. Zhou, C. R. Wiebe and L. M. D. Cranswick, *Physical Review B* 2010, 81, 224409.

[3] F. C. Coomer and E. J. Cussen, *J. Phys.: Condens. Matter* 2013, 25(8):082202.

[4] F. C. Coomer and E. J. Cussen, *Inorganic Chemistry* Vol 53, No. 2, pp. 746-755 (2014)

PTue046

Ways Out of Frustration?! The Magnetic Structures of the low and high temperature phases of $Mn_3(VO_4)_2$

Clemens, Oliver (TU Darmstadt and KIT Karlsruhe, Darmstadt, GER); Nénert, Gwilherm (PANalytical, Almelo); Wright, Adrian J. (University of Birmingham, Birmingham, GBR); Knight, Kevin S. (ISIS Facility, Didcot, GBR); Berry, Frank J. (University of Birmingham, Birmingham, GBR); Slater, Peter R. (University of Birmingham, Birmingham, GBR)

Transition metal vanadates $M_3(VO_4)_2$ (M = Mn, Ni, Co) are interesting materials due to crystallisation in a Kagomé staircase structure [1, 2]. This structure gives rise to spin frustrated interactions between edge sharing, octahedrally coordinated M ions, due to a triangular interaction situation. The magnetic structures of $Ni_3(VO_4)_2$ and $Co_3(VO_4)_2$ are well known and show ferrimagnetic incommensurate ordering [3], where for $Ni_3(VO_4)_2$ even multiferroic properties arising from a structural transition at high magnetic fields have been reported [4]. In contrast, the detailed magnetic structure of manganese vanadate (lt-$Mn_3(VO_4)_2$) was not reported and the material was only characterised regarding its magnetic properties [5] by field dependent measurements. This is explained by the fact that a facile synthesis route for the preparation as a single phase powder was only reported recently [6]. In this study, also the formation of a structurally different high temperature phase could be observed (ht-$Mn_3(VO_4)_2$), and this phase can easily stabilized by means of chemical substitution using alkali metals ($A_{2x}Mn_{3-x}(VO_4)_2$, A = Li, Na) [6, 7]. ht-$Mn_3(VO_4)_2$ shows a rather unusual structural arrangement with partially 8 fold coordinated Mn^{2+} ions (with a coordination polyhedron known as Hoard dodecahedron), and spin frustration would also be expected between neighbouring Mn^{2+} ions due to triangular interaction situations. Here we report on the determination of the magnetic structures of both lt as well as ht-$Mn_3(VO_4)_2$ by means of powder neutron diffraction studies, and the correlation with magnetic properties [8, 9].

For the soft ferrimagnet ht-$Mn_3(VO_4)_2$, magnetic properties are well explained by similar superexchange pathways between the 8-fold coordinated Mn^{2+} ions with the other octahedrally coordinated Mn^{2+} ions [8]. In contrast, lt-$Mn_3(VO_4)_2$ is known to show two different magnetically ordered states [5], which have been described as the LT1 ($T < 16$ K) and the HT1 ($16 \text{ K} < T < 25$ K) phases. The detailed structures of both magnetic phases could be determined. In this respect we showed that the small remanent magnetisation of ~ 1.5 µB per $Mn_3(VO_4)_2$ unit of the LT1 phase results from an unique spin canting within the Kagomé staircase structure [9] with moments commensurately ordering within the *ab*-plane.

---

[1] H. Fuess, E. F. Bertaut, R. Pauthenet and A. Durif, Acta Crystallogr., 1970, B26, 2036-2046.

[2] G. M. Clark, R. Morley and A. N. Pick, J. Inorg. Nucl. Chem., 1977, 39, 1841-1843.

[3] Y. Chen, J. W. Lynn, Q. Huang, F. M. Woodward, T. Yildirim, G. Lawes, A. P. Ramirez, N. Rogado, R. J. Cava, A. Aharony, O. Entin-Wohlman and A. B. Harris, Phys. Rev. B, 2006, 74, 014430.

[4] G. Lawes, A. B. Harris, T. Kimura, N. Rogado, R. J. Cava, A. Aharony, O. Entin-Wohlman, T. Yildirim, M. Kenzelmann, C. Broholm and A. P. Ramirez, Phys. Rev. Lett., 2005, 95, 087205.

[5] E. Morosan, J. Fleitman, T. Klimczuk and R. J. Cava, Phys. Rev. B, 2007, 76, 144403.

[6] O. Clemens, R. Haberkorn and H. P. Beck, J. Solid State Chem., 2011, 184, 2640-2647.

[7] O. Clemens, R. Haberkorn, M. Springborg and H. P. Beck, J. Solid State Chem., 2012, 194, 409-415.

[8] O. Clemens, A. J. Wright, K. S. Knight and P. R. Slater, Dalton Trans., 2013, 42, 7894-7900.

[9] O. Clemens and G. Nénert, Dalton Trans., in preparation.

PTue047

Li-Ion Dynamics of Layer-Structured 2H-Li$_x$NbS$_2$ studied by ^{7}Li NMR

Stanje, Bernhard (Technical University of Graz, Graz, AUT)

Layer-structured materials such as graphite (LiC$_y$) or Li$_x$(Co,Ni,Mn)O$_2$ are important electrode materials in current battery research that still relies on insertion materials. This is due to their excellent ability to reversibly accommodate small alkali ions such as Li$^+$ and Na$^+$. Despite of these applications behind, microscopic information on Li ion self-diffusion in transition metal sulfides are relatively rare. Here, we used ^{7}Li nuclear magnetic resonance (NMR) spectroscopy to study translational Li ion diffusion in the model system hexagonal (2H) Li$_x$NbS$_2$ (x = 0.3, 0.7 and 1) by means of variable-temperature NMR relaxometry. ^{7}Li spin-lattice relaxation rates and 7Li NMR spectra were used to determine Li jump rates and activation barriers as a function of Li content. Hereby, NMR spinlattice relaxation rates recorded with the spin-lock technique offered the possibility to study Li ion dynamics on both the short-range and long-range length scale. Dynamic parameters, such as jump rates and activation barriers, could be extracted from complete diffusion-induced rate peaks, which are obtained when the relaxation rate is plotted vs reciprocal temperature. The peak maximum of the three samples studied shifts towards higher temperatures with increasing Li content x in 2H-Li$_x$NbS$_2$ revealing a decrease of Li diffusivity with increasing x. Information on the dimensionality of the diffusion process was experimentally obtained by frequency dependent Rρ measurements carried out at T = 444 K, that is in the high-temperature regime of the rate peaks. A slight, but measurable frequency dependence within this limit is found for all samples; it is in agreement with predictions from relaxation models developed to approximate low-dimensional (2D) jump diffusion; thus, Li diffusivity within the van der Waals gap governs the NMR rates recorded.

PTue048

Visualization of ion motion in Fe-SrTiO$_3$ thin films by means of impedance spectroscopy under bias

Taibl, Stefanie (TU Wien, CTA - Electrochemistry, Vienna, AUT)

SrTiO$_3$ is among the most investigated perovskite-type oxides and therefore serves as model material for other -more complex- perovskites e.g. BaTiO$_3$ or Pb(Zr,Ti)O$_3$. The scientific interest in SrTiO$_3$ not only refers to polycrystalline as well as single- crystalline bulk material [1], SrTiO$_3$ recently came into the focus of research since it is a promising candidate in the field of resistive switching. Local conductivity changes after applying a high electrical field to single- and polycrystalline SrTiO$_3$ bulk samples were already measured and simulated [2,3]. Accordingly, in current literature the observed resistive switching behavior of SrTiO$_3$ thin films is also discussed in terms of field driven ion motion [4].

In this contribution we combine two methods to obtain more information on the mass and charge transport properties in slightly Fe-doped SrTiO$_3$ thin films. Electrical impedance spectroscopy (EIS) performed in a temperature range between 700°C and 300°C revealed an additional low frequency feature under anodic (inductive loop) as well as under cathodic bias (second semicircle or inductive loop). DC measurements with different cycling rates made it possible to probe the samples in two different states, providing information on samples with continuously changing stoichiometry as well as information on samples in a fixed polarization condition. By correlating the results obtained from current-voltage measurements with the impedance data we were able to quantify ion motion in these thin films even though the ionic conductivity is much lower than the electronic one.

---

[1] R. Merkle and J. Maier, Angewandte Chemie International Edition, 2008, 47, 3874-3894.

[2] S. Rodewald, J. Fleig and J. Maier, Journal of the European Ceramic Society, 1999, 19, 797-801.

[3] R. Waser, Journal of the American Ceramic Society, 1991, 74, 1934-1940.

[4] R. Waser, R. Dittmann, C. Staikov and K. Szot, Advanced Materials, 2009, 21, 2632-2663.

PTue049

A Micro-contact Electrochemical Impedance Spectroscopy Study of NASICON Type $Li_{1.5}$ $Al_{0.5}$ $Ti_{1.5}$ $(PO_4)_3$ and $LiTi_2$ $(PO_4)_3$ Single Crystals

Rettenwander, Daniel (Dept. Materials Research & Physics, University of Salzburg, Salzburg, AUT); Welzl, Andreas (Institute for Chemical Technologies and Analytics, Vienna University of Technology, Getreidemarkt 9/164EC, AUT); Pristat, Sylke (Forschungszentrum Jülich GmbH, Institute of Energy and Climate Research, Materials Synthesis and Processing (IEK-1), Jülich, GER); Tietz, Frank (Forschungszentrum Jülich GmbH, Institute of Energy and Climate Research, Materials Synthesis and Processing (IEK-1); Helmholtz-Institute Münster, c/o, Jülich, GER); Redhammer, Günther (Dept. Materials Research & Physics, University of Salzburg, Salzburg, AUT); Amthauer, Georg (Dept. Materials Research & Physics, University of Salzburg, Salzburg, AUT); Fleig, Jürgen (Institute for Chemical Technologies and Analytics, Vienna University of Technology, Wien, AUT)

NASICON-type (**NaS**uper-**I**onic **Con**ductor) solid electrolytes are known for their high Li ion conductivities, in particular systems derived from the $LiTi_2(PO_4)_3$ (LTP) system have been widely studied.[1-3] The partial substitution of Ti^{4+} by a subvalent cation such as Al^{3+}, Ga^{3+}, In^{3+}, Sc^{3+}, Y^{3+}, La^{3+}, Cr^{3+} or Fe^{3+} leads to an increase of Li^+ content and forms the high ionic conducting $Li_{1+x}M_xTi_{2-x}$ $(PO_4)_3$ system.[4,5] Among this group the $Li_{1+x}Al_{1+x}Ti_{2-x}(PO_4)_3$ (LATP) composition show the highest Li^+ conductivity and one of the highest within the group of inorganic Li+ conducting electrolytes.[6,7] The additional Li^+ occupy sites which are unoccupied in the conventional LTP structure by forming a 3D Li^+ network in the NASICON structure. One would expect that the formed Li^+ network is responsible for the improved total ionic conductivity, but instead the total ionic conductivity is dominated by the grain boundary conductivity and the grain conductivity plays just a minor role.[8] Nevertheless, the exact contribution of the grain conductivity to the total ionic conductivity and how grain conductivity is related to the crystal chemistry is not at hand.

Therefore we used for the first time micro-contact electrochemical impedance spectroscopy to exactly determine the bulk ionic conductivity of dense LTP and LATP single crystals, which are carefully studied by X-ray single crystal diffraction. This finally enables us to quantify the effect of crystal chemistry on Li-ion transport within the grain. The results of this study will be presented at the conference.

---

[1] J. Fu, *Am. Ceram. Soc.***1997**, 80, 1901.
[2] H. Aono, E. Sugimoto, Y. Sadaoka, N. Imanaka, G. Adachi, *J. Electrochem. Soc.* **1989**, 136, 590.
[3] X. Xu, Z. Wen, X. Yang, J. Zhang, Z. Gu, *Solid State Ionics***2006**, 177, 2611.
[4] P. Maldonado-Manso, E.R. Losilla, M. Martínez-Lara, M.A.G. Aranda, S. Bruque, F.E. Mouahid, M. Zahir, *Chem. Mater.* **2003**, 15, 1879.
[5] J. Fu, J. Mater. Sci. **1998**, 33, 1549.
[6] H. Aono, E. Sugimoto, Y. Sadaoka, N. Imanaka, G. Adachi, *J. Electrochem. Soc.* **1990**, 137, 1023.
[7] K. Arbi, S. Mandal, J.M. Rojo, J. Sanz, *Chem. Mater.* **2002**, 14, 1091.
[8] A.S. Best, P.J. Newman, D.R. MacFarlane, K.M. Nairn, S. Wong, M. Forsyth, *Solid State Ionics***1999**, 126, 191.

PTue050

Combined ^{6,7}Li NMR study of slow Li diffusion in monoclinic Li_2SnO_3

Langer, Julia (Institute for Chemistry and Technology of Materials, Graz University of Technology, Graz, AUT); Bottke, Patrick (Institute for Chemistry and Technology of Materials, Graz University of Technology, Graz, AUT); Wilkening, Martin (Institute for Chemistry and Technology of Materials, Graz University of Technology, Graz, AUT)

A comprehensive understanding of ion dynamics in solids plays a crucial role in many fields of today's materials research. In particular, the investigation of Li ion transport properties attracts great scientific interest since it is highly relevant for the development of new energy storage systems. Solid-state nuclear magnetic resonance (NMR) provides the necessary means to collect information ion hopping processes on different time and length scales from an atomic-scale point of view.

Here, polycrystalline Li_2SnO_3 served as a model substance to quantitatively study Li ion diffusion via ^{7}Li spin-lattice relaxation (SLR) NMR and spin-alignment echo (SAE) NMR. As conventional SLR NMR is per se sensitive to rather fast Li exchange processes, NMR measurements in the rotating frame of reference take advantage of locking frequencies in the kilohertz range that enabled us to probe Li ion dynamics on a much broader length scale. Both SLR techniques point to rather slow Li ion mobility in Li_2SnO_3. Therefore, ion transport in Li_2SnO_3 is perfectly suited to be studied by SAE NMR that is sensitive to extremely slow Li diffusion. Temperature-dependent echo decay rates directly reflecting Li jumps between the three available Li sites in the oxide, reveal Arrhenius behavior over several decades; the corresponding activation energy (0.4 eV) is in good agreement with that obtained by SLR measurements in the rotating frame of reference.

Finally, in combination with 1D and 2D ^{6}Li exchange NMR experiments, we were able to obtain a detailed picture of ion dynamics and, in particular, preferred diffusion pathways in Li_2SnO_3.

PTue051

Direct approach for impedance analysis of ion conducting glasses

Fraenkl, Max (Department of General and Inorganic Chemistry, Faculty of Chemical Technology, University of Pardubice, Pardubice, CZE); Shimakawa, Koichi (Joint Laboratory of Solid State Chemistry of Inst. of Macromolecular Chem. of the AS CR, v.v i., Prague and University of Pardubice, Pardubice, CZE); Patil, Deepak (Department of General and Inorganic Chemistry, University of Pardubice, Pardubice, CZE); Macak, Jan (Department of General and Inorganic Chemistry, Faculty of Chemical Technology, University of Pardubice, P, CZE); Vlcek, Milan (Joint Laboratory of Solid State Chemistry of Inst. of Macromolecular Chem. of the AS CR, v.v i., Prague and University of Pardubice, Pardubice, CZE); Wagner, Tomas (Department of General and Inorganic Chemistry, Faculty of Chemical Technology, University of Pardubice, Pardubice, CZE)

Solid-state ion conductors are an important class of materials. These materials attract considerable interest due to their potential applications in the field of electrolytes in batteries and fuel cells, gas sensors, etc.[1,2] Electrochemical impedance spectroscopy (EIS) is powerful method for understanding dynamics of ionic transport. Measured data are mainly analyzed by using equivalent electrical circuits (EEC) or Poisson-Nernst-Planck (PNP) equation [3]. The EEC method does not provide physical parameters such as the diffusion coefficient, the number of mobile ions, etc. The PNP approach (in principal macroscopic method) is not so popular, probably due to the high mathematical complexity. Being unhappy with these drawbacks and limitations we propose our direct microscopic approach of analysis EIS [4-6]. Studied systems are chlacogenide glasses doped with Ag. Our model is based on Dyre’s random walk theory [7]. The study shows, how helpful this approach can be to understand the electrode polarization as well as ionic transport mechanism. Proposed approach can be used for description of the various ion conductive systems.

---

[1] S. Horike, D. Umeyama, and S. Kitagawa, Accounts Chem. Res. 46, 2376 (2013).

[2] R. J. Klein, S. Zhang, S. Dou, B. H. Jones, R. H. Colby, and J. Runt, J. Chem. Phys. 124, 144903 (2006).

[3] J. R. Macdonald, Phys. Rev. 92, 4 (1953); J. Phys: Condensed Matter 22, 495101 (2010); J. Phys. Chem. A 115, 13370 (2011); J. Phys. Chem. C 117, 23433 (2013).

[4] S. Stehlik, K. Shimakawa, T. Wagner and M. Frumar, J. Phys. D: Appl. Phys. 45 (2012) 205304.

[5] D. S. Patil, K. Shimakawa, V. Zima, J. Macak, and T. Wagner, J. Appl.Phys. 113, 143705 (2013).

[6] D. S. Patil, K. Shimakawa, V. Zima, and T. Wagner, J. Appl. Physics 115, 143707 (2014) 7. J. C. Dyre, J. Appl. Phys. 64, 2456 (1988).

PTue052

Electrical properties of perovskite-type complex oxides $Ba_2Sc_2MO_8$ (M=Ti, Zr)

Kochetova, Nadezda (Institute of natural science, Ural Federal University, Ekaterinburg, RUS); Koryakin, Kirill (Institute of natural science, Ural Federal University, Ekaterinburg, RUS); Animitsa, Irina (Institute of natural science, Ural Federal University, Ekaterinburg, RUS)

Perovskite-type complex oxides with structural disordering of oxygen sublattice are of interest to investigations like oxygen-ion and proton conductors due to prospects of some practical applications. Compounds with total formula $A_3B_2^{III}B^{IV}O_8[V_o]$ such as $Ba_2Sc_2MO_8$ (M=Ti, Zr) related to this class of oxides were described earlier like oxygen-ion conductors [1]. In this study electrical properties of $Ba_2Sc_2MO_8$ (M=Ti, Zr) were investigated under air atmosphere with different water partial pressure (pH_2O) to determine the realization of proton conductivity.

The samples were prepared by solid state reaction of $BaCO_3$, Sc_2O_3 and TiO_2 (or ZrO_2) at the temperature range 900-1450°C. The structure of the sintered samples determined by X-ray diffraction measurements (Bruker D8 ADVANCE) was found to be cubic symmetry with space group *Pm3m* and cell parameters a=0.4156 nm (for $Ba_2Sc_2TiO_8$) and a=0.4220 nm (for $Ba_2Sc_2ZrO_8$).The water uptake was studied by using thermogravimetric (TG) analysis (Netzsch STA 409 PC Luxx) combined with mass-spectrometry (Netzsch QMS 403C Aeolos). The samples pedominantly treatmented under wet atmosphere were found to demonstrate weight loss around 300 – 600°C which corresponds to water removing from the structure. The water uptake calculated like an amount of water moleculs per formula unit is about 0.4 mol ($Ba_2Sc_2MO_8 {*} 0.4H_2O$).Conductivity measurements were done by AC impedance spectroscopy (Elins Z-2000) at frequency range 1 kHz – 1 MHz under dry ($pH_2O=3\cdot10^{-5}$ atm) and wet ($pH_2O=2\cdot10^{-2}$ atm) air atmospheres. The measurements were performed as a function of temperature (300 – 1000°C) and oxygen partial pressure (0.21 – 10^{-7} atm).

Temperature dependences of the total conductivity in dry atmosphere may be described by Arrenius equation with activation energy ~0.8 eV. Under wet conditions the value of the conductivity becomes to be higher at the temperatures lower 650°C; the difference reaches more than one order of magnitude. Activation energy is about 0.5 eV that is corresponds to protonic transport. The temperature interval of conductivity increasing correlates with temperatures of water intercalation in the structure of the oxides according to TG measurements.

The partial (oxygen-ion, electron, and proton) conductivities were determined from pO_2-dependencies of the total conductivity of the samples. The compounds $Ba_2Sc_2MO_8$ (M=Ti, Zr) were found to be mixed ion and electron (p-type) conductors under dry air atmosphere. According to structural features of the oxides ion transport can be attributed to an oxygen-ion type. Oxygen transport numbers calculated from pO_2-dependencies is about 20% at the investigated temperature interval (900-600°C). The magnitude of ion conductivity and the value of ion transport numbers increase in wet conditions due to appearance of proton defects and proton conductivity. The part of proton transport becomes to be about 50% at 600°C, the magnitude of proton conductivity is about $1{*}10^{-4}$ $Ohm^{-1}cm^{-1}$. Thus, the complex oxides $Ba_2Sc_2MO_8$ (M=Ti, Zr) are predominantly proton conductors at the temperatures lower 600°C at high pO_2 under wet atmosphere.

---

[1] Kurt R. Kendall, Carlos Navas, Julie K. Thomas, and Hans-Conrad zur Loye , Solid State Ionics 82 (1995) 215-223

PTue053

Electron structure as a foundation for selecting the compositions of doped lanthanum gallate as electron ionic conductors for SOFC

Chezhina, Natalia (St.Petersburg State University, Sankt Petersburg, RUS); Korolev, D. (St. Petersburg University, St. Petersburg, RUS)

Electron-ionic conductors based on lanthanum gallate doped with bivalent diamagnetic elements and d-elements are now widely studied owing to their importance in producing SOFC, oxygen sieves, and other devices of high electronics. The studies are mostly centered on the conductivity and structural aspects. Little attention is given to the state of paramagnetic atoms and their influence on the stabilization of the structure as a whole and of vacancies, thus on the conductivity of gallates.

The systematic study of magnetic properties of lanthanum gallate doped with strontium, magnesium, and various transition elements with various ratios M:Sr(Mg) showed the following:

1. A paramagnetic element is not oxidized to oxidation state +4 upon heterovalent doping with a bivalent element.
2. Heterovalent doping results in the formation of clusters in the lattice, which include paramagnetic elements, bivalent elements, and accompanying vacancies in the oxygen sublattice. The sizes of these clusters increase as the ratio M:Sr(Mg) decreases.
3. The clusters appear to stabilize the oxygen deficient structure, however, instead of increasing the oxygen conductivity, a decrease in the M:Sr(Mg) ratio results in its hampering. The reason for this is the fact that the vacancies are blocked within a large cluster by Coulomb field with strong interactions preventing the clusters from destroying even at very low concentrations of paramagnetic atoms.
4. The most optimal ratio M:Sr(Mg) appears to be 5:1 by the data of magnetic susceptibility and conductivity.
5. The calculation of the band structure of doped lanthanum gallate allowed an explanation of high electron conductivity in nickel containing systems. Thus nickel can be used as a doping element for cathodes, whereas cobalt and chromium would be promising dopants for electrolytes.

Therefore, a complex study of magnetic and electrical properties of a wide range of solid solutions shows that upon selecting the compositions of electron-ionic conductors for SOFC the sizes of clusters formed of paramagnetic elements, bivalent elements, and accompanying vacancies in the oxygen sublattice together with the electron structure of transition doping element and of the whole cluster must be taken into account.

PTue054

Extremely High Li^+ Diffusivity in NASICON-type $Li_{1.5}Al_{0.5}Ti_{1.5}(PO_4)_3$

Epp, Viktor (Institute for Chemistry and Technology of Materials, Graz University of Technology, Graz, AUT); Ma, Qianli (Forschungszentrum Jülich GmbH, Institute of Energy and Climate Research, Jülich, GER); Tietz, Frank (Forschungszentrum Jülich GmbH, Institute of Energy and Climate Research, Jülich, GER); Wilkening, Martin (Institute for Chemistry and Technology of Materials, Graz University of Technology, Graz, AUT)

The continuing demand for efficient electrochemical energy storage systems is hoped, in the medium term, to be met by rechargeable Li-based batteries. This requires improved battery characteristics in terms of power, capacity, longevity, and safety compared with the state-of-the-art Li-ion technology. Especially the last point can be addressed by the use of so-called all-solid-state batteries which do not rely on highly flammable solvent-based electrolytes but instead on solid compounds such as Li-bearing sulfides or oxides. So far, only few examples have been found whose ionic conductivities are comparable to those of liquid electrolytes.

Here, we present results on one of such promising materials *viz.* $Li_{1.5}Al_{0.5}Ti_{1.5}(PO_4)_3$ (LATP) being a NASICON-type fast ion conductor.[1] LATP was prepared by a novel sol-gel method;[2] bulk ion dynamics were studied via various time-domain ^{7}Li NMR techniques. The latter allowed for an in-depth investigation of Li-ion translational dynamics on different time and length scales. As an example, ^{7}Li NMR line-shape analysis reveals that the onset of significant Li^+ exchange processes, which are characterized by jump rates in the order of several kHz, is well below 140 K. Line shapes provide a first qualitative indication for a high ionic diffusivity in LATP. The finding is corroborated by ^{7}Li NMR spin–lattice relaxation (SLR) measurements carried out in both the laboratory and the rotating frame of reference. The diffusion-induced SLR NMR rate peaks recorded with the spin-lock technique point to a mean Li^+ jump rate in the order of 4×10^5 1/s at ca. 200 K; the corresponding activation energy is as low as 0.16 eV, thus, guaranteeing fast dynamics over a broad temperature range. Using the Einstein-Smoluchowski relation,[3,4] the jump rate determined can be translated into a bulk Li^+ self-diffusion coefficient of about 10^{-14} m^2/s. For comparison, for the majority of fast ion conductors such values are usually reached at temperatures being equal or significantly higher than 300 K. The appearance of an SLR NMR rate peak well below room temperature marks LATP as an extremely fast ion conductor. This is corroborated by additional impedance measurements showing high Li-ion conductivities of 5.3×10^{-4} and 1.04×10^{-3} S/cm in dry argon and ambient air, respectively. The difference observed points to a small influence of humidity on the grain boundary conductivity. In summary, our results reveal ultrafast Li^+ dynamics in LATP being comparable to that recently found in other potential solid electrolytes such as garnets[5,6] and argyrodites.[7,8]

---

[1] H. Aono, E. Sugimoto, Y. Sadaoka, N. Imanaka, G. Adachi, *J. Electrochem. Soc.* **137**, 1023 (1990).

[2] Q. Ma, F. Tietz, O. Guillon, German Patent DE 10 2014 012 926 (2015).

[3] A. Einstein, *Ann. Phys.* **322**, 549 (1905).

[4] M. von Smoluchowski, *Ann. Phys.* **326**, 756 (1906).

[5] R. Murugan, V. Thangadurai, and W. Weppner, *Angew. Chem. Int. Ed.* **46**, 7778 (2007).

[6] H. Buschmann, J. Dölle, S. Berendts, A. Kuhn, P. Bottke, M. Wilkening, P. Heitjans, A. Senyshyn, H. Ehrenberg, A. Lottnyk, V. Duppel, L. Kienle, J. Janek, *Phys. Chem. Chem. Phys.* **13**, 19378 (2011).

[7] V. Epp, Ö. Gün, H.-J. Deiseroth, and M. Wilkening, *J. Phys. Chem. Lett.* **4**, 2118 (2013).

[8] V. Epp, Ö. Gün, H.-J. Deiseroth, and M. Wilkening, *Phys. Chem. Chem. Phys.* **15**, 7123 (2013).

PTue055

Fast Li Ion Transport in the $Li_7P_3S_{11}$ Glass Ceramic as Seen by ^{6,7}Li NMR Relaxometry

Wohlmuth, Dominik (TU Graz, ICTM, CD Laboratory for Li Batteries, Graz, AUT); Epp, Viktor (TU Graz, ICTM, CD Laboratory for Li Batteries, Graz, AUT); Wilkening, Martin (TU Graz, ICTM, CD Laboratory for Li Batteries, Graz, AUT)

The glass ceramic $Li_7P_3S_{11}$ (LPS), intensively studied by Tatsumisago [1], is a well-known fast ion conductor [2]. Hence, it is undoubtedly a promising ceramic to be used in bulk-type all-solid-state batteries. The complex Li dynamics in LPS is, however, far from being understood completely.
To shed light on this issue, we performed temperature-variable ^{7}Li (and ^{6}Li) NMR measurements on a wide temperature range. Microscopic diffusion parameters were extracted from diffusion-induced rate peaks of an LPS sample that had been prepared by ball-milling with subsequent annealing. At 334 K the mean residence time between two successful Li jumps is in the order of 1 ns, cf. also Ref. [3]; the low-T flank of the purely diffusion-induced ^{7}Li SLR NMR peak leads to an activation energy of ca. 200 meV. This value is in good agreement with that recently reported for densified LPS powder samples investigated by impedance spectroscopy.

Surprisingly, the high-T flank of the rate peak, detectable above 350 K, is characterized by an even smaller slope. Its origin is yet unclear; most likely, it is connected to the presence of a large distribution of jump processes.

---

[1] M. Tatsumisago, M. Nagao, A. Hayashi, J. Asian Ceram. Soc., 1 (2013) 17

[2] Y. Seino, T. Ota, K. Takada, A. Hayashi, M. Tatsumisago, Energy Environ. Sci, 7 (2014) 627

[3] K. Hayamizu, and Y. Aihara, Solid State Ion., 238 (2013) 7

PTue056

High-Temperature Transformation from 1T- to 3R-Li_xTiS_2 Observed in situ with Neutron Diffraction

Wiedemann, Dennis (Technische Universität Berlin, Berlin, GER); Nakhal, Suliman (Technische Universität Berlin, Berlin, GER); Senyshyn, Anatoliy (Technische Universität München, Garching, GER); Bredow, Thomas (Universität Bonn, Bonn, AUT); Lerch, Martin (Technische Universität Berlin, Berlin, GER)

Layered titanium disulfide is used as lithium-ion intercalating electrode material in batteries. The room-temperature stable trigonal 1T polymorphs of the intercalates Li_xTiS_2 ($x \leq 1$) are widely-investigated. However, the rhombohedral 3R polymorphs, being stable at higher temperatures for large x, are less well known.

We recently reported on the synthesis of phase-pure 1T-Li_xTiS_2 ($x = 0.7$ and 0.9) and its reversible reconstructive transformation to the 3R phase between 673 and 873 K.[1] Neutron powder diffractograms, that we acquired at multiple temperature points, allowed for full Rietveld refinements resulting in good to very good fits. As proposed previously,[2] lithium ions were unambiguously located in octahedral voids at fractional coordinates 0, 0, ½ and no ordering was observed. (The same had been found for 1T-Li_xTiS_2 before.)[3] Known trends in the temperature evolution of lattice parameters were reproduced. Analyzing the Madelung parts of the lattice energies, we found the 3R polymorph to be electrostatically more stable than the 1T polymorph. However, periodic quantum-chemical calculations indicated that this approach is oversimplified due to neglect of polarization and electron correlation effects, at least for the relative stability of the polymorphs. The anomalous decrease of lattice parameters in 3R-$Li_{0.7}TiS_2$, when being heated from 873 to 973 K, is tentatively attributed to effects of lithium migration.

The insights gained do not only elucidate the structure of 3R-Li_xTiS_2, but also help to understand and control polymorphism in layered transition-metal sulfides.

This work is based upon experiments performed at the SPODI instrument operated by FRM II at the Forschungs-Neutronenquelle Heinz Maier-Leibnitz (FRM II), Garching, Germany. Financial support by the Deutsche Forschungsgemeinschaft (FOR 1277: "Mobilität von Lithiumionen in Festkörpern [molife]") is gratefully acknowledged.

---

[1] D. Wiedemann, S. Nakhal, A. Senyshyn, T. Bredow, M. Lerch, *Z. Phys. Chem.***2015**, DOI: 10.1021/acs.jpcc.5b01166.

[2] S. Nakhal, M. Lerch, J. Koopman, M. M. Islam, T. Bredow, *Z. Anorg. Allg. Chem.* **2013**, *639*, 2822–2825.

[3]J. R. Dahn, W. R. McKinnon, R. R. Haering, W. J. L. Buyers, B. M. Powell, *Can. J. Phys.* **1980**, *58*, 207–213.

PTue057

Ilmenite ceramics for advanced electrical and magnetic materials

Ryabkov, Y.I. (Institute of Chemistry, Komi Science Center, Ural Branch of RAS, Syktyvkar, RUS); Rinkevich, A.B. (Institute of Metal Physics, Ural Branch of RAS, Ekaterinburg, RUS); Krasnov, A.G. (nstitute of Chemistry, Komi Science Center, Ural Branch of RAS, Syktyvkar, RUS); Michailov, V.I. (Institute of Chemistry, Komi Science Center, Ural Branch of RAS, Syktyvkar, RUS)

Ceramic and composite materials based on titanium oxide compounds are widely used in the creation of modern photocatalytic, magnetic, electrical materials [E.S.Kim, et.al.(2011); S.Pavasupree, et.al.(2013)]. Numerous studies last decade [J.Mona (2006), C.-L.Huang (2009), L.Li (2012), etc.] show for some ilmenite titanates an unique combination of magnetic and electrical properties. In the ilmenite lattice of the ternary compounds $ATiO_3$ (A=Fe,Mn,Co,Ni), the A- and/or Ti-site oxygen octahedra share an edge with the same type of oxygen octahedra along the a-axis. AO_6-octahedra are connected to TiO_6-octahedra with face sharing along the c-axis and corner sharing along the oblique direction. Some of this compounds are known as wide-gap ($FeTiO_3$ 2,50-2,58 eV) anti-ferromagnetic semiconductor and have various potential applications, such as electrodes, catalysis support, gas sensing devices, spintronics [M.Zhang (2012)]. There has been much interest in doping comlex titanium oxides $ATiO_3$ with Fe, Mn, Ni, Co or other divalent metals in order to obtain high temperature magnetic semiconductors and new other electrical, magnetic materials with predicted properties [D.Nakatsuka, et.al. (2010)]. On the other hand $MgTiO_3$ is the base of one of the most popular dielectric materials for microwave devices, due to its high dielectric constant (ε_r =17), high quality factor (Q×f value =160,000 GHz) (K.Wakino, 1989). With partial replacement of Mg^{2+} by Co^{2+}, for the $(Mg_{0.95}Co_{0.05})TiO_3$ ceramics Q×f value grows up to 230,000 GHz (J.-H. Sohn,1994). The sensitivity of the magnetic and electrical properties of titanium-oxide phases to the chemical composition, size and shape of the particles forming materials intensively studied and widely discussed in the scientific literature [N.Naresh, et.al. (2012)]

Some of the goals of this research have been studying the conditions of synthesis the ilmenite titanates with different cation composition. There were developed the original synthesis procedure of solid solutions $A_{(1-x-y)}Mg_xFe_yTiO_3$ (A-Mn, Co, Ni at x = 0-0.2). It was confirmed the best synthetic routes are sol-gel and template synthesis (example: synthesis of nanocrystalline ceramics based $FeTiO_3$ [A.B.Gambhire, (2011)], or hydrothermal synthesis method of complex oxides [A.Simpraditpan, et.al.(2013); Q.Li, et.al.(2013)]. The synthesis of starting powders - nanoparticle with different morphology: fibers (template synthesis with modified cellulose fibers), plates (hydrothermal synthesis with tetrabutoxytitanium), particles of round shape (Pechini method) have been developed.

It was found for the majority of the ceramic titanates transmittance of EMR with the centimeter and millimeter wave lengths increases with increasing frequency, and the reflection coefficient decreases. So the values of the real (2-6) and the imaginary part (0,05-0,45) of complex permittivity were determined. The presence of magnesium atoms in the A-positions increases the value of the dielectric constant and decreases the value of the conductivity ilmenite titanates. For the fine ceramics $Mg_{0.1}Ni_{0.7}Fe_{0.2}TiO_3$ and $MnTiO_3$ both ferroelectric polarization and magnetic polarization reinforce the multiferroic properties as it was shown only for $MnTiO_3$ by X.Deng (2012). Analysis of the electrical and magnetic properties of the ilmenite titanates based on the model of 2D exchange interactions in a layered structure: A-O-A, A-O-Fe-O-A, Fe-O-Fe. The variability of the magnetic layers contents by isomorphic substitution provides the basis on which the behavior of new materials could be studied.

Work is supported by the fundamental research program of RFBR (project № 13-03-00132).

PTue058

Intercalation of water in the $LaSr_3Fe_3O_{10-\delta}$ Ruddlesden-Popper type material

Øygarden, Vegar (University of Oslo, Oslo, NOR); Fjellvåg, Helmer (University of Oslo, Oslo, NOR); Sjåstad, Anja (University of Oslo, Oslo, NOR)

Ruddlesden-Popper (RP) type oxides, $A_{n+1}B_nO_{3n+1}$, possess a wide range of technologically important properties including thermoelectricity, colossal magneto-resistance, mixed conductivity and high temperature superconductivity. RP oxides are also currently of high interest in solid oxide fuel cell (SOFC) technology. The RP structure consists of n blocks of perovskite type units (ABO_3) separated by a layer of rock salt type (AO). Certain $A_4B_3O_{10}$ (n=3, RP3) materials are prone to intercalation reactions with water, carbonate and simple alcohols after treatment in reducing atmospheres [1, 2]. The properties can be modified by careful tuning of the oxygen stoichiometry and the type and concentration of the intercalating species. Although it is known that the intercalated species locate to the rock salt layers, the process and the accompanying structural and physical changes are poorly understood. In addition to focusing on intercalation, in our work we explore novel solid solution systems with intriguing physical properties, including redox activity and vacancy ordered superstructures. This presentation will focus on $LaSr_3Fe_3O_{10-\delta}$ and demonstrate how the structural, magnetic and electrical properties are affected as a function of the intercalation of water. In particular we highlight the change from mixed to oxygen ion and protonic conductivity as a function of water content, making this material system highly interesting for use as an electrode and electrolyte material in fuel cell and battery applications.

---

[1] L. Jantsky et al., Inorg. Chem. 51 (2012) p. 9181-9191.

[2] M. Lehtimäki et al., J. Sol. State Chem. 204 (2013) p. 95-101.

PTue059

Investigation of the solid-solution Sr_2YNbO_6 - $Sr_3NbO_{5.5}$

Polt, Julia (Institut für Anorganische Chemie (Materialchemie), AUT); Kennedy, Brendan J (School of Chemistry, Sydney, AUS); Ling, Chris D (School of Chemistry, Sydney, AUS)

One major challenge of the 21st century is to ensure energy security. Solid-oxide fuel cells (SOFCs) are one technology that may help to achieve this. However, the development of new solid-state ionic conductors (SSICs) is therefore mandatory to overcome their key limitation: the need to operate at high temperatures. The use of high temperatures reduces the energy efficiency of the SOFC due to the required large power input and furthermore increases the risk of material failure caused by mechanical degradation during thermal cycling.

Most of the currently used materials are based on oxide ionic conduction through vacancies in an oxide sublattice. Our approach focuses on rarely investigated materials with oxygen-excess; the presence of oxide ions in the interstitial sites of a crystalline structure; and the possible presence of superoxide species in the normal crystalline sites. Understanding these will give us insight about the structure-property relationship of O^{2-} conduction and provide a systematic route to enhanced performance and new materials.

To this end, we are investigating the solid solution between $Sr2YNbO_6$ and $Sr_3NbO_{5.5}$. Sr_2YNbO_6 is an example of a double-perovskite where the corner sharing YO_6 and NbO_6 octahedra exhibit rock-salt like ordering. [1] Similar ordering occurs in $Sr_3NbO_{5.5}$ where the octahedral sites are occupied by Sr and Nb. [2] Through neutron diffraction studies we have found that the average structures differ in terms of the cooperative tilting of the octahedra, with Sr_2YNbO_6 being monoclinic while $Sr_3NbO_{5.5}$ is cubic. We postulate that the oxygen vacancies reduce the need for octahedral tilting, and are now working to confirm this using a combination of diffraction and spectroscopic methods, the results of which we will be presenting.

---

[1] Howard, C.J.; Barnes, P.W.; Kennedy, B.J.; Woodward, P.M. Acta Crystallographica Section B-Structural Science **2005**, 61, 258

[2] Li, M.R.; Hong, S.T. Chemistry of Materials **2008**, 20, 2736

PTue060

$La_2Mo_2O_9$-based compounds with high oxygen conductivity in $La_2Mo_2O_9$ - $Ln_2W_2O_9$ - $Ln_2Mo_2O_9$ (Ln = Pr, Nd, Sm, Gd) ternary systems

Kharitonova, Elena (M.V. Lomonosov Moscow State University, Moscow, RUS); Maslov, Anton (M.V. Lomonosov Moscow State University, Moscow, RUS); Orlova, Ekaterina (M.V. Lomonosov Moscow State University, Moscow, RUS); Voronkova, Valentina (M.V. Lomonosov Moscow State University, Moscow, RUS)

A large LAMOX family of compounds based on $La_2Mo_2O_9$, doped with various dopants in the lanthanum position and in the position of molybdenum, was discovered in 2000 by Lacorre et al. [1]. These compounds attract attention because of their high oxygen conductivity (0.06 S/cm at 800ºC) and possibility to use it in various electrochemical systems. Pure $La_2Mo_2O_9$ undergoes a reversible first order phase transition from monoclinic to high-temperature cubic phase with high oxygen conductivity. Addition of dopants promotes suppression of this phase transition. In this case a metastable cubic phase is stabilized at room temperature. The metastable cubic phase transforms into high temperature cubic phase upon heating. Stability of LAMOX compounds increases at partial substitution of Mo with W. For this purpose in present work we study phase formation, polymorphism and conductive properties of $La_2Mo_2O_9$-based compounds in $La_2Mo_2O_9$ - $Ln_2W_2O_9$ - $Ln_2Mo_2O_9$ (Ln = Pr, Nd, Sm, Gd) ternary systems.

Polycrystalline samples in the above systems were prepared by solid state reaction in air and characterized by X-ray, DSC and conductivity measurements. X-ray investigation shows that wide field of $La_2Mo_2O_9$-based compounds restricted by $La_2Mo_2O_9$ - $La_{0.6}Pr_{1.4}Mo_{0.6}W_{1.4}O_9$ - $Pr_2Mo_{0.9}W_{1.1}O_9$ - $Pr_2Mo_2O_9$ exist in Pr-contained ternary system. For Ln = Nd the above field becomes narrower and restricted by compositions $La_2Mo_2O_9$ - $La_{0.8}Nd_{1.2}Mo_{0.8}W_{1.2}O_9$ - Nd_2MoWO_9 - $Nd_2Mo_{1.86}W_{0.14}O_9$ - $La_{0.4}Nd_{1.6}Mo_2O_9$. "$Nd_2Mo_2O_9$" does not exist in pure form, but $Nd_2Mo_{2-x}W_xO_9$ solid solutions (0.14 £ x £ 1) have the same structure as $La_2Mo_2O_9$. In the system with Sm and Gd field of the existence of compound with the $La_2Mo_2O_9$ structure is significantly narrower and limited by $La_2Mo_2O_9$ - $La_{0.8}Sm_{1.2}Mo_{0.8}W_{1.2}O_9$ - $LaSmMo_2O_9$ and $La_2Mo_2O_9$ - $La_{1.2}Gd_{0.8}Mo_{1.2}W_{0.8}O_9$ - $La_{1.4}Gd_{0.6}Mo_2O_9$ triangles. So, decrease of the ion radius of rare-earth element leads to decreasing of crystallization field of $La_2Mo_2O_9$-based compounds. According to DSC data, substitution of Mo with W and La with Nd, Pr, Sm, Gd leads to disappearance of monoclinic phase and stabilization of metastable cubic phase at room temperature. Phase transition between low temperature and high temperature cubic phases was observed at 450 - 600ºC depending on dopant content. Pure $La_2Mo_2O_9$, $Pr_2Mo_2O_9$ and samples in $La_2Mo_2O_9$ - $Nd_2W_2O_9$ - $Nd_2Mo_2O_9$ and $La_2Mo_2O_9$ - $Gd_2W_2O_9$ - $Gd_2Mo_2O_9$ systems demonstrate the same conductivity behavior. The conductivity of low temperature phase obeys Arrhenius law, for high temperature cubic phase Vogel-Tammann-Fulcher law can be used to describe the conductivity. The conductivity of these samples varies weakly depending on the content of tungsten and the rare earth element. In the case of Pr and Sm contained systems the conductivity behaves different. Independently of W content, for the samples with high amount of Pr and Sm, their conductivity curves can be divided into two parts, each of which is well approximated by the Arrhenius law. The border between these two parts corresponds to a phase transition between metastable low temperature cubic phase and high temperature cubic phase. In this case conductivity of the compounds in high temperature region is significantly lower than that of pure $La_2Mo_2O_9$ and $Pr_2Mo_2O_9$.

Thus, our studies show that the behavior of the conductivity does not depend on the ionic radius of the rare earth dopant. It can be assumed that the change in behavior of the conductivity for samples with high Pr and Sm content may be related to the ability to change the valence of these elements.

---

[1] Lacorre P. Goutenoire F. Bohnke O. Retoux R. Laligant Y. *Nature*. (2000) 404 **.** 856-859.

PTue061

Phase formation and conductivity of compounds in Ln_2MoO_6 - Bi_2O_3 (Ln = Pr, Nd) systems

Kharitonova, Elena (M.V. Lomonosov Moscow State University, Moscow, RUS); Voronkova, Valentina (M.V. Lomonosov Moscow State University, Moscow, RUS); Orlova, Ekaterina (M.V. Lomonosov Moscow State University, Moscow, RUS)

Bi_2O_3-based compounds attract attention as materials with high anionic conductivity. The greatest interest is the high temperature cubic phase of Bi_2O_3, which has extremely high oxygen conductivity close to 3 S/cm [1]. At room temperature this phase may be stabilized by partial substitution bismuth with niobium, tantalum, calcium and rare earth elements. In a series of articles codoping bismuth with tungsten and rare earth was also studied and their conductivity reaches 0.05-1 S/cm at 500-800 ºC [2-4]. Codoping with rare earth and molybdenum, which is similar to tungsten crystallochemically, has not been studied. The purpose of this work - the synthesis of compounds in Ln_2MoO_6-Bi_2O_3 (Ln = Pr, Nd) system and study of their electrical properties.

Polycrystalline samples in Ln_2MoO_6-Bi_2O_3 (Ln = Pr, Nd) systems with composition $(1–x)Ln_2O_3+(1–x)MoO_3+xBi_2O_3$ were obtained by solid state synthesis in air. Maximum firing temperature was 800-1100 °C depending on sample compositions. Investigation shows, that solid solutions isostructural with cubic fluorite Bi_2O_3 phase are formed in wide area of bismuth concentrations: $0.6<x<0.9$ both for Ln = Nd and Pr. The samples with less bismuth concentration ($0.5<x<0.6$) have tetragonal structure resulted from distortion of cubic fluorite Bi_2O_3 structure. Cell parameters a and c of these tetragonal compounds close to that of cubic solid solutions. The samples with $x<0.5$ were a mixture of two tetragonal phases based on Ln_2MoO_6 and Bi_2O_3 compounds.

An intensive diffuse peak is observed on dielectric permittivity temperature dependence for all samples with cubic and tetragonal structure. The peak moves into low temperatures with decrease of bismuth concentration, from 770-800 °C ($x=0.5$) to 570 °C ($x=0.85$). The nature of this peak is not clear.

The samples with tetragonal and cubic structure demonstrate high conductivity, which, analogously Bi_2O_3, may be caused by the diffusion of oxygen anions. For the tetragonal samples with ($0.5<x<0.6$) the conductivity is weakly dependent on bismuth content and reaches 0.05 S/cm at 800 °C. For cubic samples with increasing of bismuth concentration the conductivity grows on an order of magnitude. Samples with $x=0.85$ demonstrate the conductivity close to 0.2 S/cm at 800 °C, which is comparable with the results of [2-5]. Conductivity temperature dependences for all measured samples may be approximated by Arrhenius law with activation energy near 0.8 eV.

This work was supported by Russian Foundation for Basic Research (project No. 15-02-03492).

---

[1] V.V. Kharton, E.N. Naumovich, A.A. Yaremchenko, F.M.B. Marques. J. Solid State Electrochem. 5 (2001) 160-187;

[2] N. Jiang, E.D. Wachsman, Su-Ho Jung. Solid State Ionics. 150 (2002) 347-353;

[3] A. Borowska-Centkowska, F. Krok, I. Abrahams, W. Wrobel. Solid State Ionics. 203 (2011) 22-28; [4] A. Watanabe, M. Sekita. Solid State Ionics. 176 (2005) 2429-2433.

[5] T. Takahashi, H. Iwahara. J. Appl. Electrochem. 3 (1973) 65-72.

PTue062

$La_2NiO_{4+\delta}$ as anode material for solid oxide electrolyser cells under chromium poisoning conditions

Schrödl, Nina (Chair of Physical Chemistry, Montanuniversitaet Leoben, Leoben, AUT); Egger, Andreas (Chair of Physical Chemistry, Montanuniversitaet Leoben, Leoben, AUT); Sitte, Werner (Chair of Physical Chemistry, Montanuniversitaet Leoben, Leoben, AUT)

The highly efficient conversion of electrical energy to hydrogen via high-temperature water electrolysis is not only considered as a promising means of energy storage but also as a sustainable way to produce hydrogen, especially if thermal energy from existing power plants or industrial facilities can be used in the process. Within this study, mixed conducting $La_2NiO_{4+\delta}$ (LNO) with K_2NiF_4-structure was evaluated as potential anode material for high-temperature solid oxide electrolyser cells (SOECs). Besides electrode delamination, the poisoning of the oxygen electrode by impurities such as chromium (which can be released from system components) is regarded as a major issue with respect to the long-term stability of solid oxide cell stacks. The absence of alkaline earth elements in LNO is considered to be beneficial since elements like Sr and Ba are known to segregate from the bulk material to the electrode surface, thus facilitating the formation of insulating or catalytically inactive secondary phases. The suitability and long-term stability of LNO for SOEC anode application was assessed by exposing dense samples of LNO at 800°C to a chromium source in dry and humid Ar/O_2 atmospheres and simultaneously monitoring the oxygen exchange kinetics via dc-conductivity relaxation experiments. After more than 3000 hours of degradation experiments, the test samples were extensively analysed using AFM, SEM-EDXS and XPS. The post-test analyses revealed that humidity in combination with chromium can have a detrimental effect on the morphology and composition of the sample surface, leading to a decrease in oxygen surface exchange rates. Additionally, the electrochemical characterisation of LNO as oxygen electrode was performed by impedance spectroscopy and IV-measurements on button cells with a screen-printed LNO-anode, a platinum counter electrode and a platinum reference electrode on a GDC-electrolyte. Electrochemical characterisations were conducted at 800°C and 0.2 bar pO_2. Current densities of up to -410 mA cm^{-2} were applied to simulate real-life SOEC operating conditions. For subsequent periods of 1000 hours the area specific polarisation resistance (ASR) of the cell was measured with and without the presence of a chromium source in dry and humid test gases. Post-test analyses of the cell cross section using SEM-EDXS identified a number of impurities derived from different cell components but no chromium contamination.

---

[1] A. Egger, N. Schrödl and W. Sitte, Faraday Discussions, 2015, DOI: 10.1039/C5FD00021A.

PTue063

Li diffusion pathways in LATP-based materials

Monchak, Mykhailo (Karlsruhe Institute of Technology (IAM-ESS), Eggenstein-Leopoldshafen, GER); Hupfer, Thomas (Karlsruhe Institute of Technology (IAM-KWT), Karlsruhe, GER); Senyshyn, Anatoliy (Heinz Maier-Leibnitz Zentrum (MLZ), Technische Universität München, Garching, GER); Ehrenberg, Helmut (Karlsruhe Institute of Technology (IAM-ESS), Eggenstein-Leopoldshafen, GER)

Li-ion batteries are nowadays considered as the most promising electrochemical energy storage media for mobile applications. However their further progress is seriously limited by the instability of liquid electrolytes and an active research towards batteries adopting solid lithium-ion conducting electrolytes (all-solid-state Li-ion cells) is in progress. A solid-state electrolyte with high lithium-ion conductivity at room temperature, high stability against oxidation and reduction to other cell constituents and high voltage stability is the key element in all-solid-state lithium cells.

The diversity of possible materials as solid electrolytes can be distinguished in two major classes: organic polymers and inorganic ceramics. For the latter NASICON type compounds are one of the most promising candidates [1]. The NASICON framework of $LiM_2(PO_4)_3$ compounds is built up by $M_2(PO_4)_3$ units which are bound to form the three dimensional framework of NASICON. Its framework with well developed 3D cavities is well-suited for Li diffusion in the structure. The ionic conductivity of the $LiM_2(PO_4)_3$ series is considerably enhanced, thus reaching values of 10^{-3} S/cm at room temperature, when tetravalent cations (M) are partially substituted by trivalent cations (Al, Ga, In, Fe, etc.). The highest conductivities are observed for Al-substituted $Li_{1+x}Al_xGe_{2-x}(PO_4)_3$ (LAGP) and $Li_{1+x}Al_xTi_{2-x}(PO_4)_3$ (LATP) compounds [2-4]. Further optimization of NASICON-type materials as well as the understanding of the function of trivalent cations requires certain knowledge about the crystal structure and diffusion pathways.

Series of Al-substituted $LiTi_2(PO_4)_3$ were synthesized. The powders were prepared by a water based sol-gel-process, successively calcined at up to 900°C to transform the amorphous powder into crystalline material. Localization of lithium and quantification of its content can be hardly performed by X-ray based structural methods. Therefore elastic coherent neutron scattering experiments were performed on the high-resolution powder diffractometer SPODI at the neutron source FRM II (Garching, Germany) [5] and on the D2B diffractometer at the Institute Laue Langevin (Grenoble, France). Powder diffraction data were collected at room temperature and at fixed temperatures in the range of 100-800 ºC (with a constant increment $\Delta T = 100$ ºC) upon heating. Analysis of differential Fourier maps revealed the Li2 position (0.11, 0.33, 0.08) besides the Li1 (0,0,0) in the rhombohedral modification of Al-substituted $LiTi_2(PO_4)_3$, which is in agreement with the (0.07, 0.34, 0.07) position proposed by K. Arbi et al [6]. The 3D distribution of valence mismatch and negative nuclear density maps were calculated from neutron powder diffraction data, and obtained results were discussed in the frame of Li diffusion pathways in LATP–based materials.

This work is financially supported by DFG under grant no. EH 183/15-1.

---

[1] J. W. Fergus, J. Power Sources 2010, 195, 4554-4569.
[2] J.S. Thokchom, B. Kumar, J. Power Sources 2008, 185, 480-485.
[3] H. Aono, E. Sugimoto, Y. Sadaoka et al, J. Electrochem. Soc. 1989, 136(2), 590-591.
[4] X. Xu, Z. Wen, X. Yang et al, Solid State Ionics 2006, 177, 2611-2615.
[5] M. Hoelzel, A. Senyshyn, N. Juenke et al, Nucl. Instrum. Methods Phys. Res., Sect. A 2012, 667, 32-37.
[6] K. Arbi, M. Hoelzel, A. Kuhn et al. Inorg. Chem. 2013, 52, 9290-9296.

PTue064

Li ion dynamics in nanocrystalline and structurally disordered Li_2TiO_3

Brandstätter, Harald (Institute of Chemistry and Technology of Materials, CD-lab for Li-Batteries, Graz, AUT); Wohlmuth, Domink (Institute of Chemistry and Technology of Materials, CD-lab for Li-Batteries, Graz, AUT); Bottke, Patrick (Institute of Chemistry and Technology of Materials, CD-lab for Li-Batteries, Graz, AUT); Pregartner, Veronika (Institute of Chemistry and Technology of Materials, CD-lab for Li-Batteries, Graz, AUT); Wilkening, Martin (Institute of Chemistry and Technology of Materials, CD-lab for Li-Batteries, Graz, AUT)

The monoclinic polymorph of Li_2TiO_3 (β-form) is known to be a relatively poor Li ion conductor. Up to now, no information is available on how the ion transport properties change when going from well-ordered crystalline Li_2TiO_3 to a structurally disordered form with the same chemical composition. Here, we used high-energy ball milling to prepare nanocrystalline, defect-rich Li_2TiO_3 ion dynamics have been studied via impedance spectroscopy. It turned out that ball milling, see, e.g., refs. [1,2], offers the possibility to enhance long-range ion transport in the oxide by approximately 3 orders of magnitude. Its effect on the oxide ceramic is two-fold: besides the introduction of a large number of defects, the originally µm-sized crystallites are transformed into nanocrystallites with a mean diameter of less than 50 nm. This process is accompanied by a mechanically induced phase transformation towards the α-form of Li_2TiO_3 besides that, a significant amount of amorphous materials is produced during milling. Structural disorder in nanocrystalline as well as amorphous Li_2TiO_3 is anticipated to play the capital role in governing Li ion dynamics of the sample finally obtained.

---

[1] M. Wilkening, V. Epp, A. Feldhoff, and P. Heitjans, J. Phys. Chem. C 112 (2008) 9291.

[2] D. Wohlmuth, V. Epp, P. Bottke, I. Hanzu, B. Bitschnau, I. Letofsky-Papst, M. Kriechbaum, H. Amenitsch, F. Hofer, and M. Wilkening, J. Mater. Chem. A 2 (2014) 20295.

PTue065

Light-induced stoichiometry changes in oxides at high temperatures

Walch, Gregor (Vienna University of Technology, Vienna, AUT); Rotter, Bernhard (Vienna University of Technology, Vienna, AUT); Brunauer, Georg (Vienna University of Technology, Vienna, AUT); Esmaeili, Esmaeil (Vienna University of Technology, Vienna, AUT); Opitz, Alexander Karl (Vienna University of Technology, Vienna, AUT); Summhammer, Johann (Vienna University of Technology, Vienna, AUT); Ponweiser, Karl (Vienna University of Technology, Vienna, AUT); Fleig, Jürgen (Vienna University of Technology, Vienna, AUT)

In oxides that are stable within a certain oxygen stoichiometry range oxygen exchange with the surrounding atmosphere can be brought about by different means, e.g. changing the oxygen partial pressure in the atmosphere or the temperature [1], or applying a voltage [2]. The scarce studies on the effect of light on the oxygen exchange reaction include work on Fe-doped $SrTiO_3$ single crystals and anodic TiO_2 thin films, for which the kinetics of oxygen exchange following an O_2 partial pressure jump was reported to change under irradiation with UV light [3, 4].

In the present work we study the effect of UV light on the stoichiometry of the model oxides $SrTiO_3$ and TiO_2 in equilibrium with the surrounding atmosphere, without any other driving force. This photon-driven “oxygen pumping” process could be interesting for devices harvesting light energy as well as sensors. The material under investigation was used as an electrode in a high temperature (~400°C) electrochemical cell (oxide|yttria-stabilized zirconia|porous Pt) on which current and voltage measurements were performed with and without light in atmospheres with different oxygen partial pressure.

A time-dependent voltage up to a few hundred mV results upon light. Partly, this voltage originates from a photovoltaic effect in the cell. The time-dependent voltage contribution, on the other hand, is caused by light-driven incorporation of oxygen into the crystal. This stoichiometry change leads to a cell voltage also after switching off UV irradiation and may be considered as a kind of electrode changing by light.

---

[1] M. Kuhn, S. Hashimoto, K. Sato, K. Yashiro, J. Mizusaki, Solid State Ionics, 195 (2011) 7-15.
[2] G. Holzlechner, D. Kastner, C. Slouka, H. Hutter, J. Fleig, Solid State Ionics, 262 (2014) 625-629.
[3] R. Merkle, R.A. De Souza, J. Maier, Angewandte Chemie International Edition, 40 (2001) 2126-2129.
[4] H.W. Gundlach, K.E. Heusler, Zeitschrift für Physikalische Chemie, 119 (1980) 213-224.

PTue066

Lithium diffusion in mixed conducting polymers

Woods, Michael (University of Kent, Canterbury, GBR)

Conducting polymers are a promising prospect in terms of modern day lithium ion batteries. With high electrical conductivity values not too far off that of metals in a few cases (i.e. Polyacetylene), as well as good ionic conductivity in some examples (PEG), they are now becoming more widely used in battery cells. Here, we present a study of co-block polymers in which a polymer with high electrical conductivity is linked to a polymer with lithium ion conductivity, using a combination of atomistic simulations and experiments. In particular, the PEDOT-PEG system, also referred to as Aedotron, will be discussed in detail. PEDOT-PEG exists in multiple distributions, including the multi- and tri-block forms. The latter having higher electrical conductivity. However, calculations show that the multi-block form is the energetically more stable one. A study was undertaken into the amorphous chains of PEDOT-PEG, using the experimental density. Molecular Dynamics (MD) simulations shows that the chain length controls phase separation of the two polymers. Insertion of lithium ions using different salts, with MD allows diffusion coefficients and ionic conductivity to be calculated. Diffusion coefficients show that lithium salts based on chlorine have values in the order of 9×10^{-12} m^2/s for low Li concentrations decreasing towards a value of 1×10^{-12} m^2/s for saturated systems. Lithium iodine-based systems instead on average showed diffusion coefficients of 1×10^{-12} m^2/s. These numbers are in good agreement with experimental values measured with solid-state NMR. One application of these mixed conducting polymers is to produce a wireless integrated antenna-battery. To maximise the antenna performance, the dielectic properties of the battery is one of the determining factors. Dielectric constants of the mixed conducting polymers can be calculated from First Principles and applied to simulations of the antenna design.

PTue067

Lithium ion Conduction in Disordered Non-Framework Crystalline Borohydrides

Cussen, Eddie (University of Strathclyde , Glasgow, GBR); Cascallana, Irene (University of Strathclyde, Glasgow, GBR); Gregory, Duncan (University of Glasgow, Glasgow, GBR)

Ionic conductivity in solids is a fascinating phenomenon that is of great relevance in a growing range of technologies including batteries, fuel cells and supercapacitors. A considerable research effort is involved in the search for solid Li+ electrolyte materials. Polymeric materials, in both amorphous and crystalline forms, have been found to be effective lithium electrolytes and a range of continuous framework materials including perovskites and garnets are also capable of supporting lithium conductivity through an immobile framework. The mechanism for lithium conductivity in all of these materials is usually considered in the context of isolated ion hopping events.

Recent results from our laboratories have shown that high lithium conductivity, ca. 10−4 S cm−1, can also be obtained a range of non-framework materials based on the parent phase lithium borohydride, LiBH4. At room temperature this compound adopts a fully−ordered, non−conducting orthorhombic phase that on heating to 109°C transforms into a superionic conductor with hexagonal crystal symmetry. Our synthetic approach has stabilised the highly conducting polymorph and derivatives of this compound at room temperature. Neutron diffraction has been used to investigate the structural features of the high symmetry phase that facilitate lithium movement. We will show how these compounds can be related to the classic ‘paddlewheel’ mechanism and so illustrate a cooperative mechanism for fast lithium conduction through solid lattices that have aspects of both crystalline and amorphous order.

PTue068

Local conductivities in Li ion conducting garnet-based ceramics measured by microelectrodes.

Welzl, Andreas (TU-Wien Institute of chemical technology and Analytics, Wien, AUT)

Energy storage and energy conversion with a high efficiency are key issues for future mobile devices and transportation technology. Secondary elements like lithium ion batteries are already state of the art for a large number of mobile applications. Despite the good performance of current lithium ion batteries, safety and stability problems as well as limitations in the energy density are related to the standard organic electrolytes. Being able to surpass these problems would open further options, e. g. for applications.

In the past years new solid material classes came into the focus of electrolyte research. Cubic $Li_7La_3Zr_2O_{12}$ (LLZO) garnets and it variants are among the most promising candidates for future solid electrolyte systems because of their very high lithium conductivity (about 10^{-4} - 10^{-3} S cm^{-1} [1]). Doping of the garnet is a crucial factor to achieve high conductivities. However, many details on the effects of dopants and on the role of the exact Li stoichiometry, but also on degradation phenomena are still not understood.

In this contribution, we present an electrochemical impedance spectroscopy (EIS) study of LLZO doped with different elements. To achieve a better fundamental understanding of the electrochemical processes and diffusion of lithium ions, we performed, besides overall conductivity measurements using blocking electrodes, measurements on microelectrodes of different composition and size. Varying doping materials (Ga, Al, Mo, …) and changing temperature lead to very different impedance responses in the complex impedance plane. From these measurements information on the local bulk conductivity can be determined and blocking layers near to the surface can be identified.

---

[1] Murugan, R.; Thangadurai, V. Weppner, W. Angew. Chem. Int. Ed. 2007, 46, 7778.

PTue069

Mechanochemical synthesis and characterization of the metastable, nanocrystalline F ion conductor $(Ba_xCa_y)La_{(1-x-y)}F_{(3-x-y)}$

Breuer, Stefan (TU Graz, Graz, AUT); Preishuber-Pflügl, Florian (TU Graz, Graz, AUT); Wilkening, Martin (TU Graz, Graz, AUT)

Solid ion conductors are important materials as they find applications in many electrochemical devices, *e.g.* , in lithium-ion batteries, fuel cells or in super capacitors. [1] Compared to their liquid analogues they are expected to feature a number of advantages such as longer lifetimes, higher energy densities as well as higher safety. [2] Hence, ongoing research is devoted to find new materials with enhanced ion conductivity properties. [1] Quite recently, fast ion conduction has been found for nanocrystalline binary alkaline earth fluorides such as $(Ba,Ca)F_2$. [3] Here, we tried to modify overall F ion transport further by replacing Ba and Ca with trivalent cations such as La. Thus, nanocrystalline samples of $(Ba_x Ca_y)La_{(1-x-y)} F_{(3-x-y)}$ with varying stoichiometries were synthesized via high-energy ball milling the binary fluorides in a planetary mill under dry conditions. In general, mechanochemical routes allow the preparation of non-equilibrium compounds that, in many cases, cannot be prepared via conventional high-temperature or wet-chemical synthesis methods. Structural characterization of the compounds prepared was carried out using X-ray powder diffraction. Heat treatment of the samples clearly reveal their thermodynamic metastability. This behavior was further confirmed by differential scanning calorimetry, which was employed to investigate structural transitions as well as to monitor the phase separation taking place at elevated temperatures. Finally, variable-temperature conductivity spectroscopy was used to study anion transport properties of the quaternary fluorides synthesized.

---

[1] Ahmad M. M., Yamane Y., Yamada K., *Mat. Sci. Engin.* B 178, **2013**, 965-970.

[2] Padma Kumar P., Yashonath S., *J. Chem. Sci.* 118, **2006** , 135-154.

[3] Düvel A., Ruprecht B., Heitjans P., Wilkening M., *J. Phys. Chem. C* 115, **2011**, 23784-23789.

PTue070

Mechanochemistry of Fluorine Ion Conductors: Insights into Synthesis and Ion Transport via Impedance Spectroscopy and Solid-State NMR

Preishuber-Pflügl, Florian (Institute f. Chemistry and Technology of Materials, Graz, AUT); Wilkening, Martin (Institute f. Chemistry and Technology of Materials, Graz, AUT)

Mechanochemistry is a powerful tool in solid-state chemistry, which is represented by some very recent, comprehensive reviews on this topic that outline the manifold potential of this technique.[1,2] For solid ion conductors, it has been demonstrated as a very useful method that does not only facilitate the chemical reactions itself, but also improve many of the materials' properties, such as the ionic conductivity and diffusivity.

The treatment of the reactants in, *e.g.*, planetary mills can induce chemical reactions that otherwise require high temperature synthesis methods. The driving force of the reactions is the input of mechanical energy that is dissipated by the shear, friction and impact forces of the milling balls onto the reactants. Besides the possible conversion of the starting materials, high-energy ball milling always leads to a significant reduction of the grain size yielding nanocrystalline materials that very often show improved ion transport properties compared to the coarse grained bulk materials. This effect can be attributed to the high amount of structural disorder as well as the large fraction of interfacial areas introduced during milling.

As an example, the synthesis of ternary $BaMgF_4$ will be presented, which was prepared by joint milling of the binary fluorides BaF_2 and MgF_2.[3] The very high rotation speed of 1000 rpm in a Fritsch Pulverisette 7 premium line yielded a phase pure, nano-sized polycrystalline powder. The reaction was followed *ex-situ* by solid-state ^{19}F MAS NMR spectroscopy as well as by X-ray powder diffraction. The resulting product shows enhanced ionic conductivity compared to the conventionally synthesized material. Other possible applications of mechanochemistry involve the preparation of (metastable) solid solutions. $Ba_{0.6}La_{0.4}F_{2.4}$ can be prepared from BaF_2 (cubic) and LaF_3 (tysonite structure). The milling procedure yields disordered $Ba_{0.6}La_{0.4}F_{2.4}$ crystallizing with cubic symmetry. [4] The conductivity of the material is found to be two orders of magnitude higher than that of pure BaF_2; it can be explained by the formation of anion vacancies due to the disorder resulting from the trivalent La^{3+} ions. The highest ionic conductivity of the fluorides prepared was found for tetragonal $BaSnF_4$ synthesized via a mechanochemical route with subsequent soft annealing. It is a member of the layered $MSnF_4$ (M=Pb, Sn, Sr) family that is known for their very good F ion transport properties. At room temperature, the dc F ion conductivity reaches almost $1 \cdot 10^{-3}$ S/cm. [5] For the preparation, BaF_2 and SnF_2 were mechanically treated to give a metastable, cubic BaSnF4 as an intermediate that was transformed into the highly conductive tetragonal modification via annealing at only 573 K. This procedure prevented grain growth and allowed the preservation of the nanocrystalline properties being beneficial for the very good ionic conductivity observed.

---

[1] S. L. James, C. J. Adams, C. Bolm, D. Braga, P. Collier, T. Friscic, F. Grepioni, K. D. M. Harris, G. Hyett, W. Jones, A. Krebs, J. Mack, L. Maini, A. G. Orpen, I. P. Parkin, W. C. Shearouse, J. W. Steed and D. C. Waddell, *Chem. Soc. Rev.*, **2012**, *41*, 413.

[2] V. Sepelák, A. Düvel, M. Wilkening, K-D. Becker and P. Heitjans, *Chem. Soc. Rev.*, **2013**, *42*, 7507.

[3] F. Preishuber-Pflügl and M. Wilkening, *Dalton Trans.*, **2014**, *43*, 9901.

[4] F. Preishuber-Pflügl, P. Bottke, V. Pregartner, B. Bitschnau and M. Wilkening, *Phys. Chem. Chem. Phys.*, **2014**, *16*, 9580.

[5] F. Preishuber-Pflügl, V. Epp, S. Nakhal, M. Lerch and M. Wilkening, *Phys. Status Solidi C*, **2015**, *12*, 10.

PTue071

Metal exsolution in $Ba(Fe,M)_2(PO_4)_2$ (M=Li, Co, Ni): Metal versus alkali cationic mobility

Blazquez Alcover, Ignacio (UCCS, Villeneuve d'Ascq, FRA); David, Rénald (UCCS, Villeneuve d'Ascq, FRA); Daviero-Minaud, Sylvie (UCCS, Villeneuve d'Ascq, FRA); Filimonov, Dmitry (Chemistry Department, Moscow, RUS); Huvé, Marielle (UCCS, Villeneuve d'Ascq, FRA); Masquelier, Christian (LRCS, Amiens, FRA); Roussel, Pascal (UCCS, Villeneuve d'Ascq, FRA); Kabbour, Houria (UCCS, Villeneuve d'Ascq, FRA); Mentré, Olivier (UCCS, Villeneuve d'Ascq, FRA)

If alkaline cation mobility is rather easy and at the origin of most of the Li-ion science[1], the exsolution of transition metals from solids is rare and compounds that exhibit a spontaneous extrusion of cations under mild oxidizing conditions are in very limited in number. Generally it concerns Fe^{2+} oxides, due to very favorable Fe^{2+}/Fe^{3+} redox properties, as seen for olivines LiFePO4 and Fe2SiO4, where iron emerges as Fe_2O_3 nano-clusters [2-4].

In this frame, the layered compound $BaFe^{2+}{}_2(PO_4)_2$, made of $\infty[Fe_2O_6]$ honeycomb layers with phosphate groups pointing towards the Ba-filled interlayer space[5], presents fascinating properties. It is the unique case of 2D Ising ferromagnetism between Fe^{2+} (S=2) spins (< Tc=65.5 K) and displays, on cooling, a remarkable re-entrant transition induced by the competition between the lattice Jahn–Teller instability and the energy gained through the uniaxial ferromagnetic ordering.6 Under heating with a soft oxidizing/reducing atmosphere, it shows an unexpected reversible iron exsolution, leading to different iron-deficient phases $BaFe_{(2-x)}(PO_4)_2$ and nanometric α-Fe_2O_3[7]. The exsolution is efficient and fully reversible until x=2/3, which corresponds to 12 wt% initial mass converted into nanometric iron oxide. This process is unique as the exsolution occurs with initial crystallinity preservation, even on single crystals. Single crystal XRD studies of intermediate members x=2/7, x=1/3, x=1/2 and the Fe-depleted ultimate term x=2/3, show a systematic order between Fe-ions and vacancies (V_{Fe}), denoting an unprecedent easy in-plane metal diffusion [8].The substituted phases $BaFe_{(2-y)}M_y(PO_4)_2$ (M = Co^{2+} and Ni^{2+}) have also been synthesized and characterized and Fe-exsolution is observed in same conditions. Here, M^{2+} atoms act as obstacle due to less mobility, hampering Fe_2O_3 nano-crystals growth. So, control of cations vacancies and of Fe_2O_3 size are possible by manipulation of Fe/M ratio.

To take advantage of the voids distributed in the Fe-depleted lattices, we have explored their potentiality for Li^+ (de)-intercalation. Chemical lithium insertion in the lattice has been succeed by heating the phase in $LiCO_3$ excess under H_2(3%)/Ar atmosphere at 550°C. The Li+ presence in the network was confirmed by solid-NMR, ICP analysis and single crystal X-Ray diffraction. Electrochemical Li insertion was performed in Li-ion cell batteries made with lithiated or not BaFe1.33(PO4)2 as the cathode. $BaFe_{1.33}(PO_4)_2$ shows a promising cyclability rate during the first cycles whereas the chemically lithiated phase presents a high work potential during the first charge cycle.

---

[1] M. Armand and J. M. Tarascon, Nature, 2008, 451, 652-657.

[2] S. Kondoh, M. Kitamura and N. Morimoto, American Mineralogist, 1985, 70, 737-746.

[3] S. Hamelet, P. Gibot, M. Casas-Cabanas, D. Bonnin, C. P. Grey, J. Cabana, J. B. Leriche, J. Rodriguez-Carvajal, M. Courty, S. Levasseur, P. Carlach, M. van Thournout, J. M. Tarascon and C. Masquelier, Journal of Materials Chemistry, 2009, 19, 3979-3991.

[4] S. Hamelet, M. Casas-Cabanas, L. Dupont, C. Davoisne, J. M. Tarascon and C. Masquelier, Chemistry of Materials, 2011, 23, 32-38.

[5] H. Kabbour, R. David, A. Pautrat, H. J. Koo, M. H. Whangbo, G. Andre and O. Mentre, Angewandte Chemie-Internationa al Edition, 2012, 51, 11745-11749.

[6] R. David, A. Pautrat, D. Filimonov, H. Kabbour, H. Vezin, M. H. Whangbo and O. Mentre, Journal of the American Chemical Society, 2013, 135, 13023-13029.

[7] R. David, H. Kabbour, D. Filimonov, M. Huve, A. Pautrat and O. Mentre, Angewandte Chemie-International Edition, 2014, 53, 13365-13370.

PTue072

NMR study of proton motion in fluorine-doped complex oxides with perovskite and brownmillerite structures

Animitsa, Irina (Ural Federal University, Ekaterinburg, RUS); Denisova, Tatiana (Institute of Solid State Chemistry, Ekaterinburg, RUS); Belova, Ksenia (Ural Federal University, Ekaterinburg, RUS); Tarasova, Natalia (Ural Federal University, Ekaterinburg, RUS); Nevmyvako, Roman (Institute of Solid State Chemistry, Ekaterinburg, RUS)

It was recently shown that the fluorine-doping$F^{-} \rightarrow O^{2-}$ of oxygen deficient perovskite-related complex oxides promotes much greater oxygen-ion conductivity (mixed anion effect) and as a consequence proton-conductivity can be improved in wet atmosphere [1]. Our main purpose was to study the effect of fluorine-doping on proton mobility in the solid solutions with brownmillerite $Ba_2In_2O_{5-0.5x}F_x$ ($0 \leq x \leq 0.24$) and double perovskite $Ba_4Ca_2Nb_2O_{11-0.5x}F_x$ ($0 \leq x \leq 1.0$) structures. Upon hydration by equilibration with water vapor the oxygen vacancies may be filled by oxygen from water and the hydroxide ions are formed. This process leads to dominant proton transport below 500°C.

^{1}H MAS NMR spectra were obtained on the Agilent 400 spectrometer operating at Larmor frequencies of 400.0 MHz. The protons exist in the structures as nonequivalent OH^--groups involving in different hydrogen bonding. It was established the presence of two proton environments. The F^--doping leads to increase of hydrogen bonds (as OH...O distance decreases), in other words the extending of the O–H bond allows for stronger hydrogen bonding, facilitating proton transfer.

This work was financially supported by the Grant of research in cooperation of Ural Federal University and Ural Branch of the Russian Academy of Sciences

---

[1] I. Animitsa, N. Tarasova, Ya. Filinkova, Solid State Ion., 207, (2012) 29.

PTue073

The effect of phosphate doping on local structure and ion transport of $Ba_4Ca_2Nb_{2-x}P_xO_{11}$

Animitsa, Irina (Ural Federal University, Ekaterinburg, RUS); Belova, Ksenia (Ural Federal University, Ekaterinburg, RUS); Obrubova, Anastasia (Ural Federal University, Ekaterinburg, RUS)

The strategy of doping perovskite related structures with oxyanions BO_3^{3-} , CO_3^{2-} , SiO_3^{2-} , SO_4^{2-} , PO_4^{3-} , SeO_4^{2-} has been successfully used to modify the composition and properties of complex oxides. Recent investigations showed that this doping strategy of brownmillerite led to an increase in the oxygen-ion and proton conductivity and allowed to improve the stability at elevated temperatures towards CO_2. In this work we investigated the local structure and O^{2-} and H^+ transport of double perovskite $Ba_4Ca_2Nb_{2-x}P_xO_{11}$.

The samples from homogeneity range of solid solution $Ba_4Ca_2Nb_{2-x}P_xO_{11}$ ($0 \leq x \leq 0.5$) were prepared by a solid state method from $BaCO_3$, $CaCO_3$, Nb_2O_5, $NH_4H_2PO_4$. The X-ray powder diffraction (XRD) measurements were made ona Bruker Advance D8 diffractometer with Cu K_α radiation. The cubic lattice parameter decreases with increasing concentration of PO_4^{3-}.

The total conductivity was measured in wet ($pH_2O=1.42 \cdot 10^{-2}$ atm) and dry ($pH_2O=4.5 \cdot 10^{-4}$ atm) atmosphere. The conductivity increases with x and attains the maximum value for $x = 0.1 - 0.2$, a large enhancement compared to the undoped sample was observed in wet atmosphere at intermediate temperatures .

Raman spectra were obtained using spectrometer Renishaw 1000, capacity of the laser 20 mW, scan range of 15–1000 cm^{-1}. The investigation of the Raman spectra made it possible to establish the basic relationships:

- For «dry» compositions, with increasing phosphate content the line at ~930 cm^{-1} , corresponding to $[PO_4]$ polyhedra, shifts to higher frequencies and this indicates the decrease in P–O distance. The line at ~780 cm^{-1}, assigned to the Nb–O stretching vibration, did not changed.

- For hydrated compositions, with increasing phosphate content the line at ~780 cm^{-1}, shifts to lower frequencies, indicating the increase in Nb–O distance.

- Upon hydration (for the same x) the line at ~780 cm^{-1} shifts to higher frequencies, indicating the decrease in Nb–O distance.

This work was financially supported by the Grant of fundamental and exploratory research in cooperation of Ural Federal University and Ural Branch of the Russian Academy of Sciences

PTue074

New Rock Salt type Structure from Chemical or Electrochemical insertion Reaction

Pralong, Valerie (CNRS, Caen, FRA); Freire, Melanie (CNRS CRISMAT, Caen, FRA); Lebedev, Oleg (CNRS, Caen, FRA); Raveau, Bernard (CNRS, Caen, FRA); Caignaert, Vincent (CNRS, Caen, FRA); Maignan, Antoine (CNRS, Caen, FRA)

Regarding the field of energy storage, the design of new materials that provide high energy densities and long cycle life together with being economic and environmental benign is crucial [1, 2]. Therefore, the soft chemistry used to prepare the original frameworks, new structures is in perfect appropriateness with such a target. Moreover, one of the primordial properties needed for the new materials to be a good candidate for such a challenge is the property of good ionic conduction. Our research is focused on the synthesis by soft chemistry of new “metastable” frameworks with large tunnels or layered structures at low temperature. We will discuss on our strategies to generate original framework showing ionic conductivity. The first approach is based on topotactic reactions starting from existing ionic conductors with a compact anionic framework. In this case, we will show that the lithium/sodium insertion leads to new nanoscale rock salt type structure. We will discuss our recent results on iron, manganese and vanadium based materials Li_2VO_3, Na_2VO_3, $Li_5W_2O_7$,Li_2NbO_3, … [3].

---

[1] J.M. Tarascon, M. Armand, Nature, 2001, 414, 6861, 359-367; M. S. Whittingham, Chem. Rev., 2004, 104, 4271; J. M. Tarascon, N. Recham, M. Armand, et al., Chem. Mater., 2010, 22, 3, 724

[2] B. L. Ellis, K. T. Lee, L.F. Nazar, Chem. Mater., 2010, 22, 3, 691; M. I. Saiful, L.F. Nazar, J. Mat. Chem., 2011, 21, 27, 9810

[3] V. Pralong, et al., Chem. Mat. Com., 2012, 24, 12; V. Pralong, Progress in Solid State Chem., 2009, 37, 4, 262-277; V. Gopal, et al., Electrochem. Com., 40, 100-102, 2014; V. Pralong, et al., Inorg. Chem., 53, 1, 522-527, 2014; V. Pralong, et al., Chem. Mater., 23, 7, 1915-1922, 2011

PTue075

New oxygen insertion reactions involving 1-D channels

Greaves, Colin (University of Birmingham, Birmingham, GBR); de Laune, Benjamin (University of Birmingham, Birmingham, GBR)

A_2BO_4 Ruddlesden-Popper phases have large A and small B cations in a layered arrangement where AO layers are either side of BO_2 layers. The gaps between adjacent AO layers can act as hosts for interstitial anions, e.g. O^{2-}, F^-. Oxide materials of this type have shown useful properties as cathode materials in SOFCs. Previous work has revealed that *in situ* NPD studies using high intensity diffractometers can reveal unique information concerning the defect nature of the phases as a function of temperature and oxygen partial pressure. We will use a previous study on $La_{2-x}Sr_xCo_{0.5}Ni_{0.5}O_{4+y}$ [1] as background to the main aspect of the talk which will consider a new class of oxygen-excess A_2BO_{4+y} materials. These materials relate to the mineral schafarzikite, Sb_2FeO_4 where the large A cations (Sb^{3+}) now have a lone pair of electrons. This feature is highly significant and results in a structure with strong 1-D characteristics: it contains parallel chains of edge-linked FeO_6 octahedra which form oxygen-lined empty channels into which the lone pairs of electrons on the Sb^{3+} ions are directed. The channels are therefore chemically suited to accept interstitial anions. Indeed, rare mineral species are known where S^{2-} ions occupy positions within the channels. We have shown that for materials with appropriate redox capabilities, substantial amounts of oxygen can be inserted into the channels in a reversible manner. Given that a variety of transition metal cations can occupy the chains of octahedra, the materials show promise as catalysts and electrocatalysts. Oxygen insertion occurs typically at 350°C in air/oxygen and reduction can be achieved at 500°C in N_2/H_2 mixtures. These observations provide the first report of oxygen excess phases in this class of materials. In this presentation we will discuss the nature of the oxidation process, *eg* structures and bonding, using primarily *in situ* NPD experiments but also ^{17}O NMR and Mossbauer spectroscopy.

---

[1] F Tonus et al. J. Mater. Chem. 21, 7111 (2011).

PTue076

Oxide Ion Conductors for Energy Applications: Hops and Twists in the Solid State

Evans, Ivana (Durham University, Durham, GBR)

Meeting the future energy needs of the world's growing population is one of today's most significant scientific challenges. Different types of new, renewable and sustainable energy generation have been the subject of intense research, including solar, nuclear, wind and geothermal energy. Solid oxide fuel cell (SOFC) technology is a frontrunner in the short-to-medium term race to provide sustainable energy solutions, owing to the unique combination of high efficiency, fuel flexibility and environmental safety. Two factors have prevented the widespread commercialisation of SOFCs: system cost and reliability, and both stem from the high operating temperatures of the current technology (850–1000oC). Lowering the operating temperatures is therefore a major driver in SOFC research.

We have recently reported exceptional low-temperature oxide ion conductivity in $Bi_{1-x}V_xO_{1.5+x}$(x = 0.095 - 0.087) phases, with s = 3.5 ´ 10 $^{-2}$ S/cm at 450oC, arguably the highest to-date in a stable 3D fluorite-type system. We have attributed this remarkable behaviour to the simultaneous presence of four key structural factors: a highly polarisable sublattice with vacancies, central atoms able to support variable coordination numbers and geometries, and the rotational flexibility of these coordination polyhedra, co-existing in a pseudo-cubic structure. We have found similar structural features to lead to high oxide ion conductivity in a number of other materials with complex superstructures (vanadates, molybdates, tungstates, rhenates).

The presentation will emphasise how a combination of careful diffraction-based work (powder and single crystal, X-ray, neutron and electron, in-situ studies), complementary techniques (solid state NMR, electron microscopy), computational methods and characterisation of physical properties is required to understand the complexity of next-generation functional materials.

---

[1] X. J. Kuang, J. L. Payne, J. D. Farrell, M. R. Johnson and I. R. Evans, Chemistry of Materials, 2012, **24**, 2162-2167.

[2] X. J. Kuang, J. L. Payne, M. R. Johnson and I. R. Evans, Angewandte Chemie International Edition, 2012, **51**, 690-694.

[3] C. D. Ling, W. Miiler, M. R. Johnson, D. Richard, S. Rols, J. Madge and I. R. Evans, Chemistry of Materials, 2012, **24**, 4607-4614.

[4] J. L. Payne, J. D. Farrell, A. M. Linsell, M. R. Johnson and I. R. Evans, Solid State Ionics, 2013, **244**, 35-39.

[5] I. R. Evans, J. S. O. Evans, H. G. Davies, A. R. Haworth and M. L. Tate, Chemistry of Materials, 2014, **26**, 5187-5189.

PTue077

$Pr_2NiO_{4+\delta}$: InSitu electrochemical oxygen intercalation studied by synchrotron diffraction on single crystal

Maity, Avishek (Université de Montpellier, ICGM, Montpellier, FR, Montpellier, FRA); Sendatskyi, Oles (Université de Montpellier, ICGM, Montpellier, FR, Montpellier, FRA); Dutta, Rajesh (Université de Montpellier, ICGM, Montpellier, FR, Montpellier, FRA); Ceretti, Monica (Université de Montpellier, ICGM, Montpellier, FR, Montpellier, FRA); Lebranchu, Angélique (Université de Montpellier, ICGM, Montpellier, FR, Montpellier, FRA); Chernyshov, Dmitry (ESRF, BM01A SNBL, Grenoble, FR, Grenoble, FRA); Paulus, Werner (Université de Montpellier, ICGM, Montpellier, FR, Montpellier, FRA)

$Pr_2NiO_{4+\delta}$ is one of the most promising materials for oxygen ion conducting membranes in MEIC (mixed electronic ion conductors) at moderate temperatures and even more interesting down to ambient. The underlying diffusion mechanism in RE_2MO4-type frameworks has been evidenced as being triggered by low energy phonons [1-3]. Large anisotropic displacements of the apical oxygen atoms towards the interstitial lattice sites have been evidenced for the homologous $La_2CuO_{4.07}$ by single crystal neutron diffraction, and which have been equally simulated by *ab initio* DFT calculations as the oxygen diffusion pathway showing a very shallow diffusion potential [2]. A similar scenario is present for the homologous $Nd_2NiO_{4+\delta,}$ where first-principles *ab initio* phonon calculations together with molecular dynamics simulations and inelastic neutron scattering, allowed to understand oxygen diffusion pathways activated by lattice dynamics down to ambient temperature [3]. Oxygen diffusion turned out to be extremely anisotropic for $Nd_2NiO_{4+\delta}$ and $Pr_2NiO_{4+\delta}$, showing 3 orders of magnitude difference along the Pr_2O_2 rock salt layer and perpendicular to this direction [4].

In order to correlate structural complexities as a function of the interstitial oxygen concentration δ, we explored the phase diagram of $Pr_2NiO_{4+\delta}$ by *in situ* synchrotron diffraction on an oriented needle shaped 50µm size single crystal in a specially designed electrochemical cell, taking advantage of the 2D PILATUS detector at BM01A@ESRF. The oxygen stoichiometry δ in this compound can be varied in an important range $0 < \delta < 0.25$ via an electrochemically controlled reaction, proceeding fully reversibly at RT in an alkaline aqueous electrolyte.

$Pr_2NiO_{4.0} + \delta O^{2-} \Leftrightarrow Pr_2NiO_{4+\delta} + 2\delta e^-$

We followed the electrochemical galvanostatic reduction of a twinned, orthorhombic $Pr_2NiO_{4.25}$ crystal to the final orthorhombic $Pr_2NiO_{4.0}$ phase, while passing through an intermediate $Pr_2NiO_{4.125}$ phase with tetragonal symmetry. Due to the high oxygen diffusion the crystal remained extremely homogeneous during the whole reaction. This single crystal *in situ* diffraction study allowed for the first time to explore the chemical reactivity during an electrochemically-controlled reaction accessing the whole reciprocal space, i.e. the evolution of the structure, microstructure, twin domains, including diffuse scattering.

Contrary to polycrystalline electrodes, the 50µm size single crystal reacted completely and homogeneously in less than 24h. The resulting superior oxygen diffusion is discussed with respect to the microstructure consisting of 4 twin domains but without grain boundaries.

---

[1] Paulus. W. et. al.; J. Am. Chem. SOC. 2008, *130*, 16080–16085
[2] Villesuzanne. A. et. al.; J. Solid State Electrochem. 2011, 15, 357–366
[3] Perrichon. A. et. al.; J. Phys. Chem. C. 2015, 119, 1557−1564
[4] Bassat J.-M. et al. Phys. Chem. C. 2013, 117, 26466−26472

PTue078

Synthesis, thermal stability and electrical properties of copper- or cobalt-containing bismuth titanates with the pyrochlore type structure

Koroleva, Mariya (Institute of Chemistry, Komi Science Center, UB, RAS, Syktyvkar, RUS); Piir, Irina (Institute of Chemistry, Komi Science Center, UB, RAS, Syktyvkar, RUS); Sekushin, Nikolai (Institute of Chemistry, Komi Science Center, UB, RAS, Syktyvkar, RUS)

In recent years the $Bi_2Ti_2O_7$ pyrochlore attracts attention due to its high dielectric constant $\varepsilon = 118$ (25 °C) [1] and its perspective as insulator. However, $Bi_2Ti_2O_7$ decomposes at $t \approx 612$ °C [2]. A doping of bismuth titanate with 3d-metals provides thermal stability of these compounds at high temperature $t \leq 1200$ °C. The metal containing bismuth titanates can be an electronic or electron-ion conductor. Electrical properties of Co-doped bismuth titanates have not been studied yet. The investigation of electrical properties of copper- and cobalt containing bismuth titanates with the pyrochlore-type structure is the task of this work. In our work the solid solutions $Bi_{1.6}Cu_xTi_2O_{7-\delta}$ and $Bi_{1.6}Co_xTi_2O_{7-\delta}$ first were prepared by the polymeric precursor (Pechini`s method) and a solid-state reaction methods, were examined by X-ray diffraction method using Shimadzu XRD-6000 diffractometer (CuKα emission, 10–80°, 0.050° step) and scanning electron microscopy (VEGA TESCAN 35 BU microscope). The fields of homogeneity of $Bi_{1.6}Cu_xTi_2O_{7-\delta}$ ($0.08 \leq x \leq 0.8$) and $Bi_{1.6}Co_xTi_2O_{7-\delta}$ ($0.08 \leq x \leq 0.4$) were determined. The distribution of copper and cobalt atoms in the structure was established by the comparison of pycnometric and calculated densities of the synthesized samples, and the Rietveld analysis of the diffractions results. The cobalt atoms distribute in the Bi-sites (A-sites of a pyrochlore structure) in the $Bi_{1.6}Co_xTi_2O_{7-\delta}$ system predominantly. The copper atoms distribute in the Bi-sites with $x \leq 0.4$ predominantly but with $x > 0.4$ the copper atoms (~ 25 %) can distribute in the Ti-sites (B-sites of a pyrochlore structure) in the $Bi_{1.6}Cu_xTi_2O_{7-\delta}$ system. DSC, TGA studies were executed using NETZSCH STA 409 PC/PG equipment to determine melting points of the compounds. Electrical conductivities of the compounds were study using LCR meter TM -4090 ($1 \leq \omega$ (kHz) ≤ 200, $25 \leq t$ (° C) ≤ 750) and impedance spectrometer Z-1000P. It was shown that the conductivity of $Bi_{1.6}Cu_xTi_2O_{7-\delta}$ and $Bi_{1.6}Co_xTi_2O_{7-\delta}$ increases when the cobalt and copper amount increases in the bismuth titanates. The conductivity of $Bi_{1.6}Cu_{0.8}Ti_2O_{7-\delta}$ is $3{,}2\cdot10^{-3}$ $Ohm^{-1}cm^{-1}$ at 750 °C and the conductivity of $Bi_{1.6}Co_{0.4}Ti_2O_{7-\delta}$ is $6{,}3\cdot10^{-3}$ $Ohm^{-1}cm^{-1}$ at 750 °C. The conductivity of the compounds $Bi_{1.6}Cu_xTi_2O_{7-\delta}$ (x = 0.2; 0.4; 0.6; 0.8) and $Bi_{1.6}Co_xTi_2O_{7-\delta}$ (x = 0.16; 0.32; 0.40) in the argon, air, oxygen atmospheres was determined. The conductivity of $Bi_{1.6}Cu_xTi_2O_{7-\delta}$ increases when $p(O_2)$ decreases ($t \leq 500$ °C). So, we can detect the n-type conductivity. A further increase in temperature ($t > 500$ °C) the gas atmosphere doesn`t influence on the conductivity of the samples. We assume it may be associated with the beginning of mobile oxygen (O`) migration. The conductivity of $Bi_{1.6}Co_xTi_2O_{7-\delta}$ (x = 0.16; 0.32; 0.40) increases with increasing $p(O_2)$ in the wide temperature interval ($25 \leq t$ (° C) ≤ 750). The temperature dependence on the conductivity of $Bi_{1.6}Co_xTi_2O_{7-\delta}$ obeys the Arrhenius law with the activation energy $E_a = 0.36\pm0.03$ eV. Thus, the p-type conductivity of the $Bi_{1.6}Co_xTi_2O_{7-\delta}$ pyrochlores is predominant in the temperature region $160 \leq t \leq 750$ °C. This work is supported by the RFBR (project № 14-03-31175 mol_a, project № 15-03-09173 A). References: 1 Hector A.L., Wiggin S.B. Synthesis and structural study of stoichiometric $Bi_2Ti_2O_7$ pyrochlore // J. Solid State Chem. 2004. V. 177. P. 139–145. 2 Roberto Esquivel-Elizondo J., Hinojosa B.B., Nino J.C. $Bi_2Ti_2O_7$: it is not what you have read // Chemistry Mater. 2011. V. 23(22). P. 4965-4974.

PTue079

Small change-great effect: Steep increase of Li ion dynamics in $Li_4Ti_5O_{12}$ at the early stages of chemical Li insertion (x = 0.1, x = 0.3)

Schmidt, Walter (TU Graz - Institute for Chemistry and Technology of Materials, Graz, AUT); Bottke, Patrick (Tu Graz - Institute for Chemistry and Technology of Materials, Graz, AUT); Hennige, Volker (AVL List, Graz, AUT); Gollob, Peter (AVL List, Graz, AUT); Hanzu, Ilie (Tu Graz - Institute for Chemistry and Technology of Materials, Graz, AUT); Wilkening, Martin (Tu Graz - Institute for Chemistry and Technology of Materials, Graz, AUT)

Polycrystalline $Li_{4+x}Ti_5O_{12}$ (LTO, 0 < x = 3) is one of the most promising negative electrode materials for lithium-ion batteries. It shows a flat Li insertion plateau of about 1.5 V vs. Li/Li^+; its theoretic specific capacity is approximately 175 mAh/g. The increased use of LTO, which is commercially available, is due to various properties such as low cost, satisfactory safety and easy preparation. Most importantly, upon Li insertion, the expansion of the material is almost negligible favoring a long cycle life. In samples with x = 0, Li self-diffusion, which can be microscopically probed via Li nuclear magnetic resonance (NMR), is rather low. With increasing Li insertion, however, the diffusivity increases significantly. This is accompanied by a redistribution of Li ions across the 8a and 16c sites in the spinel structure [1]. Recent ^7Li NMR studies put emphasis on samples with Li contents of x >1 [2]. As yet, there are, however, no information from NMR available answering the question of how Li self-diffusion changes when x is only slightly increased. The present results show that even at x = 0.1 ^7Li NMR spin-lattice relaxation, performed in the so-called rotating frame of reference, reveals a drastic enhancement of Li diffusivity [3], which is associated with a considerable reduction of the local hopping barrier pointing to the 8a – 16c – 8a migration pathway discussed in the literature. As a result, the largest increase in Li diffusivity is observed at the early stages of Li insertion [3]. Strong Coulomb repulsions caused by the simultaneous occupation of neighboured 8a and 16c sites might explain the enhanced Li diffusivity found.

High resolution ^6Li MAS NMR was helpful to reveal the magnetically different Li sites in LTO (8a, 16c, 16d); from the areas under the NMR lines we calculated the population ratios and, thus, followed the change in site occupancy as a function of x. Site-specific (MAS) NMR spin-lattice relaxation times and ^6Li 2D NMR experiments point to rapid exchange of the Li ions between the 8a and 16c sites. This is in contrast to the Li ions in the 16d voids; they do not participate in the fast Li diffusion process that is relevant for battery applications.

---

[1] M. Wagemaker et al. *Adv. Mater.***2006**, 18, 3169.

[2] M. Wilkening et al., *Phys Chem. Chem. Phys.***2007**, 9, 6199.

[3] Schmidt et al. *Chem. Mater.*, **2015**, 27 (5), pp 1740–1750

PTue080

Solid acid proton conductors of CsH_2PO_4 - $CsHSO_4$ - H_2O salt system

Grebenev, Vadim (A.V. Shubnikov Institute of Crystallography of Russian Academy of Sciences, Moscow, RUS); Makarova, Irina (A.V. Shubnikov Institute of Crystallography of Russian Academy of Sciences, Moscow, RUS); Komornikov, Vladimir (A.V. Shubnikov Institute of Crystallography of Russian Academy of Sciences, Moscow, RUS); Dmitricheva, Elena (A.V. Shubnikov Institute of Crystallography of Russian Academy of Sciences, Moscow, RUS); Ksenofontov, Dmitry (A.V. Shubnikov Institute of Crystallography of Russian Academy of Sciences, Moscow, RUS)

Proton subsystem and its disordering in crystals are of fundamental and practical interest. Superprotonic crystals – hydrogen containing salts with the general formula $MexHy(AO_4)_{(x+y)/2}$ (where Me = Cs, Rb, K, NH_4 and A = S, Se, P, As) can be considered as model objects for studying the proton subsystem and processes occurring in it. A promising subgroup of this set of crystals for studies includes crystals of the $CsHSO_4$ – CsH_2PO_4 salt system. The first attempts to study it were made at the end of the 1990s; these investigations were rather irregular. They were aimed at searching for new protonic conductors with a highly stable superprotonic phase, as in the $CsHSO_4$ compound, and a high conductivity, as for CsH_2PO_4. A fundamental aspect of these studies was to establish a relationship between the protonic conductivity, phase transitions, crystal structure, and changes in the proton subsystem. Applied studies were related to the possibility of using these crystals as proton exchange membranes in fuel cells.

No systematic studies of this system have been performed; therefore, phase diagrams of the $CsHSO_4$–CsH_2PO_4–H_2O system in different temperature cuts were constructed [1]; as a result, a new compound with the formula $Cs_6H(HSO_4)_3(H_2PO_4)_4$ (before was established as $Cs_5(HSO_4)_2(H_2PO_4)_3$) was obtained for the first time [2]. Studies of single crystals of the system revealed absence (0.1% at.) of solid solutions at temperatures of growing single crystals. Structures of these crystals were solved and properties were studied by means of complex of techniques also. Based on analysis of the single crystals symmetry and the chemical composition, we introduced a different classification of compounds based on the stoichiometry, according to such classification compound beta-$Cs_3(HSO_4)_2(H_x(P,S)O_4)$ [3] has the simple formula $Cs_4(HSO_4)_3(H_2PO_4)$. Large single crystals of $Cs_3(HSO_4)_2(H_2PO_4)$, $Cs_4(HSO_4)_3(H_2PO_4)$ and $Cs_6H(HSO_4)_3(H_2PO_4)_4$ were grown. It has been found structural transitions in all these crystals in a state with a high conductivity. Kinetics of these transitions is anomalously slow and more similar to the chemical reactions but decomposition of crystals was not observed. Detailed studies of the single crystals properties, taking into account the literature data [4],confirms the existence of solid solutions at high temperatures and also extends the range of the compositions of solid solutions to hydrosulphate region in comparison with the previously determined boundaries of the homogeneity by other scientists. On the basis of obtained and previously published data a fragment of T - x phase diagram $CsHSO_4$ - CsH_2PO_4 was constructed.This work was supported by RFBR grant 13-03-12216.

---

[1] V.A. Komornikov et al. // Russian Journal of Inorganic Chemistry, V.57(4), pp. 478-484 (2012).

[2] V.V. Grebenev et al. // Crystallography Reports, V.58(6), pp. 894–898 (2013).

[3] S.M. Haile, P.M. Calkins, D. Boysen // J. Solid State Chem. V139, pp. 373-387 (1998).

[4] V.G. Ponomareva et al. // Inorganic Materials 50(7), 716-722 (2014).

PTue081

Space Charge Layer Effect at Nickel/$BaZr_{0.9}Y_{0.1}O_{3-\delta}$ interfaces in Protonic Ceramic Fuel Cells

Chen, Min (University of Oslo, Oslo, NOR); Norby, Truls (University of Oslo, Oslo, NOR)

The special role of interfaces, whose importance is clearly demonstrated in the field of semiconductors, is still poorly understood in cases where solid ionic conductors are involved. In this study, the interface of a solid proton conductor $BaZr_{0.9}Y_{0.1}O_{3-\delta}$ (BZY10) to a metal phase (Nickel) is considered, which is divided into core and space charge region. A negative space charge layer (SPL), depleted of oxygen vacancies and protons, is suggested to locate on the surface of the BZY10 proton conductor. This SPL would affect the kinetics of the electrochemical reaction at the metal electrode/BZY10 electrolyte interfaces in protonic ceramic fuel cells (PCFC). Using the bias impedance spectroscopy and Butler-Volmer equation, the effect of SPL on the H2 oxidation reaction (HOR) and H2 evolution reaction (HER) at Ni/BZY10 interfaces was determined at 873 K in wet(3%H2O)-(5%H2+95%Ar). It was found that the SPL resistance (RSPL) is much bigger under anodic bias (HOR) than that under cathodic bias (HER), which (RSPL under both anodic and cathodic bias) also nonlinearly increase with increasing current density (j). In order to describe the response of the SPL under various bias conditions, an electrical potential model was established based on Poisson's equation, revealing a nonlinear relationship between RSPL and 1/j. After fitting the experiment data to the model, a Schottky barrier height V(0) of the core layer at equilibrium state (zero bias condition) was estimated to be lower than 0.025 V, which is 10 times lower than that of grain boundary cores in BZY10.

PTue082

Synthesis and characterization of donor doped barium titanate

Hofer, Johannes (Montanuniversität Leoben - Lehrstuhl für Physikalische Chemie, Leoben, AUT);
Preis, Wolfgang (Montanuniversität Leoben - Lehrstuhl für Physikalische Chemie, Leoben, AUT);
Leprich, Michael (Montanuniversität Leoben - Lehrstuhl für Physikalische Chemie, Leoben, AUT);
Sitte, Werner (Montanuniversität Leoben - Lehrstuhl für Physikalische Chemie, Leoben, AUT)

It is well known, that the positive Temperature Coefficient of electrical Resistivity (PTCR-effect) in donor doped barium titanate is governed by double Schottky-barriers (DSBs) at the grain boundaries. The width and height of these blocking potential barriers is caused by the concentrations of donor and acceptor dopants in net-donor doped barium titanate (BTO), as well as the sintering schedule of the material. During the tetragonal to cubic phase transition at the Curie-temperature T_c a steep increase of the electrical resistance over several orders of magnitude is encountered. Below T_c the DSBs are compensated by spontaneous polarization in the material.

Donor doped disk-like samples of BTO with a diameter of approximately 10 mm and a thickness of 1 mm have been prepared via a modified solid oxide as well as by a Pechini route. For the solid oxide samples a composition of $Ba_{0,9975}La_{0,0025}Ti_{1,010}Mn_{0,0005}O_3$ was chosen. The Pechini samples were synthesized to yield the composition $Ba_{0,979}La_{0,021}Ti_{1,01}Mn_{0,01}O_3$ and $Ba_{0,979}La_{0,021}Ti_{0,99}Mn_{0,01}O_3$. Sol-gel processes are useful to avoid an inhomogeneous distribution of doping elements. After preparation the powders were ball milled, uniaxial pressed to tablets with an organic wax as binder, sintered and contacted via a sputtering technique. The samples were characterized by XRD, SEM, and impedance spectroscopy. As expected, the samples with the lower doping element concentrations showed the PTCR-effect, whereas the samples with higher doping levels showed no such effect. The samples with higher doping element concentrations yielded a high dielectric constant. The fitting of the impedance data was carried out with an empiric equivalent circuit. The results of the measurements are used to develop a deeper insight in the modelling of the diffusion processes during sintering as well as the modelling of the PTCR-effect under voltage load for DC-bias and AC-variation experiments.

PTue083

Synthesis and doping studies of $Na_2M(SO_4)_2.2H_2O$ (where M = Fe, Co and Ni) for potential applications as a cathode material for Na-ion batteries

Driscoll, Laura (University of Birmingham, Birmingham, GBR)

Issues with increasing energy demand, and associated concerns regarding emissions, are placing key emphasis on the development of new materials for efficient energy generation and storage. A particular issue is efficient energy storage for both consumer devices and large scale grid applications. A key example, the Li-ion battery, provides excellent power storage for portable electronics and, more recently, applications within the automobile industry. However, due to diminishing resources and the cost of extraction, the increasing cost of lithium has prevented the implementation of Li-ion technology in large scale industrial applications [1].

It is for this reason that Na-ion technology has drawn increased attention due to similar intercalation chemistry and reduced cost due to sodium's abundance. In addition, the predominant factor dictating the viability of these systems becomes the cost per kilogram rather than power density per kilogram, once the restriction on battery size is removed.

Years of research into lithium based systems suggest that cathodes built from 3-dimensional frameworks based of metal octahedra and oxyanion tetrahedra provide the excellent cell voltages as well as increased stability leading to cathode systems such as $LiFePO_4$ [2].

Using this principle, our research has focused on the low temperature synthesis of potential sodium containing cathode materials based on sulphate frameworks, one example being the recently reported $Na_2M(SO_4)_2{\cdot}2H_2O$ (where M = Fe, Co and Ni) systems [3,4]. In addition to the synthesis of these materials, we have undertaken doping studies (eg. $SeO4^{2-}$ for SO_4^{2-}) of both the hydrated and dehydrated structures and in this presentation we discuss the effect of these doping strategies on the structure and properties.

---

[1] Palomares, V., et al., Na-ion batteries, recent advances and present challenges to become low cost energy storage systems. Energy & Environmental Science, 2012. 5(3): p. 5884-5901.
[2] Padhi, A.K., K.S. Nanjundaswamy, and J.B. Goodenough, Phospho-olivines as positive-electrode materials for rechargeable lithium batteries. Journal of the Electrochemical Society, 1997. 144(4): p. 1188-1194.
[3] Barpanda, P., et al., Kröhnkite-Type Na2Fe(SO4)2·2H2O as a Novel 3.25 V Insertion Compound for Na-Ion Batteries. Chemistry of Materials, 2014. 26(3): p. 1297-1299.
[4] Reynaud, M., et al., Design of new electrode materials for Li-ion and Na-ion batteries from the bloedite mineral Na2Mg(SO4)2·4H2O. Journal of Materials Chemistry A, 2014. 2(8): p. 2671-2680.

PTue084

Synthesis and properties of $Bi_{2-y}M_xTi_2O_{7-\delta}$ (M - Sc, In) pyrochlores

Krasnov, Aleksei (Institute of Chemistry Komi SC of UB RAS, Syktyvkar, RUS); Piir, Irina (Institute of Chemistry Komi SC of UB RAS, Syktyvkar, RUS)

High dielectric constant and low leakage current of $Bi_2Ti_2O_6O'$ make possible to use it as an insulating layer for advanced MOS transistors and for design storage capacitors in DRAM [1]. Moreover bismuth titanate pyrochlore allows for a high degree of nonstoichiometry on bismuth and oxygen O' ions so it could be promising as a solid ion-conductive material. Thermal stability of $Bi_2Ti_2O_7$ [2] can be enhanced by doping with metal cations. Substitution also influences on the properties of resulting materials [3].

The aim of this work was to determine the synthesis conditions for the preparation of single-phase Sc-, In-containing bismuth titanate pyrochlore and to study properties of the obtained compounds.

The solid solutions $Bi_{2-y}M_xTi_2O_{7-\delta}$ (y=0.4; 0.6; x= 0.2–1) have been synthesized using a solid-state reaction for the first time. The stoichiometric amounts of Bi_2O_3, TiO_2, Sc_2O_3 or In_2O_3 were initially homogenized in an agate mortar. Powder mixtures were pressed into pellets. Stepwise annealing with intermediate grindings was carried out in the air at 650 °C (5 h); 850 °C (5 h); 1000 °C (5 h); 1100 °C (12 h); 1150 °C (12 h).

The homogeneity regions $Bi_{1.4(1.6)}Sc_xTi_2O_{7-\delta}$ at $0.2 \leq x \leq 0.6$; $Bi_{1.4}In_xTi_2O_{7-\delta}$ at $0.4 \leq x \leq 0.6$; $Bi_{1.6}In_xTi_2O_{7-\delta}$ at $0.2 \leq x \leq 0.6$ have been determined by XRD and SEM methods. The amount of elements has been defined using ICP NPP. The resulting composition of the samples corresponds to the initial. According to the results DSC analyzes Sc(In)-doped bismuth titanates are stable up to the melting temperature, which depends on the nature and amount of dopant.

Rietveld analysis of $Bi_{1.6}Sc_{0.4}Ti_2O_7$ and $Bi_{1.6}In_{0.4}Ti_2O_7$ was carried out based on X-rays powder diffraction data. Models with different distribution of Sc (In) atoms on cation positions were considered. The best results of the refinement were obtained for model wherein all doped atoms are distributed in the bismuth sites and furthermore Bi, Sc, In atoms are displaced from Wyckoff position 16*c* to position 96*h* [4]. Pycnometric densitiesof these samples coincide within the error with the calculated densities corresponding to the distribution of all Sc (In) atoms in Bi sites of pyrochlore structure.

The study of electrical properties was carried out by two-probe method using AC bridge RLC MT-4090. The dependence of the conductivity on scandium (indium) and bismuth concentration has been revealed. The presence of proton transport has been observed in temperature range 240-640 ºC for compounds with defects in Bi-sites and in oxygen sublattice O' consequently. So obtained materials can be promising as high temperature proton conductors.

The work was supported by RFBR grants 15-03-09173 and 14-03-31175 mol_a.

---

[1] Hardy A., Elshocht S.V., Dobbelaere C.D. et al. // Mater. Res. Bull. 2012. V. 47. № 3. P. 511.

[2] Esquivel-Elizondo J.R. Hinojosa B.B., Nino J.C. // Chem. Mater. 2011. V. 23. № 22. P. 4965.

[3] Piir I.V., Koroleva M.S., Ryabkov Y.I. et al. // J. Solid State Chem. 2013. V. 204. P. 245.

[4] Hector A.L, Wiggin S.B. // J. Solid State Chem. 2004. V. 177. № 1. P. 139.

PTue085

Synthesis of garnet-type Li-ion conductor $Li_{7-x}La_3Zr_{2-x}Bi_xO_{12}$

Wagner, Reinhard (University of Salzburg, Salzburg, AUT); Rettenwander, Daniel (University of Salzburg, Salzburg, AUT); Tippelt, Gerold (University of Salzburg, Salzburg, AUT); Redhammer, Günther (University of Salzburg, Salzburg, AUT); Amthauer, Georg (University of Salzburg, Salzburg, AUT)

Li-stuffed oxide garnets containing more than three Li cations per formula unit receive much scientific attention as they show a high Li-ion conductivity as well as an excellent chemical and thermal stability and electrochemical inertness, in particular against Li metal. Thus, these materials are excellent candidates for solid electrolytes in Li-ion and Li-oxygen batteries.[1,2] Within this group, $Li_7La_3Zr_2O_{12}$ (LLZO) garnet is among the most promising materials. Pure LLZO occurs in at least two structural modifications: a low-temperature tetragonal phase (space group *I*41/*acd*) and a cubic high-temperature phase (space group *Ia*-3*d*). In the cubic garnet structure, Zr^{4+} occupies an octahedral site (16a), whereas La^{3+} is located at an 8-fold coordinated site (24c). Li^+ occupies a tetrahedral site (24d) as well as two other positions (octahedrally coordinated 48h sites and distorted 4-fold coordinated 96h sites) that are not occupied in the conventional garnet structure.

For use as an electrolyte, the cubic phase is much more desirable, as its conductivity is two orders of magnitude higher (10^{-4}-10^{-3} S/cm) compared to the tetragonal polymorph (≈ 10^{-6} S/cm)[3]. Unfortunately, the cubic phase is not stable at room temperature and has to be stabilized by doping of LLZO with aliovalent cations [4,5]. The ionic conductivity of LLZO and its variants is still lower compared to liquid electrolytes or solid superionic conductors, such as $Li_{1+x}Al_xTi_{2-x}(PO_4)_3$ (LATP) and $Li_{10}GeP_2S_{12}$, and has to be improved [6-8].

For Li-stuffed oxide garnets, the unit-cell parameter and the Li content are considered as crucial for the ion conductivity [9]. Therefore, we combined the high Li content of LLZO with the large unit-cell parameter (13.065 Å) of $Li_5La_3Bi_2O_{12}$ [10]. Cubic LLZO was successfully stabilized by doping with Bi^{5+}. A significant enlargement of the unit-cell parameter with increasing Bi content was confirmed by X-ray powder diffraction. A unit-cell parameter of 13.07 Å was observed for Bi-doped LLZO, compared to a unit-cell parameter of 12.97 Å for LLZO doped with Ga^{3+}, Fe^{3+} and Al^{3+} [4,5]. The reason for this different behavior is considered in the crystallographic position of the dopant elements. The long range Li-ion transport properties in the garnet as a function of the unit-cell parameter will be investigated by electrochemical impedance spectroscopy as well as ^{7}Li NMR measurements. Preliminary results about the electrochemical properties of Bi-doped LLZO will be presented.

---

[1] Cussen, E.J.; J. Mat. Chem. 2010, 20, 5167-5173.

[2] Thangadurai, V.; Narayanan, S.; Pinzaru, D.; Chem. Soc. Rev. 2014, 43(13), 4714-4727.

[3] Buschmann, H.; Dölle, J.; Berendts, S.; Kuhn, A.; Bottke, P.; Wilkening, M.; Heitjans, P.; Senyshyn, A.; Ehrenberg, H.; Lotnyk, A.; Duppel, V.; Janek, J. J. Phys. Chem. Chem. Phys. 2011, 13, 19378-19392.

[4] Rettenwander, D.; Geiger, C. A.; Tribus, M.; Tropper, P.; Wagner, R.; Tippelt, G.; Lottermoser, W.; Amthauer, G; J. Sol. State Chem. 2015; in press; DOI: 10.1016/j.jssc.2015.01.016

[5] Rettenwander, D.; Langer, J.; Schmidt, W.; Arrer, C.; Harris, K. J.; Terskikh, V.; Goward, G. R.; Wilkening, M.; Amthauer, G.; Chem. Mater. 2015, in press, DOI: 10.1021/acs.chemmater.5b00684

[6 Aono, H. Sugimoto, E.; Sadaoka, Y.; Imanaka, N.; Adachi G.; J. Electrochem. Soc. 1990, 137, 1023-1027.

[7] Knauth, P.; Solid State Ionics 2009, 180, 911-916.

[8] Kamaya, N.; Homma, K.; Yamakawa, Y.; Hirayama, M.; Kanno, R.; Yonemura, M.; Kamiyama, T.; Kato, Y.; Hama, S.; Kawamoto, K.; Mitsui, A.; Nat. Mater. 2011, 10, 682-686.

[9] Zeier, W. G.; Dalton Trans., 2014,43, 16133-16138

[10] Murugan, R.; Weppner, W.; Schmid-Beurmann, P.; Thangadurai, V.; Mat. Sci. Eng. B 2007, 143, 14-20

PTue086

The mechanism of Ag filament formation in Ag doped AsS_2 thin layer

Zhang, Bo (University of Pardubice, Department of inorganic chemistry, Pardubice, CZE)

The mechanism of Ag filament formation in Ag doped AsS_2 thin layer Resistive switching phenomena reported in 1976 has attracted considerable attention as its bears a potential for applications in resistive random access memories [1][2]. The basic mechanism of resistive switching involves creation of the conductive filament across the layer with suitable composition after application of a voltage pulse on the layer [3]. However, the direct formation of such filament in integrated vertical cell has not been observed until now. The electrically induced Ag segregation is utilized to simulate the formation and rupture of filament on planner cell [4]. In this presentation, we will show results of experiments using alternative pulse voltages for the resistive switching of Ag doped AsS_2 thin layer utilized to induce the Ag filament formation process. We will demonstrate interesting morphological (SEM and optical microscope) and electrochemical observations (current transients, impedance results). In particular, we will address formation of Ag particles on the surface upon cycling. Reference

---

[1] Y. Hirose and H. Hirose, “Polarity-dependent memory switching and behavior of Ag dendrite in Ag- photodoped amorphous As2S3 films,” Journal of Applied Physics, vol. 47. pp. 2767–2772, 1976.

[2] F. Pan, S. Gao, C. Chen, C. Song, and F. Zeng, “Recent progress in resistive random access memories: Materials, switching mechanisms, and performance,” Mater. Sci. Eng. R Reports, vol. 83, pp. 1–59, 2014.

[3] J. Kolar, J. M. Macak, K. Terabe, and T. Wagner, “Down-scaling of resistive switching to nanoscale using porous anodic alumina membranes,” J. Mater. Chem. C, vol. 2, p. 349, 2014.

[4] X. Guo, C. Schindler, S. Menzel, and R. Waser, “Understanding the switching-off mechanism in Ag+ migration based resistively switching model systems,” Appl. Phys. Lett., vol. 91, no. 133513, 2007.

PTue087

Theory of charge transport through single redox-active transition metal complexes

Kastlunger, Georg (Vienna University of Technology, Vienna, AUT); Stadler, Robert (Vienna University of Technology, Vienna, AUT)

The vision of molecular electronics is to employ small ensembles or even single molecules as active, functional building blocks in electronic circuits [1]. Besides current rectification, conductance switching is one fundamental operation required for various electronic applications, e.g. logic or memory. Most switching mechanisms are based on either conformational changes or the charging of the molecule in the junction. Organometallic compounds [2] with embodied redox-active centers are a promising class of molecules as functional electronic building-blocks since they can form stable on and off states corresponding to their respective redox states.

In our contribution we focus on a description of the electron transport through transition metal complexes on the basis of density functional theory (DFT), where a special emphasis is put on the interpretation of experimental results of our close collaborators at IBM Zürich. For the interpretation of their mechanically controlled break junction experiments a dinuclear Fe unit, {Fe}–C4–{Fe} with five different end groups was studied [3]. A voltage-induced conductance switching is found in case of weak coupling (–N=C=S) at low temperature ($T < 150$ K) while the strong hybridization of metal states and molecular orbitals for the strong coupling case of a direct C-Au bond prohibits the same intrinsic redox degrees of freedom from operating. An excellent agreement between the theoretically predicted and experimentally measured conductances of the five Fe2-complexes has been achieved and a reasonable explanation for the switching properties has been found [4].

Following these findings the influence of the metal center and their corresponding interactions with the ligands in mononuclear Fe, Mo and Ru complexes coupled covalently via a thiol anchor to Au electrodes was investigated systematically. Although voltage-induced switching is detected experimentally for all compounds the magnitude of the conductance change upon switching strongly depends on the atom type of the metal center. While the switching is rather continuous for Fe and Ru, the Mo bis(σ-arylacetylide) complex reveals an abrupt hysteretic switching resulting in on/off conductance ratios of up to 400. The reason for the different behaviour has been identified in the paramagnetic groundstate of the Mo-complex, which leads to a highly localized molecular eigenstate energetically close to the electrode's Fermi Level. Due to the small coupling between the localized state and the metal electrode an electron can hop onto the metal center of the molecule and stay there with a finite life time. As a consequence an oxidized state is created in the junction, whose I/V properties differ notably from the ground state. With the source drain bias the complex can be oxidized and reduced leading to an on/off switching.

In order to describe the two processes involved in creating hysteresis, namely coherent transport, responsible for the conductance, and electron hopping, which is the mechanism of the redox reaction, a bias dependant switching formalism based on a combination of NEGF-DFT and Marcus theory has been developed, where the two redox states are treated explicitly [5,6].The results could demonstrate the high potential of redox-active molecular building-blocks for memory applications in ultimately-scaled devices with their origins rationalized by a proper theoretical description.

---

[1] M. A. Ratner and A. Aviram, Chem. Phys. Lett. 29, 277 (1974).
[2] B. Kim et al., Phys. Chem. C, 111, 7521 (2007).
[3] F. Lissel et al, J. Am. Chem, 35, 4051 (2013).
[4] F. Schwarz, G. Kastlunger, et al., Nano Lett., 14, 5932 (2014).
[5] F. Schwarz, G. Kastlunger, et al., Submitted (2015).
[6] G. Kastlunger and R. Stadler, Phys. Rev. B 88, 035418 (2013).

PTue088

Crystal Chemistry and Physics of Perovskites with Small Cations at the A Site

Belik, Alexei (National Institute for Materials Science, Tsukuba, JPN); Yi, Wei (Institute of Physics, Beijing, CHN); Matsushita, Yoshitaka (National Institute for Materials Science, Tsukuba, JPN); Tanaka, Masahiko (National Institute for Materials Science , Tsukuba, JPN); Terada, Noriki (National Institute for Materials Science , Tsukuba, JPN); Suzuki, Hiroyuki (National Institute for Materials Science , Tsukuba, JPN); Tsujii, Naohito (National Institute for Materials Science , Tsukuba, JPN); Imanaka, Yasutaka (National Institute for Materials Science , Tsukuba, JPN); Khalyavin, Dmitry (Rutherford Appleton Laboratory, ISIS, Oxfordshire, GBR); Manuel, Pascal (Rutherford Appleton Laboratory, ISIS, Oxfordshire, GBR); Sobolev, Alexey (Moscow State University, Moscow, RUS); Presnyakov, Igor (Moscow State University, Moscow, RUS)

ABO3 perovskite-type compounds, where A3+ = Y and La-Lu and B3+ = V, Cr, Mn, Fe, Co, Ni and Ni0.5Mn0.5, and their solid solutions have been attracting a lot of attention for decades from the viewpoints of fundamental physics and practical applications. For example, some ACrO3 compounds exhibit spin-reorientation transitions, and doped ACrO3 are good oxygen-ion conductors and show sensitivity toward methanol, ethanol, some gases and humidity. ACoO3 compounds have been investigated a lot because of spin-state transitions in Co3+ ions and metal-insulator transitions; ACoO3 also exhibit thermoelectric and catalytic properties. In recent years, ABO3 perovskites have been extensively expanded to smaller A cations, such as, Mn2+, Sc3+, and In3+ with expectations to find new magneto-structural coupling [1]. Properties of ABO3 perovskites with small cations at the A site (A = Sc3+ and In3+; B = transition metals) will be reported here. ScBO3 and InBO3 perovskites extend the corresponding families of perovskites with A = Y, La-Lu, and Bi and exhibit larger structural distortions. As a result of large distortions, they show, in many cases, distinct structural and magnetic properties. It is manifested in B-site-ordered monoclinic structures of ScMnO3 [2] and InMnO3 [3]; an unusual superstructure of ScRhO3 and InRhO3 [4]; two magnetic transitions in ScCrO3 and InCrO3 with very close transition temperatures [5]; and antiferromagnetic ground states and multiferroic properties of Sc2NiMnO6 and In2NiMnO6. Features of such perovskites, such as, transition metal doping into the A site, (Sc1-xBx)BO3, their magnetic properties, crystal and magnetic structures will be discussed. Special attention will be given to new spin-driven multiferroics Sc2NiMnO6 and In2NiMnO6.

---

[1] A. A. Belik and W. Yi, J. Phys.: Condens. Matter 2014, 26, 163201.

[2] H. Y. Chen, T. Yu, P. Gao, J. M. Bai, J. Tao, T. A. Tyson, L. Wang and R. Lalancette, Inorg. Chem. 2013, 52, 9692.

[3] A. A. Belik, Y. Matsushita, M. Tanaka and E. Takayama-Muromachi, Angew. Chem. Int. Ed. 2010, 49, 7723.

[4] A. A. Belik, Y. Matsushita, M. Tanaka and E. Takayama-Muromachi, Inorg. Chem. 2013, 52, 12005.

[5] A. A. Belik, Y. Matsushita, M. Tanaka and E. Takayama-Muromachi, Chem. Mater. 2012, 24, 2197.

PTue089

Absence of superconductivity in metastable $Ca_{1-x}Pr_xFe_2As_2$ (x = 0-1) synthesized under high pressure conditions

Strobl, Katharina (LMU München, München, GER); Maak, Christian (LMU München, München, GER); Pobel, Roman (LMU München, München, GER)

Among the so called 122-compounds which crystallize in the $ThCr_2Si_2$-type structure, $CaFe_2As_2$ (Ca--122) has proven to be a special case. Its often unexpected physical behavior results from a structural instability that leads to the transformation to a so called collapsed tetragonal phase when exposed to chemical and/or physical pressure. This transformation interferes with superconductivity but can be suppressed e.g. via rare earth doping resulting critical temperatures of up to 47 K. However the superconducting volume fractions are very small.

To investigate whether this compound is in fact an intrinsic superconductor, a high pressure synthetic route has been developed. This allowed for the preparation of polycrystalline samples of $Ca_{1-x}Pr_xFe_2As_2$ covering the full range from $x = 0$--1 for the first time thus overcoming the solubility limit of $x = 0.13$. The analysis revealed a metastable phase very similar to the so called collapsed tetragonal phase at Pr-contents between 30--70%. At temperatures above 450°C it irreversibly transforms to a stable phase with a c-axis closer to those of undoped Ca--122. The transition temperature increases linearly with x up to Pr-contents of about 70%. Magnetic properties and electrical conductivity measurements show that none of the samples become superconducting, neither as-synthesized nor after heat treatment. This leads to the conclusion that the superconductivity in Pr-doped Ca-122 single crystals is not an intrinsic property and most likely stems from other mechanisms.

PTue090

Hydrothermal syntheses and single crystal X-ray structures of three new vanadium (V) tellurites CaV_2TeO_8, $Sr_4V_4Te_4O_{20}(OH)_4$ AND $Cd_2V_2Te_2O_{11}$.

Konatham, Satish (Indian Institute of Technology Madras, Chennai, IND)

Three new vanadium tellurites, CaV_2TeO_8, $Sr_4V_4Te_4O_{20}(OH)_4$ and $Cd_2V_2Te_2O_{11}$ were synthesized by hydrothermal method and characterized by single crystal and powder X- ray diffraction (XRD) technique. CaV_2TeO_8 crystallizes in the orthorhombic non-centrosymmetric space group, Ccc2. Its crystal structure exhibits two-dimensional $[V_2TeO_8]^{2-}$ anionic layers, which are composed of tetrahedral VO_4, octahedral VO_6 and disphenoidal TeO_4 moities. This structure is different from those of known AV_2TeO_8 (A = Sr, Ba) analogues. $Sr_4V_4Te_4O_{20}(OH)_4$ has discrete $[VTeO_5(OH)]^{2-}$ units, which are built from pyramidal TeO_3 and tetrahedral VO_4 moities. $Cd_2V_2Te_2O_{11}$ contains $[(V_2O_7)(TeO_2)_2]^{4-}$ anionic chains, composed of tetrahedral VO_4 and disphenoidal TeO_4 moities. Its crystal structure is different from the analogue of known$Ba_2V_2Te_2O_{11}$. Thermogravimetric, infrared absorption spectroscopic and powder XRD studies of $Sr_4V_4Te_4O_{20}(OH)_4$ revealed that it undergoes thermal loss of water to form $Sr_2V_2Te_2O_{11}$ of unidentified structure type.

PTue091

High-pressure Synthesis and Single-Crystal Structure of HP-LaOF

Glätzle, Matthias (University of Innsbruck, Innsbruck, AUT); Schweigl, Andreas (University of Innsbruck, Innsbruck, AUT); Huppertz, Hubert (University of Innsbruck, Innsbruck, AUT)

In the field of rare-earth oxide fluorides, three normal-pressure modifications are closely described in literature [1, 2]. These are the cubic high-temperature α - modification, the tetragonal β -form, and the trigonal γ -phase. Besides, a high-pressure modification of *RE*OF (*RE* = La, Pr, Nd, Sm-Gd) was up to now only described by M. Gondrand *et al.* in 1970, based on X-ray powder diffraction data collected at a temperature of 1000 °C [3].

By applying high-pressure/high-temperature conditions utilizing a 1000 t press and a Walker-type multianvil device, we were able to obtain single crystals of orthorhombic HP-LaOF for the first time. Various experiments with different reaction conditions showed that the formation of HP-LaOF only takes place when adding boron oxide to the educt mixture consisting of La_2O_3 and LaF_3. Besides that, a small amount of water seems crucial for the synthesis, which corresponds to the known issue for the synthesis of the isostructural high-pressure modification of CaF_2 [4].

Single-crystal X-ray diffraction analysis of our product showed that HP-LaOF crystallizes in the space group *Pnma* ($Z = 4$) with the parameters $a = 635.0(2)$, $b = 382.53(8)$, $c = 702.9(2)$ pm, $V = 0.17074(6)$ nm^3, $R_1 = 0.0231$, and $wR_2 = 0.0476$. For the axial ratios of HP-LaOF, we obtain values of $c/b = 1.84$ and $b/a = 1.66$. The latter clearly shows that HP-LaOF can be classified as an α-$PbCl_2$-type structure.

Like the α-$PbCl_2$ structure, the crystal structure of HP-LaOF consists of almost hexagonally closest-packed cations with four- and fivefold coordinated anions. CHARDI calculations on HP-LaOF clearly show that the oxygen ions occupy the positions of the anions exhibiting shorter distances to the rare-earth cations and have a distorted tetrahedral coordination, while the fluorine anions are square-pyramidally coordinated by the lanthanum cations.

---

[1] W. Klemm, H.-A. Klein, *Z. Anorg. Allg. Chem.* **1941**, *248*, 167.

[2] W. H. Zachariasen, *Acta Crystallogr.* **1951**, *4*, 231.

[3] M. Gondrand, J. C. Joubert, J. Chenavas, J. J. Capponi, M. Perroud, *Mat. Res. Bull.* **1970**, *5*, 769.

[4] E. Morris, T. Groy, K. Leinenweber, *J. Phys. Chem. Solids***2001**, *62*, 1117.

PTue092

High-pressure high-temperature synthesis of bulk $Si_{1-x}B_x$ alloys: two semiconductors form an unusual metal

Ovsyannikov, Sergey (Bayerisches Geoinstitut, Universität Bayreuth, Bayreuth , GER); Gou, Huiyang (BGI, Universität Bayreuth, Bayreuth, GER); Karkin, Alexander (M. N. Miheev Institute of Metal Physics, Yekaterinburg, GER); Shchennikov, Vladimir (M. N. Miheev Institute of Metal Physics, Yekaterinburg, RUS); Wirth, Richard (GFZ German Research Centre for Geosciences, Potsdam, GER); Dmitriev, Vladimir (European Synchrotron Research Facility , Grenoble, FRA); Nakajima, Yoichi (Bayerisches Geoinstitut, Universität Bayreuth, Bayreuth, GER); Dubrovinskaia, Natalia (Material Physics and Technology at Extreme Conditions, Laboratory of Crystallography, University of Bayreuth, Bayreuth, GER); Dubrovinsky, Leonid (Bayerisches Geoinstitut, Universität Bayreuth, Bayreuth, GER)

Silicon is a key technological material, and its controlled doping is one of simple and effective ways which are applied for creation of new advanced materials with tunable optoelectronic properties. Boron was known to be a dopant that can dramatically change the properties of silicon. However, a limited solubility of boron atoms in silicon matrix strongly restricted creation of bulk diamond-type structured Si-B alloys with the high boron content exceeding 0.5-1 at. %. In this work we used a high-pressure high-temperature synthesis technique to prepare bulk Si1-xBx alloys. To generate high pressures we used both Piston-Cylinder apparatuses and Multi-Anvil Presses. The samples of Si:B were prepared from silicon and □-boron crystals. We found that alloying of boron and silicon can be strongly enhanced at high temperatures above the melting point of silicon and high pressures. We could synthesize the bulk Si1-xBx alloys with a rather high boron content (e.g., 2.4 at.%).[1] We extensively investigated the electronic transport and optical properties of these alloys using several techniques, including electrical resistivity, Hall effect, magnetoresistance, Raman, infrared and optical spectroscopy, and X-ray diffraction. We found that Si1-xBx solid solutions are metals that possess very unusual optical properties, e.g., they demonstrate the antiresonant Raman spectra and the loss of the reflectivity in the near-infra-red range. Our work indicates new perspectives in creation and applications of Si1-xBx solid solutions with the diamond-type structure. This approach may be applied for doping of silicon and other materials with other dopants as well.

PTue093

High-pressure synthesis of three new Ge-rich compounds in the Ba - Ge system

Castillo, Rodrigo (MPI CPfS, Dresden, GER); Schwarz, Ulrich (MPI CPfS, Dresden, GER); Grin, Yuri (MPI CPfS, Dresden, GER)

High-pressure high-temperature methods have proven to be a suitable tool for the synthesis of novel materials [1]. These metastable compounds often exhibit unusual crystal structures with interesting chemical bonding situations, as revealed by state-of-the-art quantum chemical calculations in real space [2].

Several new binary phases made of a metallic element and silicon or germanium as majority component have been quenched at high pressures and retained to ambient conditions for characterization [3]. In this sense, by applying high-pressure to mixtures of Ba:Ge in the atomic ratio 1:5 – 6, three new compounds were obtained; $BaGe_5$ [4], $BaGe_{5.5}$ and $BaGe_6$ [5].

$BaGe_5$ was synthesized at a pressure and temperature of 15(2) GPa and 1100(100) K, respectively. The crystal structure was solved and refined in a combined study using electron and x-ray diffraction. It consists of four-bonded Ge atoms forming complex layers with two of the three symmetry-independent Ge atoms in a nearly tetrahedral environment, while the third Ge adopts a ψ-pyramid variation. This unusual coordination seems to be forced by the excess of electrons coming from the Ba atoms. In agreement with these findings, $BaGe_5$ behaves like a metal in the electronic transport properties and is diamagnetic.

$BaGe_6$ was obtained at 15(2) GPa and 1073(100) K, and a Ge-deficient variety of the same family, $BaGe_{5.5}$, was obtained at 10(1) GPa 1073 (100) K. However, their electronic and physical properties are noticeably different. The cause of this difference originates in the structure and bonding patterns, and is confirmed by electronic structure calculations; $BaGe_6$ consists of three symmetry-independent four-bonded Ge atoms and behaves like a metal. On the other hand, the semiconductor $BaGe_{5.5}$ involves incommensurate modulations of both atomic positions and site occupancy. ELI-D calculations on both compounds reveal intrinsic characteristics, such as the excess of electrons in $BaGe_6$ and the perfect electron balance in $BaGe_{5.5}$, in agreement with predictions based on the Zintl-Klemm concept and the *8-N* rule.

---

[1] (a) Livermore, L. J. Phys. Chem. C 2012, 116, 2059-2060. (b) McMahon, M. I.; Nelmes, R. J. Chem. Soc. Rev. 2006, 35, 943-963.
[2] (a) Kohout, M. Int. J. Quantum Chem. 2004, 97, 651-658. (b) Wagner, F. R.; Bezugly, V.; Kohout, M.; Grin, Yu. Chem. Eur. J. 2007, 13, 5724-5741. (c) Kohout, M. Faraday Discuss. 2007, 135, 43-54.
[3] (a) Schwarz, U.; Wosylus, A.; Rosner, H.; Schnelle, W.; Ormeci, A.; Meier, K.; Baranov, A.; Nicklas, M.; Leipe, S.; Müller, C. J.; Grin, Yu. J. Am. Chem. Soc. 2012, 134, 13558-13561. (b) Wosylus, A.; Meier, K.; Prots, Y.; Schnelle, W.; Rosner, W.; Schwarz, U.; Grin, Yu. Angew. Chem. Int. Ed. 2010, 49, 9002-9006
[4] Castillo, R.; Carrillo-Cabrera, W.; Schwarz, U.; Grin, Yu. Inorg. Chem. 2015, 54, 1019-1025.
[5] Akselrud, L.; Wosylus, A.; Castillo, R.; Aydemir, U.; Prots, Y.; Schnelle, W.; Grin, Yu.; Schwarz, U. Inorg. Chem. 2014, 53, 12699-12705.

PTue094

High-pressure synthesis, crystal structure and properties of bismuth dicalcogenides, $Bi(Se_{1-x}S_x)_2$ (x = 0, 0.5, 1.0) and its substitutions

YAMAMOTO, Ayako (RIKEN Center for Emergent Matter Science, Saitama, JPN)

Various metal dicalcogenides, MX_2 (X = S and Se), have been studied, and some of them show interesting properties by chemical modification and physical effect. For example, MoS_2 shows superconductivity by both intercalation of Rb and charge-insertion with electric field effect. In most case of tetravelent M, all chalcogen ions are divalent S^{2-}/Se^{2-}, and the structure is relatively simple such as CdI_2-type. Whereas the case of divalent M, chalcogen makes dimmer and this behaves like molecular ion (S_2^{2-}/Se_2^{2-}) as seen in pyrite-type FeS_2 and $NiSe_2$. How about is it in the case of M is trivalent? Only few MX_2 with M^{3+} were reported, because in many cases they have a formula with M_2X_3 as in Bi_2Se_3. In 1960's, Silverman reported BiS_2, BiSSe and $BiSe_2$[1] that were prepared at high pressure of 4.5 GPa. They reported the composition and the peak positions of the X-ray powder diffraction (XRD) patterns of the products, but the crystal structure and physical properties have not been clarified. In this work, we prepared single crystals of bismuth diselenide, $Bi(Se_{1-x}S_x)_2$ (x = 0, 0.5, 1.0), at 5.5 GPa, and the crystal structure, substitution chemistry and physical properties were investigated[2].

Samples were prepared from Bi_2Se_3, Bi_2S_3, Se, and S with a mole ratio of Bi : S/Se = 1.0 : 2.2–3.0. Excess S/Se was needed to suppress residual products of Bi_2Se_3/Bi_2S_3. Solid solutions, $Bi(Se_{1-y}X_y)_2$ (X = S, Te) and $(Bi_{1-y}M_y)Se_2$ (M = Pb, Sb) were also synthesized using Te, Pb and Sb. Raw materials was pressed into a cylindrical shape, placed in a BN container, and inserted to a carbon tube-heater. It was pressurized at pressures from 3.0, 5.5, and 7.5 GPa using a cubic-anvil-type press, and heated at 650˚C–1200˚C for 10–30 min. Single crystals were grown from the melt with a cooling rate of 5˚C/min from 1200˚C to 800˚C and subsequent quenching to room temperature. The crystals are of silver-black color and columnar shape. Residual Se and S were removed by washing the product with carbon disulfide.
Single X-ray analysis showed that $BiSe_2$ is in a monoclinic system (space group C2/m) with lattice parameters of a = 16.740(3) Å, b = 4.1410(11) Å, c= 12.027(3) Å, beta = 127.658(13)˚. It was confirmed that BiSeS and BiS_2 have isostructure to $BiSe_2$ with smaller unit cell parameters. A crystal structure of $BiSe_2$ can be viewed as a layered structure with stacks of neutral $BiSe_2$ blocks along the c-axis, or alternatively as a quasi-one-dimensional structure with double chains of $BiSe_5$ pyramids along the b-axis.

The characteristic feature of this structure is that two types of ions, diselenium and monoselenium ions, coexist in one compound. A bond distance of shortest Se–Se bond is 2.375 Å very close to that of the Se dimer in $PdSe_2$ (Se–Se 2.36 Å). Each Bi is coordinated with three Se^{2-} and two Se_2^{2-}, and the bond valence analysis indicated that Bi was trivalent. $(Bi_{0.9}Sb_{0.1})Se_2$ was obtained as isostracural with $BiSe_2$, whereas $Bi(Se_{1-y}Te_y)_2$ (y = 0.1, 0.33, 1.0) and $(Bi_{0.9}Pb_{0.1})Se_2$ were not obtained with same structure.

All the compounds show diamagnetism attributable to the closed-shell ion core. The electrical resistivity of these compounds is above 10^4 ohm cm below room temperature and shows a semiconducting behavior; the conductivity obeys the thermal activation rule. The energy gap as estimated by the Arrhenius plot in ranging from 0.28 to 0.69 eV, being comparable with the band gaps of Bi_2Se_3. Because the bandwidth of selenium is wider than that of sulfur, it was expected that the gap of $BiSe_2$ would be smaller than that of BiS_2. However, the values are almost the same in both $BiSe_2$ and BiS_2, while the activate energy in the mixed chalcogenide BiSSe is considerably smaller.

---

[1] Silverman, M.S. Inorg. Chem., 1965, 4, 587.
[2] Yamamoto, A. et al, Inorg. Chem., 2015, 54, 4114.

PTue095

High-pressure/High-temperature Synthesis and Characterization of the first Palladium and Platinum containing Lithium Transition-Metal Sulfides $Li_2M_3S_4$ (M = Pd, Pt)

Heymann, Gunter (Institut für Allgemeine, Anorganische und Theoretische Chemie , Innsbruck, AUT); Krammer, Hans Georg (Institut für Allgemeine, Anorganische und Theoretische Chemie, Innsbruck, AUT); Niehaus, Oliver ()Institut für Anorganische und Analytische Chemie, Münster, GER)

During the recent years, layered lithium-containing transition-metal sulfides have attracted increasing interests as potential electrode materials for lithium rechargeable batteries. Besides the traditional intercalation electrode materials, transition-metal sulfides based on conversion or alloying reactions show significantly higher specific capacities [1]. In the literature, one searches in vain for high-pressure/high-temperature investigations of this class of materials.

The new lithium transition-metal sulfides $Li_2M_3S_4$ (M = Pd, Pt) were obtained *via* multianvil high-pressure/high-temperature syntheses [2] at 8 GPa and 1150 °C starting from a stoichiometric mixture of lithium nitride, sulfur, and palladium or platinum. Single crystal analyses indicated the space group $P2_1/c$ (no. 14) with the lattice parameters and refinement results: a = 492.9(1), b = 1005.9(2), c = 614.9(2) pm, β = 110.91(3)°, $R1$ = 0.0165, $wR2$ = 0.0308 (all data) for $Li_2Pd_3S_4$ and a = 498.2(1), b = 1005.5(2), c = 613.0(2) pm, β = 110.76(3)°, $R1$ = 0.0215, $wR2$ = 0.0450 (all data) for $Li_2Pt_3S_4$. The crystal structures are built up from two distinct Pd/Pt sites, one of which is a special position (0, 0, 0), two sulfur sites, and one lithium site. The atoms Pd1/Pt1 form isolated square planar PdS_4/PtS_4 units, whereas the Pd2/Pt2 atoms form pairs of square planar PdS_4/PtS_4 units, which are connected *via* a common edge. These two structural motives built up a three-dimensional network structure by linking through common corners. The lithium atoms are positioned inside of the so formed channels. $Li_2M_3S_4$ (M = Pd, Pt) crystallizes isotypically to the minerals jaguéite, $Cu_2Pd_3Se_4$ and chrisstanleyite, $Ag_2Pd_3Se_4$, which are up to now the only representatives of this structure type [3].

Magnetic properties of $Li_2Pd_3S_4$ and $Li_2Pt_3S_4$ have been analyzed in dependence of the temperature at a constant magnetic field of 10 kOe. Both compounds show a similar behavior due to the absence of localized electrons and can be classified as Pauli paramagnetic or diamagnetic. Molar susceptibilities of -1.1×10^{-4} and 2.9×10^{-4} emu/mol have been determined at room temperature for $Li_2Pd_3S_4$ and $Li_2Pt_3S_4$, respectively. For $Li_2Pt_3S_4$, a significant amount of a Curie paramagnetic impurity (elemental platinum) has to be considered.Regarding the mobility of lithium inside the channels of the structure, solid-state NMR investigations are in progress.

---

[1] X. Xu, W. Liu, Y. Kim, J. Cho, *Nano Today* **2014**, *9*, 604-630.
[2] H. Huppertz, *Z. Kristallogr.* **2004**, *219*, 330.
[3] D. Topa, E. Makovicky, T. Balic-Žunic, *Can Mineral* **2006**, *44*, 497-505.

PTue096

Investigation on the mineraliser assisted synthesis of black phosphorus via in-situ neutron powder diffraction

Köpf, Marianne (TU München, FG Synthese und Charakt. innov. Mat., Garching b. München, GER); Kohlmann, Holger (AG Funktionsmaterialien, Universität Leipzig, Leipzig, GER); Nilges, Tom (TU München, FG Synthese und Charakt. innov. Mat., Garching b. München, GER)

Black phosphorus (*o* -P) and the delaminated monolayer (phosphorene) gained reasonable interest in material science [1]. Synthesis of black phosphorus is performed in a variety of methods: recrystallisation from Bi [2, 3], or Hg [3, 4], high pressure techniques [2, 5], melting and annealing sequences performed at higher temperatures [4, 6], or using mineralising agents. The method mentioned last was underlying an optimisation process, at first the reaction mixture consisted of P_{red}, Au, Sn and SnI_4 [7]. Further investigations showed that the formation also takes place using P_{red}, AuSn and SnI_4 [8]. Within the last step of development it was possible to eliminate the coin metal so the reaction mixture is reduced to P_{red} and the mineraliser pair Sn/SnI_4 [1, 9]. ICP measurements showed no impurities in *o* -P synthesized that way and so the quality the *o* -P produced is significantly better than the one achieved by traditional methods [1]. Within the experiments reported herein the growing mechanism of *o* -P crystals using this mineraliser pair is investigated. Our aim is to identify possible intermediates and to evaluate crystal growth kinetics.

In-situ growing experiments were carried out at D20 neutron powder diffractometer, present at Institut Laue-Langevin (ILL), in Grenoble [10, 11] and are partly published in [1]. We tried to model the reported synthesis conditions as close as possible to the laboratory conditions. Three different synthesis procedures will be described; two of them were successful leading to *o* -P, while the third one resulted in the formation of amorphous species. In the first run a very small amount of educts is used, no intermediates are detected and the synthesis is performed successfully [10]. During the second experiment [11] a few reflections of *o* -P were detected only within heating but vanished shortly after. In the last run NaCl was added for temperature calibration to the V-hull and Rietveld analysis of the resulting temperature dependent lattice parameters was carried out online during synthesis. During the last approach, synthesis of *o* -P was performed perfectly and growing conditions and parameters have been derived from the data. All experiments clearly substantiated that no crystalline intermediates are formed during the *o* -P formation. The black allotrope is crystallising directly from gaseous phase.

---

[1] M. Köpf, N. Eckstein, D. Pfister, C. Grotz, I. Krüger, M. Greiwe, T. Hansen, H. Kohlmann and T. Nilges, *J. Cryst. Growth*. **2014**, 405 6-10.

[2] P.W. Bridgman, *J. Am. Chem. Soc*. **1914**, 36, 1344-1363.

[3] Y. Maruyama, S. Suzuki, *Physica B+C*. **1981**, 105, 99-102.

[4] H. Krebs, H. Weitz, K.H. Worms, *Z. Anorg. Allg. Chem*. **1955**, 280, 119-133.

[5] W. Lu, H. Nan, J. Hong, Y. Chen, C. Zhu, Z. Liang, X. Ma, Z. Ni, C. Jin, Z. Zhang, *Nano Res*. **2014**, 853-859.

[7] Lucent Technologies Inc. *Method of making black phosphorus from red phosphorus*. Inventors: James Nelson Baillargeon, Keh-Yeng Cheng, Alfred Yi Cho, Sung-Nee George Chu, Wen-Yen Hwang. U.S. Appl. No.: 09/270,883. Family ID: 23033240.

S. Lange, P. Schmidt and T. Nilges, *Inorg. Chem*. **2007**, 46, 4028ñ4035.

[8] T. Nilges, M. Kersting and T. Pfeifer, *J. Solid State Chem*. 2008, 181, 1707ñ1711.

[9] M. C. Stan, J. v. Zamory, S. Passerini, T. Nilges, M. Winter, *J. Mater. Chem*. A. **2013**, 1, 5293.

[10] H. Kohlmann, D. Weber, M. Widenmeyer, M. Köpf, C. Ney, M. Bischoff, T. Richter, P. Wenderoth (**2013**) Crystalline metastable compounds studied by in situ neutron powder diffraction. Institut Laue-Langevin (ILL).

[11] M. Köpf, H. Auer, A. Goetze, T. Hansen, H. Kohlmann and T. Nilges (**2014**). In situ neutron powder diffraction investigation on synthesis of black Phosphorus via mineralisation route. Institut Laue-Langevin (ILL).

PTue097

Kinetics of the phase transition of $CsGaSe_2$

Friedrich, Daniel (Universität Regensburg, Regensburg, GER); Schlosser, Marc (Universität Regensburg, Regensburg, GER); Pfitzner, Arno (Universität Regensburg, Regensburg, GER)

Multinary chalcogenometallates are important materials for technical applications due to their nonlinear optical and semiconducting properties. Among the known group 13 chalcogenometallates with the composition MTQ_2 (M = alkali metal, T = triel, Q = chalcogen), $CsGaSe_2$ [1] is the only example showing a phase transition at elevated temperatures [2]. The most fascinating fact about this phase transition is a complete structural reconstruction from two-dimensional layers $[Ga_4Se_8^{4-}]$ in the low temperature phase $CsGaSe_2$-*mC*64 to one-dimensional chains $[GaSe_2^{-}]$ in the high-temperature phase $CsGaSe_2$-*mC*16 (Figure 1). Both polymorphs crystallize in the monoclinic space group *C*2/*c* (no. 15) with lattice parameters $a = 11.046(1)$, $b = 11.051(1)$, $c = 16.827(1)$, $\beta = 99.402(9)$, $V = 2026.5(3)$, and $Z = 16$ for $CsGaSe_2$-*mC*64 ($KInS_2$ structure type) and $a = 7.651(1)$, $b = 12.555(2)$, $c = 6.179(1)$, $\beta = 113.53(2)$, $V = 544.2(3)$, and $Z = 4$ for $CsGaSe_2$-*mC*16 ($KFeS_2$ structure type).

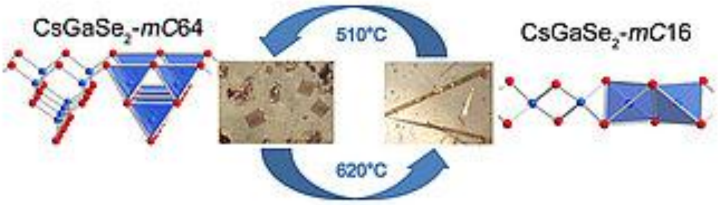

Figure 1: Schematic representation of the reversible phase transition in $CsGaSe_2$ featuring the anionic substructures in both polymorphs and the crystal shape.

The reversible phase transition of $CsGaSe_2$ was further studied *in situ* by high-temperature X-ray powder diffraction (Figure 2). The experiments were performed using a STOE Stadi P diffractometer equipped with a high temperature capillary furnace (monochromatized Mo-$K_{\alpha 1}$ radiation).

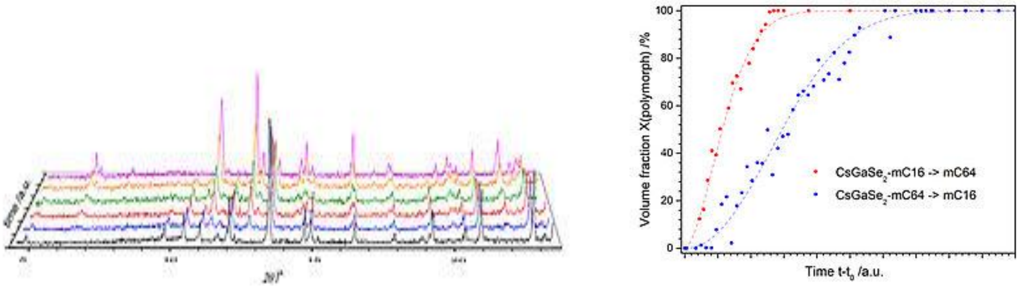

Figure 2: Left: 3D plot of the progression of the phase transition from $CsGaSe_2$-*mC*64 (front) to $CsGaSe_2$-*mC*16 (back) on an arbitrary timescale. Right: Plot of the time dependent growth of both $CsGaSe_2$ polymorphs on an arbitrary timescale corrected for the incubation time t_0.

The diffraction experiments were performed upon cooling/heating and under isothermal conditions to study the kinetics of this phase transition and to get some insight in the activation energies and crystallization behavior. The resulting data for isothermal experiments were analyzed using the JMAK-Theory of crystal growth [3]. The resulting Avrami-exponents of about $n = 2.16$ for $CsGaSe_2$-*mC*64 and $n = 1.72$ for $CsGaSe_2$-*mC*16 are in good agreement with the rod- and plate-shaped crystallites of the respective polymorphs.

---

[1] A. Kyas, Dissertation, *TH Aachen* **1981**; H. J. Deiseroth, *Z. Kristallogr.* **1984**, *166*, 283.

[2] D. Friedrich, M. Schlosser, A. Pfitzner, *Z. Anorg. Allg. Chem.* **2014**, *640*, 2356.

[3] M. Avrami, *J. Chem. Phys.* **1939**, *7*, 1103; M. Avrami, *J. Chem. Phys.* **1940**, *8*, 212; M. Avrami, *J. Chem. Phys.***1941**, *9*, 177.

PTue098

$NdLiP_4N_8$ - The First Rare Earth Nitridophosphate by Metathesis

Schnick, Wolfgang (University of Munich (LMU), Department of Chemistry, Munich, GER);
Kloß, Simon David (Ludwig-Maximilians-Universität München, Munich, GER)

Nitridophosphates are one of the largest uncharted compound classes despite their proven structural versatility, which rivals even the diversity of silicates, and their fascinating properties. To date, mainly first and second main group nitridophosphates have been thoroughly investigated. Preparation of nitridophosphates containing transition metals and rare earth elements are intriguing since open-shell systems can feature exiting properties. The lack of diversity in elemental composition within the nitridophosphates can be attributed to preparative difficulties. Common precursors like P_3N_5 exhibit a limited thermal stability and often decompose below the crystallization temperature of the targeted phases. High-pressure techniques were applied to overcome this problem and allowed the exploration of alkaline earth nitridophosphates.[1] However, the structural elucidation is laborious due to powder reaction products requiring structure solution from powder diffraction data.[2] In order to tackle the aforementioned problems, we tailored a new synthetic pathway by means of high-pressure metathesis. We targeted rare earth nitridophosphates as a model system.

Here we present $NdLiP_4N_8$, the first rare earth nitridophosphate, prepared by high-pressure solid state metathesis starting from stoichiometric amounts of NdF_3 and $LiPN_2$ at 5 GPa and 1300 °C. LiCl, formed *in situ*, is believed to act as the thermodynamic driving force powering the reaction. Moreover, the under reaction conditions molten LiF acts as a flux aiding single-crystal formation. The colorless compound crystallizes in the orthorhombic paracelsian structure type [*Pnma* (no. 62) a = 8.7305(17), b = 7.8783(16), c = 9.0881(18) Å, Z = 4].[3] The structure (Figure **a**) consists of a network of all-side vertex sharing PN_4 tetrahedra. Li resides within 4-ring channels and Nd within 8-ring channels, which run along [010]. The magnetic properties stemming from Nd^{3+} ions were studied using SQUID magnetometry (Figure **b**).

We are encouraged that these results are the basis for the discovery of a substantial amount of interesting and new rare earth and transition metal nitridophosphates thus innervating this exciting branch of chemistry.

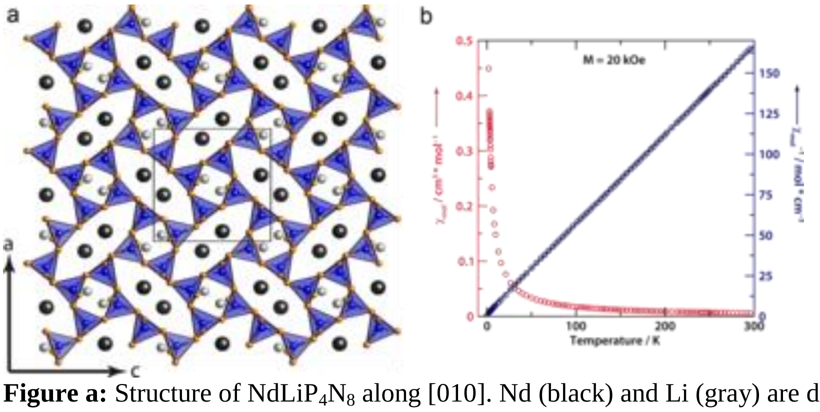

Figure a: Structure of $NdLiP_4N_8$ along [010]. Nd (black) and Li (gray) are displayed as spheres. **b:** Susceptibility measurement at 20 kOe. The data is displayed as χ_m vs. T (red circles) and χ_m^{-1} vs. T (blue circles). A linear regression (black line) was fit to the χ_m^{-1} vs. T data.

---

[1] F.J. Pucher, A. Marchuk, P.J. Schmidt, D. Wiechert, W. Schnick, *Chem. Eur. J.* **2015**, 21, 6443-6448.

[2] D. Baumann, S. J. Sedlmaier, W. Schnick, *Angew. Chemie* **2012**; *124*, 4785–4787. *Angew. Chem. Int. Ed*, **2012**, *51*, 4707-4709.

[3] J. V. Smith, *Acta Crystallogr.* **1953**, *6*, 613–620.

PTue099

Surprising Anion Topologies in Lithium Nitridophosphates

Schnick, Wolfgang (University of Munich (LMU), Department of Chemistry, Munich, GER);
Bertschler, Eva-Maria (University of Munich (LMU), Munich, GER)

Ternary lithium nitridophosphates, e. g. Li_7PN_4, $Li_{12}P_3N_9$, $Li_{10}P_4N_{10}$ and $LiPN_2$ are of interest due to their possible lithium ion mobility. These nitridophosphates can be synthesized by reaction of Li_3N and P_3N_5 at temperatures between 600 and 850 °C. In a matrix of Li^+-ions a remarkable spectrum of different P/N-anions occurrs, e. g. isolated PN_4-tetrahedra in Li_7PN_4,[1] rings or cages in $Li_{12}P_3N_9$ [2] and $Li_{10}P_4N_{10}$ [3] or a cristobalite-analogous network of corner-sharing PN_4-tetrahedra in $LiPN_2$.[4]

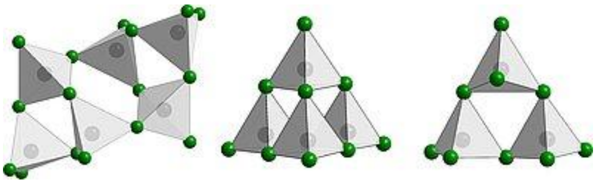

Fig. 1: $[P_6N_{16}]^{18-}$, $[P_4N_{10}]^{10-}$ and $[P_3N_9]^{12-}$ (from left to right) in nitridophosphates; P black, N green.

Recently, we have started a re-investigation of the synthesis of lithium nitridophosphates by applying the multi-anvil technique. During a systematic study we have identified two novel compounds with intriguing anion topology. By reaction of $LiPN_2$ and Li_7PN_4 at 5 GPa and above 1000 °C in a Walker-type multi-anvil press we obtained $Li_{18}P_6N_{16}$, which shows a surprising condensation of PN_4-tetrahedra. The structure of $Li_{18}P_6N_{16}$ [P, a = 5.4189(4), b = 7.5171(7), c = 9.8680(8) Å, α = 108.585(3), β = 99.414(3), γ = 104.924(3)°, Z = 1] was solved and refined from single crystal X-ray diffraction data and confirmed by Rietveld refinement. The $[P_6N_{16}]^{18-}$-anion is made up of six PN_4-tetrahedra, which are linked by shared corners, forming one *vierer*-ring[5,6] and two *dreier*-rings linked to both sides of the *vierer*-ring (Fig. 1). The Li^+-ions are tetrahedrally coordinated by N.

Unintended reaction of the crucible material *h*-BN with $LiPN_2$ and Li_7PN_4 at 5 GPa and above 1000 °C yielded $Li_{47}B_3P_{14}N_{42}$, the first mixed nitridoborophosphate. The crystal structure of $Li_{47}B_3P_{14}N_{42}$ [$P6_3/mcm$, a = 19.3036(7), c = 18.0200(7) Å, Z = 6] was solved and refined from single crystal X-ray diffraction data and confirmed by Rietveld refinement. In $Li_{47}B_3P_{14}N_{42}$ there are adamantane-type $[P_4N_{10}]^{10-}$, cyclic $[P_3N_9]^{12-}$ as well as unprecedented $[B_3P_3N_{13}]^{15-}$ anions. The latter represents a novel building unit, which is formally made up of three condensed BN_3-triangles and PN_4-tetrahedra (Fig. 2). The $[B_3P_3N_{13}]^{15-}$-anion represents a novel molecular topology with no analogue in main group chemistry.

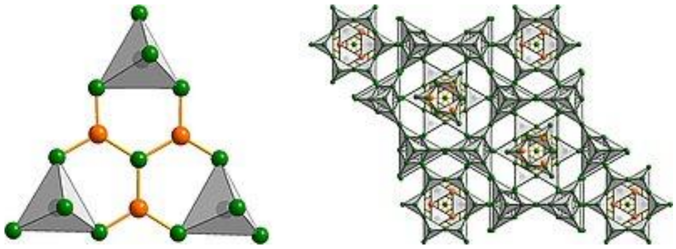

Fig. 2: $[B_3P_3N_{13}]^{15-}$ anion (left) and unit cell of $Li_{47}B_3P_{14}N_{42}$ (viewing along c, right); P black, N green, B orange, Li is omitted for clarity.

---

[1] W. Schnick, J. Lücke, *J. Solid State Chem.* **1990**, *87*,101. [2] W. Schnick, *Angew. Chem.* **1993**, *105*, 846; *Angew. Chem. Int. Ed. Engl.* **1993**, *32*, 806. [3] W. Schnick, U. Berger, *Angew. Chem.* **1991**, *103*, 857; *Angew. Chem. Int. Ed. Engl.* **1991**, *30*, 830. [4] W. Schnick, J. Lücke, *Z. Anorg. Allg. Chem.* **1990**, *588*, 19.
[5] F. Liebau, *Structural Chemistry of Silicates*; Springer, Berlin, **1985**. [6] The term *dreier* (*vierer*)ring was coined by Liebau and is derived from the German word "drei" ("vier"). A *dreier* (*vierer*) ring comprised three (four) tetrahedra centers.

PTue100

Synthesis and Characterization of the New High-Pressure Gallium Borate $Ga_2B_3O_7(OH)$

Vitzthum, Daniela (University of Innsbruck, Innsbruck, AUT); Schauperl, Michael (Institute of General, Inorganic, and Theoretical Chemistry, University of Innsbruck, Innsbruck, AUT); Strabler, Christof M. (Institute of General, Inorganic, and Theoretical Chemistry, University of Innsbruck , Innsbruck, AUT); Huppertz, Hubert (Institute of General, Inorganic, and Theoretical Chemistry, University of Innsbruck, Innsbruck, AUT)

In the system Ga–B–O(–H), there were three compounds known so far: trigonal $GaBO_3$ [1], monoclinic $Ga_4B_2O_9$ [2] and rhombohedral $B_{22}Ga_9H_{21}O_{57}$ [3]. Recently, we succeeded in synthesizing a fourth compound in this field, namely $Ga_2B_3O_7(OH)$. This new gallium borate was formed under high-pressure/high-temperature conditions of 10.5 GPa and 700 °C in a Walker-type multianvil apparatus. Its crystal structure was determined by single-crystal X-ray diffraction data collected at room temperature. $Ga_2B_3O_7(OH)$ crystallizes in the orthorhombic space group *Cmce* (Z = 8) with the lattice parameters $a = 1050.7(2)$, $b = 743.6(2)$, $c = 1077.3(2)$ pm, and $V = 0.8417(3)$ nm^3. The structure was refined to *R*-values of $R_1 = 0.0290$ and $wR_2 = 0.0774$ (all data). Vibrational spectroscopic methods (Raman and IR) were performed to confirm the presence of the hydroxyl group. Furthermore, the band gap of $Ga_2B_3O_7(OH)$ was estimated via quantum mechanical DFT calculations. These results led to the assumption that our gallium borate could be a suitable substance to split water photocatalytically, which was then tested experimentally.

---

[1] T. A. Bither, H. S. Young, J. Solid State Chem. 1973, 6, 502-508.
[2] R. Cong, T. Yang, K. Li, H. Li, L. You, F. Liao, Y. Wang, J. Lin, Acta Crystallogr. 2010, B66, 141-150.
[3] W. Gao, Y. Jing, J. Yang, Z. Zhou, D. Yang, J. Sun, J. Lin, R. Cong, T. Yang, Inorg. Chem. 2014, 53, 2364-2366.

PTue101

Thermal behavior of carbon-coated lithium iron phosphate

Krumeich, Frank (ETH Zurich, Zurich, CHE); Waser, Oliver (ETH Zurich, Zurich, CHE); Pratsinis, Sotiris (ETH Zurich, Zurich, CHE)

$LiFePO_4$ is an attractive material for Li-ion battery applications due to its high cycle stability [1]. Unfortunately, the electric conductivity of $LiFePO_4$ is low and the diffusion of the Li ions along the one-dimensional channels of its olivine structure is slow. The diffusion limitation can be surmounted with smaller particle sizes while the conductivity can be increased either by doping or by embedding LiFePO4 in a conductive matrix like carbon. A particularly promising approach is the generation of a core-shell structure in form of C-coated $LiFePO_4$ nanoparticles, in which carbon not only improves the conductivity between the electrochemically active particles but also protects the core from reacting with the electrolyte. LiFePO4 nanoparticles were produced in an enclosed flame spray pyrolysis (FSP) unit [2] and carbon-coated in-situ downstream by pyrolysis of C_2H_2 in an O_2-controlled atmosphere [3]. The thermal stability of this material was recently probed by ex-situ experiments [3]. After annealing in Ar/H_2 atmosphere at 700 °C for 4 h, the morphology and particle size are preserved while the same treatment at 800 °C leads to fusion of the core $LiFePO_4$ into larger particles being $LiFePO_4$ crystals according to X-ray powder diffraction. The carbon shells remain as empty spheres according to transmission electron microscopy [3]. To study this process in more detail, in-situ TEM was performed now with a heating holder at a Tecnai F30 (FEI, 300 kV) microscope. In the starting material, $LiFePO_4$ nanoparticles are present which have a diameter of ca. 10-60 nm and are coated with carbon shells of a few nm thickness. After heating in-situ to 800 °C, TEM images reveal drastic changes as most $LiFePO_4$ diffused out of the carbon shells sintering to larger particles of several 100 nm in diameter while leaving behind empty carbon spheres. The investigation of selected areas at intermediate temperature stages reveal that most of these morphology changes occur only above 700 °C. In particular, sintering of the $LiFePO_4$ particles is observed beyond 750 °C. In addition, crystallization of the core particles occurs around 400 °C as evidenced by electron diffraction and in accordance with in-situ X-ray powder diffraction.

We thank the Scientific Center for Optical and Electron Microscopy of ETH Zurich (ScopeM) for support and M. Cantoni (CIME, EPFL Lausanne) for lending us the heating holder.

---

[1] C. H. Mi et al., J. Electrochem. Soc. 152 (2005) A483.
[2] A. Teleki et al., Sens. Actuators B 119 (2006) 683.
[3] O. Waser et al., J. Aerosol Sci. 42 (2011) 657.

PTue102

High-Temperature Synthesis and Characterization of Rare-Earth Molybdenum-Oxynitrides

Schildhammer, Daniel (University Innsbruck - Institute of General, Inorganic and Theoretical Chemistry, Innsbruck, AUT)

While rare-earth tungsten oxynitrides are known to crystallize in many different structure types such as sheelite- [1], perovskite- [2], and defect fluorite-type [3], there are scarcely reports on the structures of the related rare-earth molybdenum oxynitrides.

Rare-earth molybdenum oxynitrides crystallizing in the pyrochlore structure type were recently reported to exhibit interesting electrical and magnetic properties. Contrary to the corresponding oxides that have electrical conductivities of a metal, the oxynitrides show a semiconducting behaviour as reported for $Sm_2Mo_2O_{7-x}N_x$. Furthermore, compounds like $Sm_2Mo_2O_{7-x}N_x$, $Y_2Mo_2O_{7-x}N_x$, and $Eu_2Mo_2O_{7-x}N_x$ show Curie Weiss behaviour concerning their magnetic susceptibilities [4-6].

In this contribution, we report on different methods for the syntheses of novel rare-earth molybdenum oxynitrides with the general formula $RE_2Mo_2O_{7-x}N_x$ and their structural characterization by Rietveld analyses of the corresponding powder diffraction data. We compare the results obtained by the conventional solid state syntheses with those obtained from the citrate and solution combustion method, as well as employing different molybdenum oxide precursors.

Furthermore, novel rare-earth molybdenum oxynitrides with the general formula $RE_6MoO_{12-3x}N_{2x}$ crystallizing in the defect fluorite structure type are reported. The colour change of the new compounds and the shifts of the reflections in the powder diffraction patterns clearly indicate different amounts of nitrogen incorporated in the same structure type depending on the applied method.

---

[1] F. Cheviré, F. Tessier, R. Marchand, Mater. Res. Bull. 2004, 39, 1091-1101.

[2] A. Fuertes, J. Mater. Chem. 2012, 22, 3293-3293.

[3] N. Diot, O. Larcher, R. Marchand, J. Kempf, P. Macaudière, J. Alloys Compd. 2001, 323-324, 45-48.

[4] G. M. Veith, M. Greenblatt, M. Croft, J. B. Goodenough, Mater. Res. Bull. 2001, 36, 1521-1530.

[5] M. J. Martìnez-Lope, M. T. Casais, J. A. Alonso, Z. Naturforsch. 2006, 164-169.

[6] M. Yang, J. Oró-Solé, A. Fuertes, J. P. Attfield, Chem. Mater. 2010, 22, 4132-4134.

PTue103

Slag to Materials - Possible Applications for Red Mud

Schmetterer, Clemens (Fraunhofer UMSICHT Institute Branch Sulzbach Rosenberg, Sulzbach-Rosenberg, GER); Wolf, Gerhard (Fraunhofer UMSICHT, Institute Branch Sulzbach Rosenberg, Sulzbach-Rosenberg, GER); Masset, Patrick (Fraunhofer UMSICHT, Institute Branch Sulzbach Rosenberg, Sulzbach-Rosenberg, GER)

Finding new applications for red mud is a topic with high technological, social and environmental relevance. Red mud is the slag obtained as a byproduct in aluminum-production and is currently deposited in settling ponds. Its high alkalinity, heavy metal content and presence of toxic substances such as As, Cd and Pb make it a potentially hazardous material. Indeed, in 2010, accidential run-off from a settling pond caused a severe environmental disaster. Several possible uses have been pursued in the past, but none has so far been successfully realized at a large scale. In this contribution, we present promising applications for red mud, the required pre-treatment and processing of the material, conditions of use, current limitations and approaches for solution. Possibilities for use include catalysis in processes such as pyrolysis, methanol synthesis, hydrogenation etc., the extraction of precious metals, and use as a cheap starting material for the making of protective coatings by thermal spraying. These applications will be discussed with respect to the composition of red mud from various sources and the presence of toxic elements.

PTue104

Alkaline-earth Metal Dependent Structural Distortion in Inverse Perovskite Nitride Arsenides

Stoiber, Dominik (University of Stuttgart, Stuttgart, GER); Niewa, Rainer (University of Stuttgart, Stuttgart, GER)

Inverse perovskites ($(A_3X)E$ (A = alkali or alkaline-earth metals; X = N, O; E = main-group element) represent a class of compounds with reversed sizes and charges in comparison to the classical oxide perovskites ABO_3 [1]. The compounds $(A_3N)As$ with A = Ca, Sr and Ba, at room temperature, crystallize as distorted perovskites in space group *Pnma* ($GdFeO_3$ structure type) [2]. $(Mg_3N)As$ represents an undistorted cubic inverse perovskite with space group *Pm*-3 *m* [3]. We have analysed the relationship between increasing structural distortion and selected alkaline-earth metals.

For synthesis of the compounds $(A_3N)As$, the binary nitrides Mg_3N_2, Ca_3N_2, Sr_2N or Ba_2N were reacted with arsenic at 800 to 1000 °C for 48 hours. Dark yellow, red and dark grey to black microcrystalline powders were received for A = Mg, Ca, Sr and Ba, respectively. The crystal structures were refined using the Rietveld-method.

In the structure of the compounds $(A_3N)As$ with A = Mg, Ca, Sr, Ba, the arsenide ions are located in a hole formed by eight (A_6N) octahedra. Only for the cubic inverse perovskite $(Mg_3N)As$ is this void cuboctahedral. Due to the increasing size of the alkaline-earth metal the space available for arsenic increases until it is no longer able to effectively fill the cuboctahedral hole. The arsenide ion is decreasing its coordination number via shifting from the central position and tilting of the (A_6N) octahedra [4]. This distortion increases in magnitude with the increasing size of the alkaline-earth metal and is realized with only minor deviations from ideal octahedral geometry. The distortion changes the coordination number of the arsenide ions from 12 in the undistorted Mg compound to about 4+4+2+2 in the most distorted variant, $(Ba_3N)As$. Thus, such semiconducting inverse perovskites can be understood with the same simple geometric relations as known for oxide-perovskites with the general formula ABO_3 [1].

---

[1] R. Niewa, *Z. Anorg. Allg. Chem.***2013**, *639*, 1699.

[2] M. Y. Chern, D. A. Vennos, F. J. DiSalvo, *J. Solid State Chem.***1992**, *96*, 415.

[3] E. O. Chi, W. S. Kim, N. H. Hur, D. Jung, *Solid State Commun.***2002**, *121*, 309.

[4] M. Y. Chern, F. J. DiSalvo, J. B. Parise, J. A. Goldstone, *J. Solid State Chem.***1992**, *96*, 426.

PTue105

Characterization of alumina-graphene composites (AGC) formed by the reaction of carbon monoxide with partially nitrided alumina powder

Jung, Joo-hei (Yeungnam University, Gyongsan, KOR); Jung, Woo-Sik (Yeungnam University, Gyongsan, KOR)

Alumina ($Al_2 O_3$) -graphene composites (AGC) were prepared by the reaction of carbon monoxide (CO) with partially nitrided alumina (PNA) powder. The PNA powder was synthesized by the carbothermal reduction-nitridation reaction of a mixture of $Al_2 O_3$ and carbon powders under a flow of nitrogen. The AGC powders were characterized by powder X-ray diffraction, scanning electron microscopy, micro-Raman and X-ray photoelectron spectroscopy, and high-resolution transmission electron microscopy. The quality and amount of graphene depended on calcination temperature and duration of calcination. Raman spectra of AGC powders showed that the intensity ratio of the D band to the G band decreased with increasing reaction temperature and duration. The AGC powders are expected to be used as a thermal conductive filler, electrically conductive paint and electromagnetic interference shielding materials.

PTue106

Development of yttria doped thoria solid electrolyte and its performance in liquid sodium systems as oxygen sensors

Lakshmigandhan, I (Indira Gandhi Centre for Atomic Research, Kalpakkam, IND); Sree Rama Murthy, A (Indira Gandhi Centre for Atomic Research, Kalpakkam, IND); Mahendran, K H (Indira Gandhi Centre for Atomic Research, Kalpakkam, IND); Ravindra Babu, M (Indira Gandhi Centre for Atomic Research, Kalpakkam, IND); Jayaraman, V (Indira Gandhi Centre for Atomic Research, Kalpakkam, IND); Gnanasekaran, T (Indira Gandhi Centre for Atomic Research, Kalpakkam, IND)

Thoria based solid electrolytes are used for measuring oxygen levels in various ambients and also for carrying out thermochemical and kinetic studies when the partial pressure of oxygen is very low (~ 10^{-6} to 10^{-25} bar at 1000^{o}C). Thoria doped with 7.5 mol% Y_2O_3 (YDT) exhibits maximum oxide ion conductivity and has been identified as the most suitable electrolyte for monitoring oxygen concentration in liquid sodium coolant of fast breeder reactors. This ceramic electrolyte based oxygen monitor has to be shaped in a suitable form followed by sintering so that it exhibits a helium leak tightness of ☐ 10^{-9} std. l/s. When the ceramic forms are produced from YDT powders prepared by conventional methods, sintering at ca.2273 K is needed to conform to this specification. A novel combustion synthesis method was developed in our laboratory for synthesis of electrolytic grade of nanocrystalline YDT powders and conditions were optimized to get sintered bodies conforming to the leak tightness specified [1]. Conditions were also optimized for soldering YDT compacts with FERNI (Fe – 50 %, Ni – 48 % and Cr – 2 %) alloy using a borate glass. The glass seal was found to be intact after several hours of exposure in liquid sodium at 723 and 748 K.

Two different configurations of sensors viz. thimble and disc type were made and tested in sodium. Thimble type sensor had the following cell configuration:

$$\text{SS, [O] Na} \mid \text{YDT} \mid \text{In/In}_2\text{O}_3\text{ , W}$$

This sensor was tested in liquid sodium at 723 K. The emf output was found to be about 680 mV, which corresponded to 2 ppm of oxygen in sodium. Analysis of sodium for oxygen impurity corroborated with the values deduced from emf output of the sensor. However, these sensors had short and unpredictable lifetimes, indicating the need to modify the design of the ceramic-to-metal seal.

Copper – cuprous oxide couple was used as the reference electrode for sensors with YDT in the form of disc. The sensor response was evaluated by maintaining sodium at different temperatures ranging from 623 to 723 K. The emf outputs exhibited by the sensors were different from the theoretically predicated values. The lifetimes of these sensors were found to be about 10000 h.

The results of these investigations will be presented in this paper.

---

[1] Development of yttria doped thoria solid electrolyte for use in liquid sodium systems, V. Jayaraman **,** D. Krishnamurthy, Rajesh Ganesan, A. Thiruvengadasami, R. Sudha, M.V.R. Prasad and T. Gnanasekaran, Ionics **13** (2007) 299 - 303.

PTue107

Synthesis, characterization and hydrogen sensing properties of $Cr_{1-x}Fe_xNbO_4$ (x = 0-1)

Sree Rama Murthy, A (Indira Gandhi Centre for Atomic Research, Kalpakkam, IND); Vinod, K (Indira Gandhi Centre for Atomic Research, Kalpakkam, IND); Gnanasekar, K I (Indira Gandhi Centre for Atomic Research, Kalpakkam, IND); Jayaraman, V (Indira Gandhi Centre for Atomic Research, Kalpakkam, IND); Umarji, A M (Indian Institute of Science, Bangalore, IND)

The change in conductivity of simple metal oxides like ZnO, SnO_2, etc., in the presence of trace levels of reducing/oxidizing gases were extensively studied by many research teams for gas sensor applications. Studies have shown that in the presence of a reducing gas like H_2, the conductivity of an n-type material increases, whereas the opposite trend is suggested for a p-type material. To improve the specificity towards a particular analyte gas in the preferred concentration range, two different approaches are suggested, a) addition of selective catalysts to speed up the chemical reaction with a particular analyte gas, b) incorporation of additives and dopants to modify the electronic properties of the base material and hence the reactivity towards different analytes can be altered. The latter approach eventually extended the scope of the investigations of the ternary and quaternary compounds including perovskites [ABO_3], pyrochlores [$A_2B_2O_7$], heterometallates [$A_nXM_{12}O_{40}$ n= 3-4] etc.

Oxides of niobium and niobium doped compounds are known to have high hydrogen storage capacity. We have explored $Cr_{1-x}Fe_xNbO_4$ (x = 0-1) , for their ability towards sensing hydrogen in various concentration levels. The compounds were prepared by conventional solid state reaction method using calculated amounts of the oxides of chromium, niobium and iron. Powder X-ray diffraction revealed the formation of substitutional solid solution up to x = 0.6. The validation of Vegard’s law in these compositions was evaluated. The morphology of the pellet samples were analysed with scanning electron microscopy and semi quantitative elemental analysis was carried out by energy dispersive analysis of X-rays (EDAX). The AC impedance of these compositions was measured in the temperature range of 423 – 723 K. The electrical conductivity was deduced from the Cole-Cole plot and the activation energy for conduction was derived from the Arrhenius plot. Oxidation states of chromium, iron, niobium and oxygen in these compositions were estimated from the X-ray photoelectron spectroscopic studies. Magnetic transitions in these compositions in the temperature range of 4 to 298 K were elucidated from vibrating sample magnetometer (VSM). The gross magnetic moment at 298 K was derived from the mass susceptibility data. Hydrogen sensing characteristics were evaluated by using thick films of these compositions. These investigations showed that some of these compositions were capable of sensing hydrogen from 100 to 4000 vppm.

The details of the results obtained from these studies will be presented in this paper.

PTue108

Electrical Conductivity, Gap Width and Sensitivity to CO_2 gas for ITO Powder and Nanoparticle

Mahmoud, Ahmed (National Research Centre, Cairo, EGY)

The A.C. electrical conductivity of powder and nanopowder samples of indium tin oxide (ITO) was measured as a function of temperature in range (298-573 K). The nanopowder samples at lower temperature possess constant conductivity. The electrical conductivity increases for the nanopowder samples with increasing temperature as well as SnO_2 content due to the higher level of electron doping, reaching a maximum at 30 wt. % of SnO_2 . However, high SnO_2 concentrations lead to a drastic drop in the conductivity. For the powder samples, as the SnO_2 content increases the conductivity decreases.

The gap width of all samples was calculated from diffuse reflectance curves and it was in the range of 3.8 - 4.3 eV for nanopowder samples and 3.1- 3.6 eV for powder samples.

The resistance and sensitivity were measured for both nanopowder and powder sample containing (In: Sn = 70:30) at 25, 40 and 60 ˚C at different times in presence of CO_2 gas and absence of CO_2. It was found that in the nano forms the ITO containing (In: Sn = 70:30) can be used as a gas sensor.

PTue109

Electrical properties of the bismuth-rich subiodides $Bi_{14}I_4$ and $Bi_{18}I_4$

Weiz, Alexander (TU Dresden, Dresden, GER); Rasche, Bertold (Technische Universität, Dresden, GER); Lê Anh, Mai (TU Dresden, Dresden, GER); Herrmannsdörfer, Thomas (Helmholtz-Center Dresden-Rossendorf, Dresden, GER); Ruck, Michael (Technische Universität Dresden, Dresden, GER)

Annealing pills of thoroughly grinded bismuth and BiI_3 at 275 °C for six days is a quick and effective route for the synthesis of $Bi_{14}I_4$ [1] and $Bi_{18}I_4$ [2]. This method allows the synthesis of single-phase products in amounts of several grams. The powder samples were analyzed via powder X-ray diffraction, energy dispersive X-ray spectroscopy and thermal analysis. The honeycomb net of bismuth atoms known from the element's structure [3] is restricted to stripes of 14 or 18 atoms width. Two terminal iodine atoms saturate each bismuth atom at the edges.

Full-relativistic DFT-based calculations of the electronic band structure, taking the strong spin-orbit coupling in to account, are consistent with previous results and indicate metallic behaviour in three dimensions [4]. Measurements of the electrical resistance in the temperature interval 2 K to 300 K with 0.5 mA and 2.0 mA confirm the predicted metallicity of $Bi_{14}I_4$ and $Bi_{18}I_4$. While the electrical resistivity of $Bi_{14}I_4$ is current independent, the resistivity of $Bi_{18}I_4$ increases with current. This dependence originates from a magneto-resistance. Up to magnetic fields of 14 T, $Bi_{18}I_4$ exhibits a positive and strictly linear magneto-resistance with $R(14\ \mathrm{T}, 2\ \mathrm{K}) / R(0\ \mathrm{T}, 2\ \mathrm{K}) = 150\ \%$.

---

[1] E. V. Dikarev, B. A. Popovkin, A. V. Shevelkov, *Z. Anorg. Allg. Chem.* **1992**, *612*, 118–122.

[2] E. V. Dikarev, B. A. Popovkin, *Dokl. Acad. Nauk SSSR* **1990**, *310*, 117–120.

[3] P. Cucka, C. S. Barrett, *Acta Crystallogr.* **1962**, *15*, 865–872.

[4] M. Lindsjö, L. Kloo, A. Kuznetzov, B. Popovkin, *Eur. J. Inorg. Chem.* **2008**, *33*, 5196–5202.

PTue110

Environmental Risk Assessment of Nanomaterials

Scott-Fordsmand, Janeck James (Department of Bioscience, Aarhus University, Aarhus, DNK);
Amorim, J.B. (Department of Biology and CESAM, University of Aveiro, Aveiro)

There is currently no unified environmental risk assessment of nanomaterials. Such an assessment framework of nanomaterials must be flexible and efficient and consider the impact of the varying properties of materials during the various life cycle stages. The proposed risk assessment includes consideration of long-term effect. Based on the initial exposure scenarios, risk assessment will, go to next tiers, where a more refined risk assessment is performed based on the available and additional obtained data. In conjunction with this assessment, an intelligent testing strategy is outlined. This presentation summarises the framework developed for the environmental risk assessment and pin-points which tools are required to guide and facilitate such a risk assessment. Further developments are needed to provide further in-depth tools for the risk assessment.

PTue111

Extended anionic frameworks in the AE-Mn-N systems. Synthesis, structure and physical properties of new nitridomanganates

Ovchinnikov, Alexander (MPI for Chemical Physics of Solids, Dresden, GER); Schnelle, Walter (MPI for Chemical Physics of Solids, Dresden, GER); Bobnar, Matej (MPI for Chemical Physics of Solids, Dresden, GER); Borrmann, Horst (MPI for Chemical Physics of Solids, Dresden, GER); Sichelschmidt, Joerg (MPI for Chemical Physics of Solids, Dresden, GER); Grin, Yuri (MPI for Chemical Physics of Solids, Dresden, GER); Hoehn, Peter (MPI for Chemical Physics of Solids, Dresden, GER)

Binary transition metal nitrides attract considerable interest due to their valuable mechanical, electrical and magnetic properties. However, chemistry and physics of multinary nitrides are far less explored. Nitridometalates represent a subfamily of multinary nitrides containing $[M_xN_y]^{n-}$ anions of typically low dimensionalities with predominantly covalent bonding stabilized by cations of electropositive metals. Transition metal atoms in such compounds usually show low coordination numbers and oxidation states [1]. Among 3*d* metals, manganese is known to display the widest variety of electronic states and coordination environments in nitridocompounds, but the nitridomanganates reported so far are mainly located in the Mn-poor regions of the corresponding phase diagrams [2].The *AE*-Mn-N ternary systems, where only alkaline-earth metal rich compounds with *0D* nitridomanganate units were known, have been reinvestigated focusing on the search for structures with extended nitridomanganate frameworks. This study was motivated by the fact that Mn displays a partial occupation of the *d*-states in all nitride compounds which is relevant to the onset of magnetism. The increase of Mn substructure dimensionality may result in a development of interesting magnetic topologies. Indeed, by increasing the Mn/*AE* ratio a condensation of the metalate structural units is observed leading to a change from *0D* (e.g. Ca_6MnN_5 [3], AE_3MnN_3 [4, 5], $Sr_8Mn_3N_8$ and $AE_8Mn_3N_9$ [6]) to *1D* ($Ba_4Mn_3N_6$), *2D* ($Ca_{12}Mn_{19}N_{23}$) and even *3D* ($AE_3Mn_{10}N_{11-x}$) structures. In total ten new phases representing each of the four dimensionality classes have been discovered and their physical properties have been characterized by means of magnetic susceptibility, electrical resistivity and electron spin resonance measurements. The one-dimensional $Ba_4Mn_3N_6$ contains infinite corrugated $[MnN_{4/2}]^{8/3-}$ chains with an ordered arrangement of Mn(II) and Mn(IV) atoms. This phase displays a typical spin-chain behaviour with a short range magnetic ordering at 120 K and a *3D* AFM ordering at ~8 K. $Ca_{12}Mn_{19}N_{23}$ is the first example of a layered nitridomanganate. Its structure possesses $Mn(II)N_4$ tetrahedra and $Mn(III)N_3$ trigonal pyramids connected via corners and edges so that Mn atoms form a distorted hexagonal net. Magnetic measurements reveal a Curie-Weiss behavior with an AFM ordering at 90 K. Cubic $AE_3Mn_{10}N_{11-x}$ compounds (*AE* = Sr, Ba), isotypic to the metallic $La_3Cr_{9.236}N_{11}$ phase [7], are the most transition metal rich nitridometalates known so far. In these nitrides Mn(II, III) atoms adopting tetrahedral and trigonal coordination by nitrogen atoms build a *3D* framework accommodating isolated $[AE_6N]^{9+}$ octahedra.The formation of extended anionic structures in the newly discovered phases is driven by an emergence of Mn-Mn bonding due to the short contacts between the metal atoms possessing partially filled *d*-states. This leads to a decrease of the magnetic moment on manganese atoms even for the compounds displaying semiconducting behavior. Presumably, other transition metals showing intermediate oxidation states in their nitride compounds (e.g., Cr, Fe) may also turn out to be good candidates for various extended nitridometalate structures.

---

[1] R. Kniep, P. Höhn in J. Reedijk & K. Poeppelmeier (Eds.), *Comprehensive Inorganic Chemistry II*, 2nd edition, Elsevier, 2013, pp. 137-160.
[2] R. Niewa, Z. Kristallogr. **217** (2002) 8.
[3] D.H. Gregory, M.G. Barker, P.P. Edwards, D.J. Siddons. *Inorg.Chem.* **34** (1995) 5195.
[4] A. Tennstedt, C. Röhr, R. Kniep. *Z. Naturforsch. B.* **48** (1993) 1831.
[5] A. Tennstedt, C. Röhr, R. Kniep. *Z. Naturforsch. B.* **48** (1993) 794.
[6] J.K. Bendyna, P. Höhn, R. Kniep. *Z. Kristallogr. - New Cryst. St.* **223** (2008) 185.
[7] S. Broll, W. Jeitschko. *Z. Naturforsch. B.* **50** (1995) 905.

PTue112

Fabrication and properties of polydimethysiloxane films for optical and triboelectric applications

Lee, Soo Hyun (Department of Electronics and Radio Engineering, Kyung Hee University, Kyung Hee, KOR); Ko, Yeong Hwan (Department of Electronics and Radio Engineering, Kyung Hee University, Kyung Hee, KOR); Yu, Jae Su (Department of Electronics and Radio Engineering, Kyung Hee University, Kyung Hee, KOR)

Recently, there has been increasing interest in triboelectric generators for energy harvesting due to high output power as well as simple and flexible device structure. Typically, the triboelectric generators are fabricated by closely separating two different triboelectric polymer and soft materials such as polydimethysiloxane (PDMS) or Kapton, which are contacted to each electronic conductive layer as an electrode. The surface morphology and interface between the polymer material and electrode play a key role in the triboelectric charge generation. On the other hand, surface nanopatterns as an antireflection layer enhance the optical transparency of layers or devices. In this presentation, PDMS layers on conductive textile (CT) were fabricated by a simple and cost-effective methodology for triboelectric generators. The optical properties were investigated by applying the nanopatterns. The multi-stacked triboelectric generators were prepared by overlapping repeatedly the PDMS coated CTs and bare CTs. Also, ZnO nanorods were synthesized on indium tin oxide/polyethylene terephthalate by the electrochemical deposition and used for the top electrode. The triboelectric properties of the fabricated samples were evaluated.

PTue113

Solution Combustion Synthesis of $CeFeO_3$ under Ambient Atmosphere

Petschnig, Lucas (Universität Innsbruck, Innsbruck, AUT); Fuhrmann, Gerda (Institut für Allgemeine, Anorganische und Theoretische Chemie, Leopold-Franzens-Universität Innsbruck, Innsbruck, AUT); Tribus, Martina (Institut für Mineralogie und Petrographie, Leopold-Franzens-Universität Innsbruck, Innsbruck, AUT); Huppertz, Hubert (Institut für Allgemeine, Anorganische und Theoretische Chemie, Leopold-Franzens-Universität Innsbruck , Innsbruck, AUT)

Rare-earth orthoferrites of the general formula $LnFeO_3$ (Ln = lanthanoides) are potential candidates for many application areas, such as high-temperature electrolysis, gas sensors, catalysis technologies and environment friendly pigments [1-5]. Although many reports exist for the synthesis of different rare-earth orthoferrites, only few are known for the cerium orthoferrite, $CeFeO_3$ [6-9]. This is mainly because cerium (III) compounds, in course of the reactions, tend to oxidise easily to cerium (IV) species generating stable CeO_2.

In this study we report the first successful synthesis of polycrystalline$CeFeO_3$ by solution combustion method under ambient atmosphere. The perovskite-type $CeFeO_3$ was obtained by using glycine as fuel from a solution of metal nitrates with almost single phase purity (93%). For comparison, the orthoferrite $CeFeO_3$ was also prepared under inert atmosphere by a conventional solid-state reaction. The products were structurally characterised by X-ray powder diffraction (XRD) and lattice parameters were determined from a subsequent Rietveld refinement. Since solution combustion is often referred as the method leading to nano-sized materials [10-12], the morphological characteristics of the products obtained through the two different synthetic methods were investigated by scanning electron microscopy (SEM). Furthermore, particle sizes were determined by laser diffraction spectroscopy.

---

[1] A. K. Opitz, A. Nenning, C. Rameshan, R. Rameshan, R. Blume, M. Hävecker, A. Knop-Gericke, G. Rupprechter, J. Fleig, B. Klötzer, *Angew. Chem.* **2015**, *127*, 2666.

[2] H. Aono, E. Traversa, M. Sakamoto, Y. Sadaoka, *Sensor. Actuat. B-Chem.* **2003**, *94*, 132.

[3] P. Ciambelli, S. Cimino, L. Lisi, M. Faticanti, G. Minelli, I. Pettiti, P. Porta, *Appl. Cat. B-Environ.* **2001**, *33*, 193.

[4] A. Delmastro, D. Mazza, S. Ronchetti, M. Vallino, R. Spinicci, P. Brovetto, M. Salis, *Mat. Sci. Eng. B* **2001**, *79*, 140.

[5] Ž. Dohnalová, P. Šulcová, M. Trojan, *J. Therm. Anal. Calorim.* **2008**, *91*, 559.

[6] F. Bertaut, F. Forrat, *J. Phys. Radium* **1956**, *17*, 129.

[7] M. Robbins, G. K. Wertheim, A. Menth, R. C. Sherwood, *J. Phys. Chem. Solids* **1969**, *30*, 1823.

[8] K. Kitayama, K. Nojiri, T. Sugihara, T. Katsura, *J. Solid State Chem.* **1985**, *56*, 1.

[9] Y. D. Tretyakov, V. V. Sorokin, A. R. Kaul, A. P. Erastova, *J. Solid State Chem.* **1976**, *18*, 253.

[10] A. S. Prakash, P. Manikandan, K. Ramesha, M. Sathiya, J. M. Tarascon, A. K. Shukla, *Chem. Mater.* **2010**, *22*, 2857.

[11] A. S. Mukasyan, P. Epstein, P. Dinka, *P. Combust. Inst.* **2007**, *31*, 1789.

[12] V. Gaikwad, J. Sheikh, S. Acharya, *J. Sol-Gel Sci. Technol.* **2015**

PTue114

Hydrofluorothermal Synthesis of Novel Transition Metal Fluorophosphate and Fluorosulfate Frameworks

Marshall, Kayleigh (University of Bath, Bath, GBR)

In the ever increasing technological world, the demand for better energy storage systems becomes ever more prevalent. Lithium-ion battery research started in the early 1980s and has progressed immensely from the first commercialised cell from Sony in 1991; comprised of a $Li_{1-x}CoO_2$ cathode, Li_xC_6 anode and operating at 3.7V at 25 °C. Cathode materials have progressed from transition metal oxides to polyanionic transition metal frameworks with iron being very popular due to its low cost and non-toxic nature, despite issues with relatively low operating voltages. The addition of fluoride into such frameworks and nanostructuring have shown to improve the electrochemical performances of these cathode materials. Mid-late first row transition metal fluorophosphate and fluorosulfate frameworks have previously been studied within the Weller group with applications towards cathode materials for both lithium and sodium ion batteries. Titanium compounds have shown to be promising as anode materials for lithium ion batteries with lithium titanium phosphate showing promising performance in aqueous electrolyte with a lithium iron phosphate cathode. Work to be presented is on the synthesis and characterisation of novel transition metal fluorophosphate and fluorosulfate frameworks (such as $K_2Ti_2F_2(PO_4)(H[PO_4]_2)$) with intentions towards anode materials and/or solid electrolytes.

PTue115

Hydrogenation of ternary intermetallic compounds MTrTt (M = Ca, Sr, Ba; Tt = Al, Ga; Tt = Si, Ge) - A chemical bonding view in position space

Wagner, Frank R. (Max-Planck Institute for Chemical Physics of Solids, Dresden, GER); Kohout, Miroslav (Max-Plank-Institut for Chemical Physics of Solids , Dresden, GER); Grin, Juri (Max-Plank-Institut for Chemical Physics of Solids, Dresden, GER); Faria, Rodolfo (Max Planck Institute for Chemical Physics of Solids, Dresden, GER)

Ternary intermetallic compounds with AlB_2-type structure such as *MTrTt* (*M* = Ca, Sr, Ba; *Tt* = Al, Ga; *Tt* = Si, Ge) incorporate hydrogen under mild conditions, which undergo subtle structural changes.[1] The hydrogenation takes a graphite-like honeycomb sheets of alternating *TrTt* atoms (separated by hexagonal *M* atoms) to a slightly puckered *TrTt*H network forming a 10-electron (valence) system. Hydrogen attaches exclusively to the *Tr* atoms.

Despite subtle structural changes upon hydrogenation, the material turns into a semiconductor. We performed topological analysis of the electron density, in the framework of Quantum Theory of Atoms in Molecules (QTAIM) [2], and electron localizability indicator (ELI-D) [3] to investigate the influence of the hydrogen incorporation on the bonding situation.

Upon hydrogenation the bond order of the *Tr*-*Tt* bonds decreases and a new *Tr*-H bond is formed. Its delocalized character however does not change. This leads to a higher charged environment, where H is negatively charged. The reduced *Tr*-H bond order is due to a competition with the surrounding *M* atoms, which also share electrons with H to a great extent. The extent of the electron sharing between H-*Tr* and H-*M* indicate that H is not an isolated ion, but instead part of the polyanionic layer. The considerable drop in *Tr* distant pair-sharing can be interpreted that local interactions become more important, which is consistent with the semiconducting behaviour. Differences in electron localizability explain the site selectivity of the hydrogenation reaction.

---

[1] Evans, M. et. al *JACS*, **2008**, *130,* 12139.

[2] Bader, R. F. W. *Atoms in Molecules: A Quantum Theory*,**2007**, USA: Oxford university Press.

[3] Kohout, M. *Faraday Discuss.* **2007**, *135,* 43.

PTue116

Hydrothermal Synthesis and Characterization of the Lutetium borate-nitrate $Lu_2B_2O_5(NO_3)_2$ - 2 H_2O

Ortner, Teresa (Institut für Allgemeine, Anorganische und Theoretische Chemie, Innsbruck, AUT); Wurst, Klaus (Institut für Allgemeine, Anorganische und Theoretische Chemie, Leopold-Franzens-Universität Innsbruck, Innsbruck, AUT); Huppertz, Hubert (Institut für Allgemeine, Anorganische und Theoretische Chemie, Leopold-Franzens-Universität Innsbruck , Innsbruck, AUT)

Borates are known to have a very wide-ranging structural chemistry. The structure motives these compounds are able to form are extended by the introduction of nitrate groups as in the borate-nitrate presented here.

The new lutetium diborate- dinitrate $Lu_2B_2O_5(NO_3)_2 \cdot 2\ H_2O$ was obtained through a hydrothermal synthesis from $Lu(NO_3)_3 \cdot H_2O$ and H_3BO_3. The compound crystallizes in the space group *P*-1 (no. 2) with the lattice parameters a = 790.45(3), b = 989.59(3), c = 1461.29(4) pm, α = 90.86(1)°, β = 101.67(1)°, and γ = 109.97(1)° (Z = 4). Isolated $[B_2O_5]^{4-}$ groups as well as NO_3^- units are linked through hydrogen bridges formed by crystal water. Unlike previously reported borate-nitrates containing early lanthanide cations *e.g.* $La[B_5O_8(OH)]NO_3 \cdot 2H_2O$ [1] or $Ce[B_5O_8(OH)]NO_3 \cdot 3H_2O$ [2 , 3] , the lutetium borate-nitrate we report displays a novel, open arrangement of borate and nitrate groups with a 1:1 ratio. In contrast to the only known hydrated lutetium borate $H_3LuB_6O_{12}$ [4] , which shows tetrahedral as well as trigonal-planar borate units, the structure of $Lu_2B_2O_5(NO_3)_2 \cdot 2\ H_2O$ is built up solely from planar BO_3 units. The four crystallographically independent nitrate groups in the presented borate-nitrate are all perpendicular to [001]. In comparison, the related lutetium nitrate hydroxide hydrate $[Ln_6O(OH)_8(H_2O)_{12}(NO_3)_6](NO_3)_2{\cdot}4H_2O$ [5 , 6] possesses eight nitrate groups that are tilted at different angles to the *ac*-plane.

---

[1] B.-C. Zhao, W. Sun, W.-J. Ren, Y.-X. Huang, Z. Li, Y. Pan, J.-X. Mi, *J. Solid State Chem.***2013**, *206*, 91-98.
[2] W. Sun, T.-T. Zhu, B.-C. Zhao, Y.-X. Huang, J.-X. Mi, *Acta Crystallogr.***2012**, *E68*, i33-i34.
[3] L. Li, X. Jin, G. Li, Y. Wang, F. Liao, G. Yao, J. Lin, *Chem. Mat.***2003**, *15*, 2253-2260.
[4] L. Li, P. Lu, Y. Wang, X. Jin, G. Li, Y. Wang, L. You, J. Lin, *Chem. Mat.***2002**, *14,* 4963-4968.
[5] G. Giester, Z. Zak, P. Unfried, *J. Alloys Compd.***2009**, *481*, 116-128.
[6] G. Giester, P. Unfried, Z. Žák, *J. Alloys Compd.***1997**, *257*, 175-181.

PTue117

Influence of binder type on the SiC-based ceramic slurries properties for casting shell moulds fabrication

Malek, Marcin (Warsaw University of Technology, Warsaw, POL)

Silicon carbide (SiC) is widely used in industry. It exhibits advantageous properties like: high strength, hardness and resistance to thermal shocks and oxidation. It is also characterized by thermal resistance and stability. It characterized by very high thermal and electrical conductivity [1]. In comparison with other ceramic powders like: aluminium oxides, zirconium oxides or mullite, SiC exhibits the highest thermal conductivity. Therefore SiC is potentially useful for fabrication ceramic shell moulds in investment casting process. SiC gives possibilities to control macro and microstructure parameters (like grain size or interdendritic distance) in cast materials, because it exhibit high thermal conductivity [2]. The aim of the study was to investigate the effect of adding three different binders on the technological properties of ceramic slurries used in manufacturing SiC shell moulds for investment casting of aircraft turbine engine parts.

This work present technological properties of ceramic slurries based on silicon carbide powder signed F400. Ceramic slurries were fabricated with three kind of binders: two kinds of water soluble polymers added in 6 wt.% amount: poly(vinyl alcohol) with molecular weight 26000g/mole used as 10 wt.% water solution and polyethylene glycol with molecular weight 1500g/mole taken as 30 wt.% water solution and water thinnable polyacrylic dispersion. Solid content was 65 wt.%. To characterize silicon carbide: SEM images, chemical composition, Zeta potential, XRF, XRD and grain size were studied. Technological properties of ceramic slurries i.e.: plate weight test, relative viscosity, dynamic viscosity, density and pH were investigated. Properties of SiC based ceramic slurries are very promising and their shell moulds are very perspective for future application as a coats of investment casting process.

Financial support of Structural Funds in the Operational Programme - Innovative Economy (IE OP) financed from the European Regional Development Fund - Project "Modern material technologies in aerospace industry", No. POIG.01.01.02-00-015/08-00 is gratefully acknowledged.

PTue118

InAlAs/InGaAs Metamorphic High-Electron-Mobility Transistor With a Sol-Gel Processed TiO_2 as Gate Dielectric

Huang, Jung-Sheng (Dept. of Electronic Engineering, I-Shou University, Kaohsiung, TWN); Lai, Cheng-Hun (Dept. of Electronic Engineering, I-Shou University, Kaohsiung, TWN); Chen, Hung-Wei (Dept. of Electronic Engineering, I-Shou University, Kaohsiung, TWN); Chang, Yu-Chi (National Cheng-Kung University, Tainan, TWN); Wang, Yeong-Her (National Cheng-Kung University, Tainan, TWN); Lee, Kuan-Wei (Dept. of Electronic Engineering, I-Shou University, Kaohsiung, TWN)

In the work, the solution-gelation (sol-gel) processed titanium oxide (TiO_2) solution was prepared by mixing three materials. First, 760 µL titanium isopropoxide was mixed with 510 µL acetylacetone, and then dissolved in 3.8 mL 2-methoxythanol to obtain the TiO_2 solution. The isolation of InAlAs/InGaAs metamorphic high-electron-mobility transistor (MHEMT) was accomplished by mesa wet etching down to the buffer layer. Ohmic contacts of the Au/Ge/Ni metal were deposited by evaporation, and then patterned by lift-off processes, followed by a rapid thermal annealing. The gate recess was etched by the H_3PO_4-based etchant to the InP etching-stop layer. For the MOS-MHEMT, a TiO_2 solution was used to generate the gate dielectric. The oxide film produced by the TiO_2 solution used the following two-step spin-coating method: 1000 rpm for 10 s and 8000 rpm for 30 s. Then, the oxide film was treated at 150 ^{o}C for 30 min. Finally, the gate pattern was defined with Au.The device using a sol-gel processed TiO_2 as gate dielectric exhibits better electrical characteristics than the referenced MHEMT. These characteristics include higher maximum drain current density, enhanced maximum transconductance, and suppressed leakage current density.

PTue119

Interaction between carbides formed in FeTiNbC alloys. Corrosion resistance.

Amara, Leïla (Laboratoire d'Electrochimie-Corrosion, Métallurgie et Chimie Minérale. Faculté de Chimie, Algiers, DZA); Madaoui, Noureddine (Division Milieux Ionisés, Centre de Développement des Technologies Avancées CDTA/ Laboratoire d'Electrochimie-Corrosion, Métallurgie et Chimie Minéral, Algiers, DZA)

The first aim of this work is to study the interaction between carbides formed in the FeNbTiC alloys, the second one is to explain the electrochemical behavior of these alloys in 3.5 wt.% aqueous NaCl solution. Arc melted ingots were elaborated using pure metals and carbon in an argon atmosphere, then submitted to a slow heating and cooling at 10K/min in differential thermal analysis (DTA) furnace. The microstructures were characterized by means of optical microscopy (OM) and scanning electron microscopy (SEM), when X-ray diffraction (DRX) and energy-dispersive X-ray spectroscopy (EDS) were used to identify the carbide phases and the matrix. The electrochemical behavior of our alloys was investigated by potentiodynamic polarization and electrochemical impedance spectroscopy (EIS). A microhardness apparatus was used to characterize another property of our samples which is the hardness of different phases formed after cooling. Our results permit to conclude that the interaction between NbC_{1-x} and TiC_{1-x} carbide phases is quite different from that of the other transition elements. Indeed, it seems to form a core-shell $(Nb,Ti)C_{1-x}$ structure when the other ones, issued from other transition elements, are separated which is the case of TaC_{1-x} and VC_{1-x} or VC an_{1-x} d TiC_{1-x} or form a continuous solid solution, as is the case of MoC_{1-x} and VC_{1-x}. The core of the mixed carbide $(Nb,Ti)C_{1-x}$ is essentially composed of titanium carbide and the shell is a niobium carbide. An intermediate zone with variable compositions and variable grey contrasts was observed in the same core-shell structure. In the other side, we noted that high carbon contents (3 wt %) could influence the electrochemical behavior of FeNbTiC alloys particularly their corrosion resistance in saline solution. Furthermore, the observation of the microstructures of the different studied alloys reveal that the alloy composed of primary carbides present a more interesting corrosion resistance than the one having a eutectic structure. On the other hand, we also noted that a low carbon level increase the hardness of our samples.

PTue120

Isothermal section and new compounds in the system Al-Fe-Ge

Reisinger, Gabriel (Institut f. Anorganische Chemie (Materialchemie), Universität Wien, Vienna , AUT); Effenberger, Herta S. (Institut f. Mineralogie und Kristallographie, Universität Wien, Vienna, AUT); Richter, Klaus W. (Institut f. Anorganische Chemie (Materialchemie), Universität Wien, Vienna, AUT)

Based on findings in the Al-Fe-Si system, which is containing eleven ternary phases, an exploratory investigation in the up to now uninvestigated Fe-poor part of the ternary phase diagram Al-Fe-Ge was performed. A partial isothermal section at 800 °C was constructed based on experimental results from powder X-ray diffraction, scanning electron microscopy and electron probe micro analysis. A significant ternary solubility for all binary Fe-Al and Fe-Ge compounds was observed. A stabilization of the binary Phase FeGe ($P2_13$, $cP8$, FeSi type) towards higher temperatures could be detected. At least three new ternary compounds have been found so far and were investigated by single crystal X-ray diffraction. We report on the crystal structures of AlFeGe ($\tau1$) (*Fddd*, $oF48$, $CuMg_2$ type), which is structurally related to the binary compound $FeGe_2$, as well as Al_3FeGe_2 ($\tau2$) ($I4/mcm$, $tI24$, Ga_5Pd type). An isostructural compound is known from the Al-Fe-Si system. The third ternary phase is $Al_8Fe_9Ge_4$ ($\tau3$) ($C\,2/m$, $mS42$), crystallizes in a new structure type related to Fe_6Ge_5. All ternary phases are exhibiting a broad homogeneity range at constant Fe content due to Al/Ge substitution.

PTue121

Luminescence spectra of Ce^{3+}-doped $LaAlO_3$ powders prepared from the La_2O_3-CeF_3-Al_2O_3 reaction system

Choi, Yeon-Hee (Yeungnam University, Gyongsan, KOR); Jung, Woo-Sik (Yeungnam University, Gyongsan, KOR)

Ce(III)-doped lanthanum aluminate ($LaAlO_3$) powders were prepared by the calcination of a mixture of lanthanum oxide (La_2O_3), cerium fluoride (CeF_3) and alumina (Al_2O_3) powders in a nitrogen atmosphere, and characterized by X-ray diffraction, photoluminescence, X-ray photoelectron spectroscopy (XPS) and scanning electron microscopy. The intense emission peak was observed at 420 (blue) nm and its intensity depended on Ce(III) concentration. The La_2O_3-CeF_3-Al_2O_3 reaction system was more effective for blue emission than the La_2O_3-CeO_2-Al_2O_3 in a reducing atmosphere. The oxidation state of the dopant Ce in $LaAlO_3$ was determined by XPS.

PTue122

Metal-Ammonia Intercalated Iron Selenide Superconductors Studied In-Situ by Powder X-Ray Diffraction

Cassidy, Simon (Department of Chemistry, University of Oxford, Oxford, GBR); Sedlmaier, Stefan (Department of Chemistry, University of Oxford, Oxford, GBR); Woodruff, Daniel (Department of Chemistry, University of Oxford, Oxford, GBR); Drakopoulos, Michael (Diamond Light Source ltd, Didcot, GBR); Ramos-Perez, Silvia (School of Physical Sciences, Canterbury, GBR); Clarke, Simon (Department of Chemistry, University of Oxford, Oxford, GBR)

In 2012, the synthesis of new superconducting phases of the kind $A_xFe_2Se_2$ (A= alkali, alkali earth, and rare earth metals) with T_cs ranging from 30 to 46 K, formed by the topotactic intercalation of A in liquid ammonia solution into the interlayer space of tetragonal FeSe.[1] In-depth structural analysis of these materials showed the '$LiFe_2Se_2$' structure to in fact contain intercalated ammonia and amide moieties along with the alkali metal, with a refined formula of $Li_{0.6}(ND_2)_{0.2}(ND_3)_{0.8}Fe_2Se_2$.[2] A further revelation was made using *in-situ* powder X-ray diffraction; when these materials are first formed in solution their structures are more ammonia rich, then of undergoing a reversible desorption of gaseous ammonia from within the crystal structure.[3]

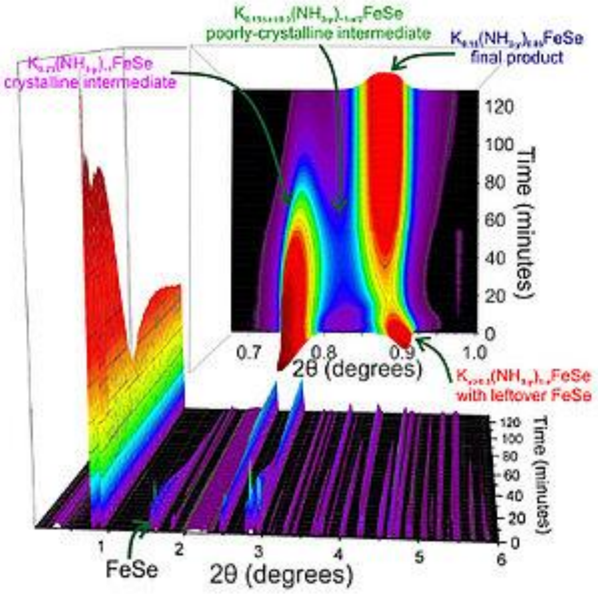

The work presented here expands on the rich structural chemistry exhibited by these metal ammonia intercalated iron selenide materials with a focus on the potassium system. The synthesis process the superconducting materials has been followed *in-situ* using X-ray powder diffraction and the analysis of the products has been carried out, *ex-situ*, using neutron powder diffraction. By following the intercalation processes with Rietveld refinements against thousands of diffraction patterns, it has been possible to reveal the existence of intermediate phases and gain information about their rates of formation, which shines new light on the product materials.

Figure 1: Evolution of the X-ray diffraction patten powder pattern for the reaction K with FeSe in ammonia.

---

[1] Ying, T. P. et al. Observation of superconductivity at 30~46 K in A(x)Fe2Se2(A = Li, Na, Ba, Sr, Ca, Yb, and Eu). Sci. Rep. 2, 426 (2012).

[2] Burrard-Lucas, M. et al. Enhancement of the superconducting transition temperature of FeSe by intercalation of a molecular spacer layer. Nat. Mater. 12, 15–9 (2013).

[3] Sedlmaier, S. J. et al. Ammonia-rich high-temperature superconducting intercalates of iron selenide revealed through time-resolved in situ X-ray and neutron diffraction. J. Am. Chem. Soc. 136, 630–3 (2014).

PTue123

New environment for a two-dimensional topological insulator with hexagonal channels hosting [BiI_2]- ions

Rasche, Bertold (TU Dresden, Dresden, GER); van den Broek, Wouter (University of Ulm, Ulm, GER); Ruck, Michael (TU Dresden, Dresden, GER)

Black shiny crystals of the new compound $Bi_{38}Pt_9I_{14}$ were grown from the melt and characterized with single crystal X-ray diffraction, energy dispersive X-ray spectroscopy, and high resolution scanning transmission microscopy. Annealing bismuth, platinum, and BiI_3 at 290 °C yielded almost single-phase samples, which were analyzed via powder X-ray diffraction and thermal analysis. The latter indicates stability of $Bi_{38}Pt_9I_{14}$ under equilibrium conditions up to 430 °C.

In $Bi_{38}Pt_9I_{14}$, the essential structural motive of the first weak three-dimensional topological insulator (TI) $Bi_{14}Rh_3I_9$ [1–3] is found in a new environment, different also to the arrangements in $Bi_{13}Pt_3I_7$ [4] and $Bi_{12}Pt_3I_5$ [5]. The honeycomb layers $[PtBi_{8/2}]^{x+}$, in which platinum-centered bismuth cubes share their edges, are known to be a two-dimensional TI if the charge is either $x = 2$ or $x = 4/3$ [1, 3]. In $Bi_{38}Pt_9I_{14}$, these intermetallic layers stack primitively, only separated by single layers of iodide ions. Thereby the hexagonal voids of the honeycombs define hexagonal tubes, which host unique triatomic anions: $[BiI_2]^-$.

Quantum chemical calculations indicate the rare oxidation state of +I for bismuth. An isolated linear $[BiI_2]^-$ ion is expected to have a strong magnetic moment originating from two unpaired electrons. However, full relativistic DFT-based calculations suggest a non-magnetic ground state with a lone-pair in the $p_{1/2}$-orbital, caused by strong spin-orbit coupling. This state is further stabilized by the crystal field of the $Bi_{38}Pt_9I_{14}$ structure. Magnetization measurements show weak diamagnetism for the compound. Electrical conductivity measurements indicate that $Bi_{38}Pt_9I_{14}$ is a semiconductor.

---

[1] B. Rasche, A. Isaeva, M. Ruck, S. Borisenko, V. Zabolotnyy, B. Büchner, K. Koepernik, C. Ortix, M. Richter, J. van den Brink, *Nat. Mater.* **2013**, *12*, 422–425

[2] B. Rasche, A. Isaeva, A. Gerisch, M. Kaiser, W. Van den Broek, C. T. Koch, U. Kaiser, M. Ruck, *Chem. Mater.* **2013**, *25*, 2359–2364.

[3] C. Pauly, B. Rasche, K. Koepernik, M. Liebmann, M. Pratzer, M. Richter, J. Kellner, M. Eschbach, B. Kaufmann, L. Plucinski, C. M. Schneider, M. Ruck, J. van den Brink, M. Morgenstern, *Nat. Phys.* **2015**, *11*, 338–343.

[4] M. Ruck, *Z. Anorg. Allg. Chem.* **1997**, *623*, 1535–1541.

[5] M. Kaiser, B. Rasche, A. Isaeva, M. Ruck, *Chem. Eur. J.* **2014**, *20*, 17152–17160.

PTue124

Protonation of $A_2Ln_2Ti_3O_{10}$ (A = K, Na, Li; Ln = La, Nd) in aqueous medium

Mechtaeva, Elizaveta (Saint Petersburg State University, Saint-Petersburg, RUS); Rodionov, Ivan (Saint Petersburg State University, Saint-Petersburg, RUS); Utkina, Tatiana (Saint Petersburg State University, Saint-Petersburg, RUS); Zvereva, Irina (Saint Petersburg State University, Saint-Petersburg, RUS)

Layered perovskite-type oxides represent a widely studied class of compounds with a number of practically significant properties, such as superconductivity, colossal magnetoresistance, catalytic and photocatalytic activity. The importance of these properties is related, first of all, to the attempts to reduce energy losses in various processes as well as to the search for ways of using solar radiation as an inexhaustible source of energy. This makes advisable a detailed study of layered perovskite-type oxides chemistry and processes occurring with them under operation conditions. Layered oxides $A_2Ln_2Ti_3O_{10}$ (A = K, Na, Li; Ln = La, Nd) in contact with aqueous solutions may undergo reversible intercalation of water molecules into the interlayer space as well as ion exchange of A^+ for H^+. These processes lead to changes in the composition of the oxides and in the structure due to the change in the interlayer space, which may affect their properties. This means that by adjusting the degree of substitution and intercalation, one can create the conditions most favorable to the process studied, for example photocatalysis. To do this one needs to know the pH values at which ion exchange occurs in layered oxides, the composition and structure of the obtained protonated compounds and stability ranges of these phases. For this reason, layered oxides $A_2Ln_2Ti_3O_{10}$ were synthesized by solid-state method and characterized by XRD, TGA and SEM. The study of ion exchange processes was carried out by means of continuous potentiometric titration of layered oxide powder suspension in water solution with hydrochloric acid. The bend observed on the titration curve corresponds to the protonation process of the layered oxide, which takes place at a high rate. It was shown that the degree of ion exchange and water intercalation and the rate of these processes at various pH depend on the layered oxide composition. Determination of the phase composition, degree of substitution and amount of intercalated water in $H_xA_{2-x}Ln_2Ti_3O_{10}\cdot yH_2O$ at different stages of titration was performed by XRD, TGA and ICP AES. We have demonstrated that the ion exchange in the layered oxides under consideration starts in an alkali medium (pH>10), accelerates at pH about 7 and proceeds thought a number of partially protonated metastable compounds. Moreover, we have shown that in acidic medium (pH<2) alkali metal ions are substituted for hydrogen ions in high degree (e.g. $H_{1,69}K_{0,31}La_2Ti_3O_{10}\cdot 0,47H_2O$). Basing on these results we can conclude that the change in pH of the medium makes it possible to control the degree of protonation in layered oxides and thus their properties. It can be useful both for the practical application of layered oxides and for the synthesis of new materials based on them.

This work was supported by the Russian Foundation for Basic Research (grant 14-03-31968)

PTue125

Syntheses and structural characterization of new quaternary vanadates of niobium and tantalum AMV_2O_8 (A = K, Rb, Tl, Cs; M = Nb, Ta)

Paidi, Anil Kumar (Indian Institute of Technology Madras, Chennai, IND)

Eight new quaternary vanadates of niobium and tantalum, AMV2O8 (A = K, Rb, Tl, Cs; M = Nb, Ta) have been prepared by solid state reactions and structurally characterized by single crystal and powder X-ray diffraction (XRD) techniques. The two cesium compounds, unlike the known CsSbV2O8 with layered yavapaiite structure[1], have a new three-dimensional structure and the other six compounds possess the known KSbV2O8 structure type. The three types of [(MV2O8)-]∞ anionic frameworks of twelve new and known A+M5+V2O8 (A = K, Rb, Cs, Tl; M = Nb, Ta, Sb) vanadates could be conceived to be built by different connectivity patterns of M2V4O18 ribbons, which contain MO6 octahedra and VO4 tetrahedra. The Raman and infrared spectroscopic studies of these eight new quaternary vanadates are presented.

---

[1] Devi, R. N.; Vidyasagar, K. *J. Chem. Soc., Dalton Trans.***1998**, 3013–3019.

PTue126

Sodium Ion Substitution in Barium Zirconate

Heppke, Eva (Technische Universität Berlin, Berlin, GER); Berendts, Stefan (Technische Universität Berlin, Berlin, GER); Nakhal, Suliman (Technische Universität Berlin, Berlin, GER); Lerch, Martin (Technische Universität Berlin, Berlin, GER)

Alkaline earth zirconates $A\mathrm{ZrO}_3$ (A = Ca, Sr, Ba) crystallize in distorted or ideal cubic Perovskite-structures depending on the ionic ratios. Hereby, the relation between crystal structure and ionic ratios can be described in first approximation by the Goldschmidt tolerance factor.[1] Additionally, different distortions of the ($B\mathrm{O}_6$)-octahedrons within the crystal structure can be expressed by the Glazer nomenclature.[2] However, one key feature of the Perovskite-structure is the tolerance towards cation and anion substitution hereby tailoring the physical-chemical properties resulting in e.g. improved ionic conductivity, electrical polarization or magnetic properties.[e.g. 3]

A new series of sodium ion substituted barium zirconates with the general formula $\mathrm{Na}_x\mathrm{Ba}_{1-x}\mathrm{ZrO}_{3-0.5x}$ (x = 0.2 to 0.4) were prepared by the Pechini method. Hereby, it turned out that sodium substitution is possible up to x = 0.4 without any impurity phase when using the Pechini method as proven by X-ray diffraction and subsequent Rietveld refinement. Furthermore, chemical composition has been determined by X-ray fluorescence spectroscopy (XRF) and the hot gas extraction method (oxygen determination). Additionally, high-temperature X-ray diffraction and simultaneously thermal analysis (TG/DTA) of the precursor mixture revealed different optimal reaction temperatures and reaction times for different sodium contents.

In forthcoming investigations the obtained materials will be characterized by temperature-dependent electrochemical impedance spectroscopy (EIS) to detect possible sodium-, oxygen-or hydrogen-ion conductivity. Furthermore, substitution of the remaining elements (e.g. oxygen by sulfur) and determination of the influence on the obtained crystal structure as also the physical-chemical properties will be carried out.

---

[1] V. M. Goldschmidt, *Naturwissenschaften* 21 (**1926**), 477.
[2] A. Glazer, *Acta Cryst. A* 31 (**1975**), 756.
[3] J. B. Goodenough, *Rep. Prog. Phys.* 67 (**2004**), 1915

PTue127

Some compositions $Pb_{1-x}Ba_x(Zr_yTi_{1-y})O_3$ with very small lead content

TAIBI, Kamel (Faculté de Chimie-USTHB, Alger, DZA)

The complex perovskite AA'(BB')O_3 are known to exhibit normal and/or relaxor ferroelectric behaviour. Many investigations have been devoted to the study of relaxation parameters in such materials in order to achieve their use in capacitors and actuators [1,2]. However, most of these materials are lead-based ceramics which present a disadvantage due to the toxicity of PbO. So, for environmental and health reasons, manufacture of such materials are more and more constrained to eliminate the lead content from these compounds. Therefore, to develop environment friendly materials, great deals of lead free materials or lead reducing compositions were examined. Among these, $Ba(Zr_yTi_{1-y})O_3$ (BZT) or $Pb_{1-x}Bax(Zr_yTi_{1-y})O_3$ (PBZT) ceramics have been found very interesting owing to their attractive ferroelectric performances. However, The first one (BZT) revealed less performant dielectric characteristics, while the second(PBZT)compositions contain relatively high lead content and remain not suitable for environmental devices. In the other hand, the simultaneous Ba-Pb and Zr-Ti substitution give rise to the better dielectric constant in comparison to undoped barium zirconate titanate (BZT). Moreover, these substituted materials were characterized by a decrease in Curie temperature and an increase of room temperature dielectric constant. In this work, we present the results of new compositions of relaxor ferroelectric with very low lead content. The compositions explored were $Ba_{1-x}Pb_x(Zr_yTi_{1-y})O_3$(BPZT) with x=0.025 and y=0.20;0.35. The effects of simultaneous cationic substitution of zirconium for titanium in the B site and of lead for barium in the A site for $BaTiO_3$ perovskite lattice on symmetry and dielectric properties were investigated. Ceramic samples were prepared by conventional mixed oxide method. Room temperature XRD analysis allowed us to determine the limits of solid solution. Dielectric measurements were performed on ceramic disks. For all samples, the temperature (85 -500K) and frequency (10^3-2.10^5 Hz) variations of the dielectric characteristics were investigated. A relaxor-like behavior with frequency dispersion is observed at high Zr content for a very low lead content which is suitable for environment devices applications.

---

[1] K. Uchino, *Ferroelectrics*, 151, 321(1994)
[1] L.E Cross, *Ferroelectrics* , 151, 305 (1994

PTue128

Structural and electrochemical impedance spectroscopic studies of anodic oxide film on zirconium fabricated in different aqueous electrolytes

Jindal, Jitender (Department of Chemistry, M D University, Rohtak, IND); Vema, Naveen (Department of Chemistry, M D University, Rohtak, IND); Singh, Krishan Chander (Department of Chemistry, M D University, Rohtak, IND); Mari, Bernabe (Universitat Politècnica de València, Camí de Vera s/n, 46022 València, Spain, Valencia, ESP)

This work reports on the growth of ZrO_2 films on zirconium in inorganic water-based electrolyte systems containing small amounts of fluoride employing a single step anodization process. observed for ZrO_2, formed in different electrolyte mixture. The barrier films were obtained in 1 M CH_3COOH+ 1 M H_3PO_4 mixture having minute pores with ridges and grooves on the surface, however highly porous spongy structures were obtained in 1 M CH_3COOH + I M H_3PO_4 + 0.2 wt % NaF electrolyte mixture. The film formed in 1 M NaH_2PO_4 + 0.2 wt % NaF was barrier and smooth. The surface morphology was determined by field emission scanning electron microscope (FESEM). The electrochemical properties of such films were investigated by electrochemical impedance spectroscopy (EIS) measurements. After fitting the EIS spectra by an appropriate equivalent circuit, the fitted parameters were determined.

PTue129

Synthesis and Characterization of Alkali Metals-doped Tin Oxide Thin Films by Sol-Gel Process

BENHEBAL, Hadj (University of Ibn-Khaldoun Tiaret, Tiaret, DZA); BENRABAH, Bedhiaf (University of Ibn-Khaldoun Tiaret, Tiaret, DZA); AMMARI, Aek (University of Ibn-Khaldoun Tiaret, Tiaret, DZA); MADOUNE, Yacine (University of Ibn-Khaldoun Tiaret, Tiaret, DZA); KHARROUBI, Abdelmalek (University of Ibn-Khaldoun Tiaret, Tiaret, DZA); KHIALI, Belkacem (University of Ibn-Khaldoun Tiaret, Tiaret, DZA); D. LAMBERT, Stéphanie (University of Liège, Liège, BEL)

In this work, we prepared thin films of tin dioxide SnO2 doped by alkali metals (lithium, sodium and potassium) to 10% by the Sol-gel technology on glass substrates from the tin dichloride dihydrate dissolved in a solution of absolute ethanol. We then performed the structural analysis on the films produced using different characterization techniques such as X-ray diffraction, electric and optical measurements such that the complex impedance spectroscopy, UV-visible, electron microscopy scanning and infrared. The experimental results have verified that the SnO2 thin films deposited are relatively uniform. The structural XRD showed that the deposited films are tetragonal structure. Optical measurements have shown that the layers of doped tin dioxide have a significantly lower optical gap than the undoped tin dioxide.

PTue130

Synthesis and In-situ X-ray Characterization of New, Metastable Cr-Sb Compounds Using Multilayered Thin Films

Regus, Matthias (University of Kiel, Kiel, GER); Mankovsky, Sergiy (Ludwig-Maximilian-University Munich, Munich, GER); Polesya, Svitlana (Ludwig-Maximilian-University Munich, Munich, GER); Barton, Bastian (Johann-Goethe-University Mainz, Mainz, GER); Kolb, Ute (Johann-Goethe-University Mainz, Mainz, GER); Ebert, Hubert (Ludwig-Maximilian-University Munich, Munich, GER); Bensch, Wolfgang (University of Kiel, Kiel, GER)

In thin multilayered films the diffusion length can be reduced dramatically which influences the reaction mechanism of a solid state reaction. The reaction mechanism changes from a diffusion-controlled to a nucleation-controlled process providing a repeating unit with sufficiently thin layers. [1, 2] Consequently new, metastable crystalline compounds can be obtained if the suitable reactions conditions are applied. [3, 4]Thin films with a Cr:Sb ratio of around 1:3 were made in an ultrahigh vacuum system using the layer-by-layer and co-deposition techniques. The characterization was done by in-situ X-ray reflectivity and X-ray diffraction experiments (XRR/XRD), energy dispersive X-ray spectroscopy (EDX) and transition electron microscopy (TEM).In the as-deposited state the samples are almost amorphous. Thermodynamic stable CrSb2 and additional Sb crystallizes at 120 °C in films with a (Cr/Sb) repeating unit of d $\geq$ 40 Å whereas a new (metastable) antimony-rich compound CrSb3 is formed in samples with thinner (Cr/Sb) double-layers (~8 Å) or co-deposited films containing 75 at-% Sb. This new phase decomposes into CrSb2 and elemental Sb at about 220 °C (Fig. 1). The crystal structure of the new phase seems to be related to orthorhombic LaCrSb3 (space group: Pbcm). [5] Our experimental results are supported by computational investigations, e.g. total energy calculations for phase stability. The orthorhombic structure seems to be preferred among other structure types considering a ferromagnetic ground state.

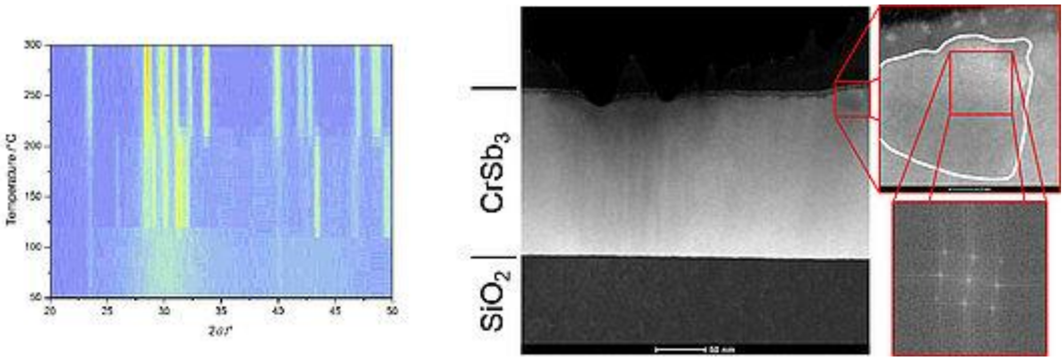

Fig. 1: Temperature-resolved in-situ XRD measurements of a film with a (Cr/Sb) repeating unit thickness of ~8 Å and 75 at-% Sb (left) and a HRTEM image including a calculated electron diffraction pattern (FFT) of a lamella from a similar, co-deposited sample (right).

---

[1] Johnson, D. C., Controlled synthesis of New compounds using modulated elemental reactants. Current Op. Solid State & Materials Sc. 1998, 3, 159–167.

[2] Johnson, C. D., Noh, M., Sellinschegg, H., Schneimiller, R., Johnson, D. C., Handbook of nanostructured materials and nanotechnology: Kinetic control of inorganic solid-state reactions resulting from mechanistic studies using elemental reactants, 2000.

[3] Williams, J. R., Johnson, M., Johnson, D. C., Composition Dependence of the Nucleation Energy of Iron Antimonides from Modulated Elemental Reactants. J. Am. Chem. Soc. 2001, 123, 1645–1649,

[4] Regus, M., Kuhn, G., Polesya, S., Mankovsky, S. et al., Experimental and theoretical investigation of the new, metastable compound Cr3Sb. Z. Kristallogr. 2014, 229, 505–515, DOI: 10.1515/zkri-2014-1744.

[5] Raju, N. P., Greedan, J. E., Ferguson, M. J., Mar, A., LaCrSb 3: A New Itinerant Electron Ferromagnet with a Layered Structure. Chem. Mater. 1998, 10, 3630–3635, DOI: 10.1021/cm9803758.

PTue131

Synthesis and characterization of mixed-metal silicophosphates

Shaqiri, Halil (Bonn University, Bonn, GER); Glaum, Robert (Bonn University, Bonn, GER)

A systematic crystal-chemical analysis of various silicophosphate structures was presented by *Schöneborn* [1]. Typical structural feature in silicophosphates $M_4[Si_2O(PO_4)_6]$ (M: Ti [1], V [2], Cr [3], Fe [4], In [5], Mo [6]) and several others are heteropolyanions $[Si_2O(PO_4)_6]^{12-}$. Remarkable are also $[M_2O_9]$ double-octahedra giving rise to direct metal-metal bonding in $Mo_4[Si_2O(PO_4)_6]$ and $Ti_4[Si_2O(PO_4)_6]$.
In our contribution we report on synthesis and characterization of several new heterometallic silicophosphates $M^{III}{}_4[Si_2O(PO_4)_6]$.

For synthesis of the silicophosphates different starting materials, according to eq. 1 to 3, were used. By isothermal heating finely ground reaction mixtures at 1000 °C for 3 to 4 weeks in sealed silica tubes microcrystalline powders were obtained. The incorporation of silica was achieved by chemical vapour transport from the wall of the tubes. Crystals were obtained by adding $PtCl_2$ and NH_4Cl forming in situ HCl as mineralizer.

$3/4\ MPO_4 + 22/9\ TiP_2O_7 + 4/9\ TiO_2 + 13/36\ TiP + 2\ SiO_2 \rightarrow Ti_{3.25}M_{0.75}[Si_2O(PO_4)_6]$ (M: Cr, Fe) (1)
$Fe(PO_3)_3 + 12/11\ Mo_2P_2O_{11} + 9/11\ MoP + 2\ SiO_2 \rightarrow Mo_3Fe[Si_2O(PO_4)_6]$ (2)
$(1\text{-}x)\ M_4(P_2O_7)_3 + xM'_4(P_2O_7)_3 \rightarrow (M_{1-x}M'_x)_4[Si_2O(PO_4)_6]$ (M, M': Fe, Cr, V) (3)

Surprisingly, dark blue $Ti_{3.25}Fe_{0.75}[Si_2O(PO_4)_6]$ (P-3, $Z = 3$, $a = 14.6658(2)$ Å, $c = 7.3837(1)$ Å) shows no homogeneity range with respect to the ratio Fe/Ti. Similarly, the silicophosphates $Ti_{3.25}Cr_{0.75}[Si_2O(PO_4)_6]$ ($a = 14.5887(8)$ Å, $c = 7.3886(4)$ Å) and $Mo_3Fe[Si_2O(PO_4)_6]$ ($a = 14.6845(9)$ Å, $c = 7.4384(7)$ Å) show no homogeneity range. Conversely, for the silicophosphates $(Fe_{1-x}Cr_x)_4[Si_2O(PO_4)_6]$, $(Fe_{1-x}V_x)_4[Si_2O(PO_4)_6]$ and $(Cr_{1-x}V_x)_4[Si_2O(PO_4)_6]$ complete miscibility ($0 \leq x \leq 1$) was observed with Vegard behavior of unit cell volume and lattice parameters.

The crystal structure of $Ti_{3.25}Fe_{0.75}[Si_2O(PO_4)_6]$ (P-3, $Z = 3$, 170 param., 4023 ind. ref., R1 = 0.029, wR2 = 0.079, Goof = 1.080) was refined from a twinned dataset (Dauphiné-Law [7]). The structure is built from face-sharing double octahedra $[M1M2O_9]$ and linear $[Si_2O_7]$ groups. These polyhedra are linked by $[PO_4]$ tetrahedra thus forming the $[Si_2O(PO_4)_6]^{12-}$ heteropolyanions. While $M1$ is exclusively occupied by titanium, for $M2$ mixed occupancy $Ti_{0.62}Fe_{0.38}$ was found.
The double octahedra exhibit asymmetric "out-of-centre" distortion of the metal cations due to electrostatic repulsion. It is noteable, that the corresponding distances $d(M1\text{-}O)$ are elongated by about 0.1 Å in comparison to the M2 site. Based on the ionic radii this leads us to the assumption of homoatomic Ti^{3+}/Ti^{4+} occupancy of site $M1$ site and heteroatomic Ti^{3+}/Fe^{2+} occupancy of site $M2$. The observed, rather short distance d(M1-M2) = 2.88 Å suggests attractive interaction besides the electrostatic repulsion between M1 and M2. The dark blue colour is presumably due to an intervalence charge transfer as in Ilmenite FeTiO3 [8].

---

[1] M. Schöneborn, *PhD Thesis*, Univ. of Bonn **2008**.
[2] A. Leclaire, H. Chaboun, D. Groult, B. Raveau, *J. Solid State Chem.***1986**, *65*, 168.
[3] R. Glaum, *PhD Thesis*, Univ. of Giessen **1990**.
[4] M. Gruß, *PhD Thesis*, Univ. of Giessen **1998**.
[5] M. Hanawa, T. Kobayashi, H. Imoto, *Z. Anorg. Allg. Chem.***2000**, *626*, 216.
[6] A. Leclaire, M. Lamire, B. Raveau, *Acta Cryst.***1988**, *C44*, 1181.
[7] W. Kleber, "*Einführung in die Kristallographie*", Verlag Technik, Berlin, **1985**.
[8] T. F. R. Barth, E. Posnjak, *Z. Kristallogr.* **1934**, 88, 265-270.

PTue132

Synthesis, characterization of ZnO and Ag-doped ZnO : Application in photocatalytic degradation of endocrine disrupting under UV irradiation

Sayadi, Sami (Laboratoire de Bioprocédés Environnementaux. , Sfax, TUN); Najjar, Wahiba (Laboratoire de Chimie des Matériaux et Catalyse., Tunis, TUN); Bechambi, Olfa (Laboratoire de Chimie des Matériaux et Catalyse, Faculté des Sciences de Tunis, Tunis, TUN); Ksibi, Zouhaier (Laboratoire de Chimie des Matériaux et Catalyse, Faculté des Sciences de Tunis, Tunis, TUN)

Zinc oxide, a typical kind of II–IV compound semiconductor with a wide band gap (3.37 eV) and a large excitation binding energy of 60 meV has garnered much attention owing to its wide potential applications in luminescence, in optics, optoelectronics, sensors, actuators, energy and biomedical sciences, and spintronics [1]. ZnO has been widely used as a photocatalyst, owing to its high activity, low cost, and environmentally friendly feature d in gas and liquid phase pollution control [2]. But the efficiency of photocatalytic degradation by ZnO should be further improved in order to meet the requirements of environmental protection.

In this work, we have successfully prepared ZnO modified oxide with various contents of silver through the hydrothermal method. Furthermore, the samples characterisation was investigated using X-ray diffraction (XRD), Nitrogen physisorption at 77K; Fourier transformed infrared spectroscopy (FTIR), UV-Visible spectroscopy and Photoluminescence spectra (PL).

Especially, the influences of Ag percentage used as dopant on the textural, structural and optical properties of the prepared catalysts have been emphasized. The photocatalytic performance of the prepared Ag-ZnO samples with various Ag contents for degradation of bisphenol A (BPA) and nonylphenol (NP) was also investigated.

Ag-doping does not change the average crystallite size with the low content of Ag and decrease with high content of Ag. The specific surface area (S_{BET}) calculated by BET method increases with increasing the Ag content. The band gap values of ZnO are slightly decreased with the increase of the Ag doping level.

The total organic carbon analysis was chosen as a mineralization index to characterize the endocrine disrupting degradation. The TOC conversion of both BPA and NP solutions over Ag doped ZnO catalysts under UV irradiation show that 1% Ag-doped ZnO exhibits the highest photocatalytic activity attributed to the most efficient charge separation proves with PL spectra . Thus, the presence of a proper content of silver can reduce electron–hole recombination and increase the photocatalytic activity.

PTue133

The First Europium(II) Oxide Hydride Iodide

Rudolph, Daniel (University of Stuttgart, Stuttgart, GER); Schleid, Thomas (University of Stuttgart, Stuttgart, GER)

Single crystals of the first europium(II) oxide hydride iodide with the composition $Eu_5O_2H_2I_4$ emerged from the reaction of equimolar amounts of oxygen-contaminated europium dihydride and europium diiodide in a sodium-iodide flux at 900 °C. The new compound crystallizes isotypically to the corresponding barium-analog $Ba_5O_2H_2I_4$ [1] in the orthorhombic space group *Cmcm* with four formula units per unit cell. The cell parameters are a = 1636.97(9) pm, b = 1369.54(7) pm and c = 604.36(3) pm at T = 100 K.

After a single-crystal X-ray diffraction measurement at ambient temperature and the following structure solution and refinement, the measurement was repeated at 100 K, because the crystal structure exhibited disordered iodide anions and there was hope to “freeze” the structure into an ordered variant at lower temperatures. However, the crystal structure obtained from the data collected at 100 K still contained disordered iodide anions, but for the description of the disorder just two instead of three partially occupied iodine positions were needed. Of course, the crystal structure was tried to solve in suitable sub-groups of *Cmcm*, but the iodine disorder remained. The presence of a merohedric twin was also contemplated, but rejected by means of symmetry considerations. It is also possible that the crystal structure can only be described properly with an incommensurate modulation.

In the crystal structure of $Eu_5O_2H_2I_4$ there are three crystallographically different Eu^{2+} cations. $(Eu1)^{2+}$ is surrounded by four hydride and four iodide anions forming a distorted square antiprism with Eu1–H distances of 243 pm and Eu1–I distances of 341 and 349 pm. The $(Eu2)^{2+}$ cation is coordinated by eight anions as well forming a distorted square antiprism, but now one of the two basal planes is built by two hydride (d(Eu2–H) = 251 pm) and two oxide anions (d(Eu2–O) = 239 pm). This distance corresponds very well to the Eu–O distances observed in europium(II) oxide iodides like Eu_4OI_6 (d(Eu–O) = 240 pm) [2] and Eu_2OI_2 (d(Eu–O) = 239 pm) [3]. The Eu2–I distances in $Eu_5O_2H_2I_4$ range between 341 and 365 pm.

The third Eu^{2+} cation is surrounded by four iodide anions being located on two fully occupied positions (Eu3–I distances: 343 and 384 pm) and by two oxide anions at a distance of 233 pm, which is amazingly short for a Eu(II)–O contact. This could be due to the completion of the coordination sphere of $(Eu3)^{2+}$ by the disordered iodide anions being on two partially occupied positions. The Eu3–I distances lie within an interval from 324 to 395 pm. The separations between the disordered iodide anions on the partially occupied positions range between 84 and 262 pm, thus being far too short to justify full occupation at the same time. By taking the refined occupation factors into account, in average two iodide anions are added to the coordination sphere of $(Eu3)^{2+}$ resulting in a coordination number of eight as well.

The crystal structure of $Eu_5O_2H_2I_4$ consists of hydride- and oxide-centered $(Eu^{2+})_4$ tetrahedra that are interconnected via common edges to form infinite columns parallel to the c axis. The building block in these columns along the a axis is composed of four *trans*-edge connected tetrahedra, namely two hydrogen-centered ones in the inner part of the columns and two oxygen-centered ones representing the outer side. These columns are separated by the disordered iodide anions along [100] and by the ordered ones along [010]. Parallel to the ab plane the columns are stacked like bricks in a wall with the iodide anions serving as mortar in between.

---

[1] O. Reckeweg, F. J. DiSalvo, *Z. Naturforsch.* **66 b** (2011) 21–26.

[2] L. Wuping, R. Dronskowski, *Acta Crystallogr.* **C 60** (2004) i23–i24.

[3] S. Hammerich, G. Meyer, *Z. Anorg. Allg. Chem.* **632** (2006) 1244–1246.

PTue134

The Incorporation of Lithium and Silicon Cations in Yttrium Tungstate

Schustereit, Tanja (Universität Stuttgart, Institut für Anorganische Chemie, Stuttgart, GER); Schleid, Thomas (Universität Stuttgart, Institut für Anorganische Chemie, Stuttgart, GER); Hartenbach, Ingo (Universität Stuttgart, Institut für Anorganische Chemie, Stuttgart, GER)

The synthesis of yttrium fluoride tungstate YF[WO_4] [1,2], a material of interest as host lattice for luminescence applications, comprises a final recrystallization step by heating the nanostructured crude product to elevated temperatures, which need to be higher than 900 °C if no flux is used. In order to reduce the applied temperature various experiments with an abundance of different fluxing agents were carried out, during which some interesting by-products were found. The desired product, however, was not yielded as crystalline phase so far. $LiY_5[SiO_4]_2[WO_4]_4$ represents one of these by-products, emerging from a recrystallization attempt using LiCl as flux and evacuated silica ampoules as container, which were attacked by the F^- anions and the Li^+ cations present in the reaction mixture. The title compound crystallizes orthorhombically in space group *Pban* with a = 512.08(4) pm, b = 1673.68(12) pm, c = 493.68(4) pm and Z = 1. Besides crystallographically unique tetrahedral $[SiO_4]^{4-}$ and $[WO_4]^{2-}$ units, the structure contains two cationic positions. While the *Wyckoff* position 2*c* is exclusively occupied by $(Y2)^{3+}$ cations, at 4 *i* both Li^+ and $(Y1)^{3+}$ cations in a 1:3 molar ratio are located. Both the cations at 2*c* and 4*i* are surrounded by eight oxide anions in the shape of trigonal dodecahedra (d_{avg}(Li/Y1−O) = 240.9 pm, d_{avg}(Y2−O) = 233.5 pm). The $[SiO_4]^{4-}$ anions exhibit 222 symmetry, thus besides four equal Si−O distances of 165.4 pm, minor angular deviations of 107 and 113° from the ideal tetrahedral angle (109.5°) are detected. The tungstate groups (symmetry: .2.) on the other hand are far from ideality, since besides four short W−O distances of 179 and 182 pm two longer ones with values of 237 pm are found, which can explain the highly stretched O2−W−O2 angle of 142° with the $(O3)^{2-}$ anions, which represent the two ligands with the long distances, widening the $[WO_4]^{2-}$ tetrahedra at that position. The polyhedra around $Li^+/(Y1)^{3+}$ and the tungstate units build up double layers according to 2D-$\{(Li/Y1)_2W_2O_{16}\}$ parallel to the *ac* plane with the $[Li/(Y1)O_8]^{13.5-}$ polyhedra being interconnected with each other via common edges and attached to the $[WO_4]^{2-}$ entities by common vertices, if the aforementioned two longer distances are not taken into account. Otherwise their connection is realized by vertices and edges. These double layers are stacked alternatingly with single layers parallel to (010) as well, constructed by $[(Y2)O_8]^{13-}$ and $[SiO_4]^{4-}$ groups, which are also vertex-connected to each other according to 2D-$\{(Y2)SiO_8\}$. The interconnection of the different layers occurs via the $[Li/(Y1)O_8]^{13.5-}$ and the $[(Y2)O_8]^{13-}$ units, also sharing common edges, showing the same structural setup as the $[CaO_8]^{14-}$ polyhedra in *scheelite*-type Ca[WO_4] [3]. This is also true for the exclusive vertex connection of the tetrahedral units $[WO_4]^{2-}$ and $[SiO_4]^{4-}$ to the trigonal oxygen dodecahedra around the alkali-, alkaline earth-, and rare-earth metal cations in these structures. However, the enlargement of the coordination sphere around the W^{6+} cations is similar to that in the *fergusonite*-type rare-earth metal tantalates [4].

---

[1] T. Schustereit, Th. Schleid, I. Hartenbach, *Z. Anorg. Allg. Chem.* **2014**, *640*, 2351.

[2] T. Schustereit, *Doctoral Thesis*, University of Stuttgart **2015**.

[3] R. G. Dickinson, *J. Am. Chem. Soc.***1920**, *42*, 85.

[4] I. Hartenbach, F. Lissner, T. Nikelski, S. F. Meier, H. Müller-Bunz, Th. Schleid, *Z. Anorg. Allg. Chem.***2005**, *631* , 2377.

The new borosulfates $Cs_2B_2S_3O_{13}$ and $Cs_3HB_4S_2O_{14}$ – on the way to the structure of vitreous B_2O_3?

Daub, Michael (Institut für Anorganische Chemie, Freiburg, GER); Hillebrecht, Harald (Institut für Anorganische Chemie, Freiburg, GER)

Recently, we reported on the first borosulfates [1-4]. Their crystal structures show a close similarity to silicates, because in all cases there are BO_4- and SO_4-tetrahedra which are linked by common corners to silicate-like building units. Because the ratio of BO_4- and SO_4-tetrahedra is between 1:4 and 1:2 a linkage between two BO_4 tetrahedra can be avoided. This is not the case for the new Cs-borosulfates. $Cs_2B_2S_3O_{13}$ is formed from B_2O_3 and CsCl in oleum at 300°C as colorless hygroscopic crystals. $Cs_3HB_4S_2O_{14}$ was obtained in small amounts as a by-product from the synthesis of $Cs[B(S_2O_7)(SO_4)]$ [2]. Both compounds were chacaterised by powder-XRD, vibrational spectra and a structure analysis. The structure of $Cs_2B_2S_3O_{13}$ or $Cs_2(B_2O)(SO_4)_3$ ($P2_1/c$, Z = 4, a = 1476.5(3), b = 671.0(1), c = 1252.8(3) pm, β = 104.60(3)°) contains layers of corner-sharing BO_4- and SO_4-tetrahedra. The BO_4-tetrahedra form dimers and with two additional SO_4 tetrahedra rings containing 10 tetrahedra. A third SO_4-tetrahedron connects two BO_4-tetrahedra of a B_2O_7 unit. The layers are stacked in direction [100]. One Cs-cation is located within the layer of thetrahedra, the second one between the layers.

In $Cs_3HB_4S_2O_{14}$ or $Cs_3H(B_2O_3)_2(SO_4)_2$ ($P6_3/m$, Z = 2, a = 656.48(2), c = 1956.69(5) pm) the SO_4-tetrahedra are isolated. Boron forms planar layers of corner-sharing tigonal-planar BO_3-units. There are two different types of BO_3-units in a ratio 3:1. The first type forms six-membered boroxol-rings B_3O_3 which are connected to layers by the second type of BO_3-units. The layers are separated by isolated SO_4 tetrahedra and Cs-cations. The "missing" proton could not be localised but was assumed to achieve electroneutrality and shows up as a O-H mode in the IR spectrum.

Both crystal structures continue the series of borosulfates to more borate-rich representatives, which result in an increased degree of condensation of the boron polyhedra. In the case of $Cs_2(B_2O)(SO_4)_3$ we observed for the first time a direct linkage of BO_4-tetrahedra to a dimeric unit B_2O_7. This motif was already known for borophosphates [5]. For $Cs_3H(B_2O_3)_2(SO_4)_2$ there is a complete separation of sulfate and borate units to isolated SO_4-tetrahedra and a planar layer B_2O_3.

Recently, Ferlat et al. [6] proposed two structure models for vitreous B_2O_3. They consist of planar layers of corner-sharing trigonal-planar BO_3-units, which were derived from a graphite-like layer. One model based on six-membered boroxol-rings, the other on BO_3 units. The B_2O_3-layer in $Cs_3H(B_2O_3)_2(SO_4)_2$ combines both motifs in equal shares, i.e. the different boron atoms are in a ratio 3:1. This ratio was already determined for vitreous B_2O_3 by the same group [7]. Therefore, the B_2O_3-layer in $Cs_3H(B_2O_3)_2(SO_4)_2$ can be considered as an crystalline model structure for viteous B_2O_3.

---

[1] H. Höppe, et al. *Angew. Chem.***2012**, *124*, 6359, *Angew. Chem. Int. Ed.***2012**, *51*, 6255.
[2] M. Daub et al. *Chem. Eur. J.***2013**, *19*, 16954.
[3] M. Daub et al. *Inorg. Chem.***2013**, *52*, 6011.
[4] M. Daub et al. *Z. Anorg. Allg. Chem.* **2014**, *640*, 2914.
[5] R. Kniep et al. *Chem. Mater.* **1998**, *10*, 2930; *Z. Anorg. Allg. Chem.***2007**, *633*, 1517.
[6] G. Ferlat et al. *Nature materials* **2012**, *11*, 925.
[7] G. Gerlat et al. *Phys. Rev. Lett.***2008**, *101*, 065504.

PTue136

Thermochemistry of New Anode Materials based on the Li-Si-O System for Li-Ion Batteries

Cupid, Damian (Karlsruhe Institute of Technology, Eggenstein-Leopoldshafen, GER)

Rechargeable lithium ion batteries are viable energy sources for electric vehicles and are also considered as vital components for smart energy grids of the future. Technological developments in Li-ion batteries have up to now focused on improving properties such as capacity, cyclability, lifetime, and safety. One way to improve the electrochemical properties is by finding new, environmentally friendly cathode and anode materials combinations which meet the aforementioned criteria.

Graphite, which has a maximum lithium storage capacity of 372 mAh/g, is currently the most widely used negative electrode material. Although Si is expected to have much higher capacities (4200mAh/g), the large volume changes which occur during lithiation/de-lithiation of pure Si leads to destruction of particle to particle contacts, electrode degradation, and poor cycling stability. One solution to reduce the volume expansion of Si anodes is by embedding nano-crystalline Si in an amorphous SiO matrix. For example, Miyachi [1] reported an initial charge capacity of 2400mAh/g for amorphous Si-O anodes corresponding to formation of a Li-Si alloy, Li-silicates and lithium oxide during lithiation.

Phase diagrams in the Li-Si-O system are essential to determine the optimal synthesis conditions of new anode materials as well as to understand phase formation and reactions during electrochemical cycling. The experimentally determined phase diagram data can also be combined with measured thermochemical data to develop a self-consistent thermodynamic description of the Li-Si-O system using the CALPHAD method to calculate open circuit voltages and coulometric titration curves at operating temperatures. The aim of our work is therefore to directly measure thermochemical and thermodynamic properties of key compounds in the Li-Si-O system.

The Li_2O-SiO_2 isopleth in the Li-Si-O system is of particular interest since all known $Li_xSi_yO_{x/2+2y}$ oxides can be found on this vertical section. In this work, commercially based $Li_xSi_yO_{x/2+2y}$ compounds were analyzed using powder-XRD and ICP-OES. The phase transformation temperatures of key $Li_xSi_yO_{x/2+2y}$ oxides in Ar and Ar/20vol.%O_2 atmospheres were determined using a combination of DTA/TGA. Heat capacities of selected compounds were measured using DSC with the continuous and step methods. Additionally, the enthalpies of drop solution of the compounds were measured using high-temperature oxide melt drop solution calorimetry performed at 700°C to be able to determine the standard enthalpies of formation of the compounds from the binary oxides and constituent elements.

---

[1] Miyachi, M., et al., Analysis of SiO Anodes for Lithium-Ion Batteries. J. Electrochem. Soc., 2005. 152(10): p. A2089-A2091.

Oxygen dynamics in $BaFeCl_{0.130(2)}O_{2.50(2)}$

Parras, Marina (Universidad Complutense de Madrid, Departamento de Química Inorgánica I, Madrid, ESP); García-García, Francisco Javier (ICTS-Centro Nacional de Microscopía Electrónica, Madrid, ESP); Serrador, Laura (Universidad Complutense de Madrid, Departamento de Química Inorgánica I, Madrid, ESP); Varela, Aurea (Universidad Complutense de Madrid, Departamento de Química Inorgánica I, Madrid, ESP); Hernando, María (Universidad Complutense de Madrid, Departamento de Química Inorgánica I, Madrid, ESP); González Calbet, José María (Universidad Complutense de Madrid, Departamento de Química Inorgánica I/ICTS-Centro Nacional de Microscopía Electrónica, Madrid, ESP)

Oxides with the perovskite structure type, either cubic or hexagonal, are studied in many respects [1]. Most of the times, the idea is to slightly modify the composition to look at the effect in the associated properties. That is possible due to the fact that the basic structures are inherently flexible [2] and then we are forced to treat them as modulated structures.

One possible way to modify the structure and composition is by introducing halides in the anion sublattice and in this communication we present our results in a crystalline phase with composition $BaFeCl_{0.130(2)}O_{2.50(2)}$ and a 10H-polytype structure type [3]. We have succeeded to prepare this compound as a single phase and therefore the magnetic properties have been studied. This compound is thermally stable up to ≈ 900ºC and it does softly lose oxygen on the heating experiments. The final composition is $BaFeCl_{0.130(2)}O_{2.34(2)}$ and the high resolution electron microscopy study reveals that the structure is undistorted.

Furthermore, when the sample is further heated the 10H phase disappears and a high temperature phase with a 4H-polytype structure type condense out. This is a very interesting case of an incommensurately modulated structure which it is also found to intergrowth with a cubic perovskite structure type. The composition is ≈ $BaFeCl_{0.13}O_{2.24}$ and like this, the whole process of transformation has to do with the oxygen content, while the ratio Ba/Fe/Cl keeps constant.

---

[1] R.H. Mitchell, Perovskites: Modern and Ancient, Almaz Press, Thunder Bay, Ontario, 2002.

[2] R.L. Withers, S. Schmid, J.G. Thompson, Prog. Solid St. Chem., 26, 1-96, 1998.

[3] M. Iorgulescu, P. Roussel, N. Tancret, N. Renault, F. Porcher, G. André, H. Kabbour, O. Mentré, 51, 7598-7608, 2012

Identification of n-type and p-type transparent conducting materials from first-principles

Villesuzanne, Antoine (IREET, University of Bolton, Bolton, GBR); Dutson, James (Plasma Quest Limited, Hook, GBR); Guo, Meilan (IREET, University of Bolton, Bolton, GBR); Twaithes, Michael (Plasma Quest Limited, Hook, GBR); Guosheng, Shao (IREET, University of Bolton / China Centre for Multi-Functional Nanomaterials, Zhengzhou University, Bolton, GBR)

Two important challenges for the design of transparent conducting oxides (TCOs) are i) the replacement of tin-doped indium oxide (ITO) due to indium scarcity and high cost, and ii) the identification of p-type TCOs. In the latter, the difficulties lie in avoiding compensating defects for charge carriers (holes) and on the high effective mass of holes, due to the flatness of the top of valence bands. For n-type TCOs, doping tin dioxide SnO_2 either with fluorine or antimony allows achieving performances comparable to ITO; however, it is highly desirable to identify more environmental-friendly formulations, avoiding those elements as dopants.

First, we have investigated the reliability of several exchange-correlation functional schemes within density functional theory (DFT), namely the generalized gradient approximation (GGA), the Tran-Blaha modified Becke-Johnson approach (TB-mBJ) and the so-called PBE0 and HSE06 hybrid schemes, as implemented in the VASP code, for the calculation of effective masses in pristine SnO2. The DFT/PBE0 hybrid scheme allowed obtaining band gap and effective masses in excellent agreement with experimental values and was retained for the subsequent calculations on doped systems, using 2x2x2 supercells. The TB-mBJ scheme can be parametrized to fit the experimental band gap in SnO_2, but the values for effective masses (band dispersion) led to only qualitative agreement with experiment.

Hybrid DFT/PBE0 calculations were then performed to investigate the effect of transition metal (n-type) doping in SnO_2, and trivalent element doping to achieve p-type conductivity. Non-oxide formulations were tested as well, and the carrier mobility was estimated based on the Bardeen-Shockley acoustic phonon-scattering model, which involves the calculation of bulk moduli and deformation potentials.

Depending on the nature of the transition metal involved, either deep impurity levels are found in the band gap (impeding transparency) or efficient n-type doping can be achieved when the transition metal d bands lie above the bottom of the Sn-character conduction band, while preserving both low effective masses and appropriate band gap for transparency in the visible spectrum. Promising results are found as well for candidates as p-type transparent conductors, in terms of low effective masses.
The thin-film deposition and characterization of the promising formulations are in progress; preliminary results will be presented.

Author Index

Participants

ABBAS	Hussien	hu_abbas2005@yahoo.com
ABDMEZIEM	Kaïssa	abdmeziemk@gmail.com
ABRIKOSOV	Igor A.	igor.abrikosov@ifm.liu.se
ALFAIFI	Bandar	ba283@exeter.ac.uk
AMANO-PATINO	Midori	midori.amanopatino@chem.ox.ac.uk
AMARA	Sif-Eddien	sifamara@hotmail.com
AMARA-ADNANE	Leïla	l_adnane@yahoo.fr
ANDRE	Rémi	remi.andre@kep-technologies.com
ANIMITSA	Irina	irina.animitsa@urfu.ru
ASABINA	Elena	elena.asabina@inbox.ru
ASSENMACHER	Wilfried	assenmacher@uni-bonn.de
ATTFIELD	J. Paul	j.p.attfield@ed.ac.uk
AZIBI	Mourad	a_mourad1983@yahoo.fr
BADER	Rosa	Rosa.Bader@plansee.com
BAE	Su-whan	suwhanbae@gmail.com
BANG	Seong-eun	kighfk@naver.com
BATTLE	Peter	peter.battle@chem.ox.ac.uk
BATUK	Dmitry	dmitry.batuk@uantwerpen.be
BELIK	Alexei	alexei.belik@nims.go.jp
BENDE	David	david.bende@cpfs.mpg.de
BENNETT	Matthew	mj.bennett@hotmail.co.uk
BENSCH	Wolfgang	wbensch@ac.uni-kiel.de
BERENDTS	Stefan	berendts@tu-berlin.de
BERTHEBAUD	David	david.berthebaud@ensicaen.fr
BERTINI	Vittorio	a1200446@unet.univie.ac.at
BERTSCHLER	Eva-Maria	Eva-Maria.Bertschler@cup.uni-muenchen.de
BEUTL	Alexander	alexander.beutl@univie.ac.at
BIMASHOFER	Gesara	sonja.g.bimashofer@gmx.at
BIZO	Liliana	lbizo@chem.ubbcluj.ro
BLACK	Ashley P.	ablack@icmab.es
BLANDY	Jack	jack.blandy@chem.ox.ac.uk
BLAZQUEZ ALCOVER	Ignacio	iblazquezalcover@gmail.com
BOEHM	Marie Lisa	mali_boehm@hotmail.com
BOLLER	Herbert	herbert.boller@aon.at
BOS	Jan-Willem	j.w.g.bos@hw.ac.uk
BOUTAMINE	Sultana	sultanadz@yahoo.fr
BOUYON	Tracy	tracy-christ.bouyon-yenda@etu.univ-amu.fr
BRANDSTÄTTER	Harald	harald.brandstaetter@tugraz.at
BREUER	Stefan	breuer@tugraz.at
BUM JAE	Lee	bjlee@cnu.ac.kr
CARIO	Laurent	laurent.cario@cnrs-imn.fr
CASCALES	Concepción	ccascales@icmm.csic.es
CASSIDY	Simon	simon.cassidy@chem.ox.ac.uk
CASTILLO	Rodrigo	castillo@cpfs.mpg.de
CHADWICK	Alan	a.v.chadwick@kent.ac.uk
CHEN	Min	min.chen@smn.uio.no

CHEREPANOV	Vladimir	v.a.cherepanov@urfu.ru
CHEZHINA	Natalia	chezhina@nc2490.spb.edu
CHOI	Yeon-Hee	dugm4041@nate.com
CIOBANU	Carmen Steluta	ciobanucs@gmail.com
CLARKE	Simon	simon.clarke@chem.ox.ac.uk
CLEMENS	Oliver	oliver.clemens@kit.edu
COOMER	Fiona	fiona.coomer@stfc.ac.uk
CUPID	Damian	damian.cupid@kit.edu
CUSSEN	Eddie	edmund.cussen@strath.ac.uk
DAVIERO	Sylvie	sylvie.daviero@univ-lille1.fr
DE LAUNE	Benjamin	b.delaune@bham.ac.uk
DE NEGRI	Serena	serena.denegri@unige.it
DE SOUSA FILHO	Paulo Cesar	pcsfilho@usp.br
DEISEROTH	Hans-Joerg	deiseroth@chemie.uni-siegen.de
DELAHAYE	Emilie	emilie.delahaye@ipcms.unistra.fr
DELSANTE	Simona	simona.delsante@unige.it
DERINGER	Volker	volker.deringer@ac.rwth-aachen.de
DONHAUSER	Hermann	h.donhauser@prager-elektronik.at
DRISCOLL	Laura	LLD788@bham.ac.uk
DRISS	Dalel	dalel.driss@cnrs-imn.fr
DUNST	Andreas	andreas.dunst@tugraz.at
DURACH	Dajana	daduch@cup.uni-muenchen.de
DUTTON	Sian	sed33@cam.ac.uk
EBNER	Gabriela	gabriela.ebner@goech.at
EFFENBERGER	Herta Silvia	herta.silvia.effenberger@univie.ac.at
EPP	Viktor	viktor.epp@tugraz.at
EREMETS	Mikhail	
EVANS	Ivana	ivana.radosavljevic@durham.ac.uk
EVANS	John	john.evans@durham.ac.uk
FARGER	Pierre	pierre.farger@ipcms.unistra.fr
FARIA	Rodolfo	faria@cpfs.mpg.de
FELDMANN	Claus	claus.feldmann@kit.edu
FELDMANN-LEBEN	Christiane	c.leben@gmx.de
FENG	Xianjuan	Xianjuan.Feng@cpfs.mpg.de
FJELLVÅG	Helmer	helmerf@kjemi.uio.no
FLANDORFER	Hans	hans.flandorfer@univie.ac.at
FOP	Sacha	r01sf12@abdn.ac.uk
FRAENKL	Max	st44390@student.upce.cz
FRANCESCONI	Maria Grazia	m.g.francesconi@hull.ac.uk
FREI	Maren	maren.frei@cpfs.mpg.de
FRIEDRICH	Daniel	daniel.friedrich@chemie.uni-regensburg.de
FUHRMANN	Gerda	gerda.fuhrmann@uibk.ac.at
FÜRTAUER	Siegfried	siegfried.fuertauer@univie.ac.at
GARCÍA-GARCÍA	Francisco Javier	javier.garcia@cnme.es
GEHRINGER	Friedrich	friedrich.gehringer@univie.ac.at
GILYOV	Artyom	a.r.gilyov@gmail.com
GLÄTZLE	Matthias	matthias.glaetzle@uibk.ac.at
GREAVES	Colin	c.greaves@bham.ac.uk

GREBENEV	Vadim	vadim_grebenev@mail.ru
GRIN	Juri	carolin.grotz@mytum.de
GROTZ	Carolin	carolin.grotz@mytum.de
GU	Mong-Wen	d02223141@ntu.edu.tw
GUESDON	Anne	anne.guesdon@ensicaen.fr
GULO	Fakhili	fgulo@unsri.ac.id
HÄBEL	Jan-Peter	jhaebel@uni-bonn.de
HAGEN	Anke	anke@dtu.dk
HALAKE	Shobha	sm.paragond@gmail.com
HANK	Zakia	z_hank@yahoo.fr
HANZU	Ilie	hanzu@tugraz.at
HARM	Sascha	sascha.harm@cup.uni-muenchen.de
HARTENBACH	Ingo	hartenbach@iac.uni-stuttgart.de
HASEGAWA	Masashi	hasegawa@numse.nagoya-u.ac.jp
HAUMANN	Sebastian	Sebastian.Haumann@chemie.uni-
HÄUSSERMANN	Ulrich	Ulrich.Haussermann@mmk.su.se
HAYWARD	Michael	michael.hayward@chem.ox.ac.uk
HECTOR	Andrew	a.l.hector@soton.ac.uk
HEINRICI	Markus	markus.heinrici@tugraz.at
HEPPKE	Eva	e.heppke@tu-berlin.de
HERING	Susanne	
HERTRAMPF	Jan	jan.hertrampf@iac.uni-stuttgart.de
HERZIG	Peter	peter.herzig@univie.ac.at
HEYMANN	Gunter	Gunter.Heymann@uibk.ac.at
HILLEBRECHT	Harald	harald.hillebrecht@ac.uni-freiburg.de
HOCH	Constantin	constantin.hoch@cup.lmu.de
HOEHN	Peter	hoehn@cpfs.mpg.de
HOFER	Johannes	johannes.hofer@unileoben.ac.at
HUANG	Rui	rhuangnju@gmail.com
HUANG	Yining	lhuang3@uwo.ca
HULLIGER	Juerg	juerg.hulliger@dcb.unibe.ch
HUPPERTZ	Hubert	hubert.huppertz@uibk.ac.at
IPSER	Herbert	herbert.ipser@univie.ac.at
IRANMANESH	mitra	mitra.iranmanesh@dcb.unibe.ch
ISAEVA	Anna	anna.isaeva@tu-dresden.de
IVANOV	Ivan	ivan.ivanov@urfu.ru
JACOB	Aurélie	a.jacob@fz-juelich.de
JANDL	Isabella	isabella.jandl@univie.ac.at
JANKA	Oliver	ocjanka@uni-muenster.de
JANSEN	Martin	m.jansen@fkf.mpg.de
JUNG	Joo-hei	joohei25@hanmail.net
JUNG-KÖNIG	Jan	jan.jung-koenig@kit.edu
KACEROVSKY	Daniel	d.kacerovsky@mbraun.de
KAINZBAUER	Peter	peter.kainzbauer@univie.ac.at
KANG	Hong Seok	hsk@jj.ac.kr
KARABYN	Vasyl	st44397@student.upce.cz
KARBSTEIN	Alexander	
KASTLUNGER	Georg	georg.kastlunger@tuwien.ac.at

KHARITONOVA	Elena	harit@polly.phys.msu.ru
KIM	Saet Byeol	saet_star@naver.com
KLEEBERG	Fabian	kleeberg@iac.uni-stuttgart.de
KLOß	Simon David	simon.kloss@cup.uni-muenchen.de
KOCHETOVA	Nadezda	Nadezhda.Kochetova@urfu.ru
KOLB	Ute	kolb@uni-mainz.de
KOLCHINA	Liudmila	Ludmila.Kolchina@yandex.ru
KOLLEK	Sarah	skollek@uni-bonn.de
KONAR	Sumit	sumit.konar@mmk.su.se
KONATHAM	Satish	satishdes5@gmail.com
KONOVALOV	Igor	9253571868@mail.ru
KÖPF	Marianne	mariannekoepf@mytum.de
KOROLEV	Dmitrii	chemdim@mail.ru
KOROLEVA	Mariia	marikorolevas@gmail.com
KOSAKA	Tomomi	tkosaka@u-gakugei.ac.jp
KRASNOV	Aleksei	alexey-krasnov@rambler.ru
KREMENETSKAYA	Olga	olga.kremenetskaya@cpfs.mpg.de
KRESSE	Georg	georg.kresse@univie.ac.at
KROUPA	Ales	kroupa@ipm.cz
KRUMEICH	Frank	krumeich@inorg.chem.ethz.ch
KUZNETSOV	Alexey	alexei@inorg.chem.msu.ru
LAI	Kwing To	kt.lai@cpfs.mpg.de
LAINÉ	Fabien	fabien.laine@ensicaen.fr
LANGER	Julia	julia.langer@tugraz.at
LEE	Kuan-Wei	kwlee@isu.edu.tw
LITTERSCHEID	Christian	christian.litterscheid@budenheim.com
LUEF	Christoph	christoph.luef@univie.ac.at
MA	Qianli	v.rostin@fz-juelich.de
MAHHOUTI	Zakaria	z.mahhouti@gmail.com
MAIER	Maria Elisabeth	maria.maier@sbg.ac.at
MAIGNAN	Antoine	
MAIGNAN	Antoine	antoine.maignan@ensicaen.fr
MARCHUK	Alexey	alexey.marchuk@cup.uni-muenchen.de
MARKER	Martin	martin.marker@univie.ac.at
MARKOVIC	Nikola	
MARSHALL	Kayleigh	K.Marshall@bath.ac.uk
MASYS	Sarunas	sarunas.masys@tfai.vu.lt
MATOS	Manuel	mmatos@deq.isel.pt
MATSELKO	Oksana	oksana.matselko@cpfs.mpg.de
MBARKI	Mohammed	mohammed.mbarki@ac.rwth-aachen.de
MECHTAEVA	Elizaveta	mechtaeva.lisa@gmail.com
MILLER	Stuart	stuart.miller@wits.ac.za
MONCHAK	Mykhailo	mykhailo.monchak@kit.edu
MORAN	Emilio	emoran@ucm.es
MORSALI	Ali	morsali_a@modares.ac.ir
MOZHARIVSKYJ	Yurij	mozhar@mcmaster.ca
MÜLLER	Ulrike	ulrike.mueller@chemie.tu-dresden.de
NAJJAR	Wahiba	wahiban@yahoo.fr

NASH	Geoffrey	gn54@sussex.ac.uk
NASH	Philip	nash@iit.edu
NASONAVA	Darya	nasonova@inorg.chem.msu.ru
NAZARCHUK	Evgeny	e_nazarchuk@mail.ru
NEDUMKANDATHIL	Reji	reji.nedumkandathil@mmk.su.se
NENTWIG	Markus	markus.nentwig@yahoo.de
NICKEL	Vera	claudia.schandelle@rockwoodlithium.com
NIEHAUS	Oliver	oliver.niehaus@uni-muenster.de
OANA	Carp	ocarp@icf.ro
ORTNER	Teresa	teresa.ortner@uibk.ac.at
OVCHINNIKOV	Alexander	alexander.ovchinnikov@cpfs.mpg.de
OVSYANNIKOV	Sergey	Sergey.Ovsyannikov@uni-bayreuth.de
ØYGARDEN	Vegar	vegar.oygarden@smn.uio.no
PACHMAYR	Ursula	urpach@cup.uni-muenchen.de
PAIDI	Anil Kumar	anilkpaidi@gmail.com
PALCUT	Marian	marian.palcut@gmail.com
PASET-PAVLOVIC	Katja	
PATHAK	Manisha	pathak@cpfs.mpg.de
PATUREAU	Pascaline	pascaline.patureau@cnrs-imn.fr
PAVLU	Jana	houserova@chemi.muni.cz
PAY GOMEZ	Cesar	cesar.paygomez@kemi.uu.se
PAYNE	David	d.payne@imperial.ac.uk
PEÑA	Alazne	alazne.pena@ehu.eus
PERZ	Martin	martin.perz@unileoben.ac.at
PESCHKE	Simon	sipech@cup.uni-muenchen.de
PET'KOV	Vladimir	petkov@inbox.ru
PETSCHNIG	Lucas	lucas.petschnig@uibk.ac.at
PFITZNER	Arno	arno.pfitzner@chemie.uni-regensburg.de
PIYR	Irina	piyr-iv@chemi.komisc.ru
POBEL	Roman	roman.pobel@cup.uni-muenchen.de
POLT	Julia	
POMPE	Constantin	constantin.pompe@chemie.uni-
PONOU	Simeon	sponou@gmail.com
POPA	Cristina-Liana	cristina.lyana@gmail.com
POSCH	Walter	walter.posch@lactan.at
PRALONG	Valerie	valerie.pralong@ensicaen.fr
PREISHUBER-PFLÜGL	Florian	preishuber-pfluegl@tugraz.at
PRODAN	Alina Mihaela	prodan1084@gmail.com
PROTS	Yurii	prots@cpfs.mpg.de
PRUTSCH	Denise	denise.prutsch@tugraz.at
RABU	Pierre	pierre.rabu@ipcms.unistra.fr
RAGOEN	Céline	ceragoen@ulb.ac.be
RAGUZ	Branimir	branimir_raguz@yahoo.de
RASCHE	Bertold	bertold.rasche@chemie.tu-dresden.de
REGOUTZ	Anna	a.regoutz@imperial.ac.uk
REGUS	Matthias	mregus@ac.uni-kiel.de
REICHMANN	Thomas	Thomas.Reichmann@kit.edu
REIN	Viktor	viktor.rein@kit.edu

REISINGER	Gabriel	gabriel.reisinger@univie.ac.at
RETTENWANDER	Daniel	daniel.rettenwander@sbg.ac.at
RICHTER	Klaus	klaus.richter@univie.ac.at
RICHTER	Verena	verena.richter@bruker.com
RITSCHER	Anna	anna.ritscher@helmholtz-berlin.de
ROEHR	Martin	martin.roehr@kit.edu
ROJO	Teofilo	trojo@cicenergigune.com
ROSHANGHIAS	Ali	ali.roshanghias@univie.ac.at
ROSLOVA	Maria	maria.roslova@chemie.tu-dresden.de
ROSSEINSKY	Matthew J.	M.J.Rosseinsky@liverpool.ac.uk
ROßKOPF	Sigrid	sigrid.rosskopf@springer.at
ROY	Subrata Chandra	scroy1979@yahoo.com
RUDOLPH	Daniel	daniel.rudolph@iac.uni-stuttgart.de
RUEFF	Jean-Michel	jean-michel.rueff@ensicaen.fr
RYABKOV	Yury	ryab2012@gmail.com
SAEZ PUCHE	Regino	rsp92@ucm.es
SAFARIFARD	Vahid	vahidsafarifard@gmail.com
SARDAR	Kripasindhu	K.Sardar@soton.ac.uk
SAUSENG	Bernhard	bernhard.sauseng@netzsch.com
SAYADI	Sami	sami.sayadi@cbs.rnrt.tn
SCHILDHAMMER	Daniel	daniel.schildhammer@uibk.ac.at
SCHMETTERER	Clemens	clemens.schmetterer@umsicht.fraunhofer.de
SCHMIDT	Walter	w.schmidt@tugraz.at
SCHMITZ	Andreas	a.schmitz@uni-bonn.de
SCHNABEL	Anke	anke@uni-bonn.de
SCHNICK	Wolfgang	wolfgang.schnick@uni-muenchen.de
SCHÖTTLE	Christian	christian.schoettle@kit.edu
SCHRÖDL	Nina	nina.schroedl@unileoben.ac.at
SCHWEINBERGER	Michaela	michaela.schweinberger@at.vwr.com
SEÑARIS-RODRIGUEZ	Maria Antonia	m.senaris.rodriguez@udc.es
SEREDA	Vladimir	vladimir.sereda@urfu.ru
SERRAS	Paula	paula.serras@ehu.eus
SESHADRI	Ram	seshadri@mrl.ucsb.edu
SHAQIRI	Halil	h.shaqiri@gmx.de
SHEVELKOV	Andrei	shev@inorg.chem.msu.ru
SITTE	Werner	sitte@unileoben.ac.at
SLABON	Adam	adam.slabon@ac.rwth-aachen.de
SLAWINSKI	Wojciech	w.a.slawinski@smn.uio.no
SOLOKHA	Pavlo	pavlo.solokha@unige.it
STAHNISCH	Andreas	office@LHVAKUUM.at
STANJE	Bernhard	bernhard.stanje@tugraz.at
STEINBERG	Simon	steinberg87@outlook.de
STERNAD	Michael	michael@sternad.com
STEURER	Walter	steurer@mat.ethz.ch
STOIBER	Dominik	stoiber@iac.uni-stuttgart.de
STOLZE	Karoline	karoline.stolze@chemie.tu-dresden.de
STROHAUER-HAHN	Martina	
TAIBL	Stefanie	stefanie.taibl@tuwien.ac.at

TAMBORNINO	Frank	frtach@cup.uni-muenchen.de
TARASCON	Jean Marie	jean-marie.tarascon@college-de-france.fr
TELEGIN	Sergey	svtelegin@imp.uran.ru
TORRALVO	María José	torralvo@ucm.es
TOUZANI	Rachid	rachid.touzani@ac.rwth-aachen.de
TRAIPHOL	Nisanart	nisanart.t@chula.ac.th
TRAIPHOL	Rakchart	rakchartt@nu.ac.th
TSIRLIN	Alexander	altsirlin@gmail.com
TSVETKOV	Dmitry	Dmitry.Tsvetkov@urfu.ru
TSVETKOVA	Nadezhda	Nadezhda.Tcvetkova@urfu.ru
TURBA	Sabrina	sturba@wiley.com
UITZ	Marlena	marlena.uitz@tugraz.at
URUSOVA	Anastasia	anastasiyapodzorova@yandex.ru
VALLDOR	Martin	martin.valldor@cpfs.mpg.de
VASYLECHKO	Leonid	crystal-lov@polynet.lviv.ua
VERCHENKO	Valeriy	verchenko@inorg.chem.msu.ru
VILLESUZANNE	Antoine	av3@bolton.ac.uk
VITZTHUM	Daniela	daniela.vitzthum@uibk.ac.at
VOLKOVA	Nadezhda	nadezhda.volkova@urfu.ru
VRESTAL	Jan	vrestal@chemi.muni.cz
WAGNER	Frank	frank.wagner@cpfs.mpg.de
WAGNER	Reinhard	reinhard.wagner@sbg.ac.at
WAGNER	Tomas	tomas.wagner@upce.cz
WALCH	Gregor	gregor.walch@tuwien.ac.at
WEIHRICH	Richard	richard.weihrich@ur.de
WEIL	Matthias	mweil@mail.zserv.tuwien.ac.at
WEIZ	Alexander	alexander.weiz@tu-dresden.de
WELLER	Mark	mtw27@bath.ac.uk
WELZL	Andreas	andreas.welzl@tuwien.ac.at
WEST	Anthony	a.r.west@sheffield.ac.uk
WIBNER	Patrick	patrick.wibner@univie.ac.at
WILKENING	Martin	wilkening@tugraz.at
WITTICH	Knut	s6knwitt@uni-bonn.de
WOHLMUTH	Dominik	wohlmuth@tugraz.at
WOLF	Silke	silke.wolf@kit.edu
WOODRUFF	Daniel	daniel.woodruff@chem.ox.ac.uk
WOODS	Michael	maw44@kent.ac.uk
WÖRSCHING	Matthias	mawoch@cup.uni-muenchen.de
YAKYMOVYCH	Andriy	andriy.yakymovych@univie.ac.at
YAMAMOTO	Ayako	ayako-yamamoto@riken.jp
YU	Jae Su	jsyu@khu.ac.kr
ZAGAYNOV	Igor	igorscience@gmail.com
ZEVALKINK	Alexandra	alex.z.williams@gmail.com
ZHANG	Bo	st44389@student.upce.cz

City Maps


U1 U-Bahn-Linie
S 1 S-Bahn-Linie
CAT City Airport Train
Lokalbahn Wien–Baden
VIB International Vienna International Busterminal
Kundenzentrum der Wiener Linien (U3 Erdberg)
Informationsstelle der Wiener Linien
Tickets-Verkaufsstelle der Wiener Linien
P+R Park & Ride
© Wiener Linien, August 2013
U1
Leopoldau
Großfeldsiedlung
Aderklaaer Straße
Rennbahnweg
Kagraner Platz
Kagran
Alte Donau
Kaisermühlen-VIC
Donauinsel
Vorgartenstraße
Praterstern
Nestroypl.
Schwedenplatz
Stephansplatz
Karlsplatz
Taubstummengasse
Südtiroler Platz Hauptbahnhof
Keplerplatz
Reumannplatz
U2
Seestadt
Aspern Nord
Hausfeldstraße
Aspernstraße
Donauspital
Hardeggasse
Stadlau
Donaustadtbrücke
Donaumarina
Stadion
Krieau
Messe-Prater
Taborstraße
Schottenring
Schottentor
Rathaus
Volkstheater
Museumsquartier
U3
Simmering
Enkplatz
Zippererstraße
Gasometer
Erdberg
Schlachthausgasse
Kardinal-Nagl-Platz
Rochusgasse
Landstraße (Bhf. Wien Mitte)
Stubentor
Herrengasse
Neubaugasse
Zieglergasse
Westbahnhof
Schweglerstraße
Johnstraße
Hütteldorfer Straße
Kendlerstraße
Ottakring
U4
Heiligenstadt
Spittelau
Friedensbrücke
Roßauer Lände
Stadtpark
Kettenbrückengasse
Pilgramgasse
Margaretengürtel
Längenfeldgasse
Meidling Hauptstraße
Schönbrunn
Hietzing
Braunschweiggasse
Unter St. Veit
Ober St. Veit
Hütteldorf
U6
Floridsdorf
Neue Donau
Handelskai
Dresdner Straße
Jägerstraße
Nußdorfer Straße
Währinger Straße-Volksoper
Michelbeuern-AKH
Alser Straße
Josefstädter Straße
Thaliastraße
Burggasse-Stadthalle
Gumpendorfer Straße
Niederhofstraße
Bahnhof Meidling
Tscherttegasse
Am Schöpfwerk
Alterlaa
Erlaaer Straße
Perfektastraße
Siebenhirten
S 1
S 2
S 3
S 7
S 40
S 45
S 50
S 60
S 80
CAT
Gerasdorf
Süßenbrunn
Siemensstraße
Strebersdorf
Jedlersdorf
Brünner Straße
Traisengasse
Nußdorf
Oberdöbling
Krottenbachstr.
Gersthof
Hernals
Breitensee
Penzing
Franz-Josefs-Bahnhof
Hirschstetten
Erzherzog-Karl-Straße
Lobau
Praterkai
Haidestraße
Rennweg
St.Marx
Geiselbergstr.
Grillgasse
Zentralfriedhof
Kaiserebersdorf
Schwechat
Kledering
Quartier Belvedere
Matzleinsdorfer Platz
Blumental
Speising
Hetzendorf
Atzgersdorf
Liesing
Wolf in der Au
Hadersdorf
Weidlingau
Purkersdorf-Sanatorium
Schedifkaplatz
Schöpfwerk
Gutheil-Schoder-Gasse
Inzersdorf Personenbahnhof
Neu Erlaa
Schönbrunner Allee
Vösendorf-Siebenhirten
W.B Wiener Neudorf, Baden (Endstation)


NIGHTLINE
Samstag, Sonntag und Feiertage.
U-Bahn
Nachtbus
ASTAX
Achtung: Eingezeichnete Haltestellen sind nur eine Auswahl!
N38
Grinzing
Sieveringer Straße
N36
Nußdorf
N35
Salmannsdorf
Agnesgasse
Glanzing
Gatterburggasse
U4
Heiligenstadt
Spittelau
N35
Nußdorfer Straße
N36
N20
Strebersdorf
U6
Floridsdorf
N29
N31
Stammersdorf
Großjedlersdorf
Fultonstraße
N20
U1
Leopoldau
Kagraner Platz
N23
N23
N23
Breitenlee
Neueßling
Kagran
N26
Hirschstetten
Am Heidjöchl
N23
Friedrich-Engels-Platz
Jägerstraße
Dresdner Straße
Traisengasse
Kaisermühlen
N90
Donaustadtstraße
U2
Aspernstraße
ab 2. Oktober 2010
Hardeggasse
Donauspital
N90
Aspern, Siegesplatz
Eßling
Guntherstraße Stadtgrenze
N26
Schüttauplatz
Donaustadtbrücke
Stadion
U2
ab 2. Oktober 2010
Taborstraße
Praterstern
N29
Schottenring
Schwedenplatz
N41
Pötzleinsdorf
Gersthof
Aumannplatz
Währinger Straße
N41
N38
Schottentor
N43
Neuwaldegg
Dornbach
Hernals
Elterleinplatz
Alser Straße
Skodagasse
N71
N43
N46
Otto-Wagner-Spital
Joachimsthalerplatz
U3
Ottakring
Thaliastraße
Strozzigasse / Piaristengasse
Volkstheater
Stephansplatz
Westbahnhof
Neubaugasse
Museumsquartier
U2
Landstraße
N49
Auhof
Baumgarten
Breitensee
N49
Hütteldorfer Straße
N54
N6
U4
Hütteldorf
Ober St. Veit
Unter St. Veit
N54
Hietzing
N60
Gumpendorfer Straße
Längenfeldgasse
Margaretengürtel
Pilgramgasse
Karlsplatz
N46
N62
360
Rennweg
St. Marx
Zippererstraße
Enkplatz
N6
U3
Simmering
Matzleinsdorfer Platz
U1
N68
Reumannplatz
N67
N66
Absbergbrücke
Laaer Berg
N68
Kaiserebersdorf
N71
Nemethgasse
Speising
N62
Edelsinnstraße
Philadelphiabrücke
Business-Park-Vienna
Raxstraße
Altes Landgut
Himberger Straße
N17
Oberlaaer Platz
Unterlaa
N17
Maurer Hauptplatz
N60
N61
Am Schöpfwerk
Computerstraße
Otto-Probst-Platz
Neu Erlaa
Vösendorf, Siebenhirten
Tarifgrenze
360
nach Baden
Birostraße
Inzersdorf Großmarkt
N67
Rodaun
N61
N66
Liesing
Atzgersdorf
Alterlaa
U6
Siebenhirten

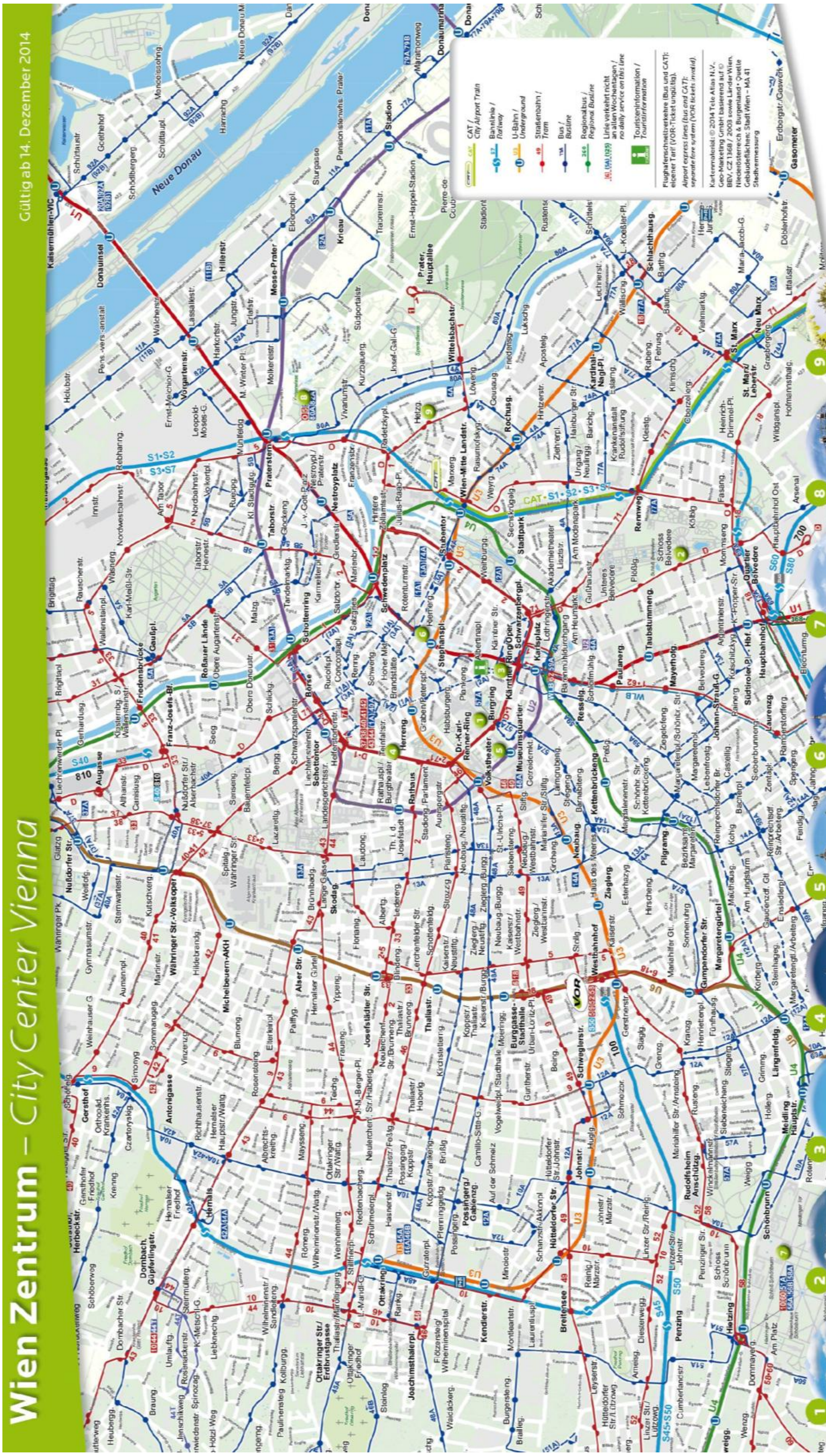
Wien Zentrum – City Center Vienna
Gültig ab 14. Dezember 2014
CAT / City Airport Train
Bahnlinie / Railway
U-Bahn / Underground
Straßenbahn / Tram
Bus / Busline
Regionalbus / Regional Busline
Linie verkehrt nicht an allen Wochentagen / no daily service on this line
Touristeninformation / Touristinformation
Flughafenschnellverkehre (Bus und CAT): eigener Tarif (VOR-Ticket ungültig).
Airport express lines (bus and CAT): separate fare system (VOR tickets invalid).
Kartenmaterial: © 2014 Tele Atlas N.V., Geo-Marketing GmbH basierend auf © BEV, CZ 1368 / 2003 sowie Länder Wien, Niederösterreich & Burgenland • Quelle Gebäudeflächen: Stadt Wien – MA 41 Stadtvermessung
Besser unterwegs
VOR Verkehrsverbund Ost-Region
1 Hofburg
2 Belvedere
3 Oper
4 Burgtheater
5 Kunsthistorisches Museum
6 Stephansdom
7 Schönbrunn
8 Riesenrad
9 Hundertwasser Haus
www.vor.at
0810 22 23 24
AnachB | VOR App
BahnhofCity Wien West